ΕΘΝΙΚΟ ΜΕΤΣΟΒΙΟ ΠΟΛΥΤΕΧΝΕΙΟ

Σχολή Πολιτικών Μηχανικών

Τομέας Γεωτεχνικής

NATIONAL TECHNICAL UNIVERSITY

School of Civil Engineering

Geotechnical Department

Διδακτορική Διατριβή

Κινηματική-Αδρανειακή Απόκριση Απλών Κατασκευών και Επικαθημένων Σηράγγων υπό Ισχυρή Σεισμική Διέγερση Επηρεασμένη από την 2-Διάστατη Γεωμετρία Εδαφικής Κοιλάδας

Ευαγγελία Γαρίνη

Δίπλωμα Πολιτικού Μηχανικού
Ε.Μ.Π., 2003

Master of Science in Civil Engineering
SUNY at Buffalo, 2005

Επιβλέπων

Καθηγητής Γεώργιος Γκαζέτας

Νοέμβριος 2011

ΕΘΝΙΚΟ ΜΕΤΣΟΒΙΟ ΠΟΛΥΤΕΧΝΕΙΟ

Σχολή Πολιτικών Μηχανικών

Τομέας Γεωτεχνικής

NATIONAL TECHNICAL UNIVERSITY

School of Civil Engineering

Geotechnical Department

Διδακτορική Διατριβή

Συστήματα Ολισθήσεως Υποβαλλόμενα σε Εγγύς-του-Ρήγματος Σεισμικές Διεγέρσεις: Ανάπτυξη Θεμελιωδών Ανελαστικών Αναλόγων

Ευαγγελία Γαρίνη

Δίπλωμα Πολιτικού Μηχανικού
Ε.Μ.Π., 2003

Master of Science in Civil Engineering
SUNY at Buffalo, 2005

Επιβλέπων

Καθηγητής Γεώργιος Γκαζέτας

Νοέμβριος 2011

ΕΘΝΙΚΟ ΜΕΤΣΟΒΙΟ ΠΟΛΥΤΕΧΝΕΙΟ

Σχολή Πολιτικών Μηχανικών

Τομέας Γεωτεχνικής

NATIONAL TECHNICAL UNIVERSITY

School of Civil Engineering

Geotechnical Department

Doctoral Thesis

Sliding Systems under Near–Fault Ground Shaking: Development and Demonstration of Inelastic Analogues

Evangelia Garini

Diploma of Civil Engineering
NTUA, 2003

Master of Science in Civil Engineering
SUNY at Buffalo, 2005

Supervised by

Prof. George Gazetas

November 2011

Table of Contents

CHAPTER 5

CHAPTER 6

CHAPTER 7

Chapter 1

Introduction and Literature Review

1.1 Sliding systems in Geotechnical engineering

Numerous earthquakes and subsequent geotechnical failures in the last decade put forward the significance of strong motion phenomena such as "directivity" and "fling". Moreover, the inelastic behaviour either of the soil or of any geotechnical structure as a whole system, reminds us of the importance of studying non-conventional inelastic systems.

Several geotechnical systems, as illustrated in Figure 1.2, develop sliding mechanisms when they respond to a dynamic excitation. For instance, the partial failure of a section in an embankment dam or in a physical slope is triggered when the shear stresses exceeds shear strength, leading to the formation of a sliding surface upon which failure is triggered. Also, with a retaining gravity wall in earthquake shaking–a Coulomb type soil prism forms behind the wall which fails by yielding and displaces horizontally. Bearing capacity problems of shallow footings can be regarded as sliding blocks on top of a horizontal base.

In structural engineering, seismic isolation of structures or of single objects perform fundamentally as sliding systems. Figure 1.3 portrays the statue of Hermes of Praxiteles

at the archaeological museum of Olympia, which is seismically isolated with a friction pendulum bearing. Dynamic response in this case, resembles the response of a block on a horizontal base, sliding with recentering mechanism.

Landslides are the most straightforward phenomenon with dominant sliding behaviour. These failures are generated by the loss of shear strength in the soil. We are interested about landslides triggered by earthquakes themselves. The size of the area affected by earthquake-induced landslides depends on the magnitude of the earthquake, its focal depth, the topography and geologic conditions near the fault, and the amplitude, frequency content and duration of ground shaking.

For example during the 2008 Wenchuan M_S 8.0 earthquake in China 3627 landslides, 2383 slope collapses, 837 debris flows have been triggerd (Figure 1.4). What is more, the 2011 Christchurch M6.3 earthquake also offer numerous cases of landslides. Figure 1.5 presents some of these sliding failures.

1.2 The Newmark analogue

In his 1965 seminal Rankine Lecture, Newmark proposed that the seismic performance of earth dams and embankments could be evaluated in terms of permanent deformations which occur whenever the inertia forces on a potential slide mass are large enough to overcome the frictional resistance at the "failure" surface and he proposed the analogue of a rigid block on inclined plane as a simple way of analytically obtaining approximate estimates of these deformations.

As aforementioned in the previous section, many applications in geotechnical earthquake engineering require use and understanding of the dynamic sliding response of a block of mass m supported on seismically vibrating base through an asymmetric frictional contact. Figure 1.1 depicts a rigid block of mass, m, resting on a plane inclined

at an angle β; the available frictional resistance (for excitation acting parallel to the slope) is:

$$F_1 = mg\,(\mu\cos\beta - \sin\beta) \qquad (1.1)$$

when the block slides downward, and

$$F_2 = mg\,(\mu\cos\beta + \sin\beta) \qquad (1.2)$$

when it moves upward. μ is the constant coefficient of Coulomb friction at the block–base interface. Therefore when an acceleration pulse acts from left to right ("upward"), the inertial force on the block acts downhill and block's acceleration can not exceed the critical value:

$$\alpha_{C_1} = \mu\cos\beta - \sin\beta \qquad (1.3)$$

Whereas in the opposite direction ("downward" base motion) the inertia acts uphill and acceleration of the block can not exceed:

$$\alpha_{C_2} = \mu\cos\beta + \sin\beta \qquad (1.4)$$

Evidently, $\alpha_{C_1} < \alpha_{C_2}$. Since the geotechnical interest is usually in relatively large values of β (e.g. $\beta > 20^o$) and small values of the coefficient of friction ($\mu < 0.70$), the ratio $\alpha_{C_2}/\alpha_{C_1} >> 1$. Thus, there is practically only one limiting acceleration: $\alpha_C = \alpha_{C_1}$ and α_{C_2} can be considered as infinitely large. This of course should not be unduly generalized: mild slopes and lined landfills, for example, will sustain both downward and upward, asymmetric sliding.

As long as the "upward" base acceleration $\alpha_H(t)$ does not exceed α_C the block remains attached to its base, with the acceleration $\alpha_H(t)$ of the base. Sliding downhill occurs whenever $\alpha_H(t) > \alpha_C$. Throughout sliding the acceleration remains constant equal to α_C. The movement continues until the velocities of the block and the ground equalize. Knowing the critical acceleration and the time history of base excitation, permanent

displacements in every sliding period are calculated by a straightforward integration process.

Thanks to the transient nature of the earthquake loading, even if the block is subjected to a number of acceleration pulses higher than its critical acceleration, it may only experience a small permanent deformation rather than complete failure.

1.3 Extensions of Newmark's analogue

Newmark's analogue had been inspired by an earlier unpublished work by R. V. Whitman in connection with the study of the displacements of the Panama Canal slopes if exposed to nuclear explosion — as revealed by Marcuson (1994) and recently reported by Reitherman (2010). Since then, the analogue has seen numerous applications and extensions.

Applications in recent years include the seismic deformation analysis of earth dams and embankments (Seed & Martin, 1966; Ambraseys & Sarma, 1967; Sarma, 1975, 1981; Franklin & Chang, 1977; Makdisi & Seed, 1978; Lin & Whitman, 1983; Constantinou & Gazetas, 1987; Yegian et al, 1991; Sawada et al, 1993; Gazetas & Uddin, 1994; Kramer, 1996; Kramer & Smith, 1997; Rathje & Bray, 1999); the displacements associated with landslides (Wilson & Keefer, 1983; Jibson, 1994; Harp & Jibson, 1995; Del Gaudio et al, 2003); the seismic deformation of landfills with geosynthetic liners (Yegian et al, 1998; Bray & Rathjee, 1998); the seismic settlement of surface foundations (Richards et al, 1982); and the potential sliding of concrete gravity dams (Leger & Katsouli, 1989; Danay & Adeghe, 1993; Fenves & Chopra, 1996).

The extension of the analogue by Richards & Elms (1979) to gravity retaining walls has met worldwide acceptance, and has found its way into seismic codes of practice. Several other generalized applications have also appeared (examples: Constantinou et

al, 1984; Ambraseys & Menu, 1988; Ambraseys & Srbulov, 1994; Stamatopoulos, 1996; Rathje & Bray, 2000; Ling, 2001; Fardis et al, 2003; Wartman et al, 2003).

1.4 Study objectives

The scope of this work is to investigate the seismic response of sliding systems utilising the Newmark analogue not only in its original configuration but including also: (i) different types of frictional behaviour of the yielding interface between the block and its base, (ii) several combinations of triggering motion. Figure 1.6 portrays these triggering combinations; base excitation can be horizontal or simultaneous vertical-and-horizontal in case of a horizontal plane, whereas for an inclined base triggering can be parallel to the plane, horizontal to the plane, or simultaneously horizontal and vertical. In addition, sliding of a rigid body on an inclined base, could occur on top of a single degree of freedom oscillator. In that way the elasticity of the base is embraced too.

Figure 1.7 illustrates the friction models utilised herein. Coulomb's law of rigid-perfectly-plastic friction with a constant coefficient of friction, μ, is extended to elasto-plastic relationships and exponentially related friction with sliding velocity. In this way, the sensitivity of sliding response is tested and thorough understanding of the phenomenon is to be achieved.

At first, a number of simple wavelets are utilised as excitation and parametrical analyses are performed. A wide variety of real accelerograms from strong earthquakes are applied as to incorporate near-fault characteristics in our research. Roughly 120 different ground motions are employed. The aim is to end up with empirical expressions to estimate sliding displacement for a minimum of ground motion information.

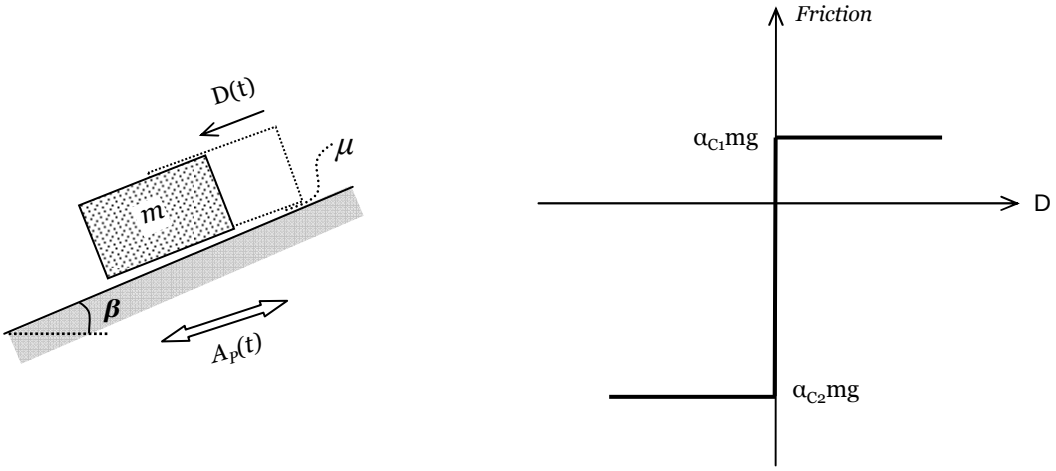

Figure 1.1 *Schematic representation of the Newmark 1965 sliding-block analogue and friction force as a function of slip displacement.*

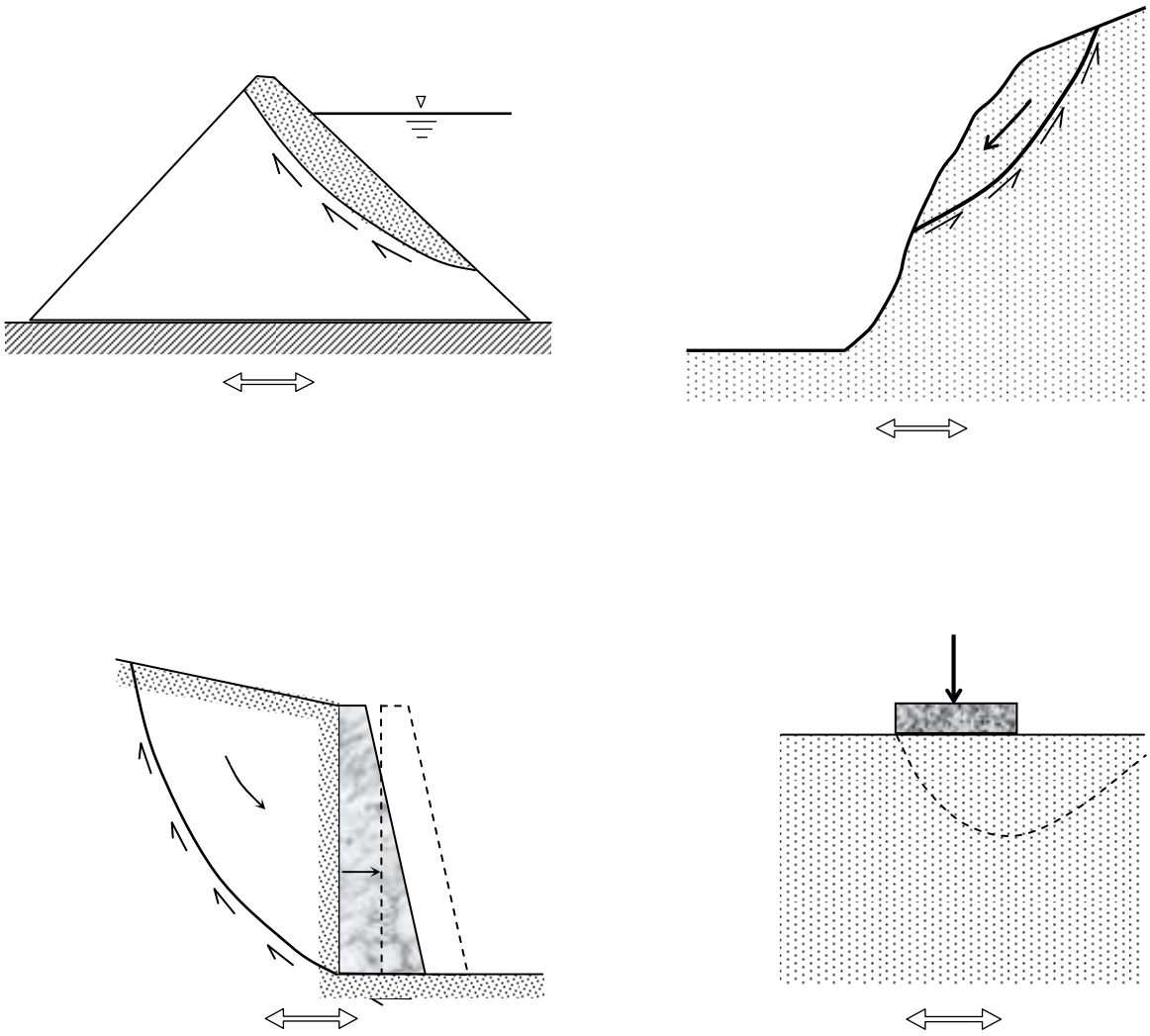

Figure 1.2 *Fundamental types of geotechnical structures that can be modelled as sliding objects on top of horizontal or slope planes.*

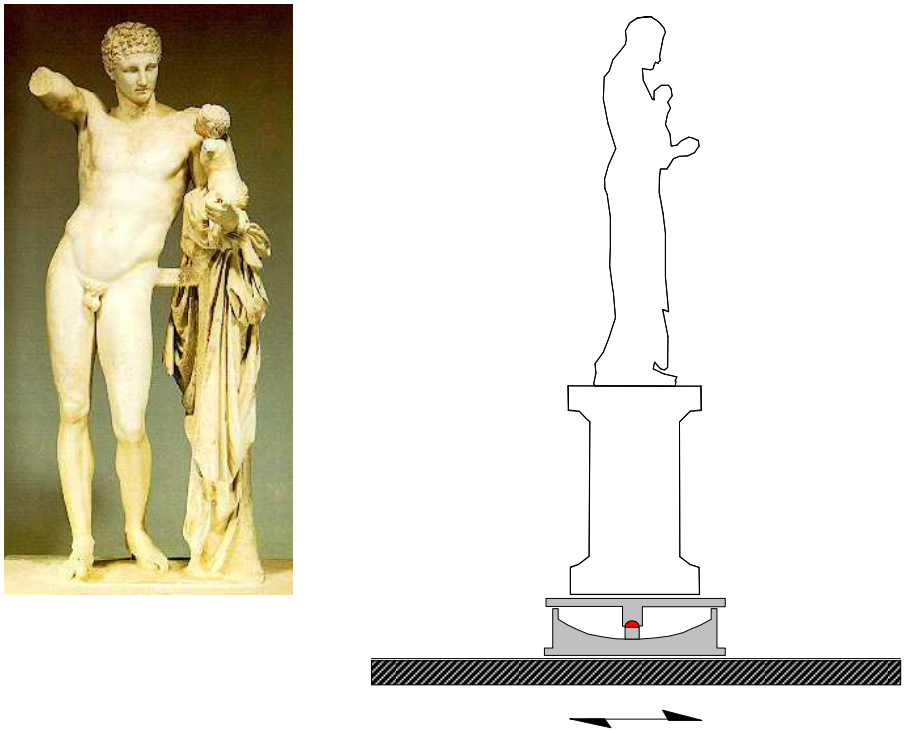

Figure 1.3 *One example of an isolated system that can be modelled as a sliding objects on horizontal plane: the isolation of the statue of Hermes at the museum of ancient Olympia.*

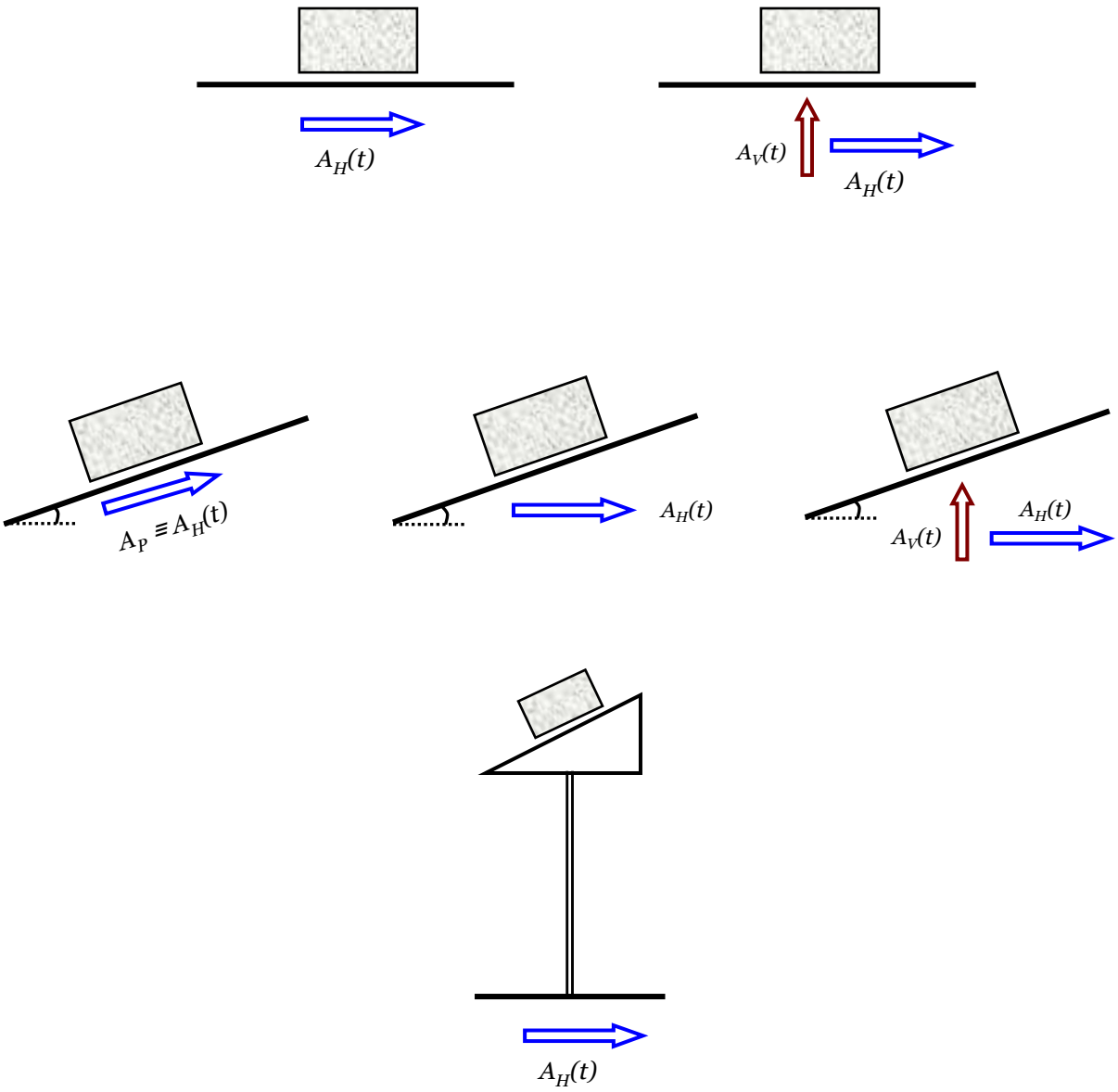

Figure 1.6 *Sketches of the sliding and excitation combinations examined.*

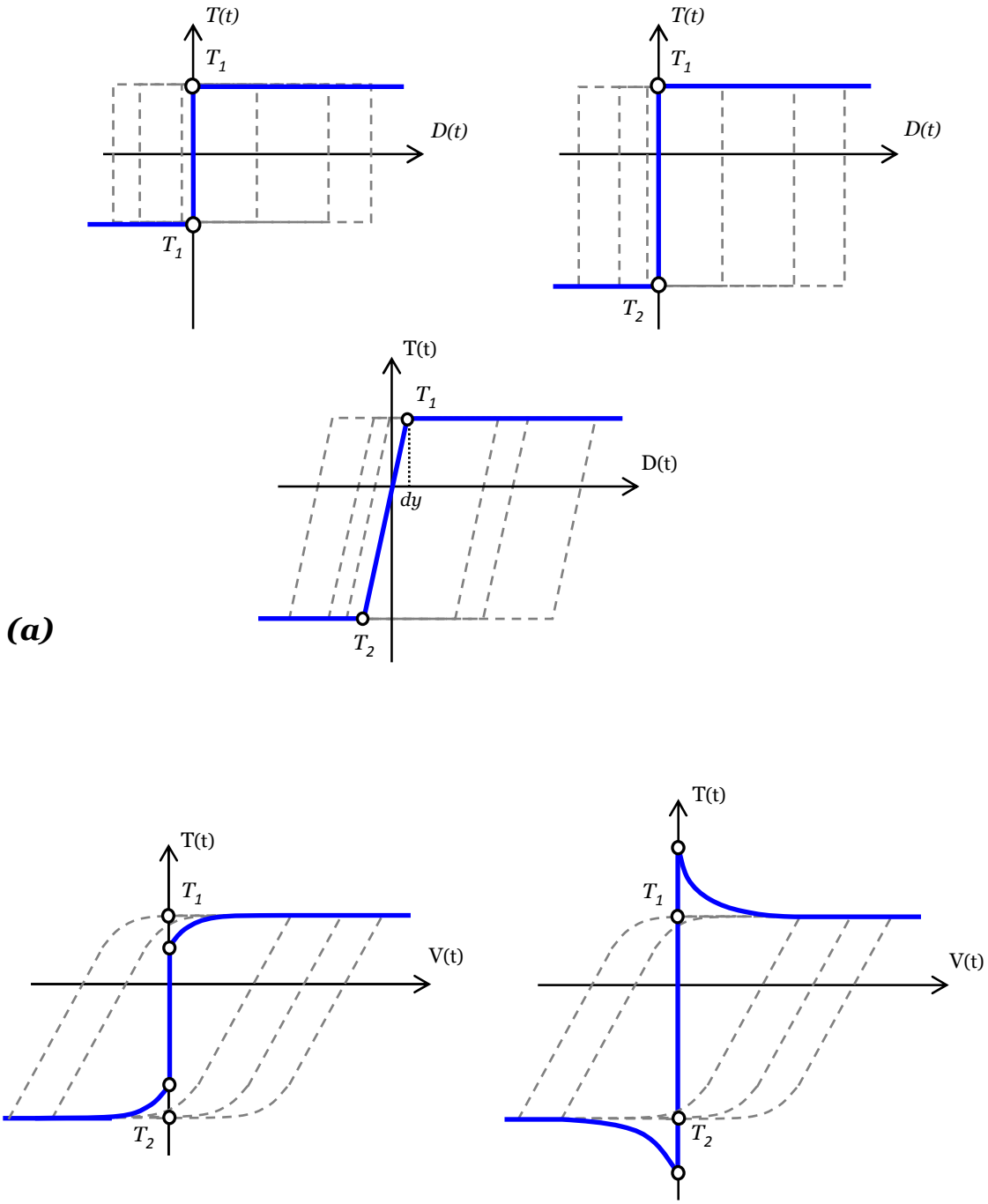

Figure 1.7 *(a) Friction-displacement and (b) friction-velocity relations governing the sliding interface between the block and its base.*

Chapter 2

Sliding Response at Near-Fault Regions

2.1 Earthquakes and Near-Fault Phenomena

Seismic wave characteristics are altered as they travel from the rupture source to the site of interest. The mechanisms that provoke wave propagation alterations are: wave dispersion at geological heterogeneities, energy dissipation, soil filtering and frequency non-linearity and topography (Silva, 1988; Aki and Richards, 1980). But these are not the only parameters that have influenced ground shaking, as fault rupture characteristics also affect the frequency and duration of earthquake ground motions.

Specifically, in the close neighbourhood of a rupturing seismic fault ground shaking may be affected by wave propagation effects known as "forward directivity" and by tectonic deformations producing a permanent ground offset known as "fling-step". The former effect is the outcome of the coherent arrival of seismic waves emitted from a seismogenetic fault when its rupturing propagates towards the site. It manifests itself with a single long–period and high–amplitude pulse occurring near the beginning of shaking, and oriented perpendicularly to the fault (Somerville, 2000). The fling-step effect is the outcome of the tectonic permanent deformation of the earth in the proximity of the fault. It manifests itself in the record with a residual displacement, oriented

parallel to the fault strike with strike-slip earthquakes and perpendicular to the fault with purely dip-slip (normal or thrust) earthquakes (Abrahamson, 2001).

Figure 2.1 is a sketch of a strike-slip event, portraying the idealized "signatures" of the two phenomena on the fault-normal and fault-parallel components of the displacement record. Two remarkable accelerograms are depicted in Figure 2.1, Sakarya (from Kocaeli 1999) and Jensen Filtration Plant (from Northridge 1994) exhibiting fling-step and forward directivity effects, respectively. The velocity time history of Sakarya contains a large pulse (0.8 m/s) of huge duration (4 s), which is consistent with the permanent ground offset of about 2 m that can be seen in the derived displacement record, and which has actually been observed in the field (with geodetic measurements). The derived velocity time history of Jensen contains several cycles with a devastating maximum velocity step $\Delta V \simeq 1.8$ m/s. The destructive capacity of this velocity increment was first elaborated by Bertero (1976).

A significant amount of research has been devoted to the two phenomena, especially in the aftermath of the Northridge, Kobe, Kocaeli, and Chi-Chi earthquakes. That research has so far focused: first, on identifying, interpreting, and mathematically representing the effects of "directivity" and "fling" on the ground motions (Singh, 1985; Somerville, 2000 & 2003; Abrahamson, 2001; Makris, 2000; Mavroeidis & Papageorgiou, 2003; Hisada & Bielak, 2003; Bray & Rondrigeuez-Marek, 2004; Howard et al., 2005); then, on developing empirical predictive relationships for the parameter characterization of the directivity or fling related pulses (Somerville et al., 1997; Bray & Rondriguez-Marek, 2004; Xie et al., 2005); and finally, on assessing the potential of directivity and fling pulses to inflict damage in a variety of geotechnical and structural systems (for example : Bertero et al., 1978; Singh, 1985; Hall et al., 1995; Gazetas, 1996;

Kramer & Smith, 1997; Iwan et al., 2000; Sasani & Bertero, 2000; Makris & Rousos, 2000; Alawi & Krawinkler, 2001; Jangid & Kelly, 2001; Pavlou & Constantinou, 2004; Shen et al., 2004; Mavroeidis et al., 2005; Xu et al., 2006; Changhai et al., 2007).

2.1.1 Directivity Effect in Acceleration Records

Earthquakes of small magnitude are frequently generated by sources that may be represented by a point, since the fault rupture extends only a few kilometres in each direction. However, for large earthquakes, fault rupture trace can be several hundred kilometres long. In the latter case, earthquake stress waves propagate in the direction of the fault rupture more intensely than in other directions.

Waves propagate away from the fault rupture with different intensity along different directions; this phenomenon is referred to as "directivity". Directivity occurs because fault rupture is a moving wave source, which travels at a finite velocity (of the order of 3 km/s) along the fault. As the fault rupture (or earthquake source) moves away from the hypocentre, it generates waves from each segment of the breaking fault. The wave energy radiates outward in all directions (expanding wavefronts).

The "constructive interference" of stress waves results in larger ground-motion magnification with shorter total duration in the direction of rupture propagation. Lower amplitude motions but longer total duration are exhibited in the opposite direction. Constructive interference, which resembles the Doppler effect, generates strong acceleration pulses at sites towards the direction of fault rupture (Singh, 1985; Somerville et al., 1997).

Rupture directivity also induces polarization of ground motion, i.e. differences between the fault-normal and fault-parallel components of horizontal ground-motion amplitudes (Stewart et al., 2001). This polarization causes more intense shaking in the

fault-normal direction than in the fault-parallel direction, especially for periods greater than 0.5 seconds (Somerville, 2000).

Figure 2.2 displays a few records with prominent directivity acceleration pulses, which are employed as triggering excitations in this study. Such pulses lead to significant velocity pulses too. However, displacement at the end of shaking is zero.

In the aftermath of the Northridge 1994 and Kobe 1995 earthquakes, Somerville et al (1997), having demonstrated that rupture directivity effects cause spatial and directional variations in ground motion at periods beyond 0.6 seconds, developed improved empirical attenuation relations to account for such effects on strong motion amplitudes and durations.

2.1.2 Fling Effect in Displacement Records

Rupture traces on the ground surface may be induced not so much by intense shaking, as by the emergence of fault rupture on the surface. Deep cracks and large gaps are generated (ranging in size from a few metres to several kilometres). Damage by fault rupture is more localized than the widespread damage caused by ground shaking.

The effects of major fault ruptures can be extreme on structures. Buildings can be ripped apart. Cracks and gaps in the ground may cause serious damage to transportation systems (highways, railways, ports and airports) and underground networks (water, wastewater and gas pipes, electric and telephone cables). Structures founded either in part or wholly on the hanging-wall or the foot-wall part may experience significantly different lateral and vertical deformations.

Fling is defined as the tectonic permanent displacement (offset) of the earth in the proximity of the seismogenic fault rupture. The fling step is significant in the parallel component of motion in close proximity to the fault, especially if the latter emerges on the

surface with a large static offset. Figure 2.3 portrays several selected records with a conspicuous fling step. Notice the resulting velocity pulses which induce the permanent displacement at the end of the motion.

The deeper nature of the two phenomena (directivity and fling) has been investigated analytically in a seminal paper by Hisada & Bielak (2003), who made use of the representation theorem and paid special attention to the superposition of static and dynamic Green's functions. They showed that fling effects (being of a static nature) attenuate very rapidly with distance from the fault, in proportion to r^{-2} *(just as static displacement in an infinite medium). That is why fling effects are hardly noticeable with "buried" faults, whose rupture does not reach close to the ground surface. By contrast, forward directivity effects are the result of constructive wave interference; hence, the associated attenuation away from the fault is much slower, on an order which ranges from* r^{-1} *to* $r^{-1/2}$ *(the former appropriate for body waves, the latter for surface waves).*

Other numerical seismic source models in combination with Green's functions have also been developed, accounting in a natural way for directivity effects (e.g., Pitarka et al., 2000 & 2002). More recent efforts to develop empirical predictive relations and parameter characterization of the directivity and fling related pulses include those of Abrahamson, 2000; Bray & Rodriguez-Marek, 2004; Xie et al., 2005; Voyagaki et al., 2008; Taflampas, 2008. At the same time the idealization and mathematical representation of near–fault pulses has attracted significant interest (see Makris & Roussos, 2000; Mavroeidis & Papageorgiou, 2003 & 2010; Howard et al., 2005; Xie et al., 2005; among others).

Numerous studies have been published to date assessing analytically and experimentally the potential of 'directivity' pulses to cause large response and inflict damage to a variety of structural systems – the latter falling mostly in the realm of

elastic or elastoplastic response (examples : Bertero et al., 1976, 1978; Hall et al., 1995; Iwan et al., 2000; Sasani & Bertero, 2000; Alawi & Krawinkler, 2000; Junwu et al., 2004; Pavlou & Constantinou, 2004; Mavroeidis et al., 2004; Makris & Psychogios, 2006; Changhai et al., 2007).

However, studies on the "destructiveness" of ground motions containing 'fling-step' pulses have been, understandably, quite limited because the phenomenon has been clearly identified and distinguished from other phenomena only recently (Abrahamson, 2001; Hisada & Bielak, 2003). Moreover, since the dominant periods of fling-steps are quite long, usually exceeding 2 sec, it was presumed (on the basis of elastic–response way of thinking) that their effects were less important than of directivity (Howard et al., 2005). It will be shown in the sequel that with strongly inelastic systems, such as the ones examined here, this may not necessarily be the case at all.

The destructive potential of long duration acceleration pulses, which is one of the outcomes of directivity and fling effects, has been demonstrated in the pioneering work of Bertero (1976) in connection with the heavy damage of the Olive View Hospital during the San Fernando 1971 earthquake. One of the significant conclusions of his research was that:

> *"The types of excitation that induce the maximum response in elastic and non-elastic systems are fundamentally different and hence one can not derive the maximum non-elastic response from the corresponding elastic one" (Bertero 1976).*

The above remark has motivated our choice of the ideally rigid–plastic constant–friction systems: in addition to their obvious direct use in earthquake engineering, they are representative of extremely–inelastic behaviour. The anticipation was that such systems

would be far more sensitive than the purely linear elastic systems (the other extreme of reality) to the peculiarity of near-fault ground shaking.

2.2 Numerical Simulation and Analyses

An idealised rigid–perfectly-plastic system was studied: the block on a sloping base, the asymmetric sliding of which is governed by Coulomb's friction 'law' with a constant coefficient μ (Figure 2.4). In addition to the obvious use of the presented results in a number of real-life seismic geotechnical problems, the examined block-on-inclined-plane model is representative of systems with highly–inelastic behaviour.

The numerical simulation performed with the finite element code ABAQUS. The analysed model consists of a mass element connecting to the base by a gap element governed by the Coulomb's frictional law. Behaviour of the gap element is determined just by the friction coefficient μ. Base node is subjected to acceleration excitation.

2.3 Sliding on Inclined Plane Subjected to Parallel Seismic Excitation

We studied the effects of 120 near-fault accelerograms on the accumulated slip of a rigid block on a plane base inclined at an angle 25^{o}. A list of these records is given in Table 1 along with some of their key properties. The parameters that are investigated and shown here, are:

- the ratio of α_{C1}/α_p of the downslope critical acceleration divided by the peak value of the base acceleration ($\alpha_{C1}/\alpha_p = 0.05 - 0.60$)
- the influence of polarity [the + or – direction of the excitation (i.e. upslope or downslope)].

Only a limited number of analyses are shown here in detail, but the results of all analyses are compiled in diagrams and compared with the available charts from the literature. In the following, results are presented classified by earthquake.

2.3.1 The M 7.0, 1995 Kobe Earthquake

The Kobe earthquake of 17th January 1995 was one of the most disastrous events ever happened in Japan. The temblor lasted for 20 seconds, registered a magnitude of 7.0, and caused at least $150 billion worth of damage. The death toll was 6,500 people. Roughly 100,000 structures were damaged or totally destroyed.

Several seismographic stations recorded the event, among which the six three-component records employed in our study: Fukiai, JMA, Nishi-Akashi, Shinkobe, Takarazuka and Takatori. These accelerograms applied without any scaling as base excitation, with their original magnitude; few of the results are presented in Figures 2.5÷2.12.

Let us discuss some of these: Figure 2.5 illustrates sliding response for the Fukiai record when imposed with its normal and reverse polarity. Fukiai is a forward directivity ground motion, characterised by large amplitude pulses of long duration (the major pulse has 0.81 g amplitude and a period of ≈1 second). The well shaped directivity pulses in acceleration induce a series of almost symmetric cycles in velocity. This symmetry of velocity explains the minor influence of polarity in slippage. It will be seen again: directivity results to symmetric velocity, thus to small polarity effect.

Figure 2.7 depicts the acceleration, velocity and displacement response to the JMA-90o component. JMA is also a forward directivity record and is another example of the aforementioned conclusion: minor polarity effect as a consequence of symmetric

velocity. The same applies in case of Shinkobe (Figure 2.9) and Takarazuka (Figure 2.10) records.

2.3.2 The M 6.7, 1994 Northridge Earthquake

The Northridge earthquake struck the region of San Fernando Valley in southern California on 17th January 1994. The moment magnitude of the event was 6.7. Rupture occurred along a south-dipping, blind thrust fault; therefore no surface faulting was produced. The earthquake resulted in 57 deaths, and structural damage of more than $20 billion. Northridge earthquake was the costliest seismic disaster in U.S. history.

Ground shaking had been recorded in several hundred stations across the Los Angeles and San Fernando valleys. The highest ever instrumentally recorded acceleration in North America, registered at 1.78 g in the Tarzana station which is located 6 km from the epicentre. However, Tarzana is located at the top of a small hill and this suggests intense topographical amplification of earthquake motion (Spudich et al., 1996). This is the reason we exclude Tarzana record from our study. Nevertheless, the ten strongest (by means of acceleration) records are utilised as base triggering.

Figures 2.13÷2.28 display some of the results. Figures 2.13 and 2.14 demonstrate the polarity influence of the Jensen Filtration Plant record. Both horizontal components of Jensen (22o and 292o) exhibit forward directivity pulses of medium amplitude (≈ 0.4 g and 0.6 g, respectively) but of large period. The induced velocity step in Figure 2.13 reaches 2.0 m/s and the subsequent sliding displacement is 4.55 m in normal polarity case, and 2.90 m in reverse polarity. So, now polarity affects the slippage. Why? Because the velocity is asymmetric to the horizontal axis. The asymmetry in velocity makes polarity important.

To make this clear, we will discuss the sliding response to the Pacoima Dam downstream record – this is an extreme example of asymmetric velocity. Figure 2.18 outlines the acceleration, velocity and displacement time histories of a sliding system subjected to the Pacoima Dam downstream motion with its normal and reverse polarity. Notice that the major velocity pulse of 0.45 m/s is located only in one side of the horizontal axis. Therefore, polarity difference climbs up to 200%. The same is true for the Rinaldi ground motion (Figures 2.21 and 2.23). The maximum velocity pulse of 1.66 m/s is one-sided resulting in polarity response differences of up to 220% (Figure 2.21). What is more, this intense polarity effect is valid for all the critical acceleration ratios as Figure 2.23 demonstrates. On the contrary, as we already show for Kobe records, symmetric velocities lead to minor polarity effect (Figures 2.20 and 2.24).

2.3.3 The M 6.5, 1979 Imperial Valley Earthquake

The Imperial Valley earthquake that occurred on 15th October 1979 in the U.S-Mexico border in California, was a seismic event of moderate magnitude, M = 6.5. It was triggered by right-lateral slip on the NW trending Imperial fault. Faulting produced approximately 30 km of surface rupture, which extended from about 4 kilometers north of the border to about 4 kilometers south of Brawley. The maximum lateral displacement was about 50 cm and the maximum vertical displacement was 20 cm. Damage from the earthquake estimated to be only $30 million, due to the sparsely populated area.

The earthquake was recorded by a large number of advantageously distributed accelerographs of a Strong Motion Stations Array. The records from stations No 4, 5, 6, 7 and 9 are used as base input excitations. Figures 2.29 ÷ 2.39 graphically present the asymmetric sliding response results for these records.

Figure 2.29 illustrates the slippage occurred from the No. 4 (140^o component) accelerogram. The particular record is characterised by strong forward directivity pulses in acceleration time history. Three distinctive long period cycles appeared between 5 and 8 seconds, as evidents of directivity. As a consequence, substantial velocity pulses are shaped. The other component of No.4 record–the 230^o–is depicted in Figure 2.30 when applied with normal and inverted polarity at the base of an inclined plane. The major directivity pulse of 0.36 g induce a velocity pulse of a step of 1.5 m/s. Sliding displacement difference between opposite polarities is very small and it can be explained by the velocity symmetry. The same outcome pictured in Figure 2.31 for the No.5 (230^o component) excitation.

On the contrast, the No.5, 140^o component is a special example of detailed pulse sequence importance on asymmetric sliding response. Even thought velocity time history exhibits a generally symmetric shape, the induced slippage in case of reversed motion is two times larger than the normal polarity produced displacement (Figure 2.32). The yellow shaded velocity pulse is responsible for this difference: is one-sided, not followed by one of similar amplitude and duration; thus local asymmetry due to pulse sequence details, results to polarity discrepancy. So, it is not only the global velocity symmetry that counts for polarity influence but local symmetry too.

2.3.4 The M 7.3, 1992 Landers Earthquake

On 28^{th} June 1992 a large earthquake shook Southern California. The Landers earthquake occurred in the Mojave Desert on a series of right-lateral strike-slip faults. Surface faulting was observed along a 70 km segment from Joshua Tree to near Barstow with as much as 5.5 meters of horizontal displacement and as much as 1.8 meters of vertical displacement.

Although this earthquake was much more powerful than the 1994 Northridge earthquake, its location in the Mojave Desert meant that damage and loss of life were significantly less than what they could have been. Nonetheless, the Landers earthquake is a well-recorded event, providing numerous records from which we select two to use as excitation: the Lucerne and Joshua Tree records. Analyses results are pictured in Figures 2.40÷2.45.

The Joshua Tree accelerogram and the derived velocity time history have many cycles. Figure 2.40 illustrates the sliding response for normal and reverse polarity triggering of the Joshua Tree record. 39 sliding incidents occur in case of normal polarity excitation, accumulating a slippage of 2.16 m. A slight smaller displacement of 2.08 m is built up after 41 slip events, in reversed polarity triggering. It is worthy of notice that the velocity time history is symmetric, therefore no polarity effect is expected. That proves to be true for all acceleration ratios a_C/a_H as displayed in Figure 2.42.

Figure 2.43 presents the response for a_C/a_H = 0.05 for the Lucerne 275^o record. The high-spiked accelerogram of Lucerne seemed at first glance to be "innocent" in terms of sliding potential. Nevertheless, its velocity revealed the fling affected motion that results to 1m residual ground displacement. The high frequency accelerogram is hiding a significant velocity step of 1.8 m/s, which is responsible for the 2.3 m induced slippage.

2.3.5 The M 6.6, 1971 San Fernando Earthquake

The M6.6 San Fernando earthquake occurred on 9th February 1971 in a sparsely populated area of the San Gabriel Mountains at the outskirts of the San Fernando valley. The event has been charged for the loss of 65 lives, and damage has been estimated at $505 million. The earthquake created a zone of discontinuous surface faulting, which

partly follows the boundary between the San Gabriel Mountains and the San Fernando Valley. Within the entire length of the surface faulting (which extended roughly for about 15 kilometers) the maximum vertical offset measured on a single scarp was about 1 meter, the maximum lateral offset about 1 meter, and the maximum shortening (thrust component) about 0.9 meters. About 1 000 landslides were generated by the earthquake.

Asymmetric sliding response of the Pacoima Dam ground motion is presented to Figures 2.46 and 2.47. Acceleration, velocity and displacement time histories of a rigid block sliding on top of an inclined plane with critical acceleration ratio $a_C/a_H = 0.1$ *are portrayed in Figure 2.46. The Pacoima Dam* 164^o *record exhibits a peak value of 1.23 g that little contributes to slippage. However, the three acceleration cycles between 7 and 8.5 seconds play important role in the final sliding displacement; not with their solely peak values but through their duration and mean amplitude. Additionally, the previous small acceleration pulses even though seem insignificant induce large velocity pulses. Therefore, contribute to the accumulated slippage.*

2.3.6 The M 6.9, 1992 Erzincan Earthquake

It occurred on 13^{th} *March 1992 close to Erzincan in northeast Turkey. The earthquake was focused on the North Anatolian Fault and caused the deaths of over 500 people together with severe damage to many thousands of properties. Landslides and avalanches blocked a number of roads in the epicentral area. Peak measured accelerations in the three directions close to the centre of Erzincan were approximately 0.50 g, 0.40 g and 0.25 g (vertically). Predominant periods were about 0.30 s, 0.95 s and 0.15 s, respectively. Figures 2.48÷2.51 display the sliding response triggered by the Erzincan horizontal components.*

In particular, the importance of reversing the polarity of the EW component is illustrated in Figure 2.48. Observe the slightly non symmetric velocity time history of the record, which results in a moderate displacement difference due to polarity. The same is also valid for the other Erzincan component.

2.3.7 The M 7.1, 1989 Loma Prieta Earthquake

The 1989 Loma Prieta earthquake occured on October 18, 1989 and was the first major event to occur along the San Andreas fault zone since the 1906 earthquake. It had a moment magnitude of 6.9 and a surface wave magnitude of 7.1. The Loma Prieta earthquake ruptured the southernmost 40 km of the 1906 break, in right-lateral strike slip and reverse slip motion. The fault rupture did not break the ground surface. The earthquake caused damage throughout the San Francisco Bay area. The death toll was 62. The cost was 6 to 8 billion dollars.

Two records are applied as base excitation: the Hollister City Hall and the Los Gatos Presentation Center accelerograms. Figures 2.52 ÷2.56 display the sliding response from these records. As mentioned before, for symmetric velocity triggering, polarity effects are minimal. That is demonstrated in Figure 2.53 for the Hollister record for all four critical acceleration ratios a_C/a_H.

2.3.8 The M 7.5, 1999 Chi-chi Earthquake

A devastating thrust-fault earthquake, named Chi-Chi Earthquake (or Ji-Ji earthquake in some articles), struck central Taiwan on 21 September 1999. It is unique for its rupture length of 105 km and upheaval of 9.8 m. Death toll reached 2500 and the financial loss was estimated to be of the order of $11 billion. There were thousands of landslides in the mountainous terrain within and adjacent to the fault. A total of 436

slope failure were investigated and documented in the reconnaissance report coordinated by NCREE.

The earthquake was produced by thrusting along the (essentially unrecognised before the event) Chelongpu Fault in the western part of the island. The fault stretches along the foothills of the Central Mountains in Nantou and Taichung County. Some sections of land near the fault were raised as much as 8 m. Near the northern end of the fault, a 7 m high waterfall was created by the earthquake.

Strong shaking lasted for more than 40 seconds with a peak horizontal acceleration of 0.99 g (east-west direction of Station TCU084) and a peak vertical acceleration of 0.71 g (Station CHY080). Due to an extensive network of sensors and monitoring stations, the quake was perhaps the best recorded and analysed event in history. Ten records along the fault are utilised herein and are schematically pictured in Figure 2.57. Their peak ground characteristics can be seen in Table 1. Fault and epicentral distances of each of these ten stations presented in Table 2. Analyses results in terms of time histories are illustrated at Figures 2.58 ÷2.78, whereas summary plots of all analyses are displayed at Figures 2.79÷2.91. Some of these figures are discussed in detail in the following paragraphs.

Figure 2.60 portray the asymmetric yielding response induced by the fling and forward directivity affected TCU 052-NS record. The particular accelerogram is characteristic of the records of Chi-chi earthquake: The peak acceleration is as low as 0.43 g *but the accelerogram is plenty of low amplitude, large period pulses which generate intense velocity pulses of substantial magnitude. Thus, an one-sided velocity*

pulse of 2.7 m/s step and ≃ 8 seconds duration. As already explained, the non symmetric shape of velocity leads to substantial polarity influence (Figure 2.61).

On the contrary, some of the 1999 records, such as the one depicted in Figure 2.62, include numerous acceleration pulses–the outcome of forward directivity– with no fling imprints. The TCU 065-EW record has a peak ground acceleration of 0.76 g *with many cycles of total duration of 40 seconds. The velocity time history is symmetric as in case of TCU 065-NS and 067-EW records (see Figures 2.64 and 2.65 respectively). Therefore, the polarity effect is small enough to neglect it.*

Arguably, the most famous (or notorious) record of the Chi-chi event is the TCU 068: both EW and NS components exhibit strong fling (mainly) and forward directivity (secondarily) features. Particularly, Figure 2.66 demonstrates the sliding response for the TCU 068-EW record. The peak acceleration of 0.45 g *is of little significance comparing with the large period, low amplitude cycles illustrated with the yellow shaded area in the figure. The acceleration cycles "built" an enormous velocity pulse of 3.75 m/s step. This remarkable velocity pulse is one-sided, characteristic of fling affected ground motions. As expected, the polarity effect is impressive: from the 12.60 m sliding displacement for normally imposed record, the slippage is reduced to 5.62 m for inversed polarity (Figure 2.67). The NS component of the TCU 068 appears the highest peak ground velocity and velocity step worldwide: PGV = 3 m/s and ΔV = 3.95 m/s (Figure 2.68). Also for the NS component the polarity effect is detrimental. By reversing the acceleration subjected motion, slippage becomes five times larger.*

All analyses data are summarised in Figures 2.79÷2.91. The irrelevance of epicentral distance to the induced displacement portrayed in Figure 2.84, whereas fault distance seems to be better indicator of sliding potential (Figure 2.83). Figure 2.85 illustrates in

physical and logarithmic scale the sliding response for different acceleration ratios versus the Makdisi & Seed (1979) curves for seismic events of M=7.5. Obviously, Chi-chi overpasses by orders of magnitude the Makdisi & Seed curves–an indication of the near-fault characteristics of records, not included in the database of Makdisi & Seed study.

2.3.9 The M 7.0, 1976 Gazli Earthquake

The 17th May 1976 Gazli earthquake (M_s = 7.0) in the former USSR, has both seismological and engineering importance. Hartzell (1980) performed waveform modelling of long-period Rayleigh waves, indicating that Gazli earthquake was triggered by a thrust mechanism of 78°. The fault area is estimated to be 150 km^2; the average dislocation, 3.3 meters. Strong directivity effects due to a propagating rupture are present in both components of the Karakyr record. Figures 2.92÷2.94 picture the sliding response to the Karakyr record. Both the 0° and 90° components exhibit small polarity effects, thanks to the almost symmetric velocity time histories.

2.3.10 The M 7.4, 1999 Kocaeli Earthquake

On August 17, 1999, the earthquake (also called "Izmit" earthquake) struck the Kocaeli area in the Northwest Turkey. The death toll estimated 45,000 people and the hardest hit cities were Gölcük, Avcilar, Yalova, and Adapazari. The earthquake epicenter was located near Gölcük on the notorious North Anatolian Fault—a strike-slip fault. The earthquake had a rupture length of 150 kilometers extending almost from the city of Düzce all the way to Yalova. The maximum right-lateral offsets were measured to be about 4 m. The rupture had also a vertical component ranging between 10 to 150 cm (more details in Erdik, 2000, 2001; Erdik et al., 2004).

During the Kocaeli earthquake several stations recorded the ground motions. Among them, the three records employed in our study: Sakarya, Yarimca, and Duzce. It has been observed that the amplitudes of ground motions are larger for the soil sites (Yarimca, Düzce) than for the rock sites (Sakarya). All three records were affected by rupture directivity. Düzce station was in the forward directivity direction of the eastern segment of the fault and as expected, the fault normal motion is dominant. Sakarya and Yarimca records display strong velocity pulses and a static displacement of 2.0 m and 1.5 m, respectively, in the E-W component. The N-S component of the Yarimca record also displays a significant static offset (1.2 m), indicating some movement to the north. Figures 2.95÷2.102 present the results of the sliding analyses performed in our study.

The Sakarya record is a fling affected motion of relatively small peak acceleration of 0.33 g but with significant velocity pulse, as Figure 2.95 displays. Inside the high frequency spiked accelerogram hides a large velocity pulse of $\Delta V = 1$ m/s. This one-sided velocity pulse is the signature of fling effect, which induces 1 m of yielding displacement for critical acceleration ratio $a_C/a_H = 0.05$.

Yarimca record is fling affected too. In this case, peak acceleration is even smaller than Sakarya's, just 0.23 g (Figure 2.99). However, the velocity pulse is greater: $\Delta V = 1.37$ m/s and longer duration. Thus, larger slippage induced. Both Sakarya and Yarimca records, present asymmetric velocities. So, polarity effect has importance as Figures 2.96, 2.97, and 2.98 depict.

2.3.11 The M 7.4, 1978 Tabas Earthquake

The 1978 Tabas earthquake struck on September 16, 1978 in central Iran. The death toll was approximately 30,000 and the worst damage was to the town Tabas, which was

at the epicentre of the quake and completely flattened. 40 villages within a 48 km radius were damaged. Berberian et al. (1979) determined the focal mechanism of this earthquake to be thrust with 127° strike azimuth and 62° SW dip angle. The 1978 Tabas earthquake was registered on 11 accelerograph stations, with source distances ranging from 3 to 350 km and corresponding recorded peak accelerations ranging from 0.95 down to 0.01 g, respectively (Mohajer - Ashjai & Nowroozi, 1979).

In our study the Tabas LN and TR records are employed as illustrated in Figures 2.103÷2.105. The Tabas station accelerogram is a forward directivity record. High spiked acceleration time histories include long duration directivity pulses that revealed in velocity. The velocity pulses are two-sided, in other words symmetric, as consequence of the directivity.

2.3.12 The M 5.7, 1986 San Salvador Earthquake

The San Salvador Earthquake struck El Salvador on October 10, 1986 at 11:49 am local time, causing considerable damage to the capital San Salvador and to the neighbouring Honduras and Guatemala. About 1,500 people are believed to have been killed. Although of 'moderate' magnitude, the earthquake was a shallow event right under San Salvador, leading to the destruction of many structures. Focal mechanisms and aftershock distributions from locally recorded seismic data indicate that the earthquake was caused by near-surface, left-lateral slip on a N25°E trending fault located directly beneath the city of San Salvador (Harlow et al., 1993). Although strong ground motion lasted for only 3 to 5 sec, horizontal ground accelerations of up to 0.72 g were recorded.

Ground shaking from three stations are studied: the National Geographical Institute (NGI), the Geotechnical Investigation Center (GIC), and the Institute of Urban Construction (IUC) records. Figures 2.106÷2.114 describe the results from sliding analyses. GIC-90^o, IUC-180^o and NGI-270^o records exhibit substantial polarity differences in slippage as Figures 2.107, 2.111, and 2.113 are portray respectively.

2.3.13 The M 7.2, 1999 Duzce Earthquake

On November 12, 1999 at 6:57 pm (local time), a magnitude M_w 7.2 earthquake struck the Düzce-Bolu area of Turkey, 70 km east of Adapazari and 170 km northwest of Ankara. Preliminary estimates of casualties are 894. The Düzce earthquake ruptured a 40 km long fault segment of the North Anatolian fault system immediately to the east of the August 17, 1999 Kocaeli rupture.

Sliding analyses results are displayed in Figures 2.115÷2.119. Both Duzce and Bolu records are directivity affected and indicate symmetric two-sided velocity time histories. Therefore, polarity is of negligible importance for these excitation.

2.4 Summary and Polarity Effect

By the providing data of all the previously discussed analyses several conclusions can be drawn. Classification and statistical presentation of them follows in next chapter. Herein we limit the processing to time histories description. Nonetheless, a thorough understanding can be achieved. The mechanisms in which directivity and fling influence the sliding response become stark and clear, whereas the general tendencies of the phenomena are emerged too. Figures 2.120÷2.124 portray all the analyses information in a condensed manner.

It is evident that for all excitations, as the critical acceleration ratio a_C/a_H increases the sliding displacement decreases (see Figures 2.120 and 2.121). The explanation is straightforward: the larger the ratio a_C/a_H becomes, the higher the coefficient of friction μ is, so the block slides more difficult producing smaller displacement.

Figure 2.122 picture the polarity factor versus the critical acceleration ratio, a_C/a_H. As polarity factor we define the ratio of sliding displacement triggered by a particular record with the polarity that induces the greater slippage, divided by the yielding displacement of the opposite polarity:

$$Polarity \quad Factor = \frac{\max\left\{\begin{matrix} D^+ \\ D^- \end{matrix}\right\}}{\min\left\{\begin{matrix} D^+ \\ D^- \end{matrix}\right\}} \qquad (2.1)$$

By definition, polarity factor takes positive values larger than unity. Figure 2.122 illustrates the polarity factor of all records with respect to critical acceleration ratio. The picture can be divided in two major regions: the first, for $a_C/a_H \leq 0.2$ polarity factor is bounded between unity and 3. The second region applies for $a_C/a_H \geq 0.2$, where polarity factor takes so large values that can not be limited. As a concluding remark, polarity effect could has major importance in the large a_C/a_H region and should not be neglected.

Near-fault phenomena affect the inclined sliding system in similar ways in terms of induced slippage but in different ways in case of polarity. Both forward directivity and fling records include long period and large amplitude velocity pulses that result in substantial sliding displacement. However, forward directivity records appear two-sided symmetric velocity pulses, leading to minimal polarity influence. On the contrary, fling accelerograms present one-sided asymmetric velocity pulses, which trigger slippage strongly affected by the imposed polarity of the record. In other words, two

theoretically identical slopes in the same area, standing one opposite from the other when subjected to the same ground shaking may perform differently. This difference can be two or ten times larger or smaller depending on the type of excitation, its details, sequence of pulses, etc.

At this point, we have to remember that nature is not always favouring us with records containing only forward directivity pulses unconjectured of fling effects. The Chi-chi records are a great example of accelerograms influenced by fling and directivity too. Nevertheless, velocity asymmetry is a good first indicator of polarity potential.

Table 2.1: *List of significant earthquake records bearing the effects of 'directivity' and 'fling', utilized as excitations in this study.*

Earthquake, Magnitude	***Record Name***	***PGA*** (*g*)	***PGV*** (*m/s*)	***PGD*** (*m*)
Kobe - Japan, (16 *January* 1995) M_W = 7.0 M_{JMA} = 7.2	*Fukiai*	0.763	1.232	0.134
	JMA-0°	0.830	0.810	0.177
	JMA-90°	0.599	0.761	0.199
	Nishi Akashi-0°	0.509	0.357	0.091
	Nishi Akashi-90°	0.503	0.356	0.109
	Shin Kobe-NS	0.422	0.688	0.169
	Takarazuka-0°	0.693	0.682	0.274
	Takarazuka-90°	0.694	0.853	0.167
	Takatori-0°	0.611	1.272	0.358
	Takatori-90°	0.616	1.207	0.328
Imperial Valley – California, (15 *October* 1979) M_W = 6.8	*No* 4-140°	0.485	0.374	0.202
	No 4-230°	0.360	0.766	0.590
	No 5-140°	0.519	0.469	0.353
	No 5-230°	0.379	0.905	0.630
	No 6-140°	0.410	0.649	0.276
	No 6-230°	0.439	1.098	0.658
	No 7-140°	0.338	0.476	0.246
	No 7-230°	0.463	1.093	0.447
	No 9 *Differential Array*-270°	0.352	0.712	0.458
	No 9 *Differential Array*-360°	0.480	0.408	0.140
Landers - California, (28 *June* 1992) M_W = 7.3	*Lucerne*-0°	0.785	0.319	0.164
	Lucerne-275°	0.721	0.976	0.703
	Joshua Tree-0°	0.274	0.275	0.098
	Joshua Tree-90°	0.284	0.432	0.145
San Fernando - California, (9 *February* 1971) M_S = 6.6	*Pacoima Dam*-164°	1.226	1.124	0.361
	Pacoima Dam-254°	1.160	0.536	0.111
Erzincan - Turkey, (13 *March* 1992) M_S = 6.9	*Erzincan* (*Station* 95)-*EW*	0.496	0.643	0.236
	Erzincan (*Station* 95)-*NS*	0.515	0.839	0.312
Loma Prieta - California, (17 *October* 1989) M_S = 7.1 M_w = 6.8	*Los Gatos Presentation Center*-0°	0.563	0.948	0.411
	Los Gatos Presentation Center-90°	0.605	0.510	0.115
	Saratoga Aloha Avenue-0°	0.512	0.412	0.162
	Saratoga Aloha Avenue-90°	0.324	0.426	0.275
Gazli - USSR, (17 *May* 1976) M_S = 7.0	*Karakyr*-0°	0.608	0.654	0.253
	Karakyr -90°	0.718	0.716	0.237

(*Table* 1 *continues*)

(*Continue of Table* 1)

Earthquake, Magnitude	***Record Name***	***PGA*** (g)	***PGV*** (*m/s*)	***PGD*** (*m*)
Northridge - California, (17 *January* 1994) M_w = 6.8	*Jensen Filtration Plant*-22°	0.424	0.873	0.265
	Jensen Filtration Plant-292°	0.592	1.201	0.249
	L.A. Dam-64°	0.511	0.637	0.211
	L.A. Dam-334°	0.348	0.508	0.151
	Newhall Firestation-90°	0.583	0.524	0.126
	Newhall Firestation-360°	0.589	0.753	0.182
	Pacoima Dam (downstream)-175°	0.415	0.456	0.050
	Pacoima Dam (downstream)-265°	0.434	0.313	0.048
	Pacoima Kagel Canyon-90°	0.301	0.379	0.095
	Pacoima Kagel Canyon-360°	0.432	0.452	0.069
	Rinaldi-228°	0.837	1.485	0.261
	Rinaldi-318°	0.472	0.627	0.166
	Santa Monica City Hall-90°	0.883	0.403	0.102
	Santa Monica City Hall-360°	0.369	0.232	0.059
	Sepulveda VA-270°	0.753	0.848	0.186
	Sepulveda VA-360°	0.939	0.766	0.149
	Simi Valley Katherine Rd-0°	0.877	0.409	0.053
	Simi Valley Katherine Rd-90°	0.640	0.378	0.051
	Sylmar Hospital-90°	0.604	0.744	0.165
	Sylmar Hospital-360°	0.843	1.027	0.256
Chi-Chi Taiwan, (20 *September* 1999) M_w = 7.5	*TCU* 052-*EW*	0.350	1.743	4.659
	TCU 052-*NS*	0.437	2.186	7.319
	TCU 065-*EW*	0.450	1.298	1.820
	TCU 065-*NS*	0.554	0.876	1.254
	TCU 067-*EW*	0.487	0.973	1.953
	TCU 067-*NS*	0.311	0.536	0.849
	TCU 068-*EW*	0.491	2.733	7.149
	TCU 068-*NS*	0.353	2.892	8.911
	TCU 075-*EW*	0.324	1.143	1.692
	TCU 075-*NS*	0.254	0.360	0.414
	TCU 076-*EW*	0.335	0.706	1.223
	TCU 076-*NS*	0.416	0.617	0.662
	TCU 080-*EW*	0.968	1.076	0.186
	TCU 080-*NS*	0.902	1.025	0.340
	TCU 084-*EW*	0.986	0.923	0.910
	TCU 084-*NS*	0.419	0.486	0.966
	TCU 102-*EW*	0.297	0.870	1.478
	TCU 102-*NS*	0.168	0.705	1.062

(*Table 1 continues*)

(*Continue of Table 1*)

Earthquake, Magnitude	***Record Name***	***PGA*** (g)	***PGV*** (*m*/s)	***PGD*** (*m*)
Kocaeli - Turkey, (17 *August* 1999) M_w = 7.4 M_S = 7.8	*Duzce*-180°	0.312	0.474	0.285
	Duzce-270°	0.358	0.464	0.176
	Sakarya-EW	0.330	0.814	2.110
	Yarimca-60°	0.231	0.906	1.981
	Yarimca-330°	0.322	0.867	1.493
Tabas - Iran, (16 *September* 1978) M_S = 7.4	*Tabas-LN*	0.836	0.978	0.387
	Tabas-TR	0.852	1.212	0.951
San Salvador – El Salvador, (10 *October* 1986) M_S = 5.4 M_w = 5.7	*National Geographical Institute*-180°	0.392	0.566	0.206
	National Geographical Institute-270°	0.524	0.753	0.116
	Geotechnical Investigation Center-90°	0.681	0.793	0.119
	Geotechnical Investigation Center-180°	0.412	0.602	0.201
	Institute of Urban Construction-90°	0.380	0.441	0.173
	Institute of Urban Construction-180°	0.668	0.595	0.112
Duzce - Turkey, (12 *November* 1999) M_S = 7.5 M_w = 7.2	*Bolu*-0°	0.728	0.564	0.231
	Bolu-90°	0.822	0.621	0.135
	Duzce-180°	0.348	0.600	0.421
	Duzce-270°	0.535	0.835	0.516

Table 2.2: *Epicentral distance and distance from the fault of all the Chi-chi earthquake records that utilized as excitation ground motions.*

The Chi-chi 7.5 Earthquake – Taiwan, 20 September 1999		
Record Name	***Epicentral Distance*** *[km]*	***Distance from the Fault*** *[km]*
TCU 052-EW	35	0.24
TCU 052-NS	35	0.24
TCU 065-EW	25	0.98
TCU 065-NS	25	0.98
TCU 067-EW	27	0.33
TCU 067-NS	27	0.33
TCU 068-EW	43	1.09
TCU 068-NS	43	1.09
TCU 075-EW	20	1.49
TCU 075-NS	20	1.49
TCU 076-EW	15	1.95
TCU 076-NS	15	1.95
TCU 080-EW	30	6.95
TCU 080-NS	30	6.95
TCU 084-EW	5	10.5
TCU 084-NS	5	10.5
TCU 102-EW	43	1.79
TCU 102-NS	43	1.79
TCU 129-EW *	13	1.18
TCU 129-NS *	13	1.18

* *The high peak accelerations recorded at TCU 129 station during the 1999 Chi-chi earthquake, was due to the effects of the concrete recording pier at station TCU 129 and not due to the source, path, or site effects of the event. Hence, the peak acceleration values should not be used in studies of peak acceleration attenuation. However, the records are still useful, especially the integrated velocity and displacement time-histories, for other studies. [Wen et al, 2001]*

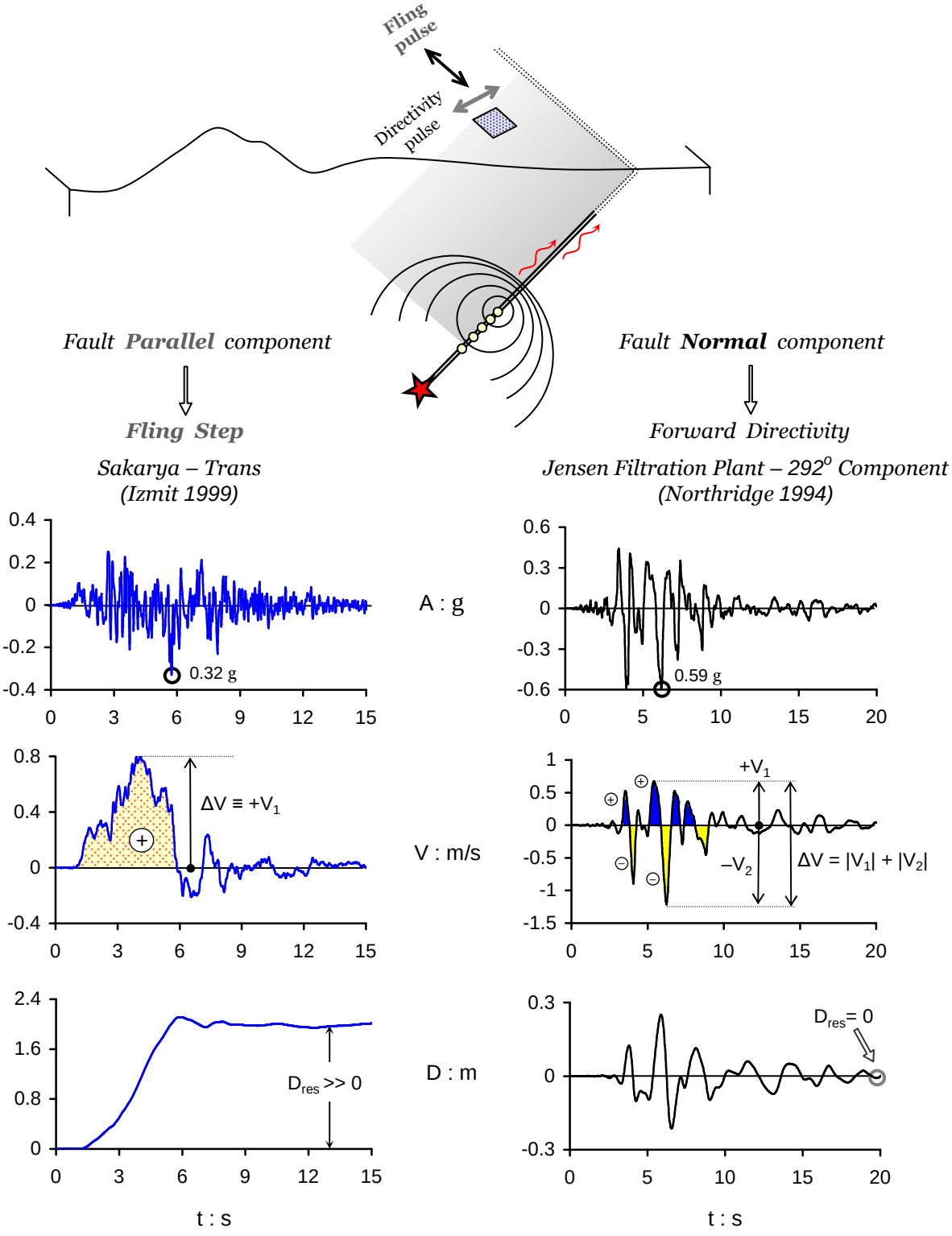

Figure 2.1 *Schematic explanation of the 'fling-step' and 'forward-directivity' phenomena as reflected in two characteristic records: the fling affected Sakarya ground motion (left) and the directivity affected Jensen Filtration Plant time-history (right).*

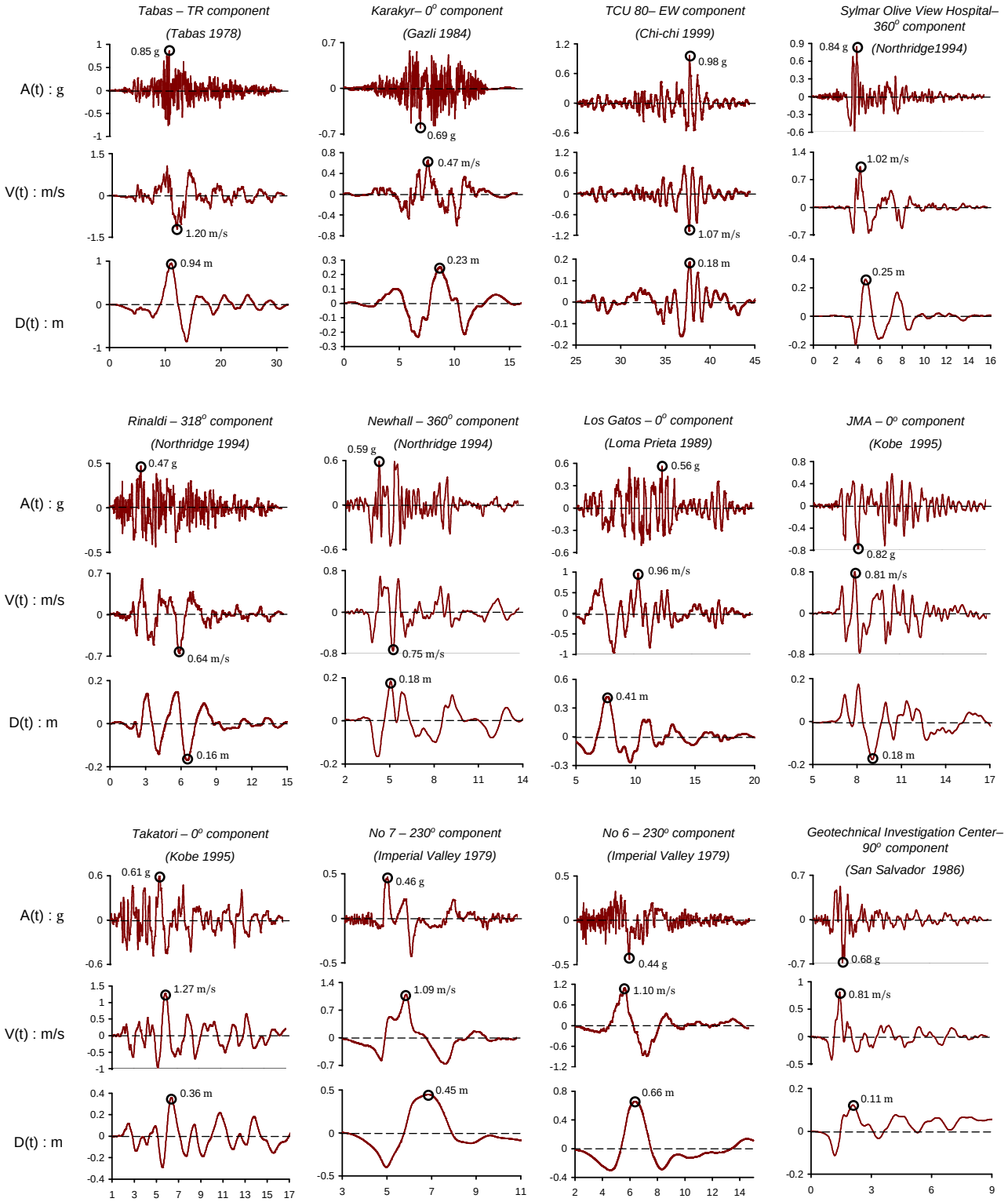

Figure 2.2 *Selection of records with prominent directivity acceleration pulses, employed as triggering excitations to this study.*

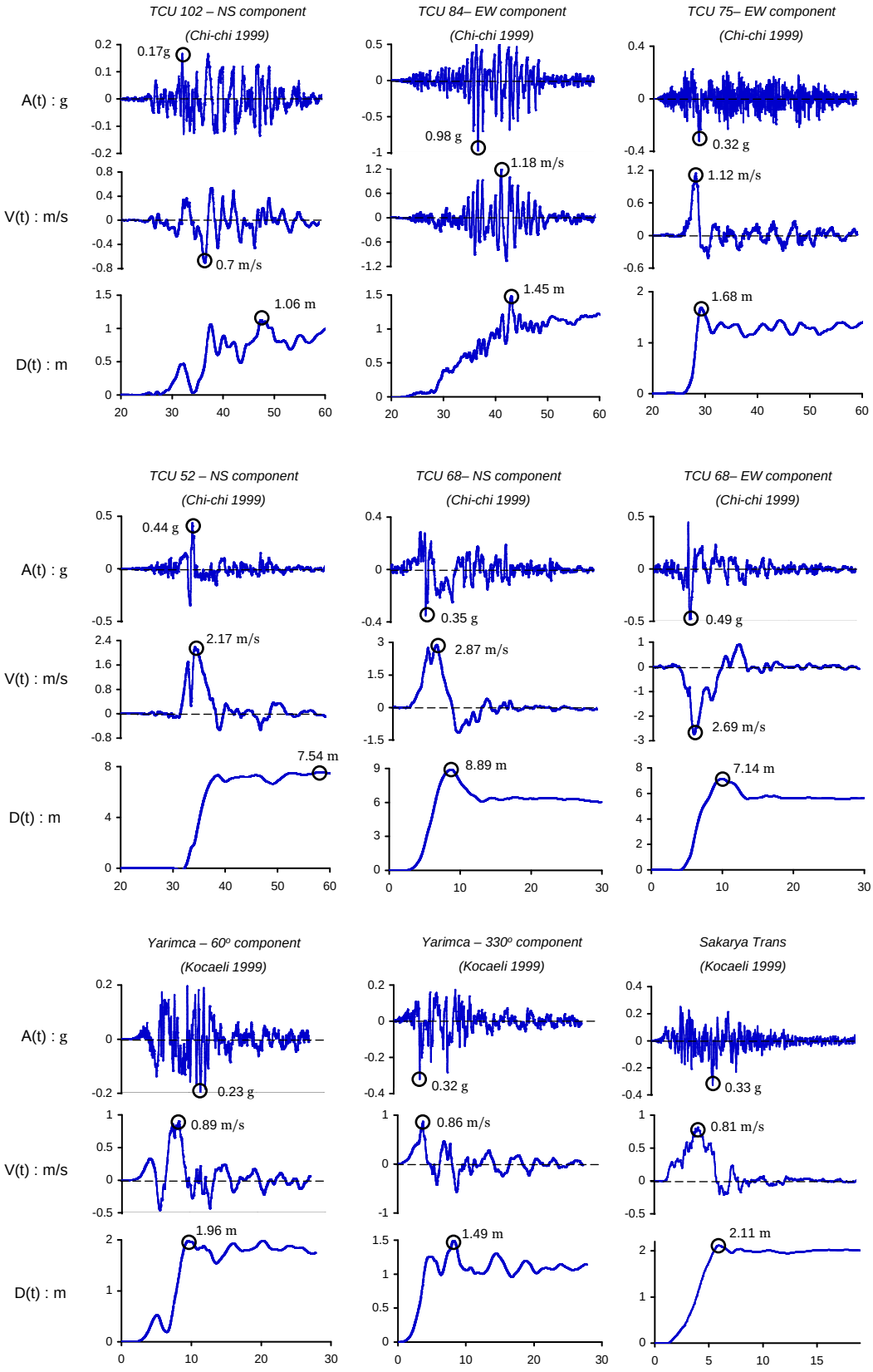

Figure 2.3 *Selection of records strongly affected by fling, employed as triggering excitations to this study.*

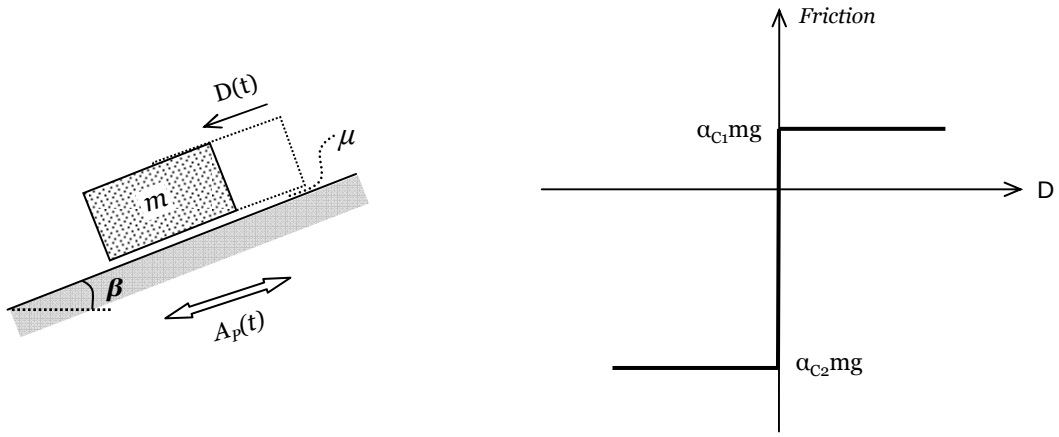

Figure 2.4 *Schematic representation of the Newmark 1965 sliding-block analogue and friction force as a function of slip displacement.*

Excitation Records from

the Kobe M_w = 7.0 Earthquake

16 January 1995, Japan

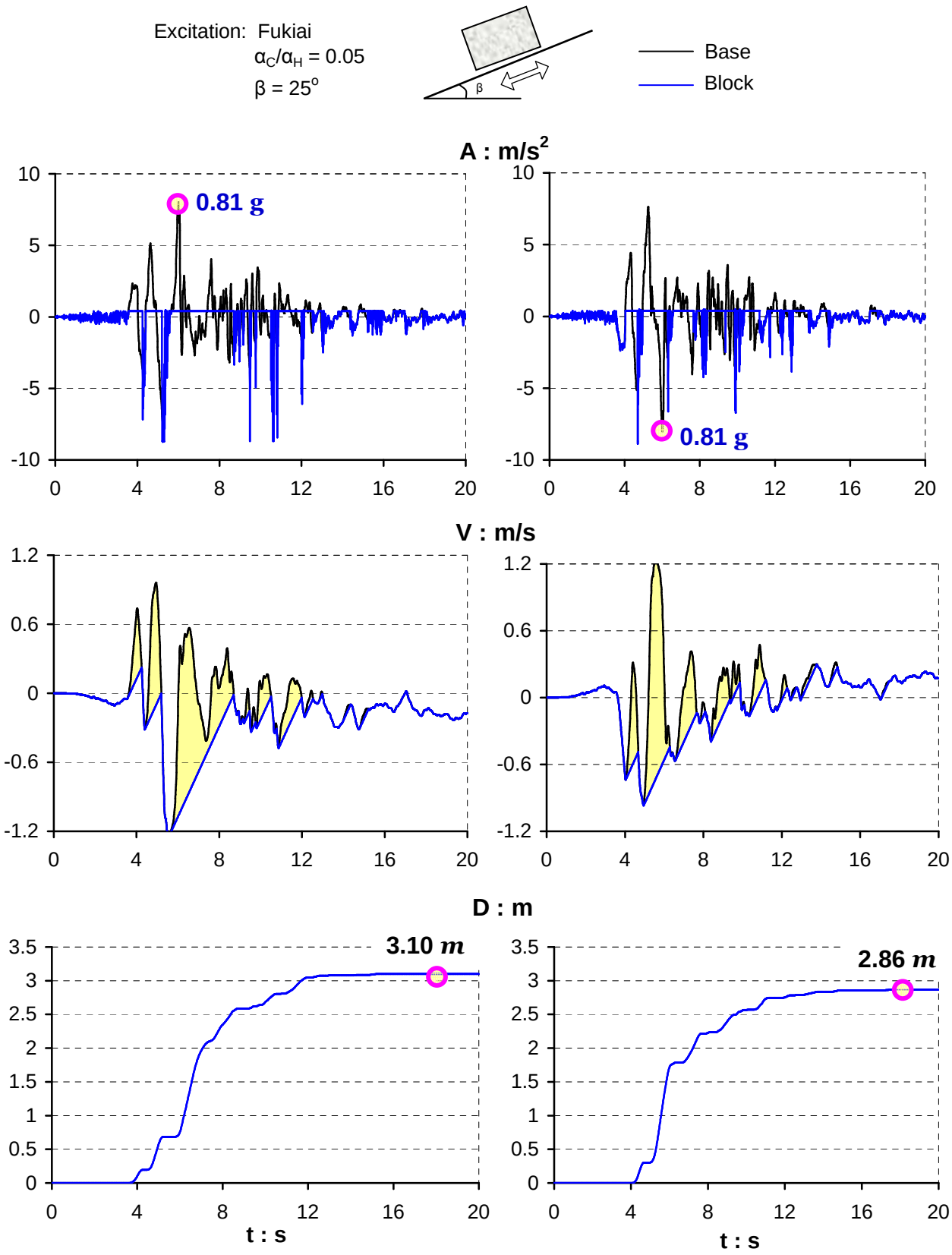

Figure 2.5 *Another group of excitations that exhibit almost symmetric velocity time-history are those with a small number of acceleration pulses induced by forward directivity (not fling) phenomena. The Fukiai record imposed with its normal (left column) and reversed (right column) sign. As expected the response difference due to polarity is quite small. (a_C/a_H = 0.05 and $\beta = 25^o$)*

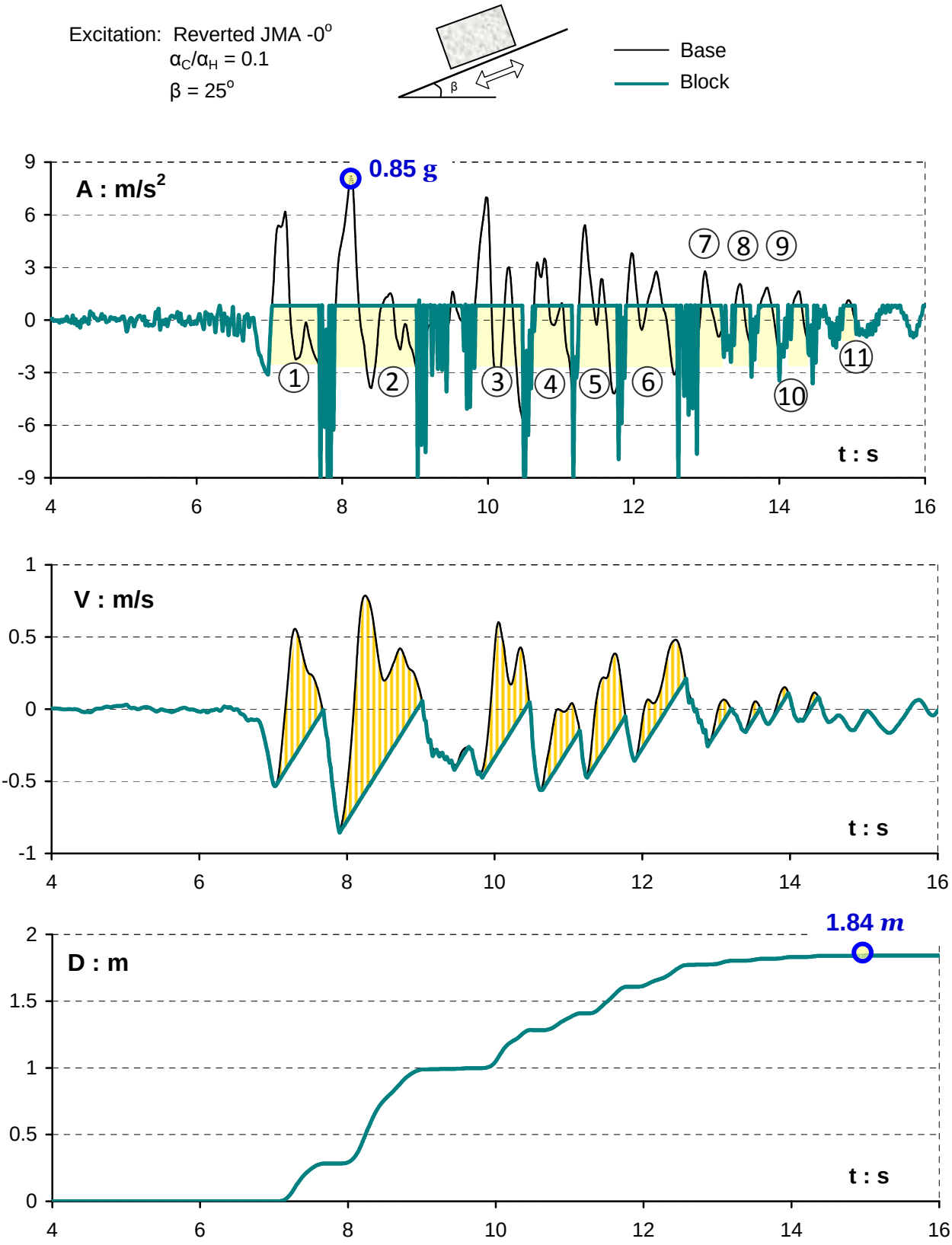

Figure 2.6 *Asymmetric response time histories of a rigid block resting on an 25⁰ inclined plane when subjected to the reversed polarity JMA 000 record. ($a_C/a_H = 0.1$)*

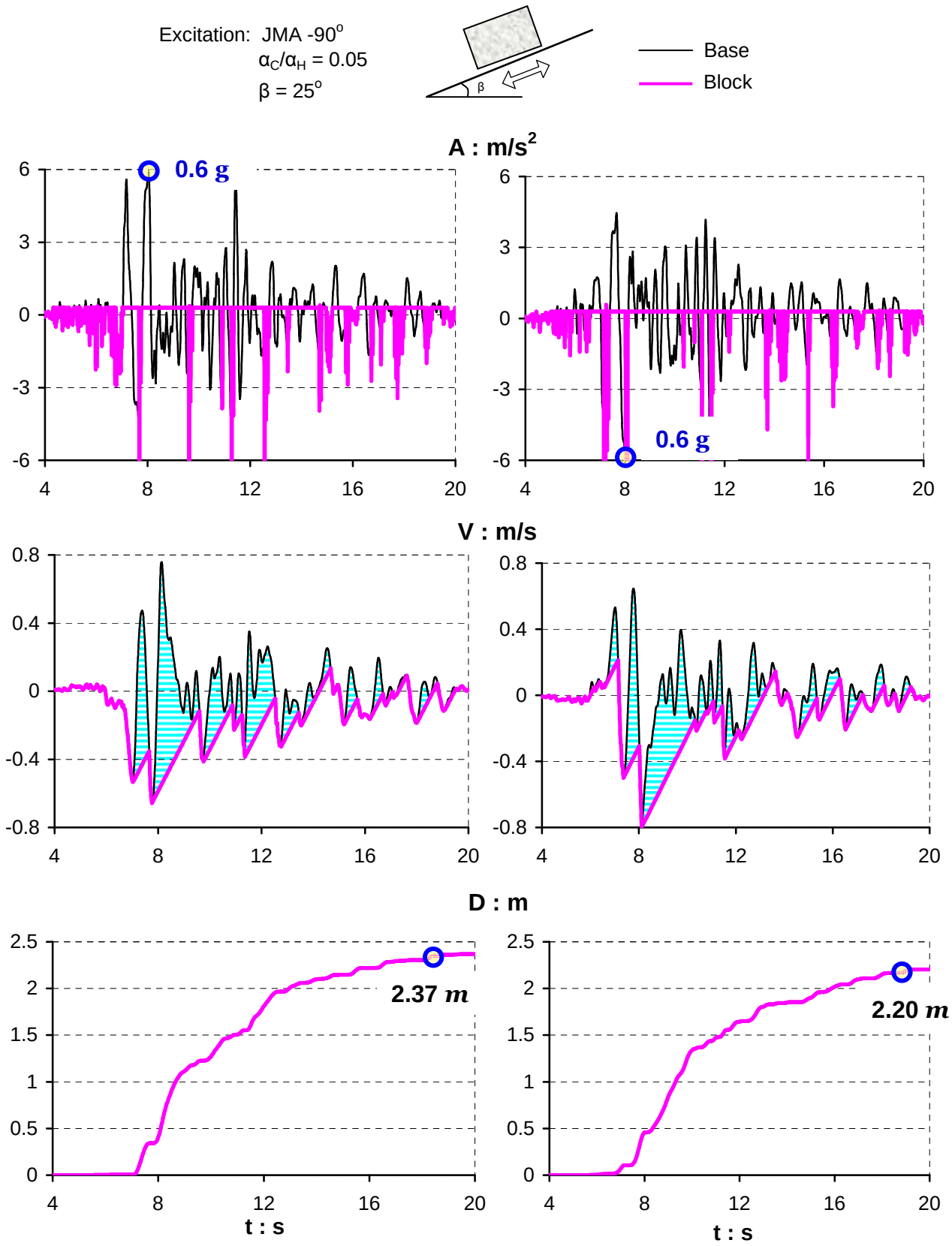

Figure 2.7 *Minimisation of the polarity effect for the JMA-090 record : symmetric velocity time-history with lot of cycles. The record imposed with its normal (left column) and reversed (right column) sign. (a_C/a_H = 0.05 and $\beta = 25^o$)*

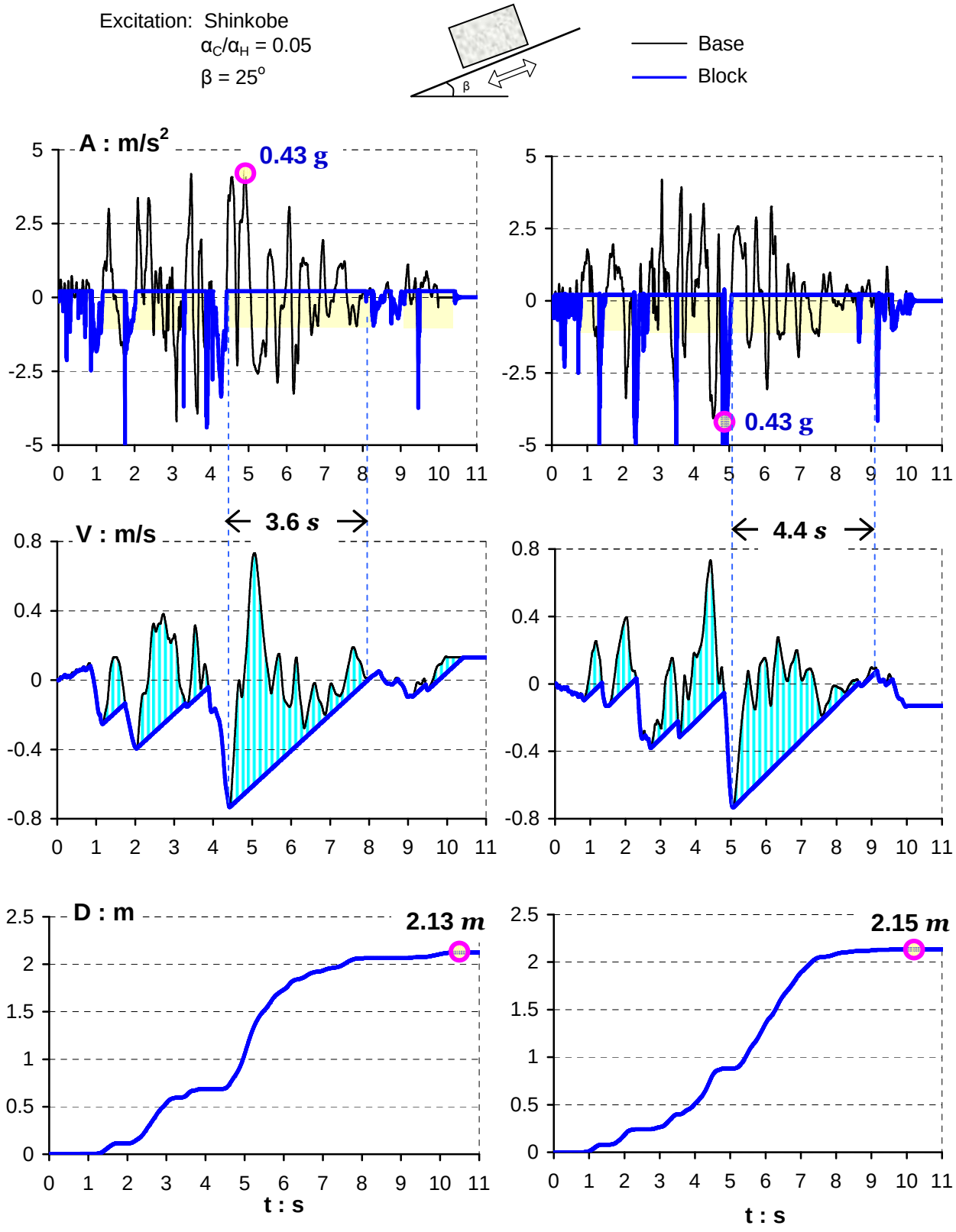

Figure 2.9 *Quite symmetric velocity time-history with a small number of acceleration pulses induced by strong forward directivity (not fling) phenomena. The Shinkobe record imposed with its normal (left column) and reversed (right column) sign. Response difference due to polarity is negligible. (a_C/a_H = 0.05 and $\beta = 25^o$)*

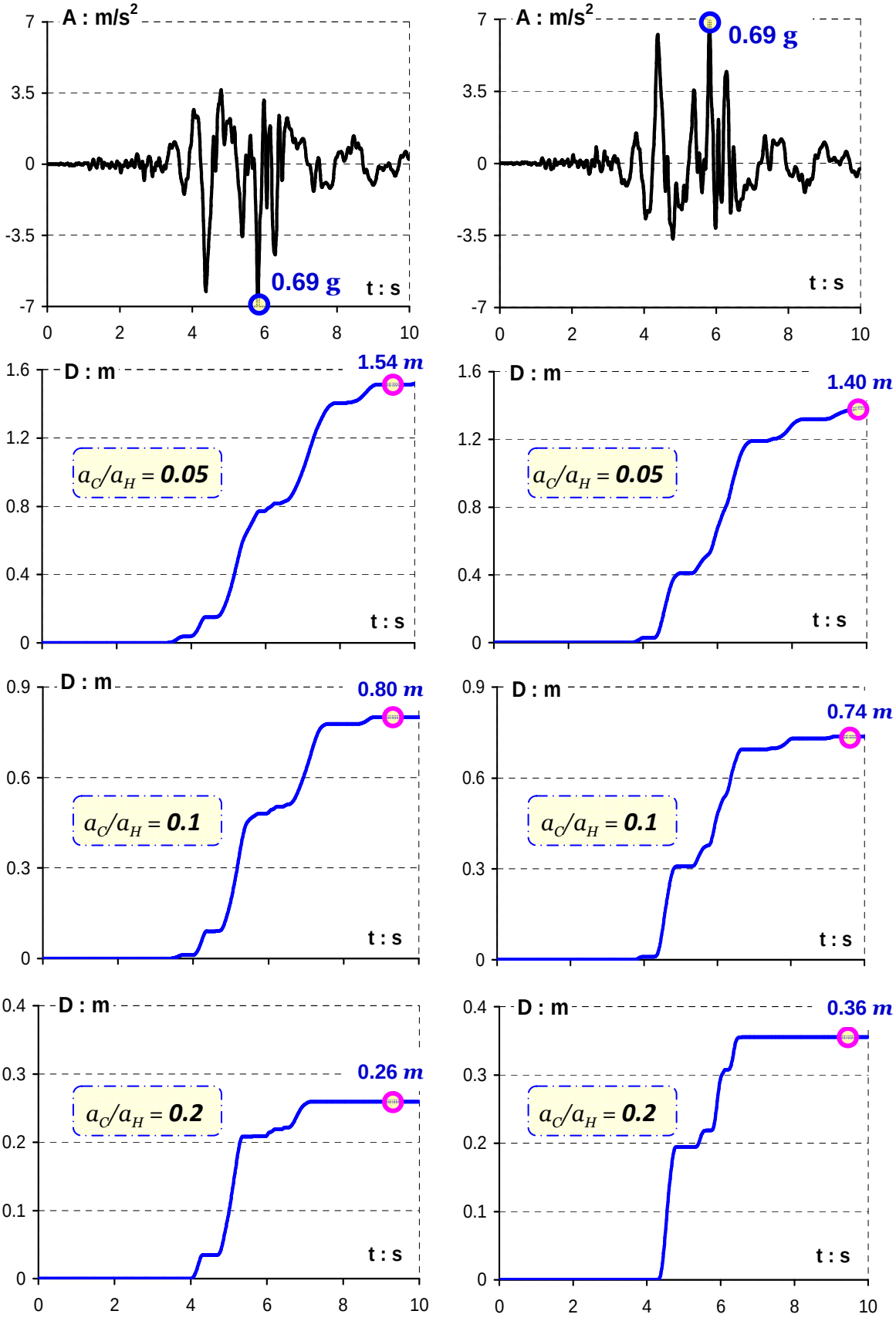

Figure 2.10 *Sliding displacement response for three acceleration ratio, a_C/a_H, values induced by the Takarazuka–0° record imposed with its normal (left column) and reversed (right column) sign. ($\beta = 25^o$)*

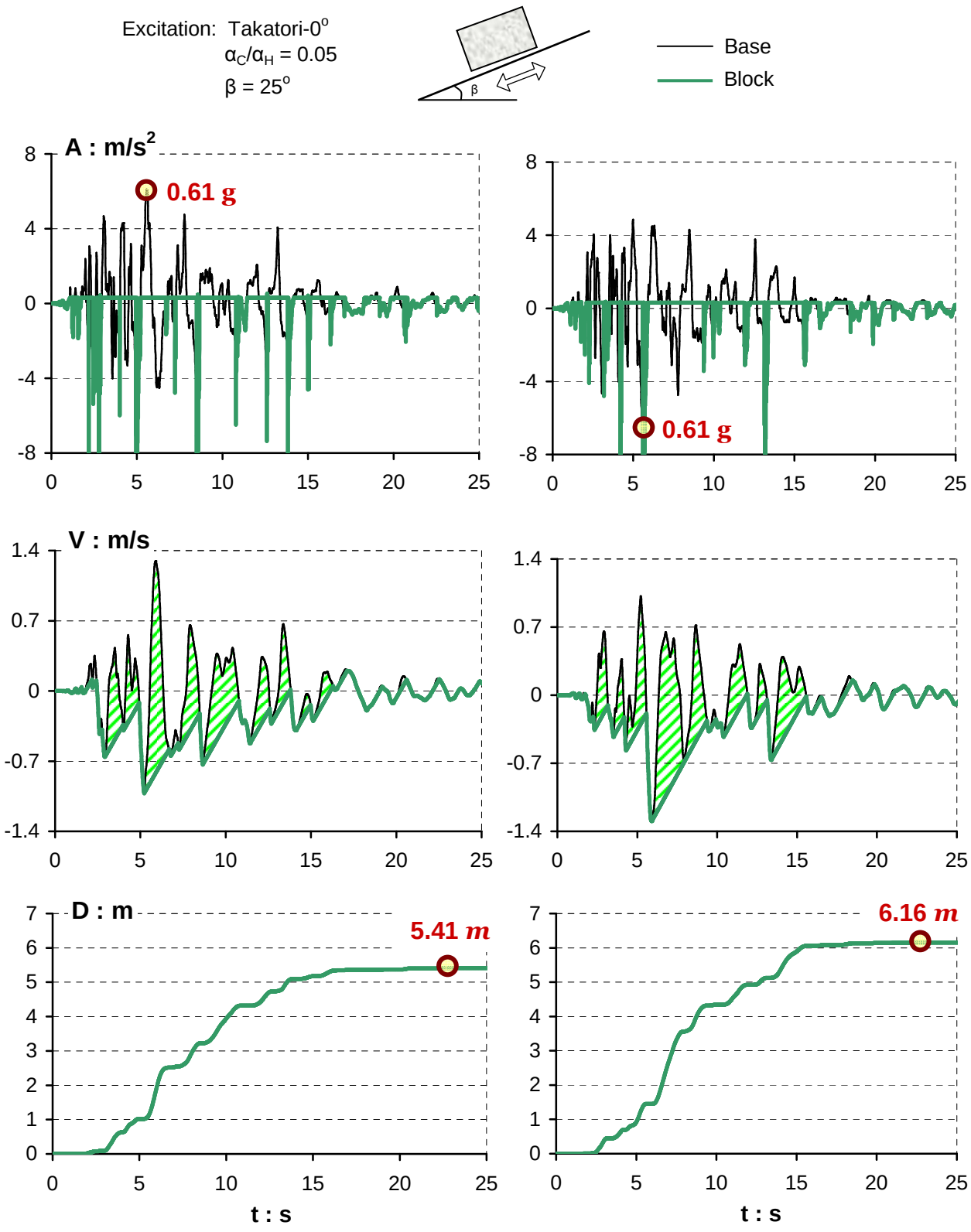

Figure 2.11 *Quite symmetric velocity time-history with well defined directivity acceleration pulses. The Takatori–0° record imposed with its normal (left column) and reversed (right column) sign. The polarity effect does not prevail.*

Excitation Records from

the Northridge $M_w = 6.7$ Earthquake

17 January 1994, California

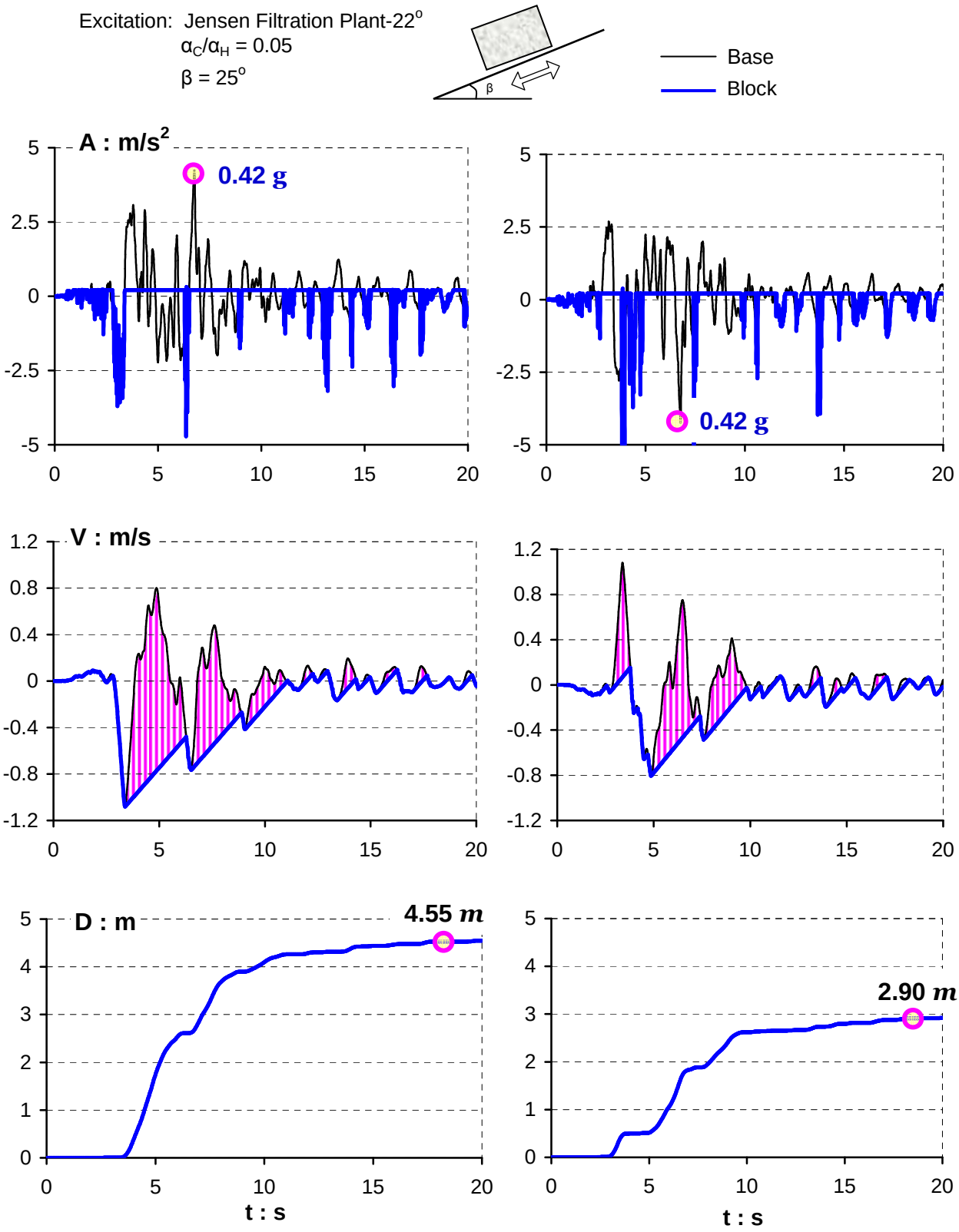

Figure 2.13 *The strong directivity affected record of Jensen-22°, exhibits several well-shaped acceleration and velocity pulses. The displacement response difference due to polarity is close to 60%. (a_C/a_H = 0.05 and β = 25°)*

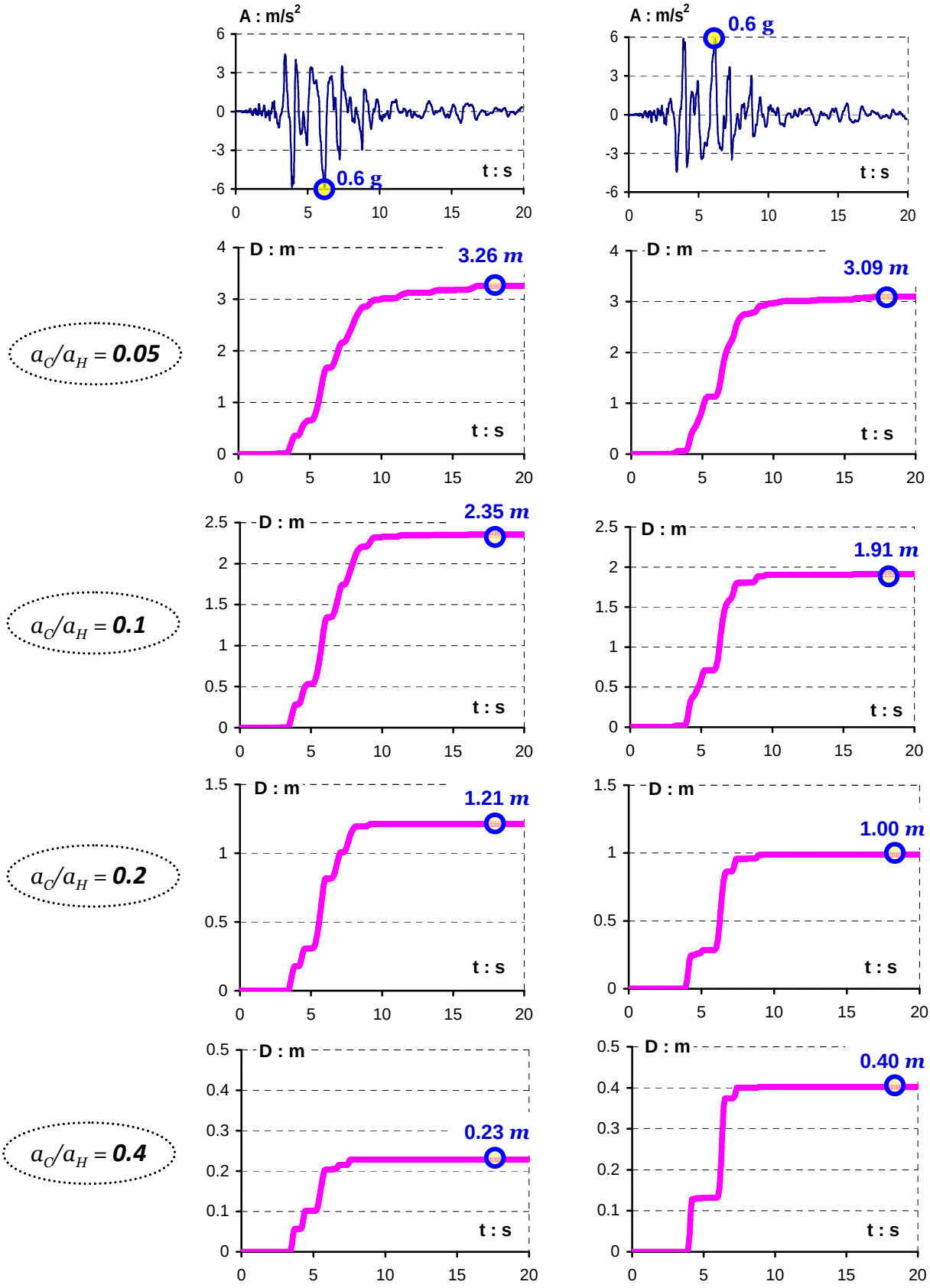

Figure 2.14 *Asymmetric sliding response for four acceleration ratio, a_C/a_H, values induced by the Jensen–292° record imposed with its normal (left column) and reversed (right column) sign. ($\beta = 25^o$)*

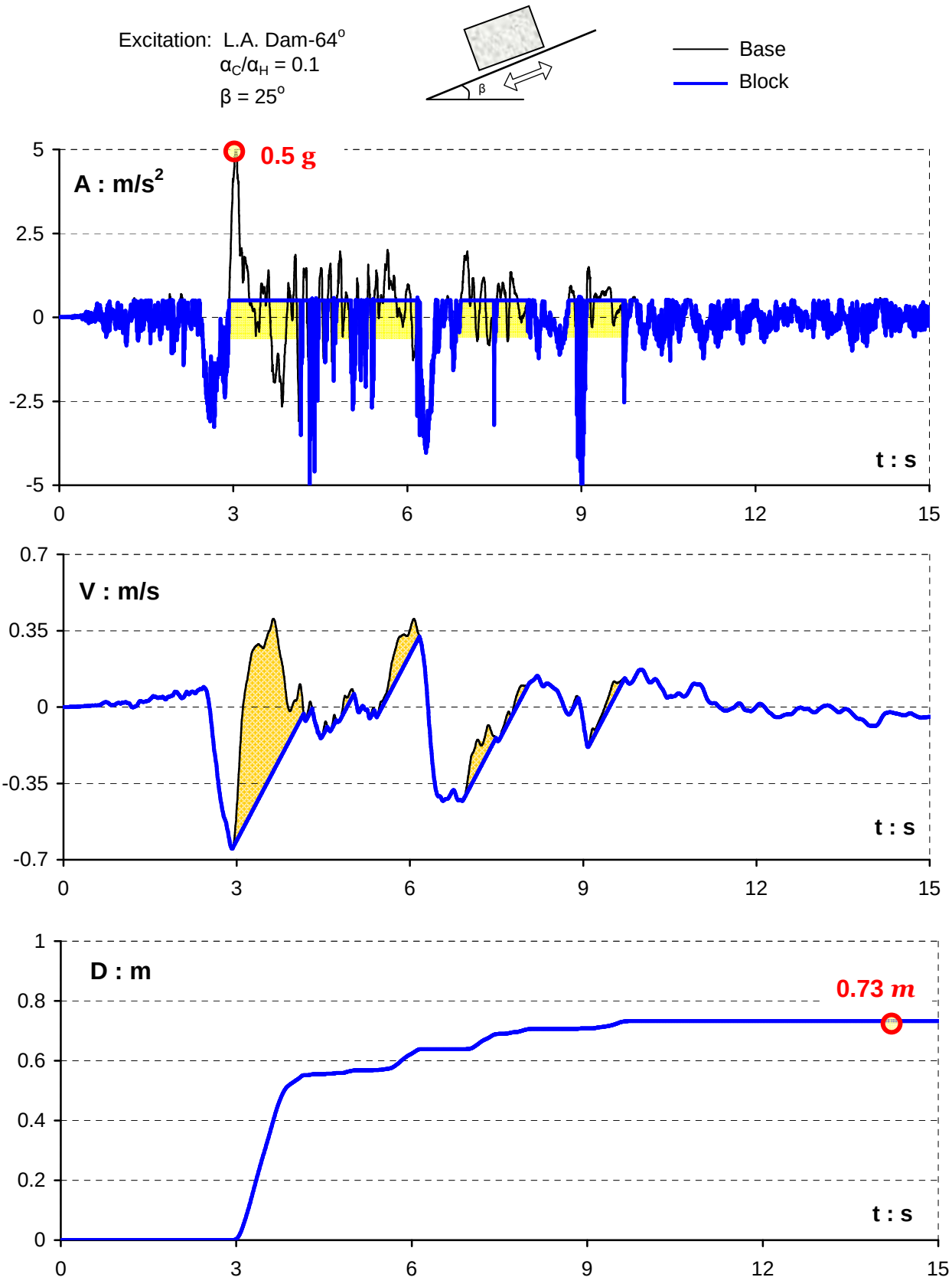

Figure 2.15 *Acceleration, velocity, and sliding displacement time histories of a rigid block resting on an 25^0 inclined plane when subjected to the L.A. Dam-64^o record. (a_C/a_H = 0.1)*

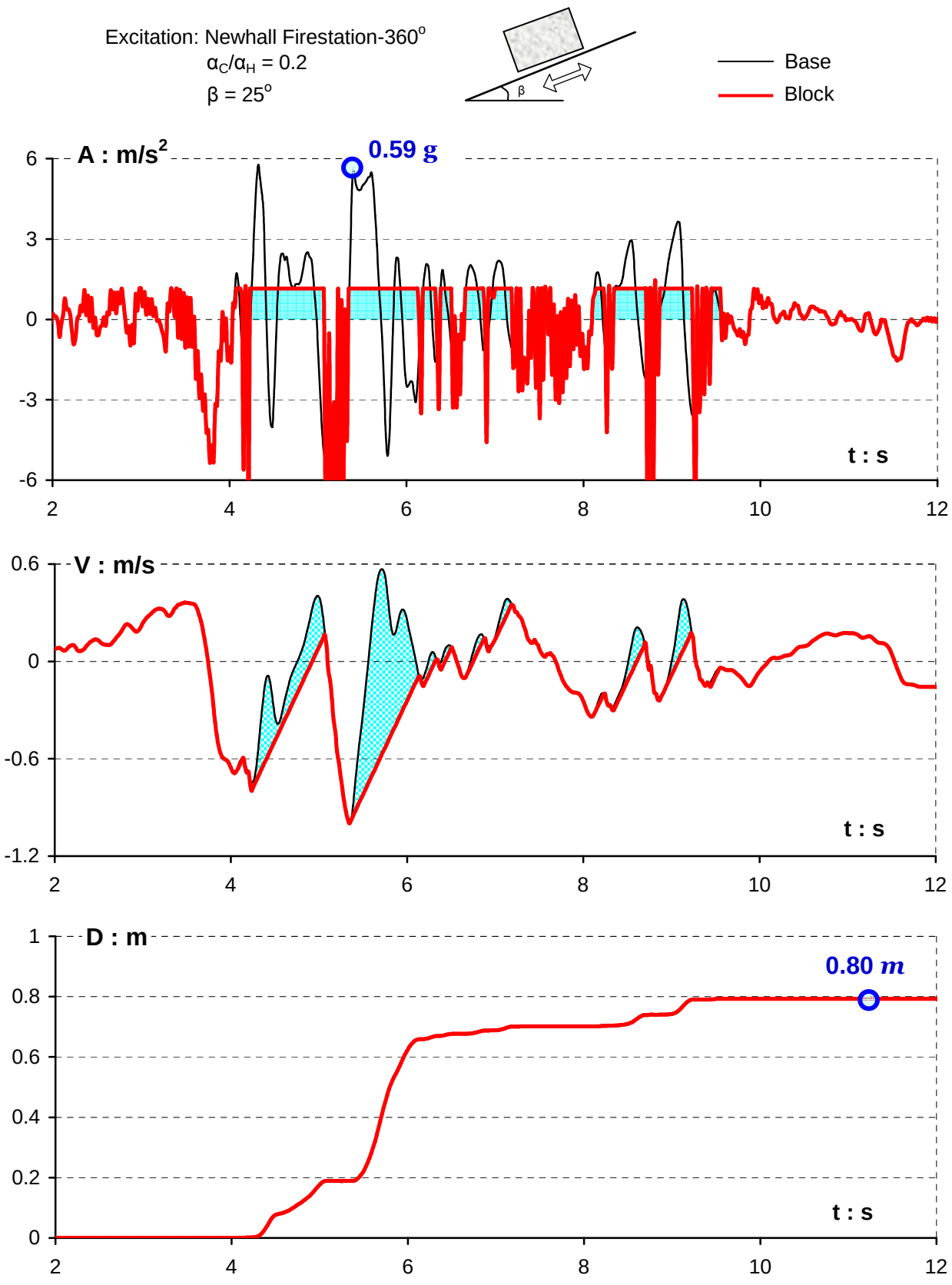

Figure 2.16 *Asymmetric response of a rigid block resting on an 25⁰ inclined plane when subjected to the Newhall Firestation-360° record. This record presents strong directivity acceleration pulses and as a consequence a highly asymmetric velocity. (a_C/a_H = 0.2)*

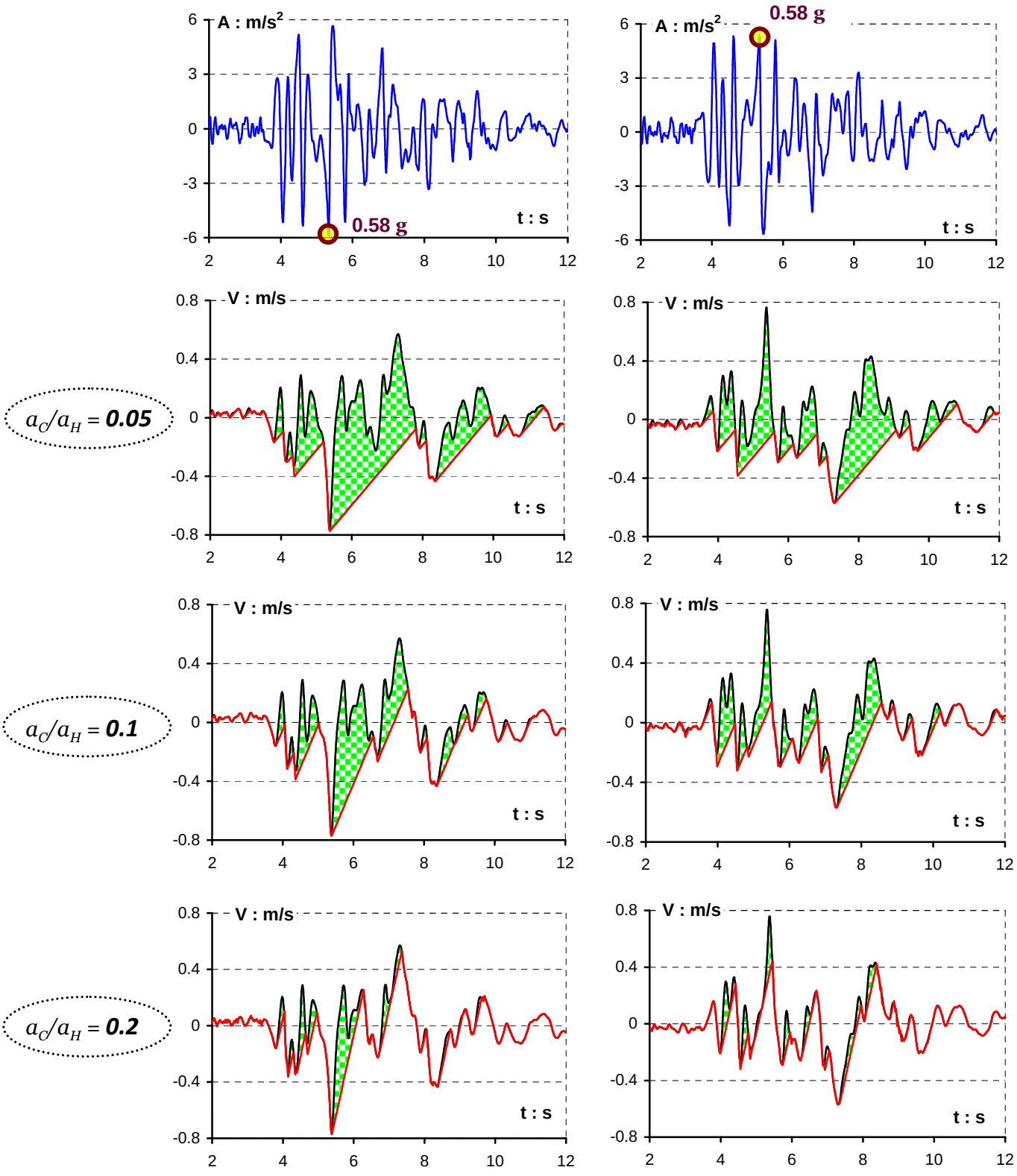

Figure 2.17 *Velocity response for different acceleration ratios, a_C/a_H, induced by the Newhall Fire station–90° record imposed with its normal (left column) and reversed (right column) sign. ($\beta = 25^o$)*

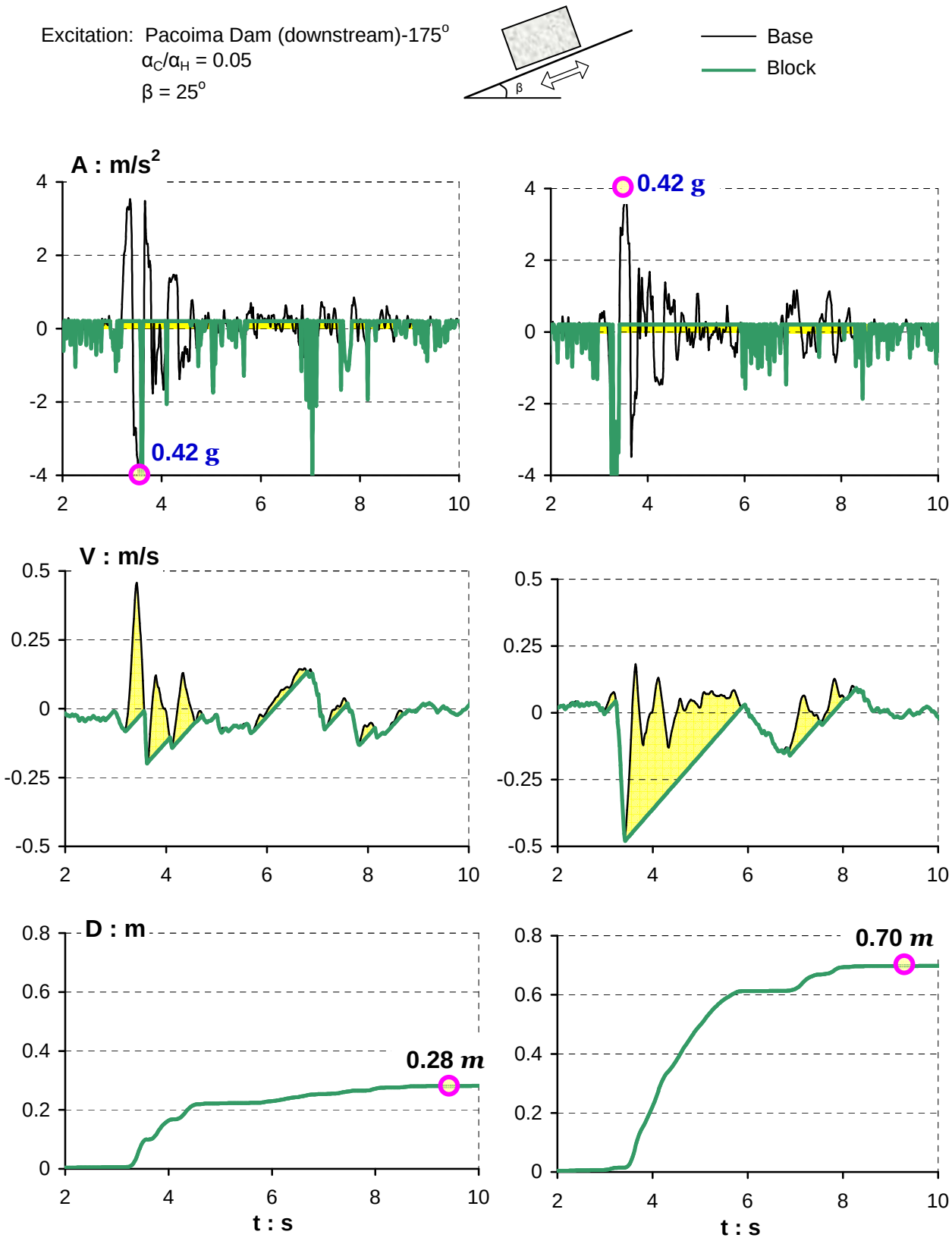

Figure 2.18 *The strong directivity affected record of Pacoima Dam Downstream-175°, exhibits several well-shaped acceleration pulses. Observe the highly asymmetric velocity time history. The displacement response difference due to polarity is over 200%. (a_C/a_H = 0.05 and β = 25°)*

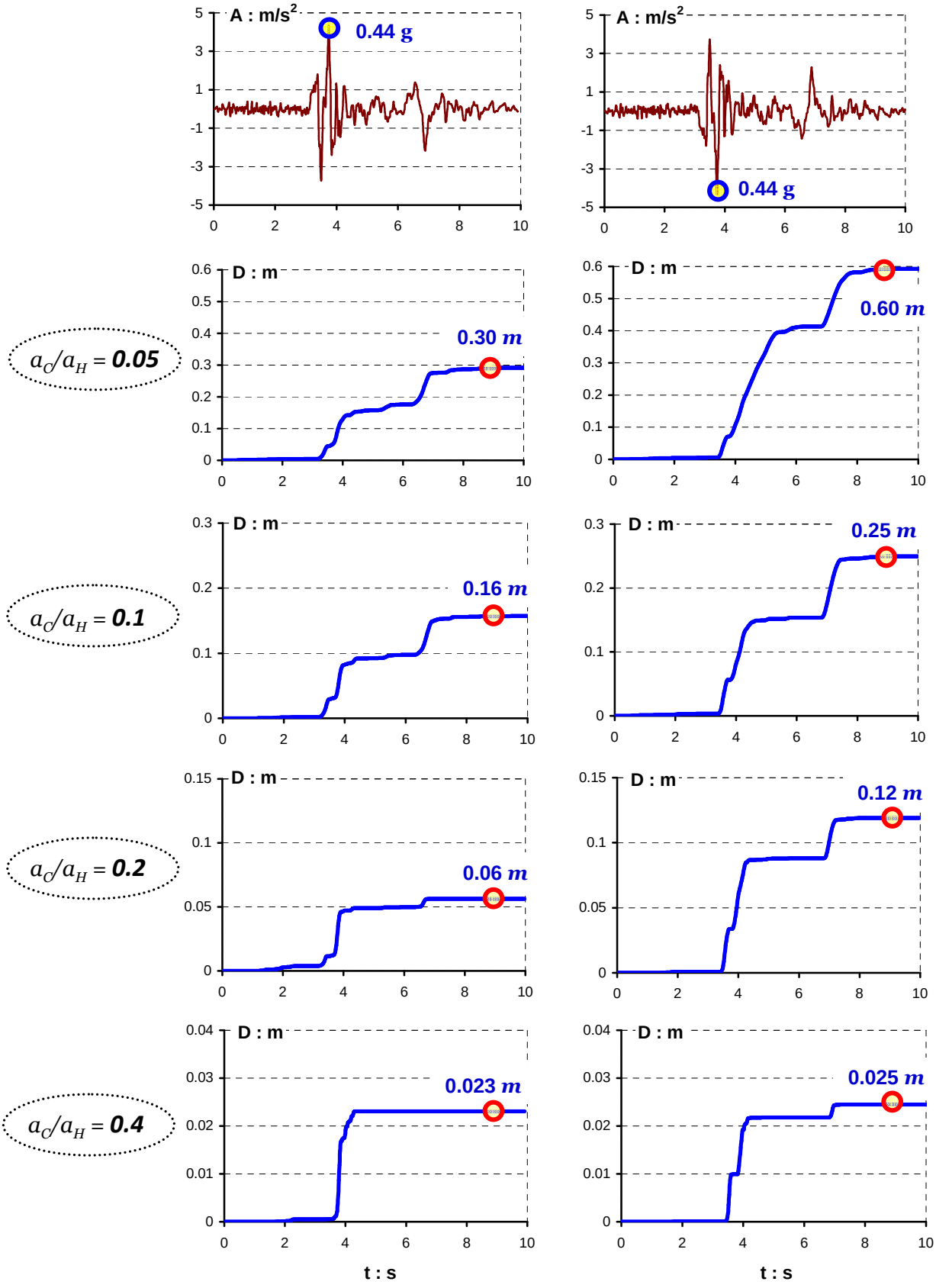

Figure 2.19 *Asymmetric sliding response for four acceleration ratio, a_C/a_H, values induced by the Pacoima Dam downstream–265° record imposed with its normal (left column) and reversed (right column) sign. ($\beta = 25^o$)*

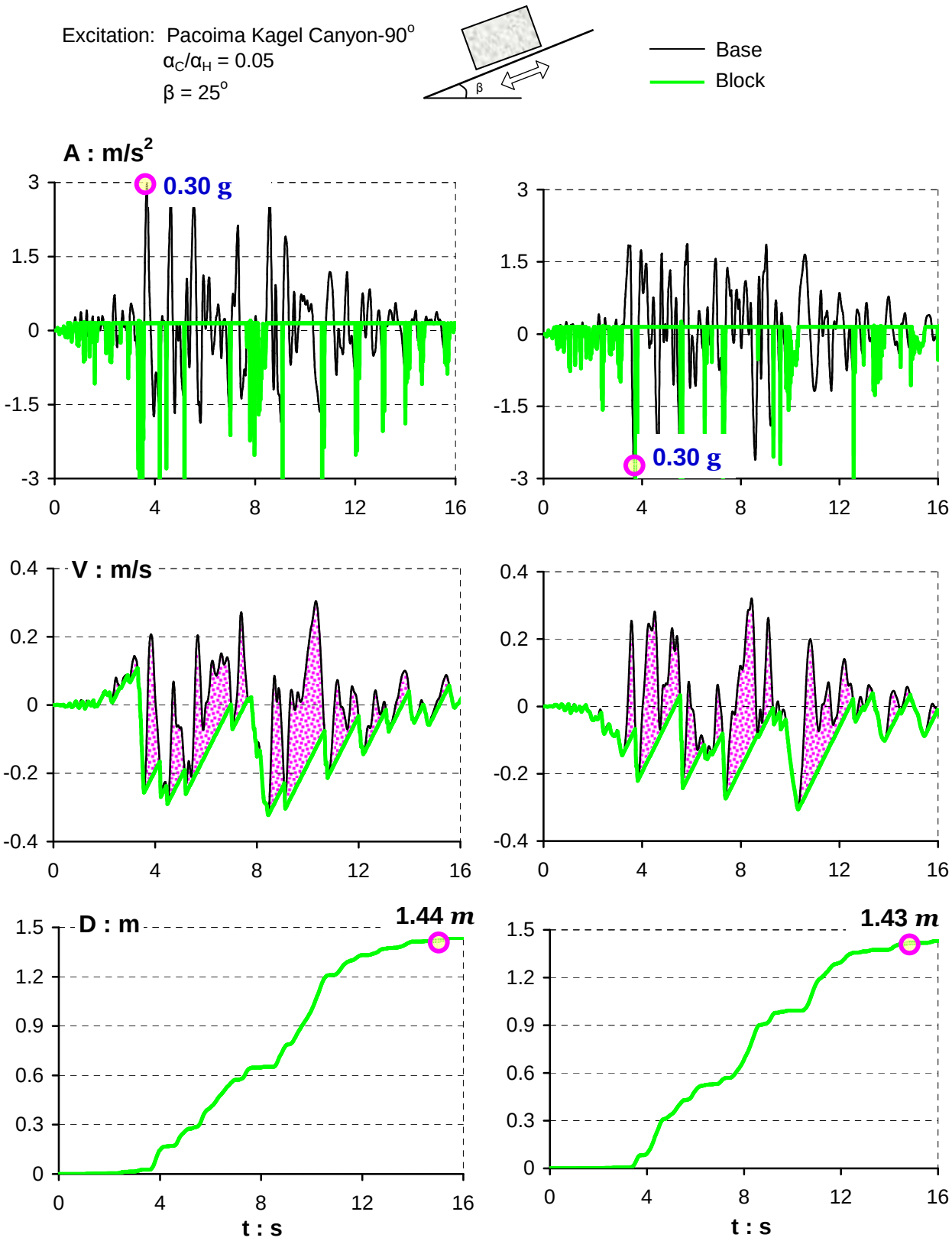

Figure 2.20 *The Pacoima Kagel Canyon-90° record presents a symmetric velocity time history, that minimises the polarity influence on sliding response.* *($a_C/a_H = 0.05$ and $\beta = 25^o$)*

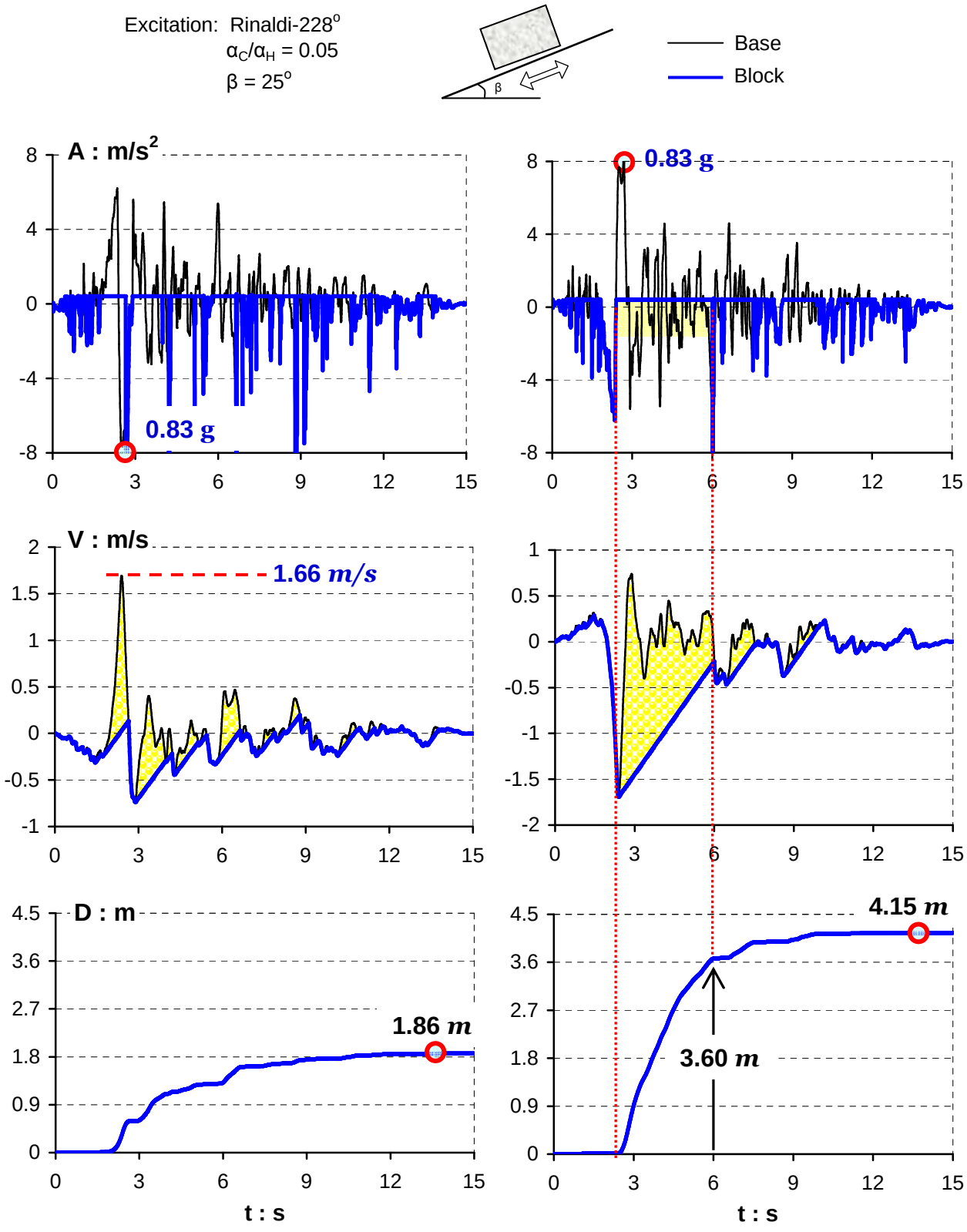

Figure 2.21 *The strong directivity affected record of Rinaldi-228°, is characterised by one long-period acceleration pulse (starting at 1.7 s and ending at 3.6 s). Observe the highly asymmetric velocity time history. The displacement response difference due to polarity is over 200%. (a_C/a_H = 0.05 and β = 25°)*

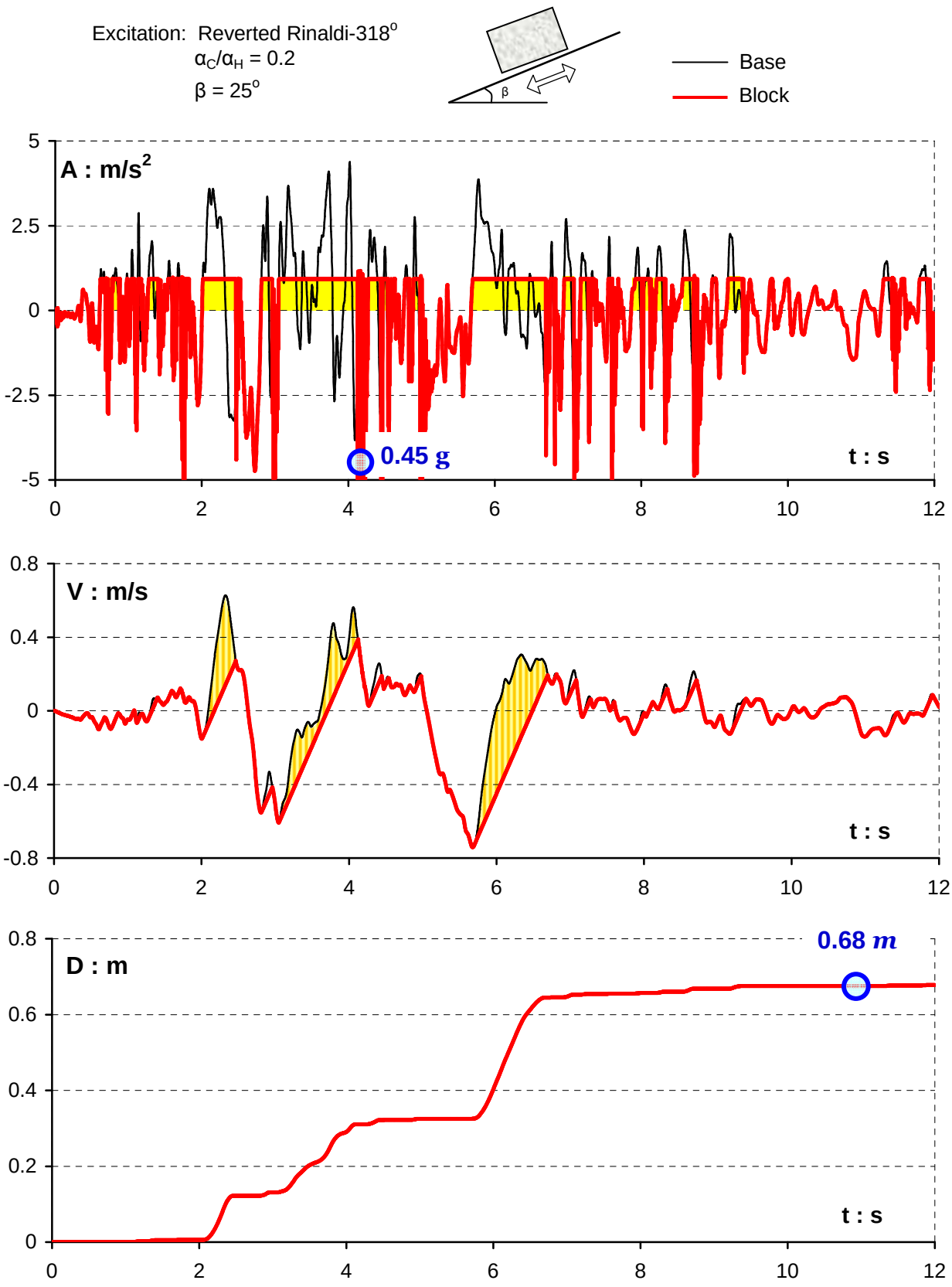

Figure 2.22 *Asymmetric response of a rigid block resting on an 25⁰ inclined plane when subjected to the reversed polarity Rinaldi-318° record. (a_C/a_H = 0.2)*

Excitation Records from the

Imperial Valley $M_w = 6.5$ Earthquake

15 Octomber 1979, California

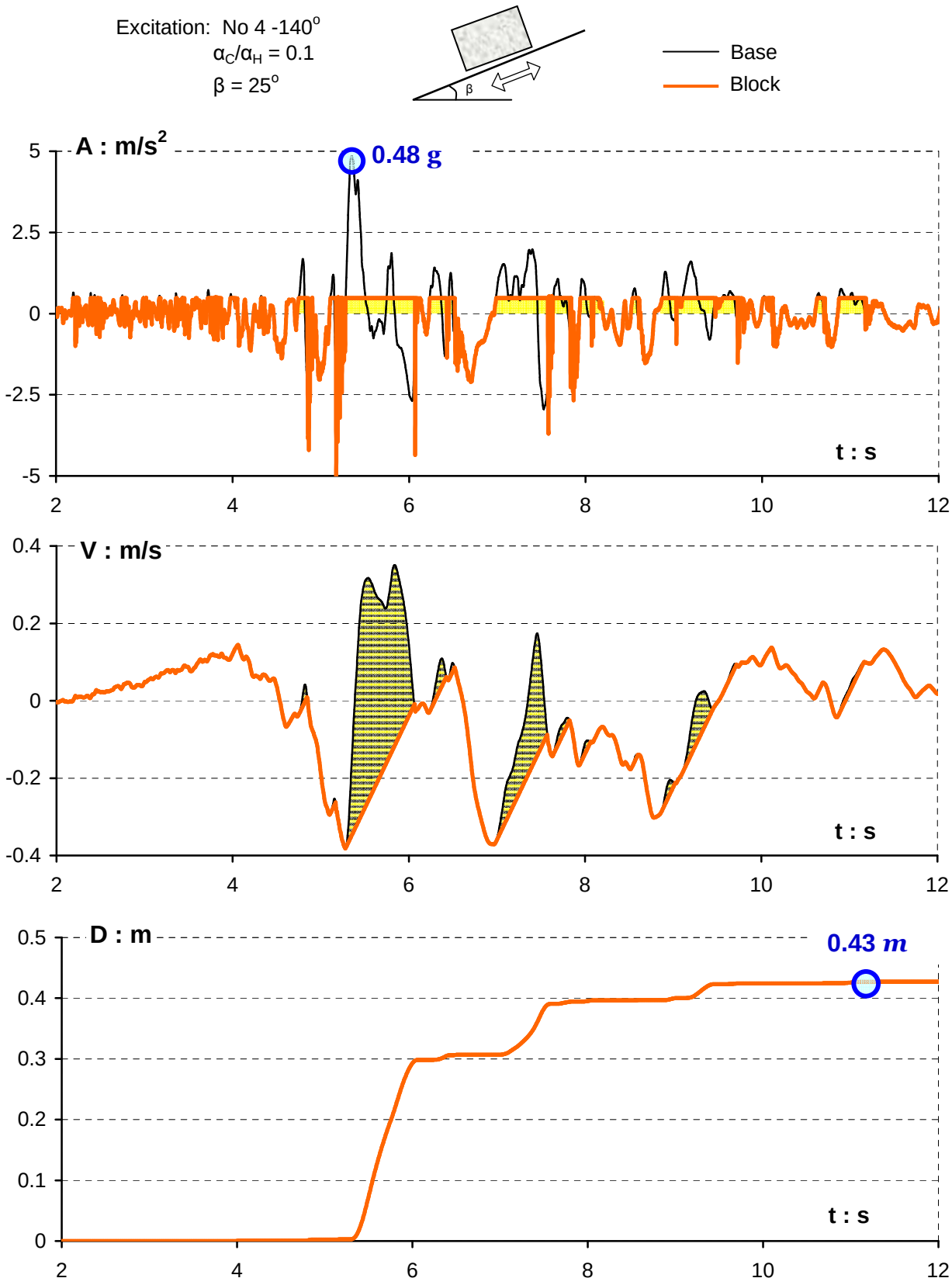

Figure 2.29 *An other example of strong affected directivity motion: block slippage on an 25^0 inclined plane when subjected to the Imperial Valley No 4-140° record. This record includes a number of long-period acceleration pulses (starting at the moment of 5 sec until 9 sec) that result to a series of well-shaped symmetric velocity pulses as well. ($a_C/a_H = 0.1$)*

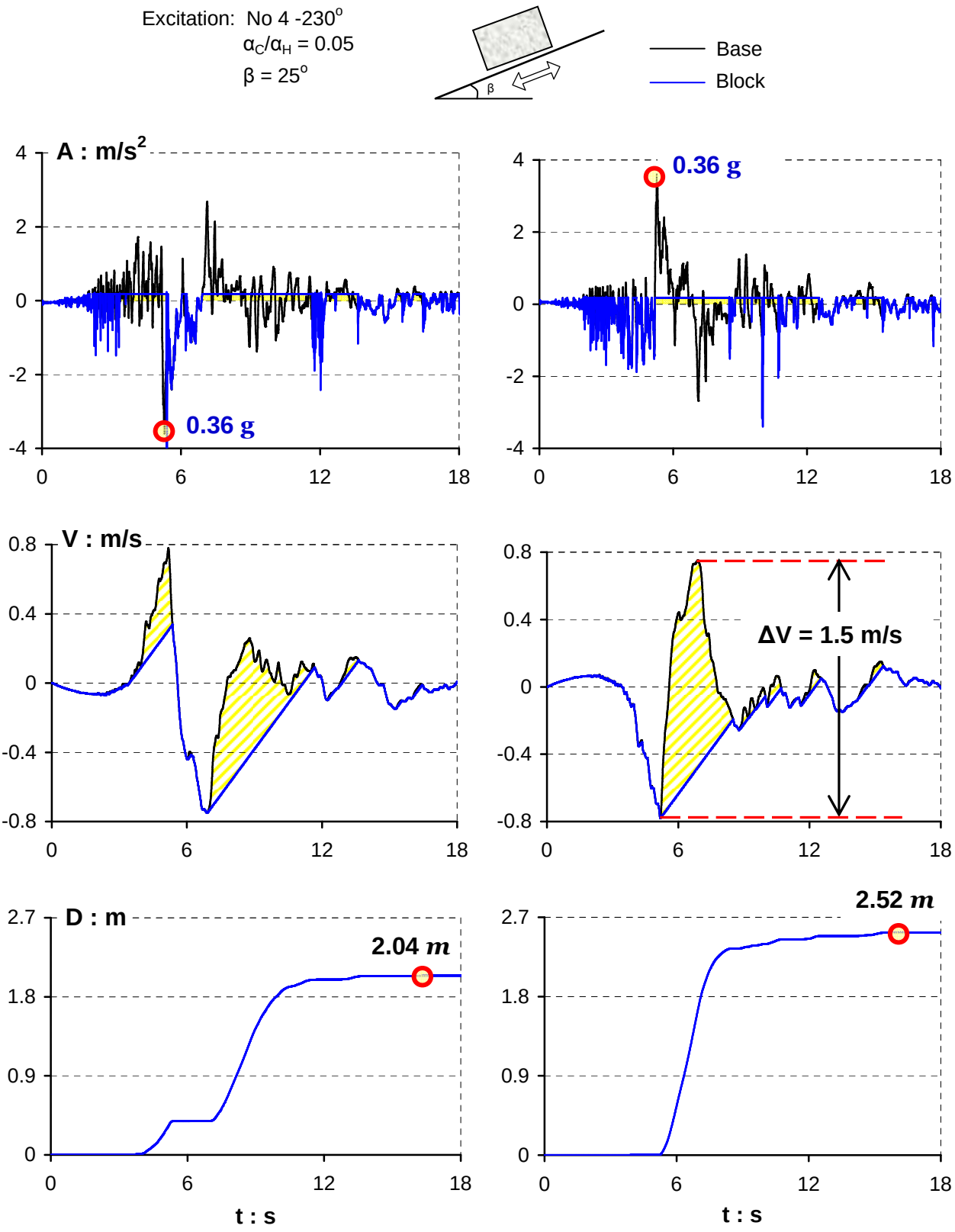

Figure 2.30 *The forward directivity affected record of Imperial Valley No 4-230°. The velocity time-history exhibits one symmetric long-duration pulse, responsible for the most of the slippage. As expected, the sliding difference due to polarity is small – less than 25%.* ($a_C/a_H = 0.05$ *and* $\beta = 25^o$)

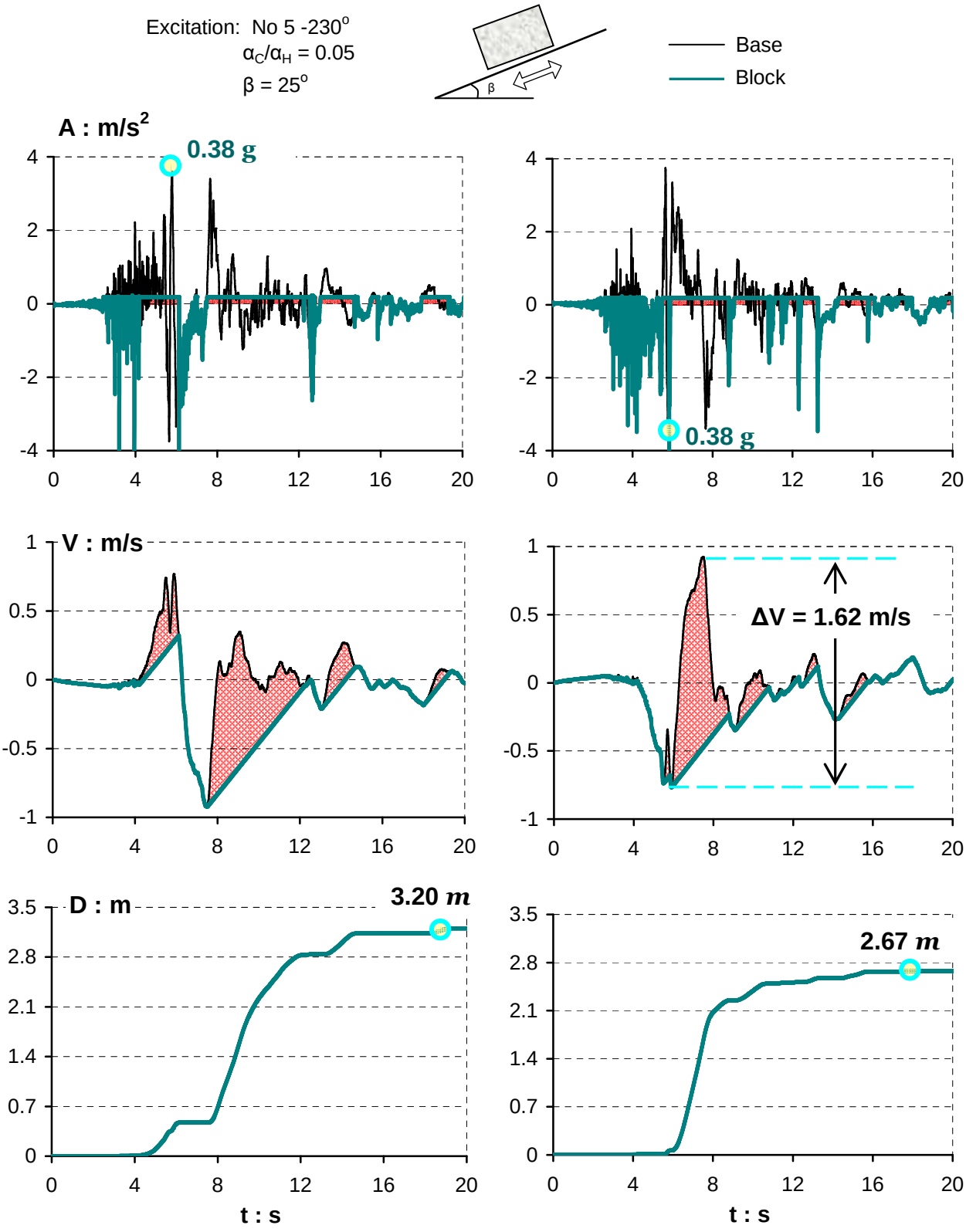

Figure 2.31 *A similar case: the Imperial Valley No 5-230° record. Also, the velocity time-history exhibits one symmetric long-duration pulse, which is responsible for the most of the slippage. Furthermore, the difference due to polarity is less than 20%. ($a_C/a_H = 0.05$ and $\beta = 25^o$)*

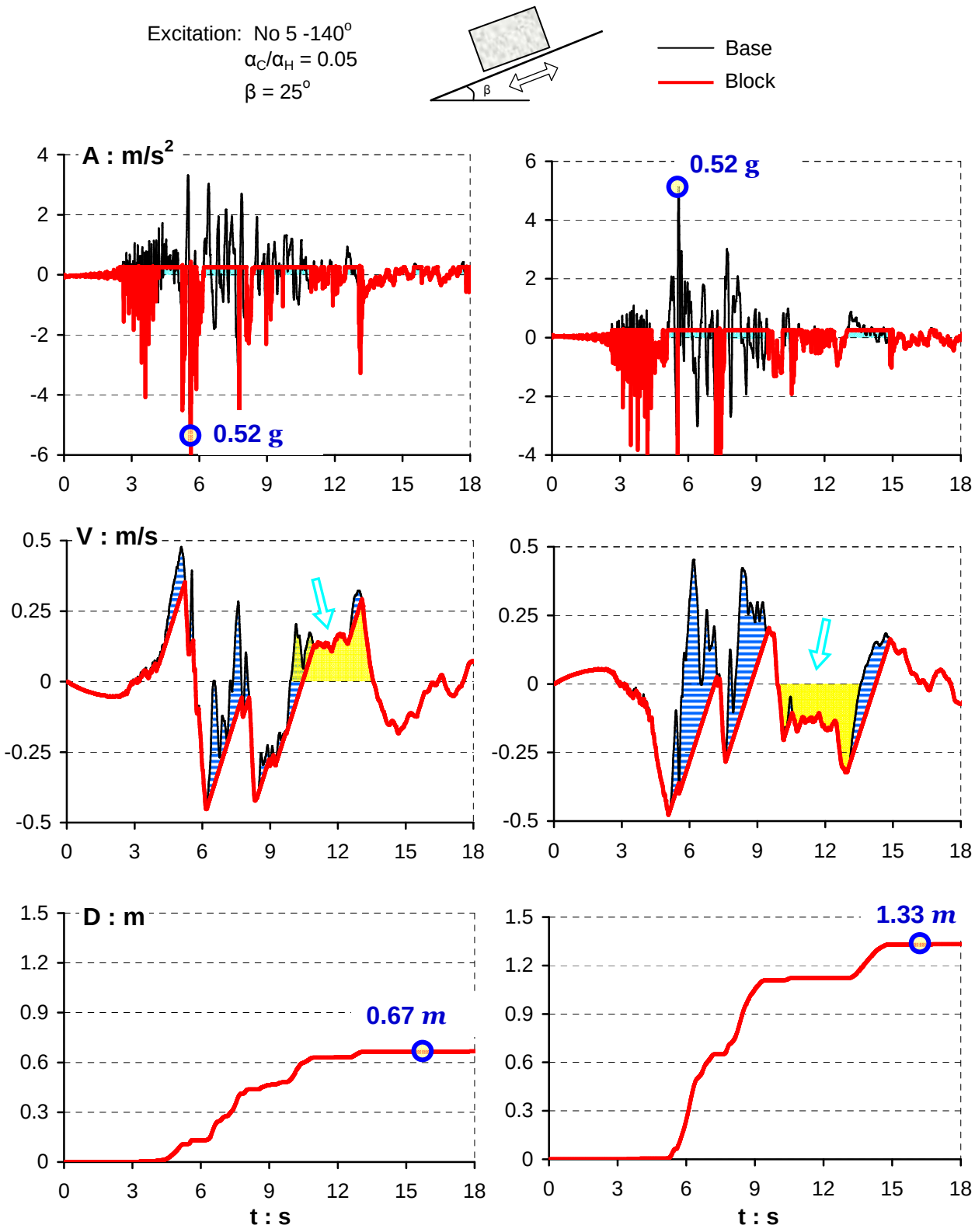

Figure 2.32 *The opposite case: the Imperial Valley No 5-140°. There is not only one velocity pulse triggering the slippage but several of them. What is more, the velocity pulse starting at 9 sec and ending at 15 sec does not sequel by one of opposite sign, thus generating the asymmetry in velocity. The polarity effect is prominent, leading to a quantitative difference of almost 200%.* ($a_C/a_H = 0.05$ *and* $\beta = 25^o$)

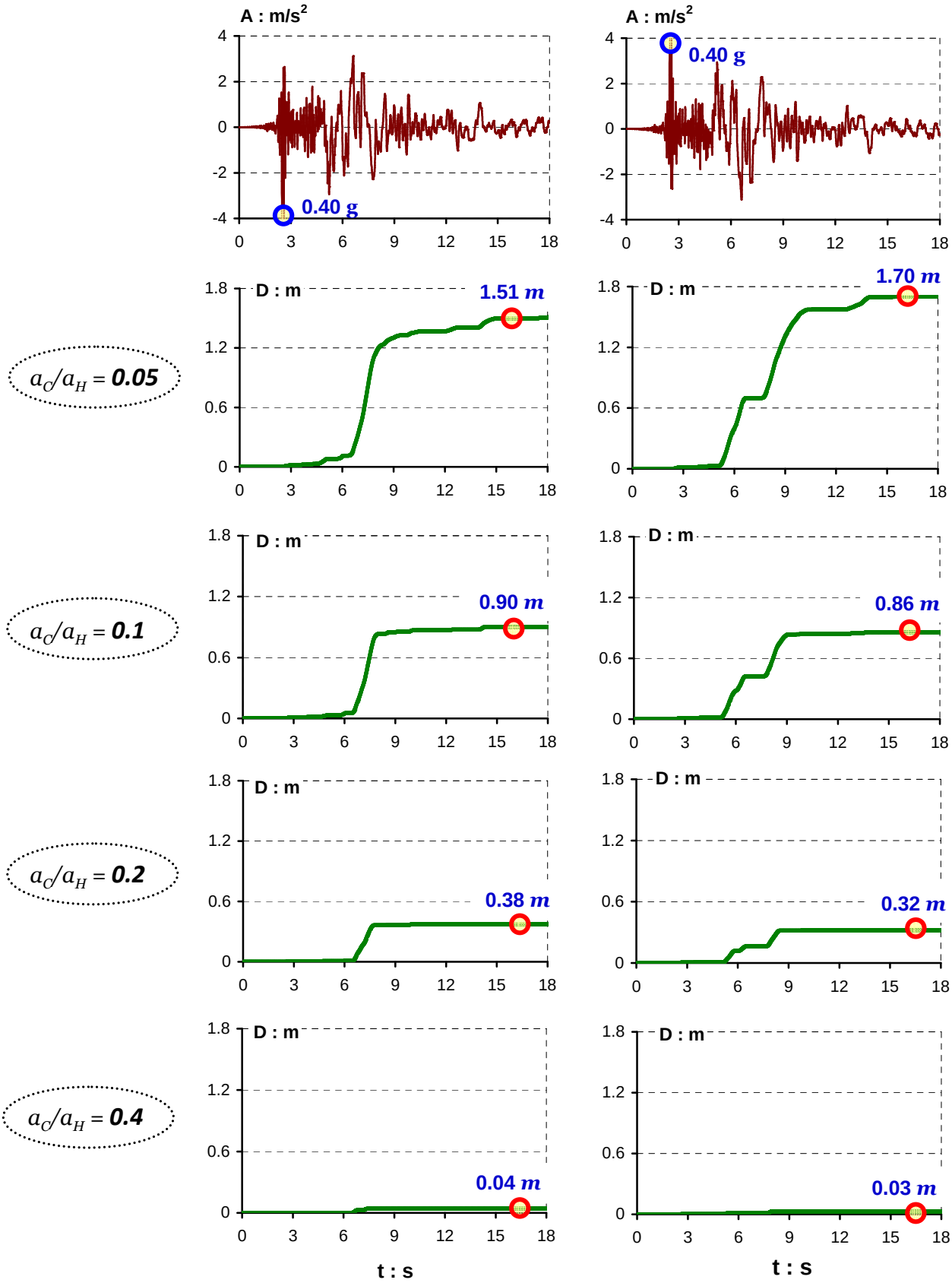

Figure 2.33 *Sliding displacement response for four acceleration ratio, a_C/a_H, values induced by the Imperial Valley No 6–140° record imposed with its normal (left column) and reversed (right column) sign. ($\beta = 25^o$)*

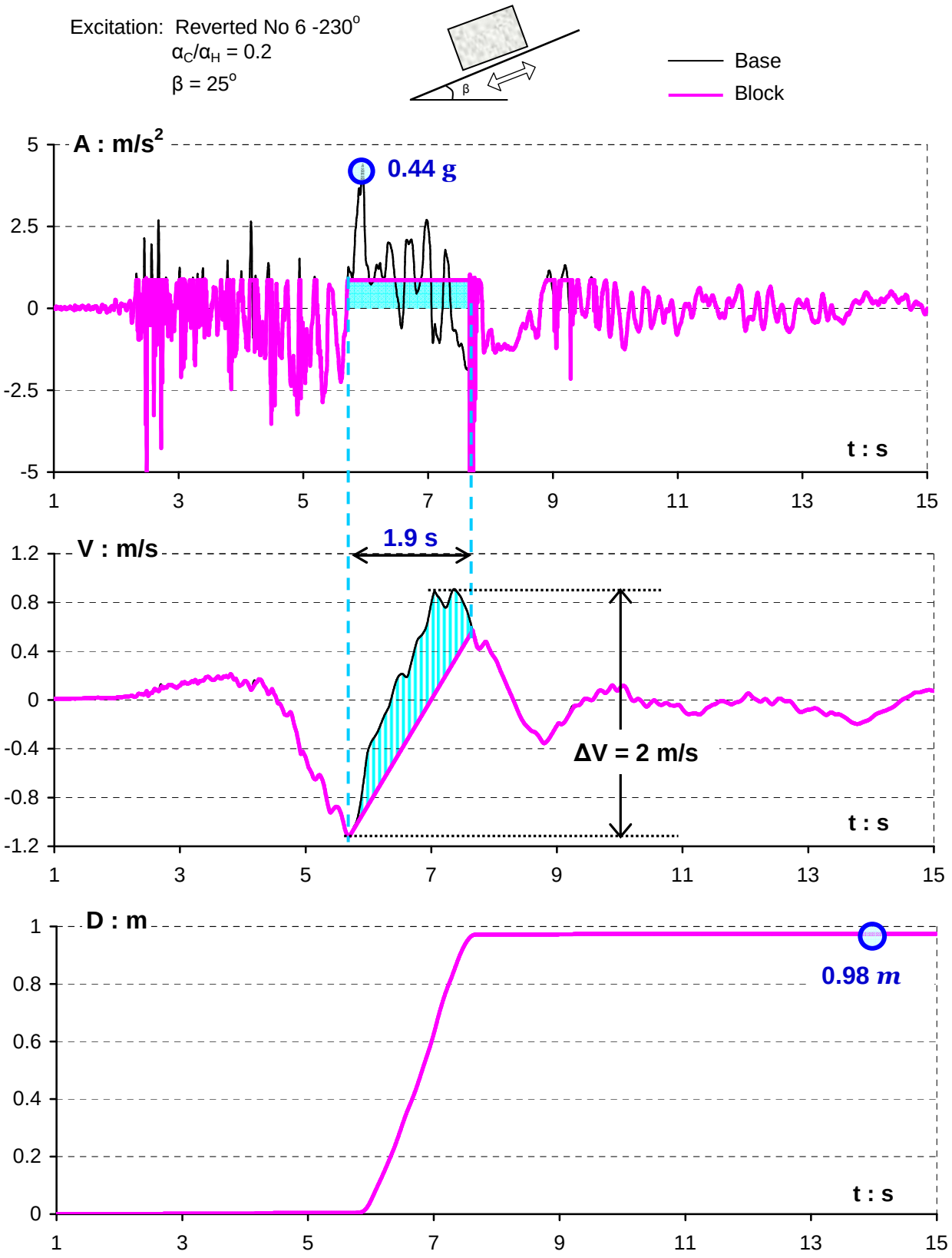

Figure 2.34 *Sliding response on an 25^0 inclined plane when subjected to the inverted Imperial Valley No 6-230° record. Notice in this ground motion the long-period acceleration pulses starting at 5 sec until 10 sec, that result to one well-shaped long-period velocity pulses as well. That particular velocity pulse is responsible for the only sliding event which occurred with $a_C/a_H = 0.2$.*

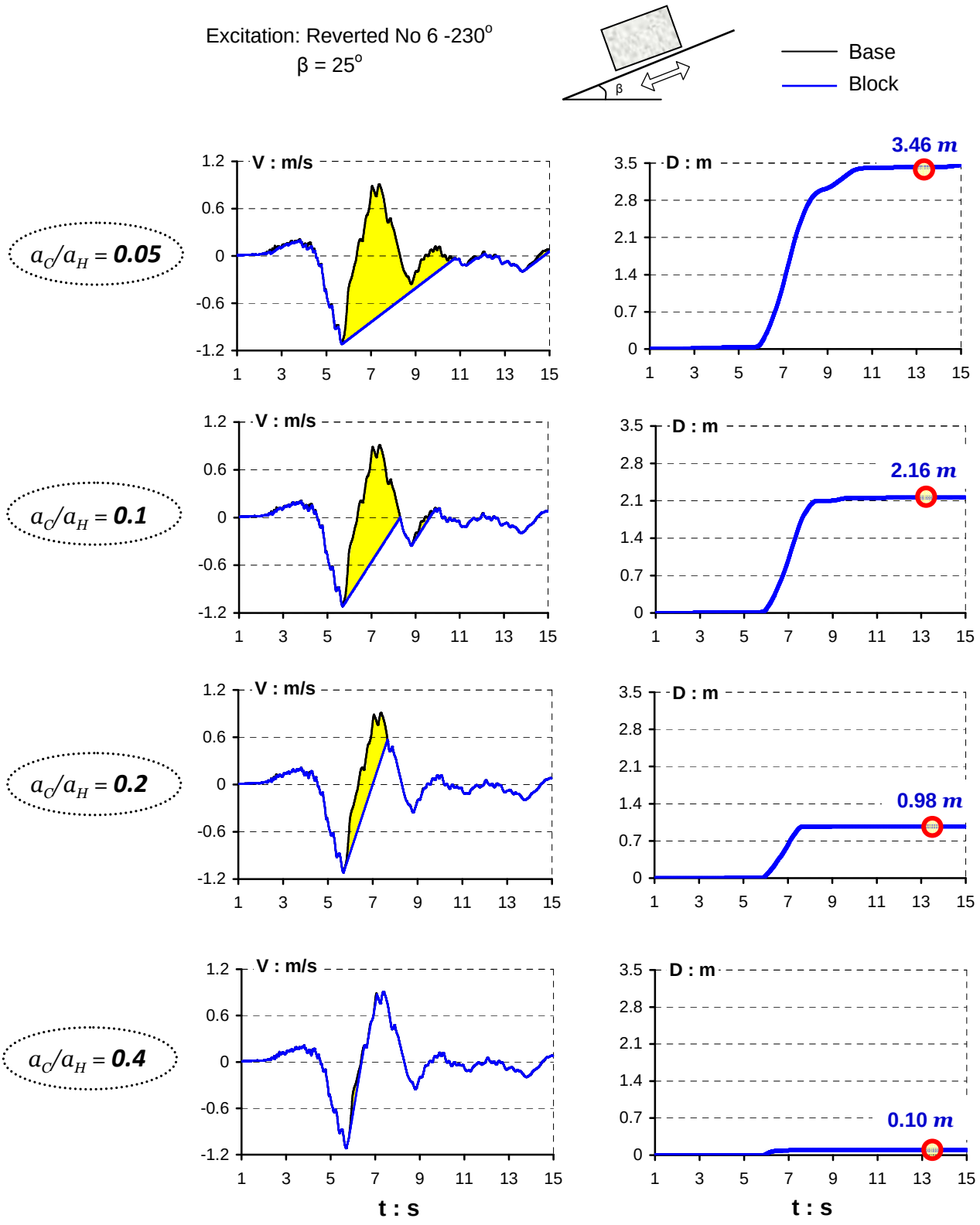

Figure 2.35 *Velocity and displacement time-histories for four acceleration ratio, a_C/a_H, values induced by the Imperial Valley No 6–230° record imposed with its reversed polarity. ($\beta = 25^o$)*

Excitation Records from

the Landers M_w = 7.3 Earthquake

28 June 1992, California

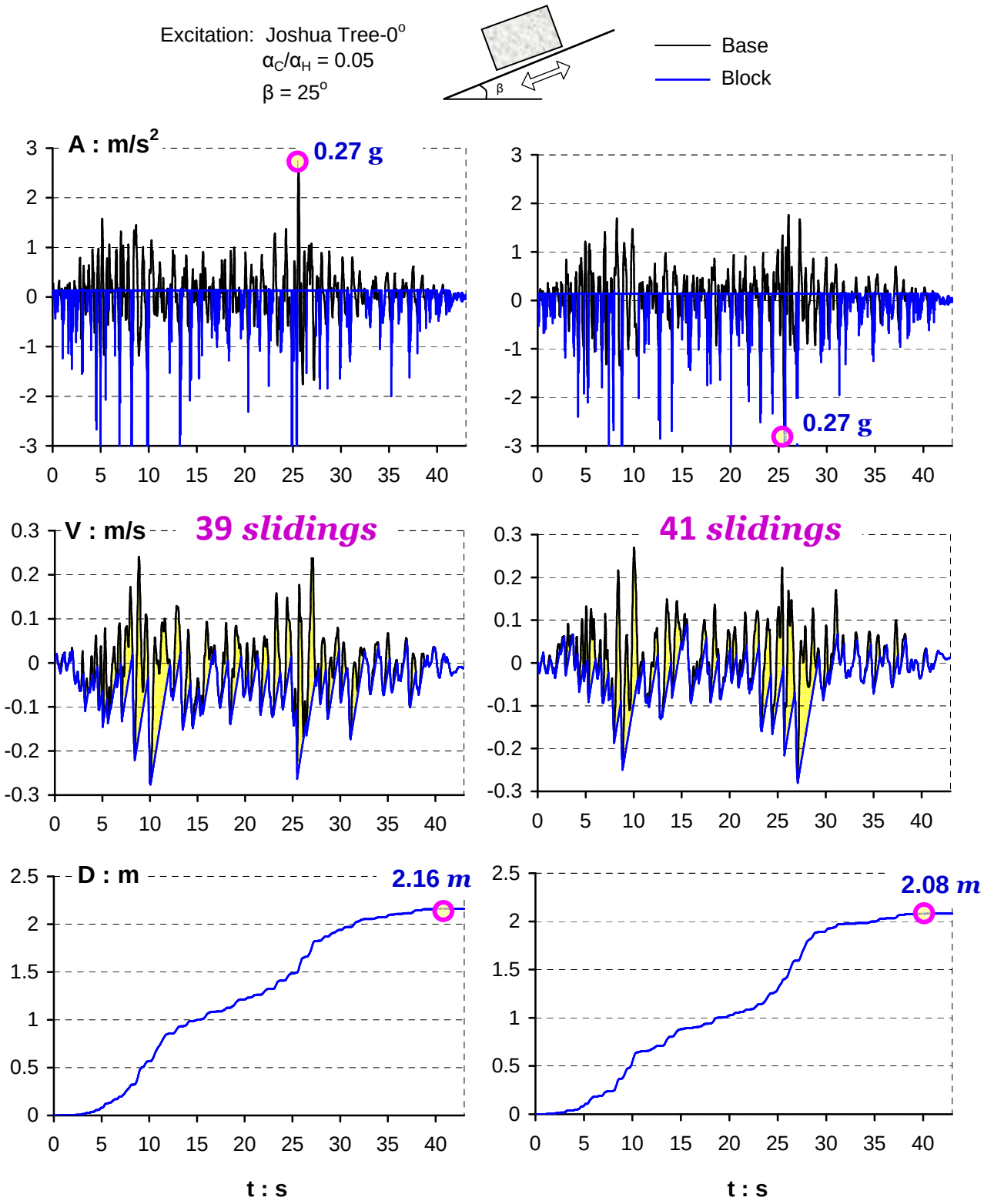

Figure 2.40 *Another example of a ground motion with lots of cycles and symmetric velocity time-history: the Joshua Tree-0° record. The polarity effect is almost negligible. (a_C/a_H = 0.05 and $\beta = 25^o$)*

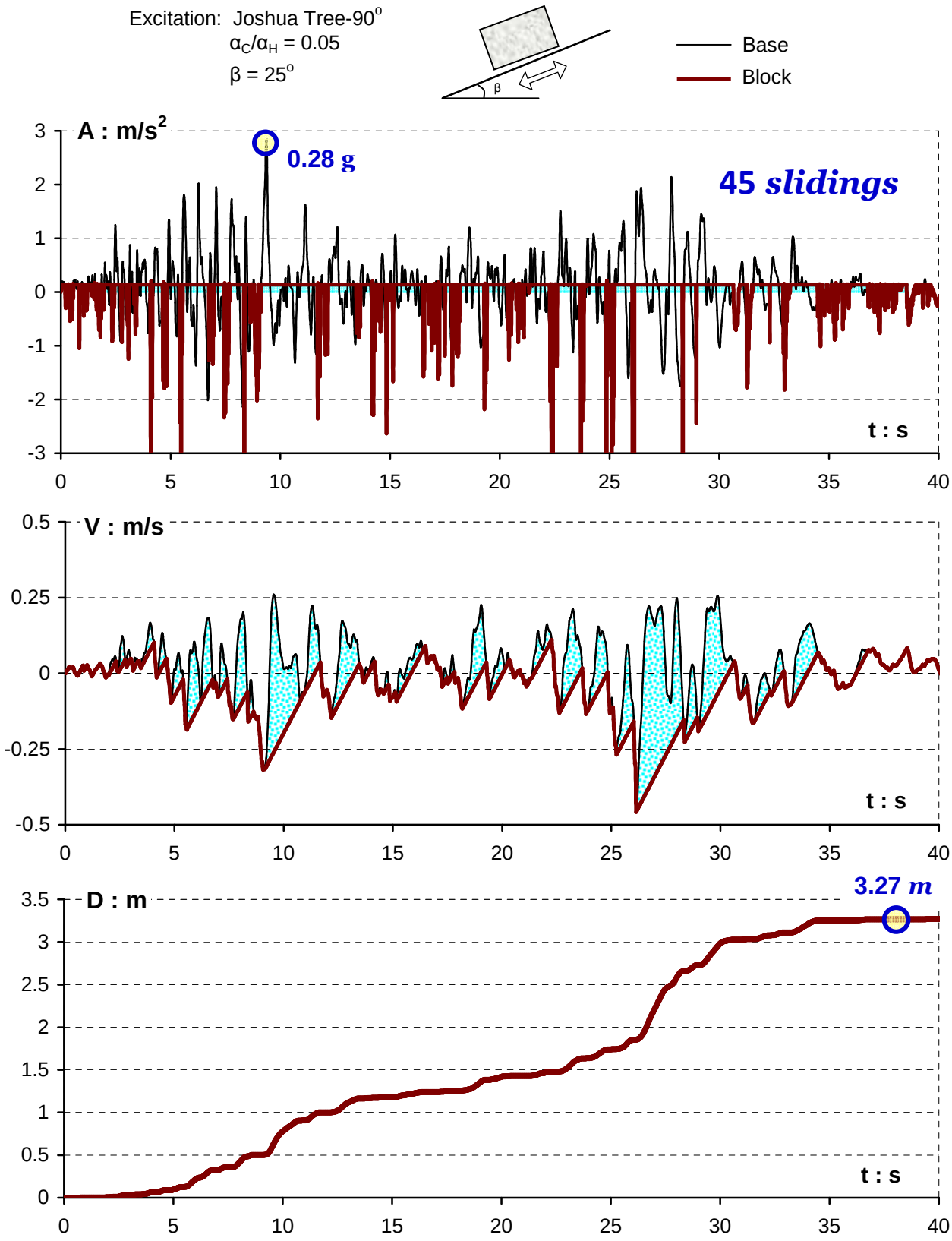

Figure 2.41 *The sliding response induced by the Joshua Tree-90° record is representative of the accumulative character of asymmetric sliding systems, such as our block on an 25⁰ inclined plane. The particular record consists of numerous acceleration pulses exceeding the critical yielding acceleration a_c. In each cycle an additional slippage induced, thus increasing the total displacement. After 45 slips the total displacement builds up to 3.27 m.*

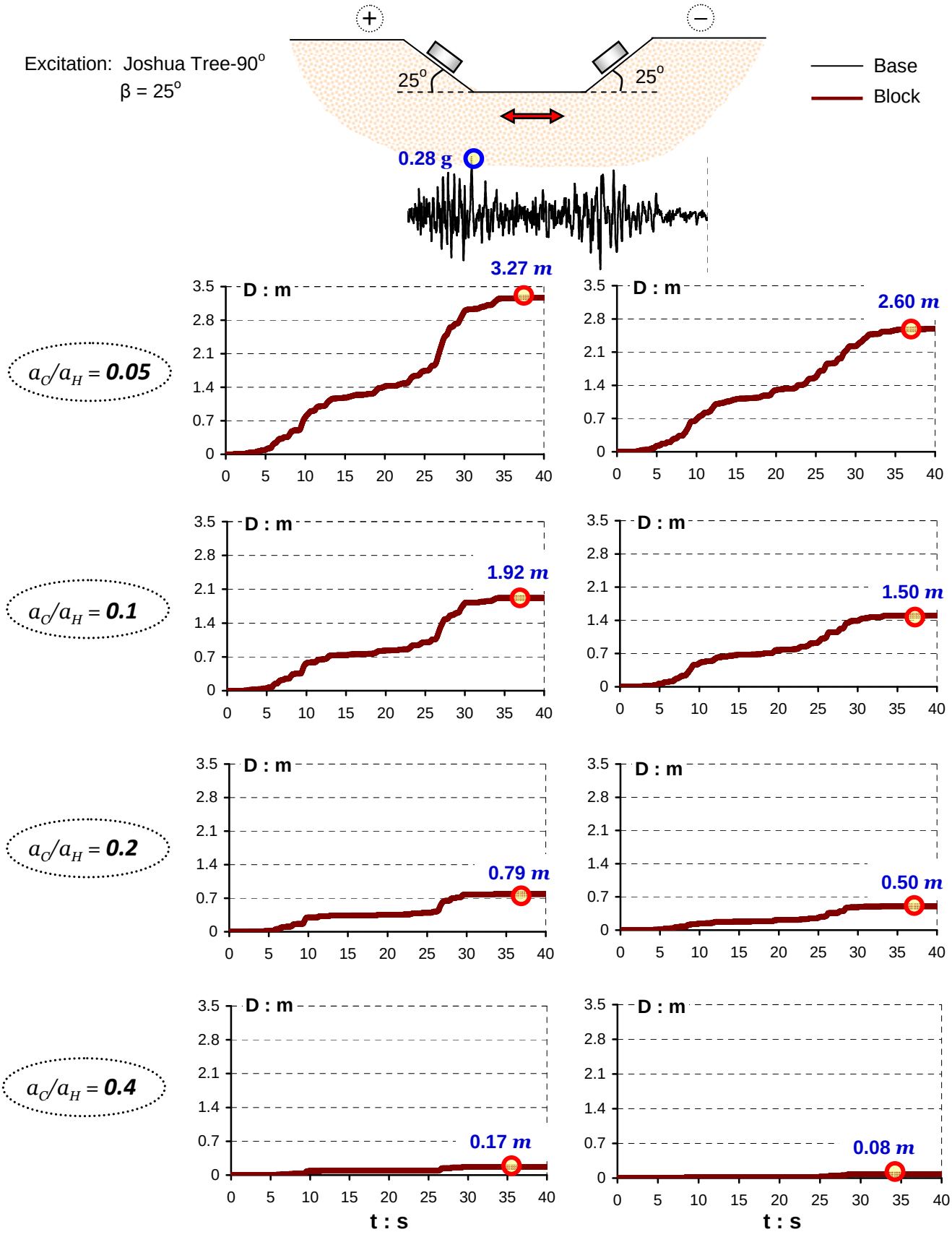

Figure 2.42 *Sliding displacement response for four acceleration ratio, a_C/a_H, values induced by the Joshua Tree–90° record imposed with its normal (left column) and reversed (right column) sign. ($\beta = 25^o$)*

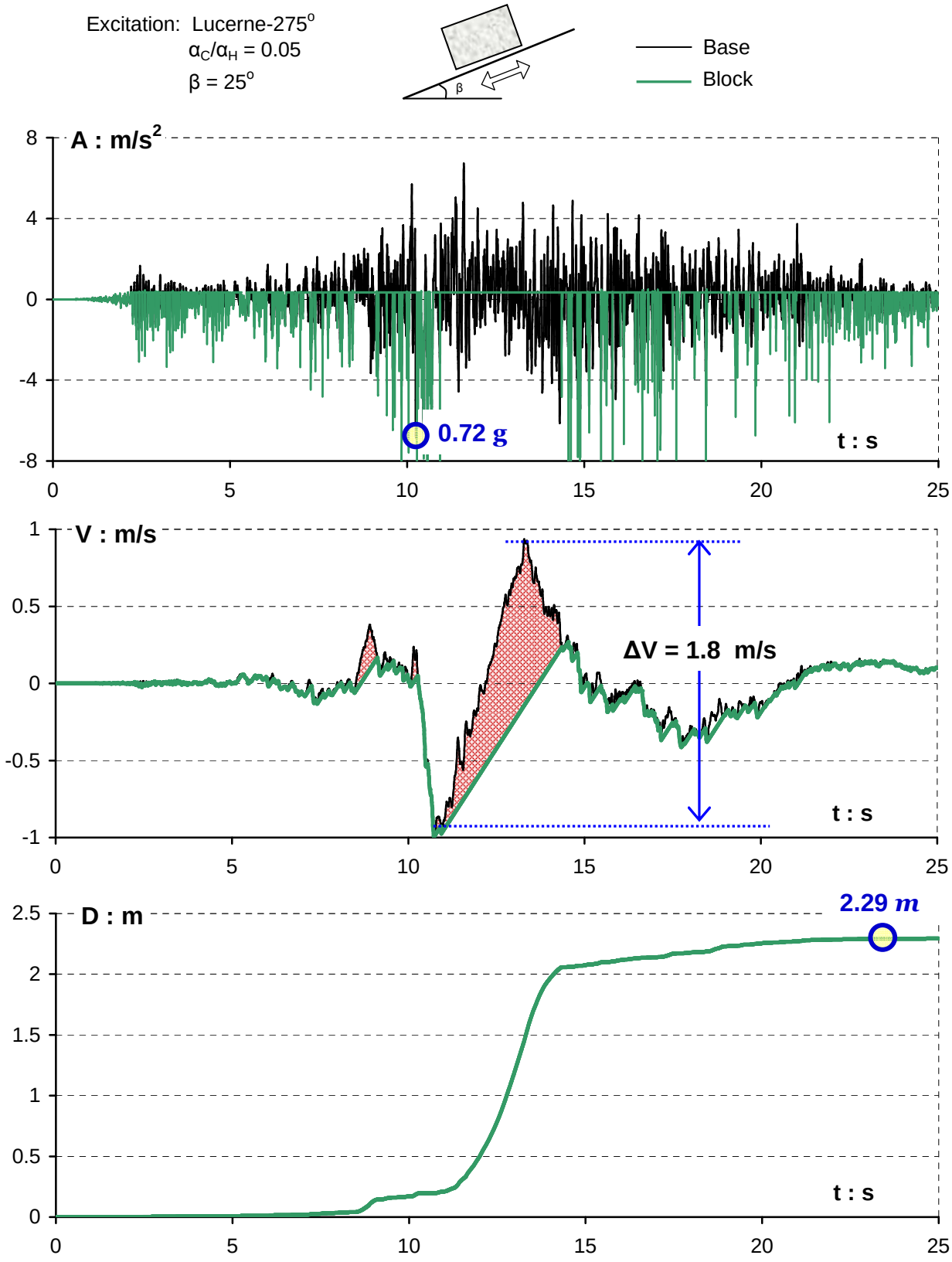

Figure 2.43 *The Lucerne-275° record is a fling affected motion with a peaked high frequency accelerogram. Behind all those peaks, a large period acceleration pulse is hiding. This pulse is responsible for the detrimental velocity pulse with a step of 1.8 m/s and with 5 seconds duration. The particular velocity pulse triggers the main sliding event.*

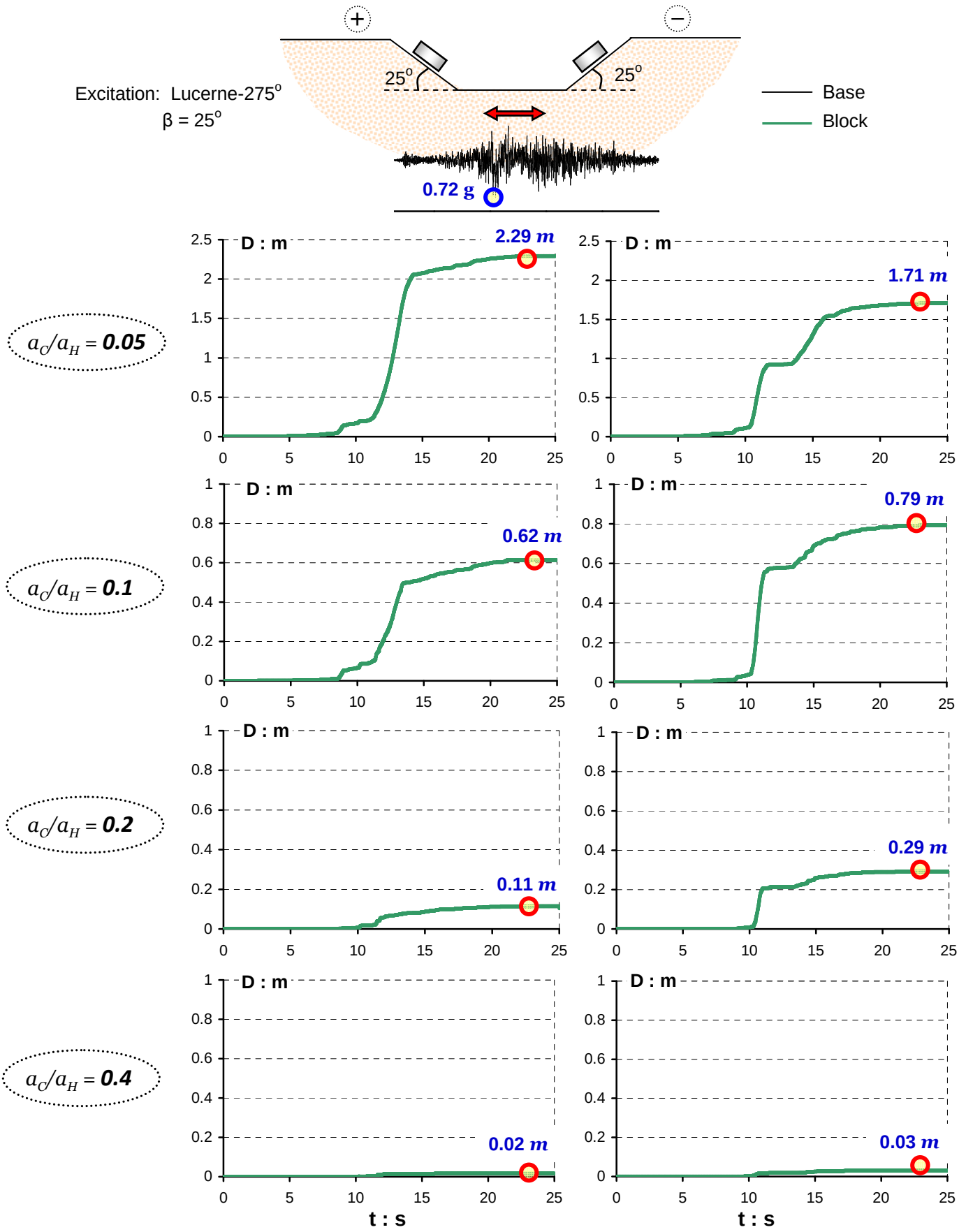

Figure 2.44 *Sliding response for four acceleration ratio, a_C/a_H, values induced by the Lucerne–275° record imposed with its normal (left column) and reversed (right column) sign. ($\beta = 25^o$)*

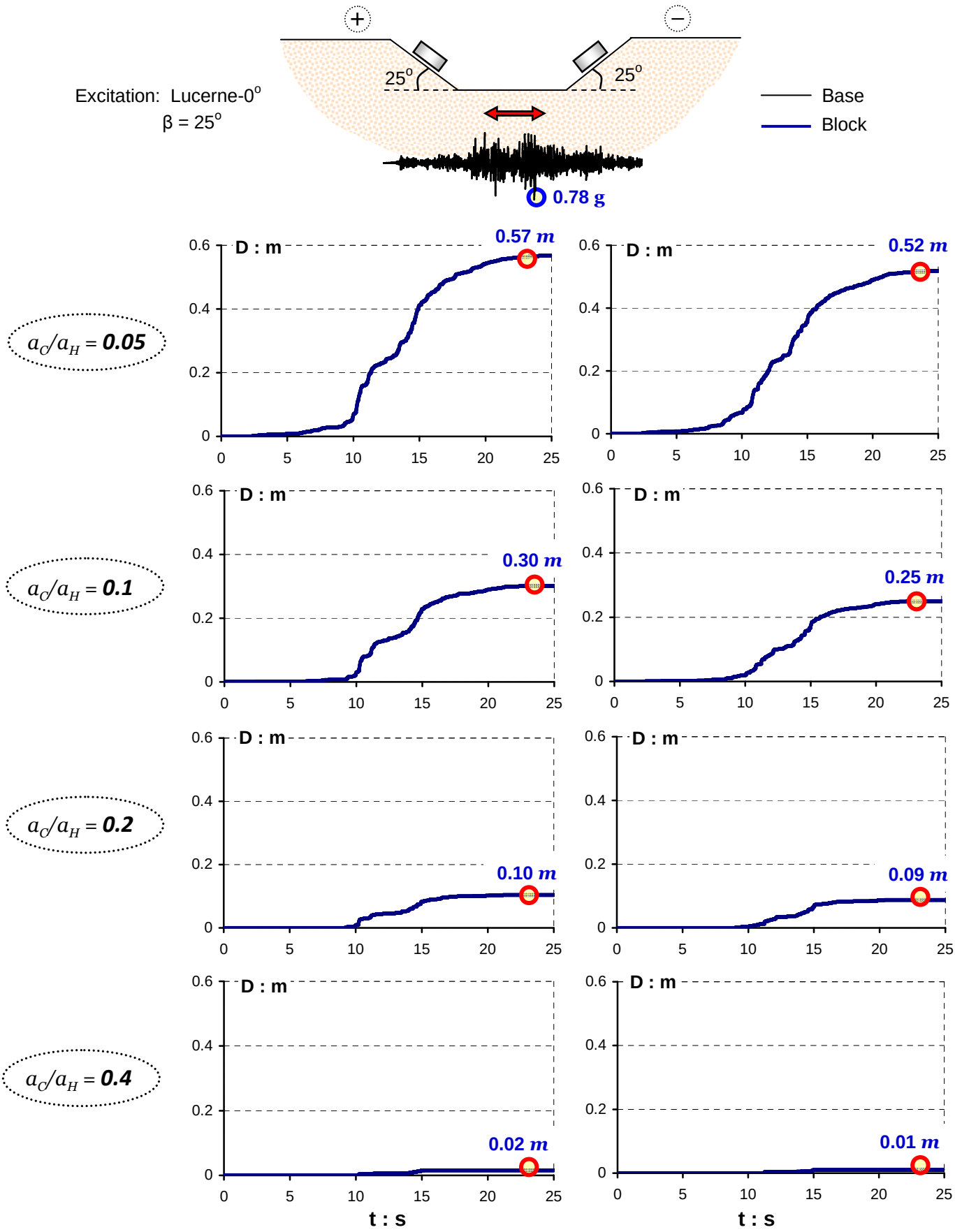

Figure 2.45 *Sliding response for four acceleration ratio, a_C/a_H, values induced by the Lucerne–0° record imposed with its normal (left column) and reversed (right column) sign. (β = 25°)*

Excitation Records from

the Loma Prieta M_s = 7.1 Earthquake

17 October 1989, California

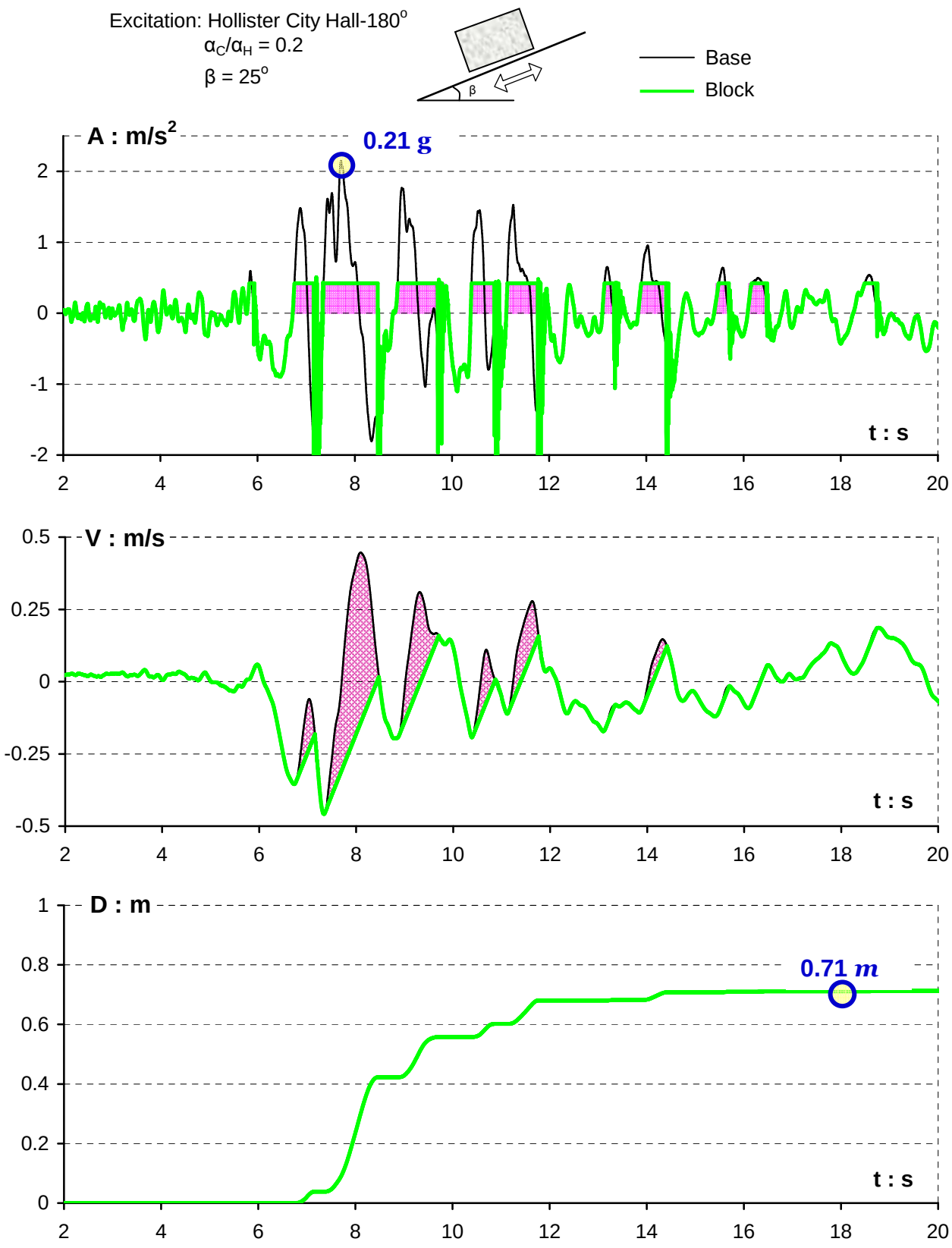

Figure 2.52 *Acceleration, velocity and displacement time-histories of the inclined base (black line) and of the sliding block (light green line) for the triggering motion of Hollister City Hall-180° record.*

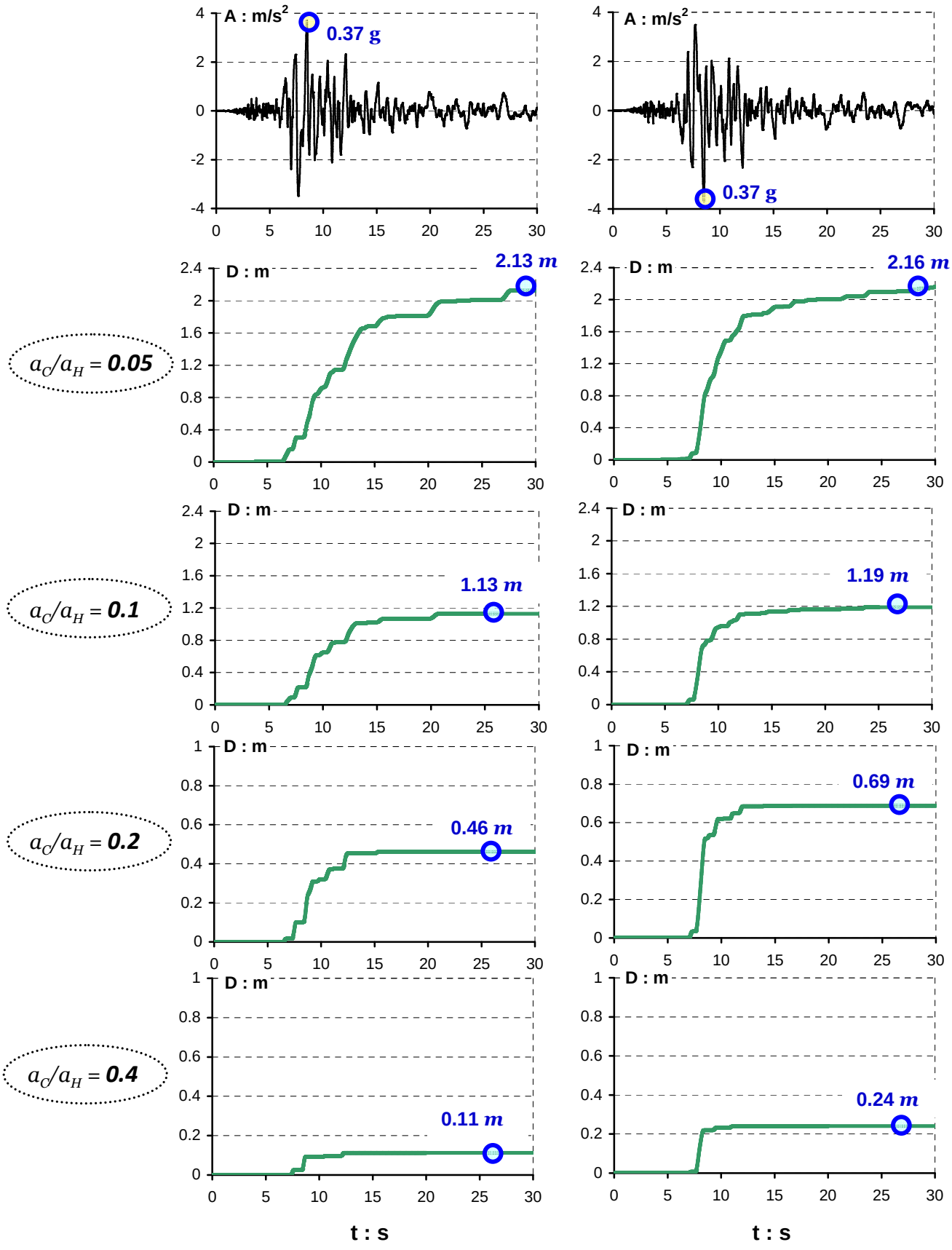

Figure 2.53 *Sliding displacement response for different acceleration ratios, a_C/a_H, induced by the Hollister South & Pine–0° record imposed with its normal (left column) and reversed (right column) sign. ($\beta = 25^o$)*

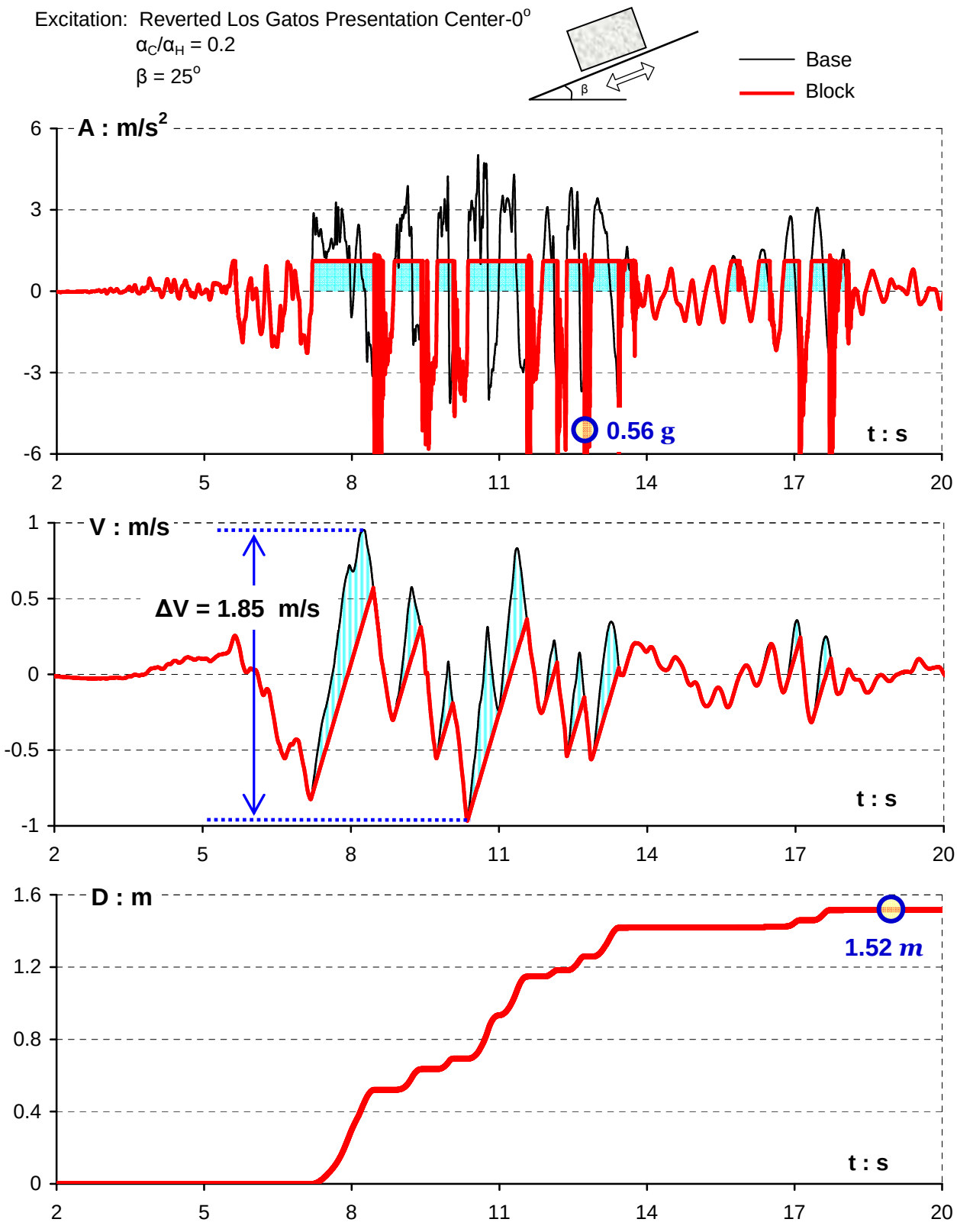

Figure 2.54 *Acceleration, velocity and displacement time-histories of the inclined base (black line) and of the sliding block (red line) for the reversed motion of Los Gatos Presentation Center-0° record.*

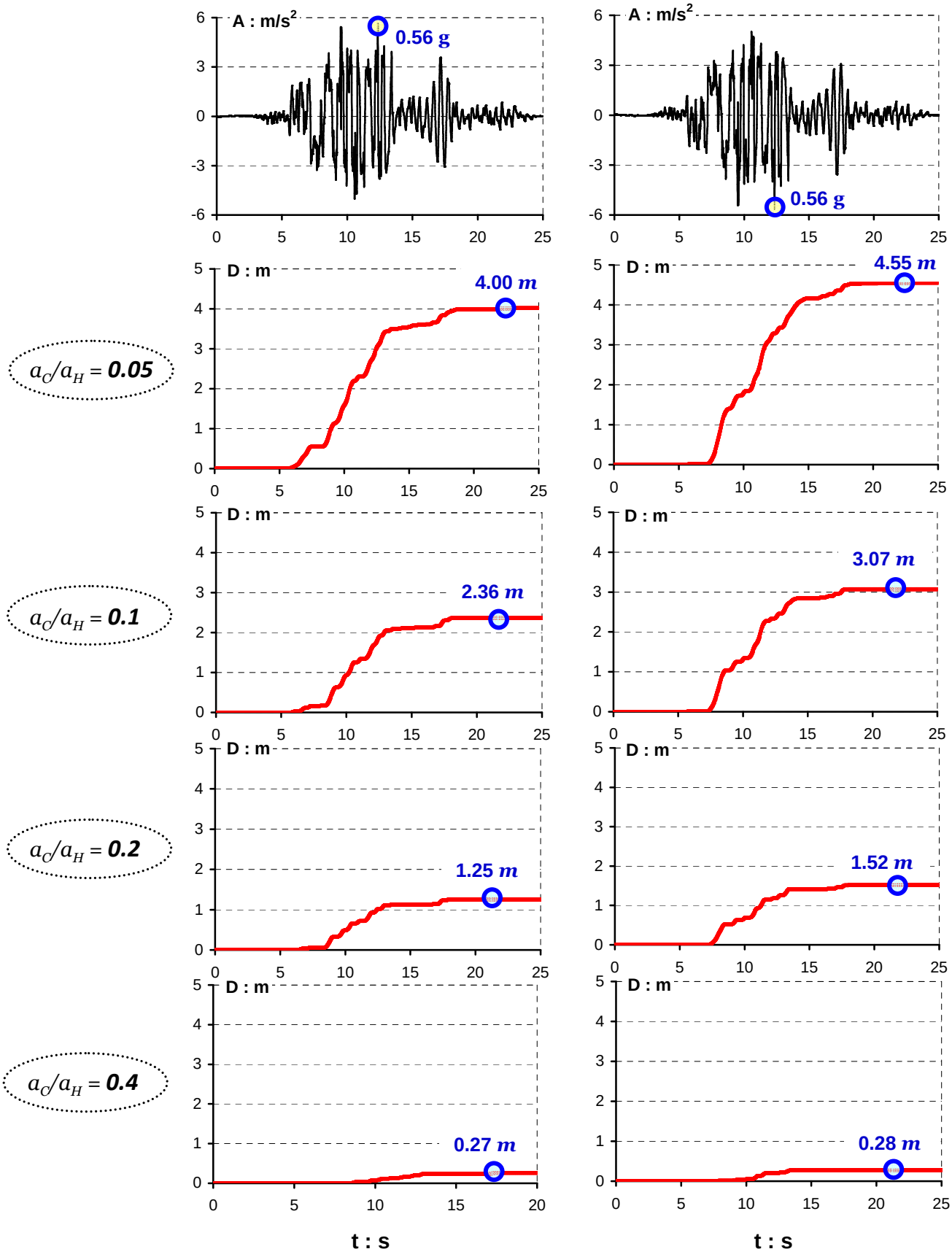

Figure 2.55 *Sliding displacement response for different acceleration ratios, a_C/a_H, induced by the Los Gatos Presentation Center–0° record imposed with its normal (left column) and reversed (right column) sign. ($\beta = 25^o$)*

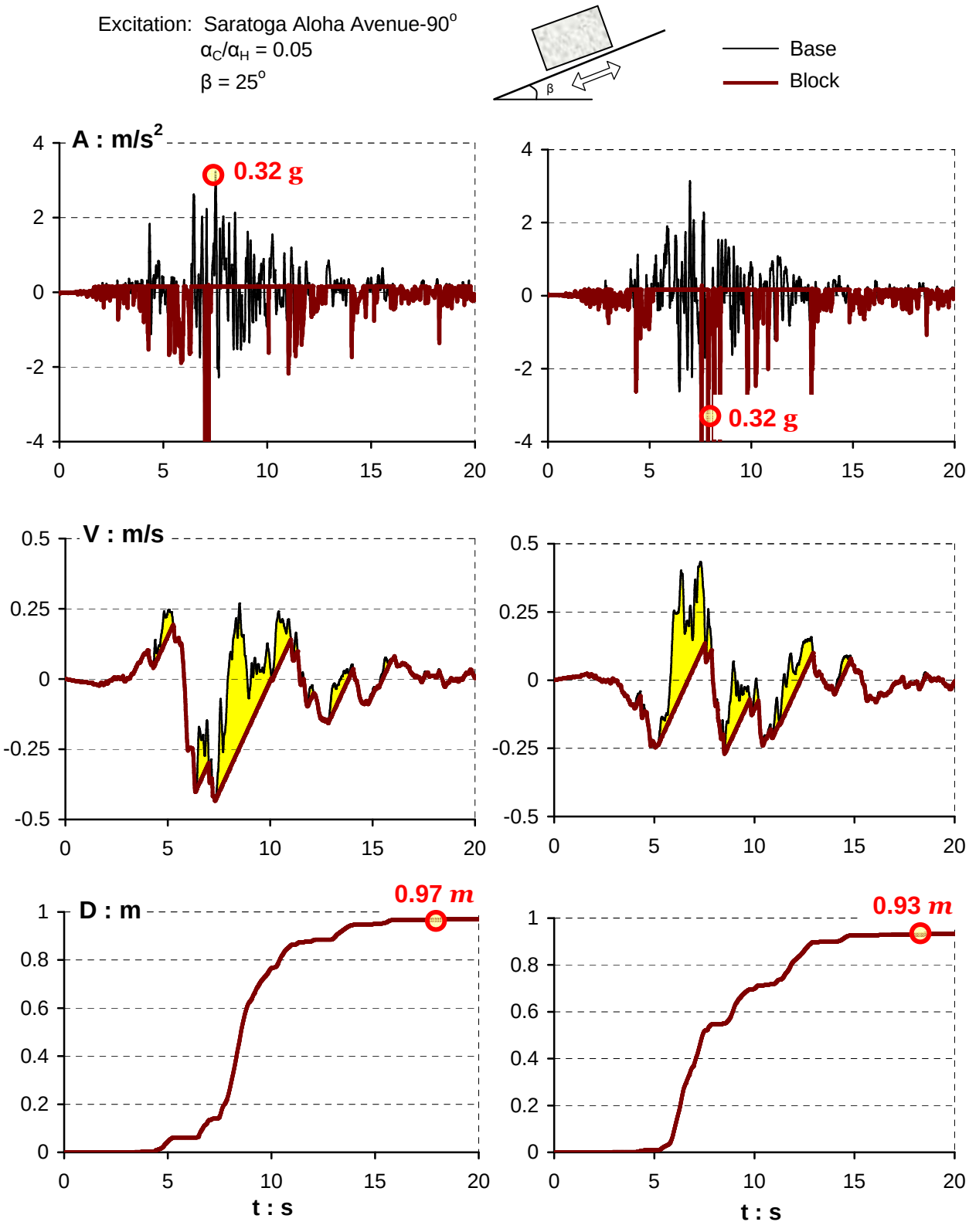

Figure 2.56 *Sliding response in terms of acceleration, velocity and slippage time-histories triggered by the Saratoga Aloha Avenue-90° record: when applied with its normal (left column) and reversed (right column) polarity. As it can be seen, the polarity effect is negligible. (a_C/a_H = 0.05 and β = 25°)*

Excitation Records from

the Chi-chi M_w = 7.5 Earthquake

20 September 1999, Taiwan

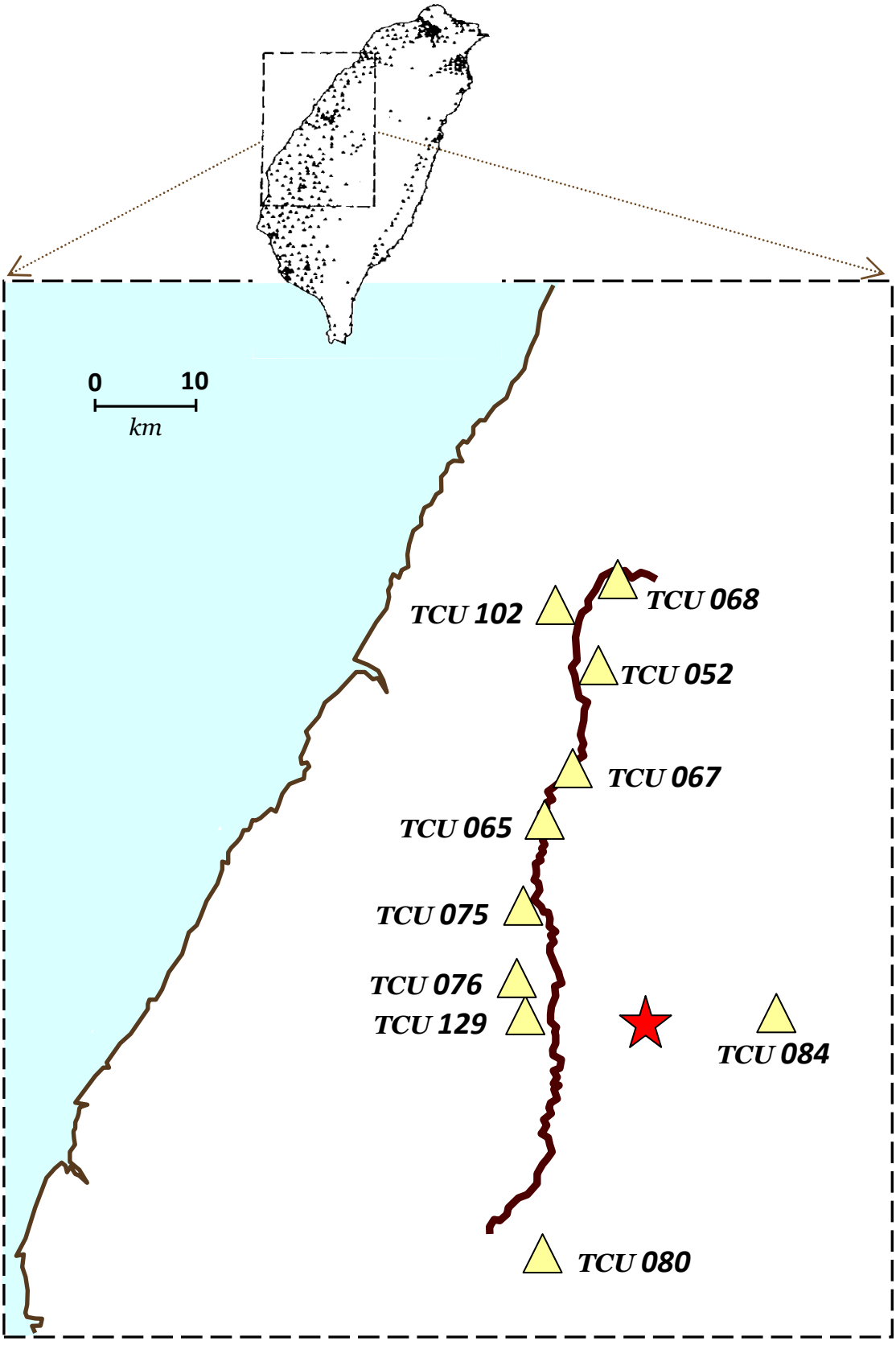

Figure 2.57 *Locations of the TCU real time strong-motion records from the 1999 Chi-chi earthquake, that we utilised as excitations in our study. The "star" indicates the location of the main shock.*

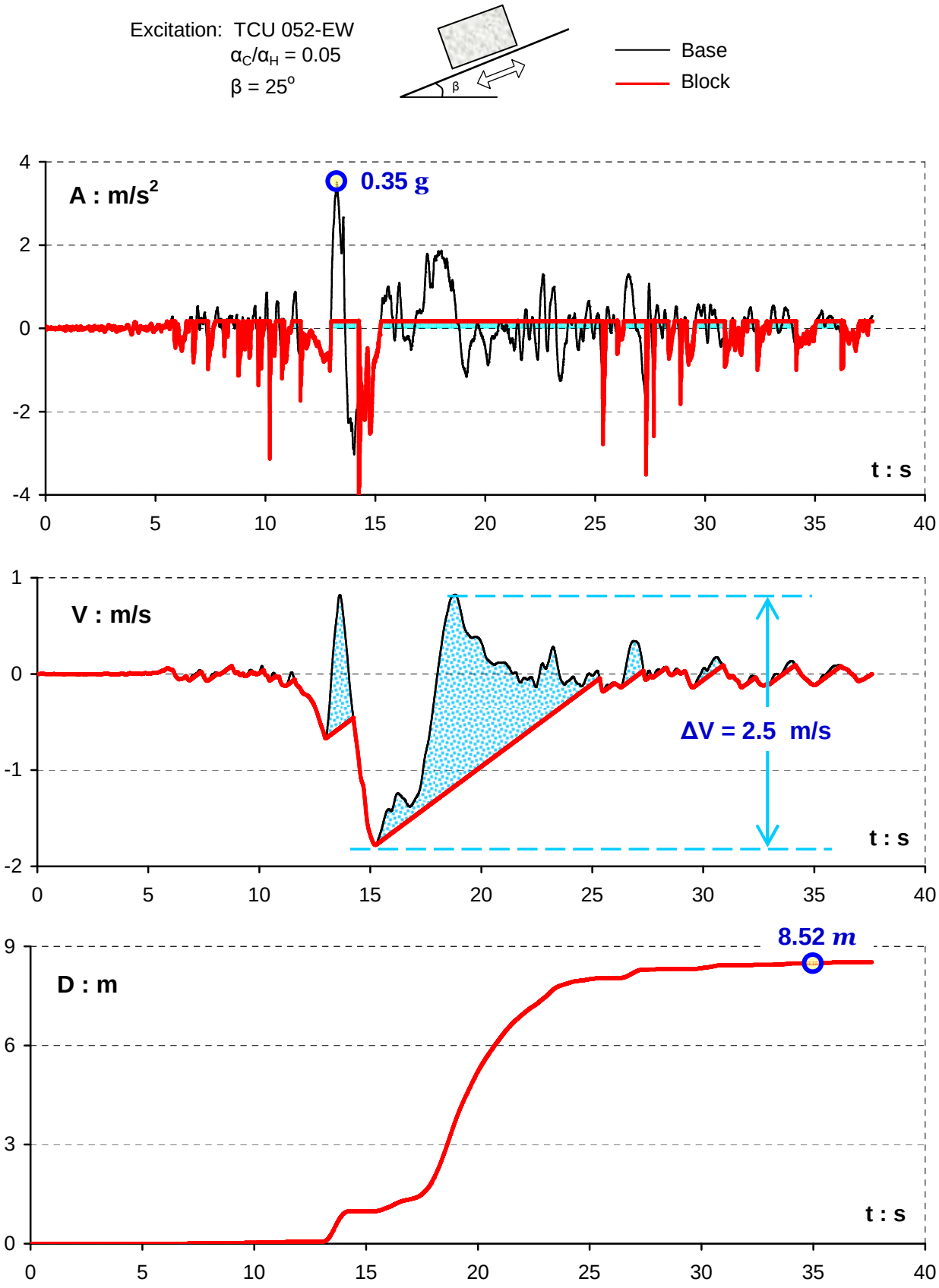

Figure 2.58 *Acceleration, velocity, and slippage time histories of a rigid block resting on an 25^0 inclined plane when subjected to the TCU 052-EW record. ($a_C/a_H = 0.05$)*

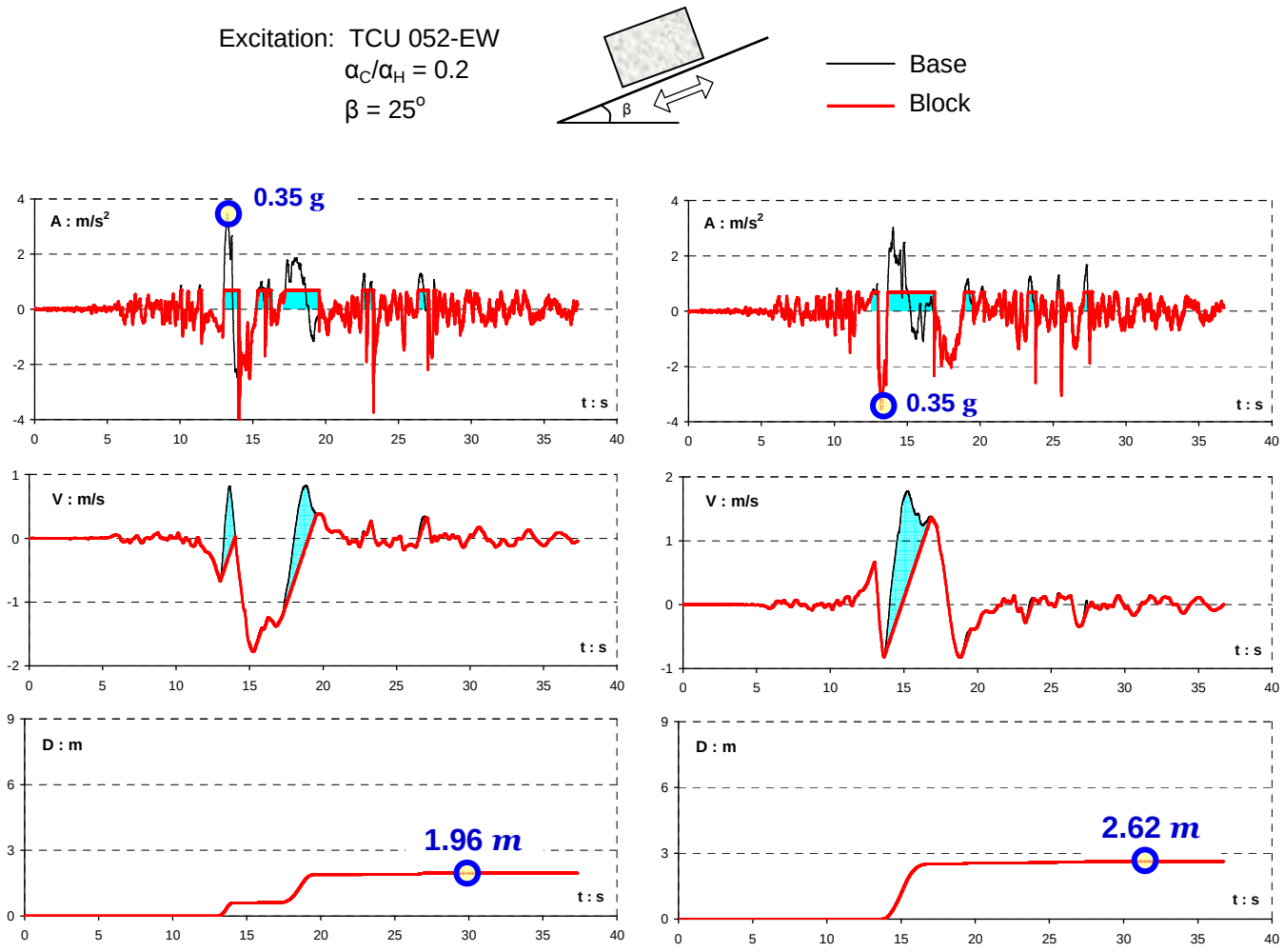

Figure 2.59 *The polarity effect: the time histories response for the TCU 052-EW record imposed with its normal (left column) and reversed (right column) sign. ($a_C/a_H = 0.2$ and $\beta = 25^o$)*

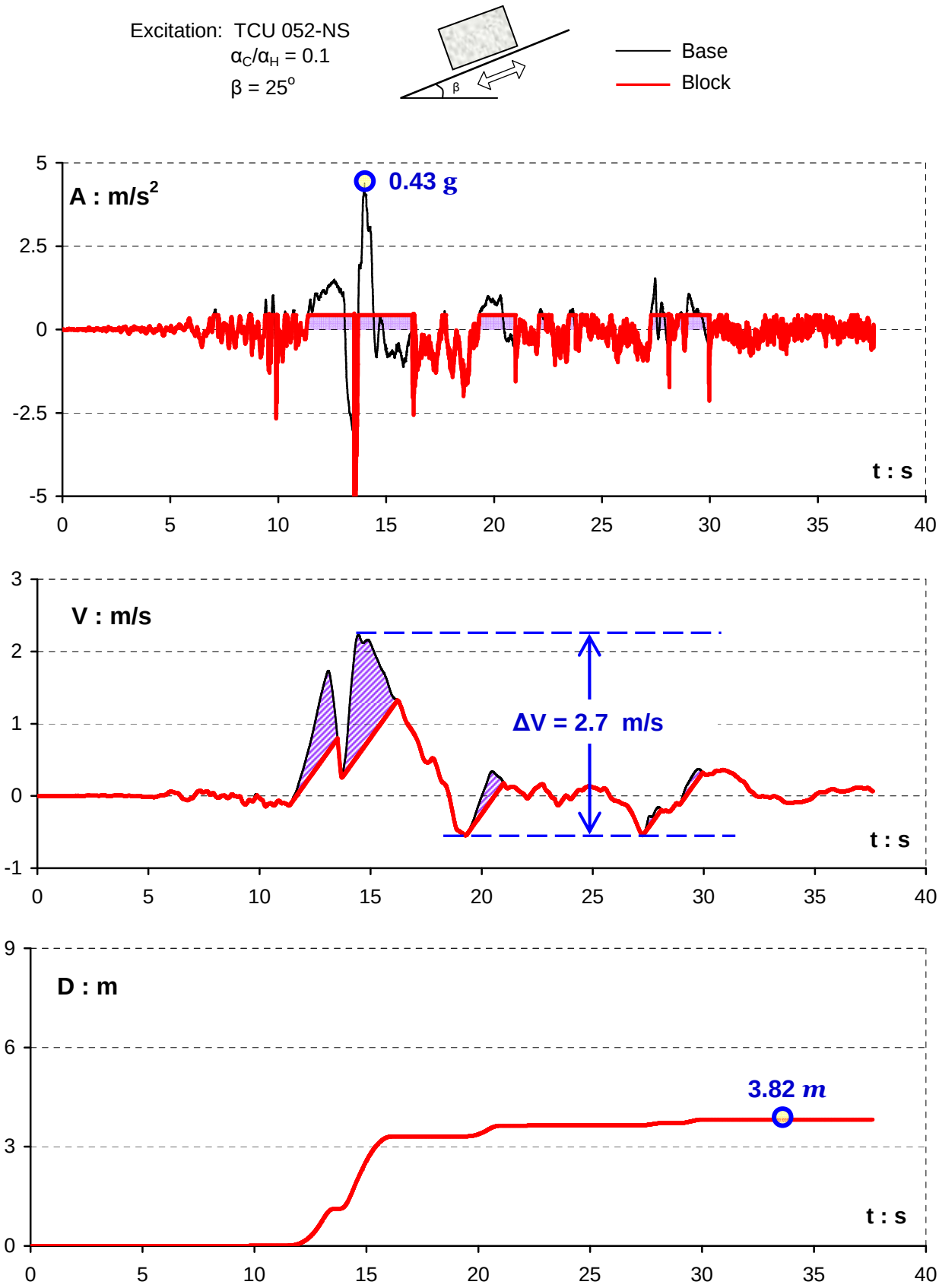

Figure 2.60 *Acceleration, velocity, and slippage time histories of a rigid block resting on an 25^0 inclined plane when subjected to the TCU 052-NS record. (a_C/a_H = 0.1)*

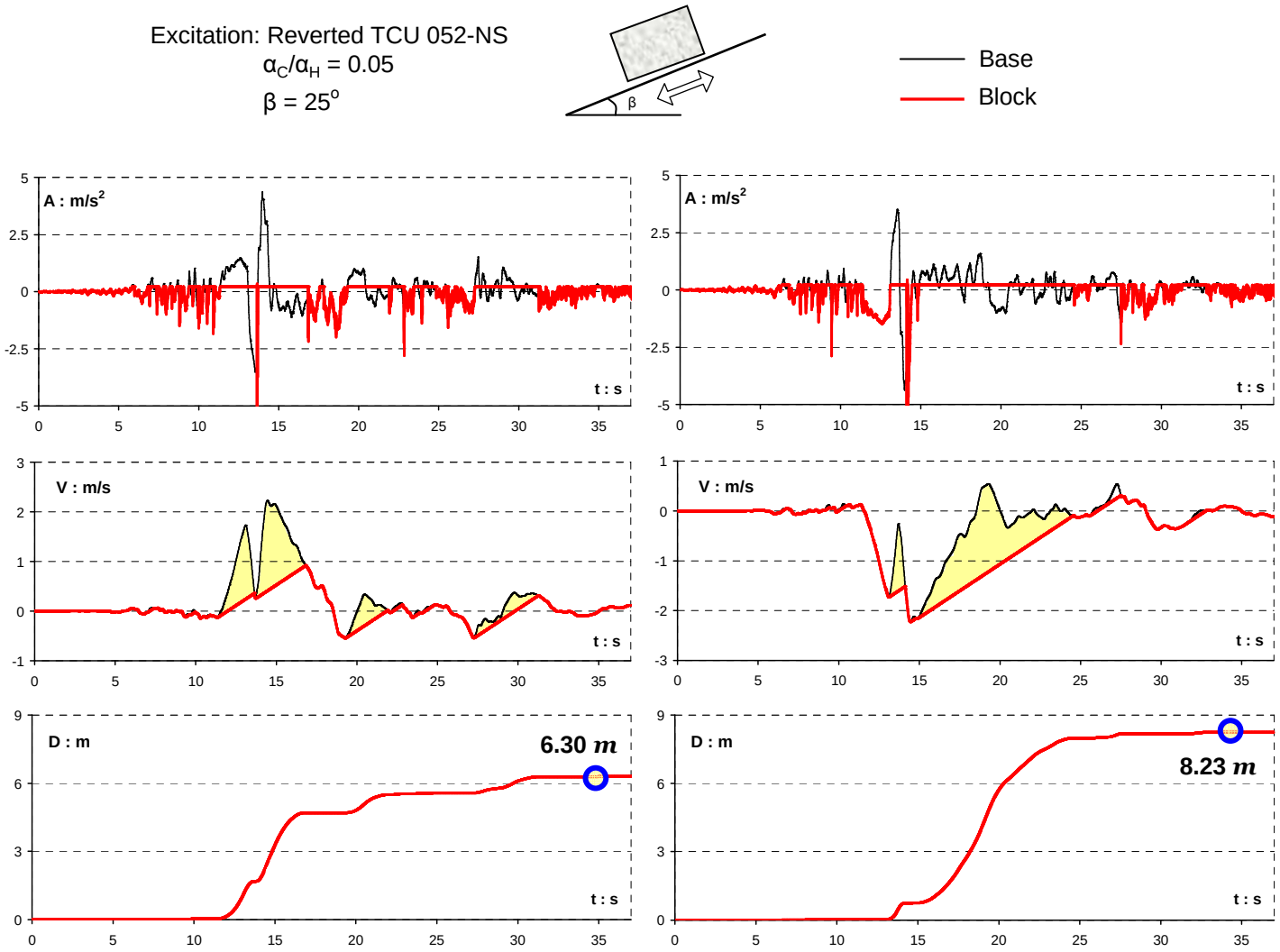

Figure 2.61 *The polarity effect: the time histories response for the TCU 052-NS record imposed with its normal (left column) and reversed (right column) sign. ($a_C/a_H = 0.05$ and $\beta = 25^o$)*

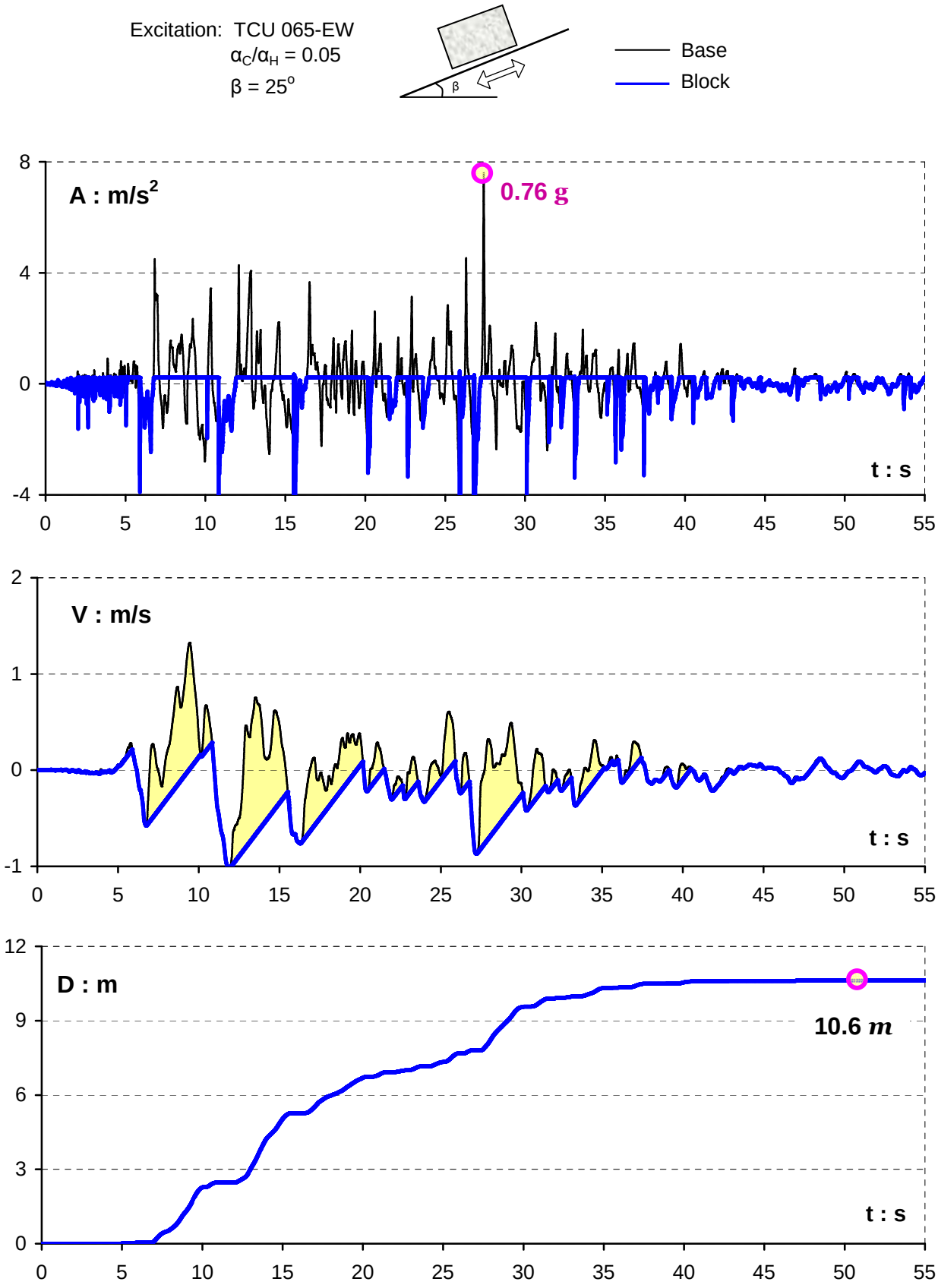

Figure 2.62 *Acceleration, velocity, and slippage time histories of a rigid block resting on an 25^0 inclined plane when subjected to the TCU 065-EW record. ($a_C/a_H = 0.05$)*

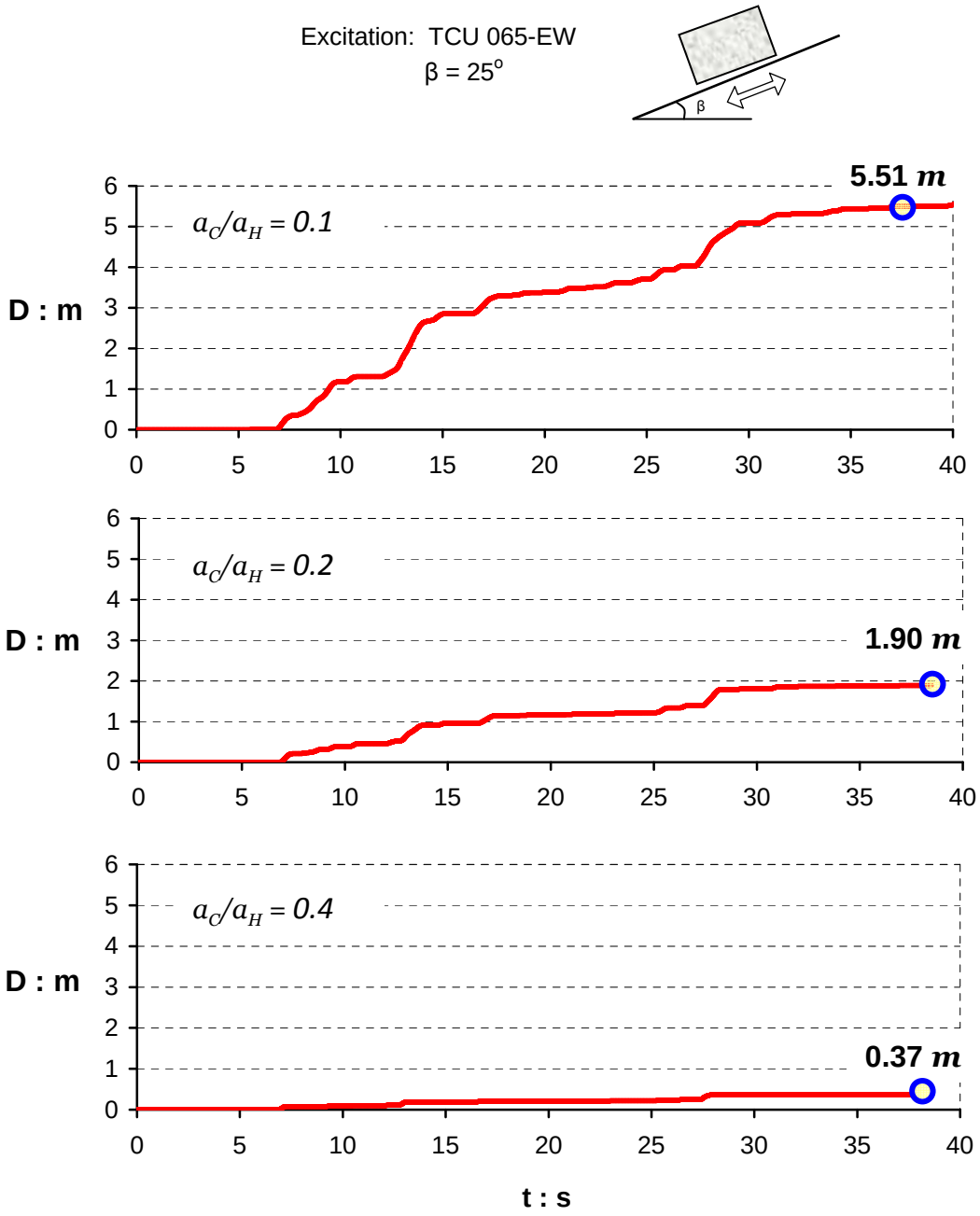

Figure 2.63 *Accumulated sliding displacement for different critical acceleration ratios a_C/a_H. The triggering motion is the TCU 052-EW record. As the acceleration ratio increases the slippage decreases. However, even for a relatively large ratio of 0.4 the induced sliding almost reaches 0.4 m which may be critical for any kind of structure.*

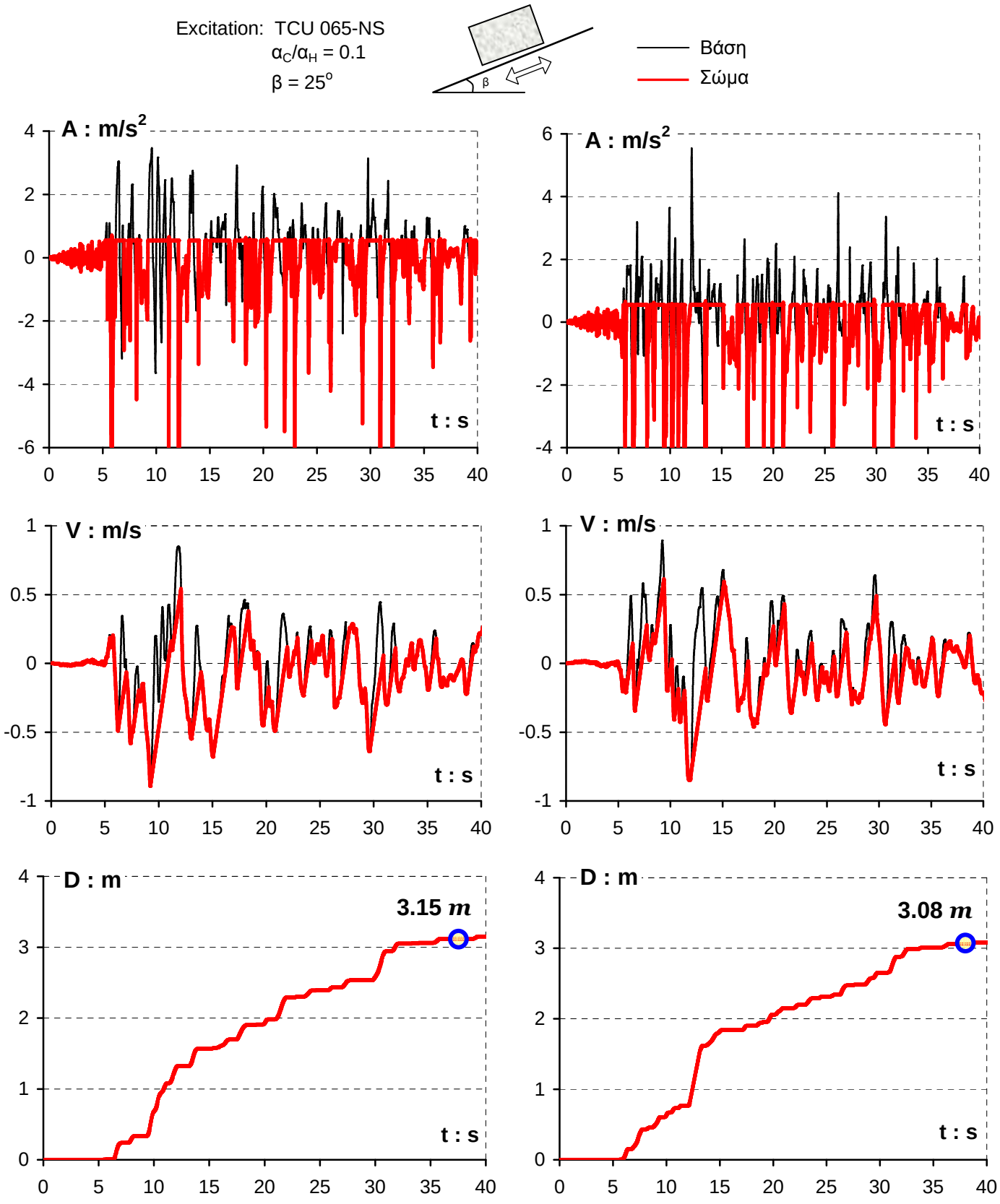

Figure 2.64 *The polarity effect is limited in case of strong ground motions with numerous directivity acceleration pulses that result to an almost symmetric velocity time-history. A particular example is illustrated in this figure where the TCU 065-NS record imposed with its normal (left column) and reversed (right column) sign.*

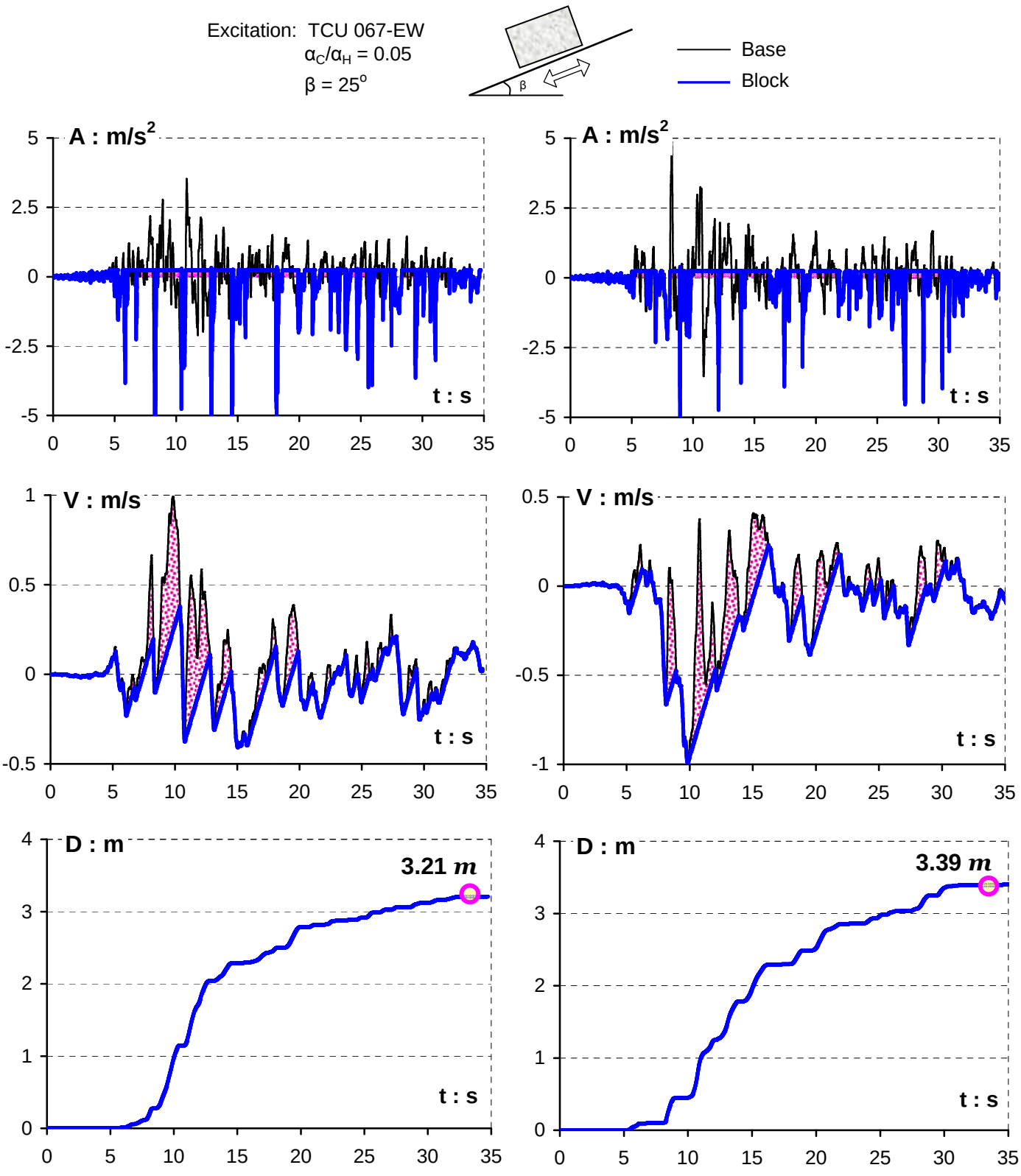

Figure 2.65 *The polarity effect is limited in case of strong ground motions with numerous directivity acceleration pulses that result to an almost symmetric velocity time-history, such as the TCU 067-EW record. As the ratio a_C/a_H increases the little asymmetric details of the velocity in topical scale are vanished. The higher the symmetry of velocity time-history (in local and global scale), the least significance of polarity effect in small acceleration ratios.*

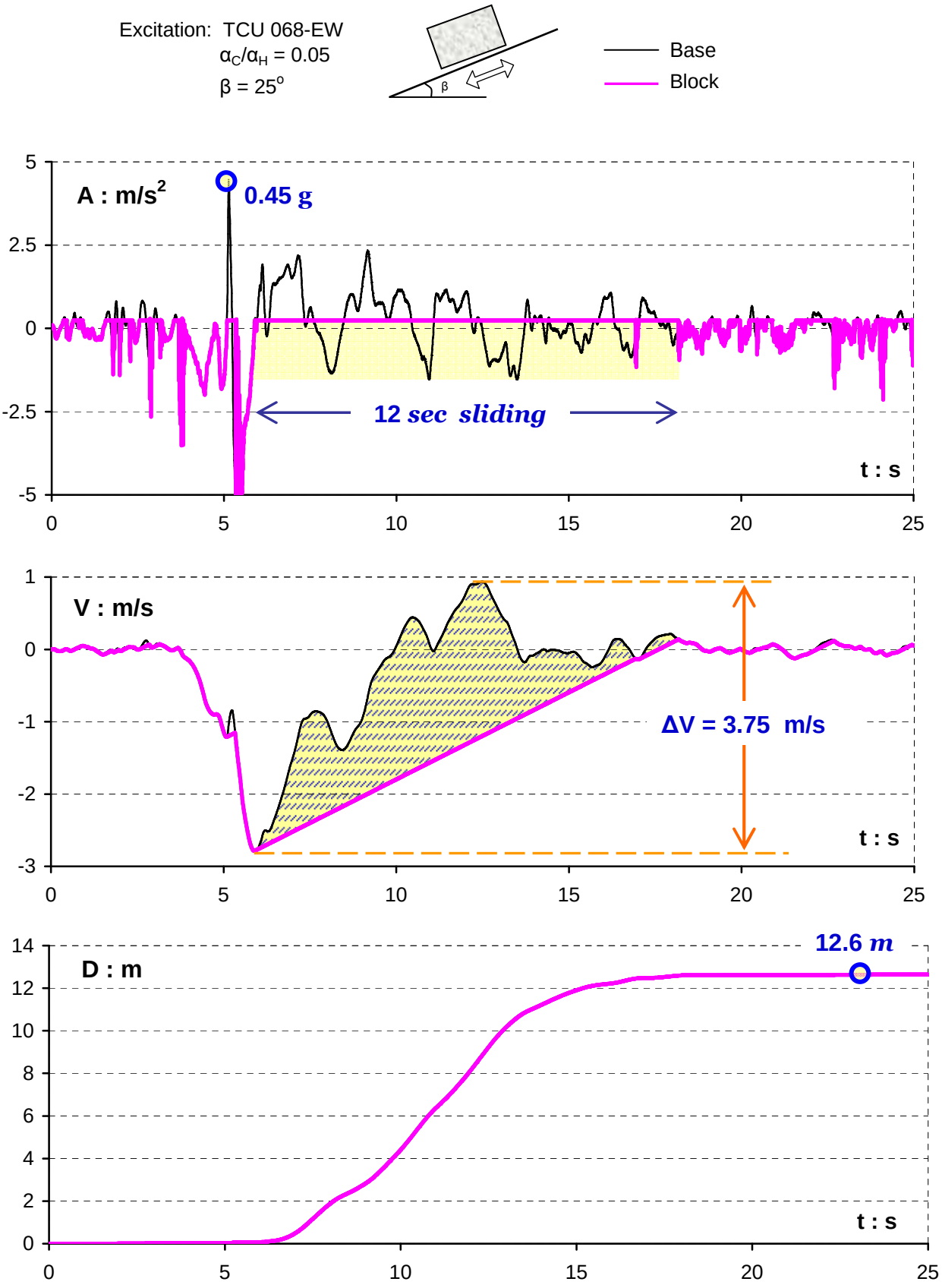

Figure 2.66 *Acceleration, velocity, and slippage time histories of a rigid block resting on an 25^0 inclined plane when subjected to the TCU 068-EW record. ($a_C/a_H = 0.05$)*

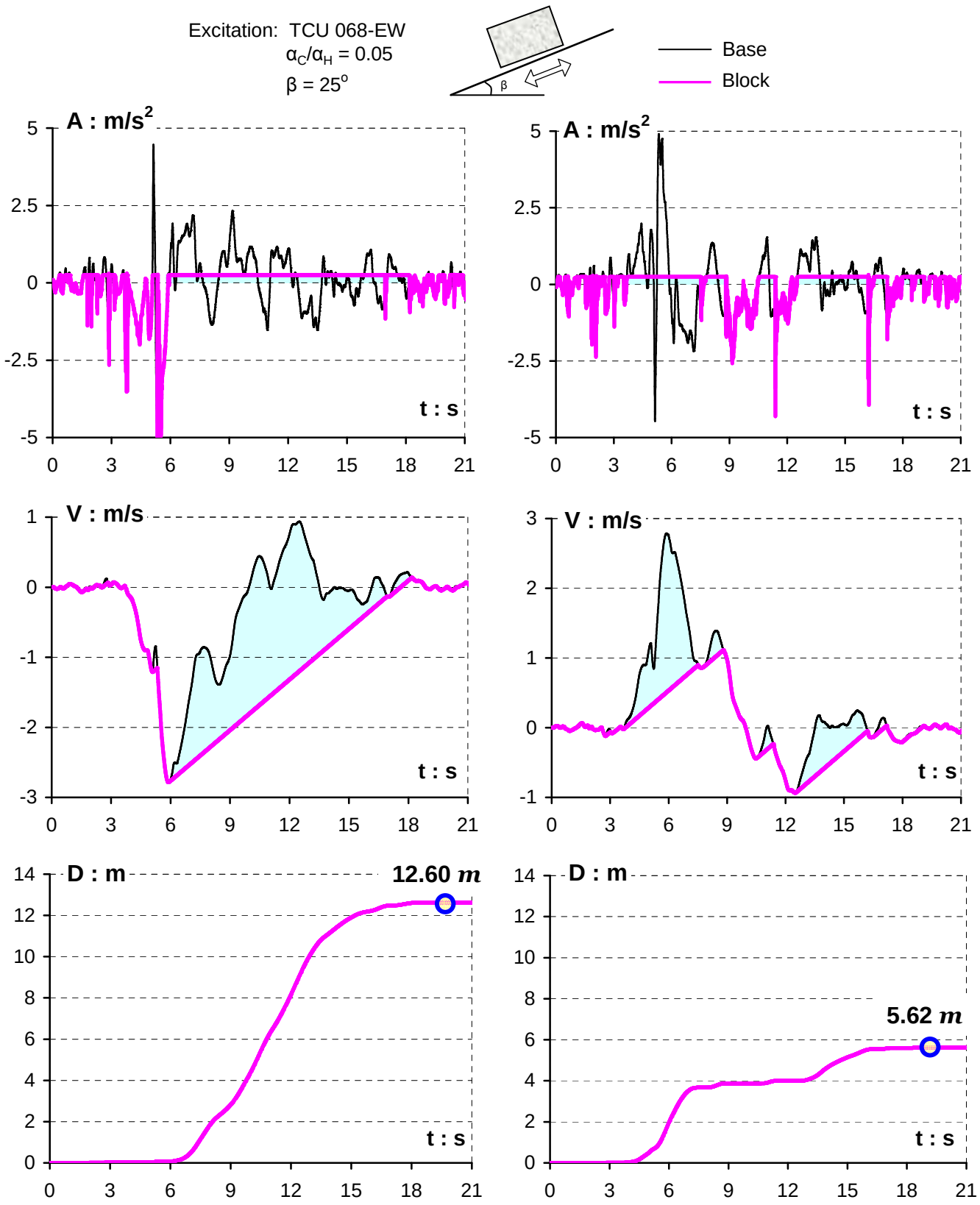

Figure 2.67 *One case of strong polarity effect: time histories response for the TCU 068-EW record imposed with its normal (left column) and reversed (right column) sign. The TCU 068-EW record is characterised by asymmetric velocity time-history which give rise to a startling polarity difference in slippage by a factor of 2.5; an index of the polarity sensitiveness of a record could be the permanent ground displacement at the end of the motion.*

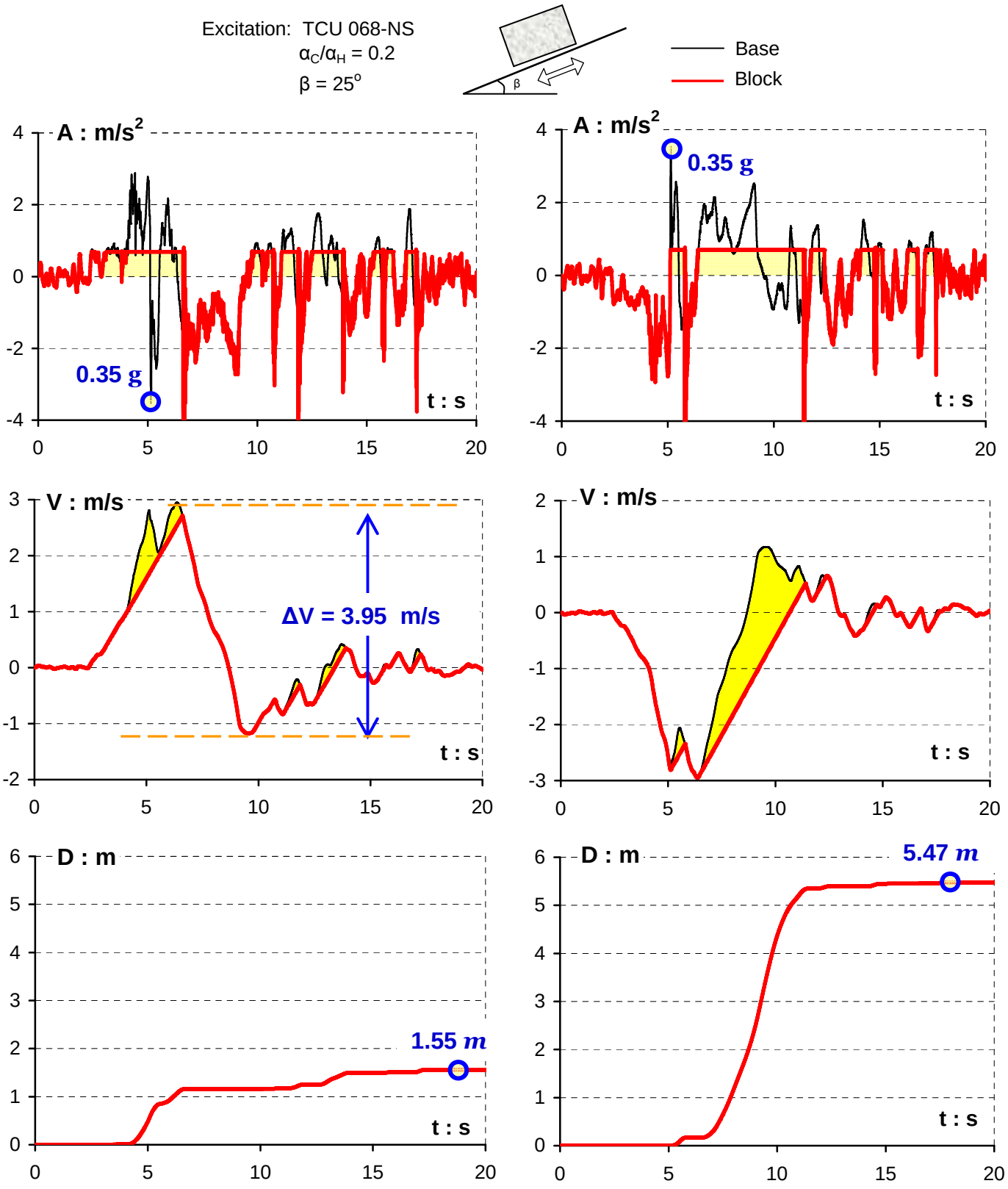

Figure 2.68 *Strong polarity effect even for large acceleration ratios a_C/a_H : time histories response for the TCU 068-NS record imposed with its normal (left column) and reversed (right column) sign. ($a_C/a_H = 0.2$ and $\beta = 25^o$)*

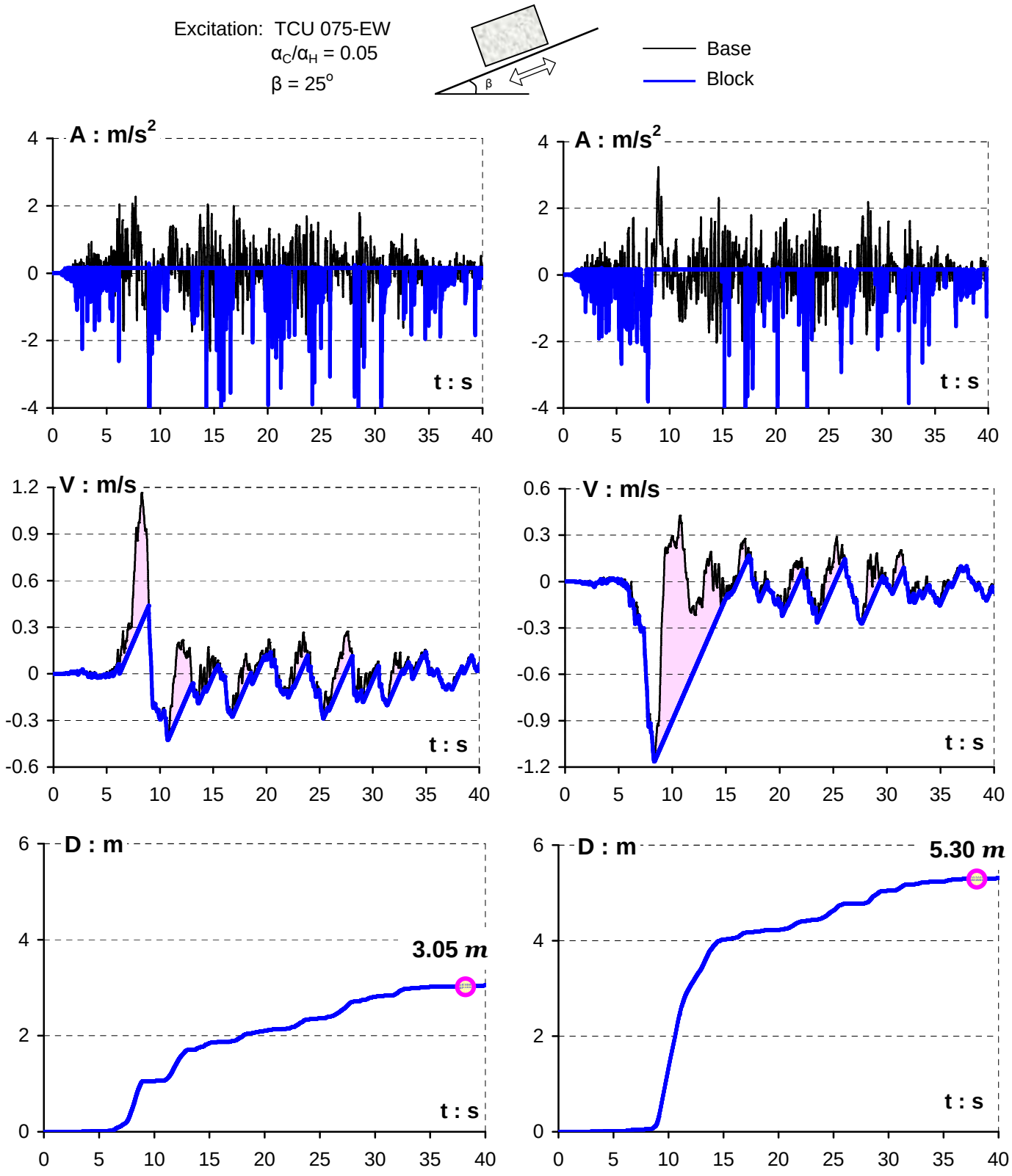

Figure 2.69 *The polarity effect: response time histories for the TCU 075-EW record imposed with its normal (left column) and reversed (right column) sign.* *(a_C/a_H = 0.05 and β = 25°)*

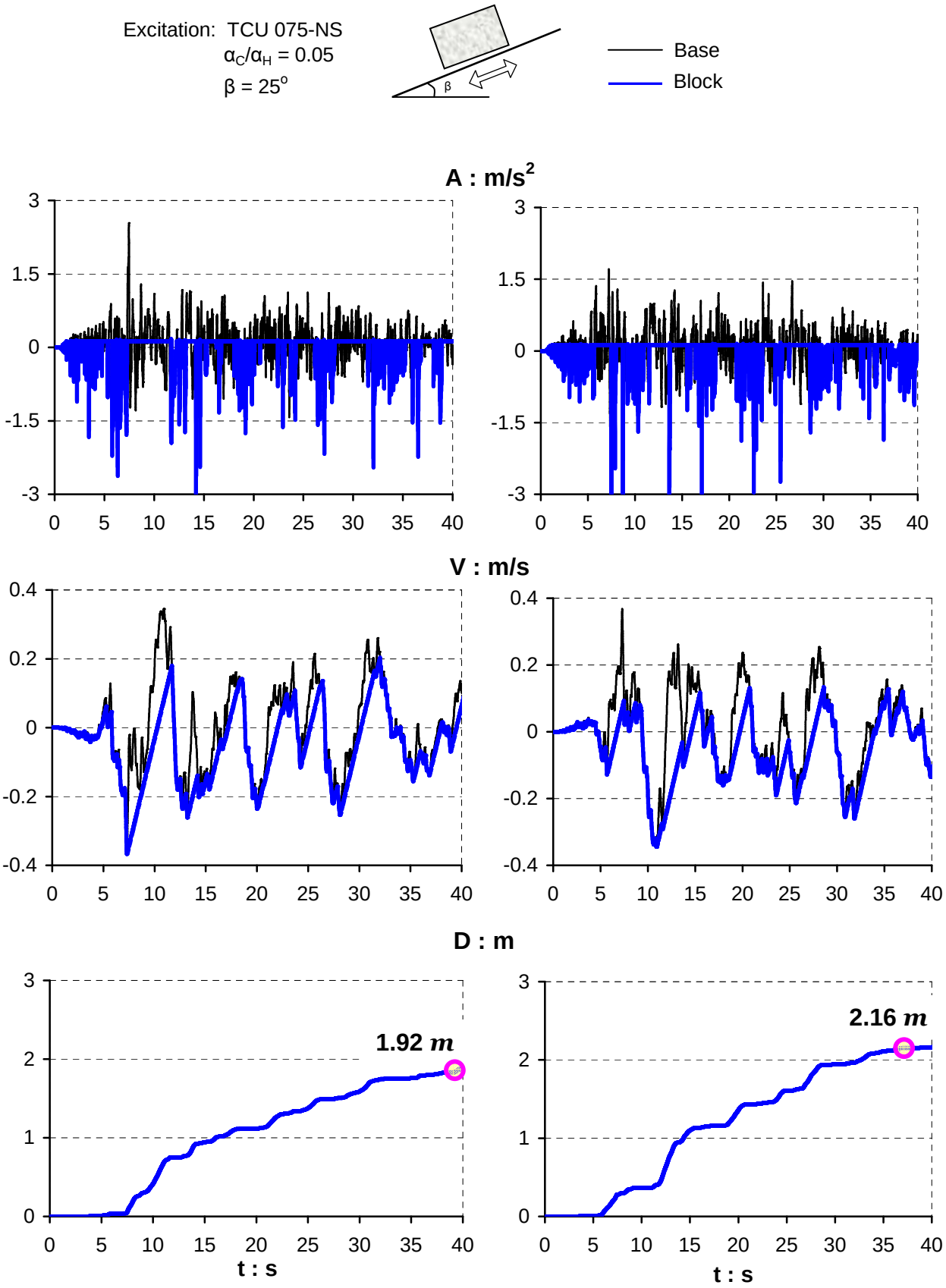

Figure 2.70 *In the previous figure is shown that the asymmetric velocity of the TCU 075-EW leaded to significant polarity effect. On the contrary, the other component TCU 075-NS of the recorded station, characterised by a symmetric velocity time-history. Thus, polarity effect is almost negligible.*

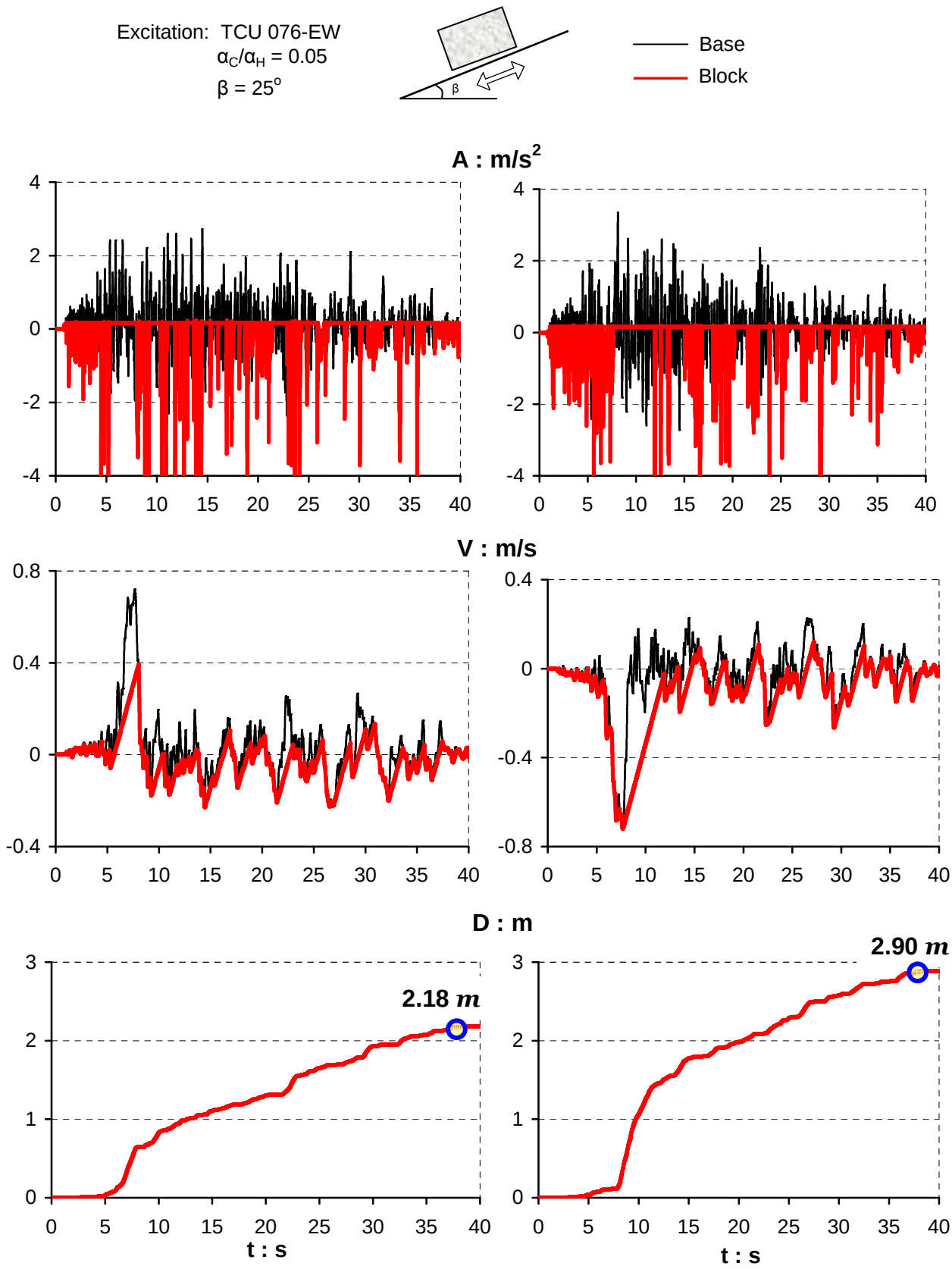

Figure 2.71 *Acceleration, velocity, and sliding displacement time histories for the TCU 076-EW record imposed with its normal (left column) and reversed (right column) sign. ($a_C/a_H = 0.05$ and $\beta = 25^o$)*

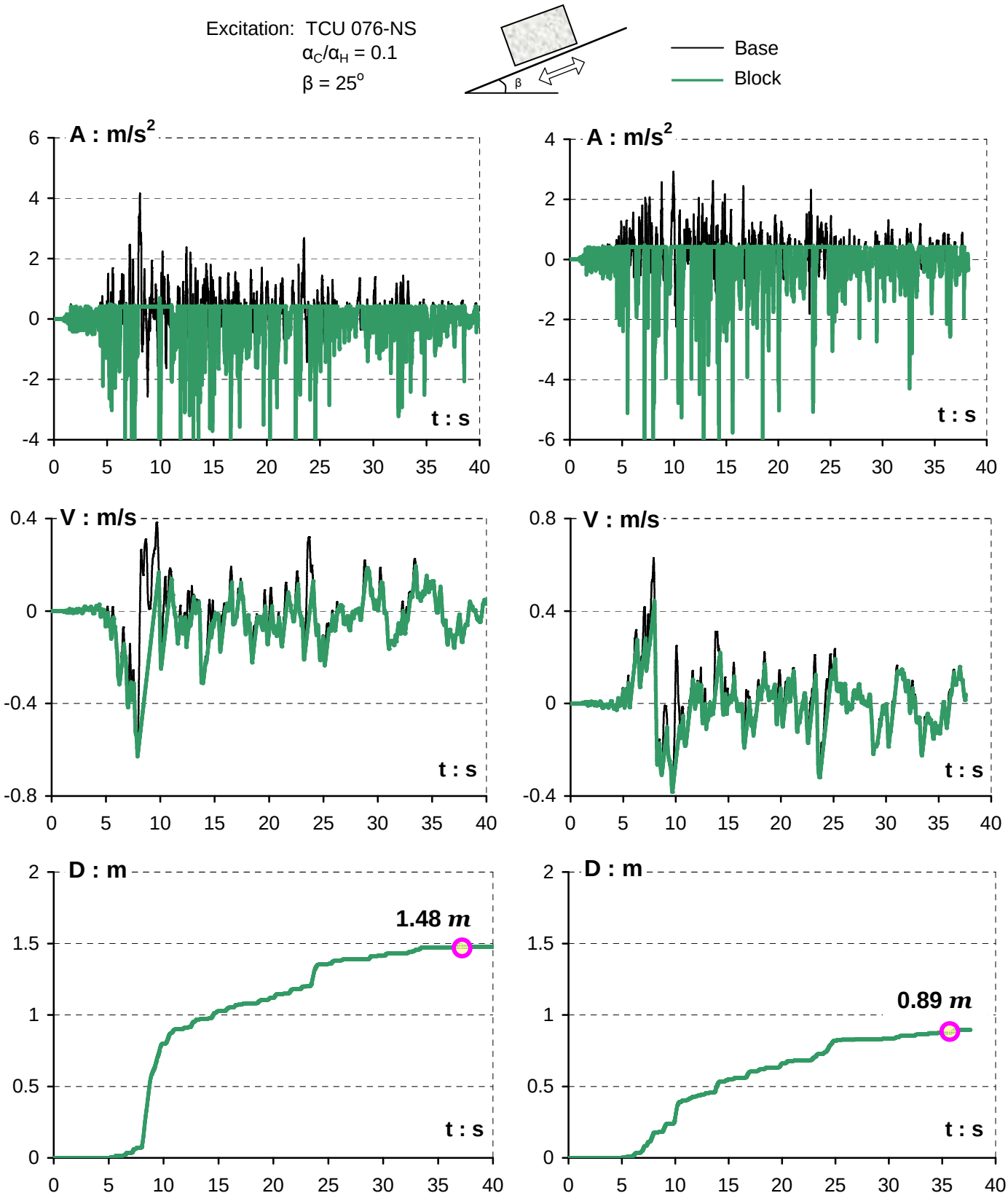

Figure 2.72 *Acceleration, velocity, and sliding displacement time histories for the TCU 076-NS record imposed with its normal (left column) and reversed (right column) sign. (a_C/a_H = 0.1 and $\beta = 25^o$)*

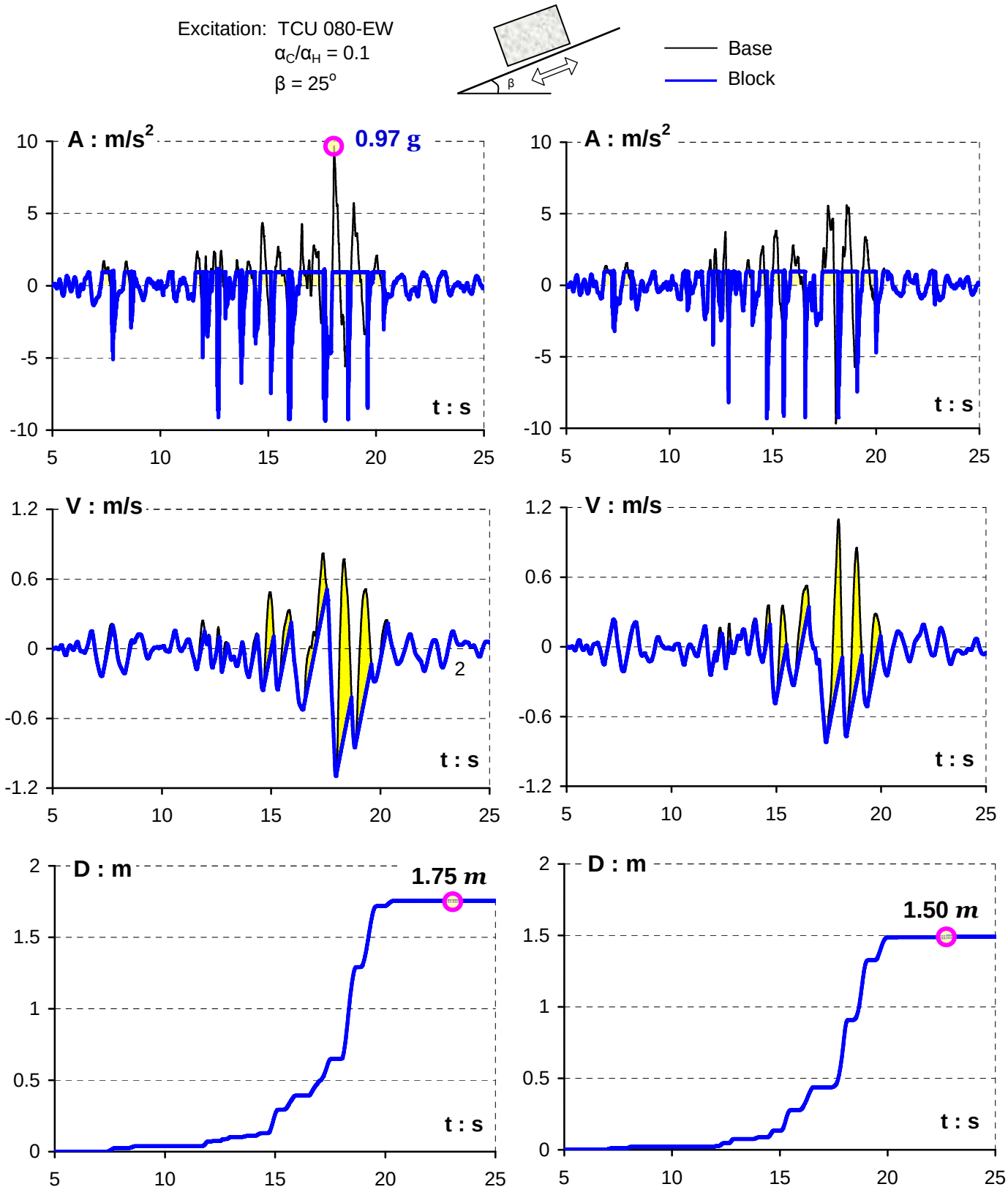

Figure 2.73 *Another case of an excitation with almost symmetric velocity time-history: the TCU 052-EW record imposed with its normal (left column) and reversed (right column) sign. As expected the response difference due to polarity is minimal. (a_C/a_H = 0.1 and $\beta = 25^o$)*

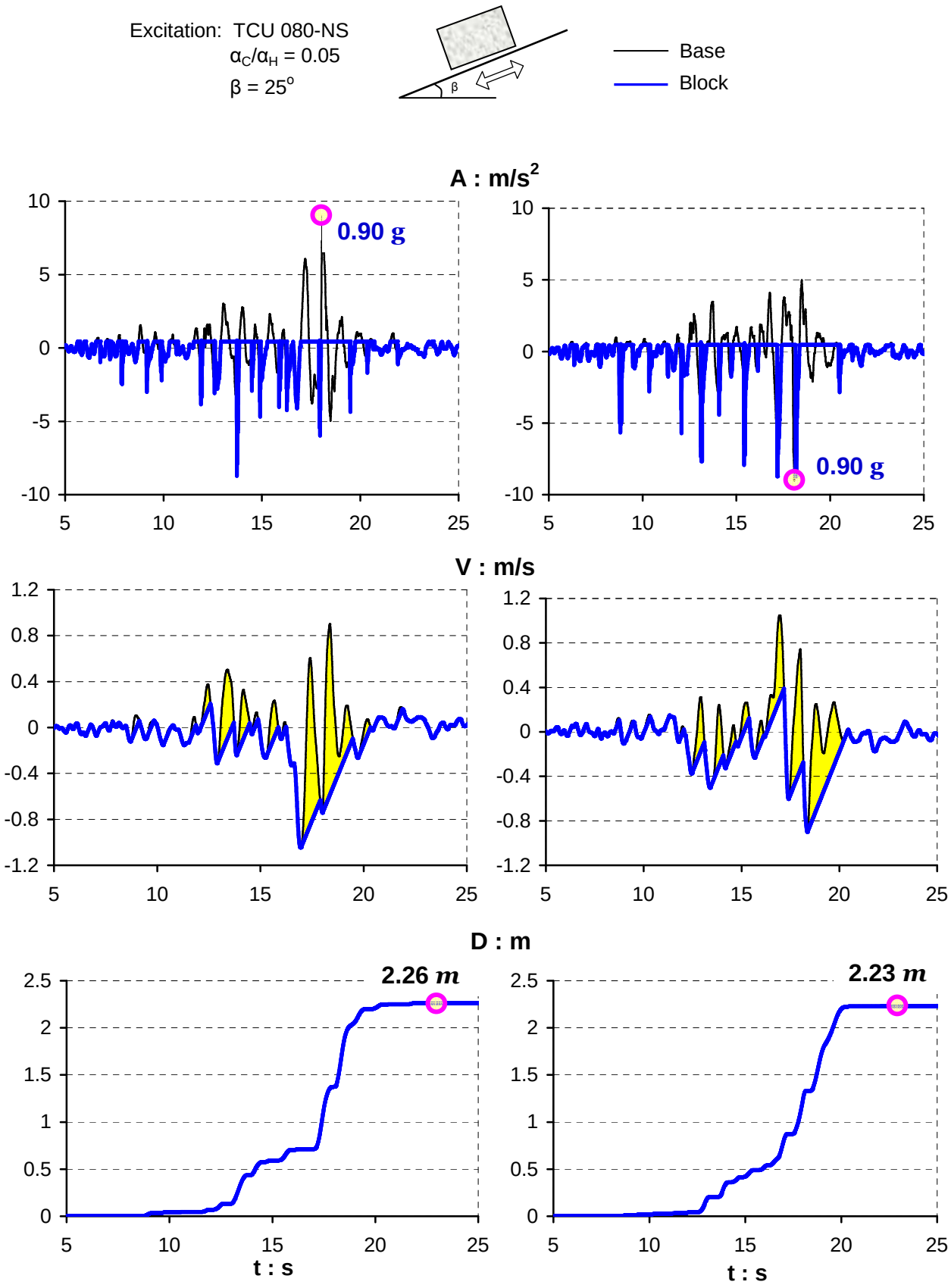

Figure 2.74 *Also, the NS component of the TCU 052 record presents to have symmetric velocity time-history: imposed with its normal (left column) and reversed (right column) sign. As expected the response difference due to polarity is minimal.* ($a_C/a_H = 0.05$ *and* $\beta = 25^o$)

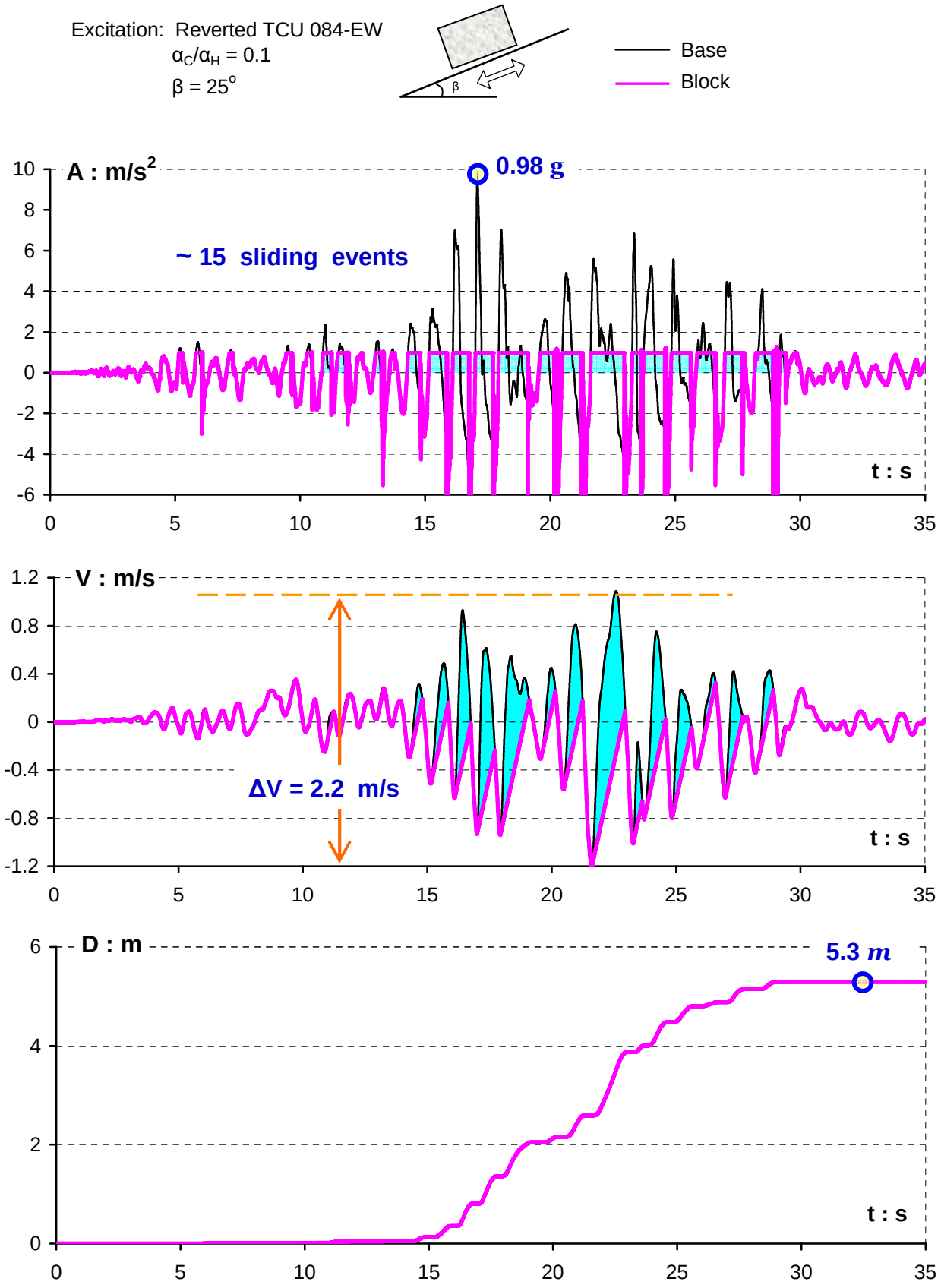

Figure 2.75 *Acceleration, velocity, and slippage time histories of a rigid block resting on an 25^0 inclined plane when subjected to the reversed polarity TCU 085-EW record. (a_C/a_H = 0.1)*

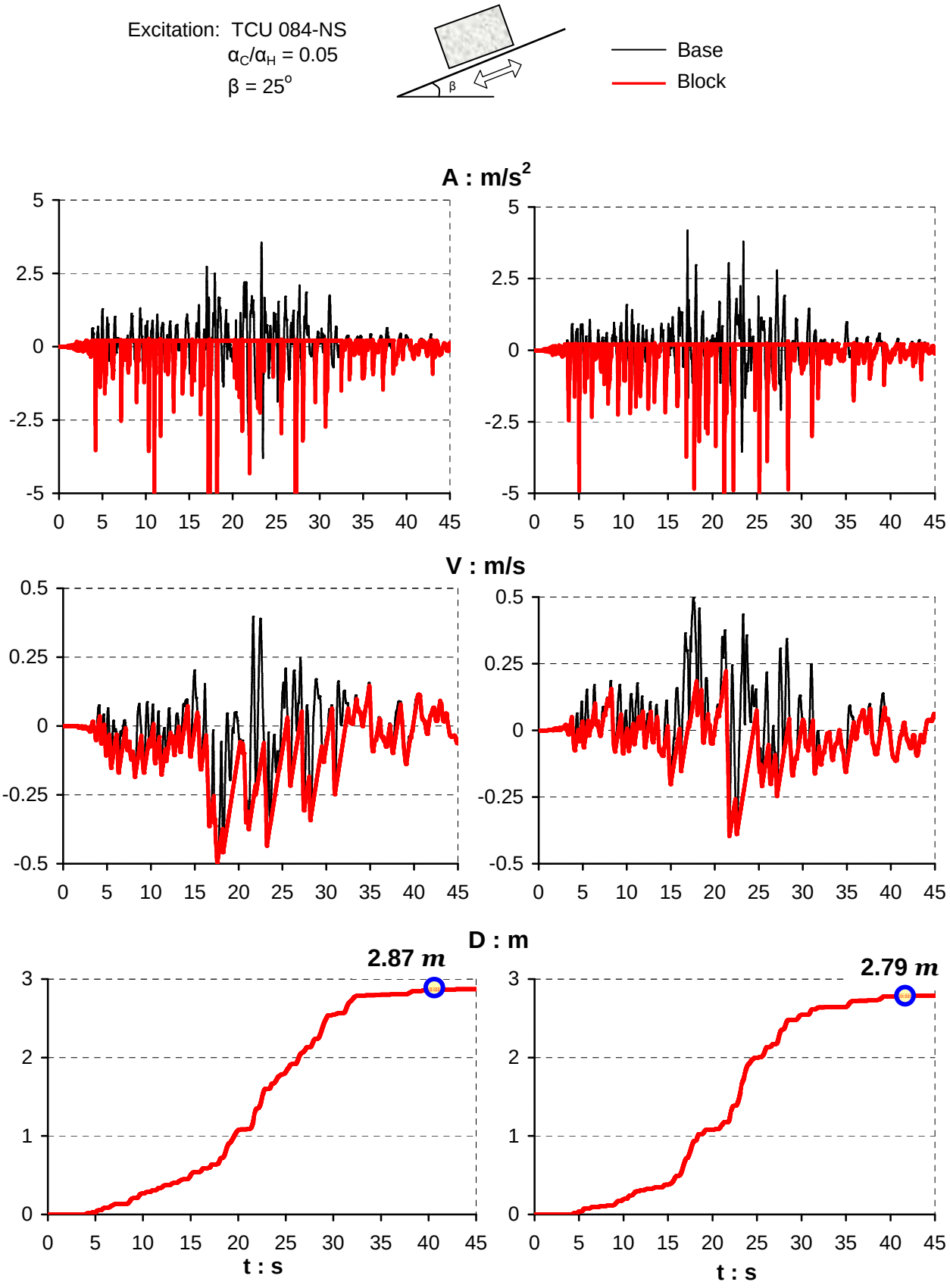

Figure 2.76 *Detailed time histories response for the TCU 084-NS record imposed with its normal (left column) and reversed (right column) sign.*
($a_C/a_H = 0.05$ and $\beta = 25^o$)

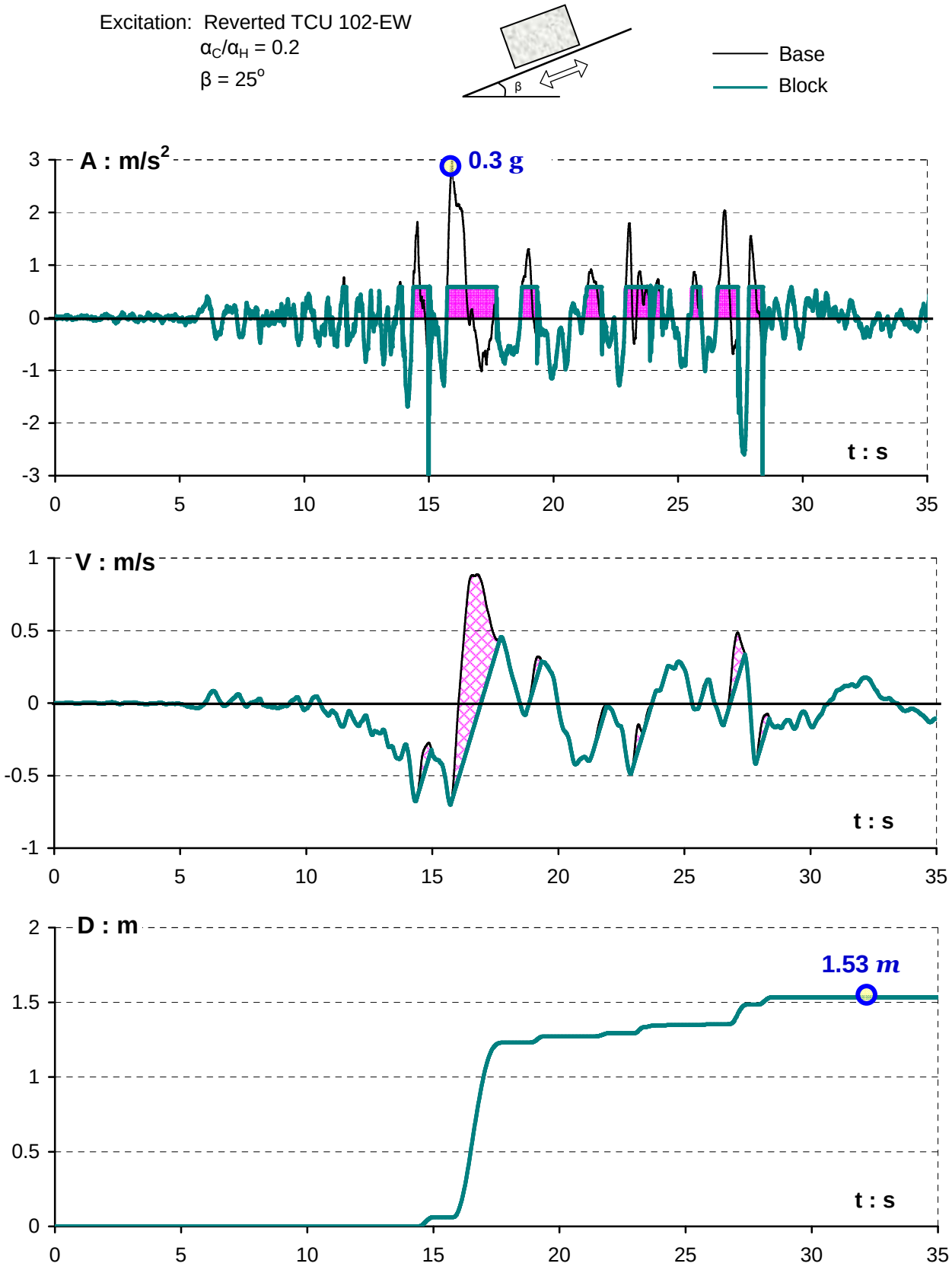

Figure 2.77 *Even for relatively large acceleration ratios of* $a_C/a_H = 0.2$ *several excitations with small PGAs, such as the TCU 052-EW record in this depiction, can trigger a slippage of 1.5 m or greater which is unacceptable for the most of our structures.*

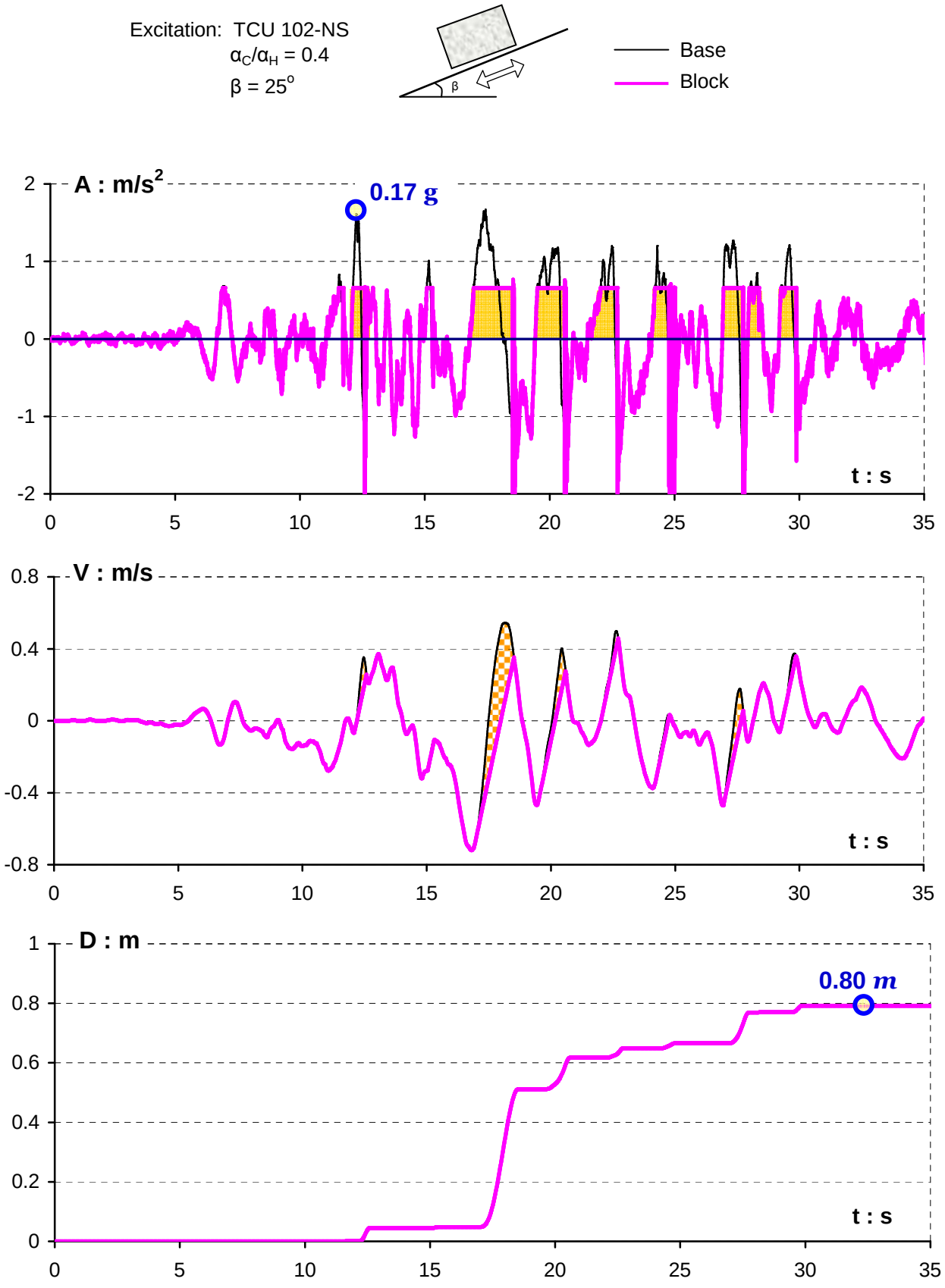

Figure 2.78 *The other component of the TCU 102 record (NS component) with PGA = 0.17* g *for* $a_C/a_H = 0.4$ *leads to 0.8 m of sliding displacement.*

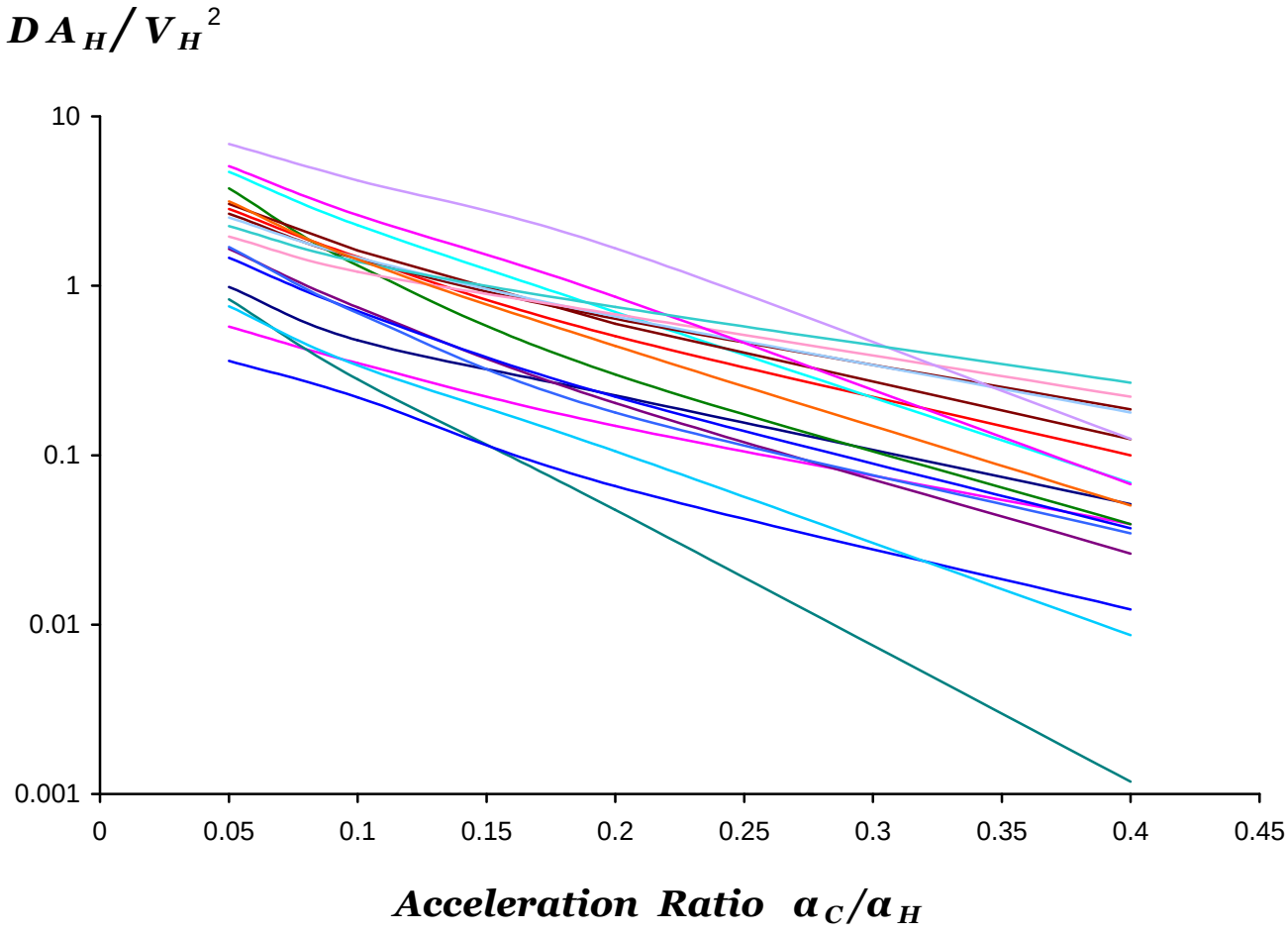

Figure 2.79 *Normalised sliding displacement triggered by the Chi-chi 1999 earthquake records with respect to the critical acceleration ratio* a_C/a_H. ($\beta = 25^o$)

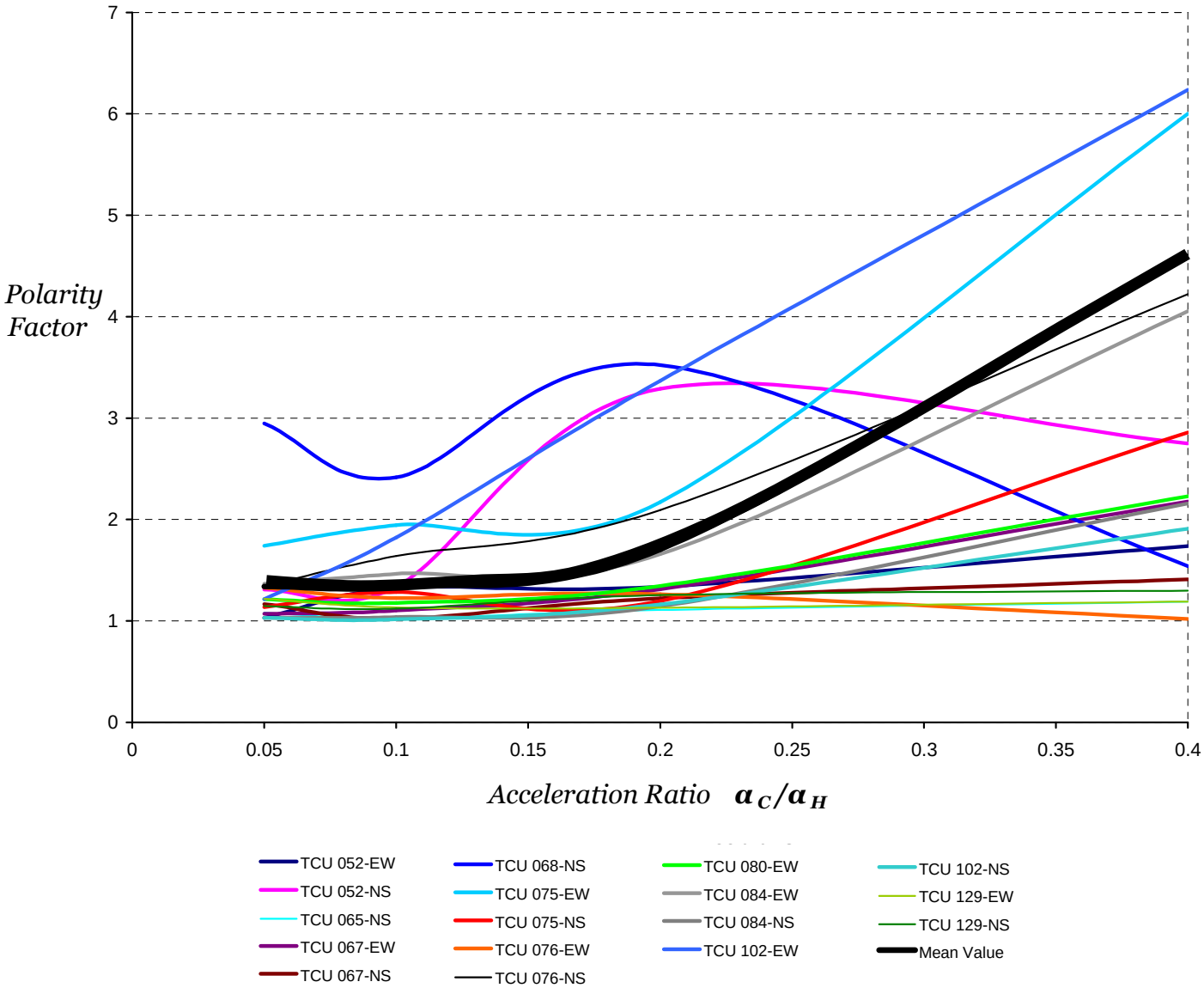

Figure 2.90 *The polarity factor for all the Chi-chi records. With black solid line is illustrated the mean curve. Notice that the polarity factor can be as large as six; thus by reverting the polarity of the excitation, the slippage becomes six times greater.*

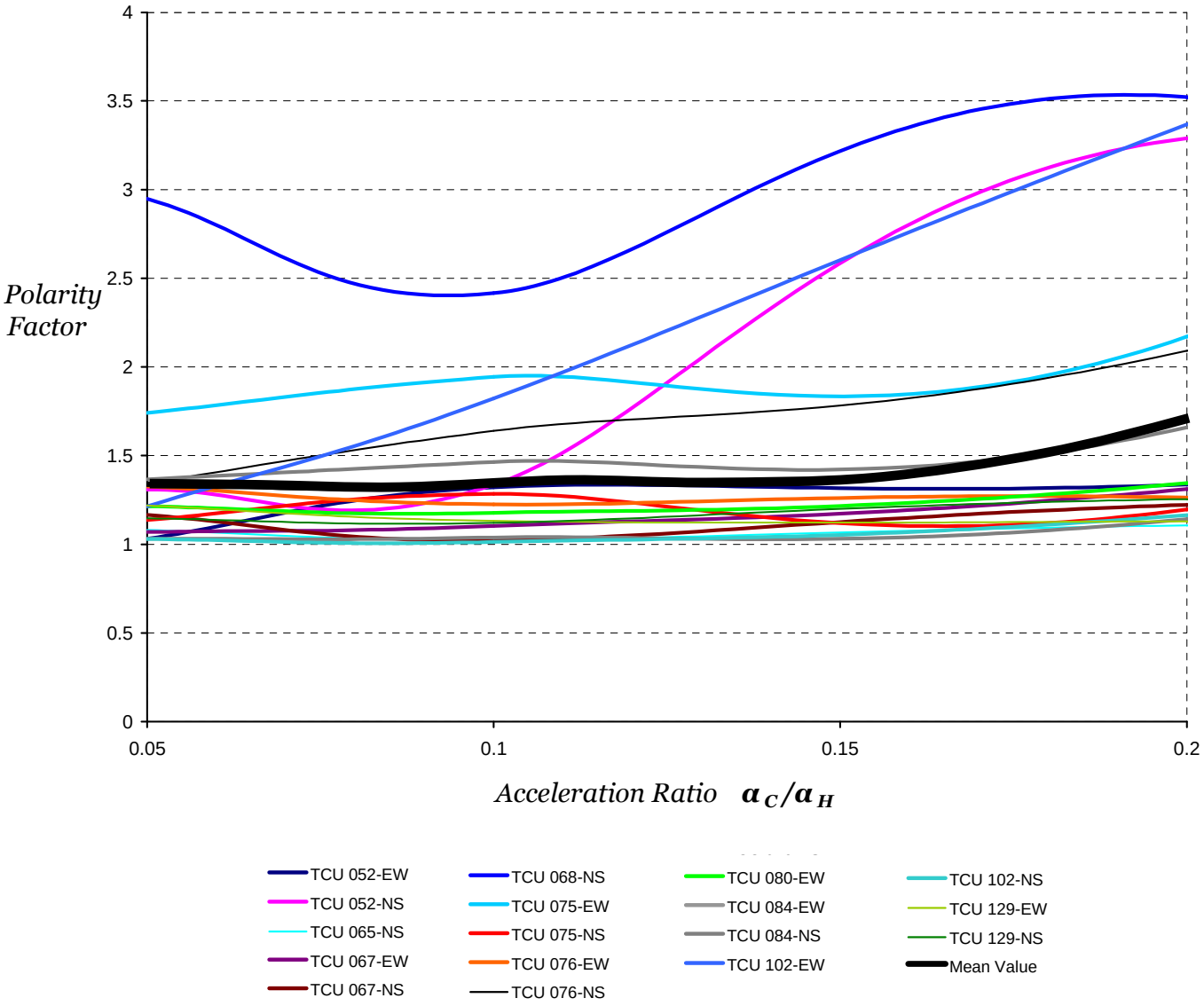

Figure 2.91 *The polarity factor shown in the previous figure, zoomed in a smaller window for a detailed view between the acceleration ratios of 0.05 and 0.2. With black solid line is illustrated the mean curve.*

Excitation Records from

the Gazli M_s = 7.0 Earthquake

17 May 1976, USSR

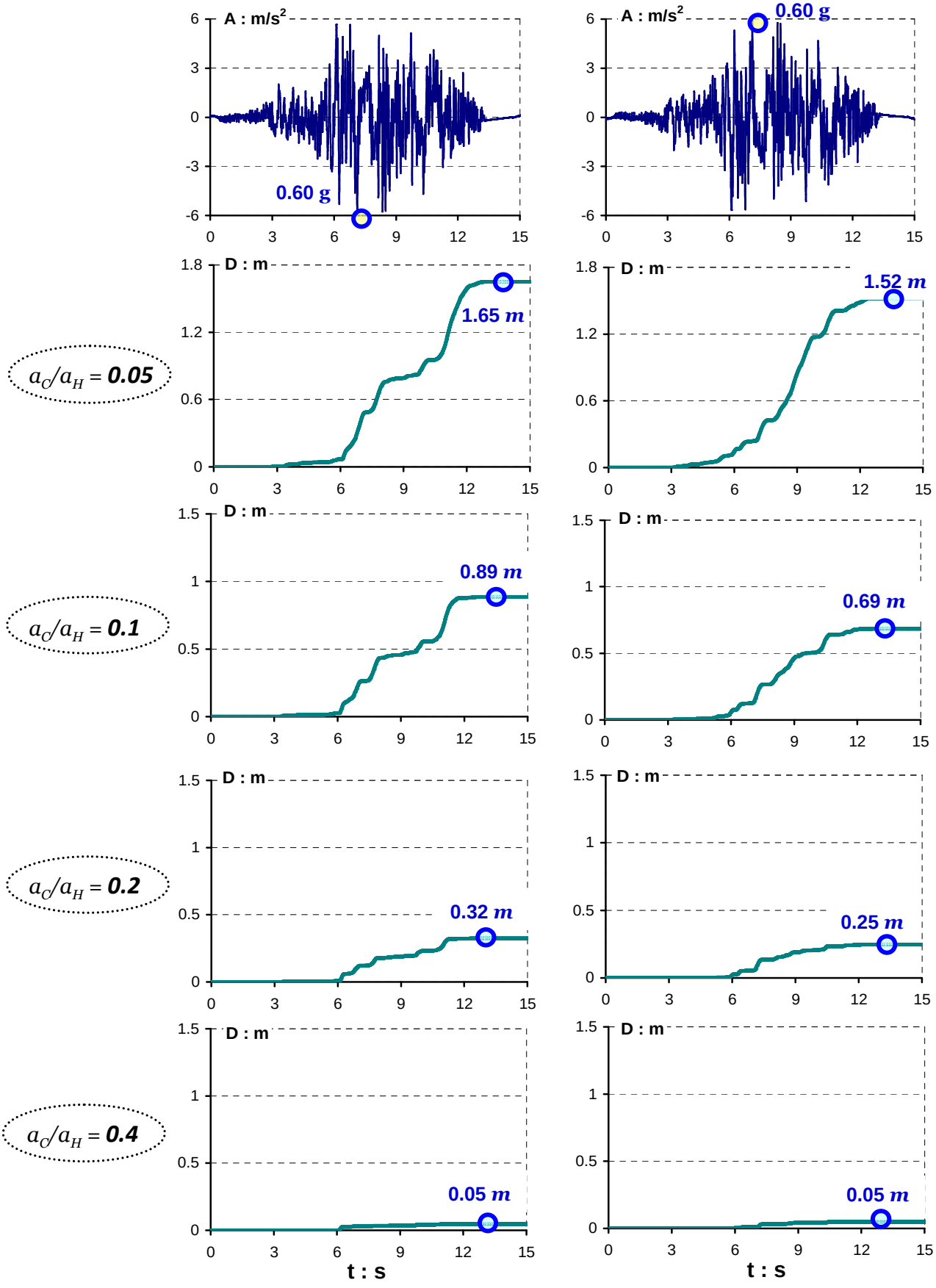

Figure 2.92 *Sliding displacement response induced by the Karakyr–0º record imposed with its normal (left column) and reversed (right column) sign. ($\beta = 25^o$)*

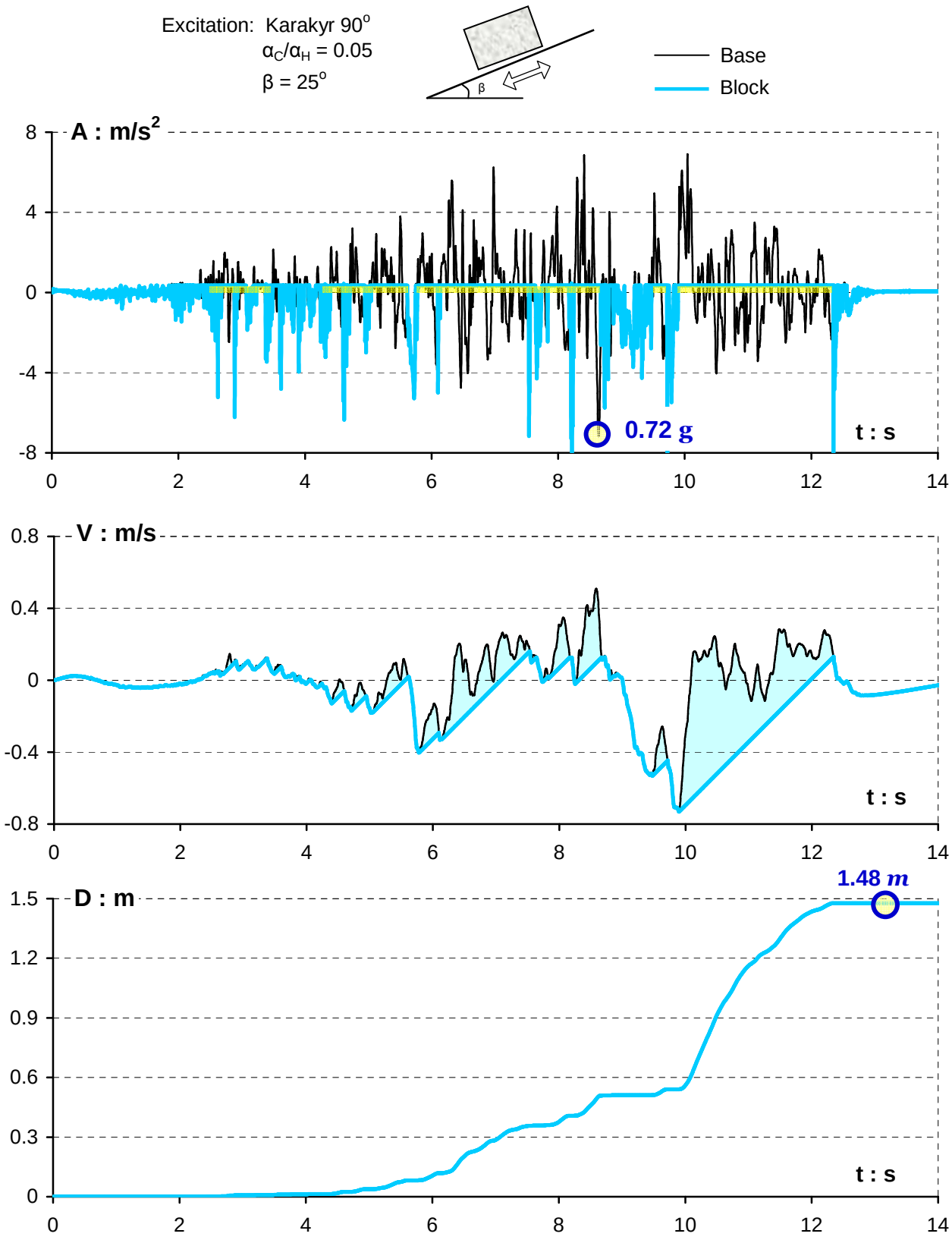

Figure 2.93 *Acceleration, velocity and displacement time-histories of the inclined base (black line) and of the sliding block (light blue line) for the triggering motion of Karakyr-90° record.*

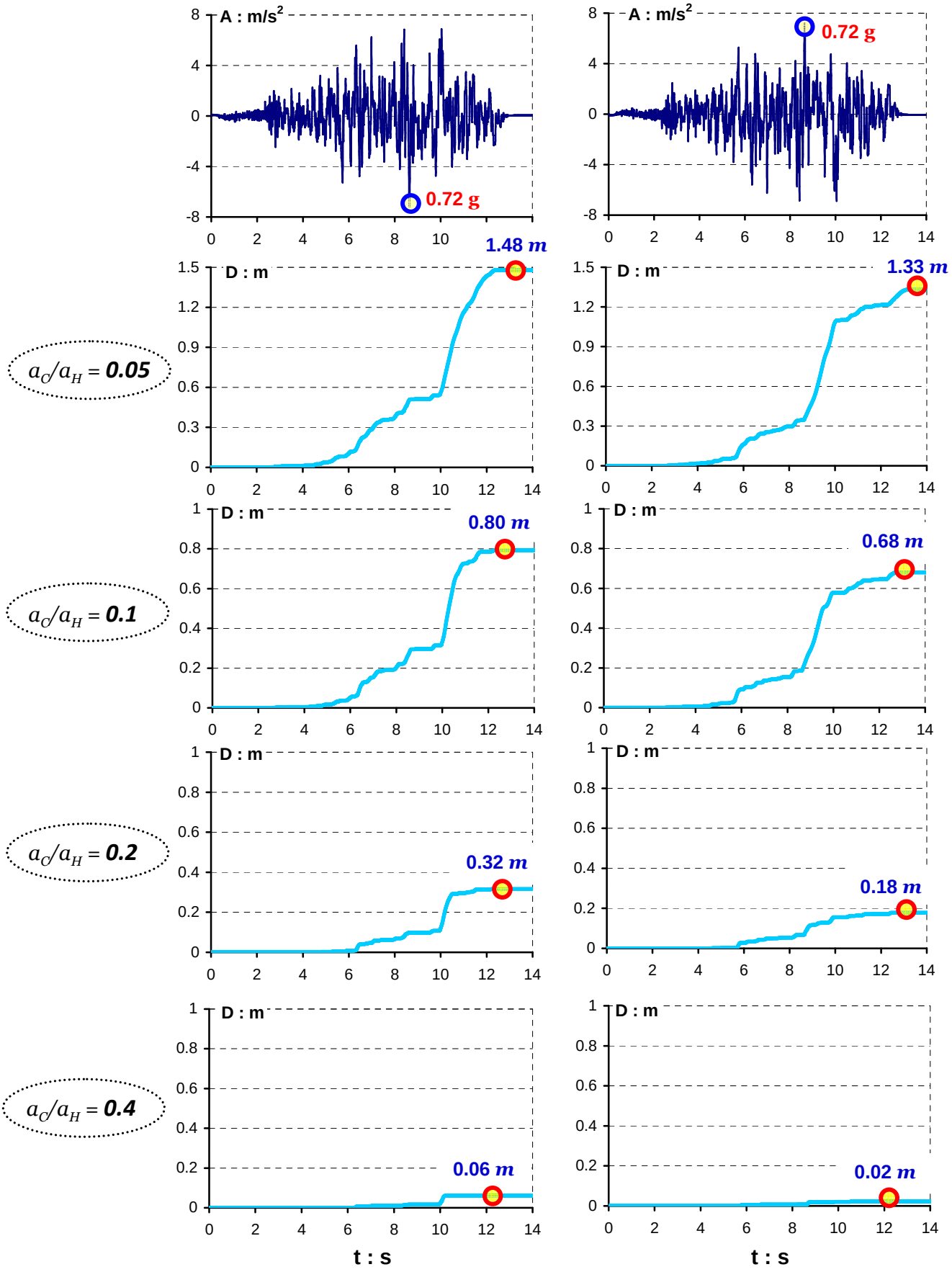

Figure 2.94 *Sliding displacement response induced by the Karakyr–90° record imposed with its normal (left column) and reversed (right column) sign. ($\beta = 25^o$)*

Excitation Records from

the Kocaeli M_w = 7.4 Earthquake

17 August 1999, Turkey

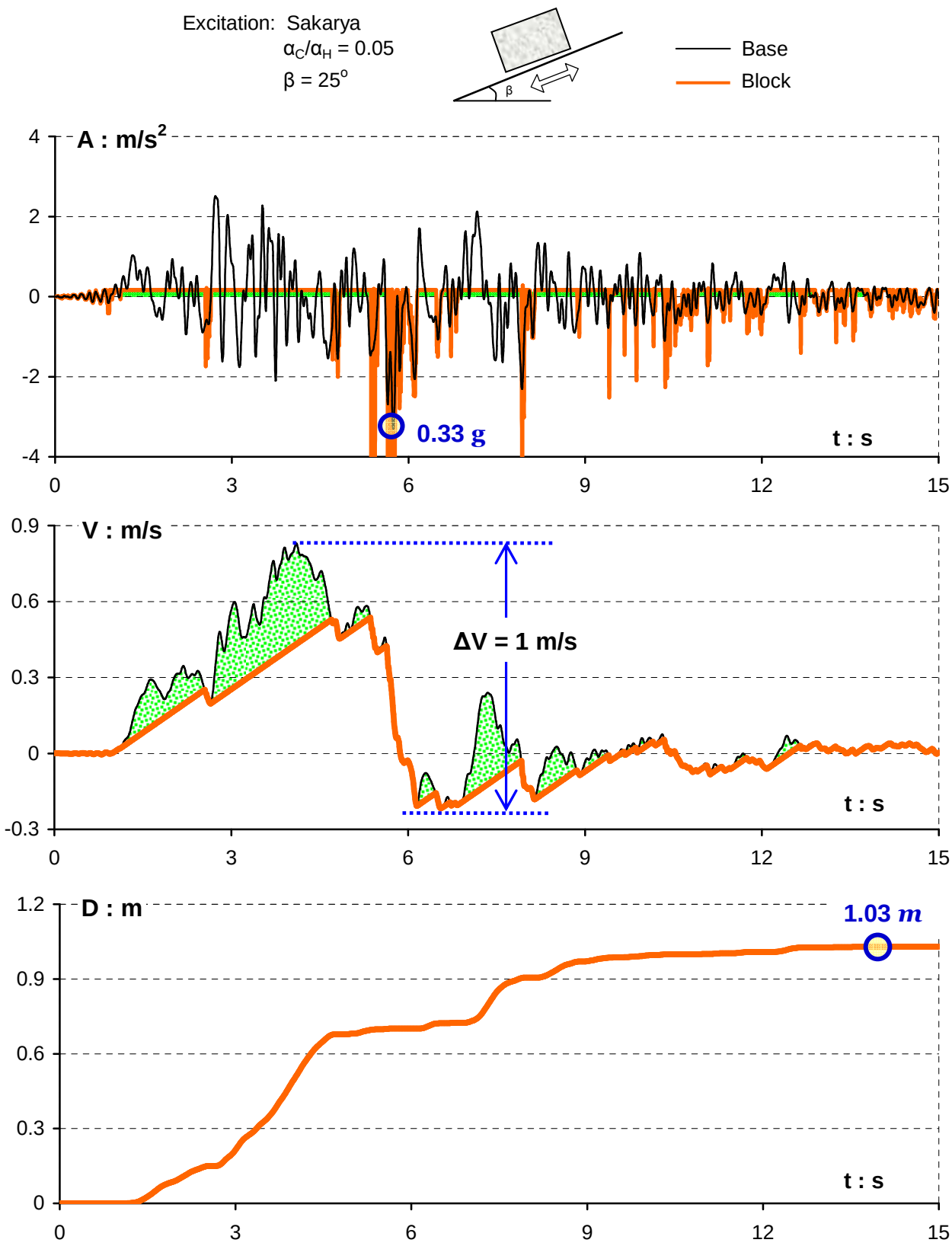

Figure 2.95 *Sliding response of a block subjected to the Sakarya ground motion. This particular record under a spiked high-frequency accelerogram hides some long period pulses which induce a large velocity pulse of 0.8 m/s magnitude (a step of 1 m/s) and 4.9 sec duration. As a consequence, a permanent ground displacement of 2 m at the end of the record reflects the fault's offset. The block slides 1 m relatively to its base.*

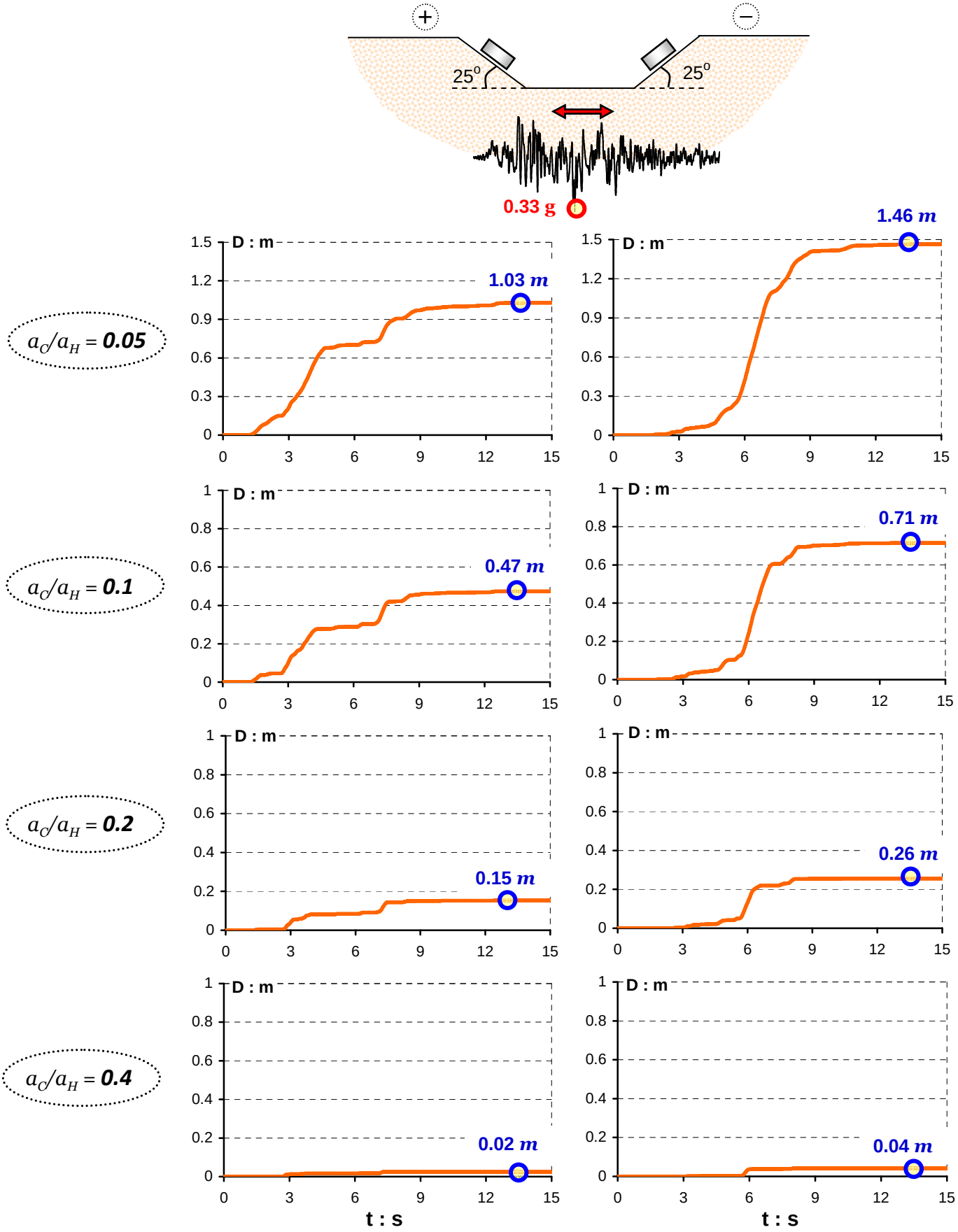

Figure 2.96 *Sliding response for four acceleration ratio, a_C/a_H, values induced by the Sakarya record imposed with its normal (left column) and reversed (right column) sign. ($\beta = 25^o$)*

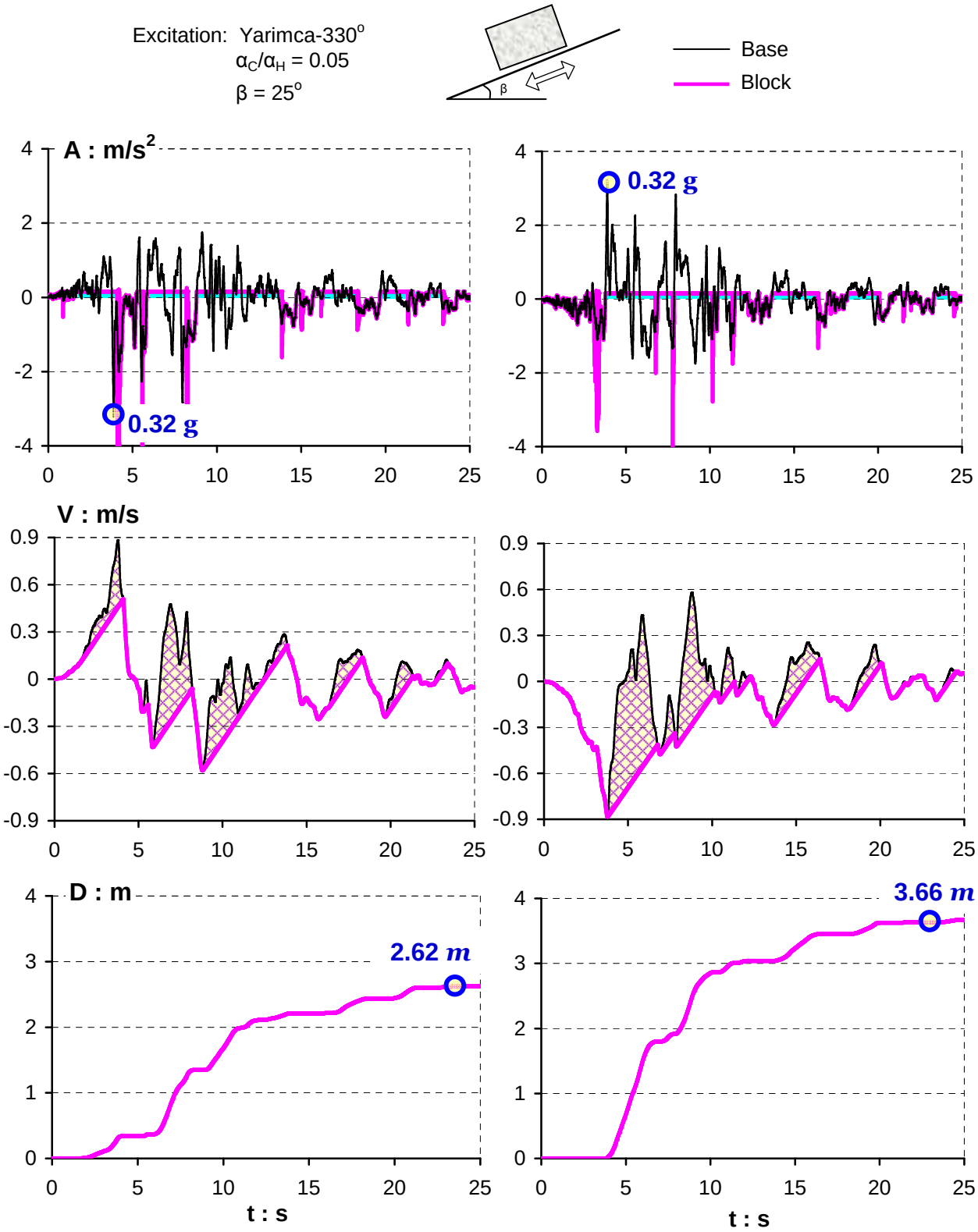

Figure 2.97 *An example of a ground motion with strong directivity effects: the Yarimca-330° record. The accelerogram is characterised by small peak values but numerous of long duration pulses. Therefore, the large velocity pulses of high amplitude and long period. As a result, the polarity effect present to be significant.* (a_C/a_H *= 0.05 and* β *= 25°)*

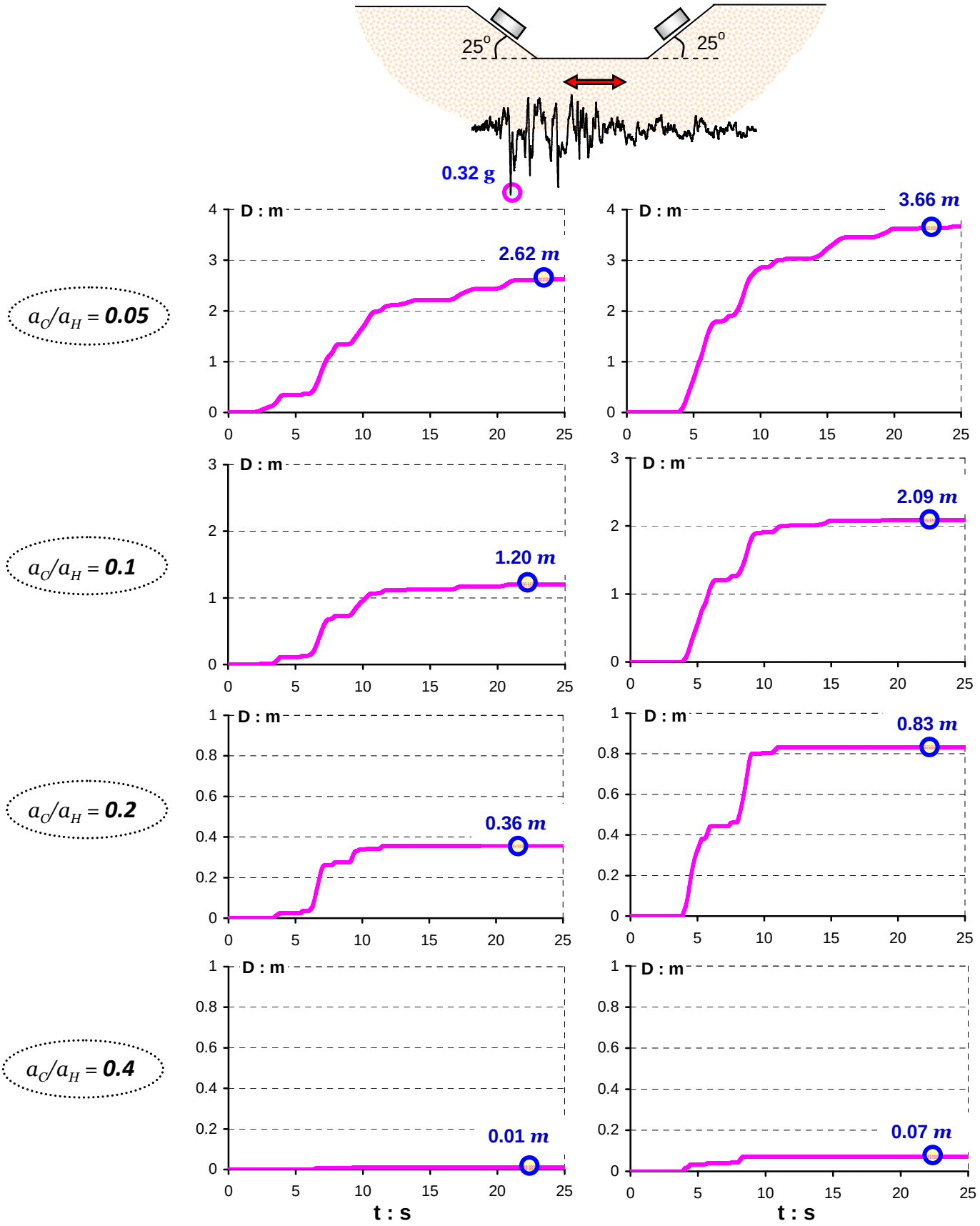

Figure 2.98 *Polarity effect in terms of slippage induced by the Yarimca-330° record imposed with its normal (left column) and reversed (right column) sign. Notice that as the acceleration ratio increases the polarity effect increases too. For a_C/a_H = 0.4 the polarity ratio reaches to 700 %.*

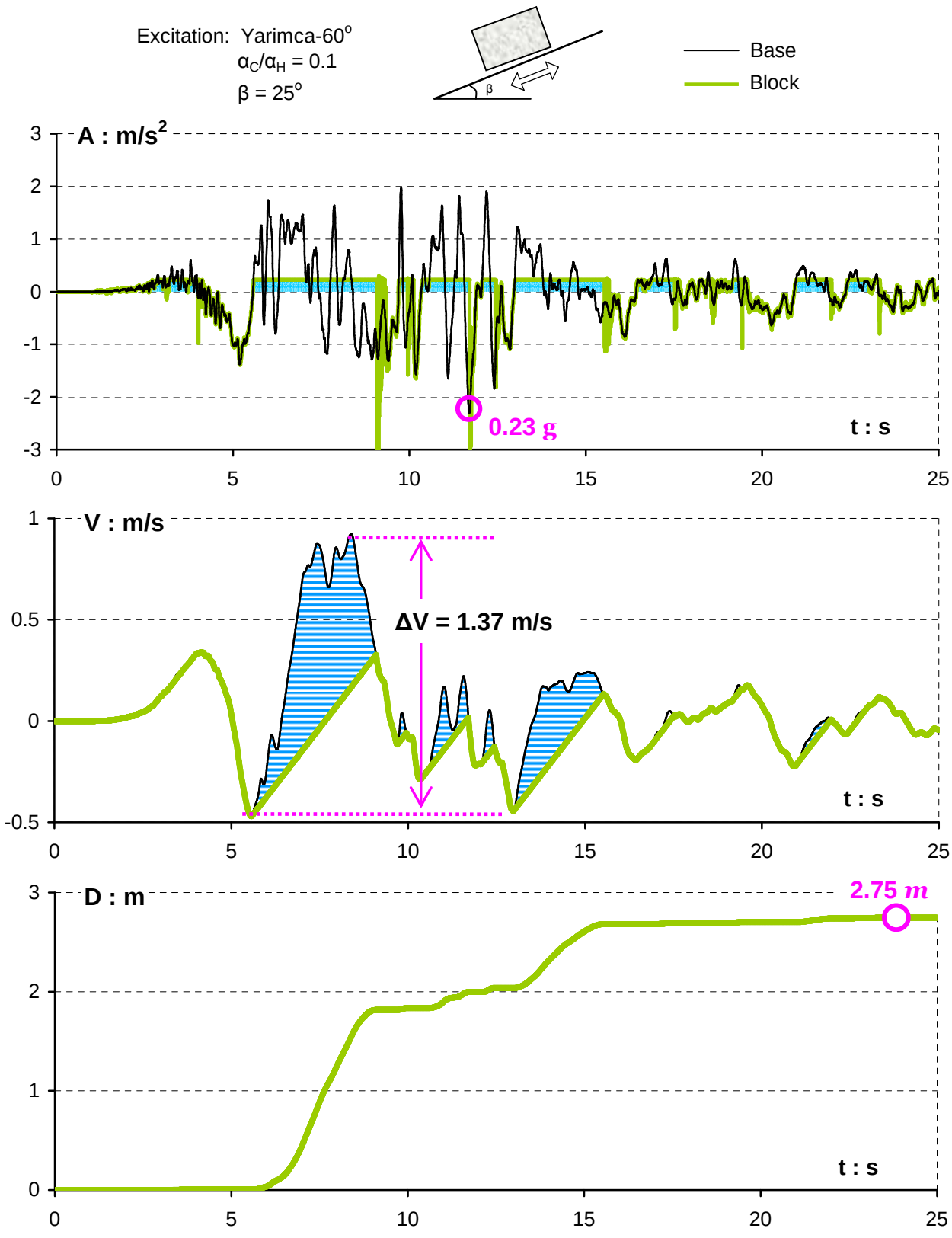

Figure 2.99 *The forward directivity affected Yarimca-60° record. A series of long period acceleration pulses generates a large velocity pulse with a step of 1.37 m/s and 4 s duration. Herein, the sliding response of a rigid block is illustrated for a critical yielding acceleration ratio of 0.1, resulting in 2.75 m slippage.*

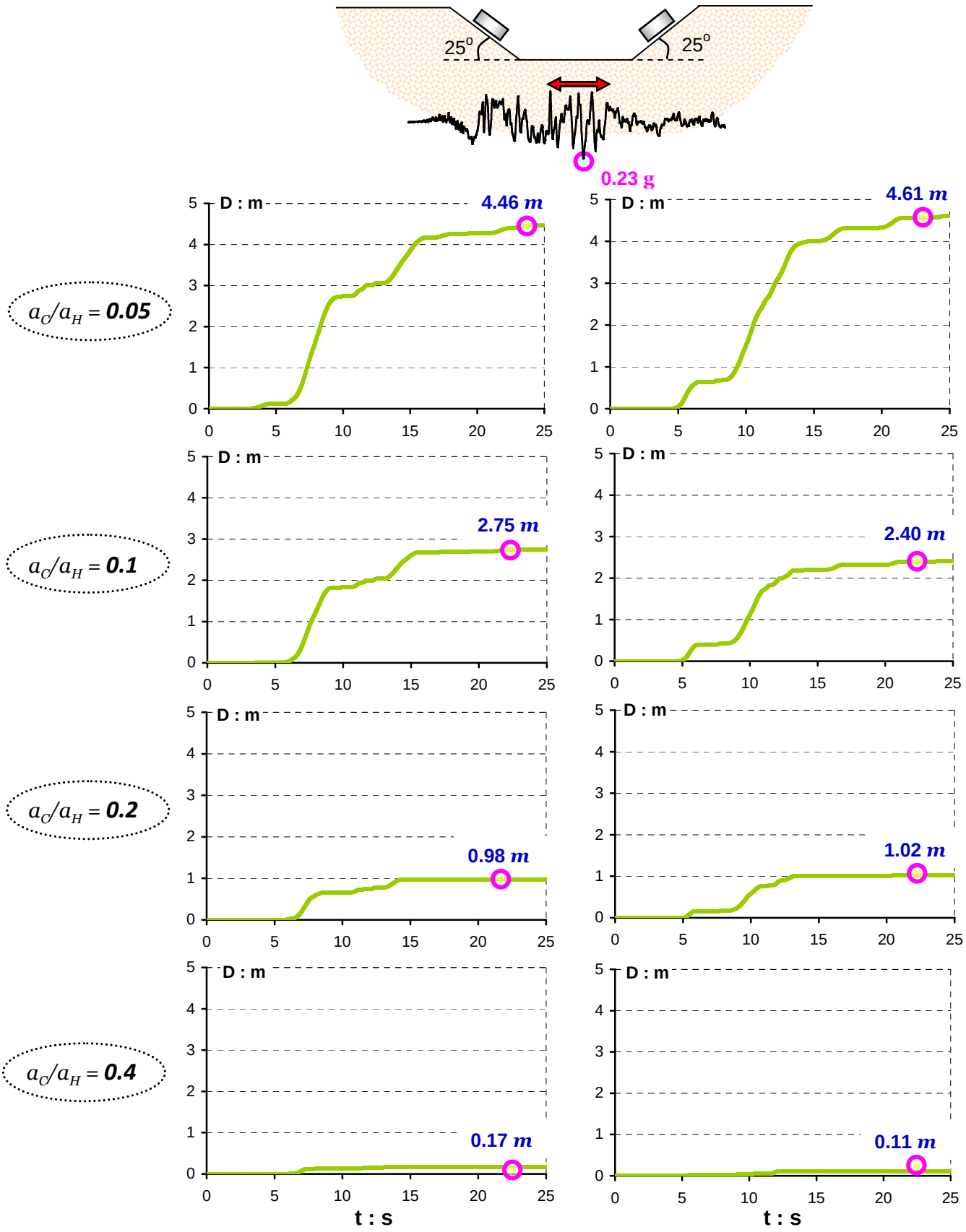

Figure 2.100 *Polarity effect in terms of slippage induced by the Yarimca-60° record imposed with its normal (left column) and reversed (right column) sign. Notice the paradoxical behaviour of polarity: for a_C/a_H = 0.05 the reversed record triggers the larger displacement, for a_C/a_H = 0.1 the original polarity record outweighs, for a_C/a_H = 0.2 the reversed record surpasses again and another alteration follows for a_C/a_H = 0.4*

Summary Results

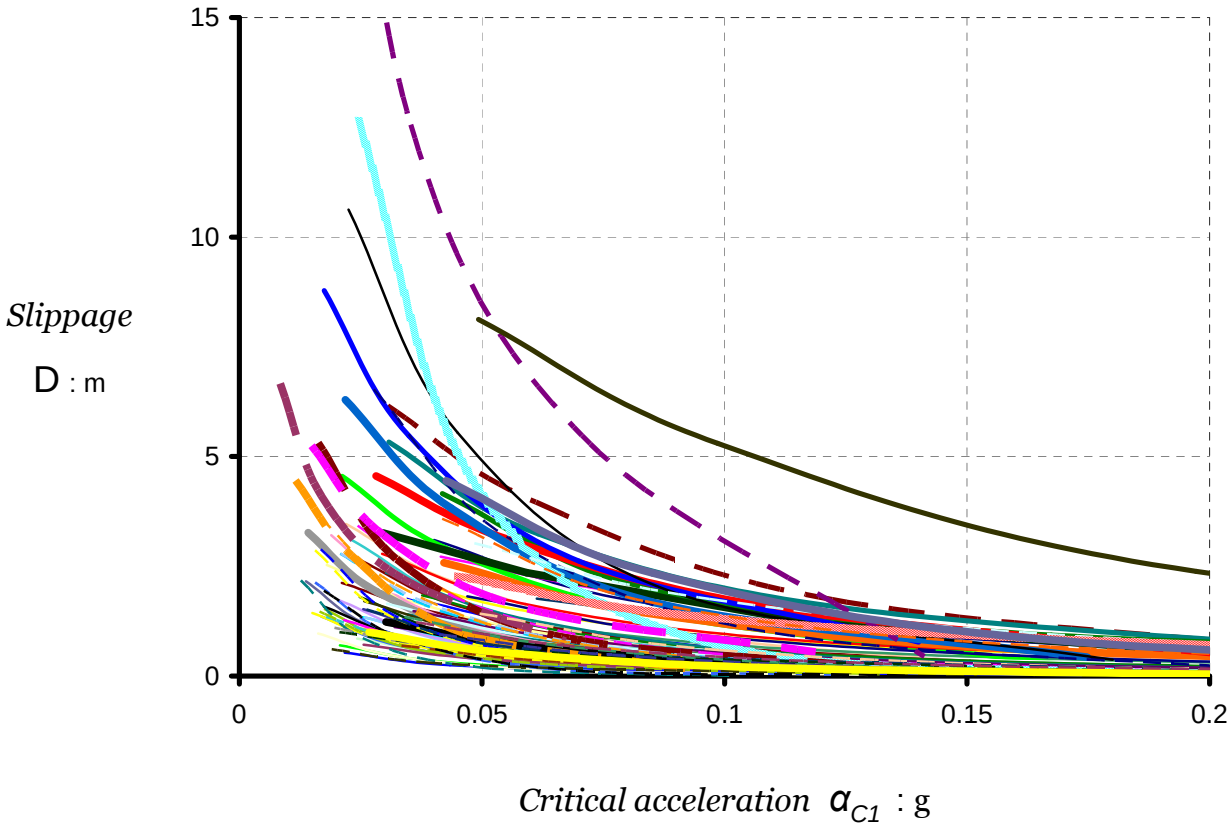

Figure 2.120 *Summary depiction of sliding displacement, triggered by the 98 near-fault ground motions utilised in this study, for various levels of yielding acceleration.*

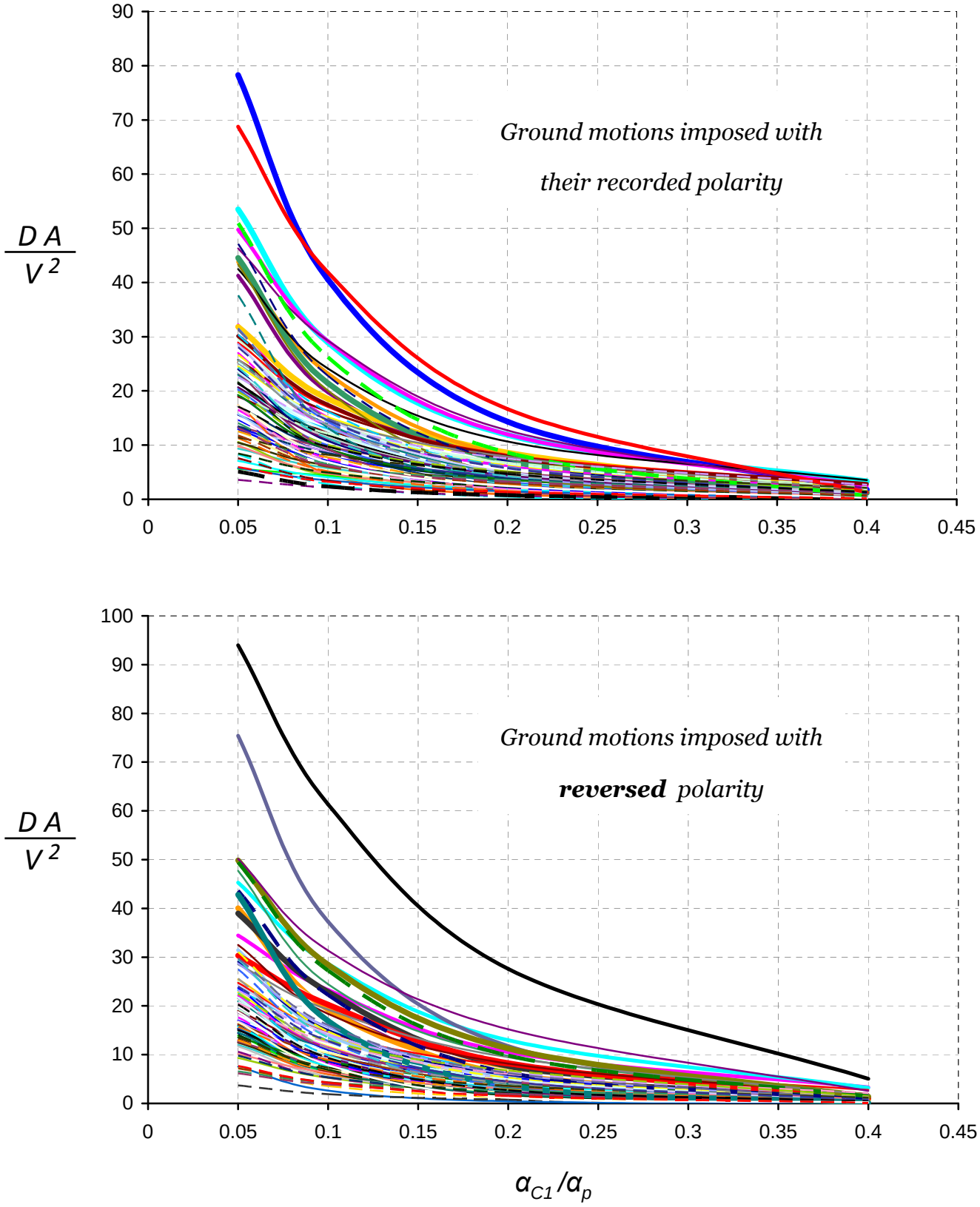

Figure 2.121 *Dimensionless ratio of slippage plus maximum input acceleration over the square of maximum velocity (of excitation), for all the 98 recorded ground motions.*

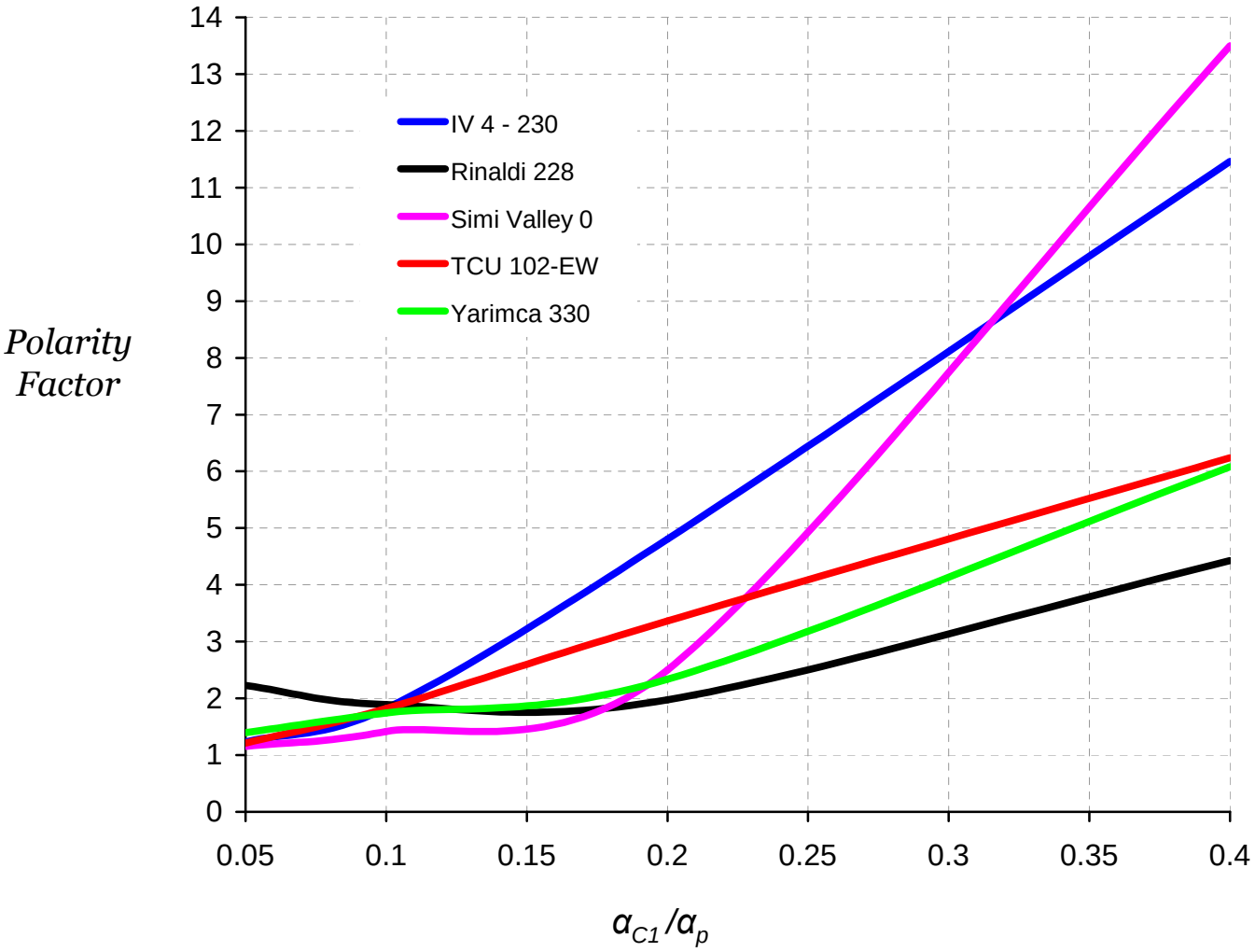

Figure 2.123 *For most of the excitation cases (see a juxtaposition at the next figure) the polarity factor increases as acceleration ratio* a_{C1}/a_P *increases too.*

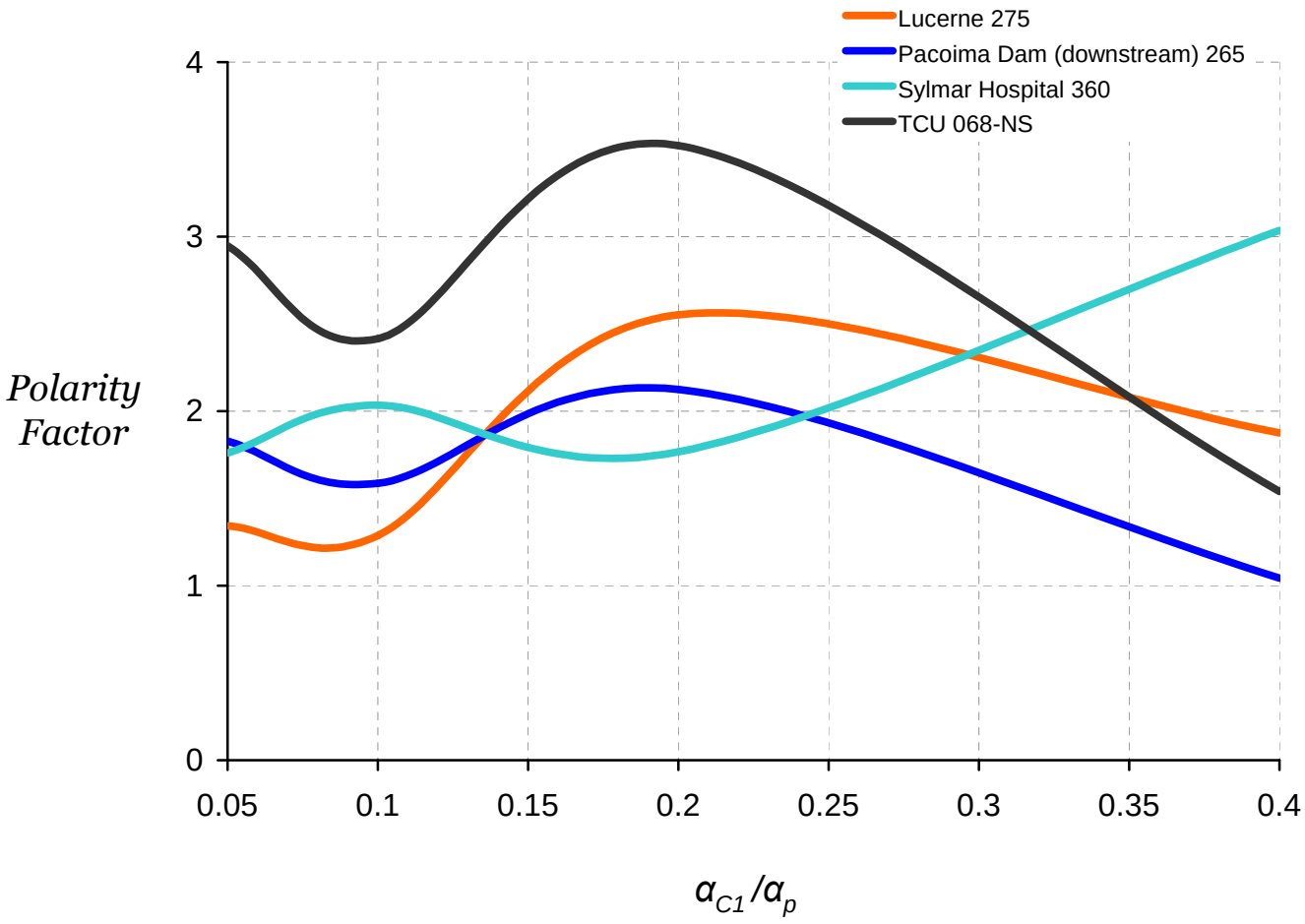

Figure 2.124 *The variation of polarity factor is not (for every input excitation) monotonically dependent on acceleration ratio a_{C1}/a_P. For instance, as illustrated herein the polarity factor can obtain local maximum and minimum values; therefore it can be a locally increasing and decreasing function of a_{C1}/a_P.*

Chapter 3

Sliding Spectrum and Damage–Potential Indices

3.1 Descripion of available Damage Ponential Indices (DPI)

Earthquake records contain information on the seismic intensity and potential destructiveness of ground shaking. Numerous parameters of a ground motion have been proposed over the years to serve as indices of the "damage potential" of a ground motion. They are often called "Damage Potential Indices" (DPI).

Several such DPI are tested herein against the amount of slippage induced by a ground motion. Specifically, the examined indices include: the Arias intensity (I_A); the Housner intensity (I_H); the RMS acceleration, or velocity, or displacement (A_{RMS}, V_{RMS}, D_{RMS}); the characteristic intensity (I_C); the specific energy density (S_E); the cumulative absolute velocity (CAV); the sustained maximum acceleration and velocity (SMA and SMV respectively); the acceleration and velocity spectrum intensity (ASI and VSI); the acceleration parameter A_{95}; the predominant period (T_P); the mean period (T_{mean}); the significant duration (D_{sig}); the "destructiveness potential factor" (P_D), and the ratio $V_{max}{}^2/A_{max}$ of the peak velocity squared divided by PGA. Next all these parameters are presented in detail and are listed in Table 3.1:

- *Arias Intensity, I_A, is proportional to the integral of the squared ground acceleration A(t) time history:*

$$\mathrm{I_A} = \frac{\pi}{2g}\int \mathrm{A}^2(t)dt \qquad (3.1)$$

- *Housner Intensity, I_H, is the integral of the pseudo-velocity spectrum over the period range [0.1 s, 2.5 s] :*

$$\mathrm{I_H} = \int_{0.1}^{2.5} S_V(T, \xi = 5\%)dT \qquad (3.2)$$

where $S_V(T,\xi)$ is the pseudo-velocity response spectrum (Housner, 1952).

- *RMS acceleration, A_{RMS}, is the square root of the mean acceleration:*

$$\mathrm{A}_{RMS} = \sqrt{\frac{\int \mathrm{A}^2(t)dt}{\mathrm{T}_D}} \qquad (3.3)$$

where T_D is the length of the record and A(t) is the acceleration time history.

- *RMS velocity, V_{RMS}, is the root mean square of velocity:*

$$V_{RMS} = \sqrt{\frac{\int V^2(t)dt}{\mathrm{T}_D}} \qquad (3.4)$$

where T_D is the length of the record and V(t) is the velocity time history.

- *RMS displacement, D_{RMS}, is the root mean square of displacement:*

$$D_{RMS} = \sqrt{\frac{\int D^2(t)dt}{\mathrm{T}_D}} \qquad (3.5)$$

where T_D is the length of the record and D(t) is the displacement time history.

- *Characteristic Intensity, I_C, is defined as:*

$$\mathrm{I}_C = \left(\mathrm{A}_{RMS}\right)^{3/2}\sqrt{\mathrm{T}_D} \qquad (3.6)$$

where T_D is the length of the record.

- *Specific Energy Density, S_E , is calculated from the expression:*

$$S_{\mathrm{E}} = \frac{\beta_S \rho_S}{4} \int V^2(t) dt \qquad (3.7)$$

where V(t) is the ground velocity time history, β_S is the wave velocity and ρ_s is the mass density of the recording site (Sarma, 1971).

- *Cumulative Absolute Velocity, CAV, is defines as:*

$$CAV = \sum_{i=1}^{N} \mathrm{H}\left(PGA_i - \mathrm{A}_{\min}\right) \int_{t_i}^{t_{i+1}} \left|\mathrm{A}(t)\right| dt \qquad (3.8)$$

where A(t) is the ground acceleration, N is the number of 1-second time windows in the time series, PGA_i is the PGA (in g) during time window i, t_i is the start time of time window i, A_{min} is an acceleration threshold (user-defined, but usually taken as 0.025g) to exclude low amplitude motions contributing to the sum, and H(x) is the Heaviside step function (unity for x>0, zero otherwise).

- *Sustained Maximum Acceleration, SMA, is the third highest absolute peak in the acceleration time history, proposed by Nuttli (1979).*
- *Sustained Maximum Velocity, SMV, is the third highest absolute peak in the velocity time history, proposed by Nuttli (1979).*
- *Acceleration Spectrum Intensity, ASI, is calculated as:*

$$ASI = \int S_{\mathrm{A}}\left(5\%, \mathrm{T}\right) d\mathrm{T} \qquad (3.9)$$

where $S_A(5\%,T)$ is the spectral acceleration for 5% damping and T is natural period [see Kramer (1996)].

- *Velocity Spectrum Intensity, VSI, is calculated from:*

$$VSI = \int S_V\left(5\%, \mathrm{T}\right) d\mathrm{T} \qquad (3.10)$$

where $S_V(5\%,T)$ is the spectral pseudo-velocity for 5% damping and T is natural period [see Kramer (1996)].

- *Acceleration parameter A_{95} is the level of acceleration which contains up to 95% of the Arias Intensity [Sarma & Yang (1987)].*

- *Predominant Period, T_P, evaluated using the 5% damped acceleration response spectrum, and corresponds to the period of the maximum spectral acceleration, as long as $T_P > 0.20$ sec.*

- *Mean Period, T_{mean}, is defined based on the Fourier amplitude spectrum. The mathematical expression is:*

$$T_{mean} = \frac{\sum\left(\frac{C_i^2}{f_i}\right)}{\sum C_i^2} \qquad (3.11)$$

where C_i is the Fourier amplitude for each frequency f_i within the range 0.25–20 Hz.

- *Significant Duration, D_{signif}, is the interval of time between the accumulation of 5% and 95% of Arias Intensity.*

- *Destructiveness Potential Factor, P_D, is the ratio between the Arias Intensity I_A and the square of the number of zero crossings per second of the accelerogram ν_o^2:*

$$P_D = \frac{I_A}{\nu_0^2} = \frac{\pi}{2g}\frac{\int A^2(t)dt}{\nu_0^2} \qquad (3.12)$$

as introduced by Araya & Saragoni (1984) and by Crespellani et al. (2003).

- *Modified Destructiveness Potential Factor, P_G, is the ratio between the Arias Intensity I_A and the square of the number of zero crossings per second $\nu_o^{2'}$ in the "significant" region of the accelerogram. We define as "significant" the part of record*

that includes all the directivity and fling acceleration pulses. Of course, the directivity or/and fling section of the record can not be strictly accurate because depends on our judgement.

Apart from the seismological parameters described above, the sliding displacement on an inclined plane is utilized as an additional destructiveness index representative of the inelastic response of structural systems. Thus, the simplified model used in our study as a fundamental analogue of inelastic systems: a rigid block of mass, m, resting on an inclined plane with a coefficient of friction, μ. The base is subjected to strong ground motion excitation in the form of recorded earthquake acceleration time histories. The block response is ideally-perfectly-plastic. Accelerations lower than the critical yielding acceleration, $a_C = \mu\cos\beta - \sin\beta$, ($\beta$ = the inclination angle) are transmitted through the friction interface to the block. For higher accelerations than a_C the friction interface can not transmit these accelerations and sliding begins. It occurs essentially only in the downward direction for inclination angles over 15^o. Every acceleration cycle contributes to sliding displacement downhill. At the end of each record, yielding displacements accumulate to a final slippage, D.

As already mentioned, excitation is applied parallel to sliding surface. Each accelerogram is imposed with its recorded sign (normal polarity) and with opposite sign (reversed polarity).

3.2 The Arias Intensity versus Sliding Response

In the (seemingly endless) search of the profession for reliable indexes of "destructiveness" of ground motions, i.e., for motion parameters indicative of the severity of a particular shaking, 'Arias Intensity' has enjoyed a rather significant popularity. The definition has already been given (Table 3.1) and it has been correlated with, among

other measures of damage, one-directional sliding displacement of rigid blocks (Jibson, 1994 ; Kramer, 1996) or flexible slopes (Travasarou, 2004).

An attempt is made here to correlate I_A of some severe near-fault motions with the permanent slip they produced on a steep (25^o) slope. Such permanent (residual) slip is a direct measure of the "damage" to the respective geotechnical structure (slope, retaining wall, etc) by the specific excitation.

Figures 3.1÷3.5 display D (in metres) as a function of the yield acceleration a_{C1} (recall that for $\beta = 25^o$, $a_{C1} = \mu cos25^o - sin25^o$). No scaling or any other modification to the ground motions was made. What appears as scatter in the results of each record, arises solely from the change in polarity (+ or − direction) of each specific record. The Arias Intensity of each motion is written directly on each relevant pair of curves.

Figures 3.1 and 3.2 present the sliding response for triplets of records with different Arias intensity. The top plot of Figure 3.1 portrays the response of the Imperial valley No 6, the Lucerne, and the Shinkobe records. Interestingly, the sliding response of the record with the lower Arias intensity, I_A=1.8, IV No 6, exceeds the slippage induced by excitations with nearly four times larger Arias indensity (Lucerne, I_A = 6.8). Therefore, the Arias I_A value is not a reliable indicator of sliding displacement of a particular ground motion.

The same conclusion is drawn not only by comparing ground motions of different earthquake events but also for records of a single event (Figure 3.3). In the top plot of this figure, the slippage of three records of the Chi-chi earthquake is shown. Response of TCU 084-EW with I_A = 19.5 is smaller than the sliding displacement triggered by TCU 068-NS with I_A = 3.3, for small a_{C1} values.

Although, admittedly, the presented data in this paper are rather limited for a statistically robust statement, and the selection of "severe" motions was somewhat arbitrary, one can still draw a first conclusion of potential interest: Arias Intensity can not alone be a reliable predictor of slip, especially with motions containing acceleration pulses of large duration (directivity or, especially, fling related).

This implies an order of magnitude or more error, if I_A is used for prediction of the potential repercussions of the two motions. This conclusion is in accord with the observation by Sarma and Kourkoulis (2004) and Crespellani et al (1997). The latter, proposed for slope deformation a corrected measure of motion "destructiveness" based on Arias Intensity along with the average rate of zero-crossing of the record. Questions are raised on the applicability of empirical correlations between D and I_A such as those presented by Jibson (1994) and Del Gaudio et al (2003).

3.3 Other DPI versus sliding response

Figures 3.6 ÷ 3.18 present the influence of every DPI (except Arias intensity that was already discussed in the previous part) on sliding rigid block displacement, D, triggered by near-fault ground motions subjected at the base of a 25^o inclined plane. A correlation expression is also provided for each plot along with the standard error, R.

R is a correlation coefficient giving a good idea about how closely one variable is related to another. The closer a correlation coefficient is to zero, the weaker the relationship is and the less able we are to predict what happens to one variable based on knowledge of the other. As the correlation coefficient approaches unity the relationship is closer and accurately we can predict one variable from the other.

Table 3.2 displays the correlation coefficient, R, for all the examined DPIs. Several conclusions can be drawn:

(i) "time" indices (mean period, predominant period, significant duration) are invariable poorly correlated with slippage;

(ii) the acceleration indices are also deficient descriptors of slippage;

(iii) the velocity indices (peak ground velocity, RMS velocity, cumulative absolute velocity, sustained maximum velocity and velocity spectrum intensity) are in fairly good correlation with sliding response;

(iv) Arias and Housner intensity relate satisfactorily with displacement–even though Arias intensity could lead to major errors for the sliding of a particular record; in a large statistical scale the trend is matched; and

(v) the spectral displacement at the period of 2 sec and the "destructiveness potential factor" are in good agreement with sliding response.

3.4 The sliding spectrum concept

The need for an objective quantitative index of the intensity of seismic response has prompted the development of the elastic spectrum, which was latter extended to constant-ductility inelastic spectrum.

In case of sliding systems governed by the Coulomb's friction law, we introduce the idea of equivalent sliding motions for a given displacement level, and present particular shortcomings of elastic response spectra for such anelastic systems.

The concept of equivalent sliding motions is as follows: for a given predetermined level of sliding displacement and yielding acceleration a_C, we obtain the appropriate scaled ground motions that induce this predetermined slippage. For instance, Figure 3.19 illustrates all the records that for an inclined system ($\beta = 25^o$) with $A_C = 0.05$ g induce a sliding of 20 cm. So, the JMA record (90^o component) must be down-scaled to a PGA = 0.13 g to lead to a sliding of 20 cm; while for the same slippage, the Simi Valley record

(component 0^o) must be doubled from 0.13 g to 0.26 and the Institute of Urban Construction record (IUC 90^o) to 0.27 g. Figures 3.21, 3.23, and 3.25 present the equivalent sliding motions giving sliding displacements of: 0.5 m, 1 m, and 1.5 m. Notice that as the common level of sliding increases (a_C decreases), the acceleration discrepancy among the records becomes starking. In case of yielding on a horizontal base ($\beta = 0^o$) with $A_C = 0.15$ g, the equivalent ground motions that induce maximum sliding of 3 cm are shown in Figure 3.32.

To demonstrate the weakness of elastic response spectrum in capturing the behavior of inelastic systems (such as those in our study), for every "equivalent" sliding record we compute the elastic spectrum. Thus, in Figures 3.20, 3.22, 3.24, 3.26, and 3.27 portray the elastic spectra of the equivalent set of ground motions giving a slippage of 20 cm, 50 cm, 1 m, and 1.5 m, respectfully. As can be seen, the differences among the "equivalent" sliding spectra are significant. For example, in Figure 3.24 the elastic spectrum of the Sakarya record scaled to induce sliding of 1 m, is almost three times larger than the elastic spectrum of the down-scaled Jensen Filtration Plant record (component 22^o) that triggers the same slippage. In other words, these two elastic spectra have the same inelastic response for our system!

Furthermore, an elastic response spectrum does not always reflect the importance of the detailed sequence of acceleration pulses. Figures 3.28 ÷ 3.31 illustrate the acceleration time histories and the corresponding elastic spectra of four particular records that induce a sliding displacement of 1 m. The excitations are applied with their recorded and reversed polarity. The elastic response spectrum is of course independent of the polarity of motion: normal and reversed records have identical spectra. However, in asymmetric sliding the polarity has significant effect on the resulting slippage. Figure 3.30 pictures

the equivalent normal and reversed polarity Rinaldi 228° acceleration time histories and their elastic spectra. The Rinaldi record scaled to 0.41 g triggers 1 m sliding displacement when applied in one direction, while when reversed it must be reduced to half, 0.22 g. So, two elastic spectra of identical shape but different magnitude (one half the other) result in almost exactly the same slippage !

To conclude, the use of elastic spectrum as a representative index of the destructiveness of a motion is limited. The need of more resilient indicators emerges for inelastic systems.

3.5 Comparison with literature results

It is worth comparing the results of our study against the classical relevant charts for sliding published by Makdisi & Seed (1978), Sarma (1975), and Crespellani et al. (1996). The comparison is portrayed in Figures 3.34 ÷ 3.50. Evidently, for small a_C/a_H values (< 0.30), these classical curves, based on statistically processing a number of (mostly "usual") records, can not adequately predict the extreme slippage produced with motions strongly affected by fling and directivity phenomena. Our data, admittedly not of a sufficient number to allow derivation of a reliable design diagram, do nevertheless point out that the upper bound of sliding displacements may be substantially higher than is usually considered on the basis of widely-used, if older, charts.

3.5.1 Correspondence with the Makdisi & Seed charts

Makdisi & Seed (1976) computed the permanent displacements of a sliding block by utilising the Newmark analogue, and they proposed design curves for the estimation of embankment deformation for different magnitudes of earthquakes. Figures 3.34 ÷ 3.37 illustrate the results we obtained for all the ground motions utilised in our study, and

compared with the Makdisi & Seed Curves. Our data are categorised in those induced by directivity-affected records and those by fling-affected ground motions. As it can be seen, the near-fault induced displacements exceed by far the curves of Makdisi & Seed. For the flinged triggered response, in particular, Makdisi & Seed curves underestimate by more than an order of magnitude the permanent slippage (Figure 3.35) !

Figures 3.36 and 3.37 depict our results for the seismic events of magnitude 6.0 ÷ 6.8 and 6.9 ÷ 7.7 respectively. Upper bound curves for each magnitude level are provided too:

$$D_{res} = 3000 \exp\left[-10\,\alpha_{C1}/\alpha_P\right] \ , \quad for \ 6.0 < M < 6.8 \qquad (3.13)$$

$$D_{res} = 500 \exp\left[-7\,\alpha_{C1}/\alpha_P\right] \ , \quad for \ 6.9 < M < 7.7 \qquad (3.14)$$

3.5.2 Comparison with the dimensionless results of Sarma

Sarma (1975) suggested that earthquake triggered displacements can be calculated by using simple pulses. Dimensionless sliding displacements were given in terms of the critical acceleration ratio for the cases of rectangular, triangular and half-sine excitation pulses. These curves were utilised as envelopes to design dams and embankments. Their analytical expressions are:

For a rectangular pulse of duration T/2 and amplitude a_P g :

$$\frac{4D_{res}}{\alpha_P g \mathrm{T}^2}\left[\frac{\cos\varphi}{\cos(\beta-\theta-\varphi)}\right] = \frac{1}{2}\left(\frac{\alpha_{C1}}{\alpha_P} - 1\right) \qquad (3.15)$$

For a triangular pulse of duration T/2 and amplitude a_P g :

$$\frac{4D_{res}}{\alpha_P g \mathrm{T}^2}\left[\frac{\cos\varphi}{\cos(\beta-\theta-\varphi)}\right]=\begin{cases}\dfrac{1}{24}\left[4(1-\alpha_{C1}/\alpha_P)(1-\lambda\,\alpha_{C1}/\alpha_P)-(1-\lambda(\alpha_{C1}/\alpha_P)^2)\right](\alpha_P/\alpha_{C1}) \\ \qquad for \quad 0\le\alpha_{C1}/\alpha_P\le\left[1-\sqrt{(1-\lambda)}\right]/\lambda \\ \dfrac{1}{6}\left[(1-\alpha_{C1}/\alpha_P)^3\left(2-2\sqrt{(1-\lambda)}-\lambda\right)\right] \\ \qquad for \quad \left[1-\sqrt{(1-\lambda)}\right]/\lambda\le\alpha_{C1}/\alpha_P\le 1\end{cases} \qquad (3.16)$$

where $\lambda T/2$ is the time at which the maximum acceleration occurs.

For a half sine pulse of duration T/2 and amplitude a_P g :

$$\frac{4D_{res}}{\alpha_P g \mathrm{T}^2}\left[\frac{\cos\varphi}{\cos(\beta-\theta-\varphi)}\right]=\begin{cases}(\alpha_{C1}/\alpha_P-\sin q)^2/\left(2\pi^2\,\alpha_{C1}/\alpha_P\right) \quad , \\ \qquad for \quad 1\ge\alpha_{C1}/\alpha_P\ge 0.725 \\ \left[\alpha_{C1}/\alpha_P+\mu-\pi+\cos^2(\mu/2)\cot(\mu/2)\right]/\pi^2 \quad , \\ \qquad for \quad 0\le\alpha_{C1}/\alpha_P\le 0.725\end{cases} \qquad (3.17)$$

$$where \quad q=\mu+(\cos\mu-\cos q)\frac{\alpha_{C1}}{\alpha_P}, \quad \mu=\sin^{-1}\left(\frac{\alpha_{C1}}{\alpha_P}\right)$$

In all the above equations, β is the inclination of sliding plane to horizontal; θ is the angle of inertia force to horizontal (= $\tan^{-1}a_P$); and φ is the effective shear strength parameter of the soil.

Figures 3.38 ÷ 3.40 compare the results of our analyses with the Sarma curves. Notice in Figure 3.38, that the slippage induced by near-fault ground shaking overshadows Sarma's curves both in normal and logarithmic scales. When a different normalisation is applied: $D(D_H^{1.5}\ A_H^{0.5})/V_H$ versus A_{C1}/A_H, the displacement surplus is decreased

substantially, and in fact the rectangular pulse leads to results that exceed slightly the highest numerical values (see Figures 3.39 and 3.40).

3.5.3 Comparison with Crespellani

Crespelani et al (1996) calculated the slippage of Newmark's block produced by the horizontal components of 155 worldwide earthquake records. The displacements were correlated with the "destructiveness potential factor", P_D. Furthermore, regression analysis led to equations for estimating the displacements of gravity retaining walls:

$$D_{res} = 34.08 \frac{V^2}{\alpha_P g} \exp\left(-7.74 \alpha_{C1} / \alpha_P\right) \qquad (3.18)$$

where V = the peak velocity of the ground motion.

Our results are plotted in comparison with Crespellani's in Figures 3.41÷ 3.46. The record database in Crespellani's study include ground motions from earthquake events in Italy, Greece, Mexico and United States. On the other hand, we focus on time histories with strong near-fault effects. As a consequence, in Figures 3.43, 3.44 and 3.45 (for yielding acceleration values of 0.05, 0.1 and 0.2 g respectively), the results of our analyses are located in the extension of Crespellani's results for all three yielding accelerations. Motions with forward directivity and fling effects were not included in Crespellani's study. If the mean line proposed by Crespellani is prolonged in higher P_D regions, then near source response could also be expressed by the same expressions.

3.6 Proposed upper-bound expressions to estimate seismic induced sliding

Apart from the expressions provided in section 3.5.1 for slippage in terms of the two parameters: earthquake magnitude range and critical acceleration ratio; herein there

will be presented sliding displacement estimation expressions as function of only one parameter: the modified "near-source" destructiveness potential factor, P_G:

$$\begin{cases} D_{res} = 0.60(P_G)^{0.87}, & for \quad A_C = 0.05g \\ D_{res} = 0.25(P_G)^{0.87}, & for \quad A_C = 0.10g \\ D_{res} = 0.10(P_G)^{0.87}, & for \quad A_C = 0.20g \end{cases} \qquad in\ (m) \qquad (3.19)$$

from which a simple, single expression is derived:

$$D_{res} = 0.0126(P_G)^{0.87}(A_C/g)^{-1.3} \qquad in\ (m) \qquad (3.20)$$

Figures 3.47 and 3.48 illustrate in logarithmic scale all analyses results versus P_G.

Table 3.1: *List of seismological indices employed to quantify the destructiveness of the imposed ground motions.*

Seismological Index	***Definition***
Arias Intensity, ***I_A***	$I_A = \frac{\pi}{2g}\int A^2(t)dt$ *A(t)= ground acceleration.*
Housner Intensity, ***I_H***	$I_H = \int_{0.1}^{2.5} S_V(T, \xi = 5\%)dT$ *$S_V(T, \xi)$ = pseudo-velocity spectrum.*
RMS Acceleration, ***A_{RMS}***	$A_{RMS} = \sqrt{\frac{\int A^2(t)dt}{T_D}}$ *T_D = length of record, A(t) = ground acceleration.*
RMS Velocity, ***V_{RMS}***	$V_{RMS} = \sqrt{\frac{\int V^2(t)dt}{T_D}}$ *T_D = length of record, V(t) = ground velocity.*
RMS Displacement, ***D_{RMS}***	$D_{RMS} = \sqrt{\frac{\int D^2(t)dt}{T_D}}$ *T_D = length of record, D(t) = ground displacement.*
Characteristic Intensity, ***I_C***	$I_C = (A_{RMS})^{\frac{3}{2}}\sqrt{T_D}$ *T_D = length of record.*
Specific Energy Density, ***S_E***	$S_E = \frac{V_S \rho_S}{4}\int V^2(t)dt$ *V_S = wave velocity, ρ_S = mass density.*
Cumulative Absolute Velocity, ***CAV***	$CAV = \sum_{i=1}^{N} H(PGA_i - A_{\min})\int_{t_i}^{t_{i+1}} \lvert A(t)\rvert dt$ *N = number of 1-second time windows in the time series, PGA_i = PGA of time window i, t_i = start time of window i, A_{min} = acceleration threshold (user-defined but commonly 0.025g), and H(x) = Heaviside step function (unity for x>0 and 0 otherwise).*

Sustained Maximum Acceleration, ***SMA***	*the third highest absolute peak in the acceleration time-history.*
Sustained Maximum Velocity, ***SMV***	*the third highest absolute peak in the velocity time-history.*
Acceleration Spectrum Intensity, ***ASI***	$ASI = \int S_A(5\%, T)dT$ *$S_A(5\%,T)$ = spectral acceleration for 5% damping, T = natural period.*
Velocity Spectrum Intensity, ***VSI***	$VSI = \int S_V(5\%, T)dT$ *$S_V(5\%,T)$ = spectral pseudo-velocity for 5% damping, T = natural period.*
Acceleration Parameter A_{95}	*the level of acceleration which contains up to 95% of the Arias Intensity.*
Predominant Period, T_P	*the period of the maximum spectral 5% damping acceleration.*
Mean Period, T_{mean}	$T_{mean} = \frac{\sum\left(\frac{C_i^2}{f_i}\right)}{\sum C_i^2}$ *C_i = Fourier amplitude for frequency f_i in the range 0.25–20 Hz.*
Significant Duration, D_{sig}	*is the interval of time between the accumulation of 5% and 95 % of Arias Intensity.*
Destructiveness Potential Factor, P_D	$P_D = \frac{I_A}{\nu_0^2} = \frac{\pi}{2g}\frac{\int A^2(t)dt}{\nu_0^2}$ *I_A = Arias Intensity, ν_0^2 = square of the number of zero crossings per second of the accelerogram.*
Modified Destructiveness Potential Factor, P_G	$P_G = \frac{I_A}{\nu_0'}$ *ν_0' = number of zero crossings per second of the velocity time-history.*

Table 3.2: *Correlation index, R, between asymmetric sliding response, D, and seismic indices of destructiveness, covering the parametric range of our study. The best DPIs for each a_C level are emphasized.*

Destructiveness Potential Index, DPI	a_{C1} = **0.05 g**	a_{C1} = **0.10 g**	a_{C1} = **0.20 g**
Distanse from the Fault, R_F	0.04	0.01	0.003
Peak Ground Acceleration, ***PGA***	0.09	0.18	0.29
Peak Ground Velocity, ***PGV***	0.59	0.32	0.15
Peak Ground Displacement, ***PGD***	0.31	0.10	0.001
Arias Intensity, I_A	0.46	0.64	0.75
Destructiveness Potential Factor, P_D	0.58	0.73	0.69
Modified Destructiveness Potential Factor, P_G	0.69	0.56	0.36
Housner Intensity, I_H	0.52	0.67	0.71
RMS Acceleration, A_{RMS}	0.23	0.25	0.24
RMS Velocity, V_{RMS}	0.54	0.26	0.12
RMS Displacement, D_{RMS}	0.07	0.03	0.004
Spectral Displacement at Period of 1 s, $S_{D/(T=1\ s)}$	0.36	0.53	0.61
Spectral Displacement at Period of 2 s, $S_{D/(T=2\ s)}$	0.61	0.61	0.45
Spectral Displacement at Period of 3 s, $S_{D/(T=3\ s)}$	0.31	0.19	0.05
Spectral Displacement at Period of 4 s, $S_{D/(T=4\ s)}$	0.23	0.08	0
Characteristic Intensity, I_C	0.39	0.51	0.55
Specific Energy Density, S_E	0.49	0.23	0.07
Cumulative Absolute Velocity, ***CAV***	0.44	0.51	0.52
Sustained Maximum Acceleration, ***SMA***	0.16	0.23	0.29
Sustained Maximum Velocity, ***SMV***	0.53	0.36	0.16
Acceleration Spectrum Intensity, ***ASI***	0.08	0.17	0.30
Velocity Spectrum Intensity, ***VSI***	0.53	0.68	0.73
Acceleration Parameter, A_{95}	0.11	0.19	0.27
Predominant Period, T_P	0.17	0.15	0.14
Mean Period, T_{mean}	0.15	0.07	0.002
Significant Duration, D_{sig}	0.001	0.003	0.006

Arias Factor

can be an reliable index

of Sliding Response ?

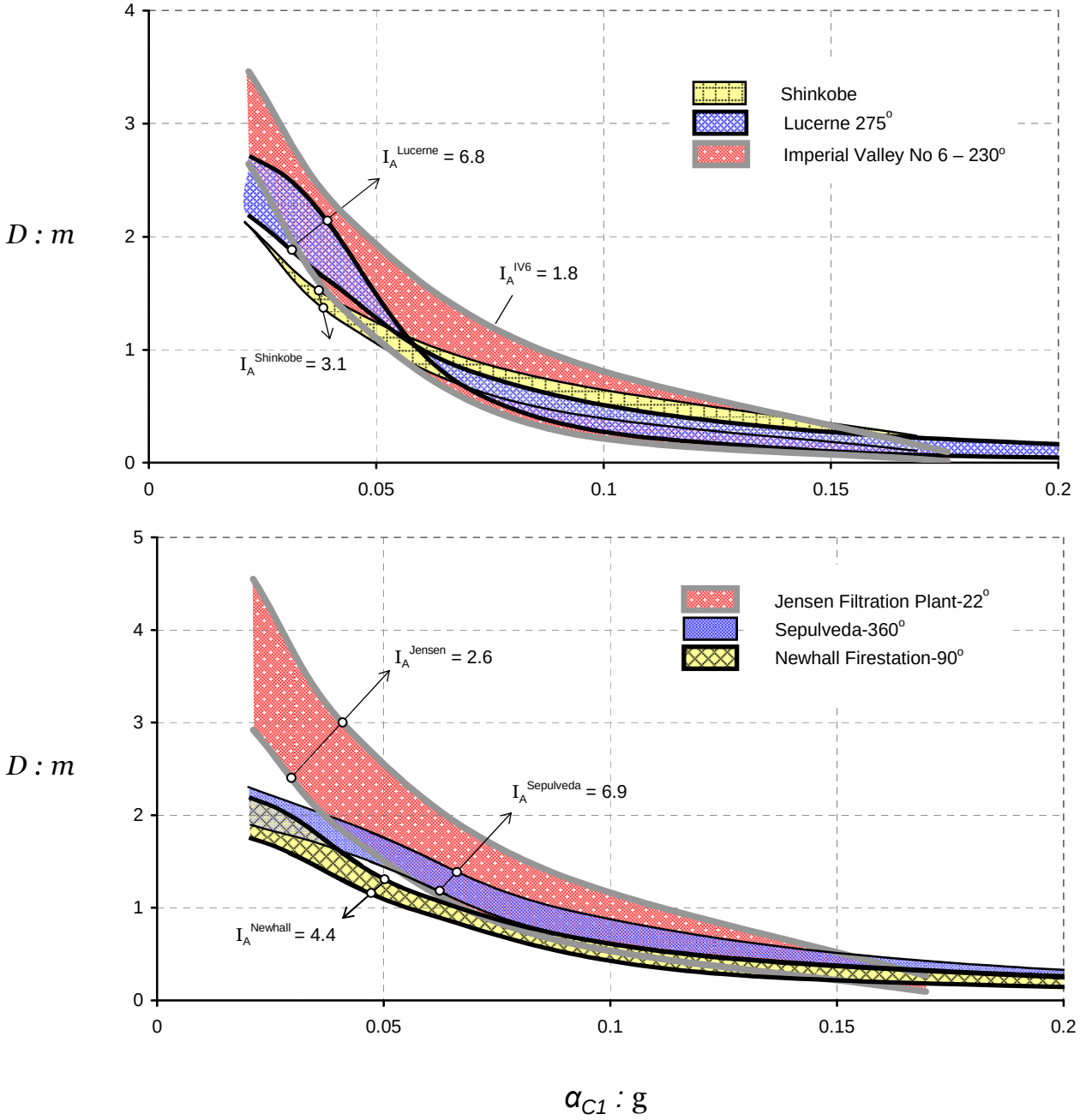

Figure 3.1 *Influence of the absolute value of critical acceleration on sliding displacement for several groups of records. Each excitation is imposed with both polarities and labelled with its Arias Intensity value.*

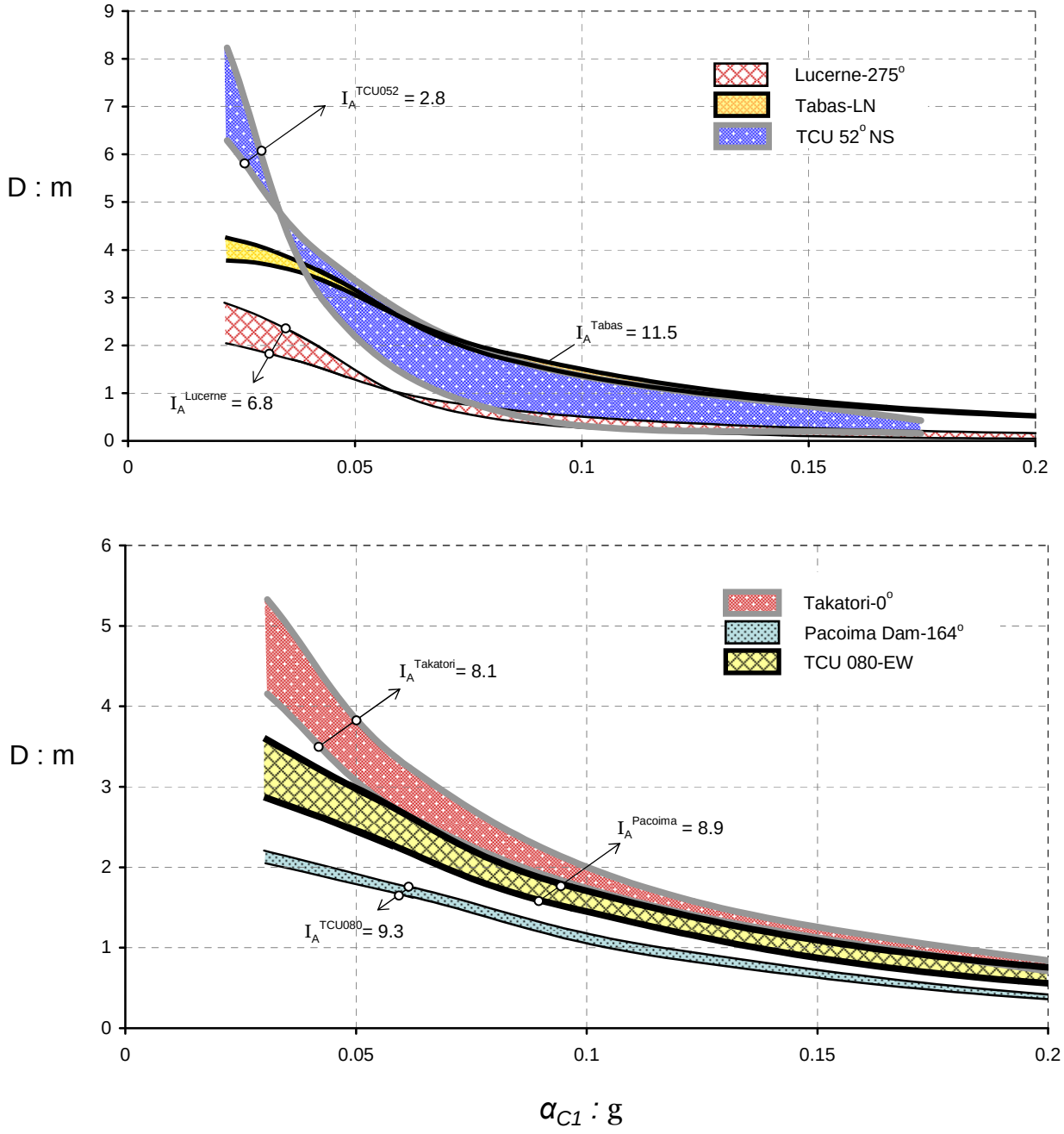

Figure 3.2 *Sliding displacement versus critical acceleration for two different groups of records. Ground accelerations imposed with both polarities. Notice that as Arias Intensity increases, the induced slippage does not necessarily increases too.*

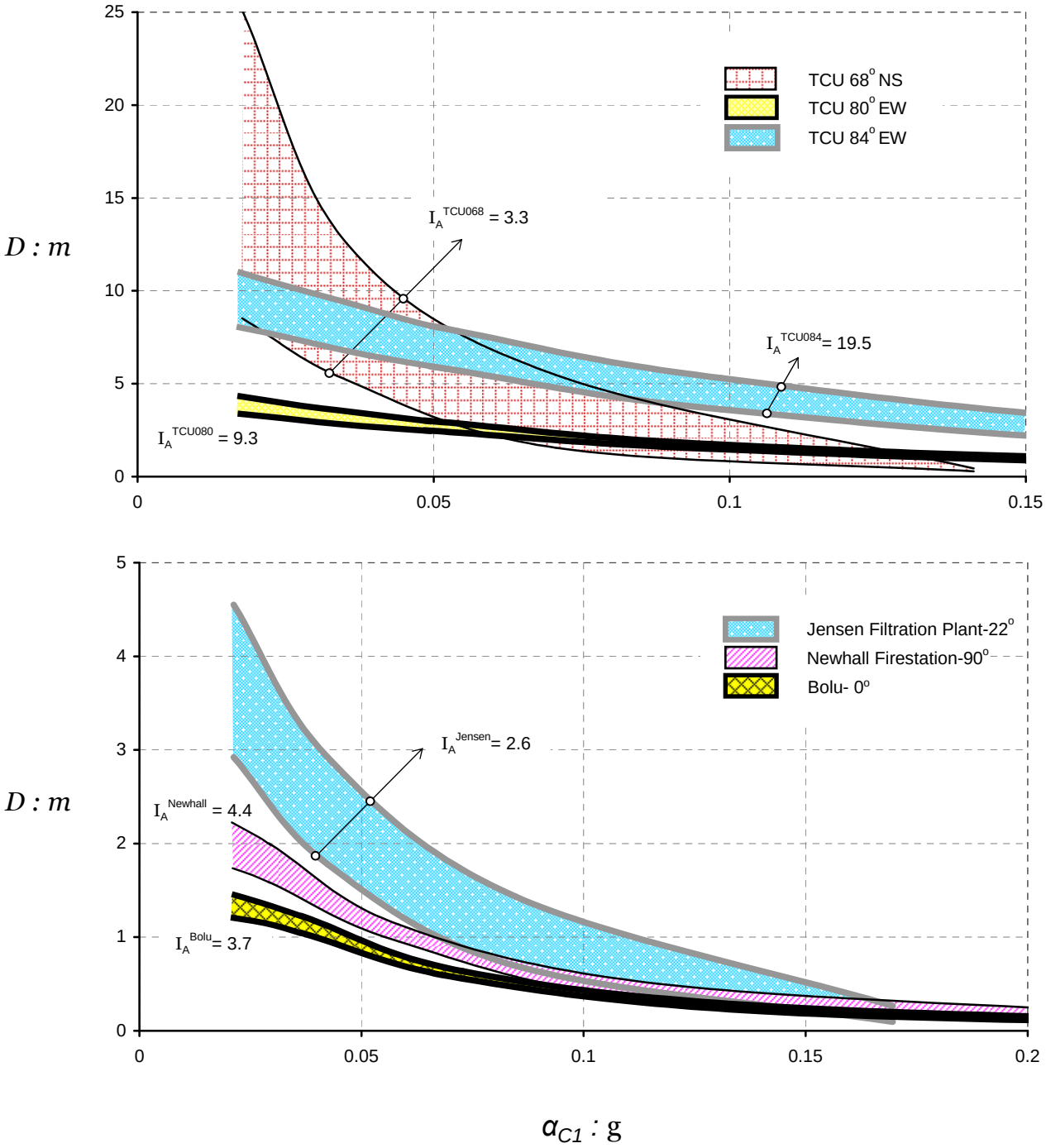

Figure 3.3 *Induced slippage with respect to critical acceleration : No convincing correlation could be found between the accumulated slip and the Arias Intensity, I_A, of the records. A "mere" reversal of polarity, while leaving I_A unchanged, may lead to differences by a factor of 3 or more.*

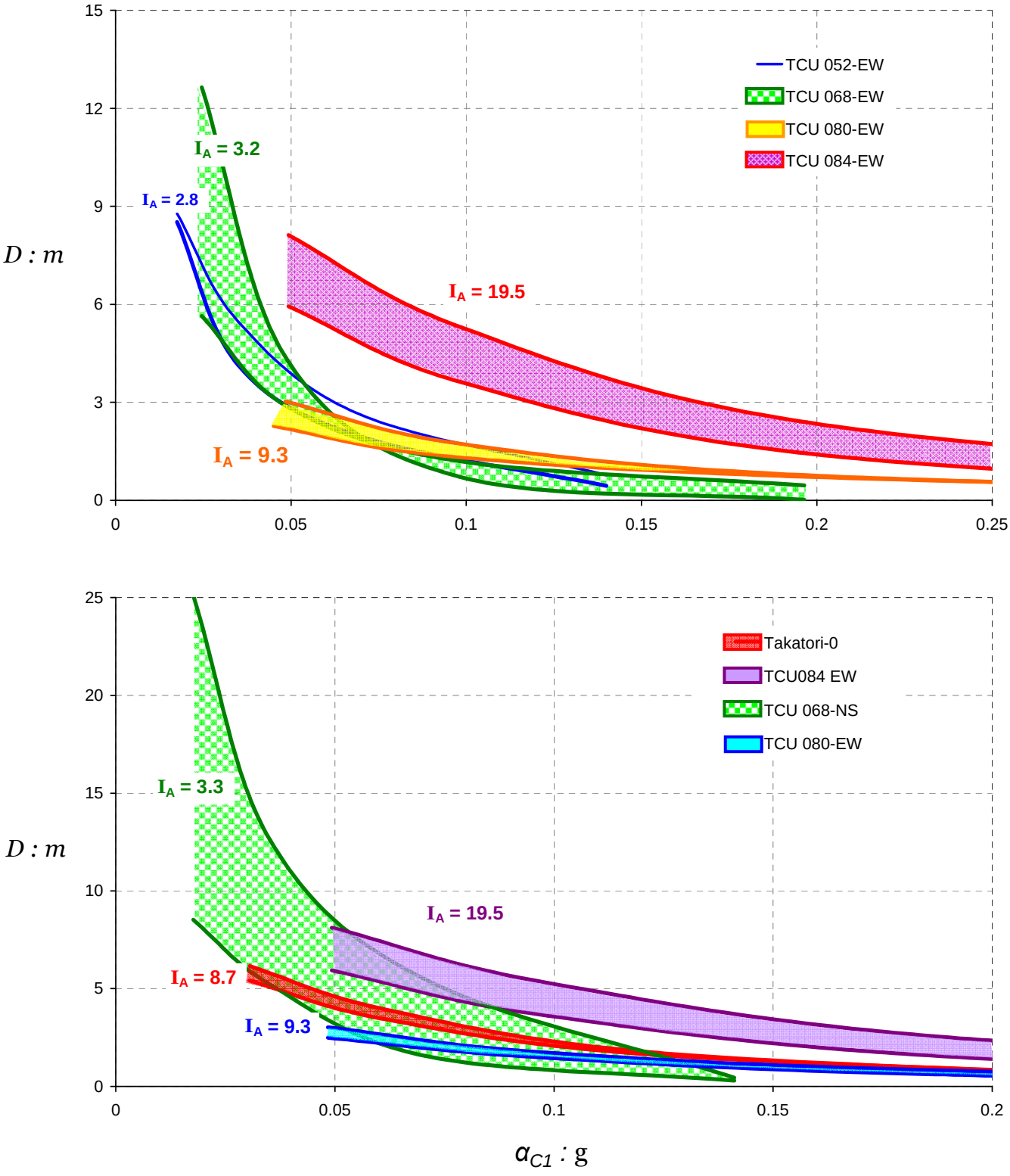

Figure 3.4 *Induced slippage with respect to critical acceleration : No convincing correlation could be found between the accumulated slip and the Arias Intensity, I_A, of the records. Here the case of the most destructive Chi-chi records compared among them (top figure) and with the strongest Kobe motion of Takatori (bottom).*

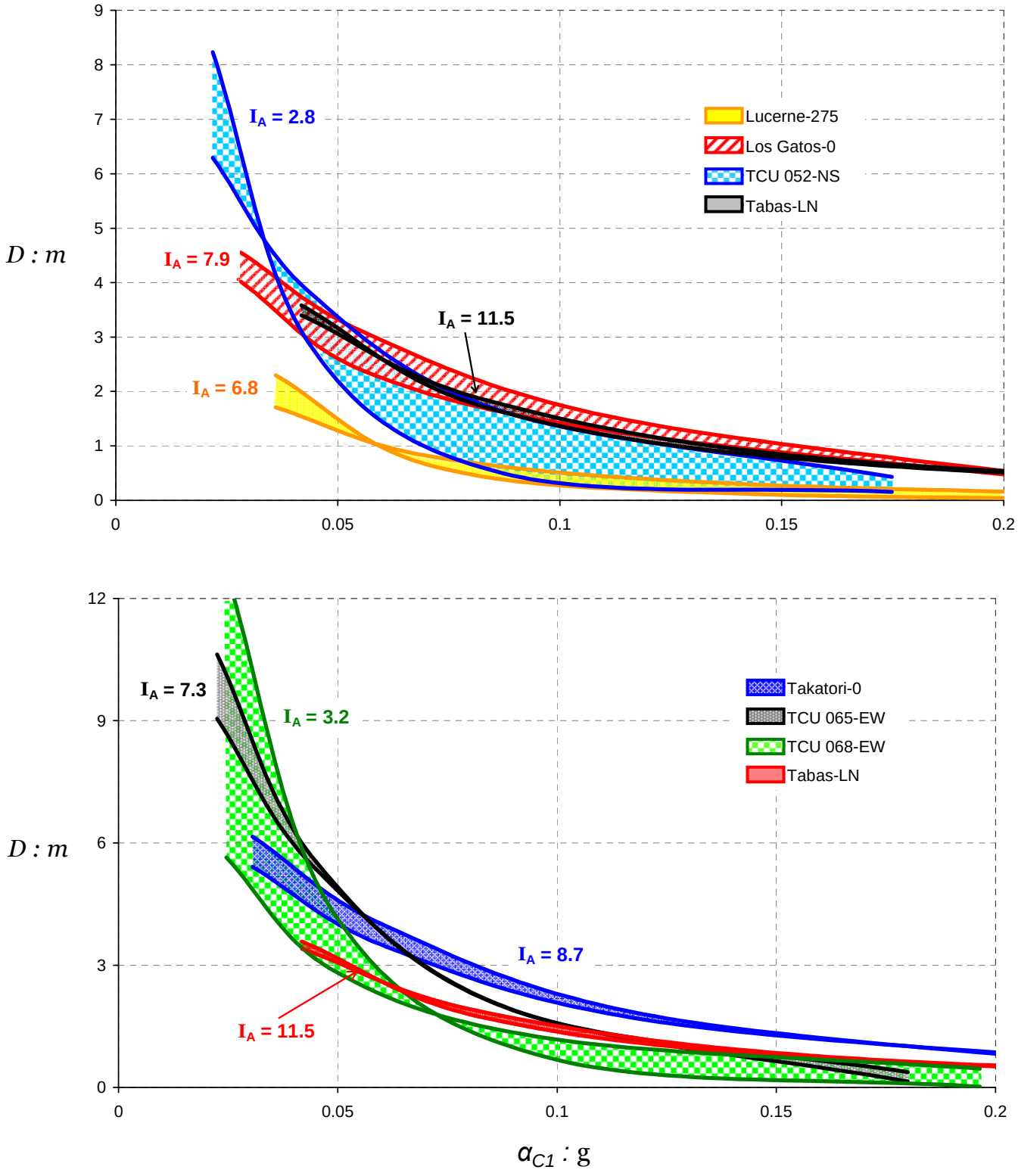

Figure 3.5 *Induced slippage with respect to critical acceleration : the case of Tabas record. Even though the Arias Intensity, I_A , of the particular motion is as high as 11.5 it can not surpass numerous other excitations with I_A significantly lower (more than four times smaller).*

Seismological Parameters and Sliding Response

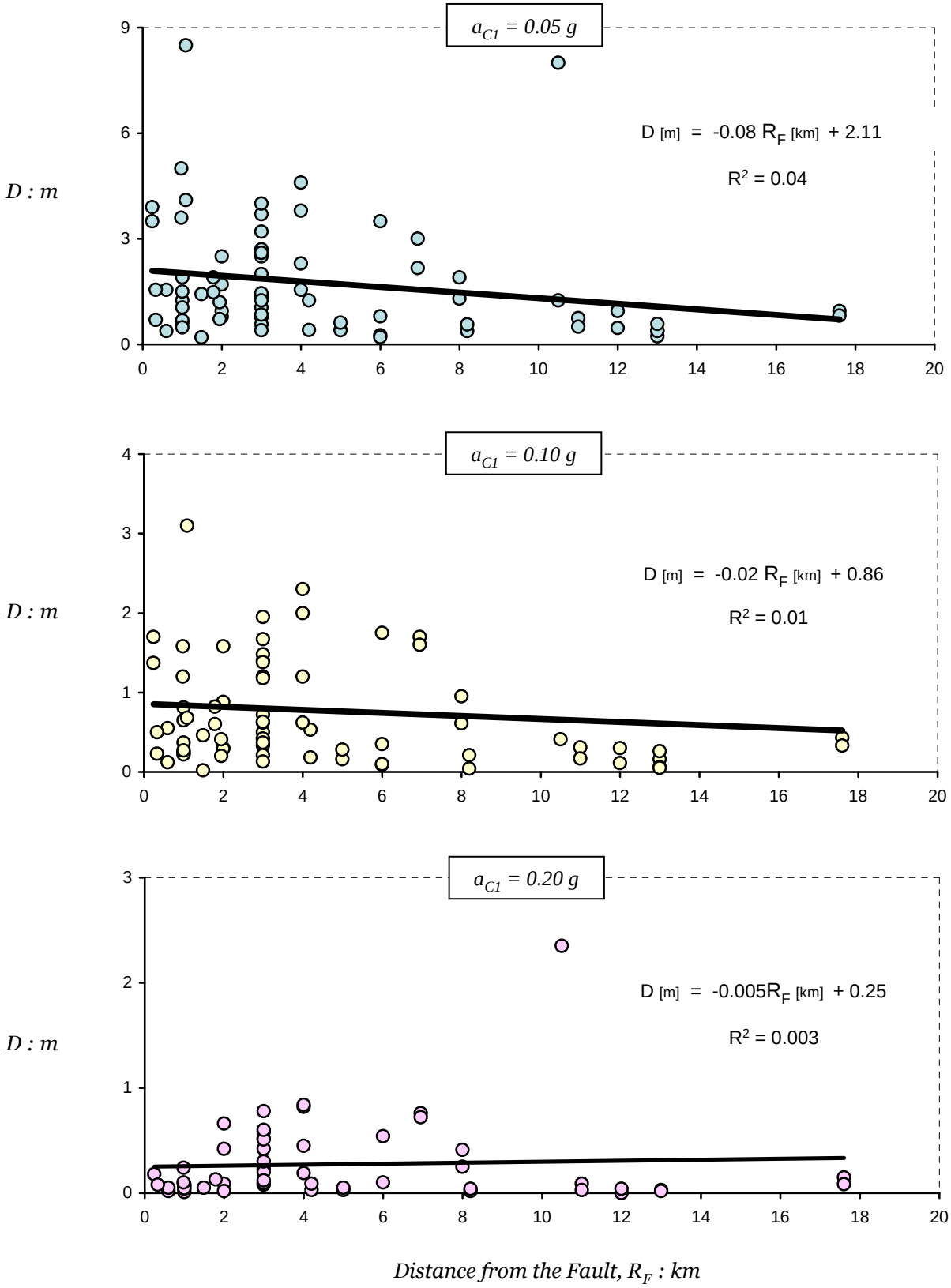

Figure 3.6 *Slippage, D, induced by ground motions recorded at a distance, $R_{F,}$ from the fault. No correlation is achieved by near-fault motions utilized in this study.*

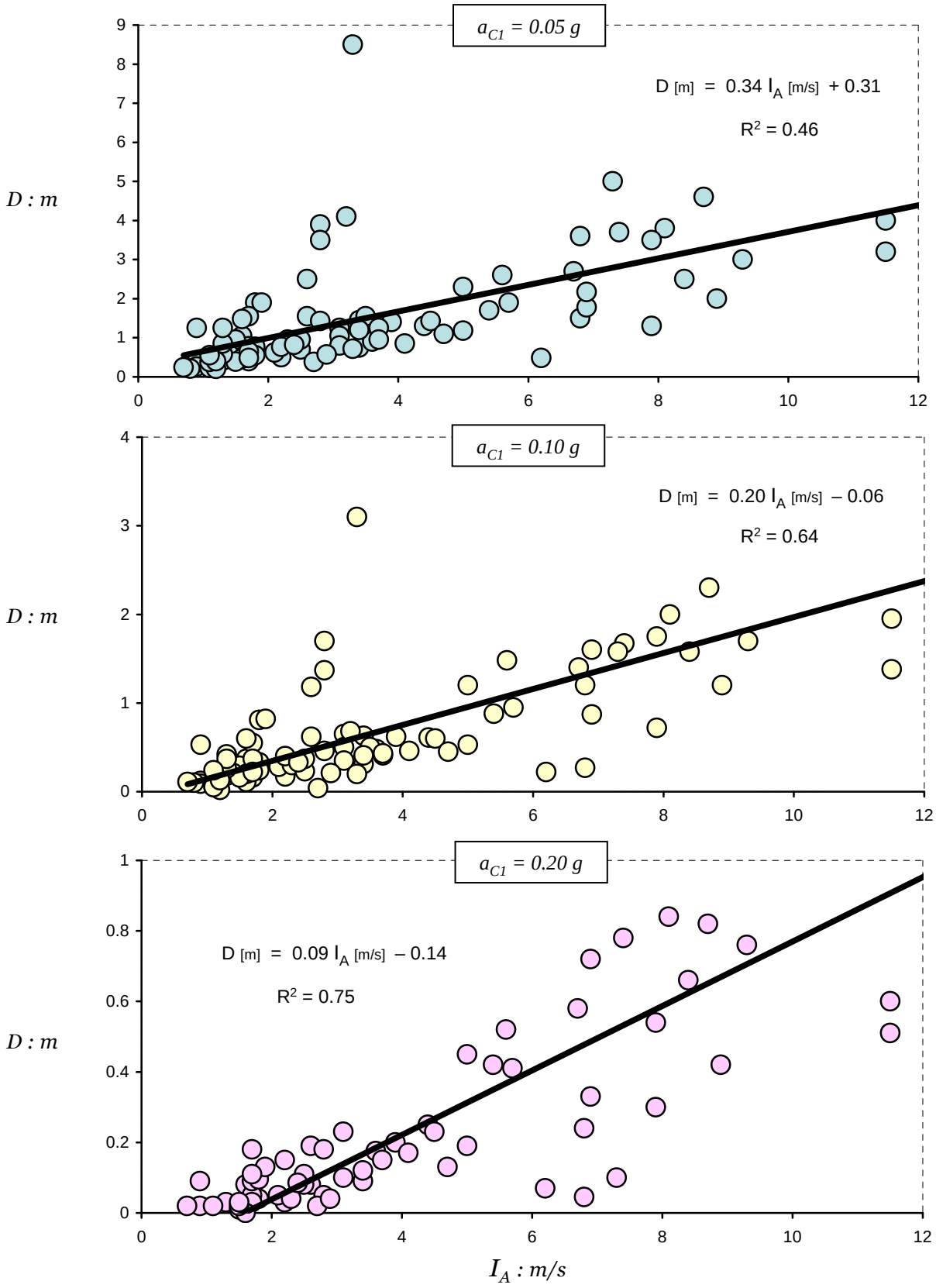

Figure 3.7 *Correlation between the Arias Intensity, I_A, of the records utilized as excitation in our study and the triggered sliding displacement, D, for three values of critical acceleration a_{C1}. A linear trend line is plotted for each case, with the correlation index, R2, stated.*

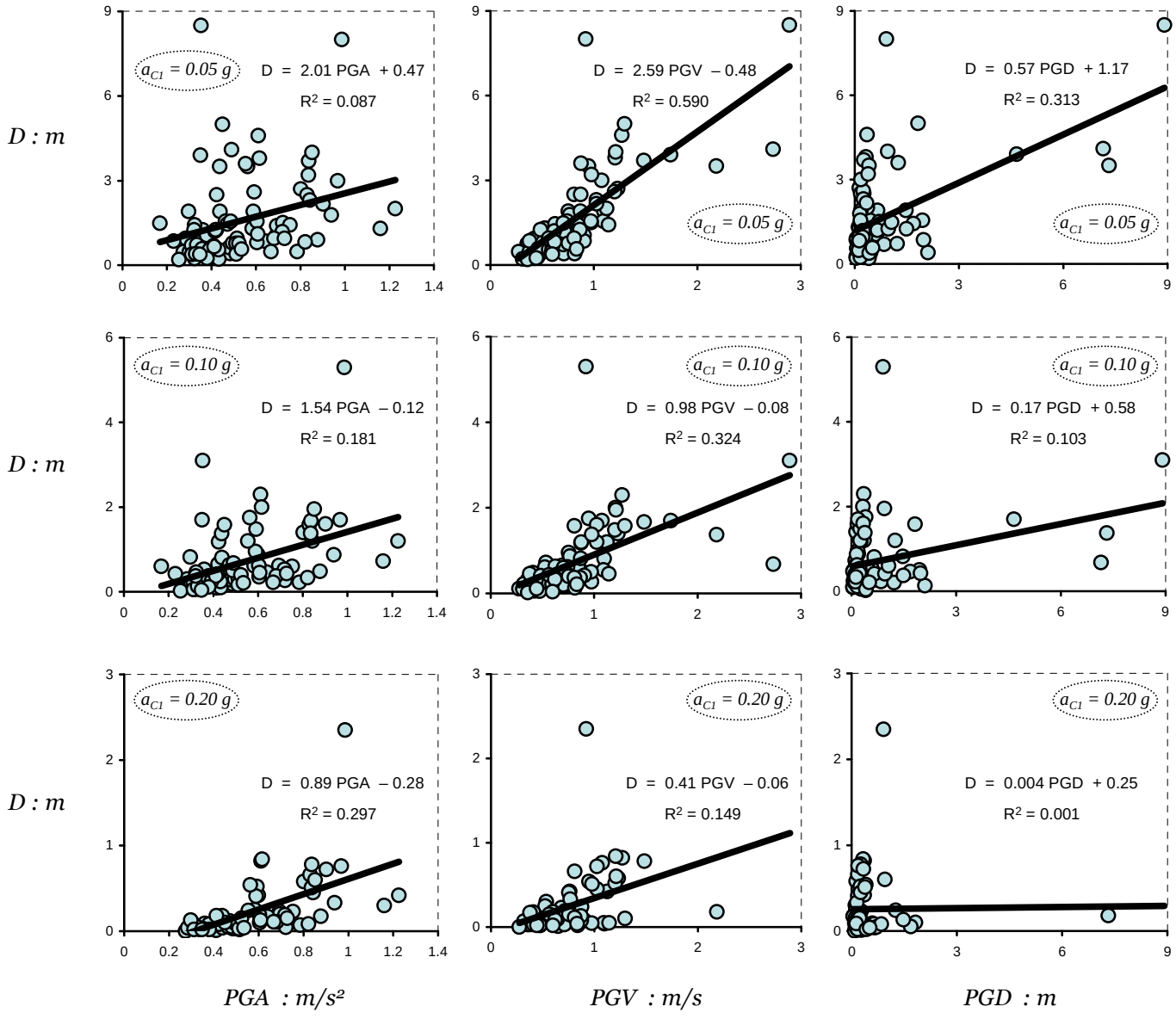

Figure 3.8 *Slippage, D, with respect to the most widely used ground motion characteristics: (a) peak ground acceleration–in the first column from the left, (b) peak ground velocity–in the second column, and (c) peak ground displacement–in the last column to the left.*

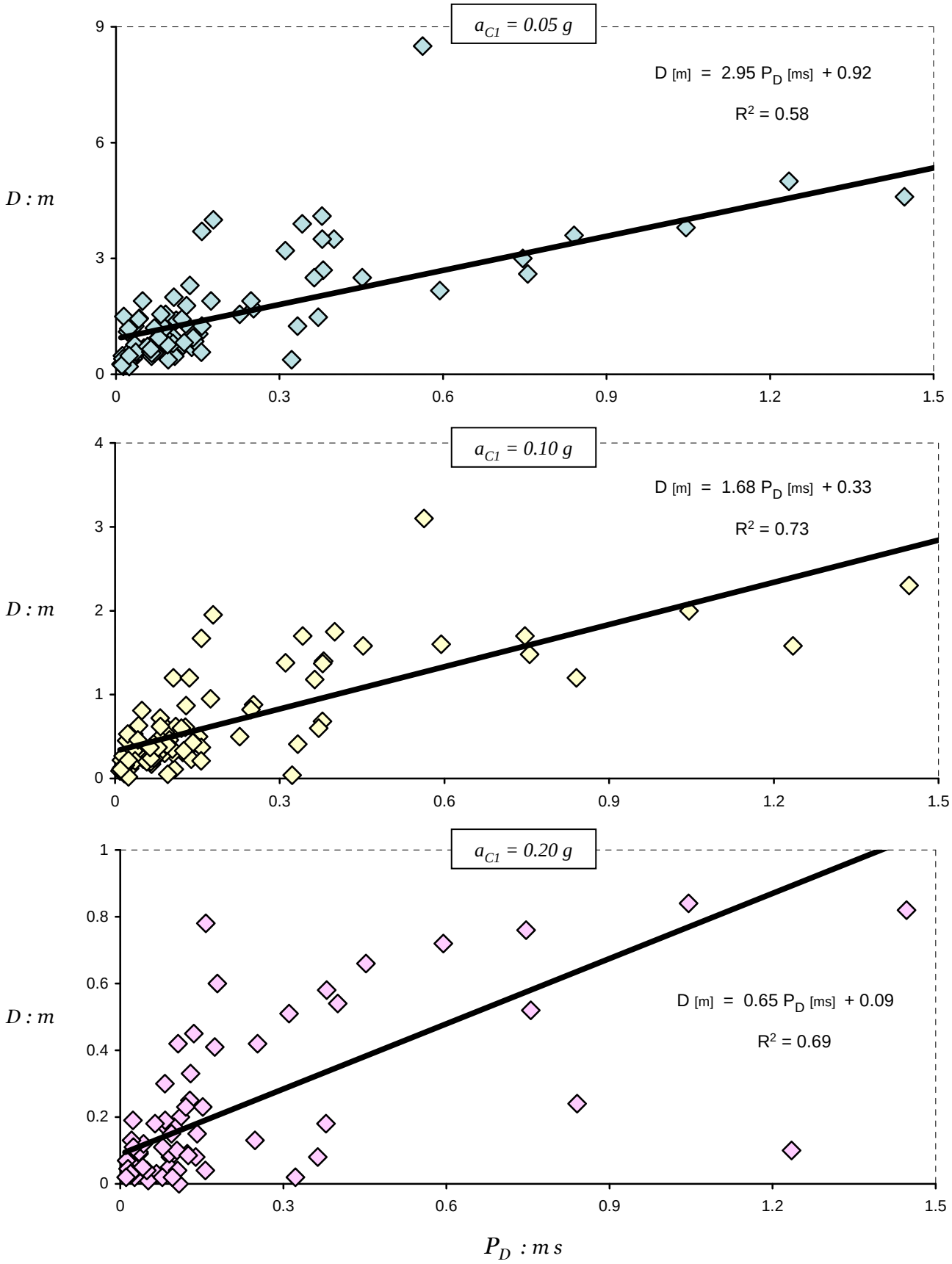

Figure 3.9 *The influence of potential destructiveness factor P_D (as defined by Araya & Saragoni, 1984) on sliding displacement D, for three levels of critical yielding acceleration a_{C1}: 0.05* g, *0.1* g, *and 0.2* g.

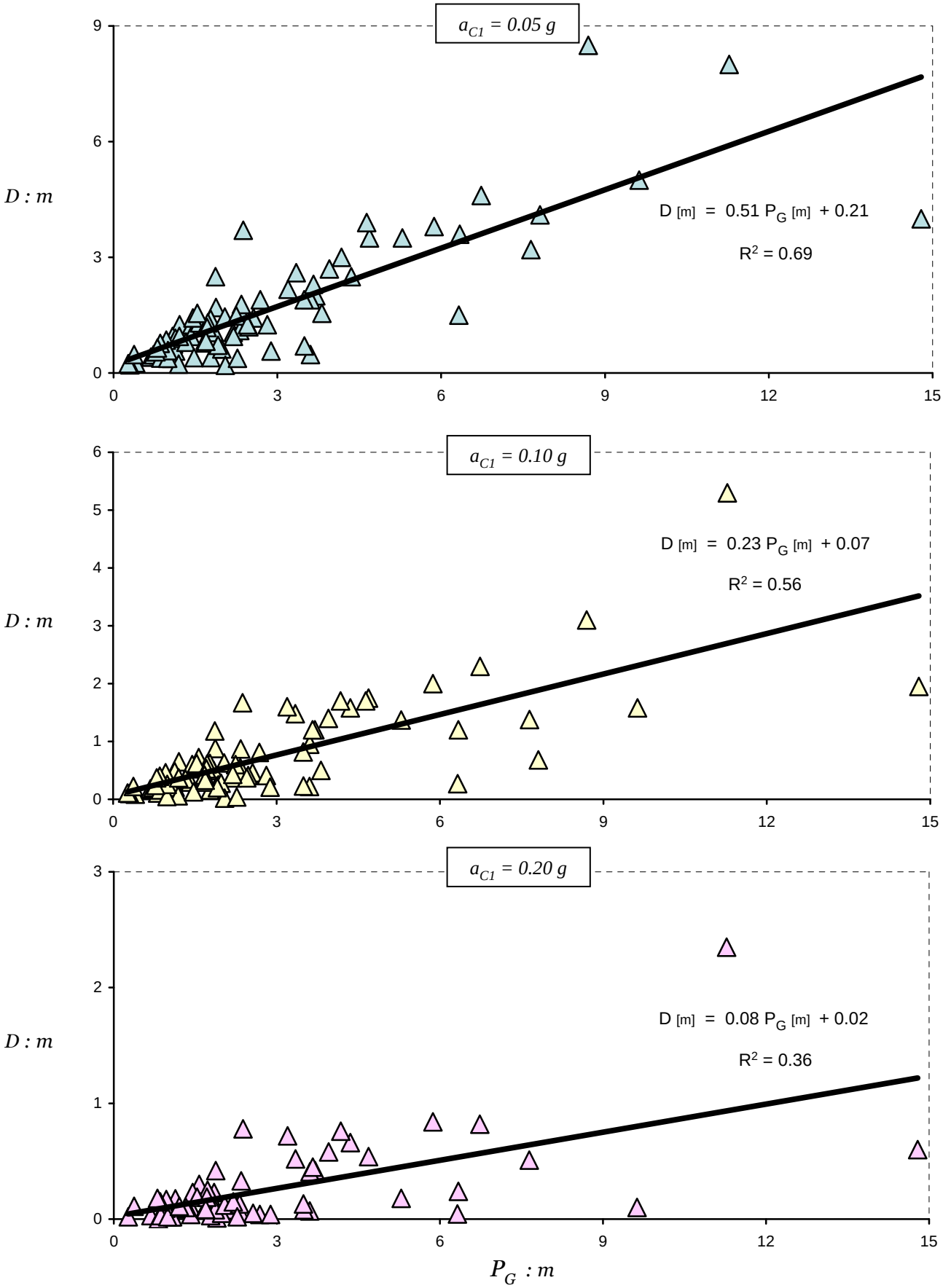

Figure 3.10 *Effect of the "velocity modified"-potential destructiveness factor, P_G, on sliding displacement D, for three levels of critical yielding acceleration a_{C1}.*

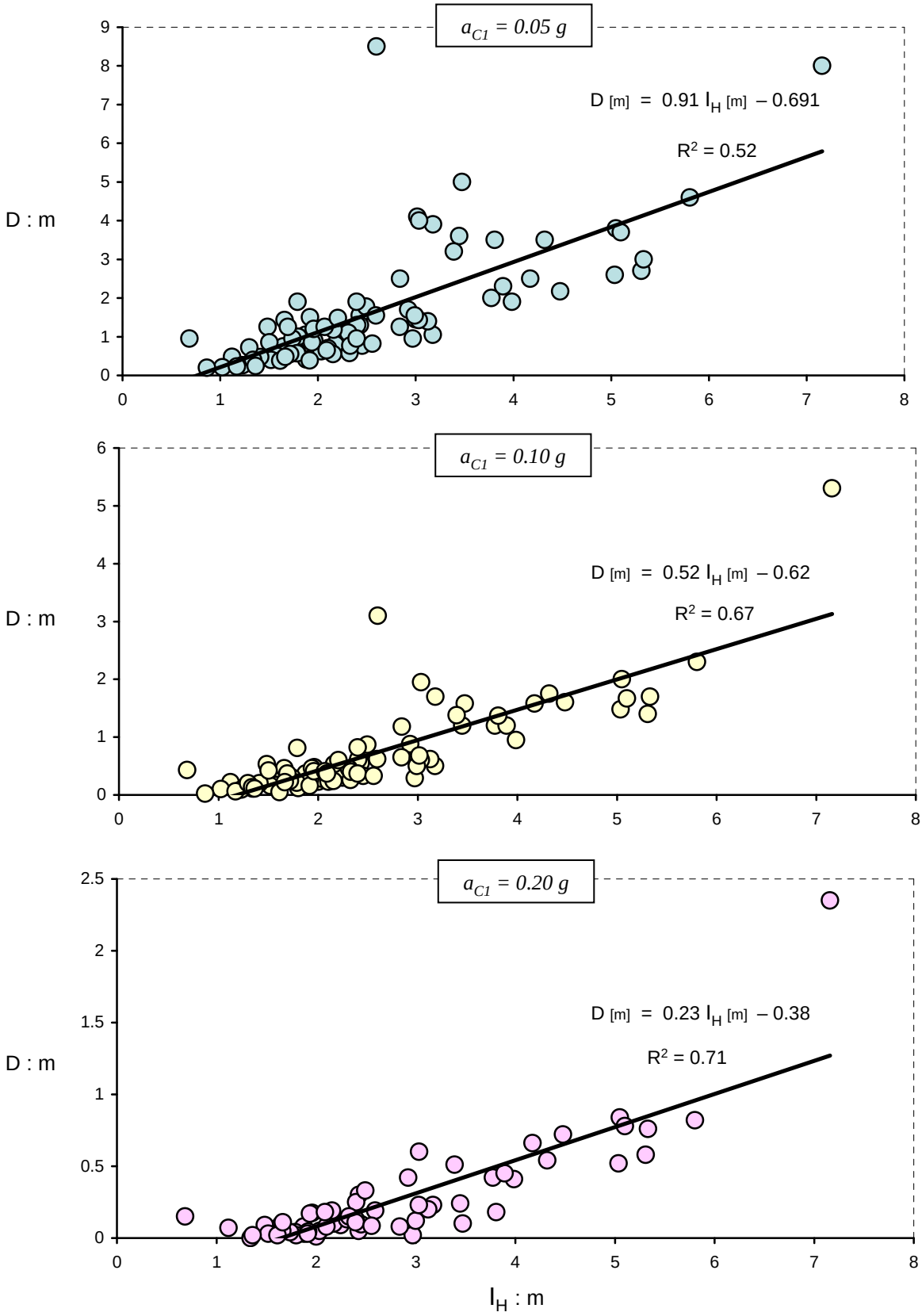

Figure 3.11 *Correlation between the Housner Intensity, I_H, of the records utilized as excitation in our study and the triggered sliding displacement, D, for three values of critical acceleration a_{C1}. A linear trend line is plotted for each case, with the correlation index, R^2, stated.*

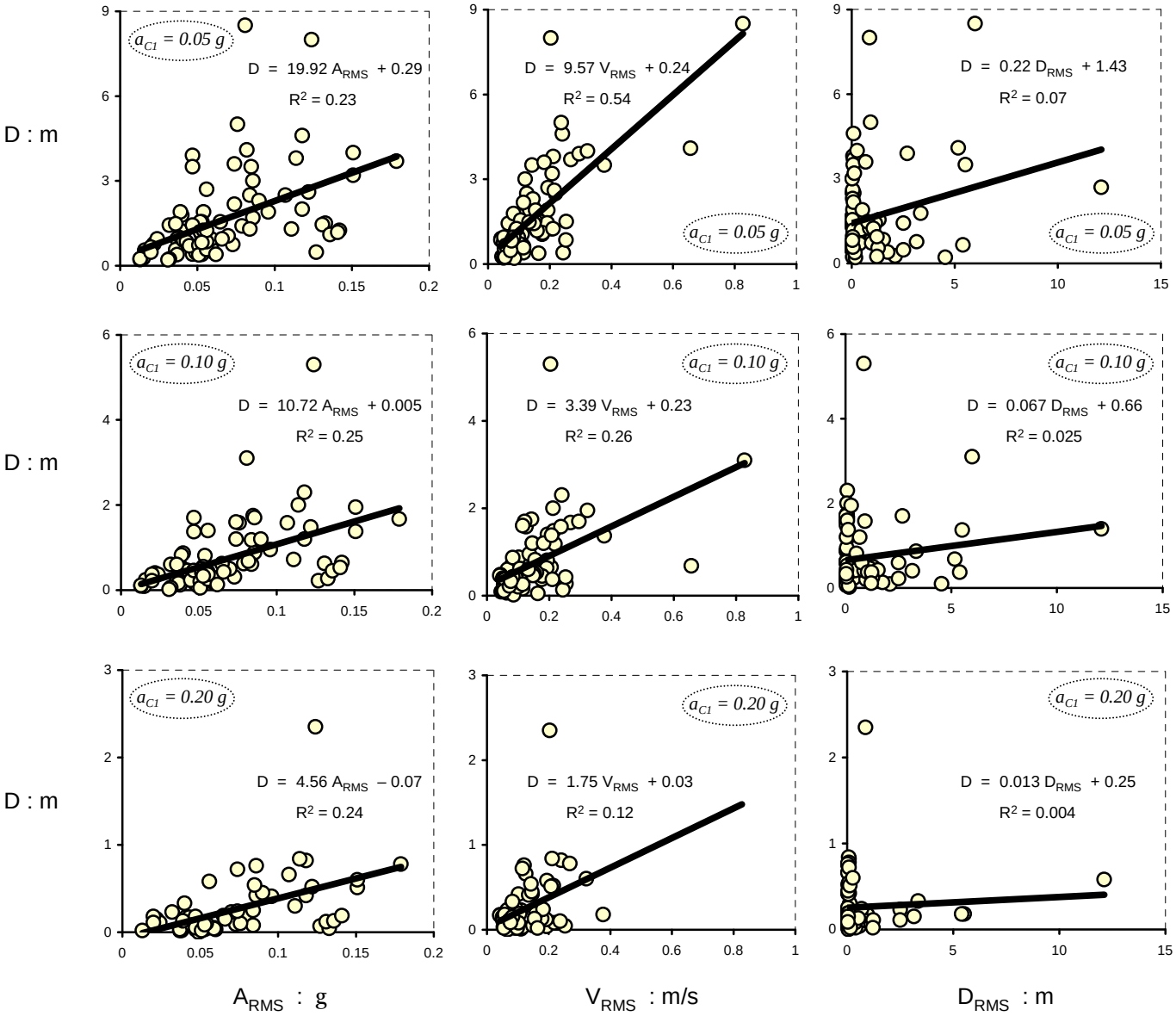

Figure 3.12 *Slippage, D, in connection with the Root Mean Square values: (a) RMS acceleration–in the first column from the left, (b) RMS velocity–in the second column, and (c) RMS displacement–in the last column to the left.*

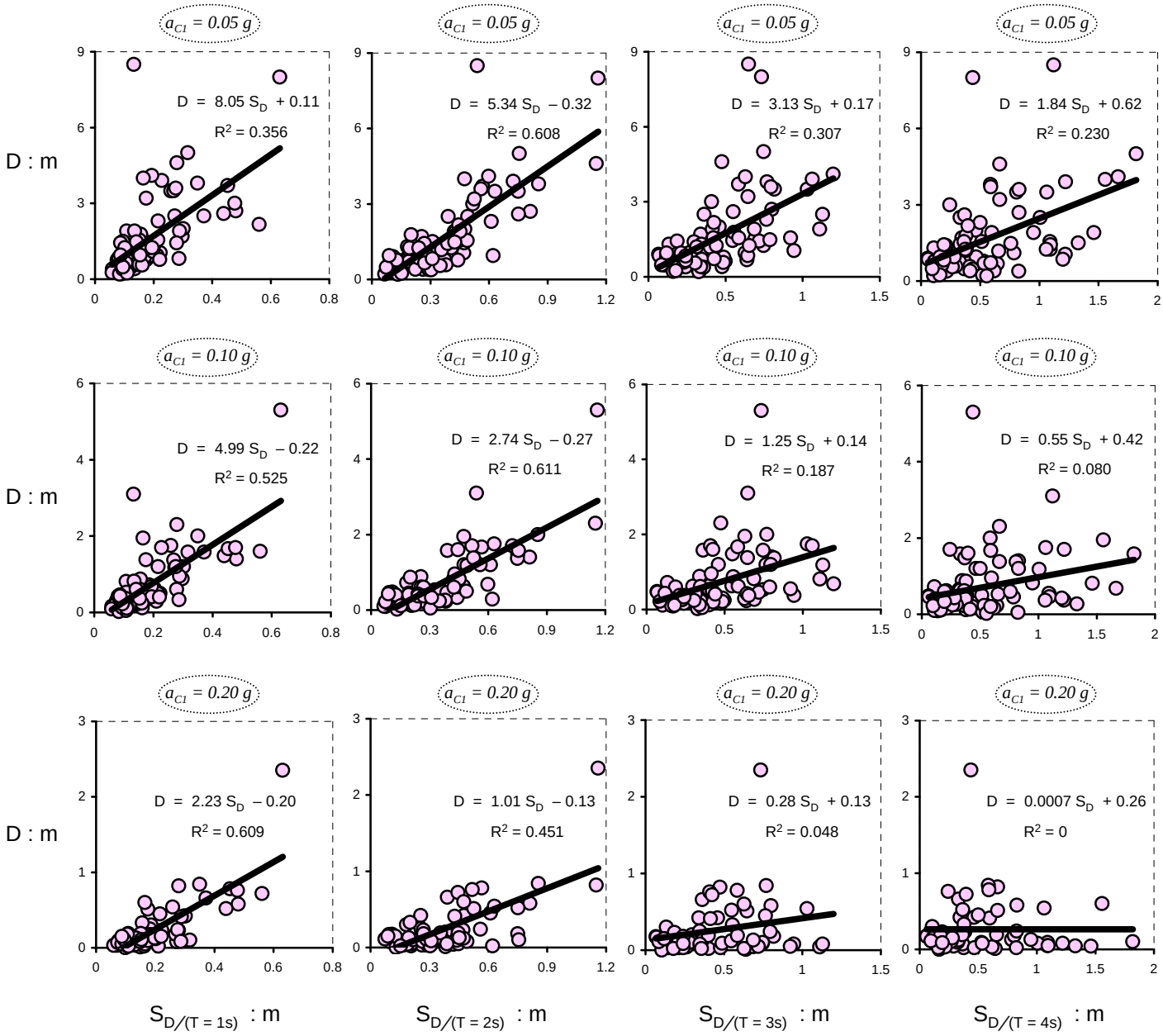

Figure 3.13 *Correlation of slippage, D, with its corresponding spectral displacement at four different periods, T: (a) for period of 1 sec–in the first column from the left, (b) for period of 2 sec–in the second column, (c) for period of 3 sec–in the third column, and (d) for period of 4 sec–in the last column to the left.*

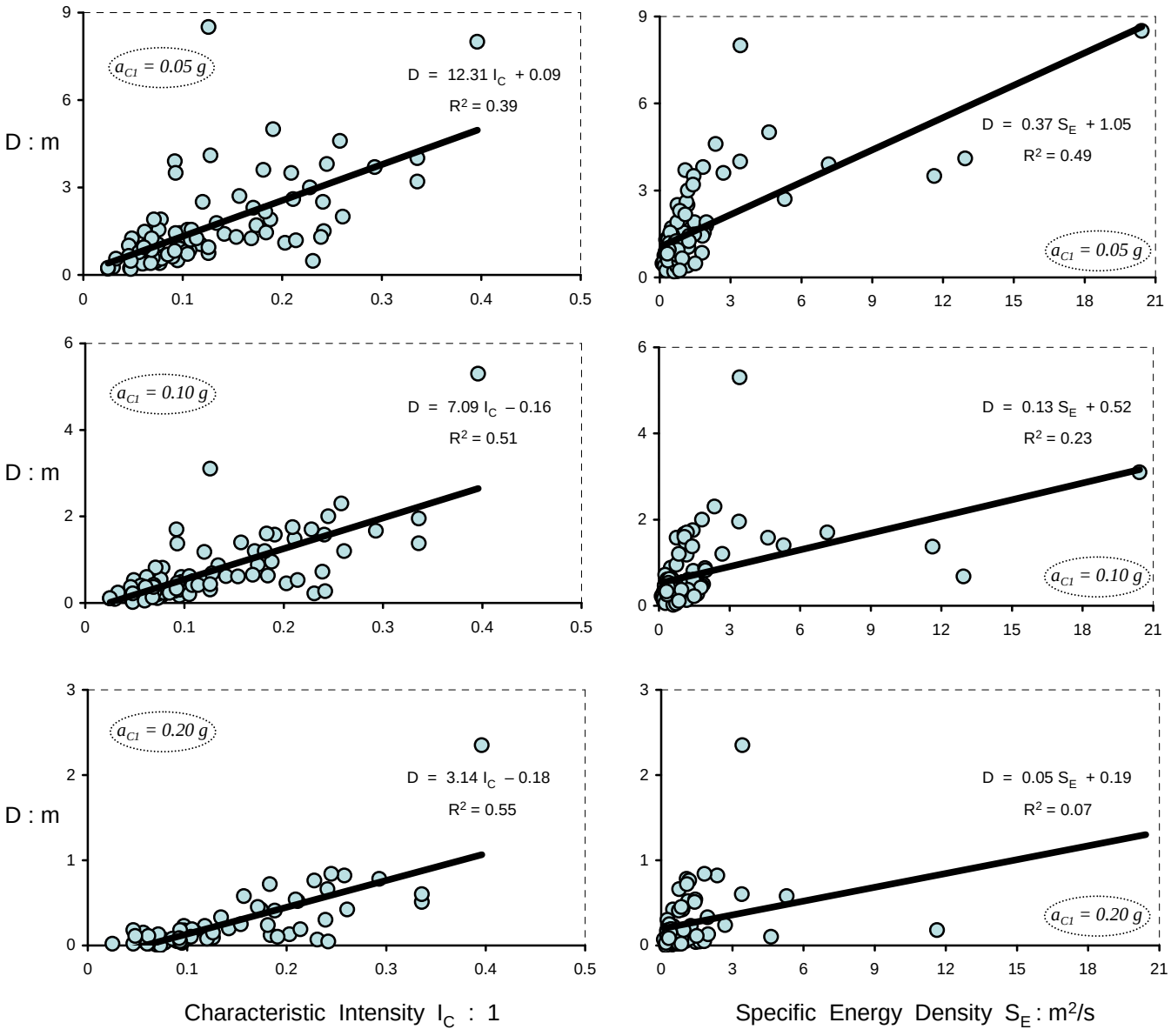

Figure 3.14 *Influence of the dimensionless parameter of characteristic intensity, I_C , on slippage, D, at the left hand-side and effect of specific energy density, S_E, at the right. Observe the poor correlation of the induced slippage with the energy density value of each earthquake event.*

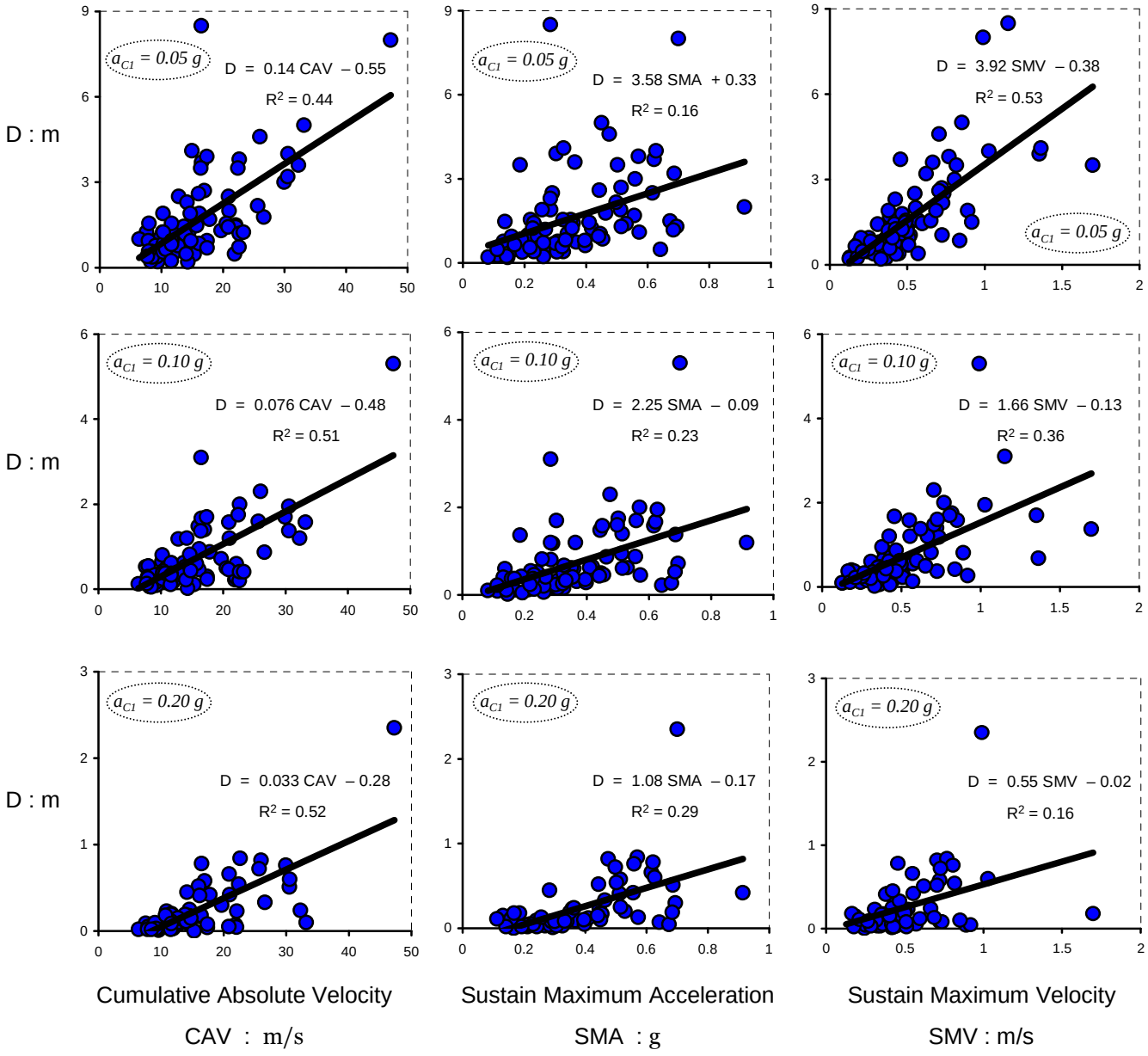

Figure 3.15 *Slippage, D, as a function of : (a) the cumulative absolute velocity–in the first column from the left, (b) the sustained maximum acceleration–in the second column, and (c) the sustained maximum velocity–in the last column to the left.*

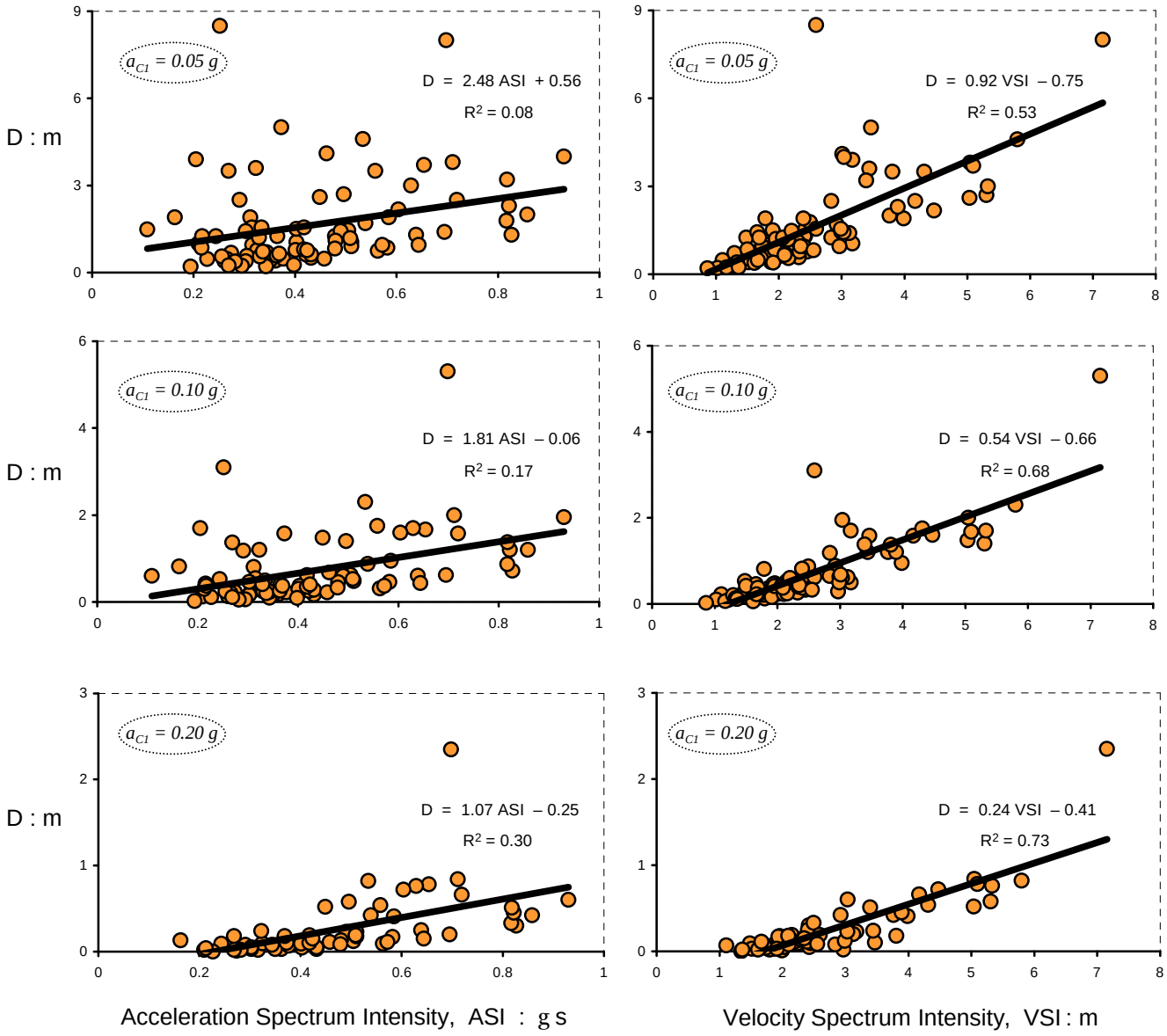

Figure 3.16 *Effect of acceleration spectrum intensity, ASI, and velocity spectrum intensity, VSI, on slippage, D, as illustrated at the left and right hand-side columns respectively.*

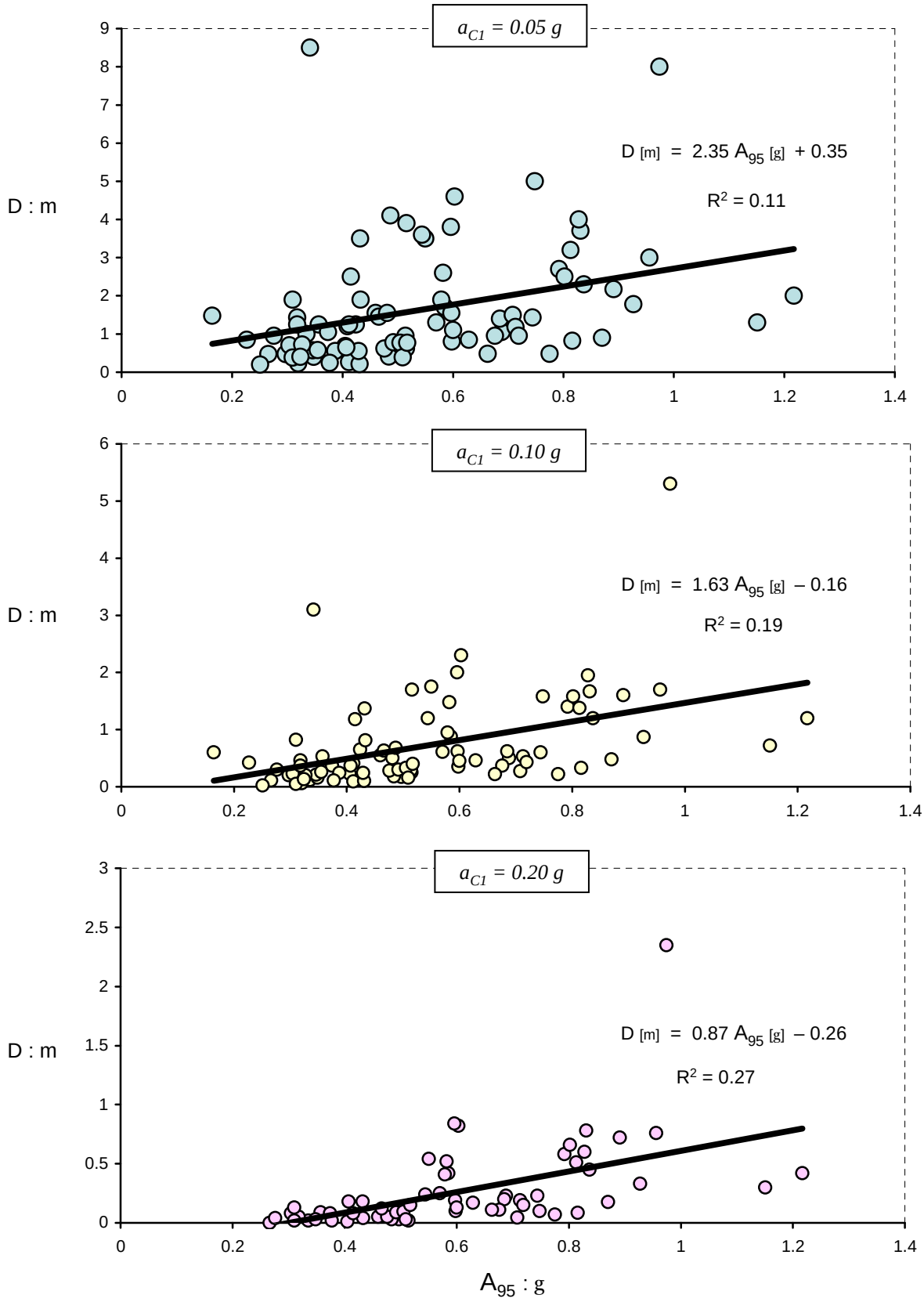

Figure 3.17 *Correlation between the acceleration parameter, A_{95}, and the triggered sliding displacement, D, for three values of critical acceleration a_{C1}. A linear trend line is plotted for each case, with the correlation index, R_2, stated.*

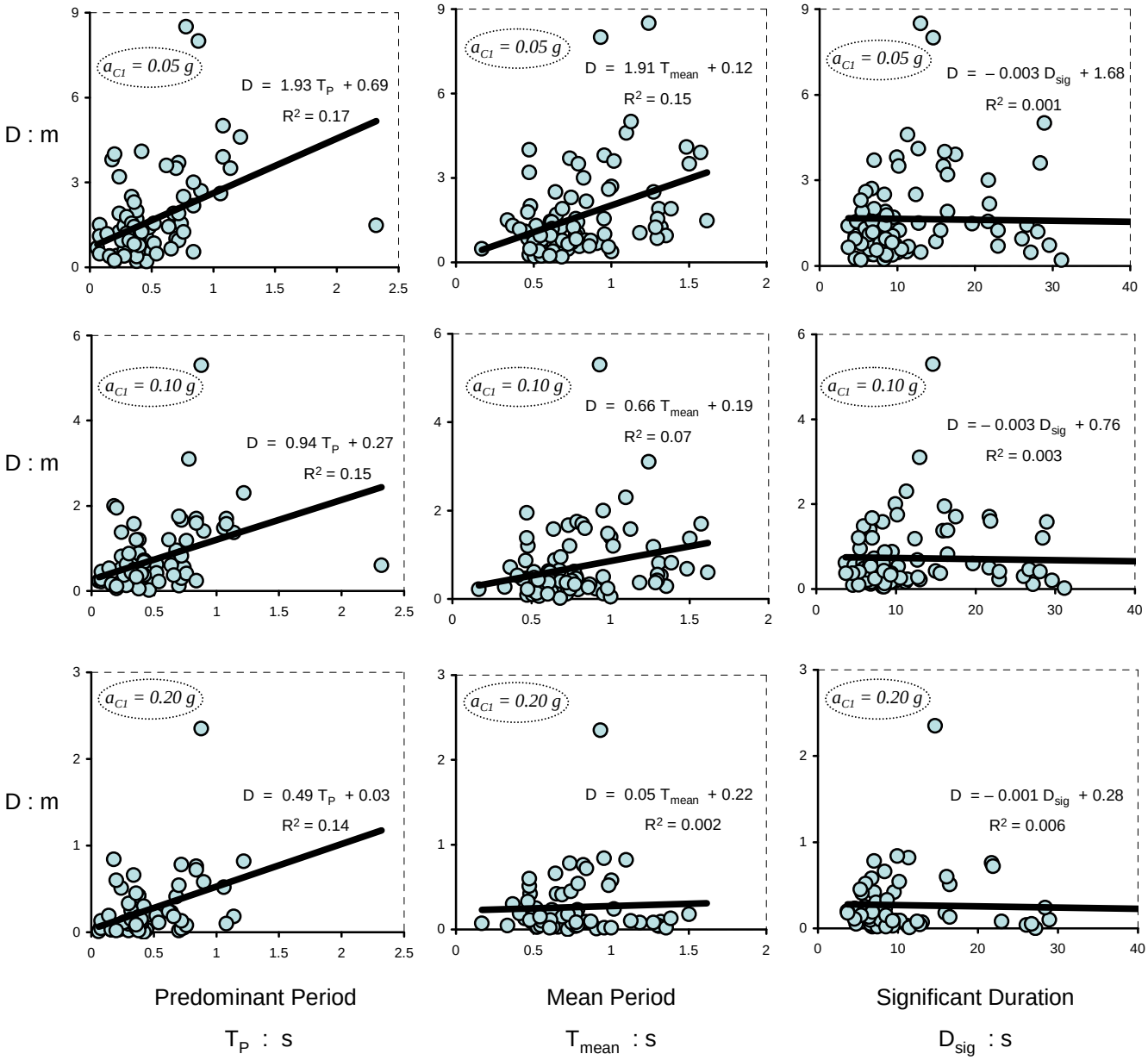

Figure 3.18 *Slippage, D, in connection with: (a) the predominant period of the ground motion–in the first column from the left, (b) the mean period–in the second column, and (c) the significant duration of the record–in the last column to the left.*

Sliding Displacement and Response Spectrum

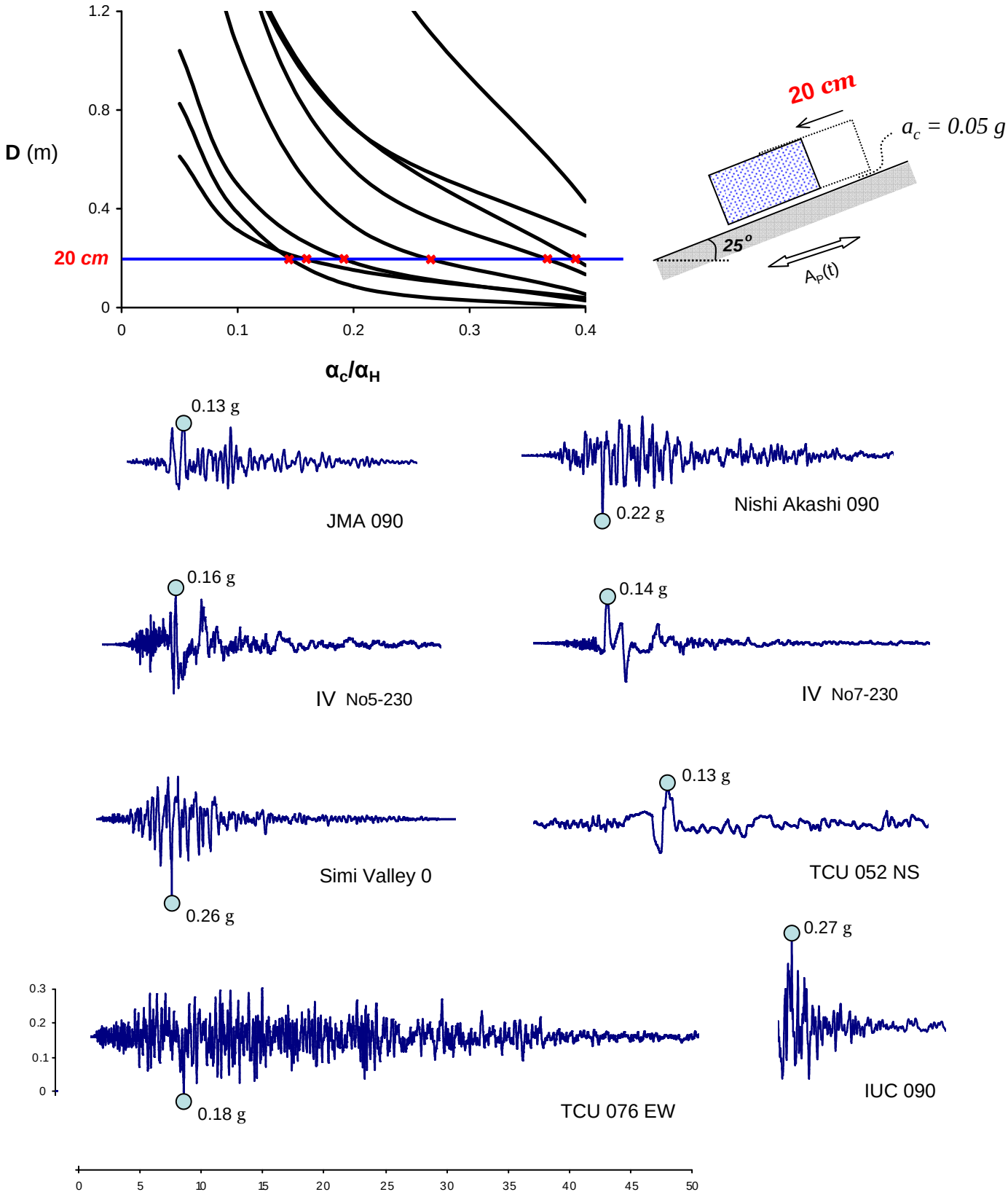

Figure 3.19 *Equivalent acceleration records (with their peak values marked with circle) that induce a slippage of 20 cm to a rigid block with critical yielding acceleration* $a_C = 0.05$ g*, on an inclined base of 25° inclination.*

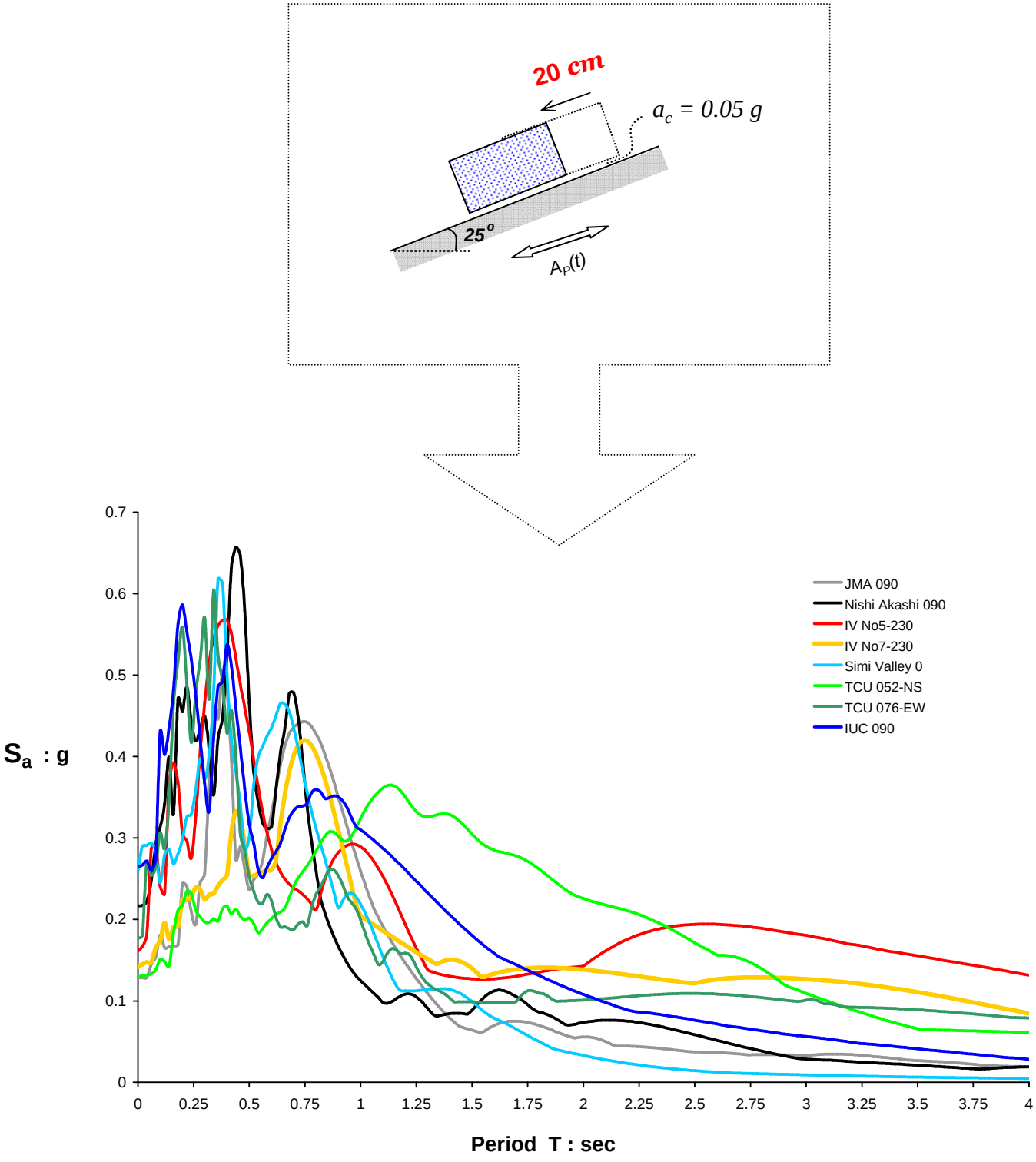

Figure 3.20 *Elastic response spectra of the equivalent acceleration time histories triggering 20 cm of sliding on an inclined base of 25° inclination (a_C = 0.05 g).*

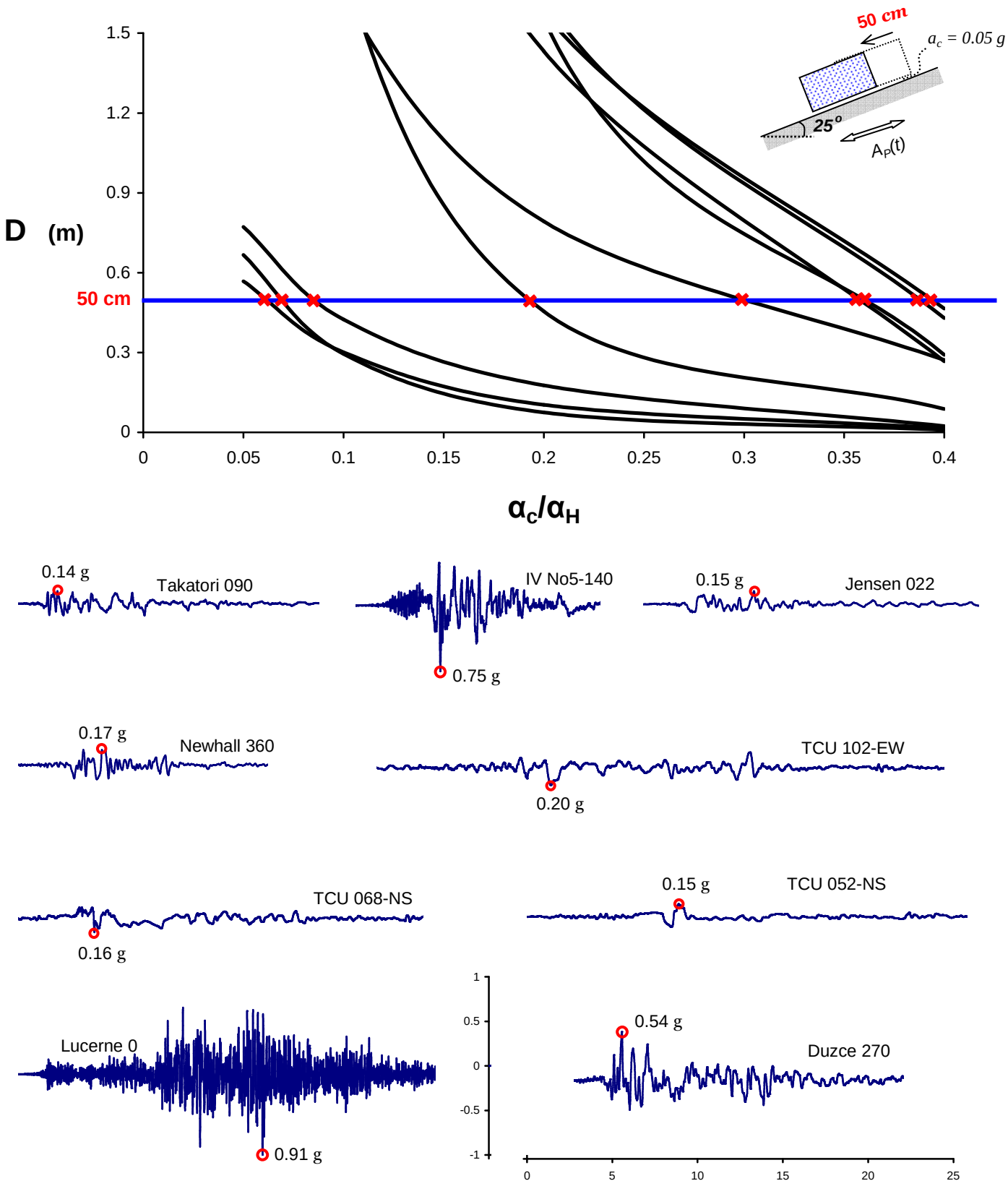

Figure 3.21 *Equivalent acceleration records (with their peak values marked with circle) that induce a slippage of 50 cm to a rigid block with critical yielding acceleration a_C = 0.05 g, on an inclined base of 25° inclination.*

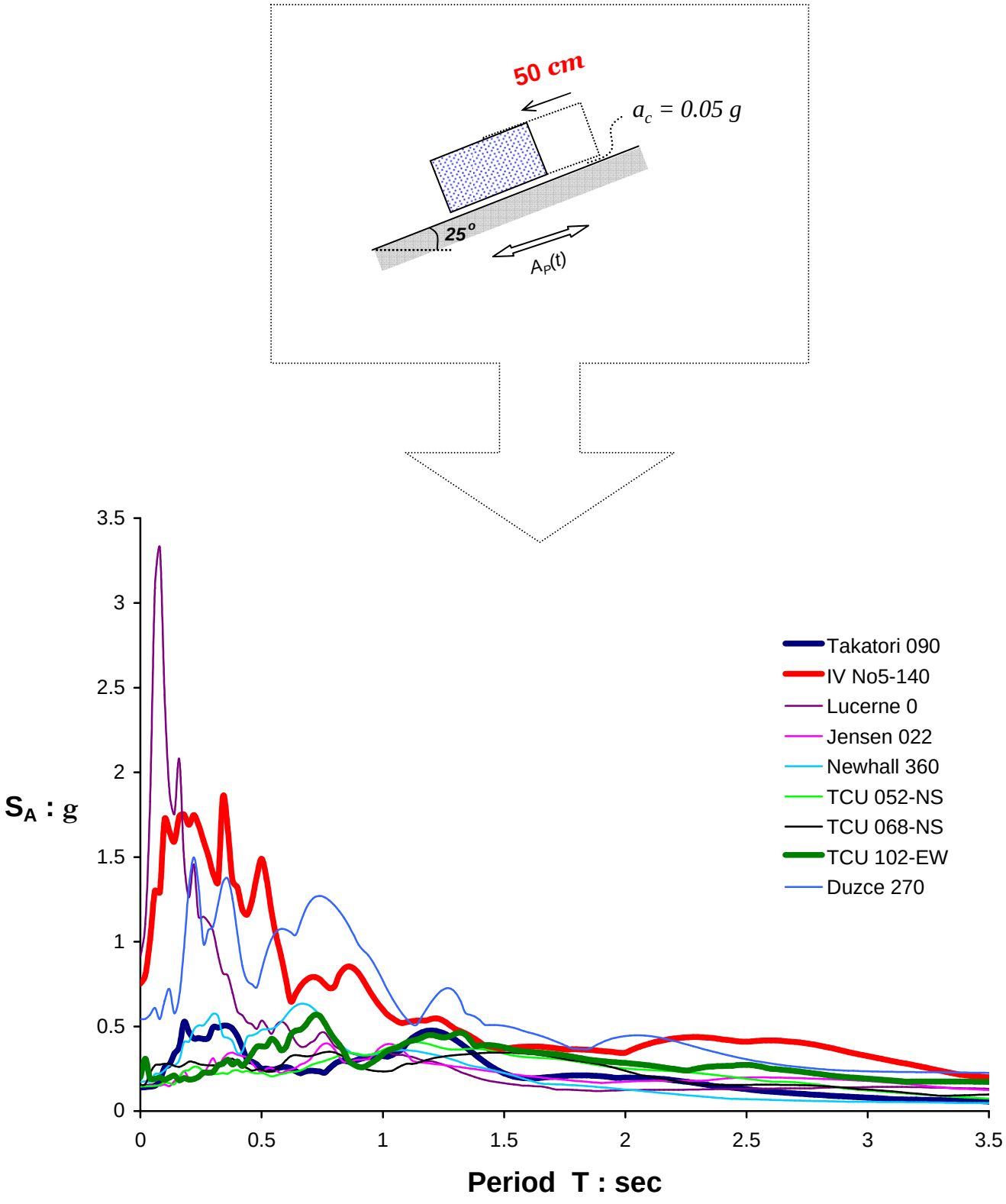

Figure 3.22 *Elastic response spectra of the equivalent acceleration time histories triggering 50 cm of sliding on an inclined base of 25° inclination (a_C = 0.05 g).*

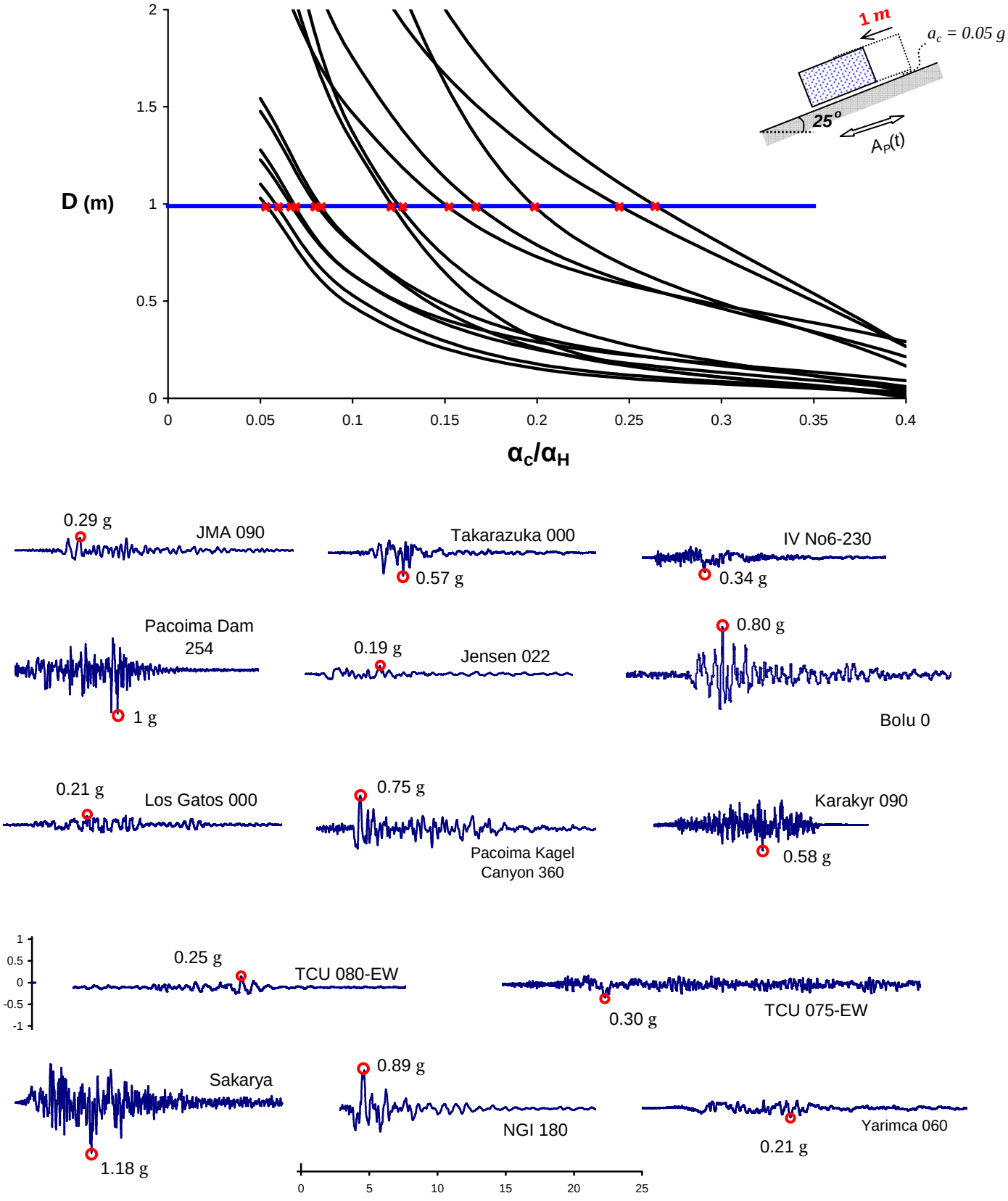

Figure 3.23 *Equivalent acceleration records (with their peak values marked with circle) that induce a slippage of 1 m to a rigid block with critical yielding acceleration a_C = 0.05 g, on an inclined base of 25° inclination.*

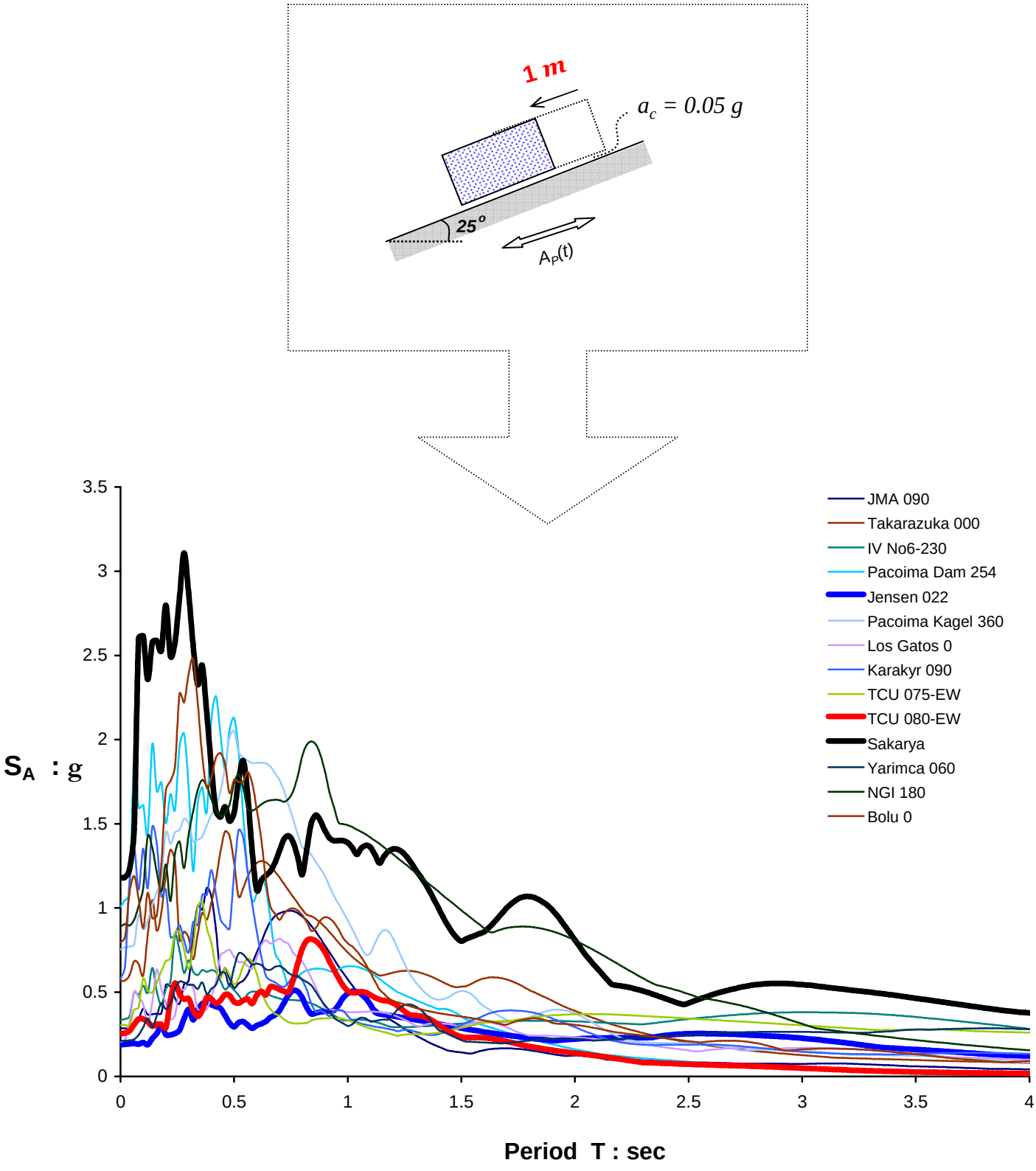

Figure 3.24 *Elastic response spectra of the equivalent acceleration time histories triggering 1 m of sliding on an inclined base of 25° inclination (a_C = 0.05 g).*

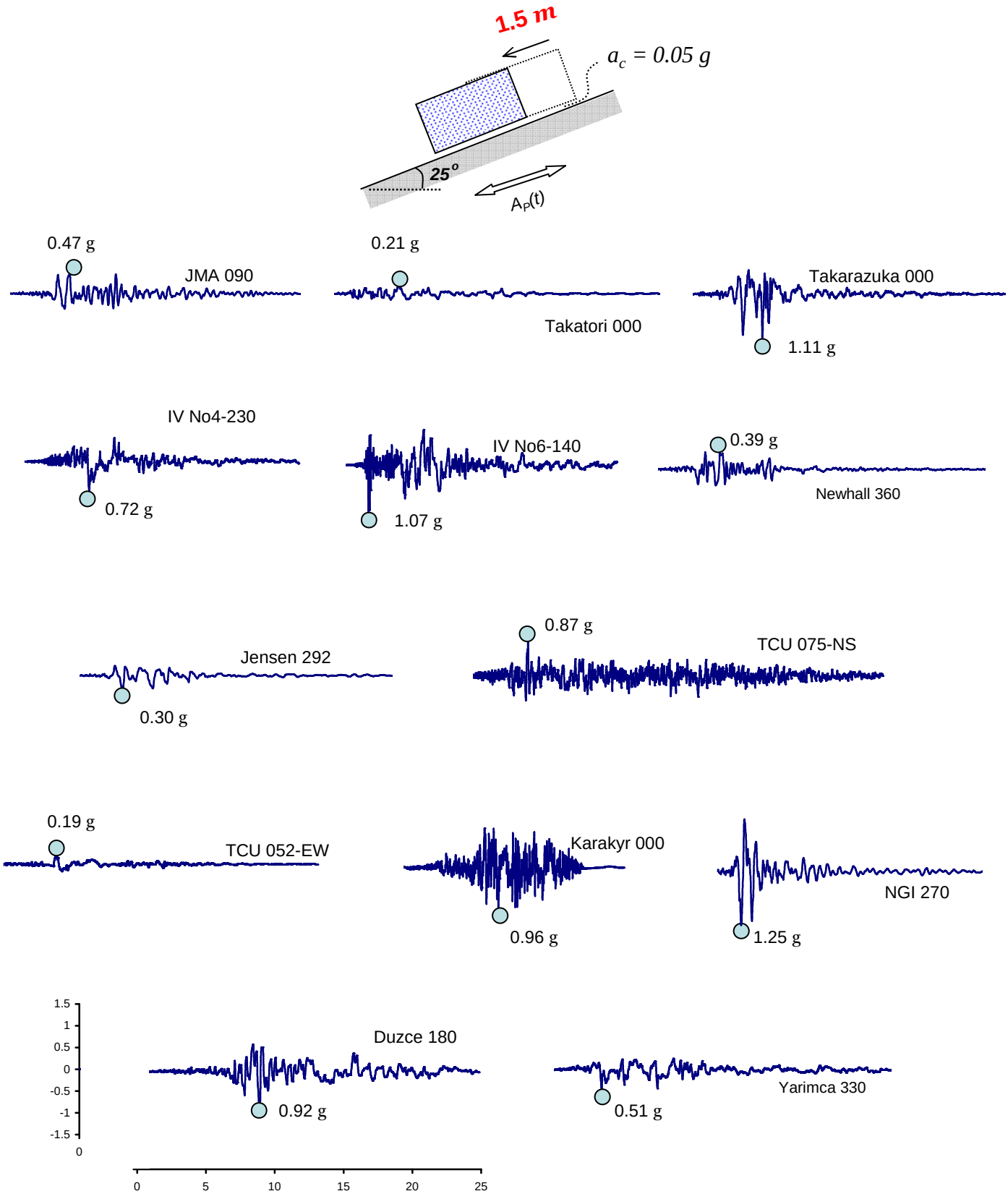

Figure 3.25 *Equivalent acceleration records (with their peak values marked with circle) that induce a slippage of 1.5 m to a rigid block with critical yielding acceleration a_C = 0.05 g, on an inclined base of 25° inclination.*

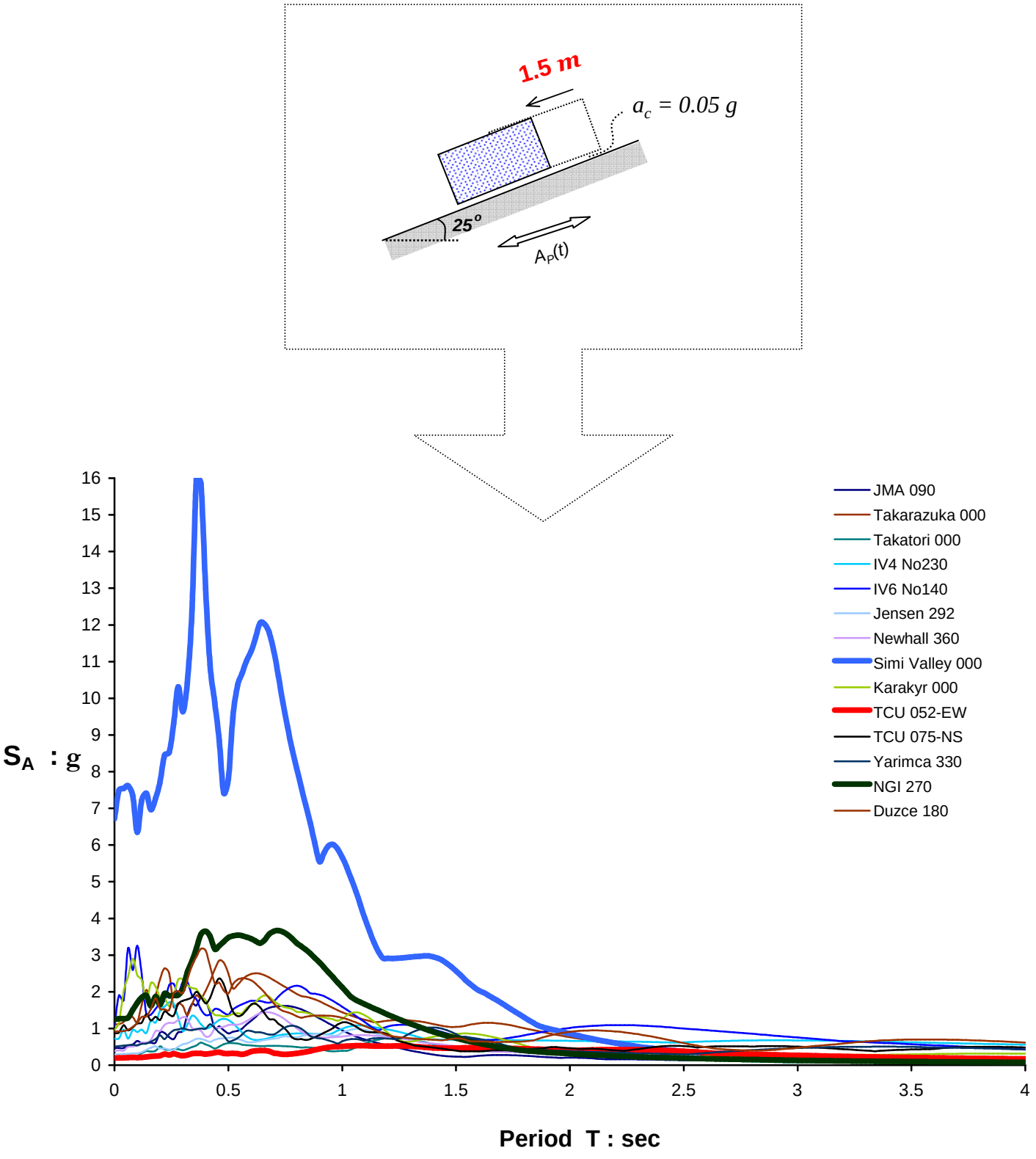

Figure 3.26 *Elastic response spectra of the equivalent acceleration time histories triggering 1.5 m of sliding on an inclined base of 25° inclination (a_C = 0.05 g).*

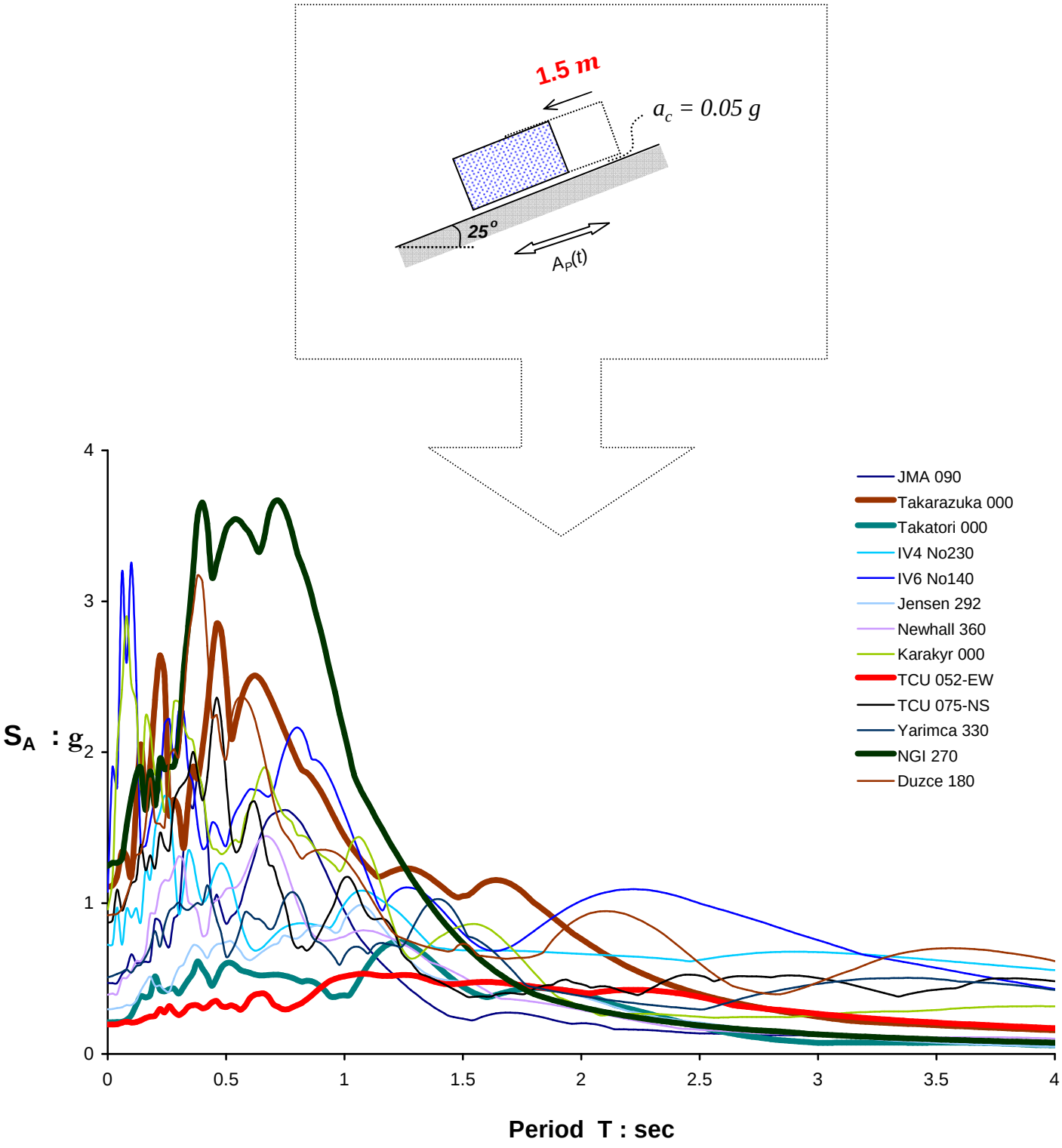

Figure 3.27 *Duplication of the exact previous figure in smaller scale on the vertical axis to demonstrate in detail the spectra of each ground motion.*

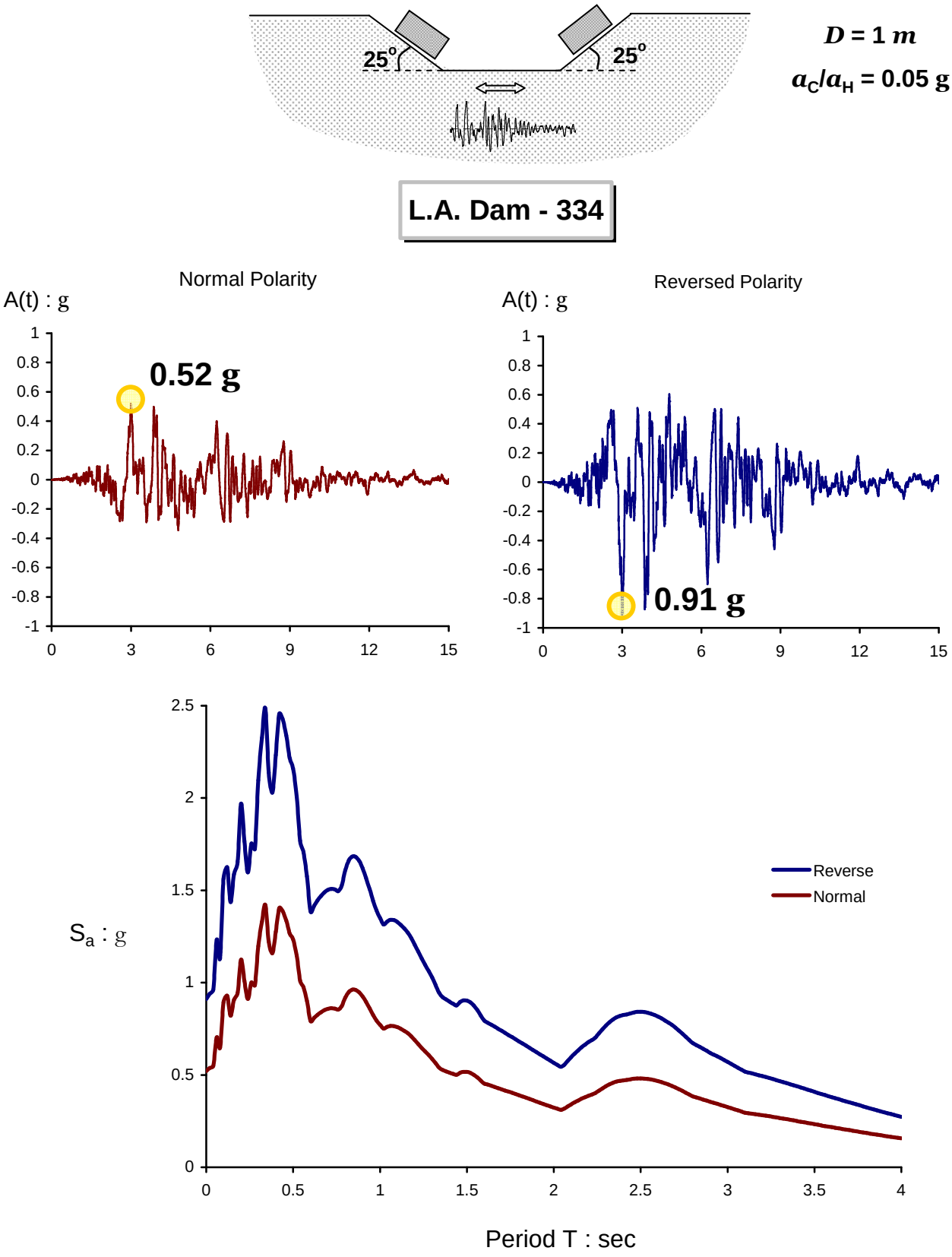

Figure 3.28 *The L.A. Dam 334° record applied with its normal polarity induces 1 m of slippage (a_C = 0.05 g, β = 25°). The equivalent reversed polarity accelerogram has to be increased up to a peak value of 0.91 g to result in the same displacement. Also the elastic response spectra of the motion are illustrated.*

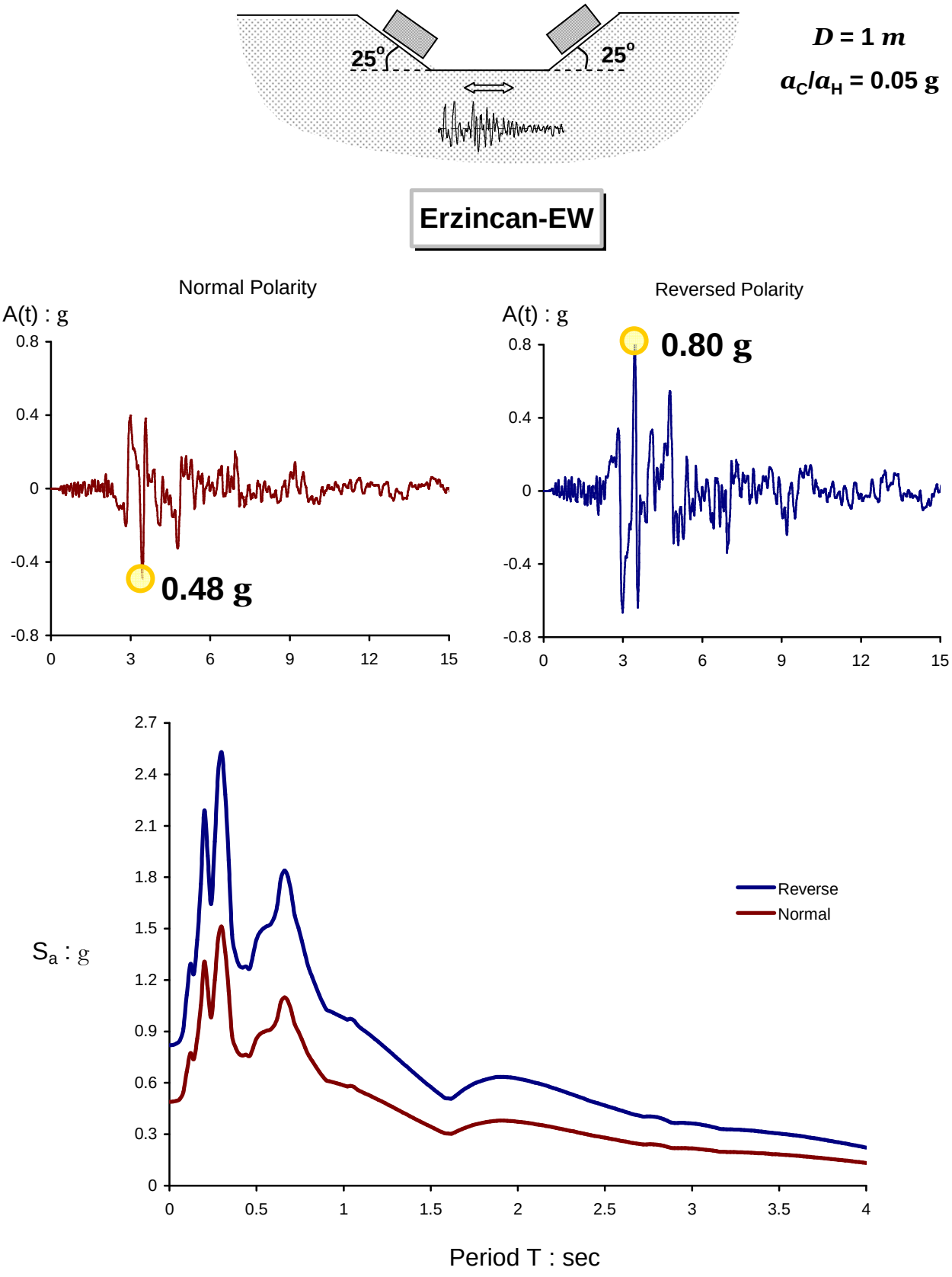

Figure 3.29 *The Erzincan-EW record applied with its normal polarity induces 1 m of slippage (a_C = 0.05 g, β = 25°). The equivalent reversed polarity accelerogram has to be increased up to a peak value of 0.80 g to result in the same displacement. Also the elastic response spectra of the motion are illustrated.*

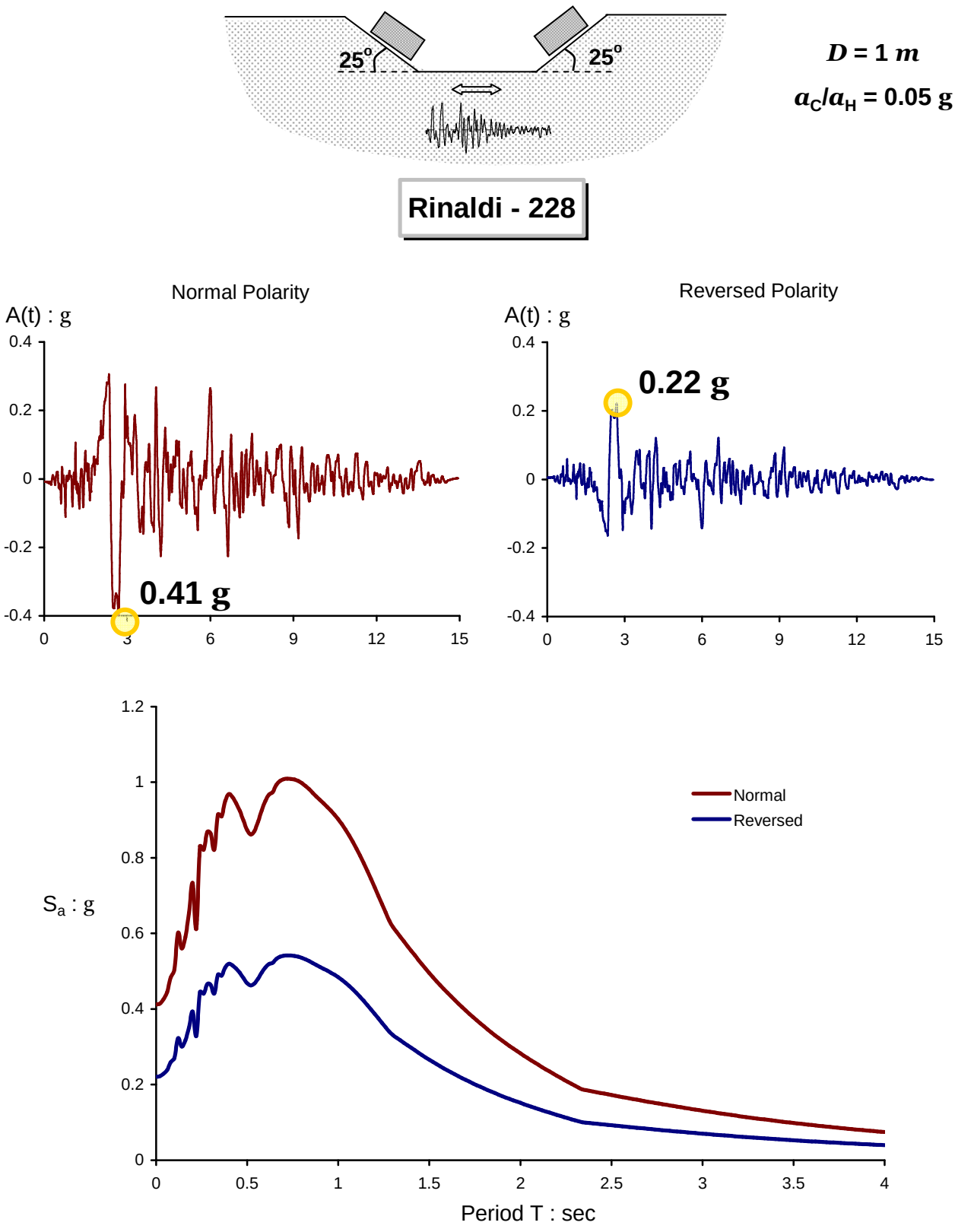

Figure 3.30 *The Rinaldi 228° record applied with its normal polarity induces 1 m of slippage (a_C = 0.05 g, β = 25°). The equivalent reversed polarity accelerogram has to be reduced down to 0.22 g to result in the same displacement. Also the elastic response spectra of the motion are illustrated.*

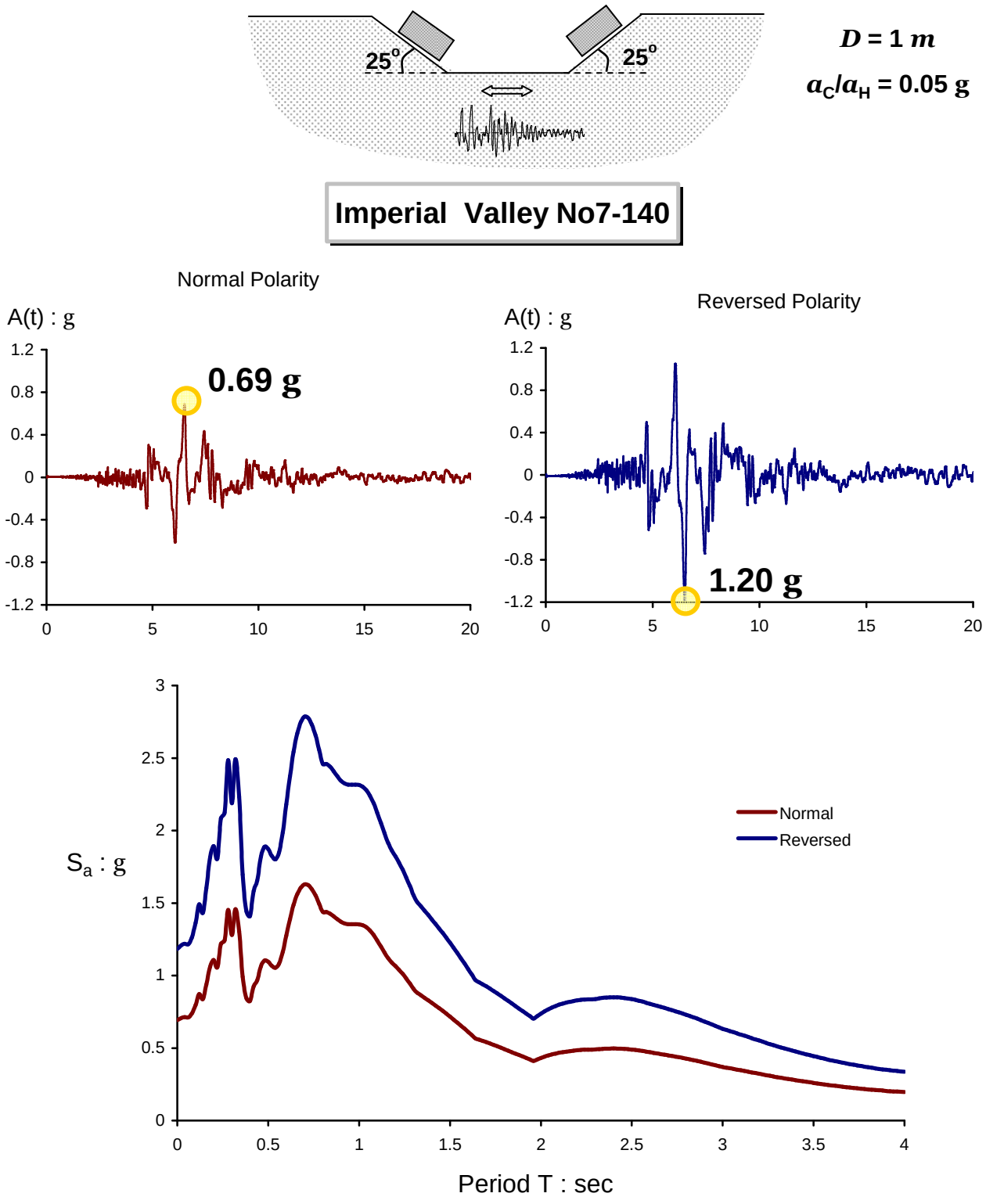

Figure 3.31 *The Imperial Valley No7-140° record applied with its normal polarity induces 1 m of slippage (a_C = 0.05 g, β = 25°). The equivalent reversed polarity accelerogram has to be increased up to a peak value of 1.20 g to result in the same displacement. Also the elastic response spectra of the motion are illustrated.*

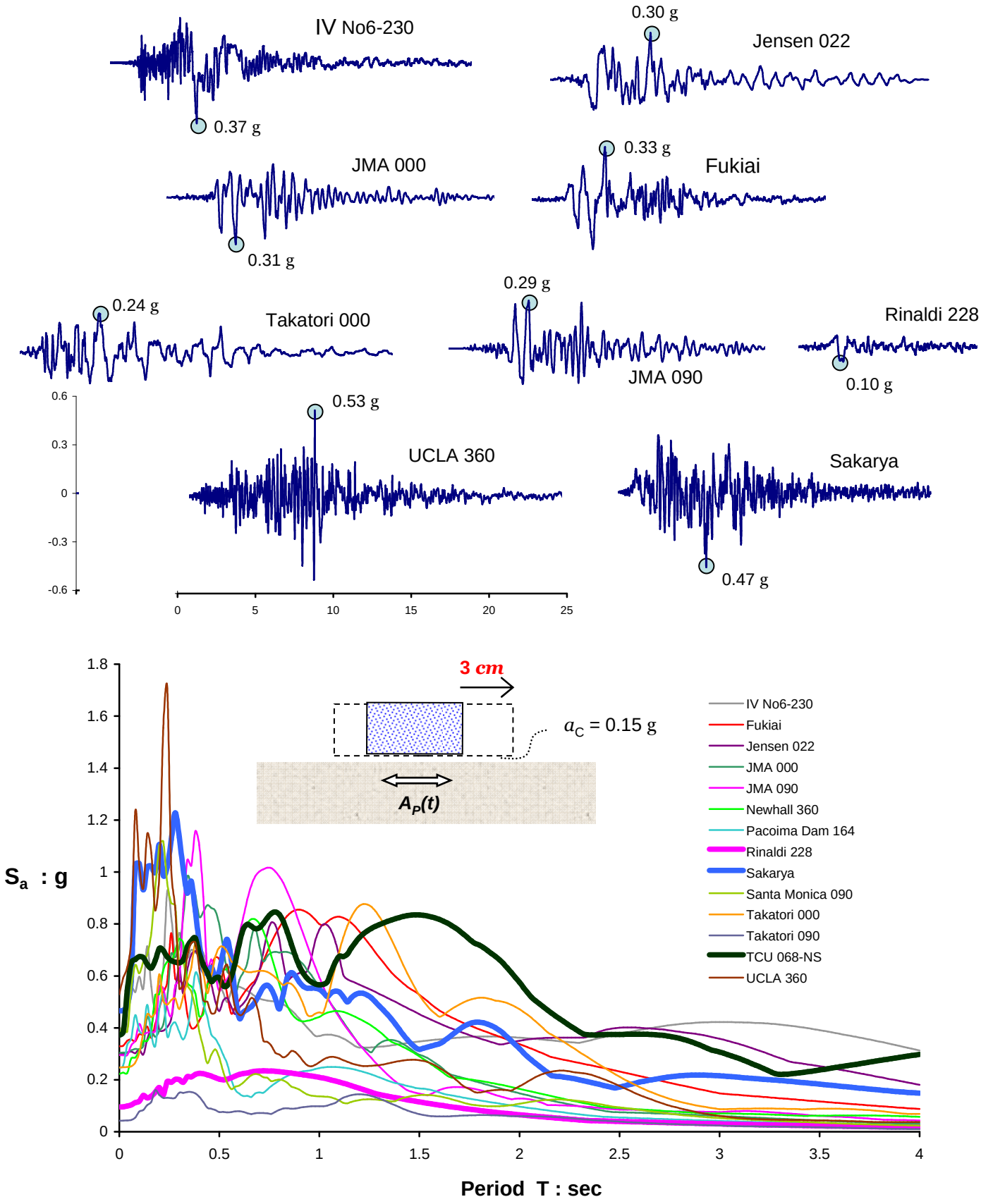

Figure 3.32 *Equivalent acceleration records (with their peak values marked with circle) that induce a maximum slippage of 3 cm to a rigid block with critical yielding acceleration a_C = 0.15 g, on a horizontal base. In addition their elastic response spectra are presented.*

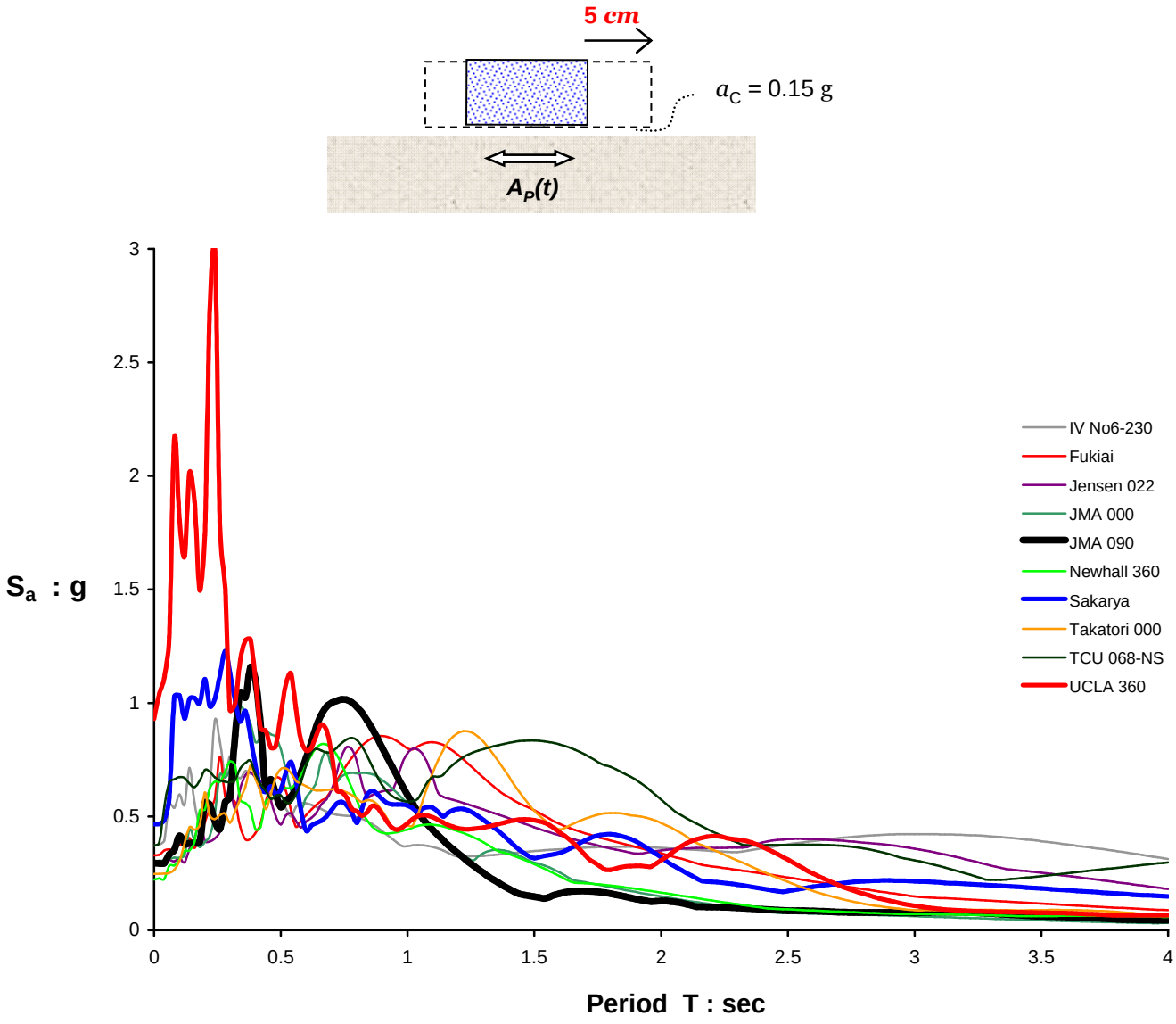

Figure 3.33 *Elastic response spectra of the equivalent acceleration records (with their peak values marked with circle) that induce a maximum slippage of 5 cm to a rigid block with critical yielding acceleration* a_C *= 0.15* g*, on a horizontal base.*

Comparison with Literature Results

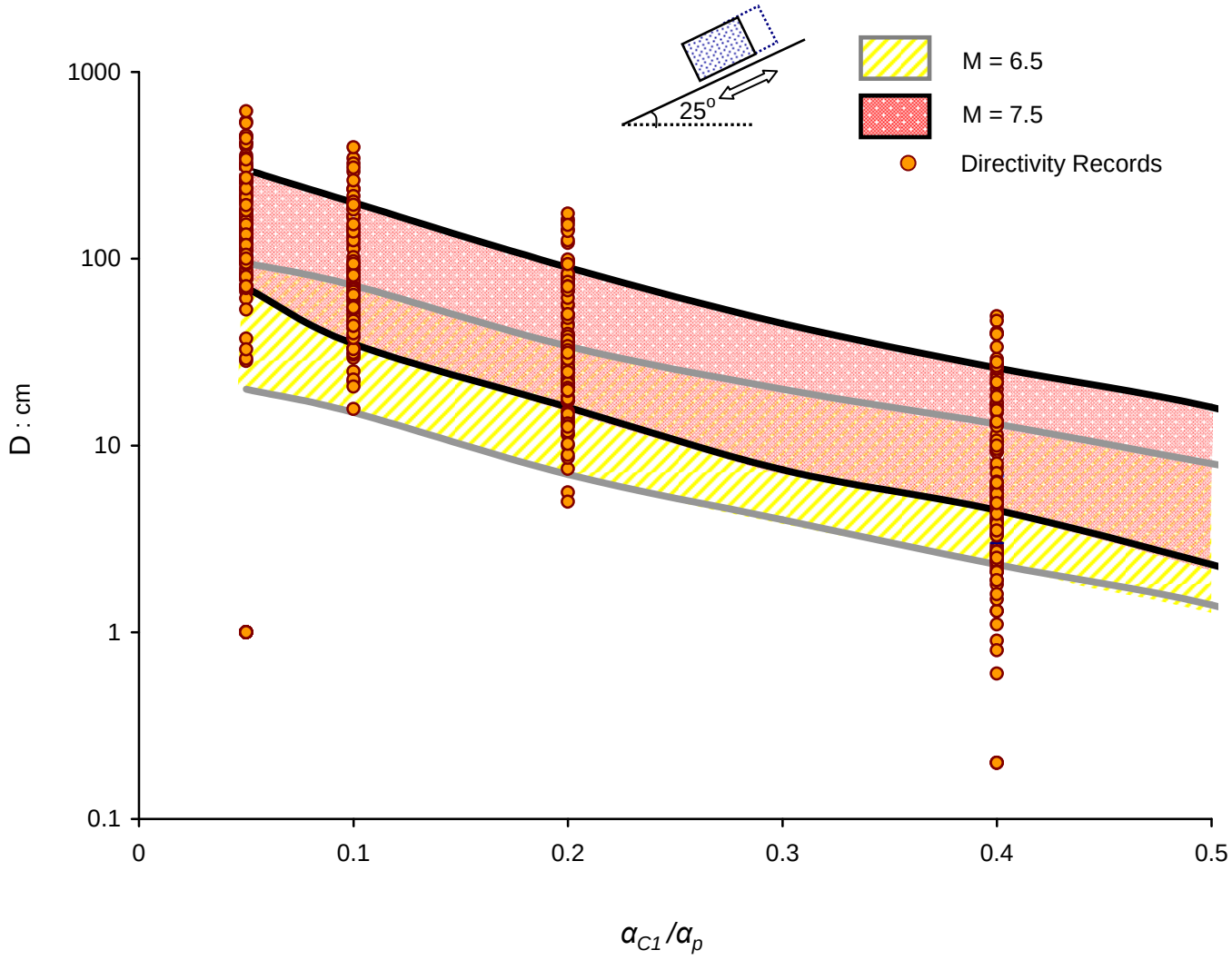

Figure 3.34 *Comparison of the widely-used results of Makdisi & Seed (1976) with the computed sliding response induced by records influenced by forward directivity effects.*

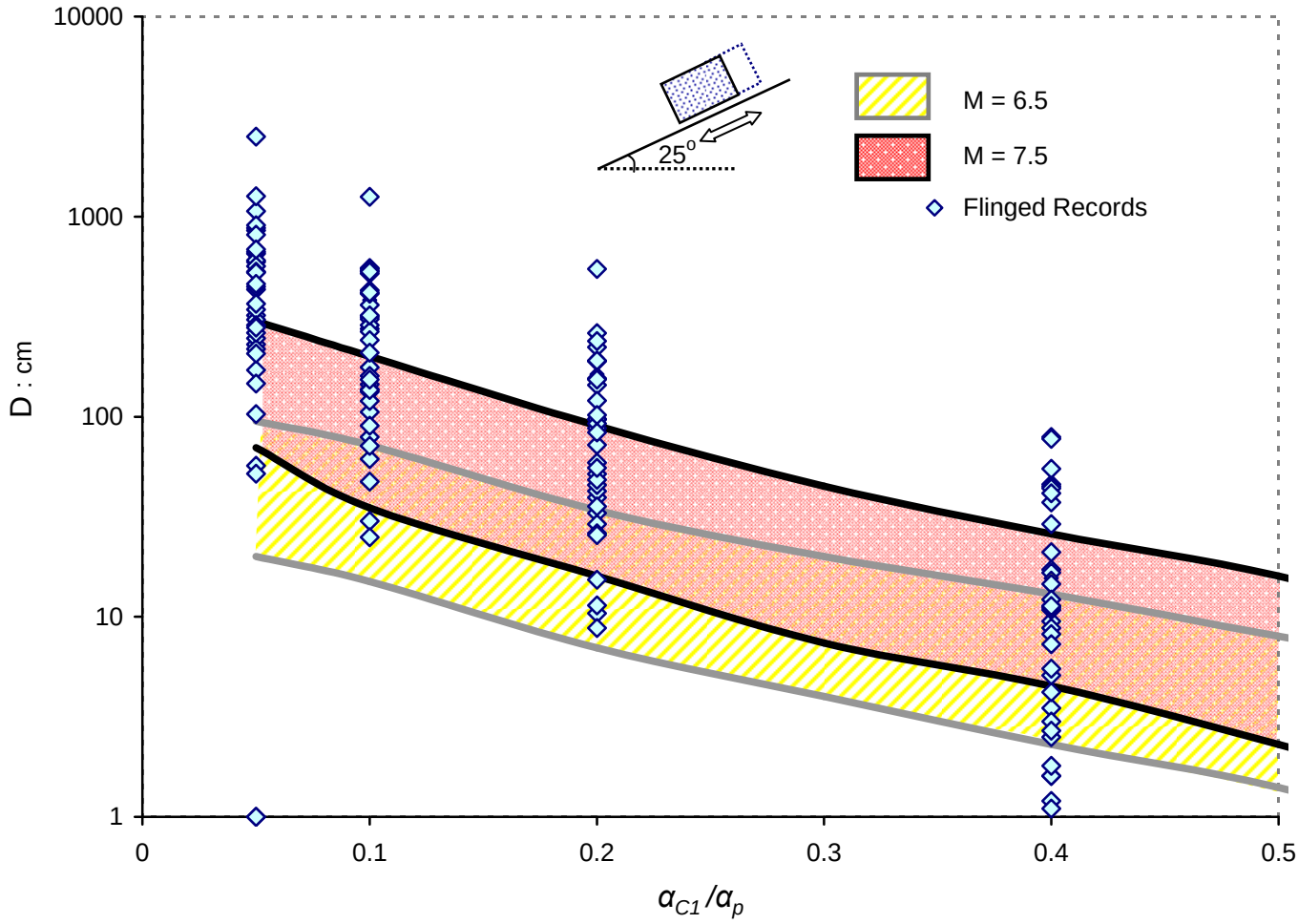

Figure 3.35 *Comparison of the widely-used results of Makdisi & Seed (1976) with the computed sliding response induced by records influenced by fling-step effects. Notice the exceedance in displacements for small acceleration ratios that can be as large as two orders of magnitude.*

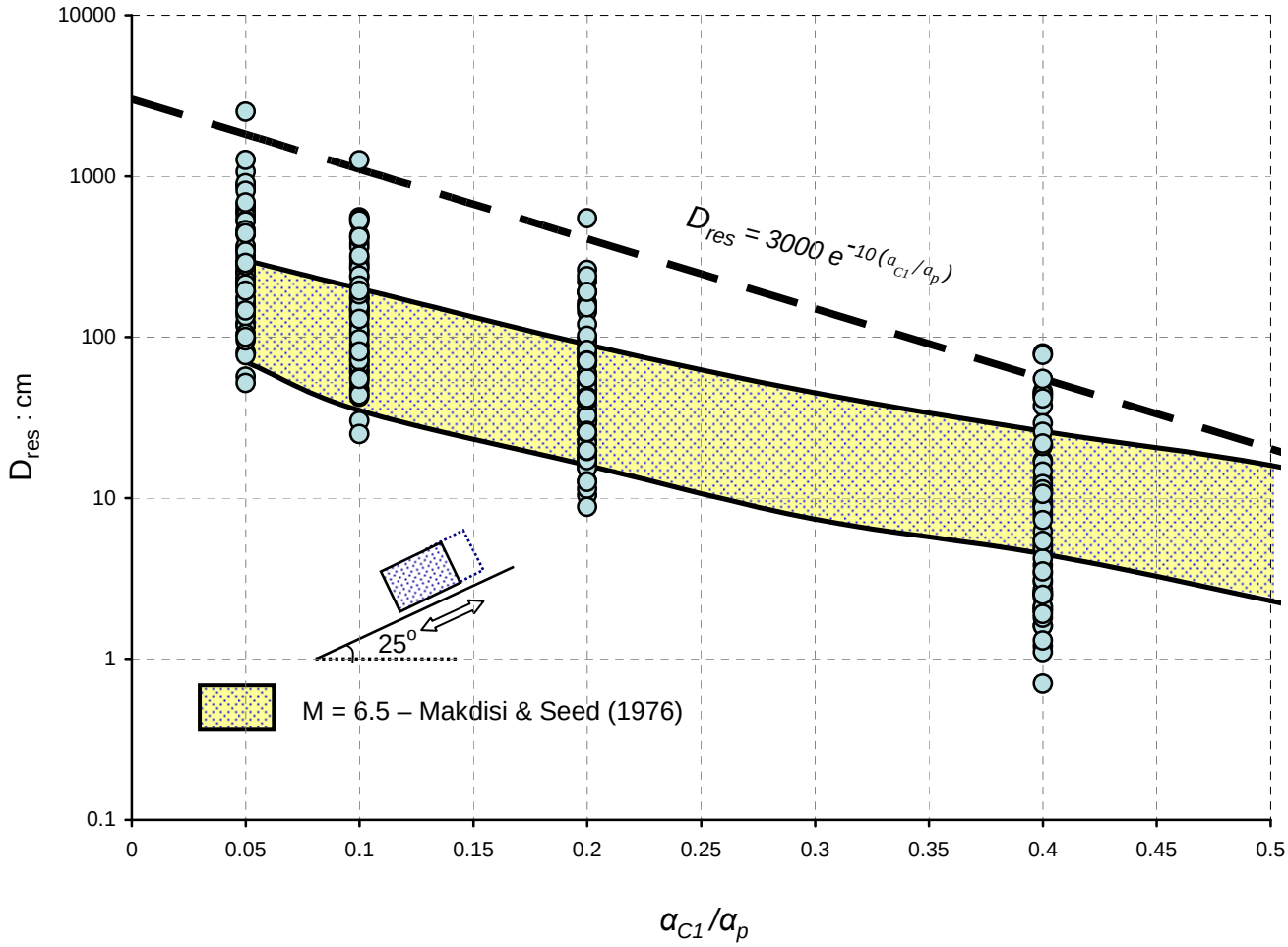

Figure 3.36 *Comparison of the widely-used results of Makdisi & Seed (1976) with the computed sliding response induced by records corresponding to earthquake events of magnitude 6.0–6.7. Each excitation is imposed with the + and – polarity. The black, dashed line represent an upper bound in displacements triggered by such events.*

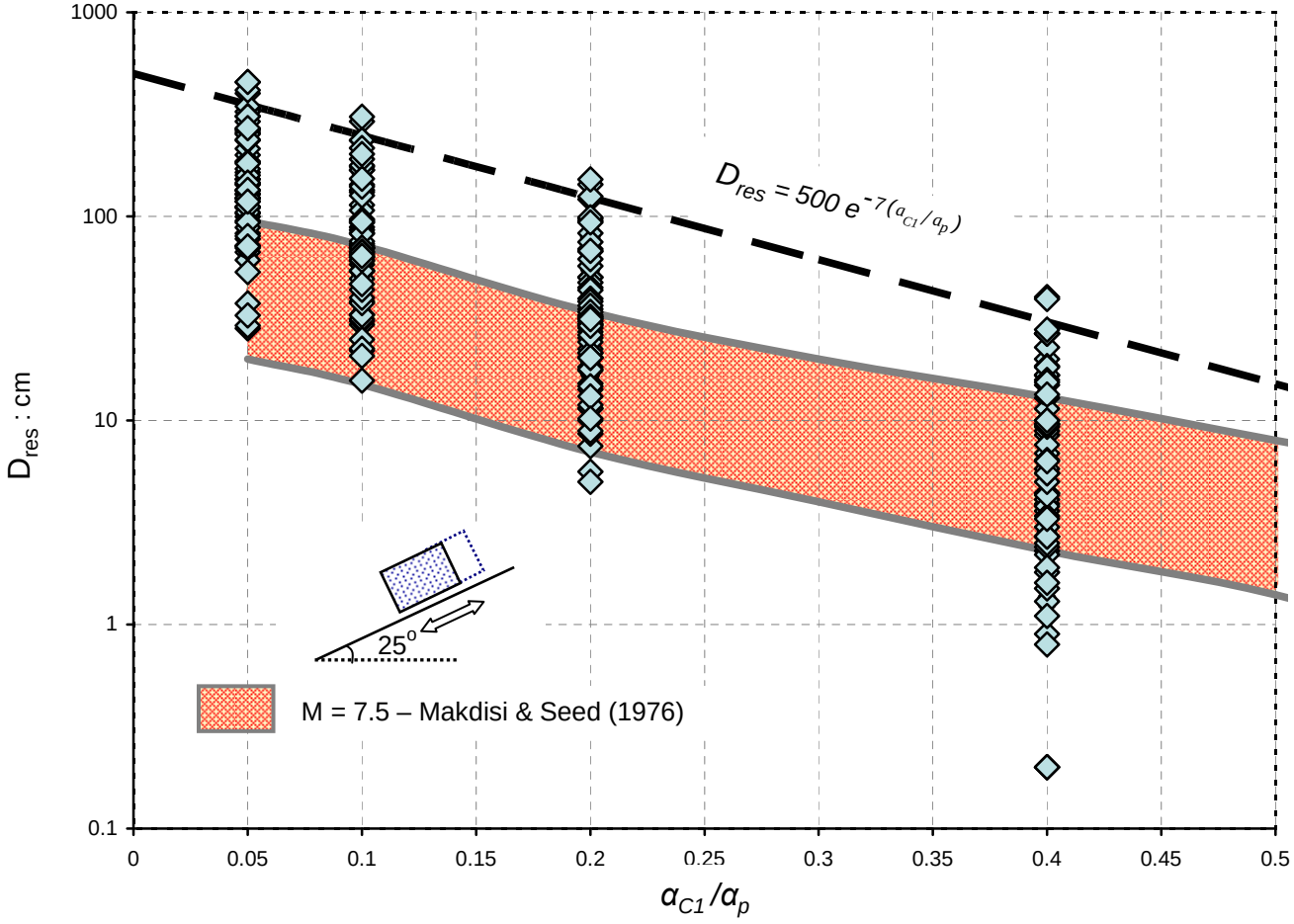

Figure 3.37 *Comparison of the widely-used results of Makdisi & Seed (1976) with the computed sliding response induced by records corresponding to earthquake events of magnitude 6.9–7.7. Each excitation is imposed with the + and – polarity. Evidently, some of the utilized severe near-fault records lead to much larger slip especially at small α_{C1}/α_p ratios. For the Chi-Chi records the superiority reaches one order of magnitude. An upper bound estimation of slippage for an earthquake of 7.5 magnitude, is also given with the bold, dashed line.*

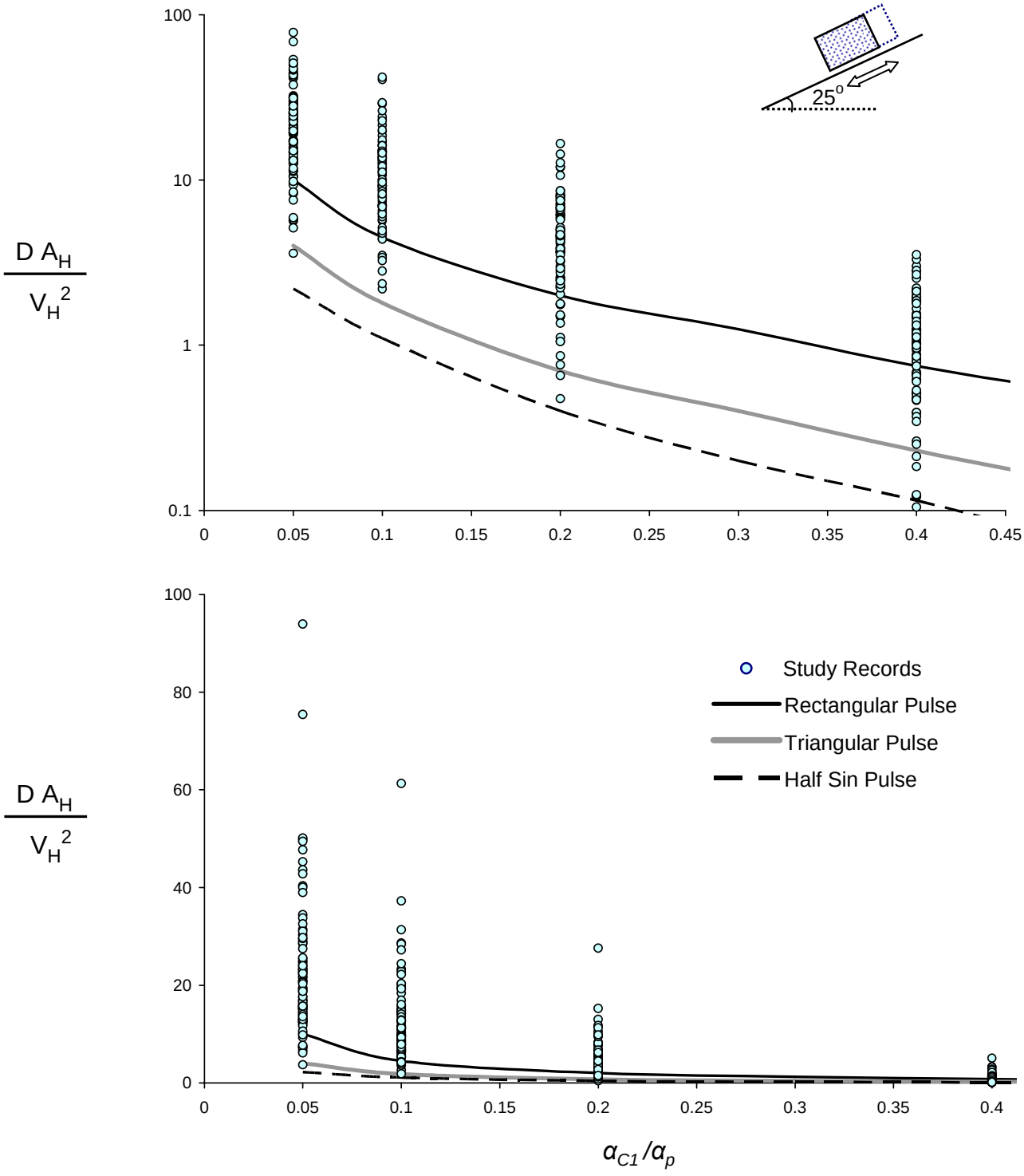

Figure 3.38 *Comparison of the dimensionless sliding response triggered by the records utilised in our study with the results of Sarma (1975) for slippage induced by fundamental pulses (of rectangular, triangular, and half sinus shape). The top plot presents the results in logarithmic scale, and the bottom figure in normal scale to emphasise the magnitude of difference between our results and those by Sarma.*

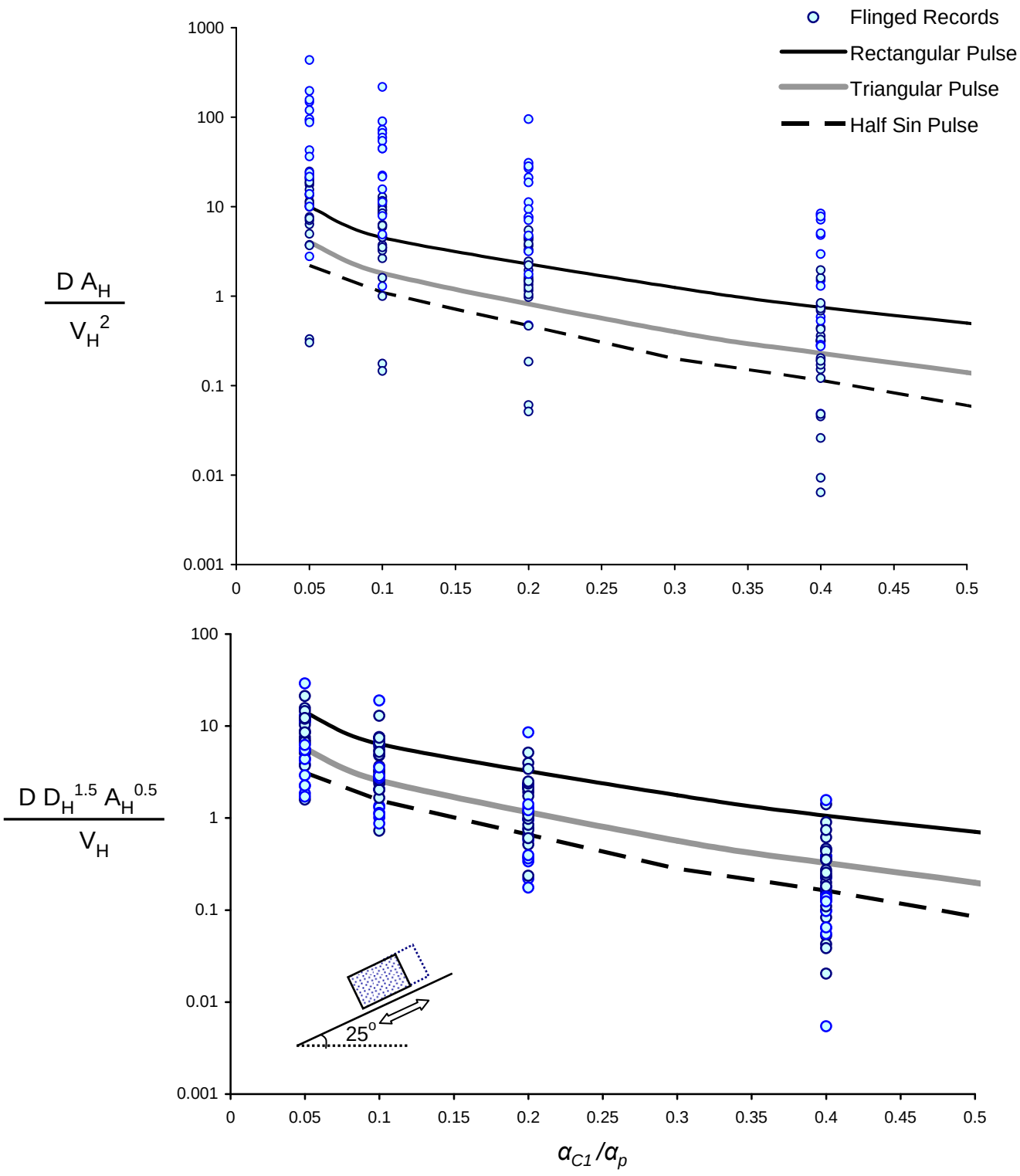

Figure 3.39 *Comparison of the dimensionless sliding response triggered by fling-step affected records with the results of Sarma (1975) for slippage induced by fundamental pulses (of rectangular, triangular, and half sinus shape). The top plot presents the results in the normalisation form utilised by Sarma, and the bottom figure in a new normalisation that reduces the scatter of the data (thus it is preferred by us).*

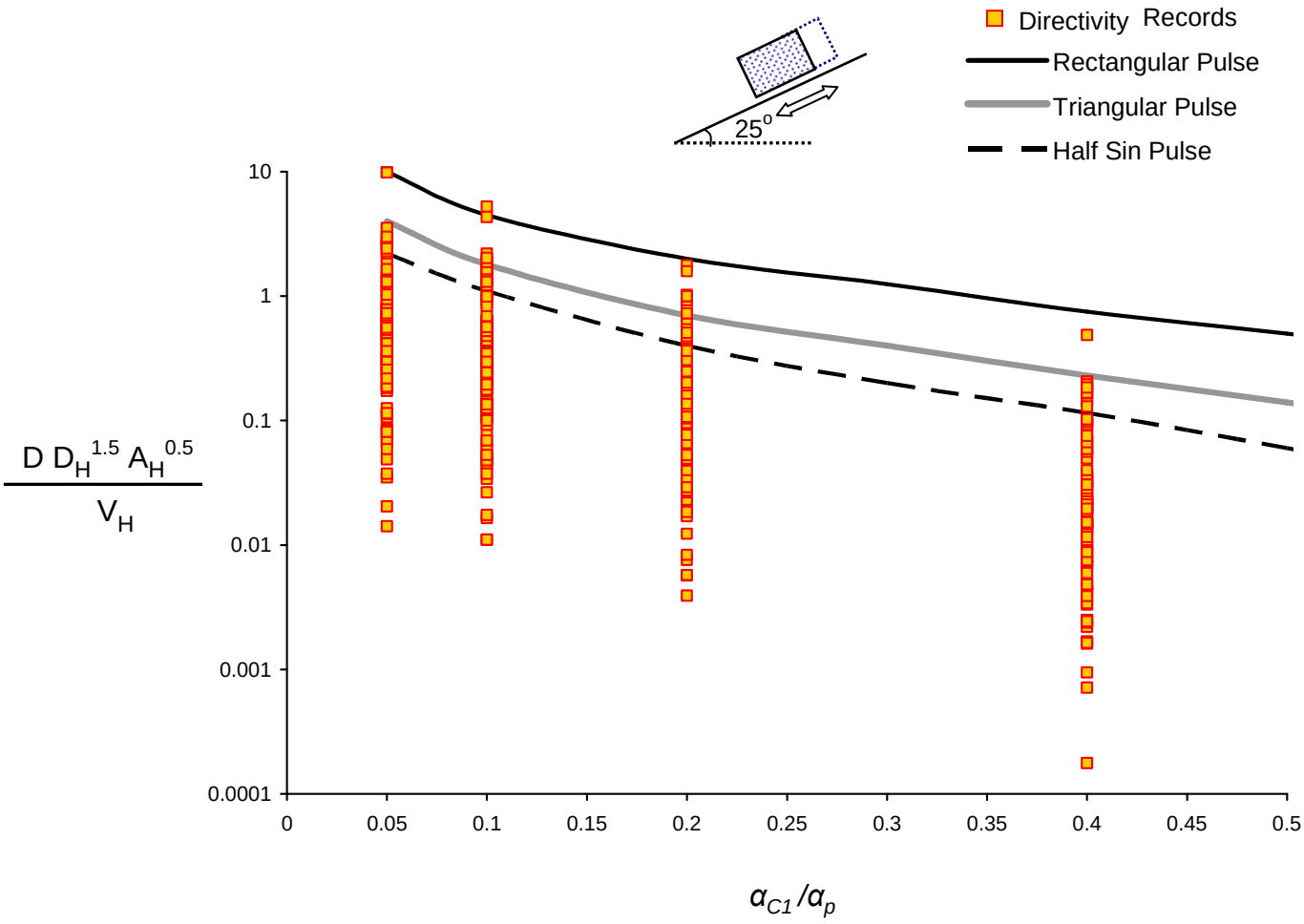

Figure 3.40 *Comparison of the dimensionless sliding response triggered by directivity affected records with the results of Sarma (1975) for slippage induced by fundamental pulses (of rectangular, triangular, and half sinus shape).*

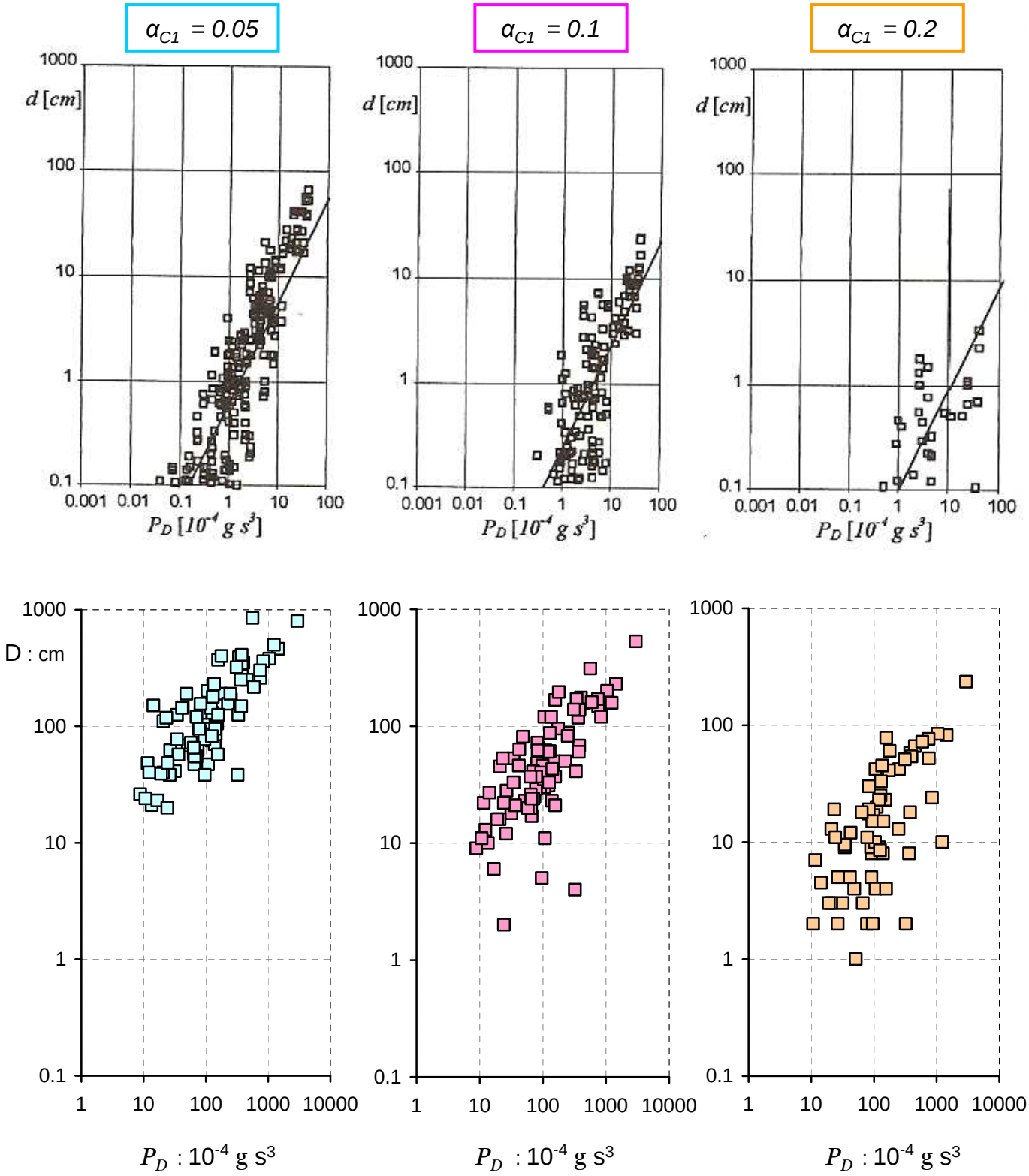

Figure 3.41 *Calculated final displacements of the sliding block versus destructiveness potential factor, P_D, for three different values of critical acceleration a_C. The top row figures picture the results of Crespellani et al (1996); whereas the bottom row shows the results of our study.*

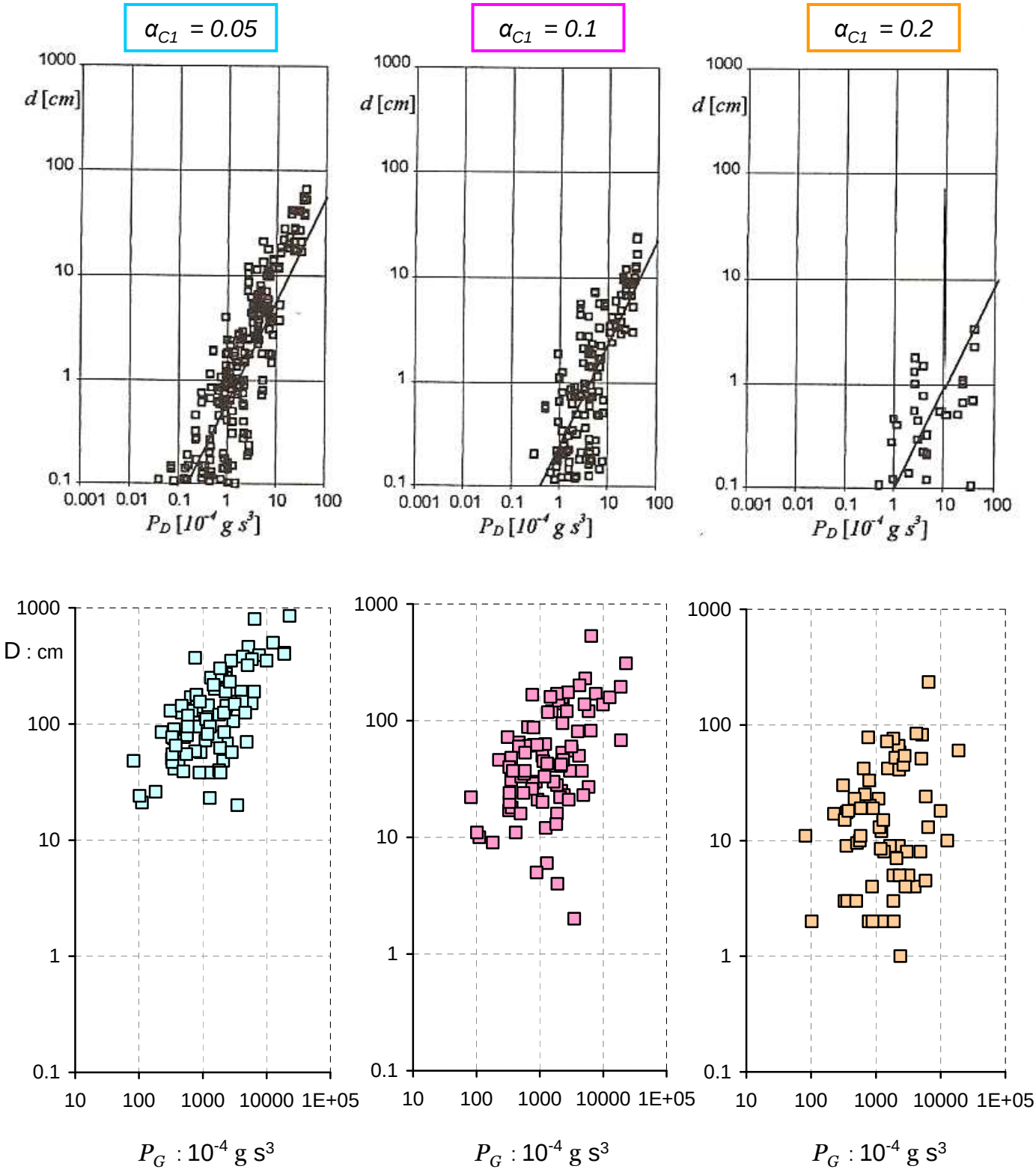

Figure 3.42 *Sliding displacements versus "near-fault" modified destructiveness potential factor, P_G, for three different values of critical acceleration a_C. The top line figures picture the results of Crespellani et al (1996); whereas the bottom ones illustrate the results of our study. [Notice that the horizontal axis between top and bottom figures is different. However, the vertical axis is the same.]*

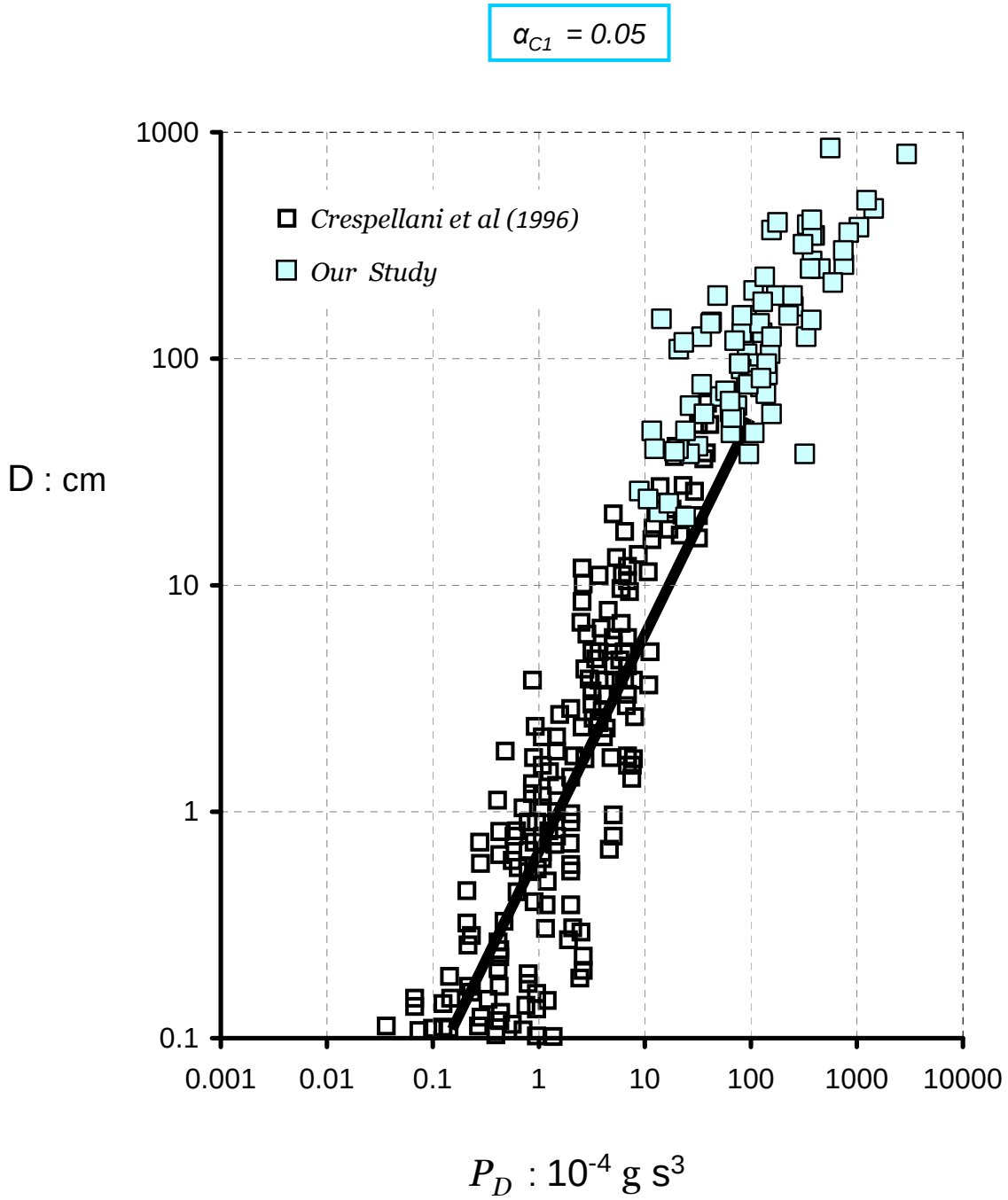

Figure 3.43 *Plot of sliding displacement results of Crespellani et al (white squares) and our study (light blue squares) in the same graph, for yielding acceleration of* 0.05 g.

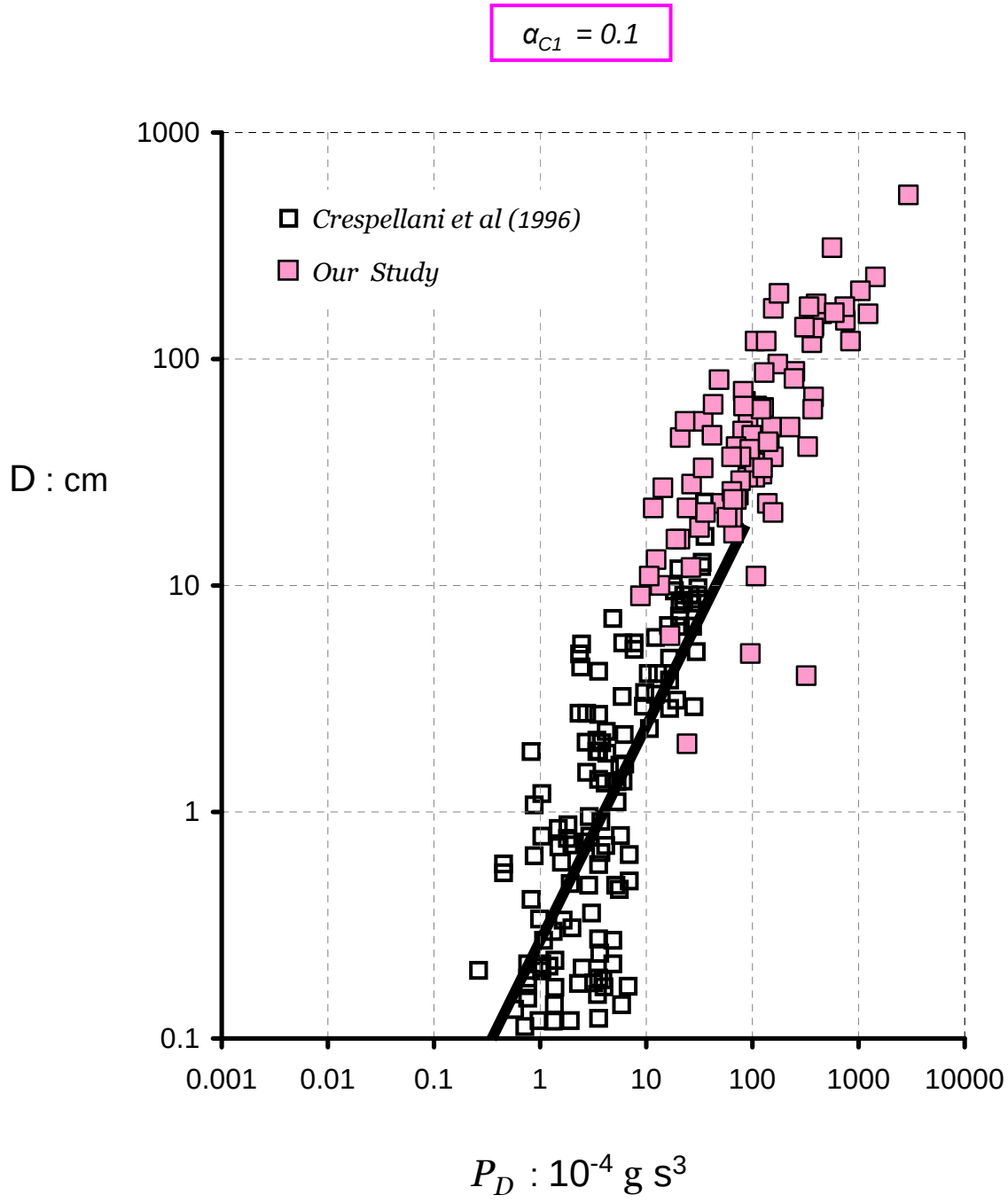

Figure 3.44 *Plot of sliding displacement results of Crespellani et al (white squares) and our study (pink squares) in the same graph, for yielding acceleration of* 0.1 g.

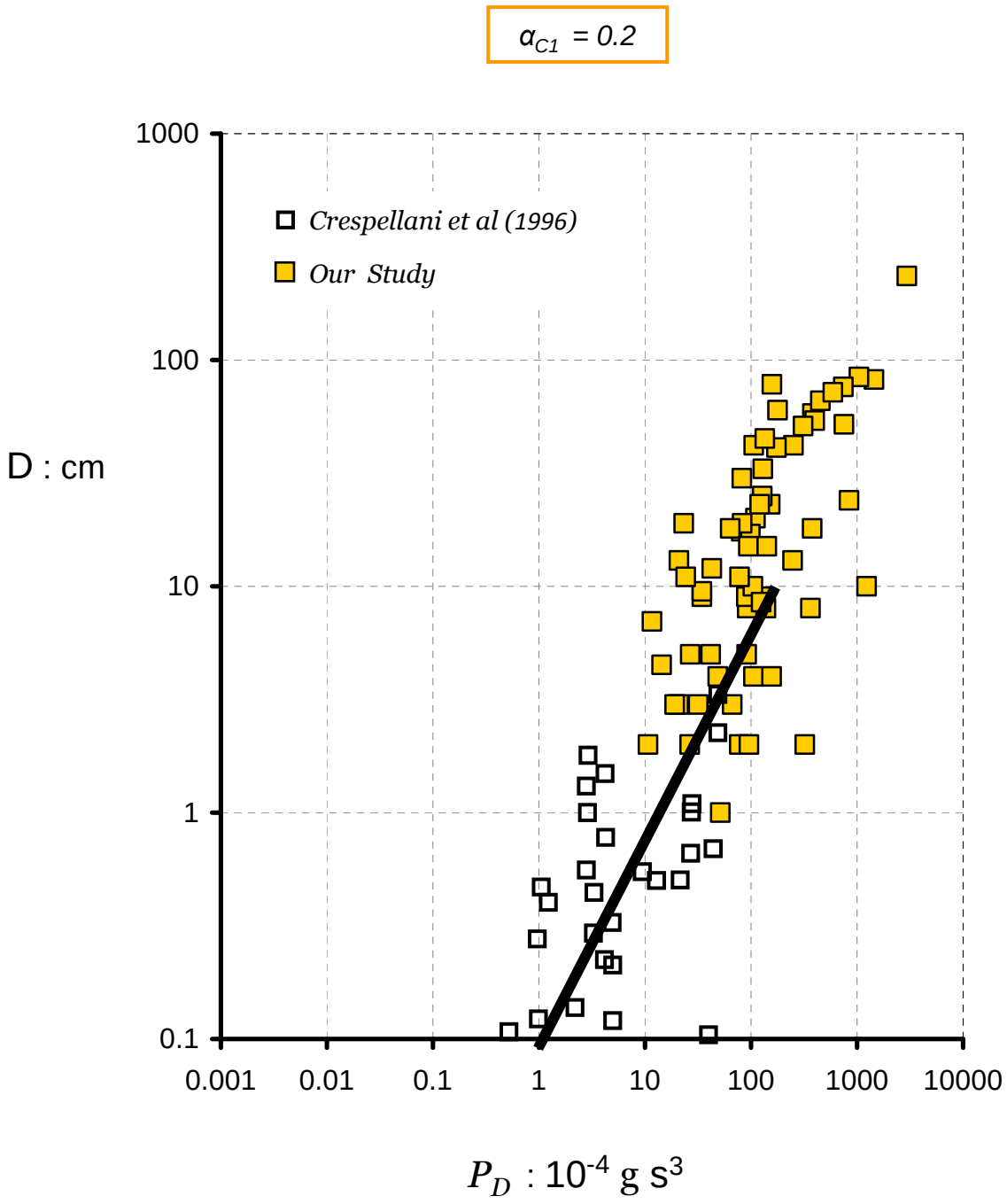

Figure 3.45 *Plot of sliding displacement results of Crespellani et al (white squares) and our study (orange squares) in the same graph, for yielding acceleration of* 0.2 g.

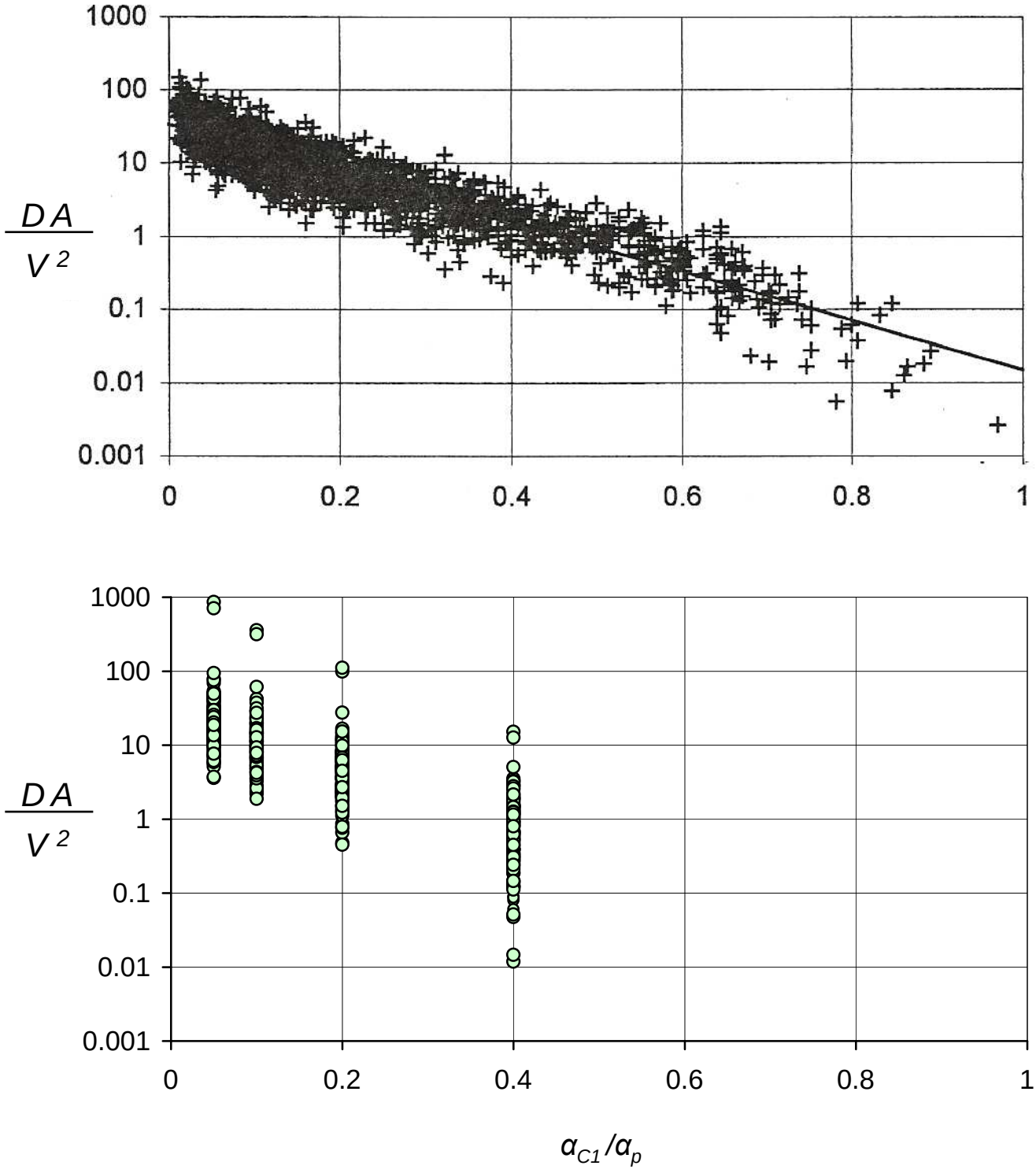

Figure 3.46 *Dimensionless slippage as a function of critical acceleration ratio. The top figure pictures the results of Crespellani et al (1996); the bottom presents the results of our study.*

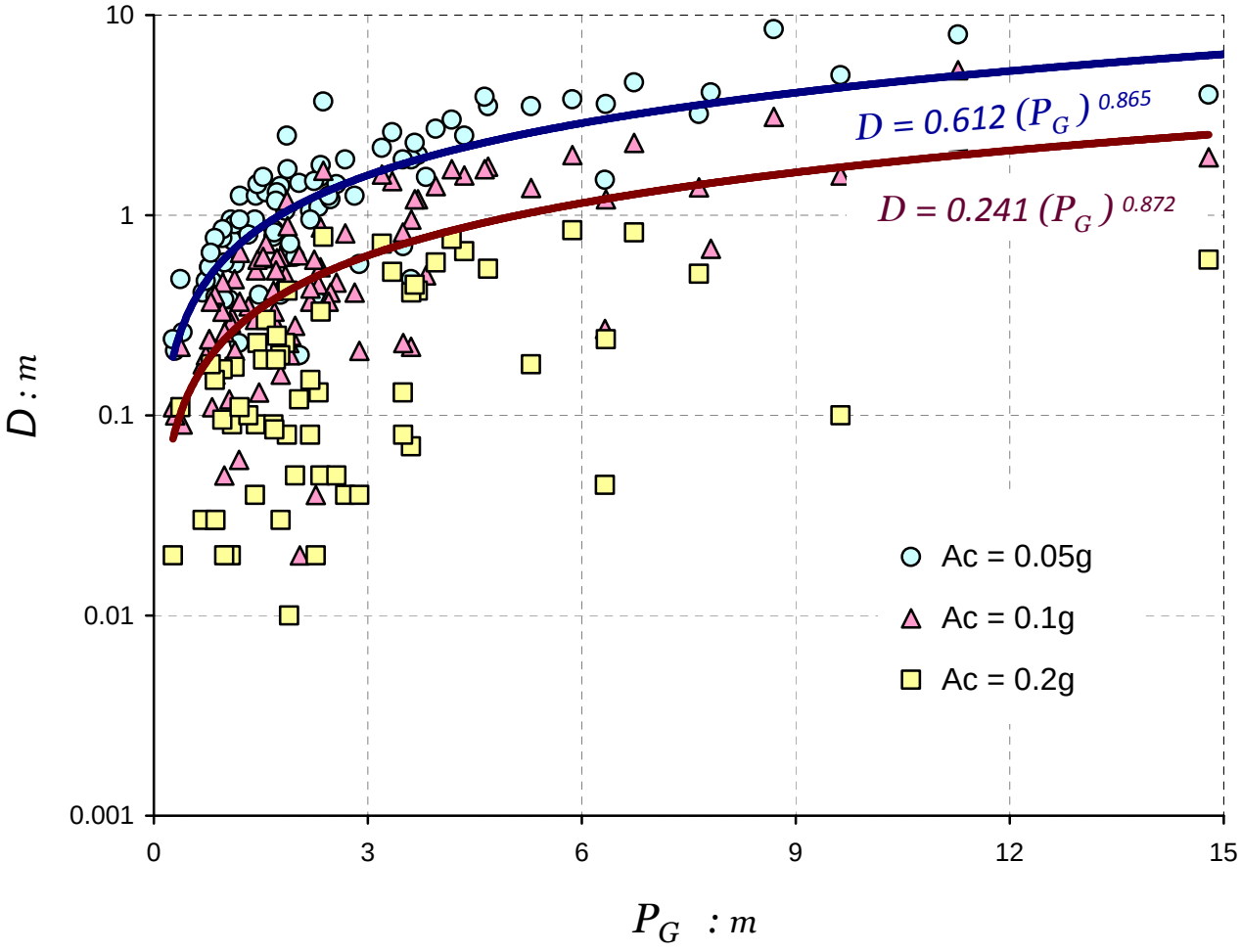

Figure 3.47 *Accumulated displacements of the sliding block versus a "near-source" modified destructiveness potential factor, P_G , for three different values of critical acceleration A_C. Two regression curves are presented: one as an upper bound (blue curve) and a second one as median (dark red line).*

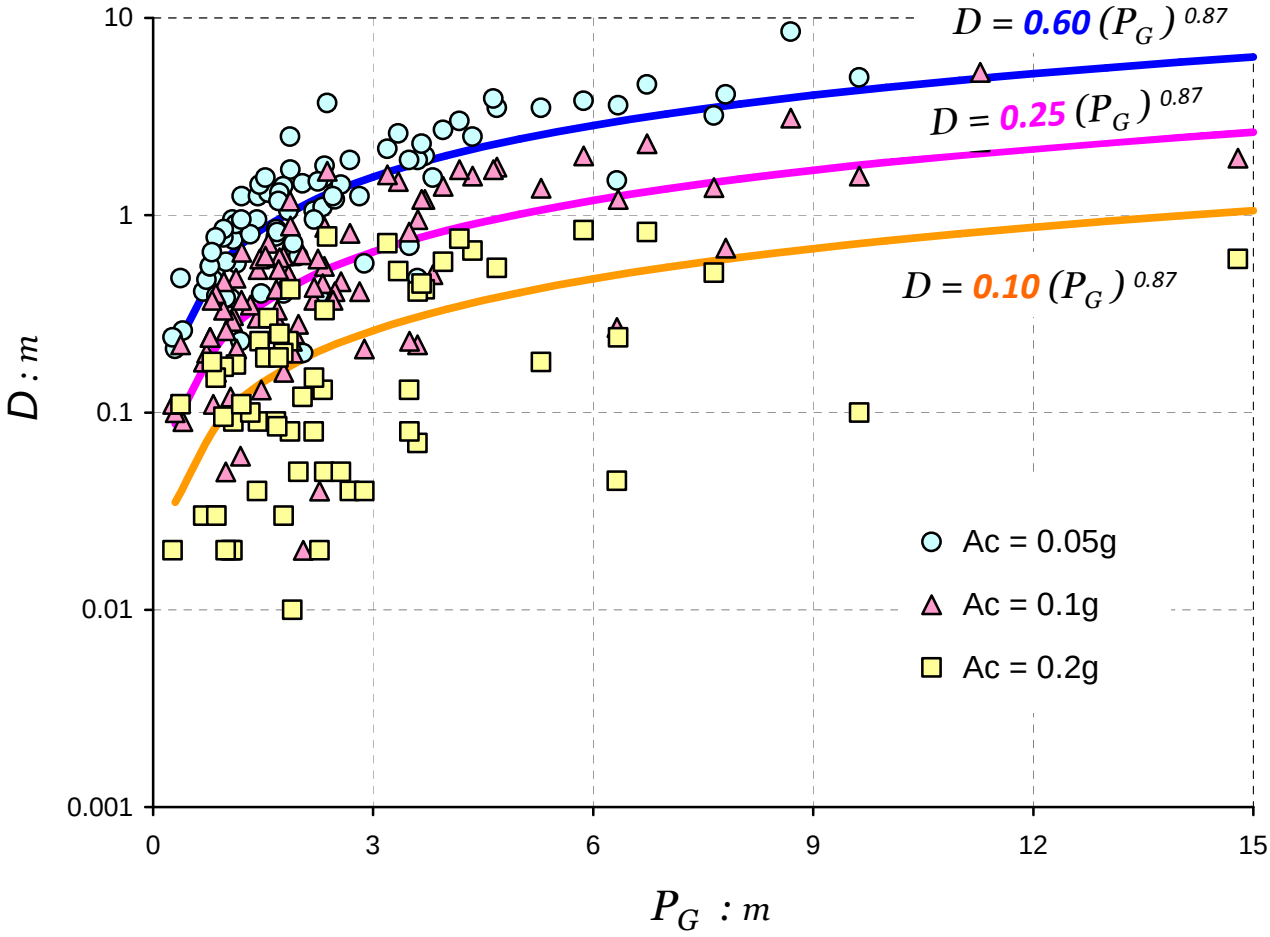

Figure 3.48 *Accumulated displacements of the sliding block versus a "near-source" modified destructiveness potential factor, P_G, for three different values of critical acceleration A_C. For each value of sliding acceleration a regression curve is given: the expression in blue for a_C = 0.05, the one in magenta for 0.1, and the orange for 0.2 respectively.*

Chapter 4

Influence of Vertical Acceleration on Asymmetric Sliding

4.1 Horizontal Excitation of Inclined Base

In the previous chapters we deal with the case of a sliding rigid block on top of a sloping plane subjected to seismic excitation parallel to the interface. The parallel direction of the triggering motion is an assumption made also by most researchers who studied this system. Herein, this assumption is abandoned: excitation is applied horizontally.

Figure 4.1 (a) depicts a rigid block of mass, m, on a plane inclined at an angle β, whereas the two components of the excitation are shown in Figure 4.1 (b). From the dynamic equilibrium of the rigid block (see Figure 4.2), the critical sliding acceleration can be obtained:

$$a_{C_1} = (\mu \cos\beta - \sin\beta) - \mu \, a_H \sin\beta \qquad (4.1)$$

when the inertial component parallel to the sliding interface is downward. Observe that the quantity inside the parenthesis is the downhill yielding acceleration in case of excitation parallel to the slope, a_P. With this notation, the previous equation simplifies to:

$$a_{C_1} = a_P - \mu \, a_H \sin\beta \qquad (4.2)$$

On the other hand, if the inertial component parallel to the sliding interface is acting upward, the critical yielding acceleration is:

$$a_{C_2} = (\mu \cos\beta + \sin\beta) + \mu \, a_H \sin\beta \qquad (4.3)$$

Similarly, the quantity ($\mu\cos\beta + \sin\beta$) represents the uphill critical yielding acceleration for excitation exclusively parallel to the slope. It remains true that: $a_{C_1} < a_{C_2}$, and the notation: $a_{C_1} = a_C$ will be employed from now on. Therefore, a rigid block can slide more easily downwards ($a_C < a_P$) and with more difficulty upwards, when the input excitation acts horizontally rather than parallel to the slope.

The explanation is quite obvious: as the parallel (to sliding plane) component of acceleration tends to move the block downhill, the normal component of developing inertia acts upwards, reducing the perpendicular reaction of the inclined plane. As a consequence, the frictional resistance of the interface is reduced and sliding is triggered at lower accelerations. Exactly the opposite occurs in case of upward sliding. Thus, the downward-sliding acceleration, a_{C1}, is time dependent, since it is affected by the normal to the slope component of motion.

Every time the threshold a_C is exceeded sliding occurs (downward or upward depending on the excitation direction). The block moves with constant acceleration a_C until its velocity coincides with the velocity of its base. Integrating the block-base relative velocity with respect to time, the permanent slippage of the block is computed. Every time a_C is exceeded, the factor of safety against sliding is momentarily exceeded; so the block slides along the slope. Even though upward sliding can happen, as we have already presented in the previous chapters, in practice for inclination angles greater than about 20^o only downhill sliding is practically observed. In every yielding period the induced

permanent displacement is added to the previous ones, resulting in an accumulated permanent slippage at the end of shaking.

In the sequence, a wide variety of real accelerograms are utilised as excitation and parametric analyses are performed. Twenty-two different ground motions are employed. Figures 4.3 ÷ 4.27 summarize the results obtained from all the analyses. The most characteristic cases are discussed in the next two sections.

4.1.1 Effect of the acceleration component normal to sliding interface

The normal acceleration component is completely coupled with the horizontal acceleration, and hence with the sliding direction of the block. In particular, when the horizontal excitation acts to the right then the perpendicular component is directed downward and the parallel component upward; the opposite is true when the horizontal acceleration is reversed. Therefore, the main effect of horizontally imposed excitation is to have a time dependent yielding acceleration, a_C *.*

Figure 4.3 pictures the sliding response triggered by the horizontally imposed Jensen Filtration Plant (22° component). The critical acceleration ratio is $a_C/a_H = 0.1$*. The yield acceleration of the block varies with time as shown in the acceleration time histories with the solid pink line. As a result, the block velocity during sliding is not linear, as was the case with excitation parallel to slope. The Jensen record induces six sliding periods as illustrated with the (turquoise) shaded areas in the velocity time histories of Figure 4.3. The resulting yielding displacement reaches 3.75 m. For the same excitation but with* $a_C/a_H = 0.05$*, the sliding response for parallel and horizontally acting acceleration is pictured in Figure 4.4. Notice that horizontal excitation leads to 1 m greater slippage than for parallel imposed record.*

Fluctuation of yielding acceleration as a result of the normal component of horizontally imposed acceleration can be starkly observed in Figure 4.6, where sliding is induced by the reversed polarity Rinaldi record for $a_C/a_H = 0.1$. In velocity time histories, inside the dashed eclipse a region is shown where a_C is remarkably reduced as a consequence of normal component of horizontal acceleration. This is shown also in Figure 4.7, where parallel and horizontal triggered sliding is presented side by side.

4.1.2 Slippage induced by parallel versus horizontally acting acceleration

When ground motions act horizontally, the resulting yielding displacement is generally larger than the slippage triggered by the same excitation when applied parallel to the slope (for the same ratio a_C/a_H). The explanation is straightforward: even if 100% of the acceleration functions as triggering force than the smaller 90%, for the parallel and horizontally imposed ground motion respectively (Figures 4.5, 4.9, 4.12, 4.15, 4.18), by far a more significant influence has the yielding acceleration which is smaller in horizontally than in parallel applied excitation. Thus, in Figure 4.8 one can easily observe that for all sliding acceleration ratios the response induced by the horizontally applied Rinaldi record is greater than if applied parallel. Figure 4.14 shows the same trend with the Takatori motion.

Figure 4.11 displays the acceleration, velocity and displacement time histories of a sliding block and its base, when subjected to the JMA record horizontally or parallel to the base (for $a_C/a_H = 0.05$). The velocity step in case of parallel acting accelerogram is $\Delta V = 1.61$ m/s, larger than the 1.43 m/s of the horizontal excitation. Nevertheless, the induced slippage is almost 25 % greater in the latter case! The same is valid for the Takatori ground motion as presented in Figure 4.13.

An exception is depicted in Figures 4.16 and 4.17: when an inclined sliding system undergoes the TCU 065-EW motion, the horizontally triggered displacement is smaller. The reason is that the particular record is a peculiar motion. It includes a sequence of rapidly alternating positive and negative acceleration cycles of equal importance, which during a sliding period reduce and increase the yielding acceleration, a_C *.*

However, such behaviour can not be generalised. In general, the presence of the normal component of the horizontal acceleration $a_H(t)$ *results in approximately 30% larger sliding compared with the one induced with parallel excitation.*

4.1.3 Influence of inclination

Figures 4.21÷4.27 depict the (asymmetric) sliding response of the block for various angles β. As it can be seen in Figures 4.22, 4.24 and 4.26, the steeper the slope the greater the induced slippage. This was expected, considering that as the inclination increases (while keeping a_C / a_H *the same), upslope yielding becomes increasingly difficult. However, the change of base angle β from* 15^o *to* 25^o*, results in a small variation of permanent displacement (of the order of 20%).*

As it can be seen in Figure 4.21, for $\beta = 5^o$ *the block does sometimes slide uphill, in addition to the dominant downhill motion. Notice a major upward slip at 3.8 seconds, illustrated between red dashed lines in Figure 4.21. For* $\beta = 15^o$ *and* 25^o *the block slides only downward. Besides, as portrayed in Figure 4.22, in case of* $\beta = 5^o$ *the velocity of the block has a nearly constant gradient during all yielding periods–meaning that* a_C *is not varying with time—reflecting that for such a small angle β the influence of the fluctuation term,* $\mu a_H(t) \sin\beta$*, on the critical acceleration* a_C *is negligible. On the contrary, for* $\beta = 25^o$ *the block velocity (bold black line in Figure 4.23) is strongly fluctuating during sliding.*

4.2 Simultaneous action of horizontal and vertical excitation

An objective of our research is to investigate the role of large vertical accelerations acting simultaneously with horizontal accelerations, as is appropriate for near-fault motions. Earthquake engineers have always been concerned about the effects of the vertical component of ground acceleration. In recent years the issue of the possible effects of vertical acceleration on different systems, such as bridges and buildings, has been debated. Large vertical accelerations recorded in numerous earthquakes have fuelled the discussion on the subject. Geotechnical engineers appear to have accepted the important role of vertical acceleration for retaining structures and slopes. The vectorial synthesis of α_H and α_V appears as a natural fact in many papers and textbooks on the subject. But is α_V really significant for sliding systems ?

To explore the subject, a comprehensive parameter study has been conducted using actual horizontal and vertical acceleration time histories. An extensive summary of the results is discussed here.

In presence of both horizontal and vertical acceleration, the inertial components acting on the block are: two parallel to the slope and two normal to it (see Figure 4.28). When an upward horizontal excitation is imposed on the mass, the latter begins to slide downward if the following "yielding" acceleration is reached:

$$a_{C1}(t) = (\mu \cos\beta - \sin\beta) - \mu\, a_H(t) \sin\beta \pm \mu\, a_V(t) \cos\beta \qquad (4.4)$$

in which $a_V(t)$ is the vertical acceleration at time t. On the other hand, if the horizontal excitation acts downhill, the block starts yielding uphill if the following "yielding" acceleration is reached:

$$a_{C2}(t) = (\mu \cos\beta + \sin\beta) + \mu\, a_H(t) \sin\beta \pm \mu\, a_V(t) \cos\beta \qquad (4.5)$$

The term: $\mu\, a_V(t) \cos\beta$, in Equations (4.4) and (4.5) can be positive or negative while the rest of the expression remains unchanged; implying that for a particular direction of the horizontal record, the vertical acceleration is independent of the horizontal. Therefore, in our analyses, vertical excitation will be imposed with both polarities as shown in Figure 4.28 to investigate the importance of vertical acceleration on sliding response.

4.2.1 A note on the selected vertical motions

In actual records, the vertical component of the ground acceleration is invariably of much higher frequency content than its horizontal components; a fact arising from the nature of the P and S waves which dominate the vertical and horizontal ground motion, respectively. Exceptions to this rule are not rare, especially in near fault recordings which can bear the fault rupture signs not only on the horizontal accelerations but on vertical too. For instance, observe the vertical acceleration recorded at Rinaldi station during Northridge earthquake and compare it with the horizontal component of the same station (Figure 4.29): the forward directivity effect appears in both components, with a long period pulse starting approximately at 2 seconds (shaded area).

Furthermore, vertical time-histories with extraordinary (for vertical accelerations) long-duration pulses, such as the record TCU-068 of the Chi-Chi 1999 earthquake (Figure 4.36), have been also chosen for our analysis. Totally, eleven pairs of horizontal and vertical earthquake records have been employed as excitations; their peak values are presented in Table 4.1. Acceleration, velocity and displacement time histories of the utilised vertical records are portrayed in Figures 4.30÷4.40. These seismic motions have been recorded within a few kilometres from the fault (where the vertical component is

usually at its strongest). Both horizontal and vertical components are imposed simultaneously and are plotted in the same scale in Figures 4.41÷4.45.

4.2.2 Significance of vertical component

Sliding response in terms of time histories for the simultaneous horizontal and vertical excitations is illustrated in Figures 4.46 ÷ 4.81. Slippage induced by the Jensen record reaches up to 3.78 m (for a_C/a_H = 0.1) as pictured in Figure 4.46. In the acceleration time history notice the rapid variation of the critical acceleration, a_C, as a result of the vertical acceleration. These micro-fluctuations of a_C can be observed clearly in Figure 4.47, where response of only horizontal or of vertical and horizontal excitation is plotted side by side. Also, all the sliding response time histories induced by the Jensen horizontal component when imposed in parallel or horizontally and by the simultaneous action of the horizontal and vertical components (with both vertical polarities) are displayed in Figure 4.48. The same summary diagrams are provided for the Rinaldi, JMA, Takatori, and TCU 065 excitations in Figures 4.52, 4.58, 4.63, and 4.69 respectively.

It is interesting to focus on the Chi-Chi record, the vertical acceleration of which seems to be particularly severe, containing a strong and exceptionally long-period pulse (0.3 g and 2.5 sec) which leads to uncommonly high (for vertical motion) spectral acceleration values [Figure 4.36]. Yet the analysis reveals their minor significance: the effect of such a vertical excitation is a mere 4% decrease in slippage for a_C/a_H = 0.1, as Figure 4.73 depicts. The same is true for every acceleration ratio of a_C/a_H examined (Figure 4.74).

Figures 4.50, 4.51, 4.56, 4.57, 4.61, 4.62, 4.68, 4.72, 4.74, 4.76, and 4.79 illustrate the general trend that by increasing the ratio a_C/a_H, while keeping the inclination β and the

maximum imposed acceleration a_H constant, leads to decreasing slippage. The results are qualitatively the same (but not quantitatively, as it will be shown later) whether the excitation acts parallel to the sliding surface or horizontally, with vertical acceleration present or not. In addition, the reduction of slippage is almost proportional to the ratio a_C/a_H.

When the ratio a_C/a_H is doubled (keeping all the other parameters constant), the sliding displacement reduces by roughly a factor of two. For instance, in Figure 4.76, the results in the left column are for exclusively-horizontal excitation (Duzce record) and demonstrate that for $a_C/a_H = 0.1$ and $\beta = 25^o$ the yielding displacement of the block is 0.55 m while for $a_C/a_H = 0.2$ (and same β) the corresponding displacement becomes 0.27 m, almost half of the previous case.

Except from the detailed time histories presented in the previous paragraph, Figures 4.82÷4.100 are summing up all the results of our analyses. Resulting curves of the slippage, D, versus a_C/a_H, which indicate the effect of vertical acceleration in asymmetric sliding, are portrayed in Figures 4.82÷4.92. Three curves are compared in each plot: one for excitation by the horizontal component alone (continuous bold line), a second curve for simultaneous excitation by the horizontal and vertical components when the vertical applied with one polarity (dashed line), and the third one also for simultaneous excitation of horizontal and vertical acceleration with reversed polarity (continuous dotted line). Apparently, even the occurrence of very strong vertical accelerations is of negligible significance for the slippage of rigid blocks ! A consistent conclusion can be drawn from the Figures 4.93÷4.98.

The presence of vertical acceleration results in additional fluctuation of the critical yielding acceleration a_C (i.e., besides the fluctuations induced by the horizontal excitation

itself). Such variations arise from the time-dependent term [μ $a_V(t)$ cosβ]. Vertical acceleration varies independently of the horizontal acceleration, so it can reduce or increase the critical yielding acceleration a_C regardless of the role of the horizontal acceleration. However, the vertical excitation can not reverse the sliding direction of the block, which is solely controlled by the horizontal excitation.

Eventually, the final displacement of the sliding block triggered by vertical and horizontal motions deviates less than 10% from the corresponding displacements when only horizontal acceleration acts (see Figures 4.99 and 4.100). What is more, the slippage in many of the cases is smaller if both vertical and horizontal excitation are imposed (negative region at Figures 4.99 and 4.100) !

The aforesaid conclusion, of non-importance of vertical excitation for sliding, is fully verified: in all studied cases, despite record-high vertical accelerations far exceeding the usual values, slippage of the block is practically unaffected by the vertical component.

4.3 Conclusions

Whether on a horizontal or on an inclined base, the slippage of a rigid block subjected to near-fault directivity or fling affected motions is sensitive not only to the peak acceleration, peak velocity, or dominant frequency, of the main excitation pulse(s) that such motions contain, but also :

- *on the unpredictable detailed sequence of strong pulses*
- *on the polarity (+ or –) of the horizontal component of acceleration.*

Such a sensitivity of sliding to details of the excitation has not been pointed out by previous researchers (e.g. Franklin & Chang 1977, Yegian et al 1991, Kramer & Lindwall 2004, Bray & Travasarou 2006) who compiled the results of huge number of analyses and performed statistical analyses to derive design sliding curves.

By contrast, the slippage is not affected to any measurable degree by even the strongest vertical components of accelerograms! Even when the two components (horizontal and vertical) are identical in amplitude and their peak values coincide in time (a very severe and rather unlikely incident, artificially imposed in the analyses), the vertical excitation still has a minor effect (see Fardis et al 2003). In fact it could not be a priori determined whether this effect would be positive or negative.

Table 4.1: *Pairs of horizontal and vertical earthquake records employed as excitations at the base of sliding mass. Both components are imposed simultaneously.*

Earthquake, Magnitude	***Record Name***	**PGA** (g)	**PGV** (m/s)	**PGD*** (m)
Kobe 1995, $M_W = 7.0$ $M_{JMA} = 7.2$	*JMA - 0°*	*0.830*	*0.810*	*0.177*
	JMA - Up	*0.341*	*0.380*	*0.100*
	Takatori - 0°	*0.611*	*1.272*	*0.358*
	Takatori - Up	*0.274*	*0.162*	*0.053*
Loma Prieta 1989, $M_S = 7.1$	*Gilroy Array No1 - Trans*	*0.473*	*0.339*	*0.081*
	Gilroy Array No1 - Up	*0.209*	*0.139*	*0.056*
Lefkada 2003, $M_W = 6.3$	*Lefkada - Trans*	*0.426*	*0.354*	*0.396*
	Lefkada - Up	*0.189*	*0.110*	*0.072*
Chi-Chi 1999, $M_w = 7.5$	*TCU 065 - EW*	*0.450*	*1.298*	*1.820*
	TCU 065 - Up	*0.261*	*0.680*	*0.564*
	TCU 068 - NS	*0.353*	*2.892*	*8.911*
	TCU 068 - Up	*0.504*	*0.221*	*4.462*
Landers 1992, $M_w = 7.3$	*Lucerne - 275°*	*0.721*	*0.976*	*0.703*
	Lucerne - Up	*0.818*	*0.465*	*0.263*
Kocaeli 1999, $M_w = 7.4$	*Duzce - 270°*	*0.358*	*0.464*	*0.176*
	Duzce - Up	*0.209*	*0.224*	*0. 241*
Northridge 1994, $M_w = 6.8$	*Rinaldi - 228°*	*0.837*	*1.485*	*0.261*
	Rinaldi - Up	*0.852*	*0.517*	*0.120*
	Jensen Filtration Plant - 22°	*0.424*	*0.873*	*0.265*
	Jensen Filtration Plant - Up	*0.395*	*0.346*	*0.095*
	Newhall Fire Station - 360°	*0.589*	*0.753*	*0.182*
	Newhall Fire Station - Up	*0.505*	*0.366*	*0.157*

**Final ground displacements of the fling–affected records are in accord with Boore (2001) and geodetic measurements.*

Block Sliding from Horizontal Acceleration Records When Imposed Horizontally to an Inclined Sliding Surface

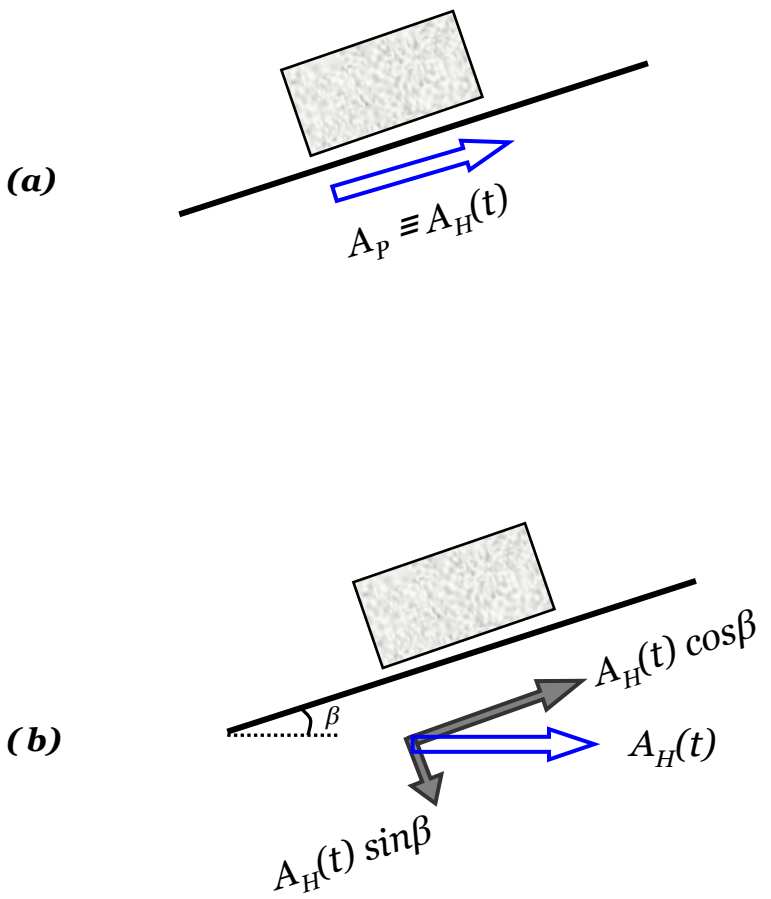

Figure 4.1 *The horizontal acceleration is applied, as the sketches illustrate, in two ways: (a) parallel to the sliding surface, and (b) horizontally, i.e. at an angle with the sliding surface which is equal to β. In the latter case, the horizontally applied excitation is analysed into a parallel and a perpendicular component.*

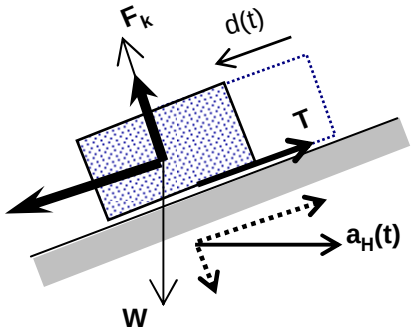

Figure 4.2 *Forces acting on a rigid block that tends to slide downwards when subjected to upwards horizontal excitation.*

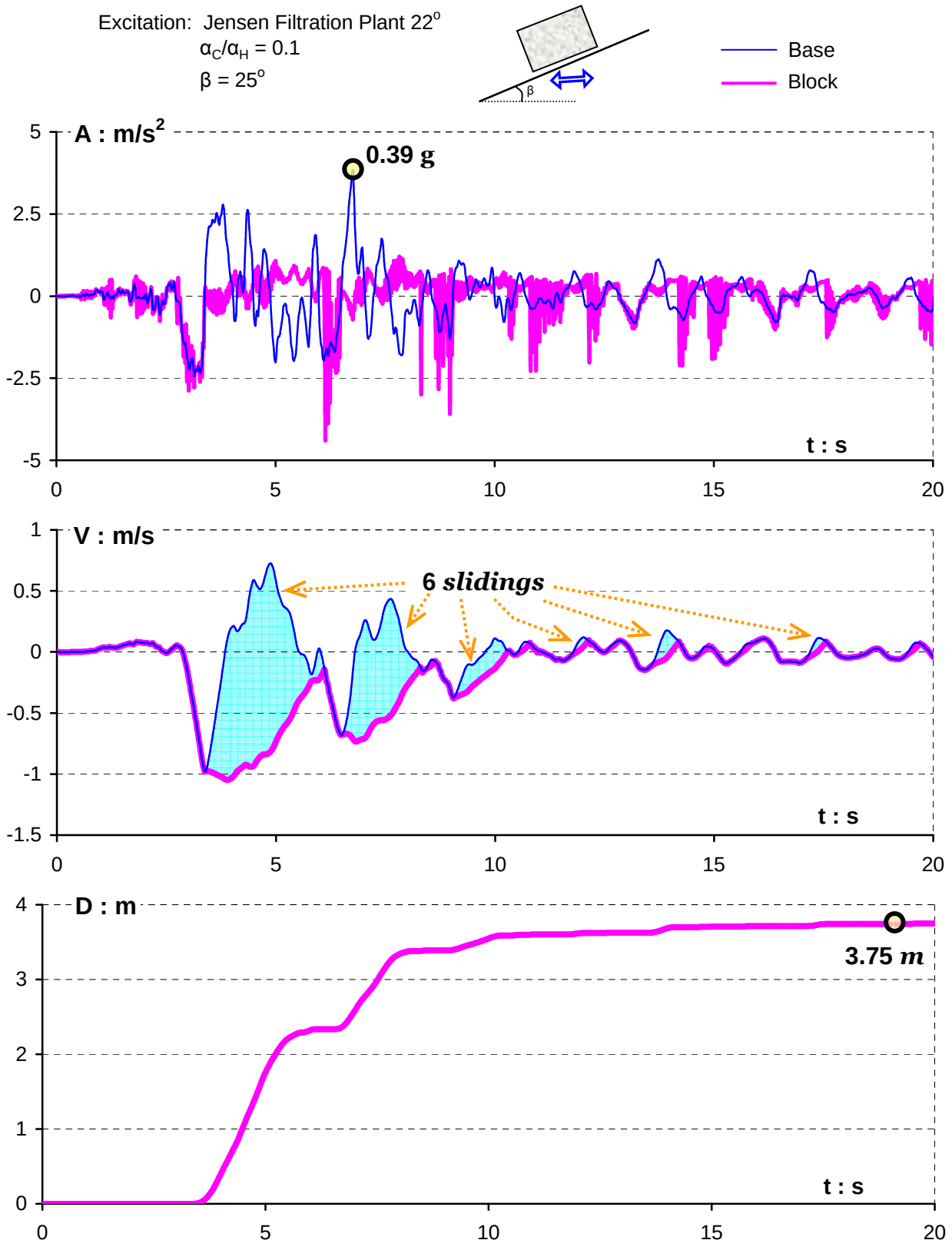

Figure 4.3 *Asymmetric response time histories of a rigid block resting on an 25^0 inclined plane when subjected to the horizontally acting Jensen Filtration Plant– 22^0 record. ($a_C/a_H = 0.1$) The light blue shaded area at the velocity time histories represents the slippage triggered at each yielding period.*

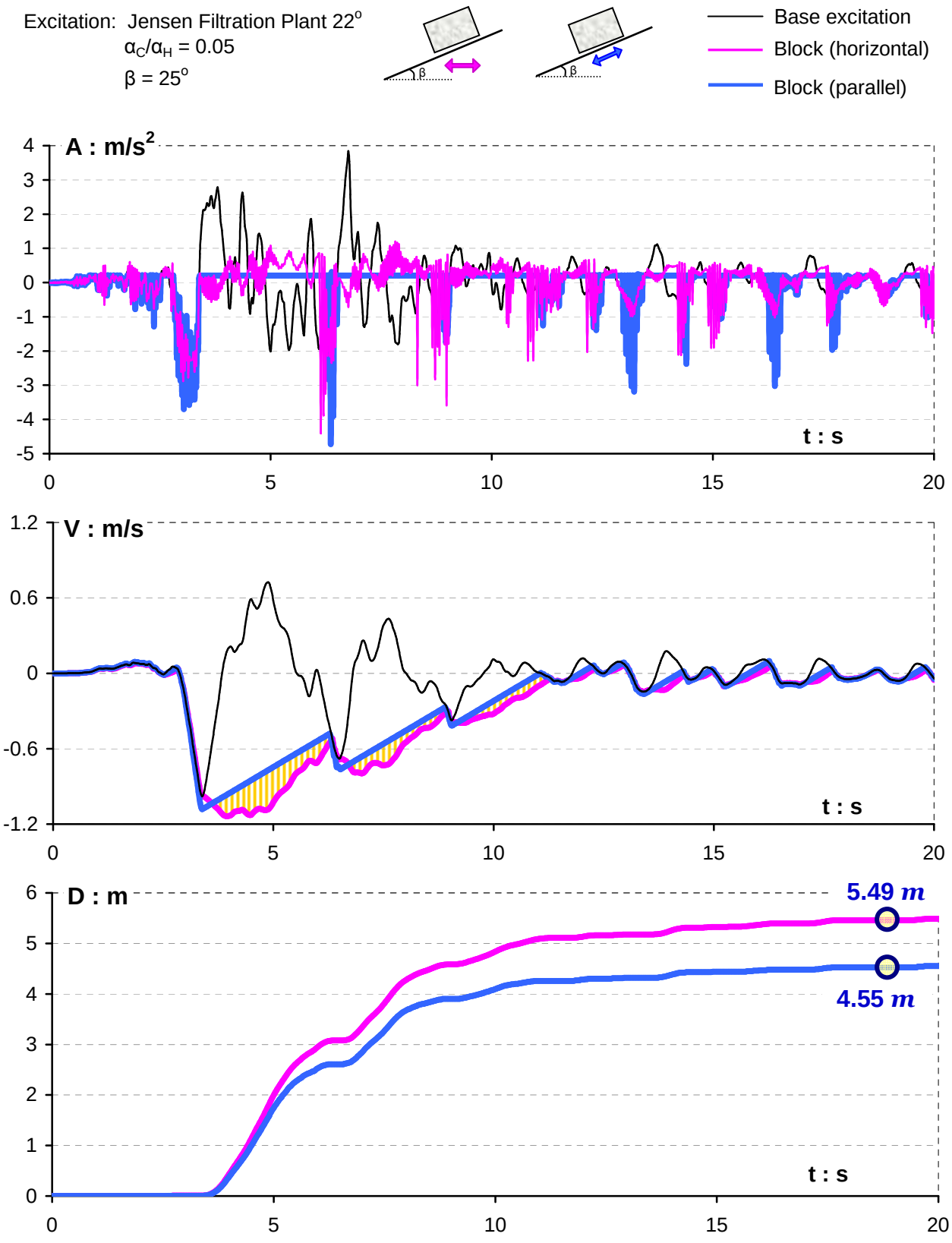

Figure 4.4 *Acceleration, velocity, and sliding displacement time histories of a block rested on a 25^0 inclined plane subjected to the Jensen Filtration Plant -22^0 horizontal record. The light blue line represents the block's response when the excitation imposed parallel to the plane. The solid pink line corresponds to the response when the input motion acts horizontally to the plane. ($a_C/a_H = 0.05$)*

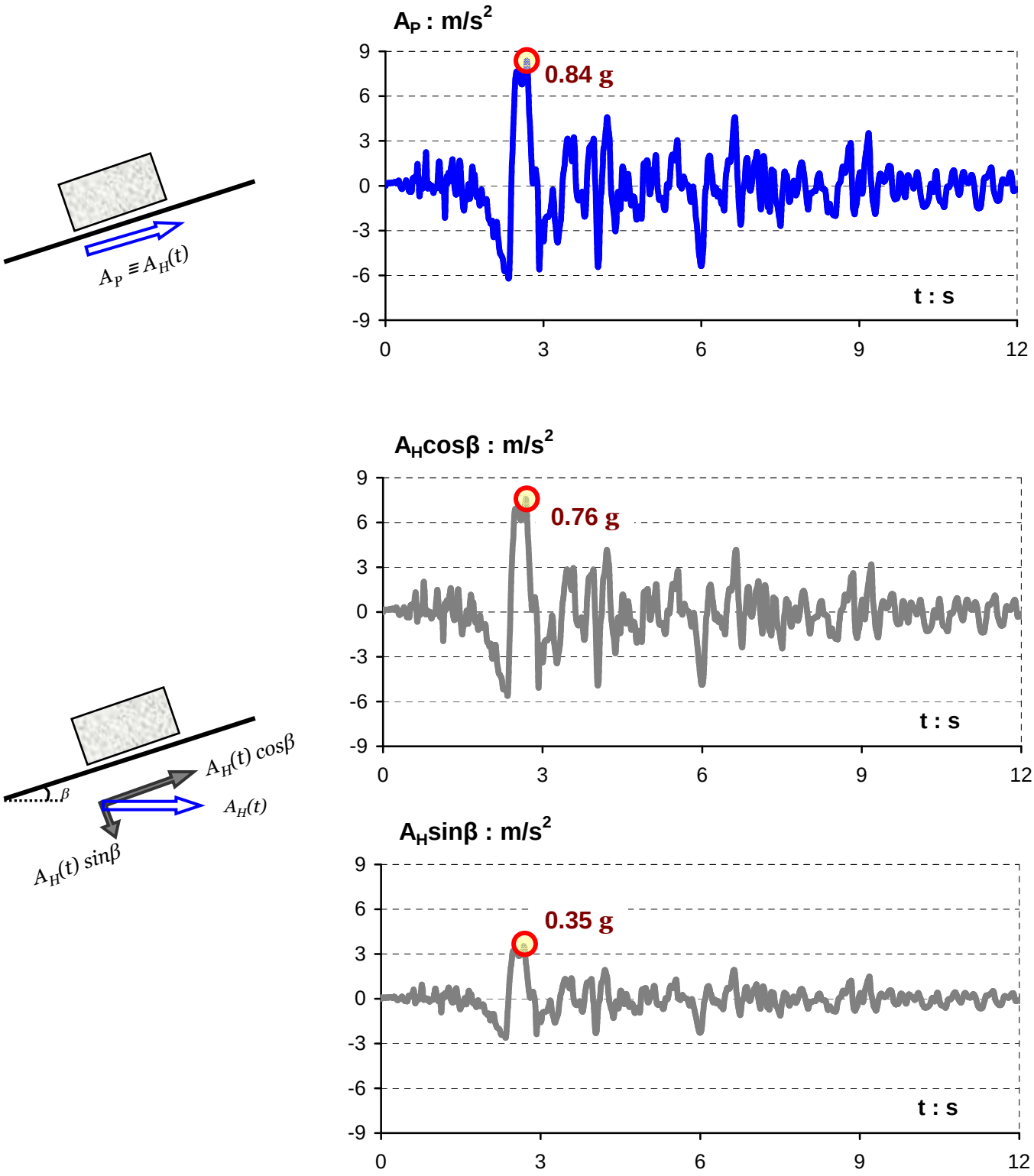

Figure 4.5 *Excitation time histories depending on the direction they apply relatively to the sliding surface. At the top figure, the solid blue line pictures the reversed Rinaldi-228º acceleration acting parallel to the slope. However, for the two bottom plots, when horizontal acceleration is applied horizontally to the plane it can be further analyzed to a parallel and a perpendicular component. The parallel component of horizontal acceleration is somewhat smaller:* $A_H cos\beta = A_H cos25^0 = 0.906A_H$ *and the perpendicular component is:* $A_H sin\beta = A_H sin25^0 = 0.422A_H$.

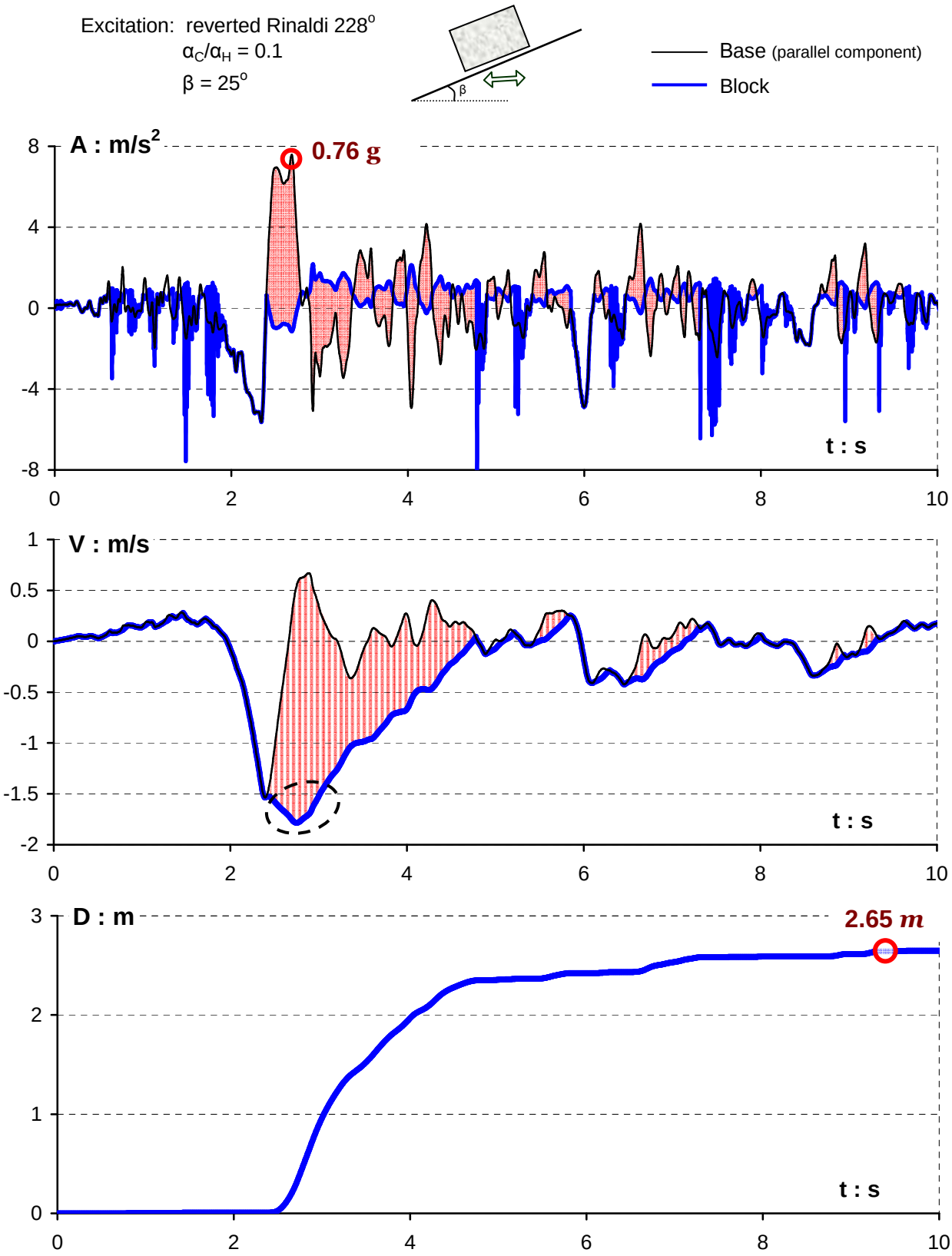

Figure 4.6 *Asymmetric response time histories of a rigid block resting on an 25^0 inclined plane when subjected to the horizontally acting reversed polarity Rinaldi -228^0 record. The red shaded area in acceleration time histories reflects the excess of the relative velocity of the block when sliding on the plane ($a_C/a_H = 0.1$).*

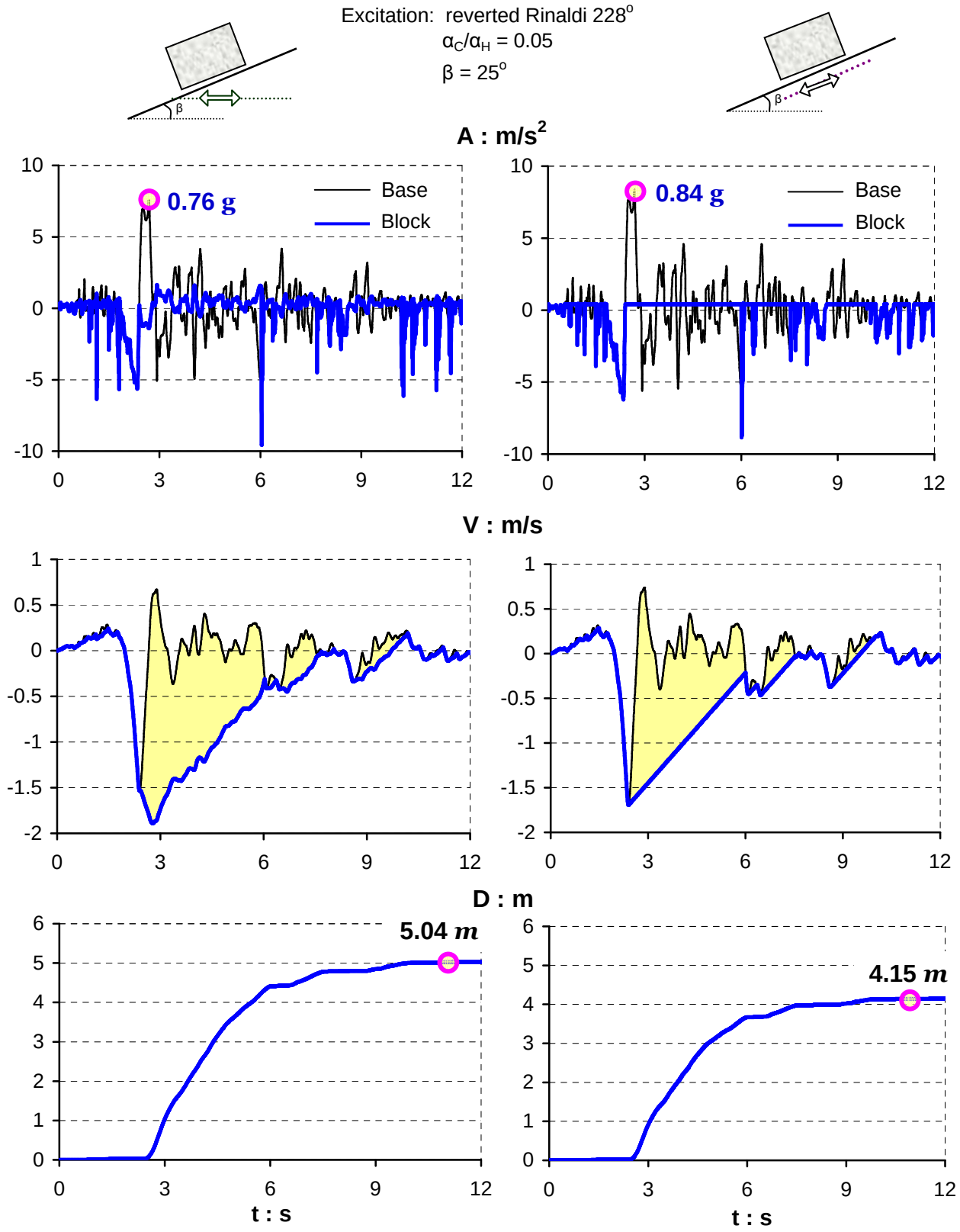

Figure 4.7 *The reversed horizontal Rinaldi –228^0 record imposed parallel (right column) and horizontally (left column) to the slope. The response difference due to directionality of the applied motion is significant. When the excitation is horizontally employed, even if the parallel component is reduced by a factor of cosβ; the importance of the perpendicular component that fluctuates the yielding acceleration prevails. As a result, the induced slippage is larger than the one caused by the parallel applied excitation (a_C/a_H = 0.05 and β = 25^o).*

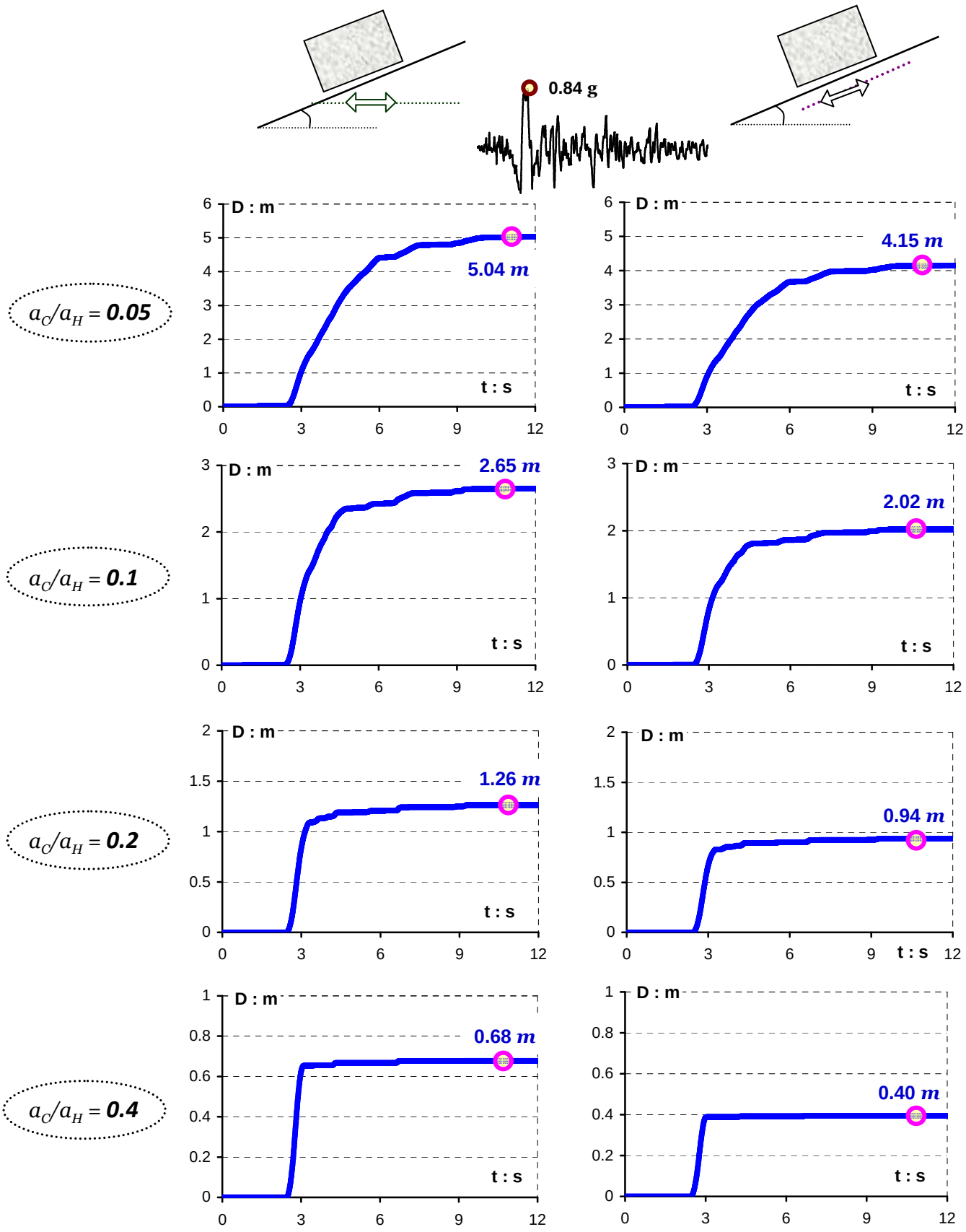

Figure 4.8 *The directionality effect on asymmetric sliding for four acceleration ratios, a_C/a_H . The triggering excitation is the reversed Rinaldi–228° record imposed parallel to the sliding surface (right column) and horizontally (left column). [$\beta = 25^o$]*

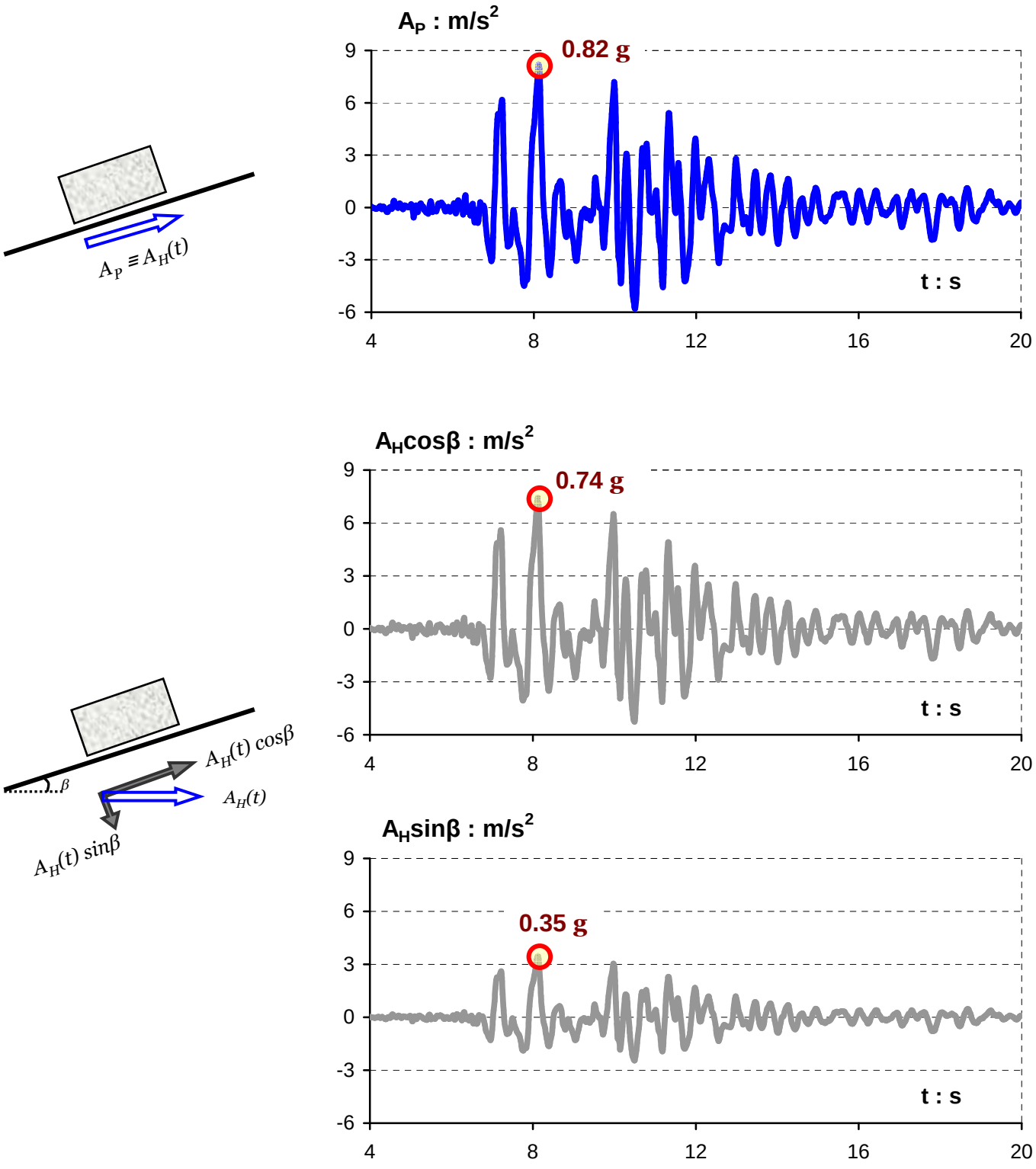

Figure 4.9 *Excitation time histories depending on the direction they apply relatively to the sliding surface. At the top figure, the solid blue line pictures the horizontal acceleration of the reversed JMA –0^0 record acting parallel to the slope. The two bottom plots portray the two components of the horizontally imposed acceleration. The parallel component of horizontal acceleration is: $A_H\cos\beta = A_H\cos 25^0 = 0.906A_H$ and the perpendicular component is: $A_H\sin\beta = A_H\sin 25^0 = 0.422A_H$.*

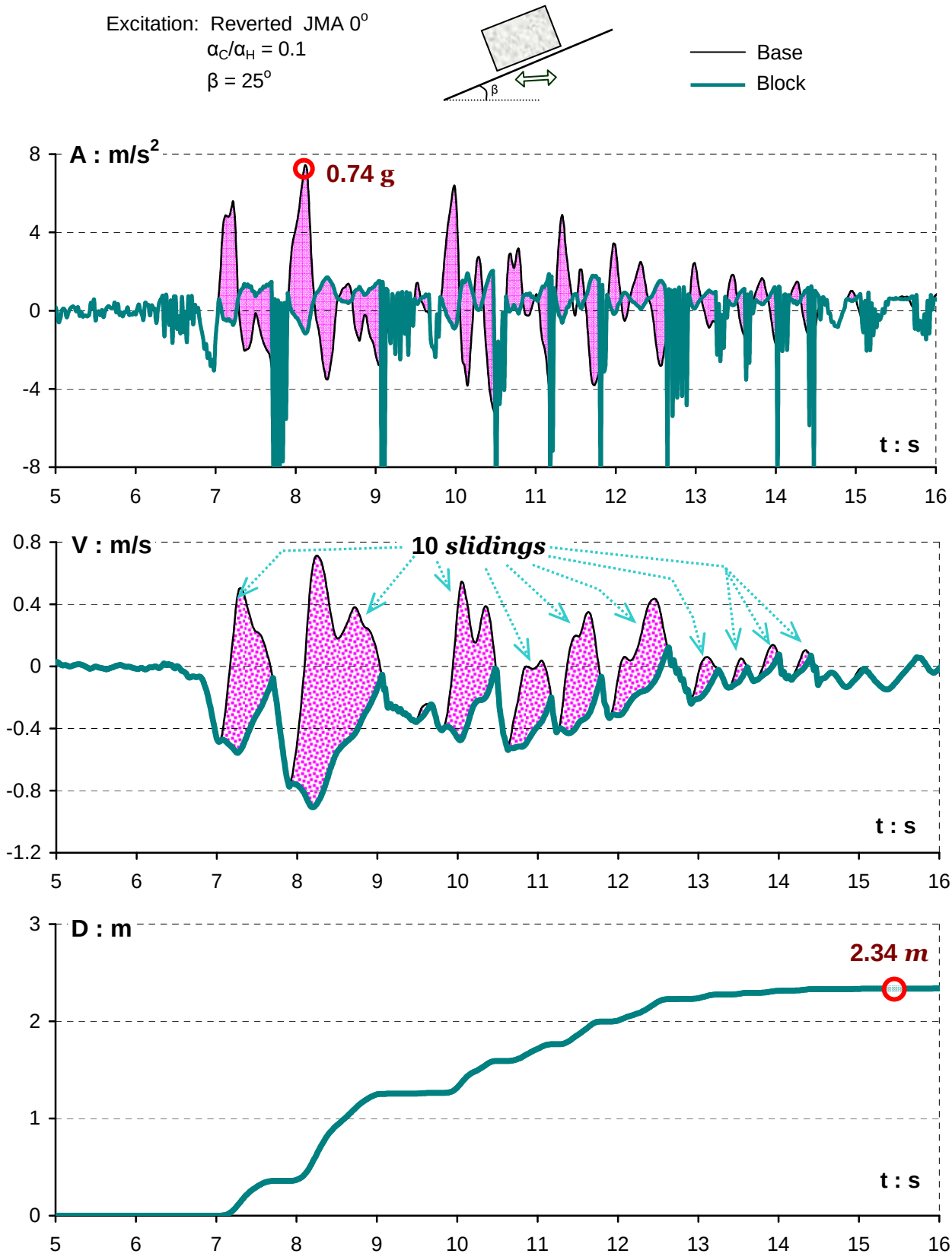

Figure 4.10 *Asymmetric response time histories of a rigid block resting on an 25^0 inclined plane when subjected to the horizontally acting reversed polarity JMA–0^0 record. The red shaded area in acceleration time histories reflects the excess of the relative velocity of the block when sliding on the plane ($a_C/a_H = 0.1$).*

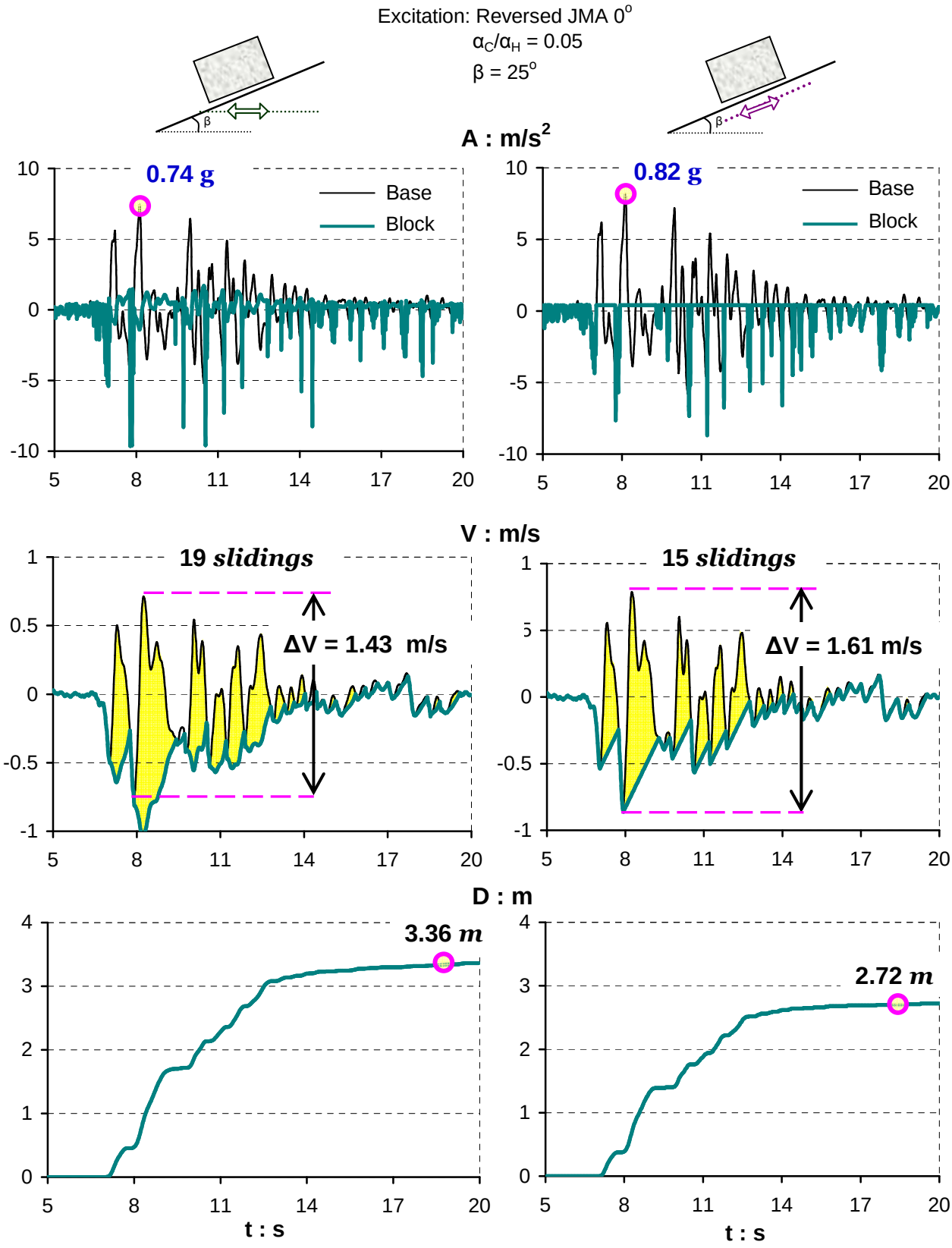

Figure 4.11 *The reversed horizontal JMA–0^0 record imposed parallel (right column) and horizontally (left column) to the slope. The response difference due to directionality of the applied motion is significant. Notice that for parallel imposed motion the number of yielding events are fewer than for horizontally employed excitation ($a_C/a_H = 0.05$ and $\beta = 25^o$).*

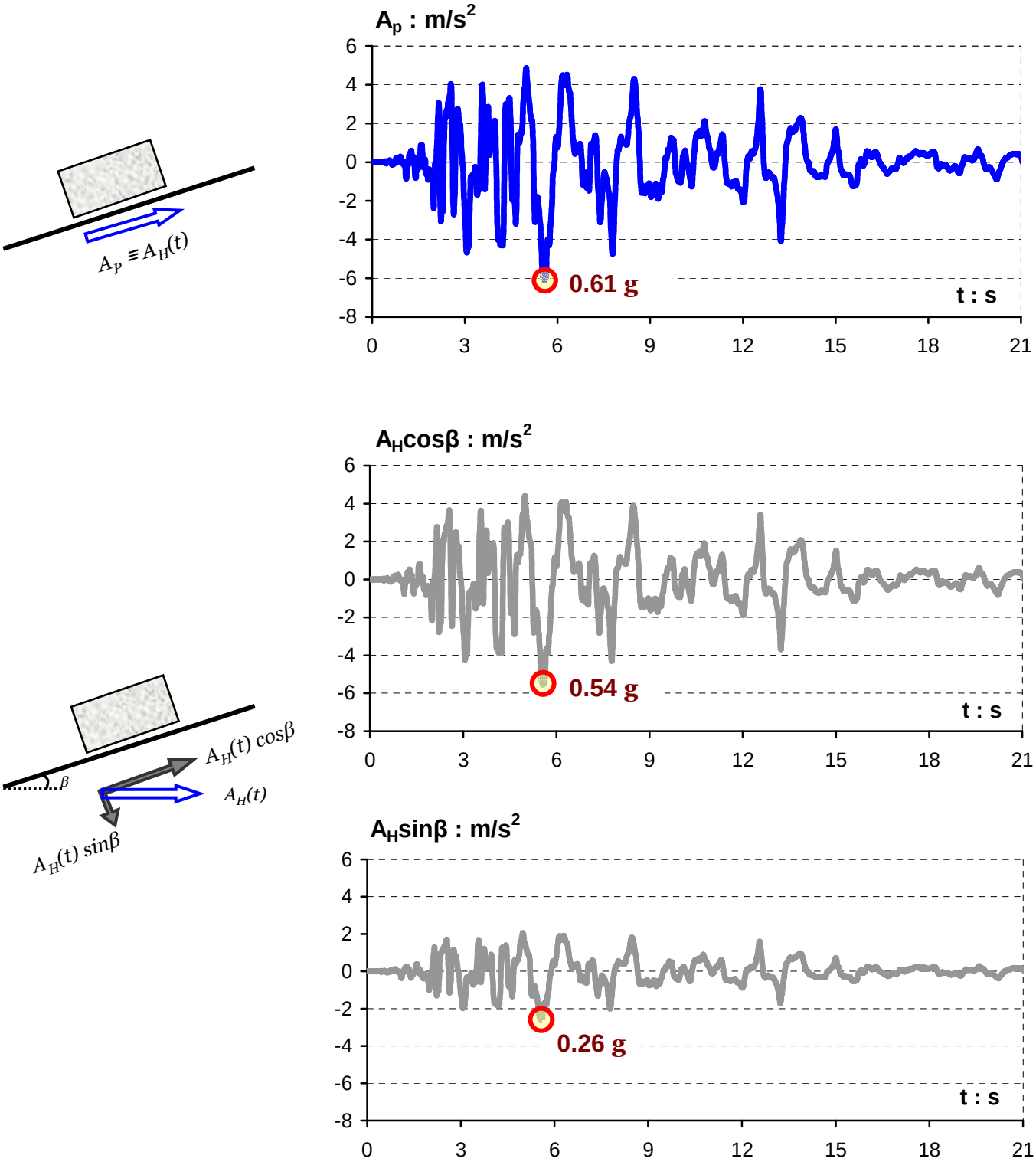

Figure 4.12 *Excitation time histories depending on the direction they apply relatively to the sliding surface. At the top figure, the solid blue line pictures the horizontal acceleration of the reversed Takatori –0^0 record acting parallel to the slope. The two bottom plots portray the two components of the horizontally imposed acceleration. The parallel component of horizontal acceleration is: $A_H cos\beta = A_H cos25^0 = 0.906A_H$ and the perpendicular component is: $A_H sin\beta = A_H sin25^0 = 0.422A_H$.*

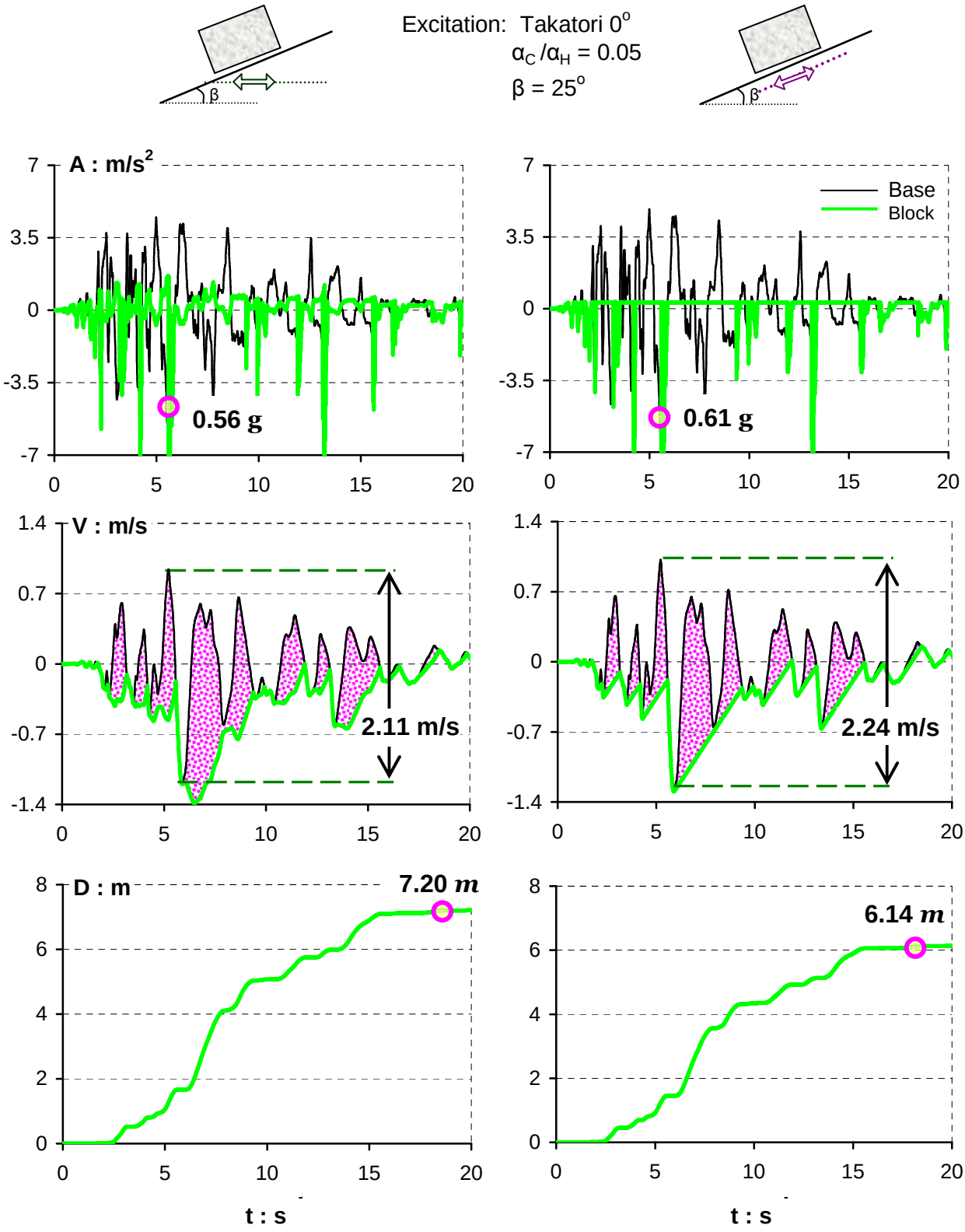

Figure 4.13 *The reversed polarity Takatori–0⁰ record imposed parallel (right column) and horizontally (left column) to the slope. The directionality response difference is quite significant as the slippage from the horizontally applied acceleration is almost 20% larger than that of the parallel excitation. ($a_C/a_H = 0.05$ and $\beta = 25^o$)*

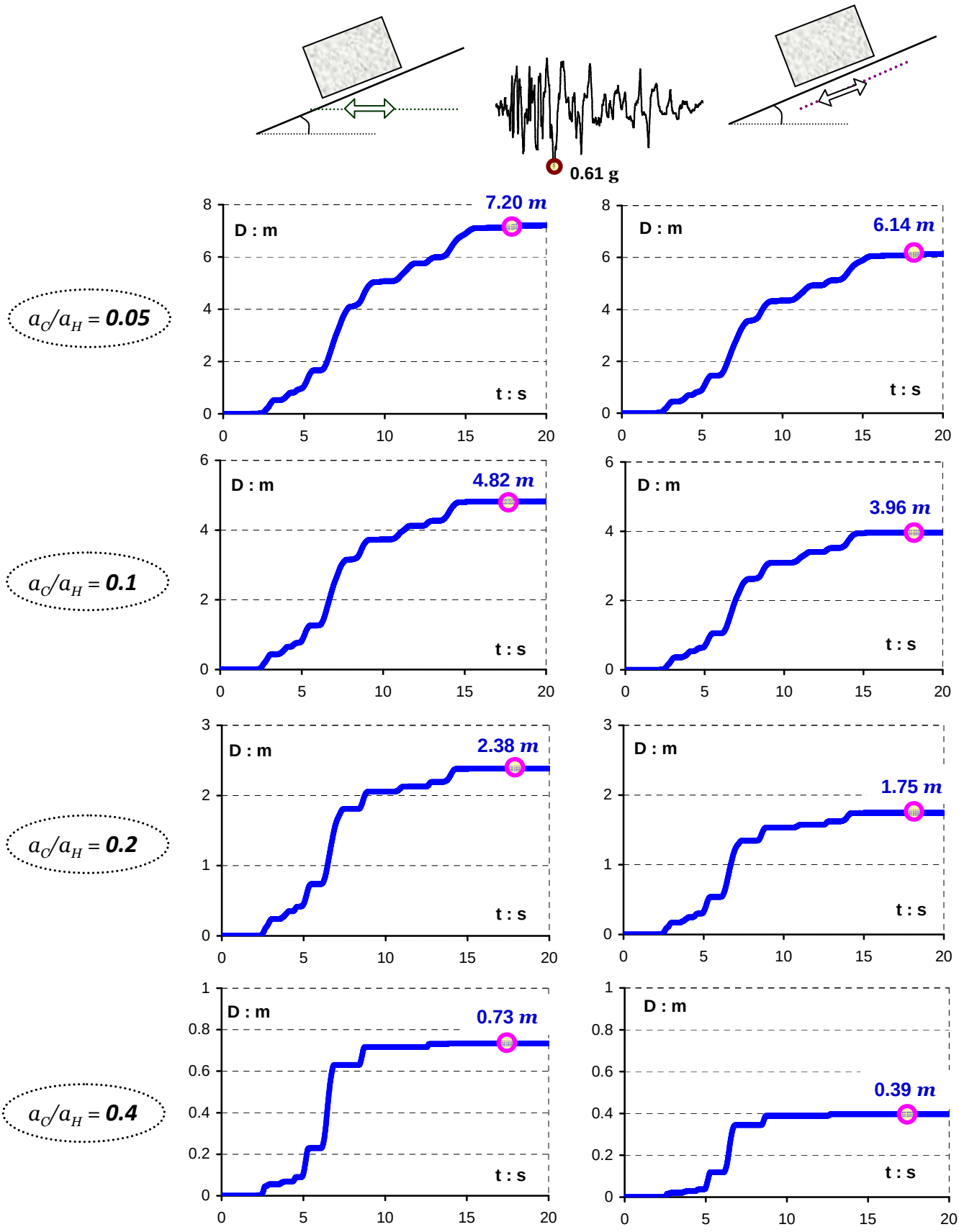

Figure 4.14 *The directionality effect on asymmetric sliding for four acceleration ratios, a_C/a_H . The triggering excitation is the reversed Takatori–0° record imposed parallel to the sliding surface (right column) and horizontally (left column). [$\beta = 25^o$]*

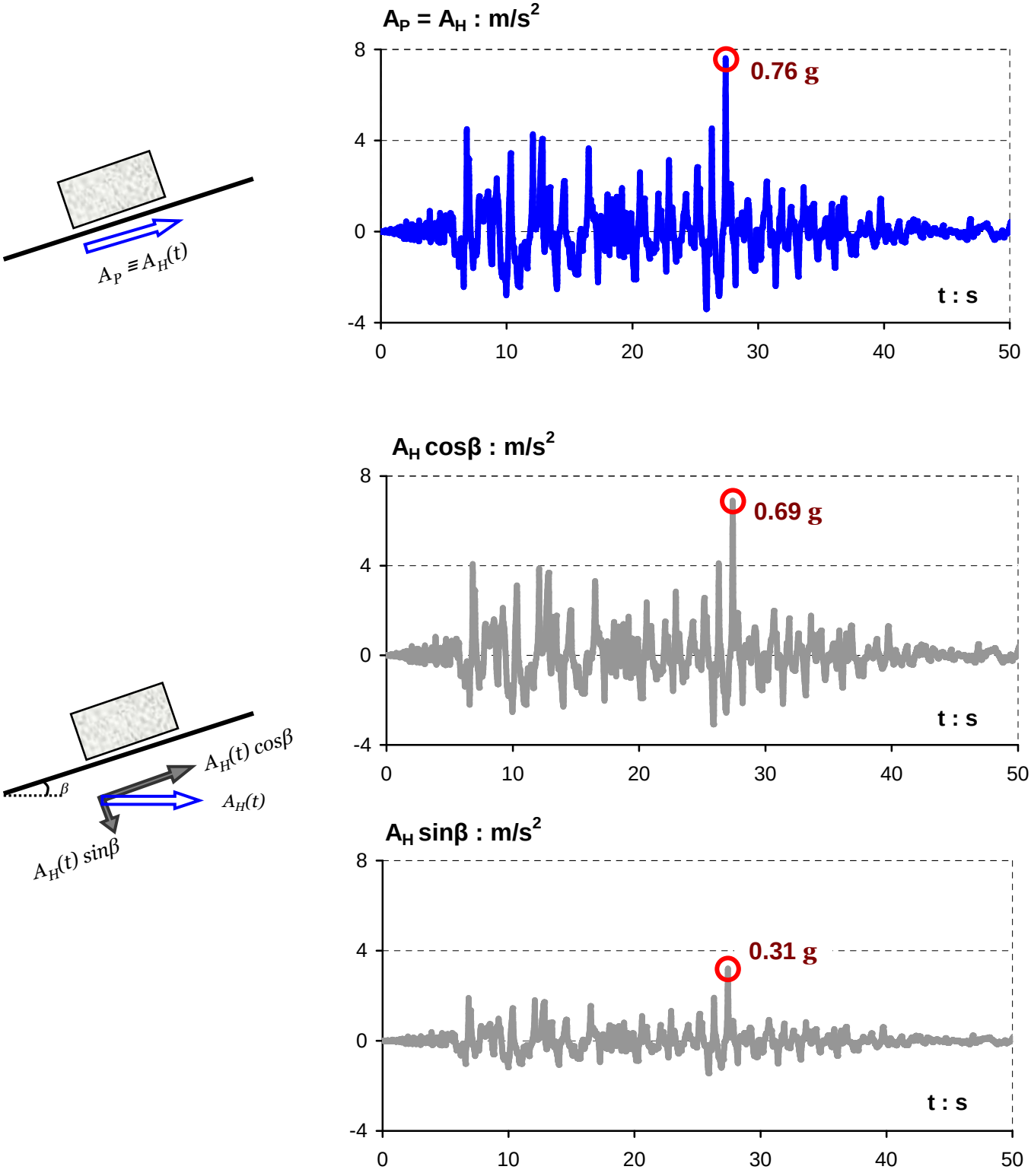

Figure 4.15 *Excitation time histories relatively to the direction they apply relatively to the sliding surface. At the top figure, the solid blue line pictures the TCU 065-EW acceleration acting parallel to the slope. However, for the two bottom plots, when horizontal acceleration is applied horizontally to the plane it can be further analyzed to a parallel and a perpendicular component. The parallel component of horizontal acceleration is somewhat smaller:* $A_H cos\beta = A_H cos25^0 = 0.906A_H$ *and the perpendicular component is:* $A_H sin\beta = A_H sin25^0 = 0.422A_H$.

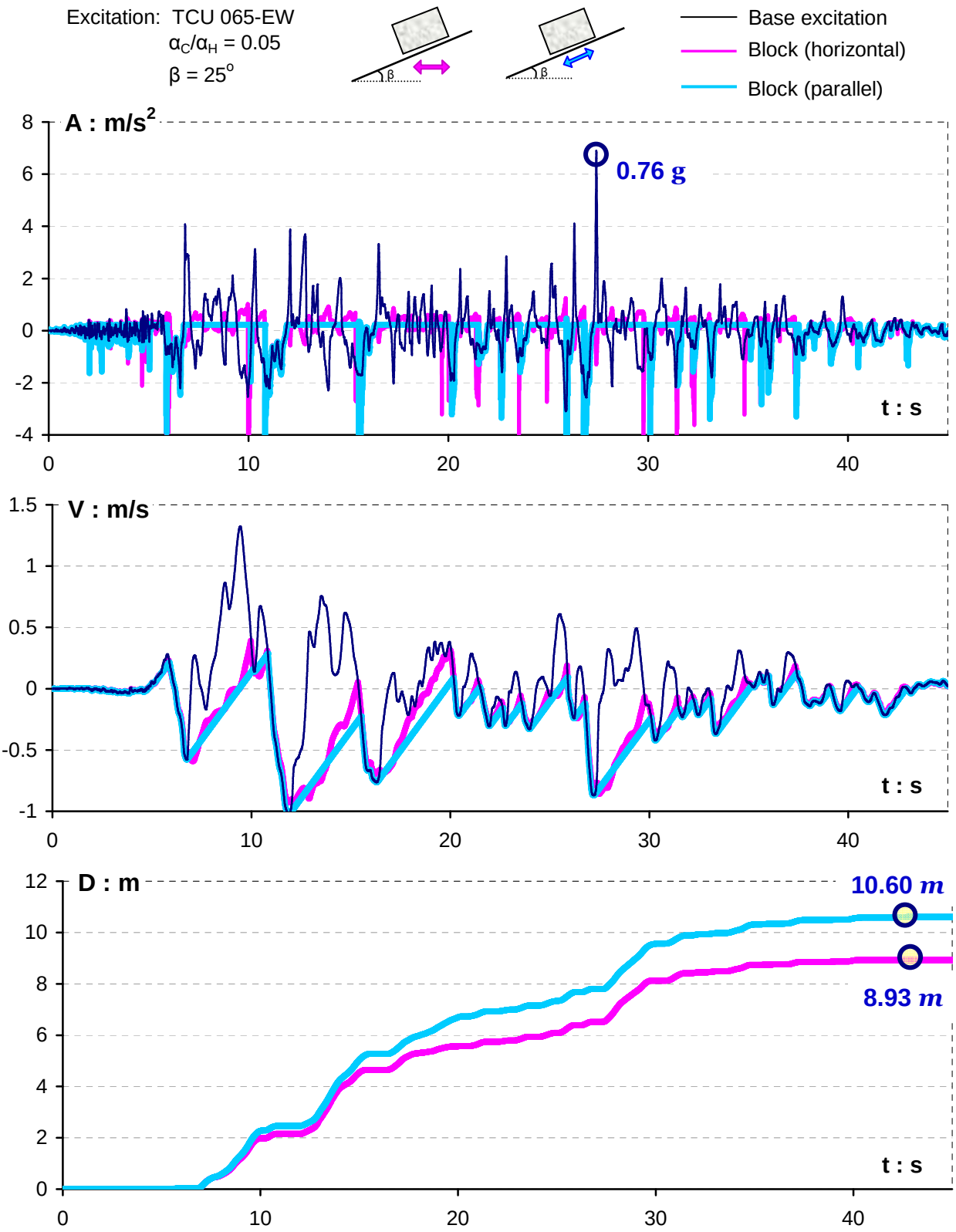

Figure 4.16 *Acceleration, velocity, and sliding displacement time histories of a block rested on a 25^0 inclined plane subjected to the TCU 065 –EW record. The light blue line represents the block's response when the excitation imposed parallel to the plane, whereas the solid pink line when the input motion acts horizontally to the plane. ($a_C/a_H = 0.05$)*

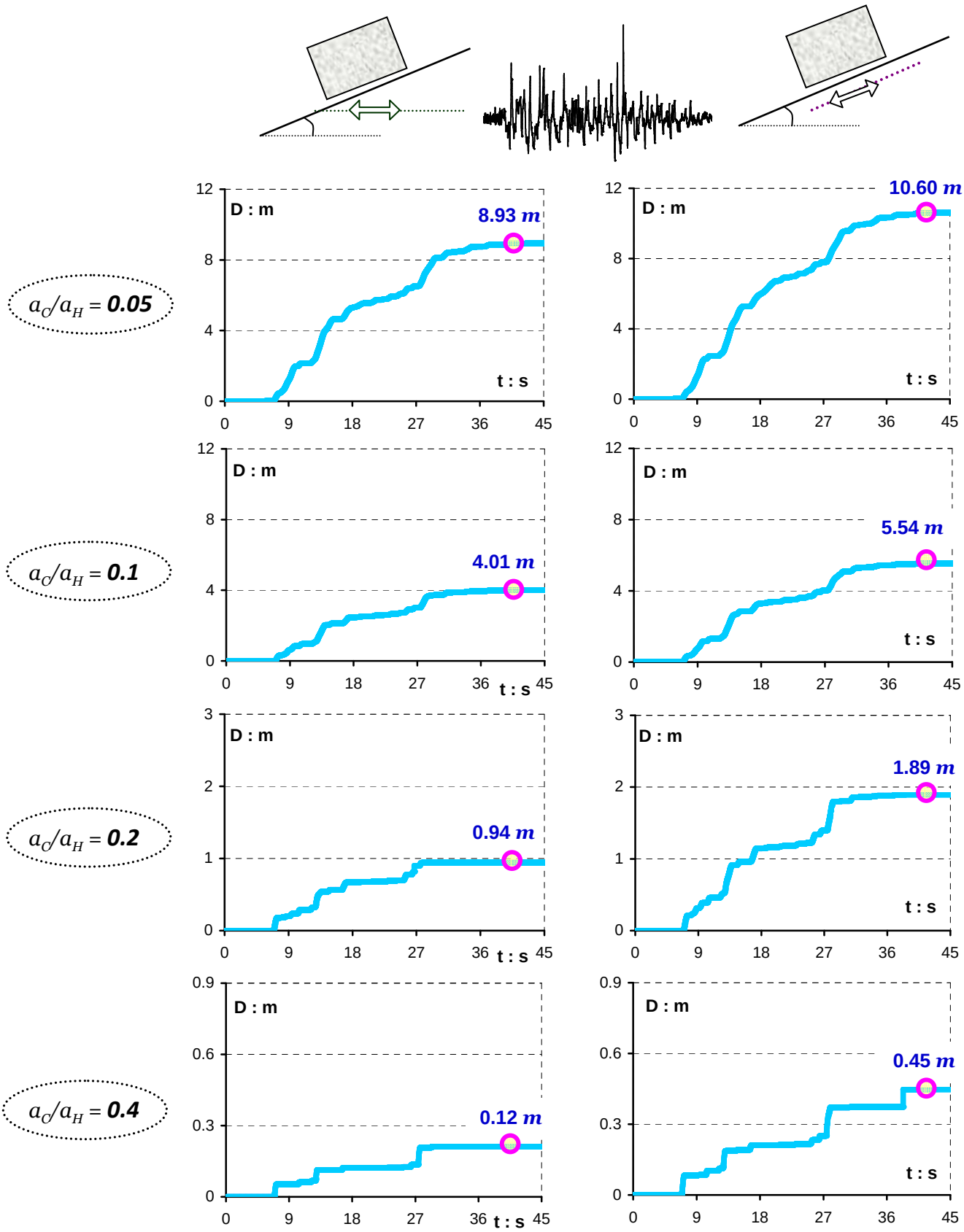

Figure 4.17 *The directionality effect on asymmetric sliding for four acceleration ratios, a_C/a_H. The triggering excitation is the reversed TCU 065–EW record imposed parallel to the sliding surface (right column) and horizontally (left column). [$\beta = 25^o$]*

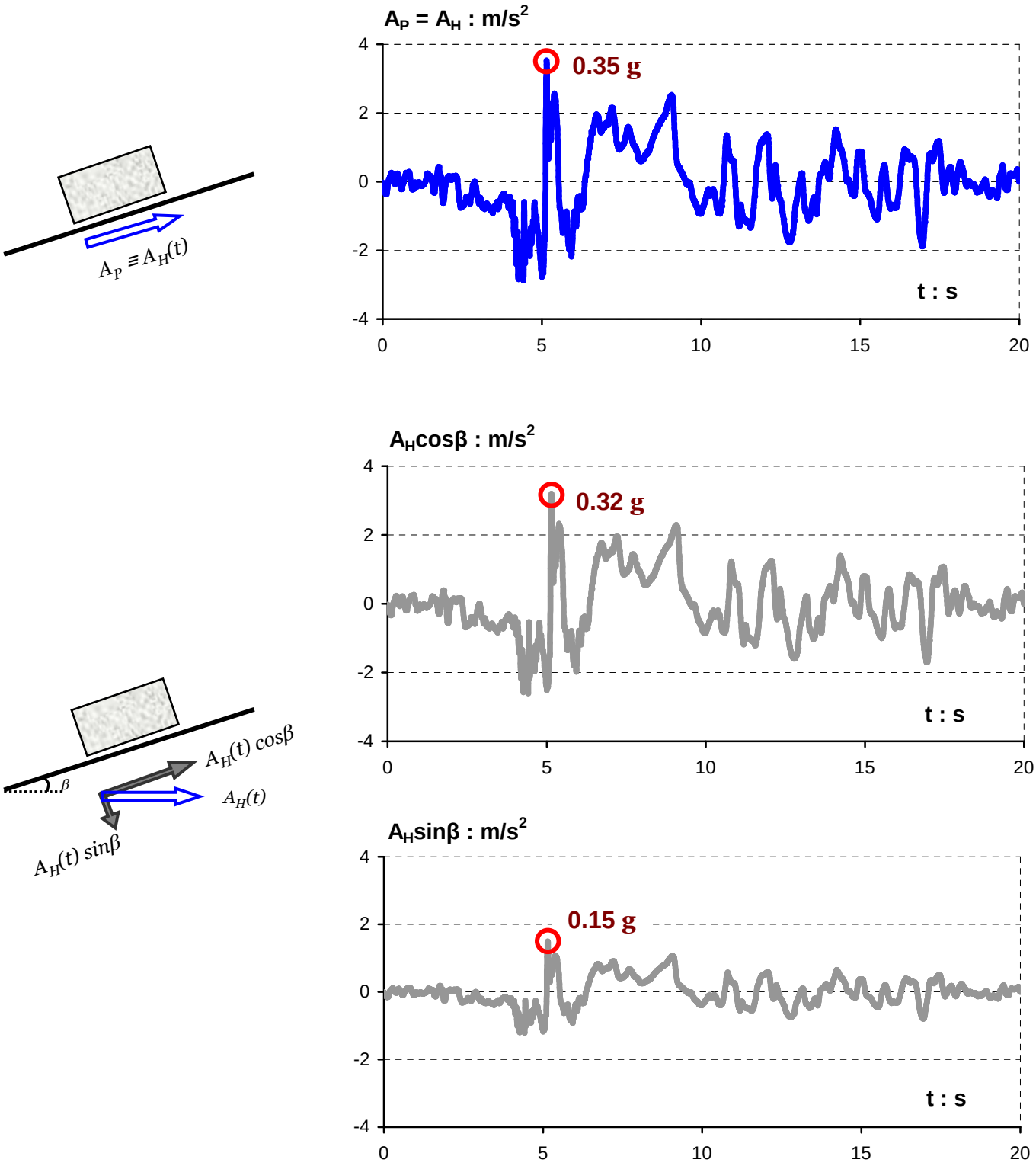

Figure 4.18 *Excitation time histories relatively to the direction they apply relatively to the sliding surface. At the top figure, the solid blue line pictures the reversed polarity TCU 068-NS record acting parallel to the slope. In the two bottom plots horizontal acceleration is applied horizontally to the plane. The parallel component of horizontal acceleration is somewhat smaller:* $A_H\cos\beta = A_H\cos 25^0 = 0.906A_H$ *and the perpendicular component is:* $A_H\sin\beta = A_H\sin 25^0 = 0.422A_H$.

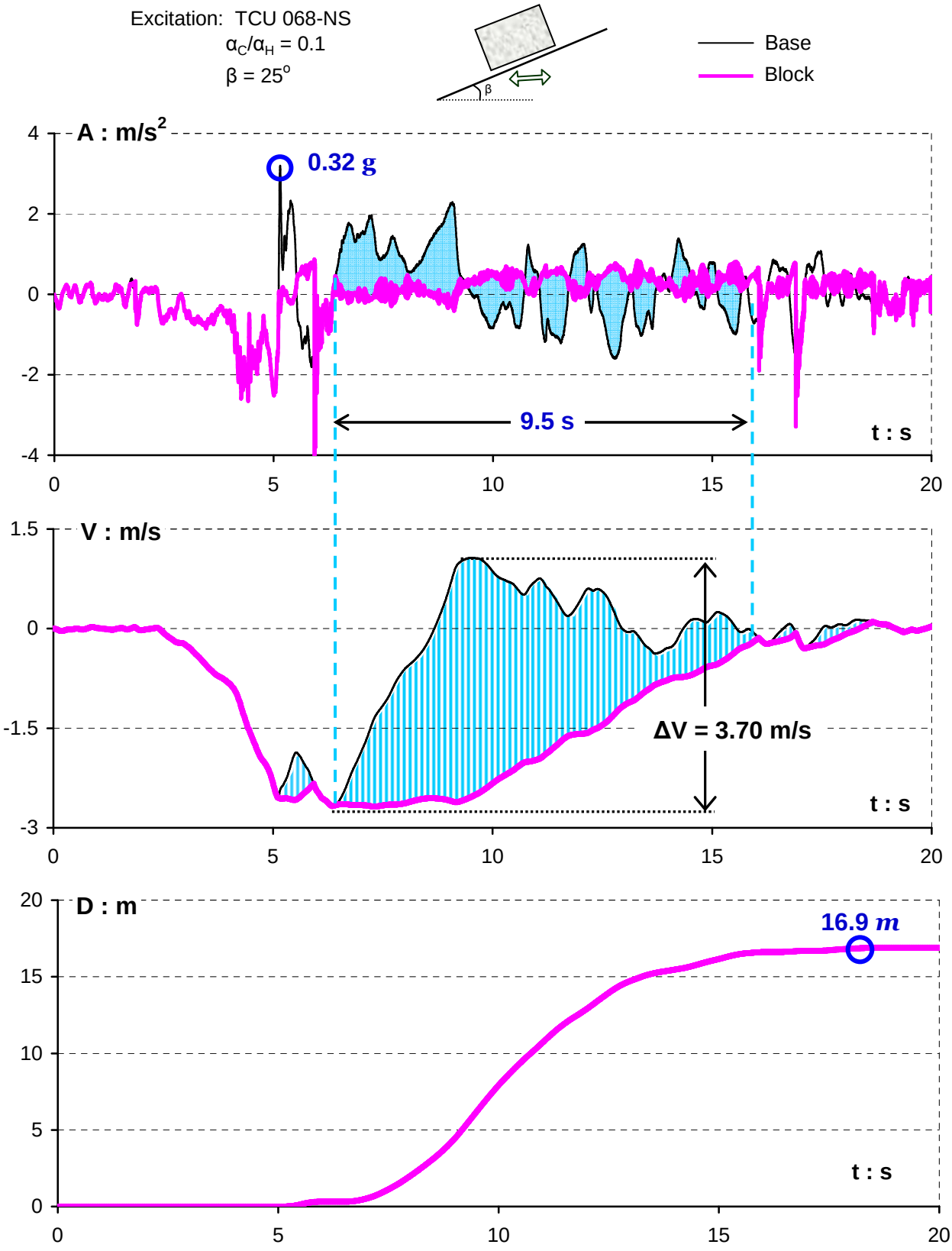

Figure 4.19 *Asymmetric response time histories of a rigid block resting on an 25^0 inclined plane when subjected to the horizontally acting reversed polarity TCU 068–NS record. The light blue stripped area in velocity plot is equal to the displacement induced when sliding occurs ($a_C / a_H = 0.1$).*

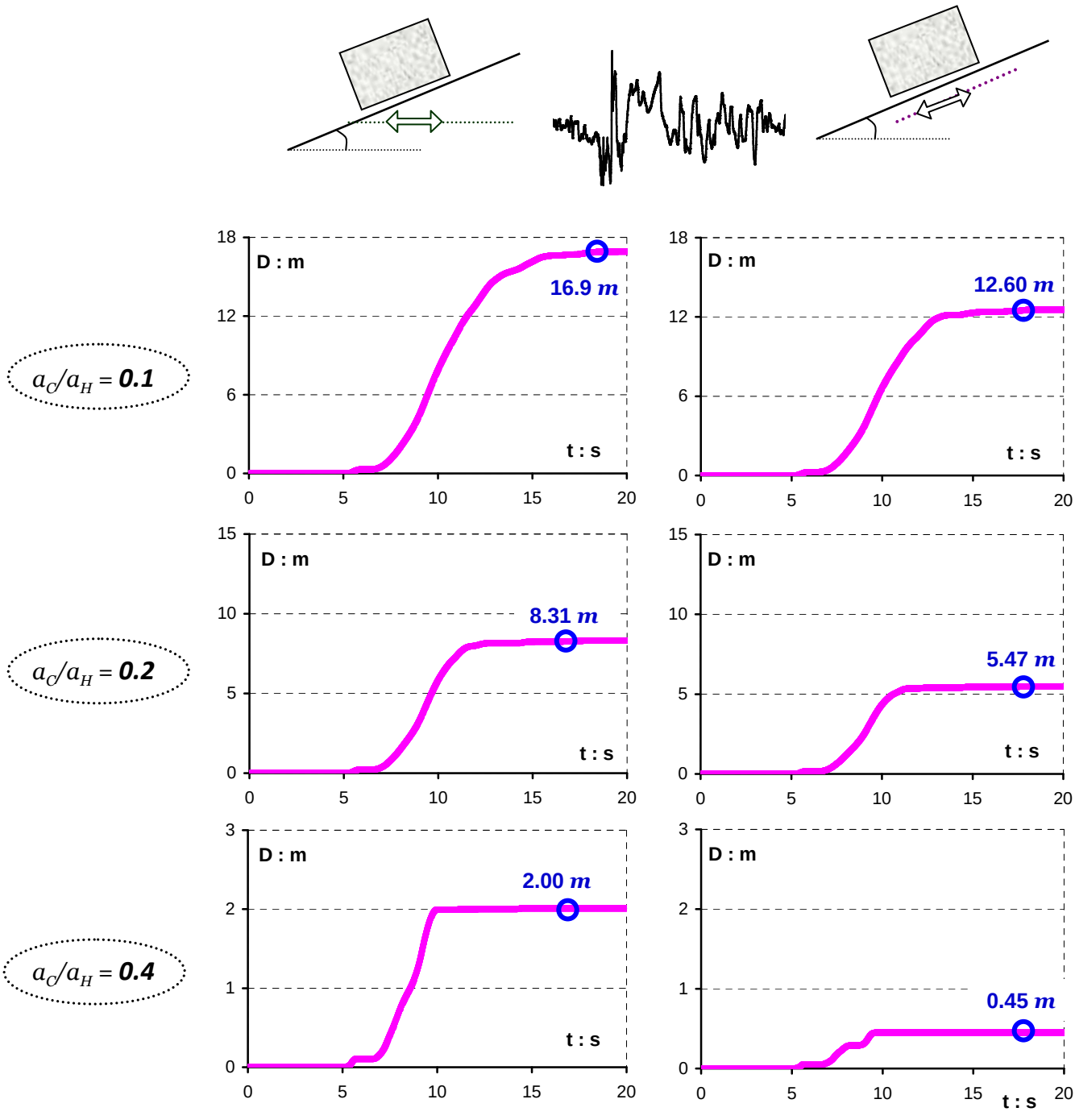

Figure 4.20 *The directionality effect on asymmetric sliding for three acceleration ratios, a_C/a_H . The triggering excitation is the reversed TCU 068–NS record imposed parallel to the sliding surface (right column) and horizontally (left column). [$\beta = 25^o$]*

The Effect of Inclination

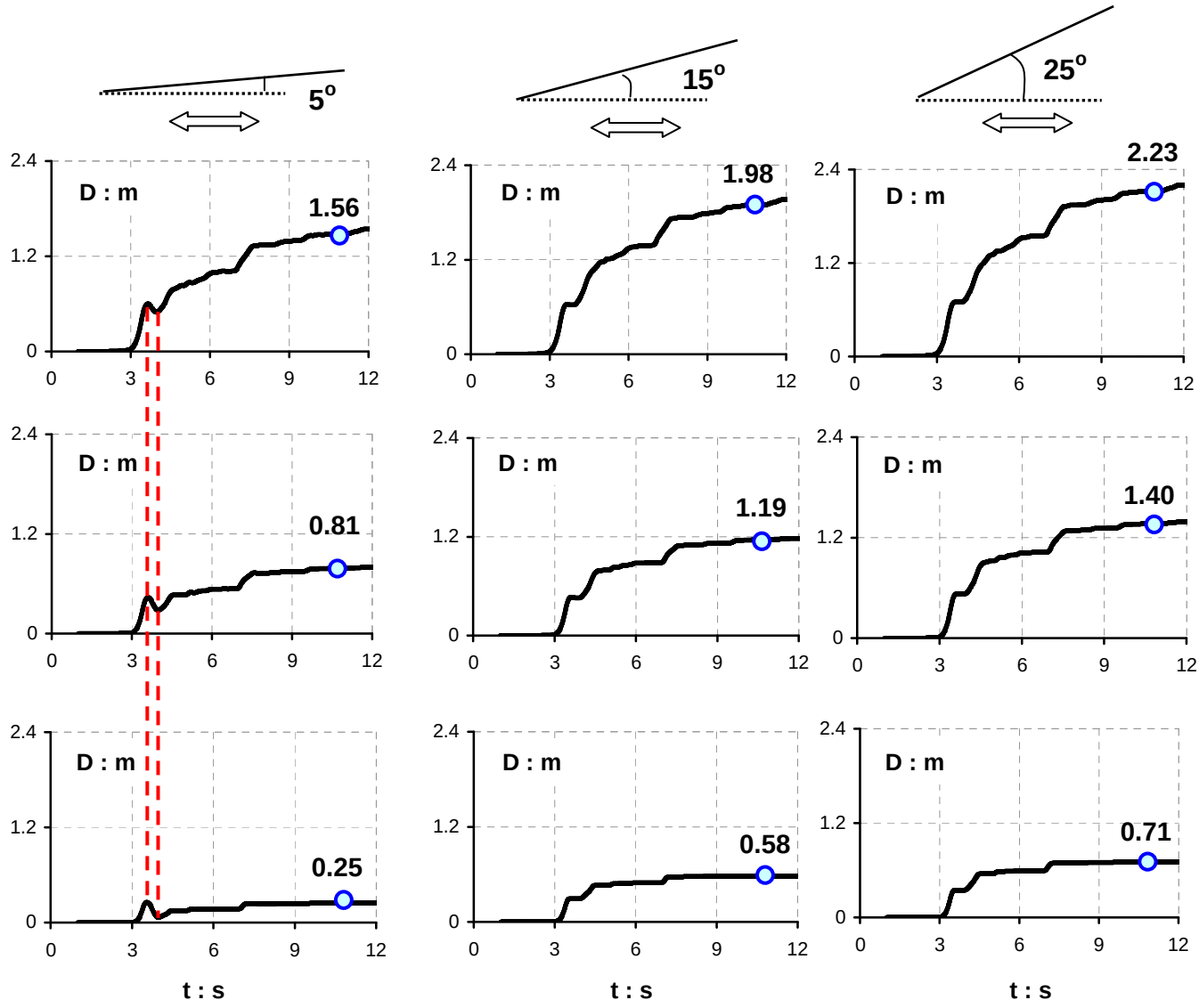

Figure 4.21 *Effect of slope inclination to sliding response induced by the Rinaldi ground motion when imposed horizontally to the plane. The three plots of the first top line correspond to a ratio $a_C / a_H = 0.05$, whereas of the middle and bottom line to ratios of 0.1 and 0.2, respectively. In case of $\beta = 5^o$, the small inclination allows uphill sliding of the block (e.g. between the dotted lines in figure).*

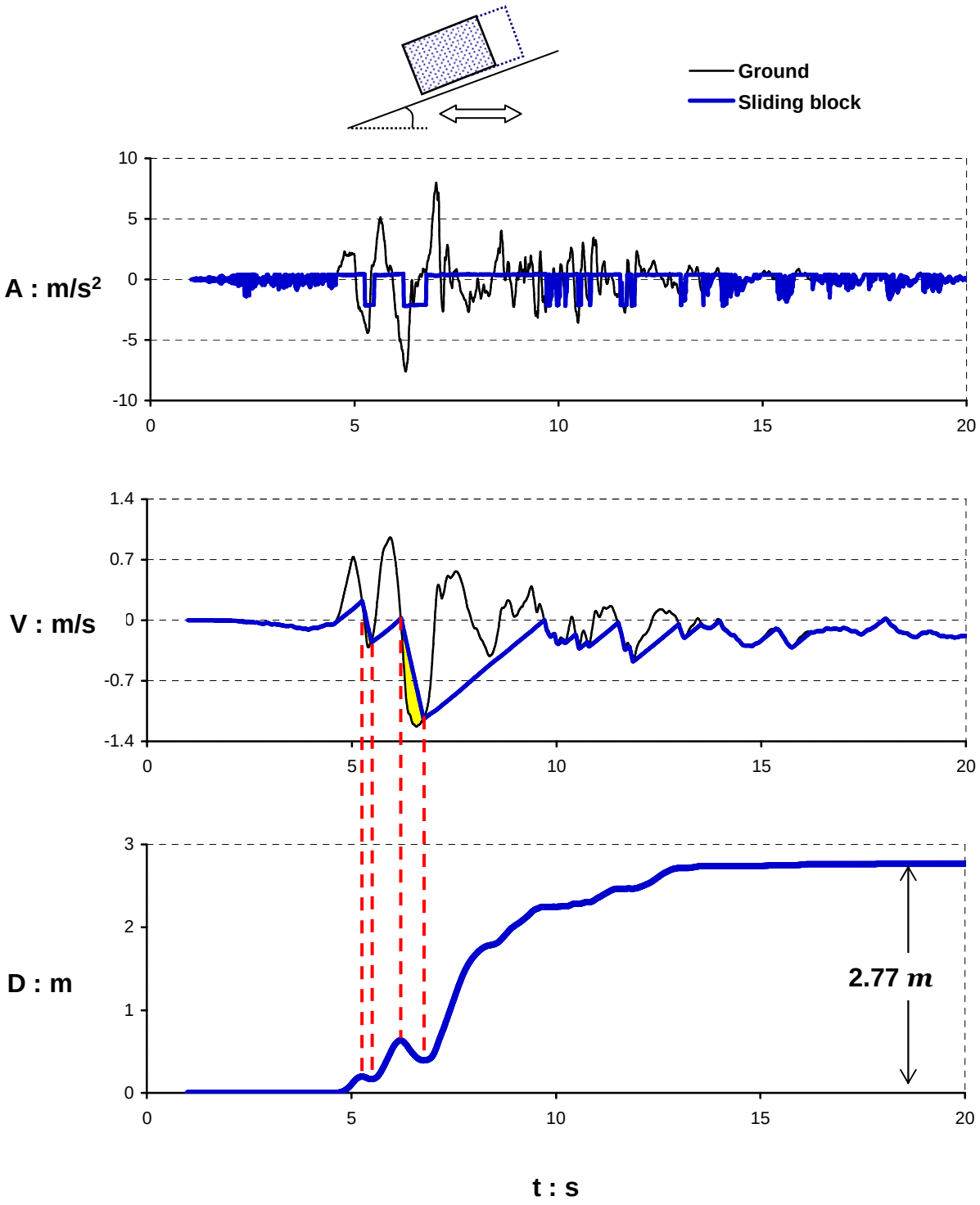

Figure 4.22 *Acceleration, velocity and displacement response of the sliding block when subjected to the exclusively horizontal excitation of Fukiai station (inclination $\beta = 5^o$ and acceleration ratio $a_C / a_H = 0.05$). The mild slope of the plane "permits" upward sliding which occurs twice in this particular case: observe a small uphill slip at 5.2 sec, and a second larger one from 6.2 sec to 6.5 sec (indicated by dotted lines).*

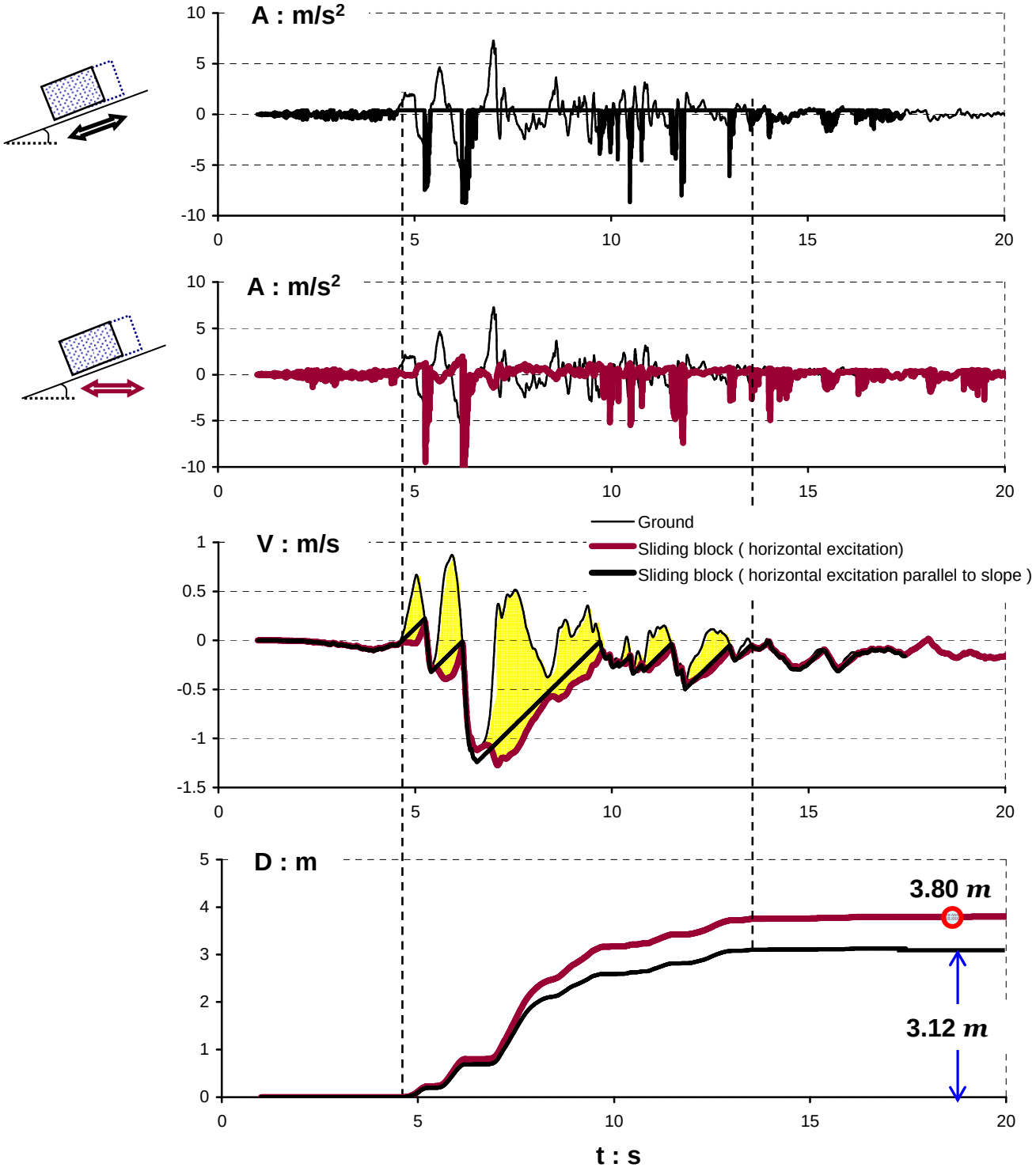

Figure 4.23 *Asymmetric sliding response for the Fukiai record imposed either horizontally or in-parallel to the slope ($\beta = 25^o$ and $a_C/a_H = 0.05$). Note that slippage begins at 4.8 sec and reaches its peak at 12 sec, a time instant which coincides with the duration of the major directivity pulses in velocity and acceleration.*

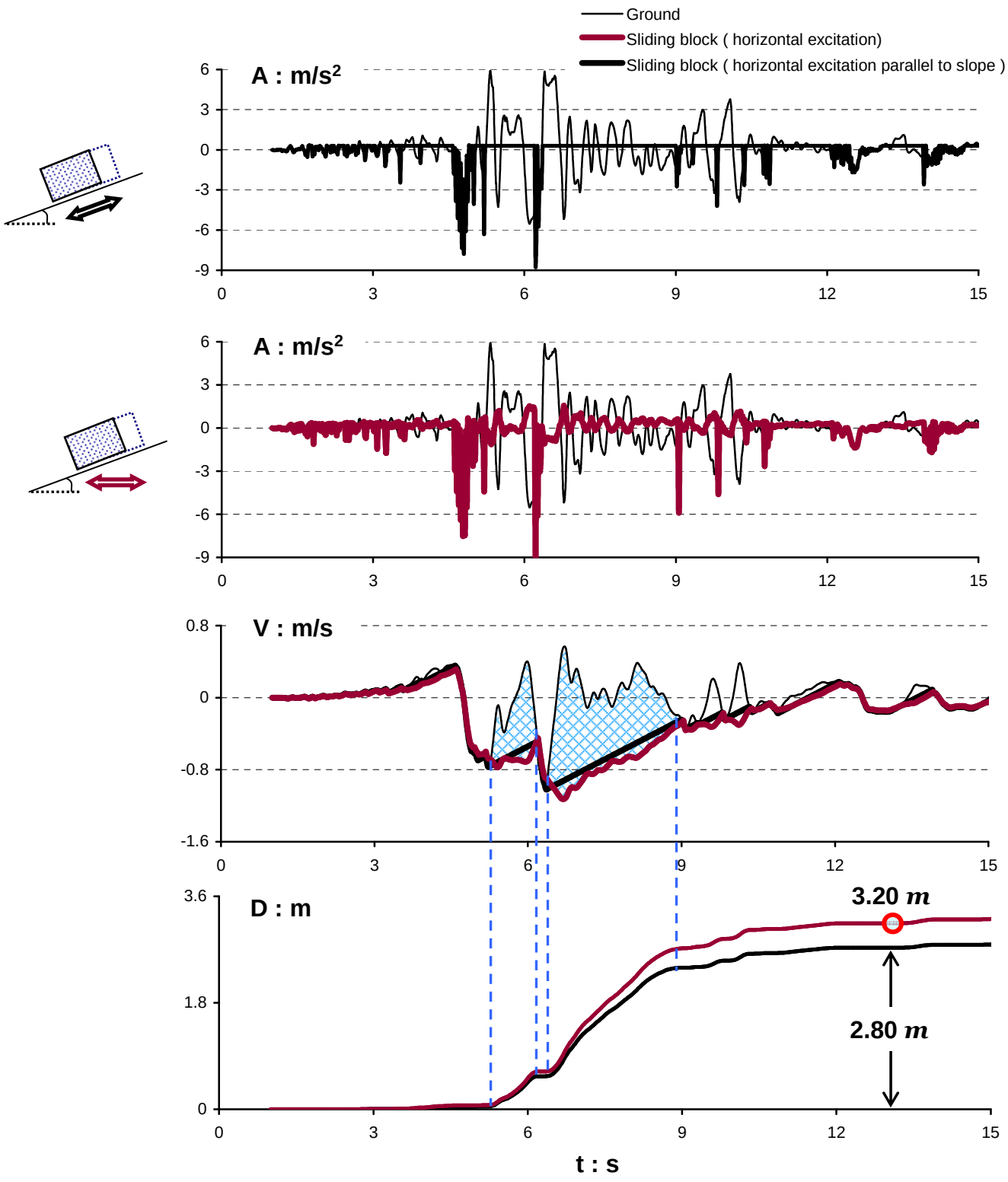

Figure 4.24 *Asymmetric sliding response for the Newhall (360 component) horizontal ground motion imposed either horizontally or in-parallel to the slope (β = 25º and a_C/a_H = 0.05). Two prevalent sliding episodes are conspicuous in the velocity and slippage time-histories (indicated with dotted lines). When the input excitation acts horizontally, the yielding acceleration of the block fluctuates around the critical acceleration value for parallel excitation.*

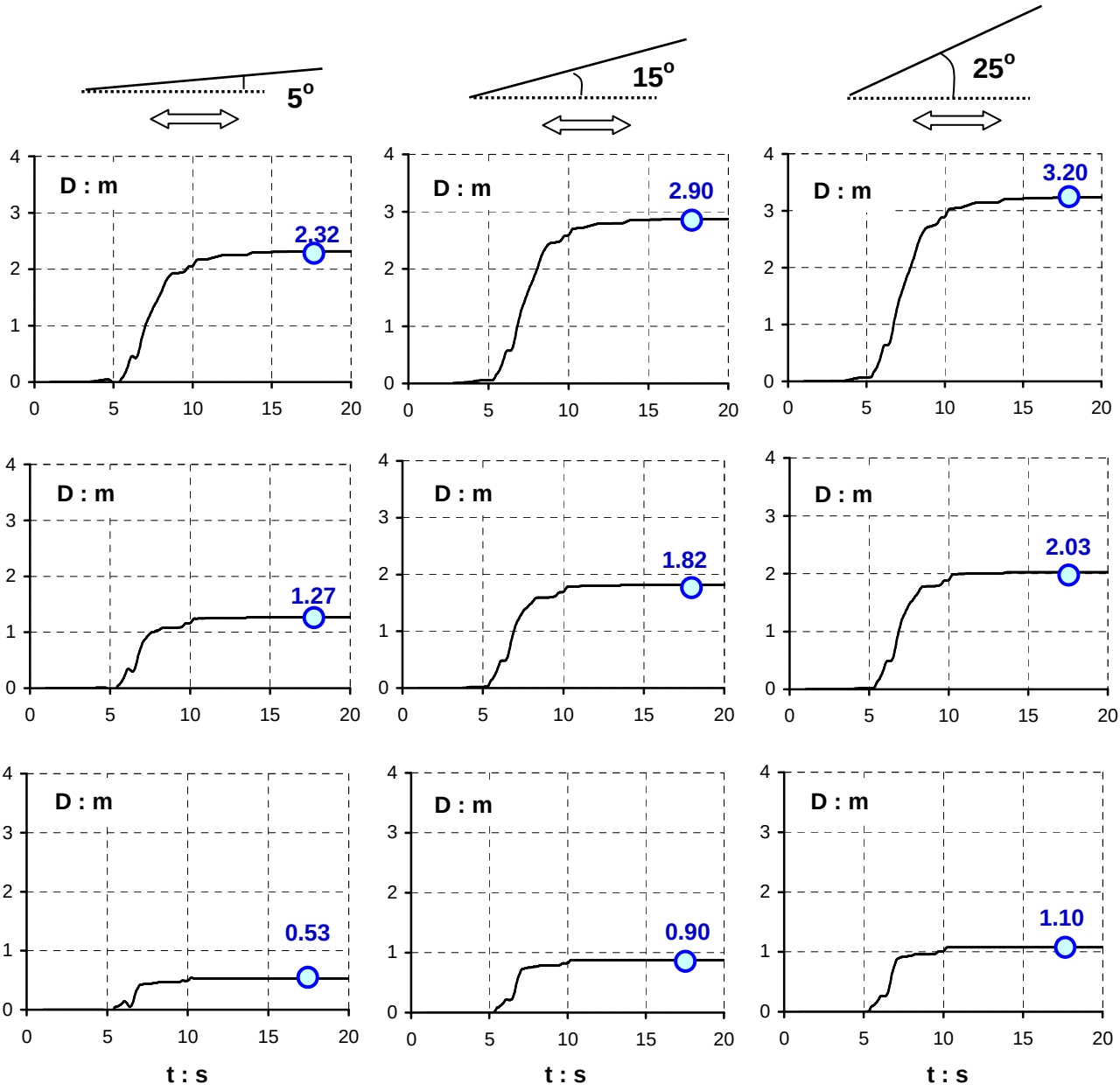

Figure 4.25 *Effect of slope inclination to slippage triggered by the Newhall ground motion imposed horizontally. The three plots of the first top line correspond to a ratio $a_C/a_H = 0.05$, whereas the slippage plots of the middle and bottom line correspond to critical acceleration ratios of 0.1 and 0.2, respectively. In case of $\beta = 5^o$, a small upward slip occurs at approximately 7 seconds, while for $\beta = 15^o$ and 25^o only downward sliding is induced.*

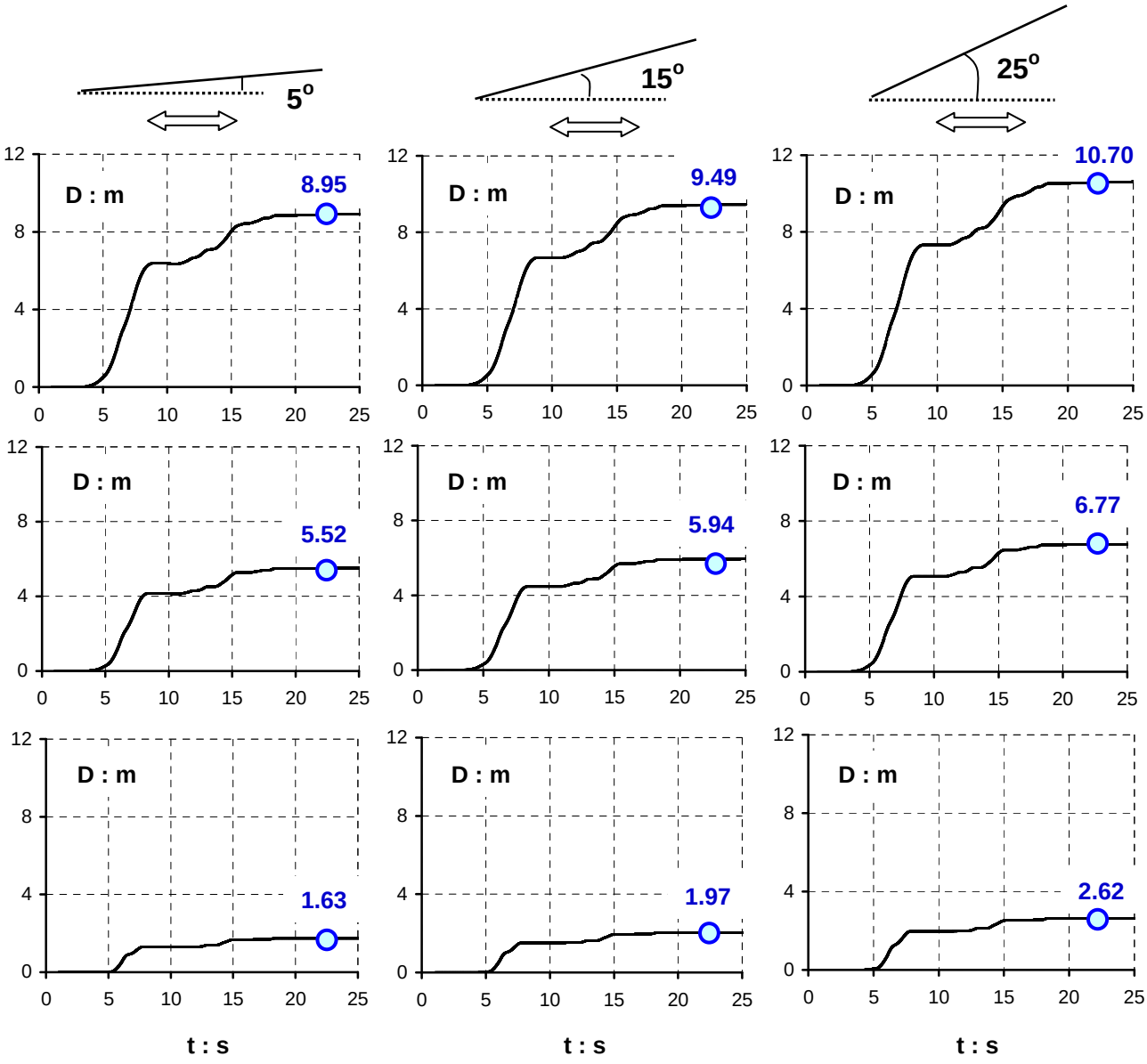

Figure 4.26 *Effect of slope inclination to slippage triggered by the TCU 068 (north-south) ground motion when imposed horizontally. The three plots of the first top line correspond to a ratio $a_C/a_H = 0.05$, whereas the slippage plots of the middle and bottom line correspond to critical acceleration ratios of 0.1 and 0.2, respectively.*

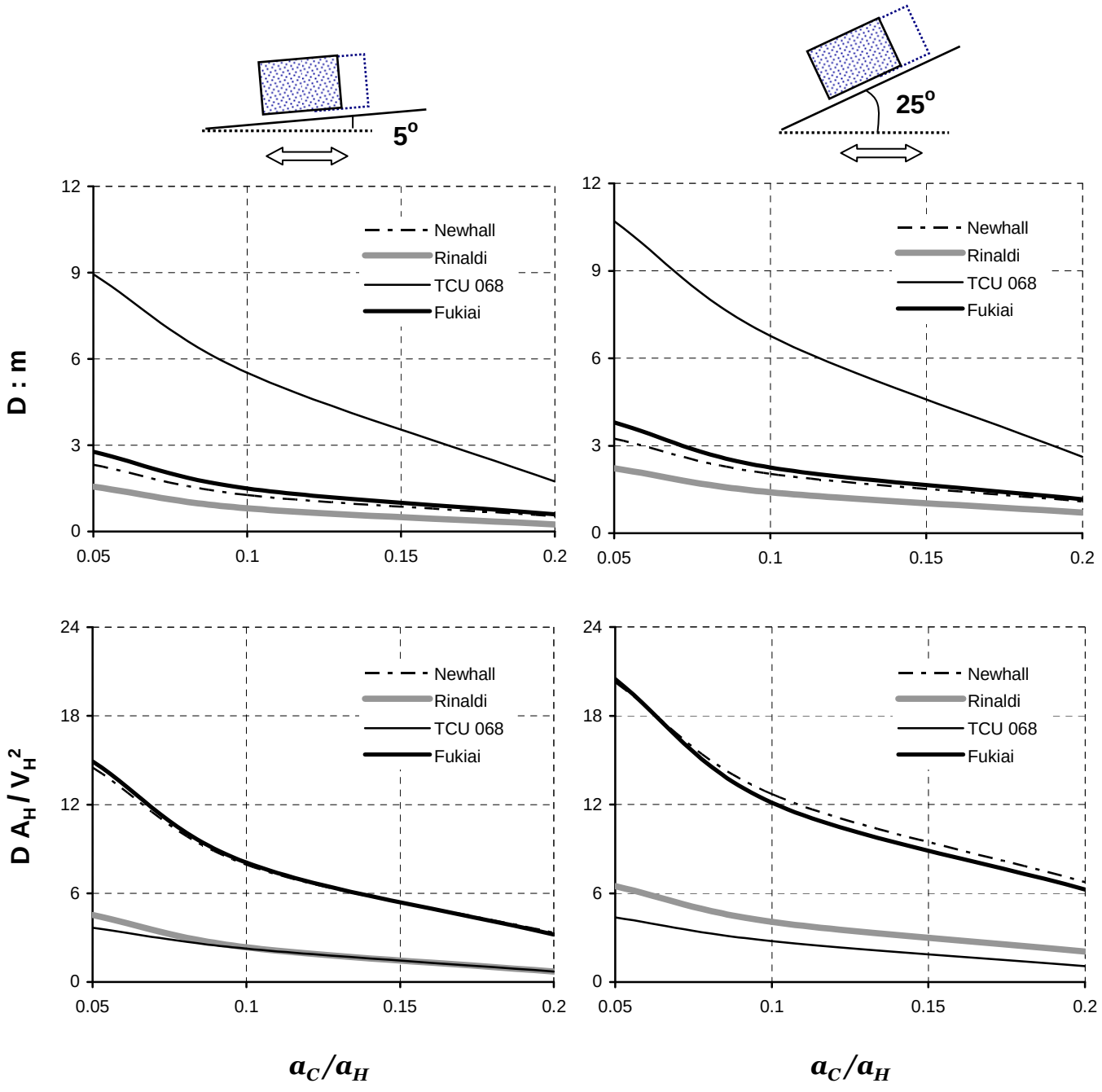

Figure 4.27 *Asymmetric sliding spectra of steep (β = 25°) and soft (β = 5°) slopes induced by four horizontally applied near-fault ground motions. The triggered slippage is presented in absolute (top two plots) and normalized (bottom) form.*

Block Sliding from Simultaneous Action of Horizontal and Vertical Acceleration Records

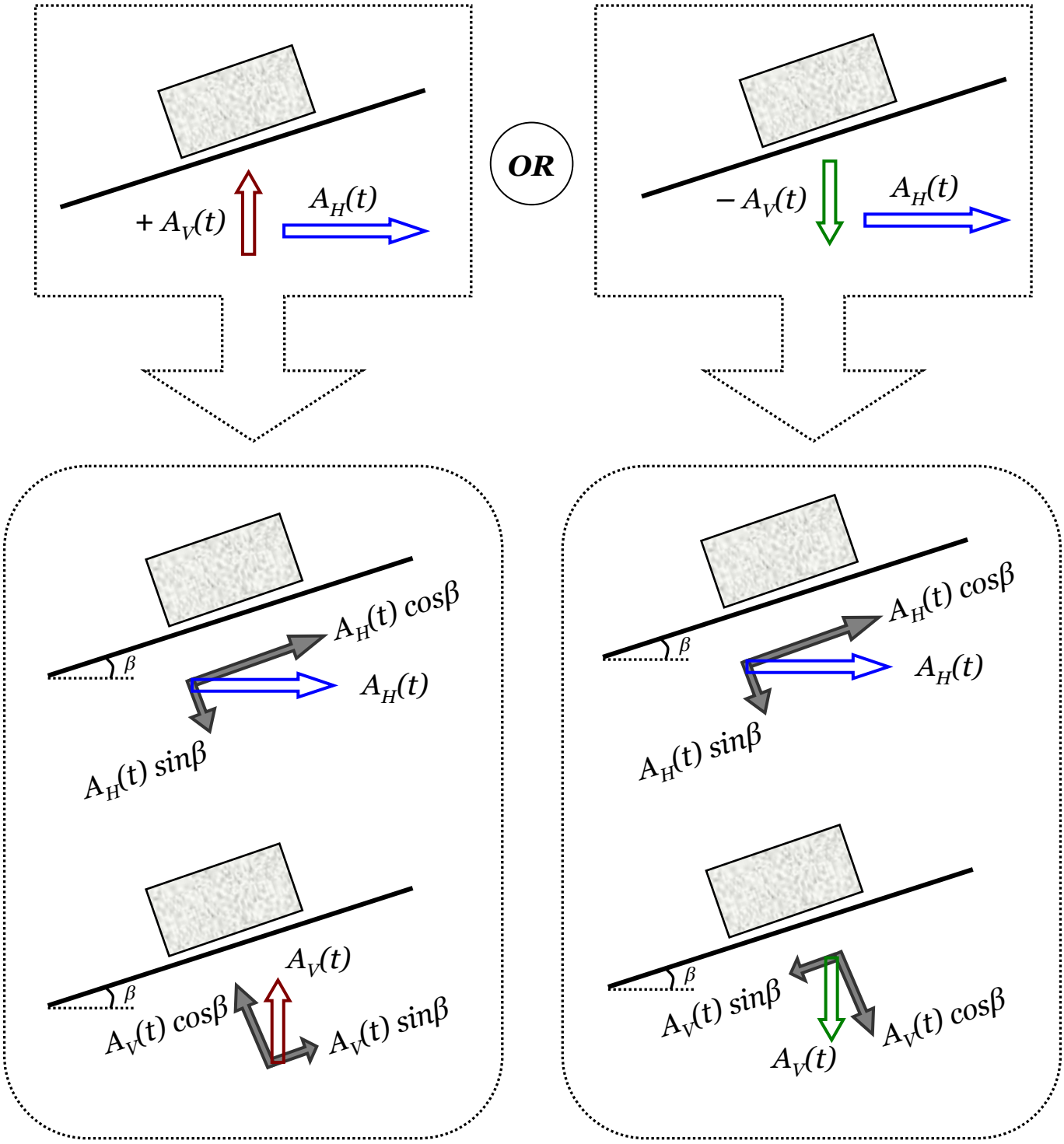

Figure 4.28 *Schematic configurations of the application of the vertical acceleration in terms of polarity, when the horizontal component is acting with its most detrimental polarity.*

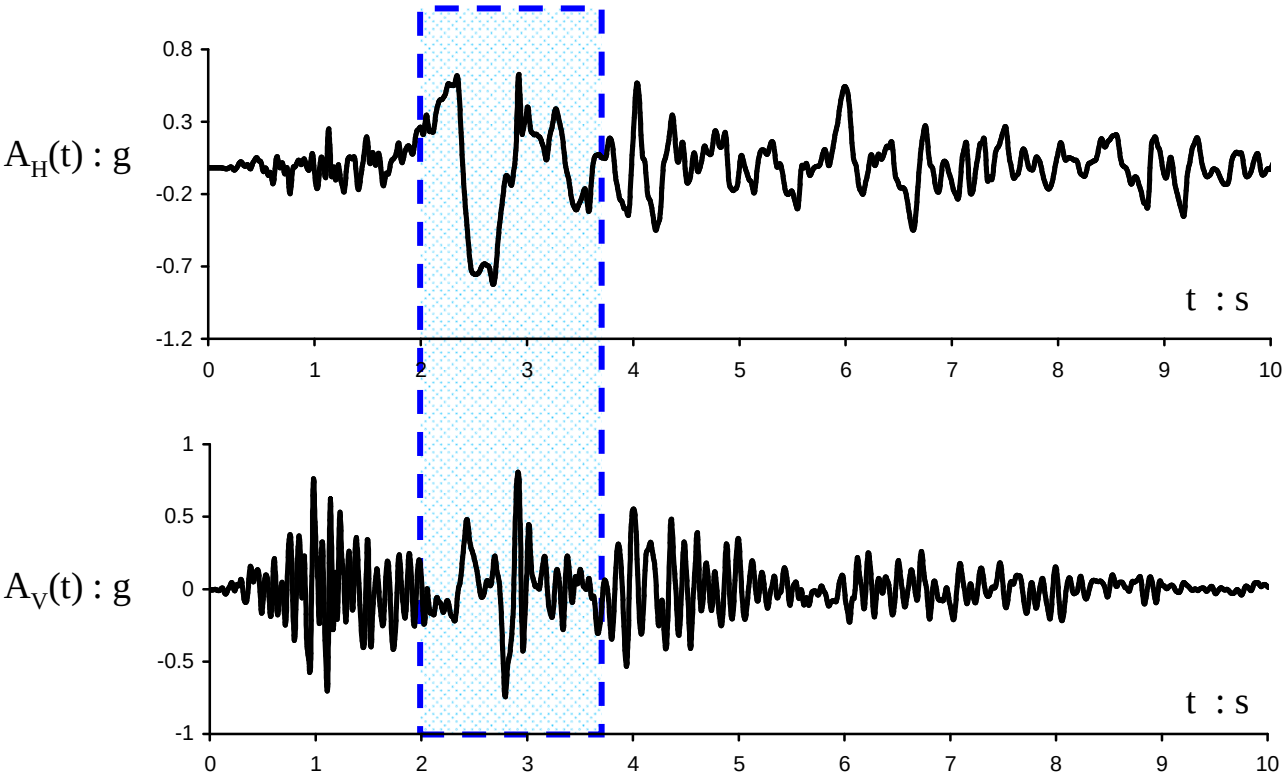

Figure 4.29 *The Rinaldi horizontal (228 component) and vertical records of the 1994 Northridge earthquake. The forward directivity effect appears in both components through a long period pulse starting approximately at 2 seconds (shaded area).*

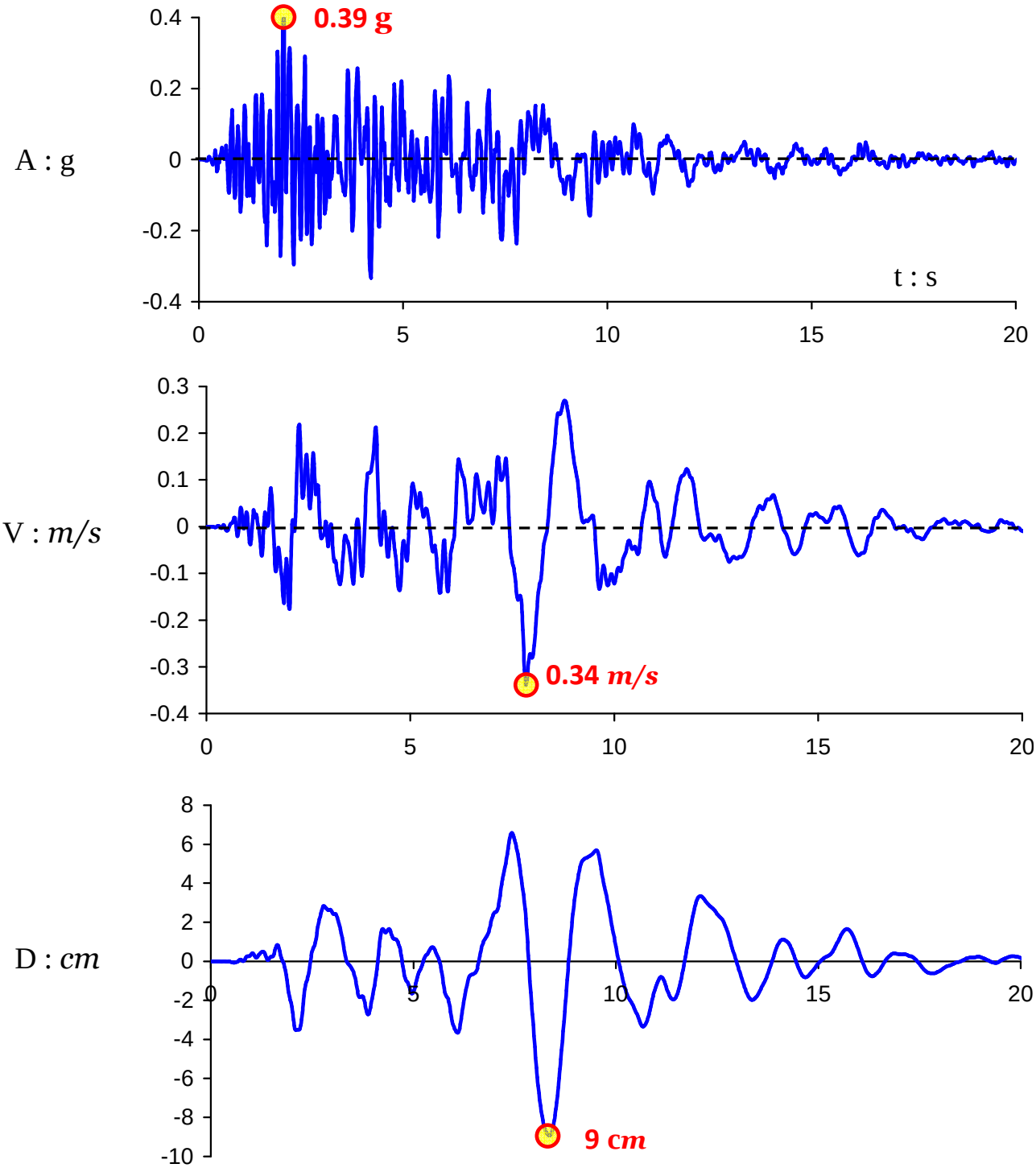

Figure 4.30 *Acceleration, velocity and displacement time-histories of the Jensen Filtration Plant vertical ground motion of the 1994 Northridge Earthquake. The peak values are circled.*

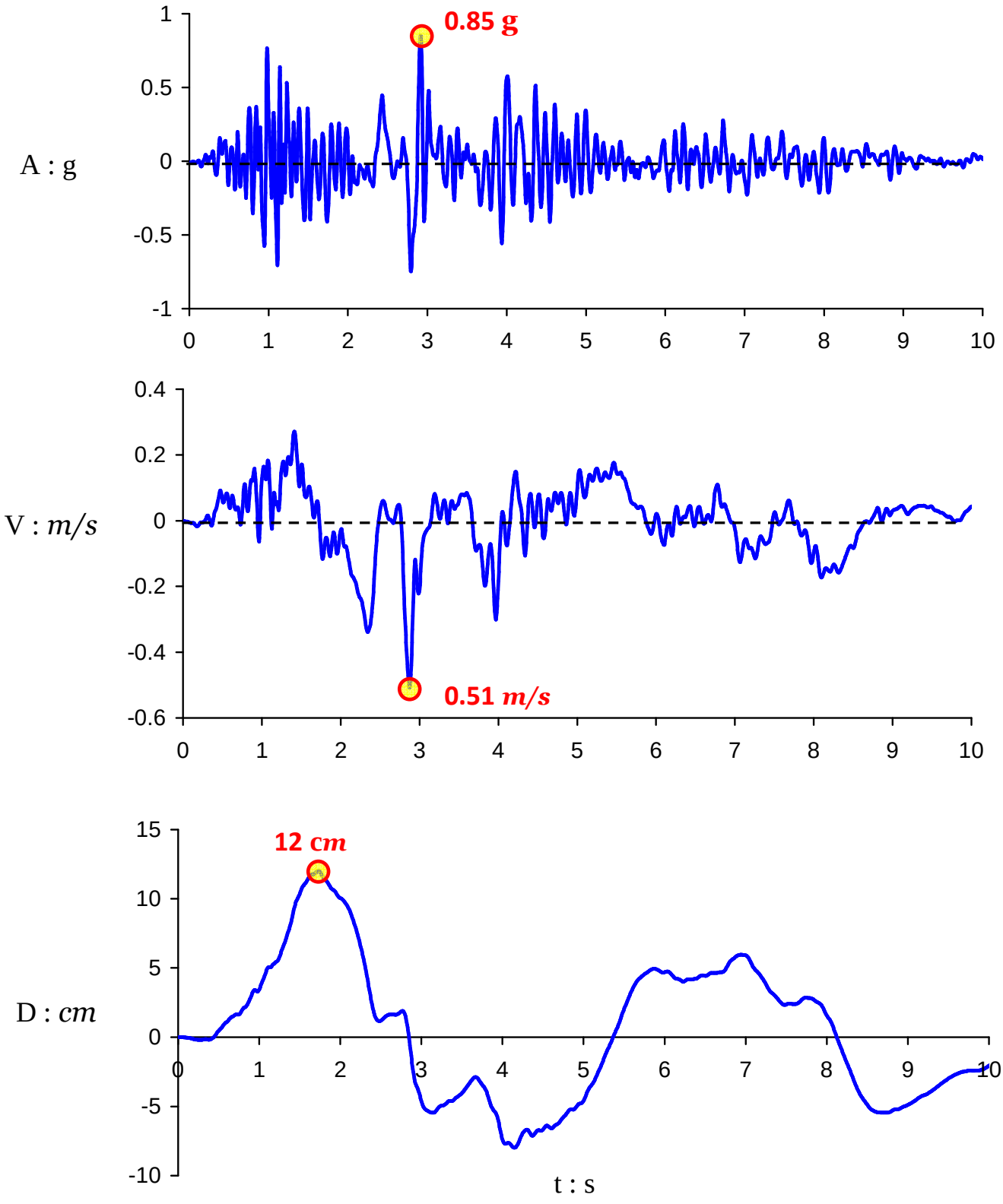

Figure 4.31 *Acceleration, velocity and displacement time-histories of the Rinaldi vertical ground motion of the 1994 Northridge Earthquake. The peak values are circled.*

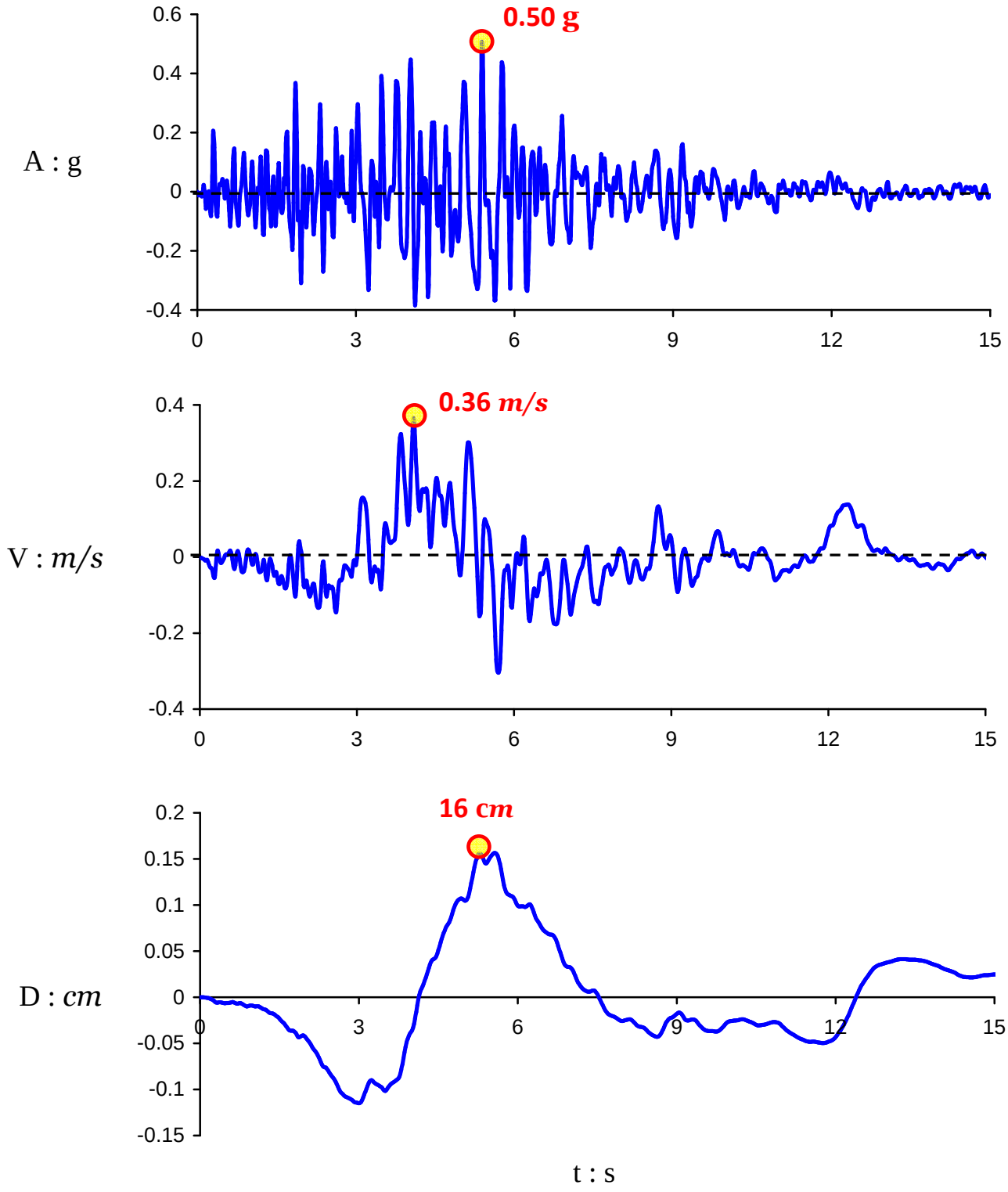

Figure 4.32 *Acceleration, velocity and displacement time-histories of the Newhall vertical ground motion of the 1994 Northridge Earthquake. The peak values are circled.*

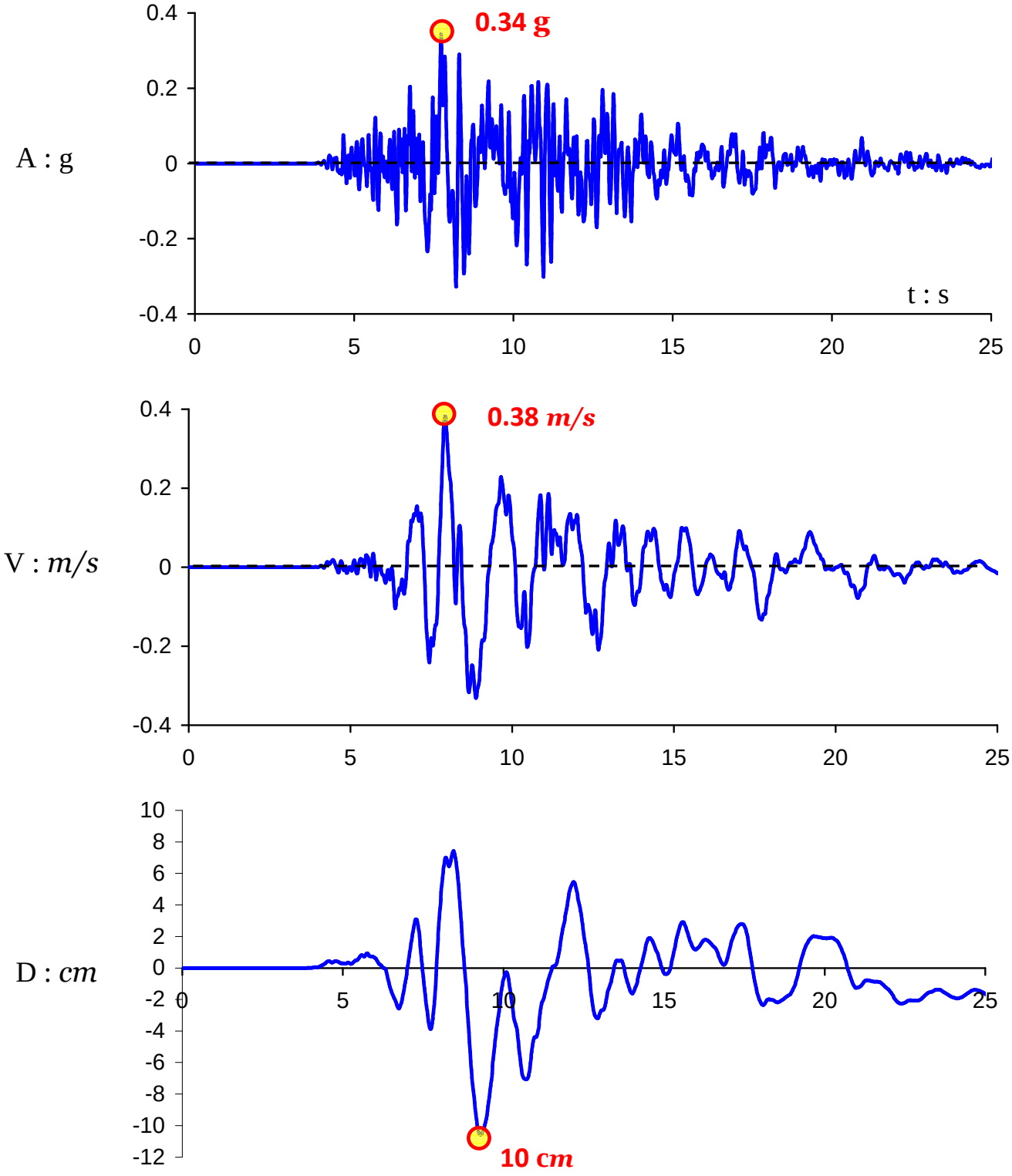

Figure 4.33 *Acceleration, velocity and displacement time-histories of the JMA vertical ground motion of the 1995 Kobe Earthquake. The peak values are circled.*

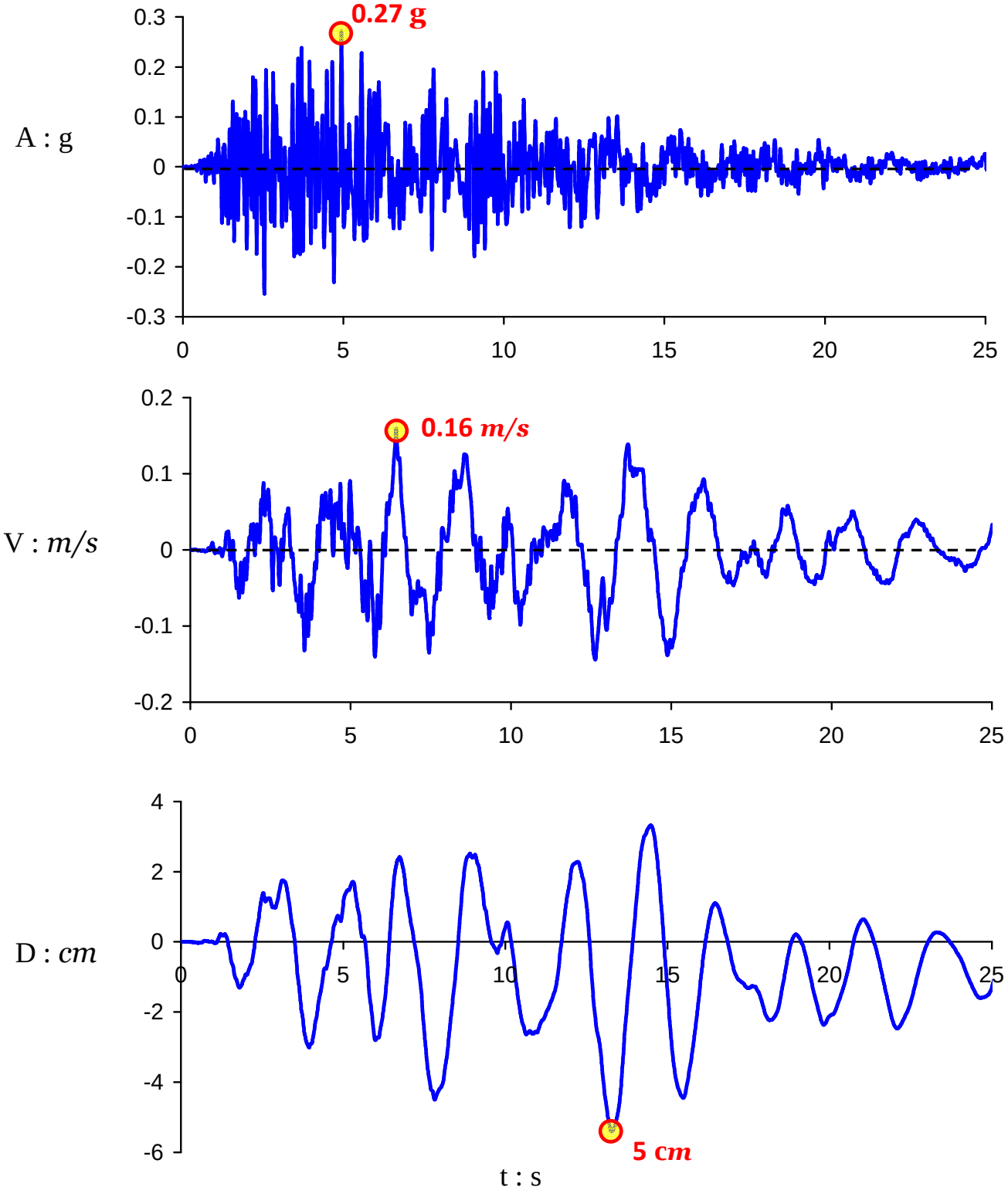

Figure 4.34 *Acceleration, velocity and displacement time-histories of the Takatori vertical ground motion of the 1995 Kobe Earthquake. The peak values are circled.*

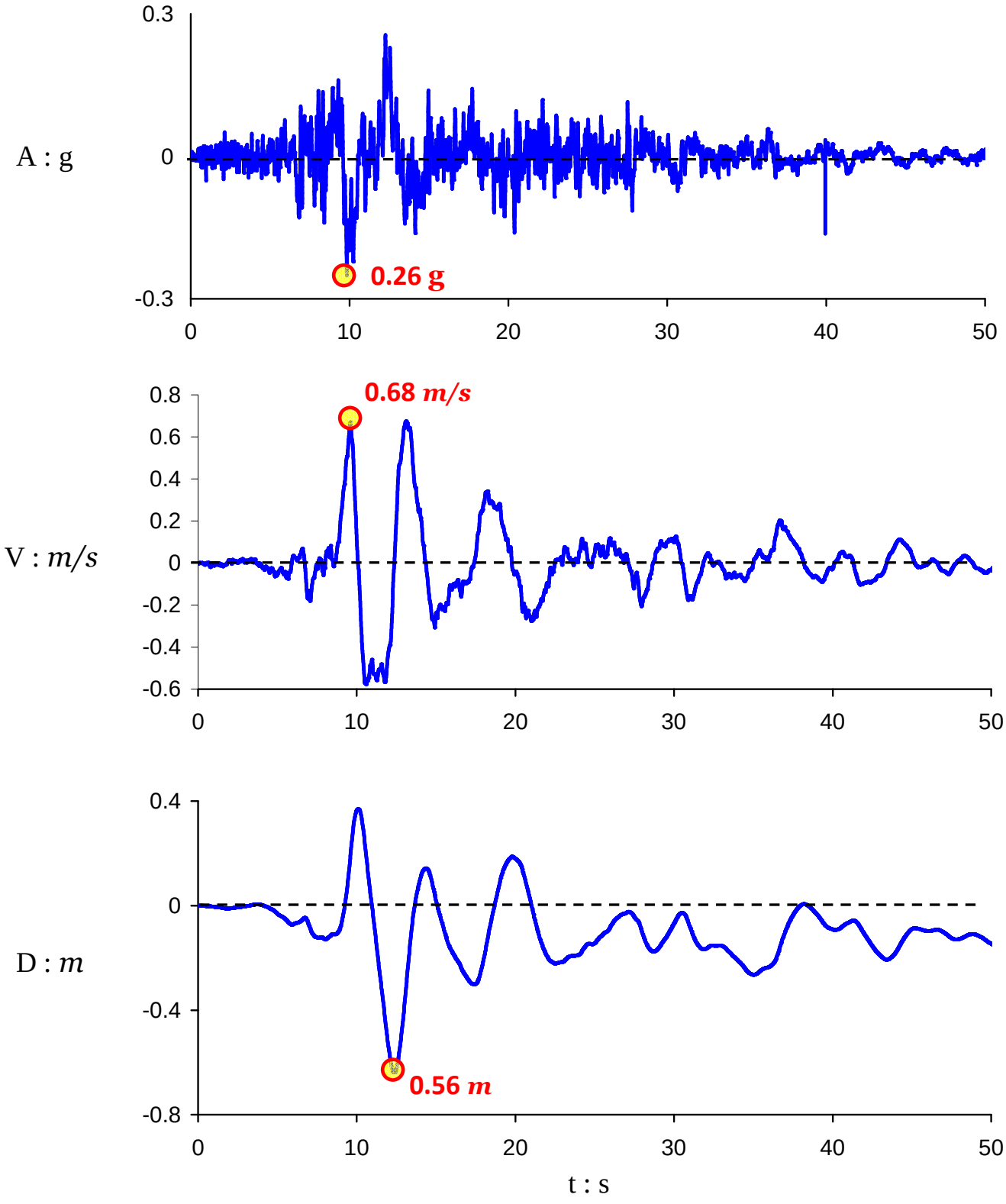

Figure 4.35 *Acceleration, velocity and displacement time-histories of the TCU-065 vertical ground motion of the 1999 Chi-chi Earthquake. The peak values are circled.*

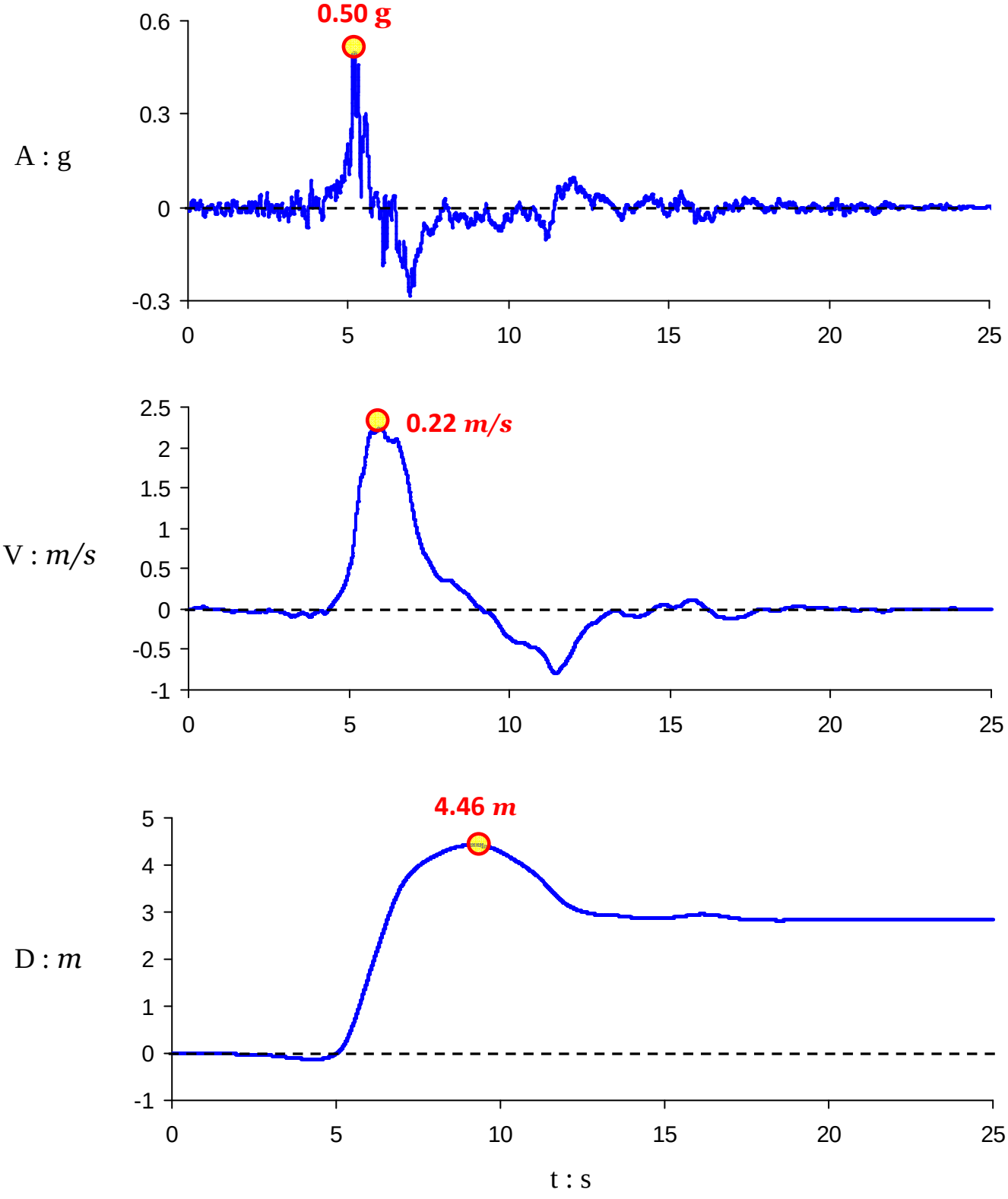

Figure 4.36 *Acceleration, velocity and displacement time-histories of the TCU-068 vertical ground motion of the 1999 Chi-chi Earthquake. The peak values are circled. Notice the residual vertical displacement at the end of motion, which reflects the vertical offset of the fault at the particular recording station.*

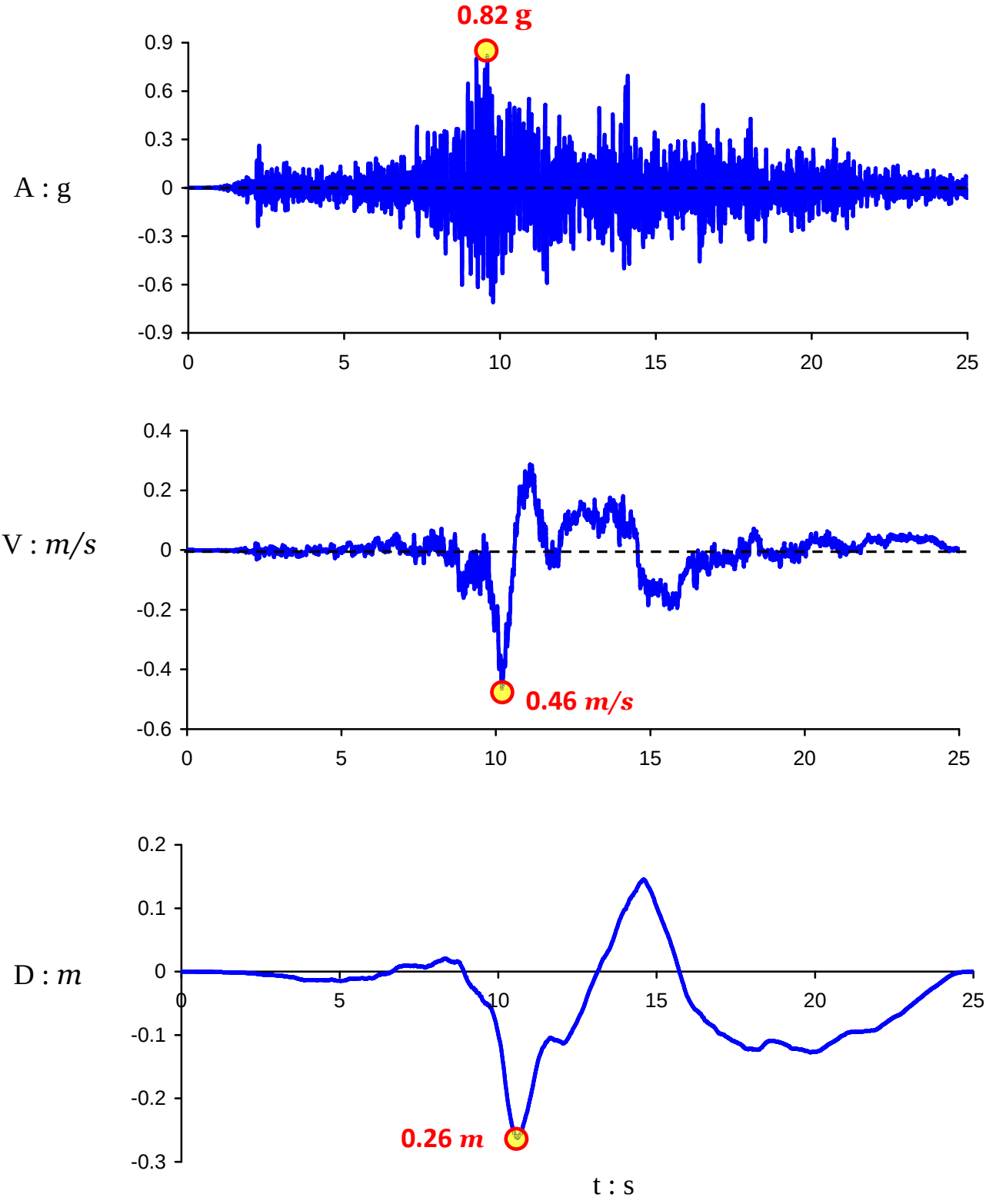

Figure 4.37 *Acceleration, velocity and displacement time-histories of the Lucerne <u>vertical</u> ground motion of the 1992 Landers Earthquake. The peak values are circled.*

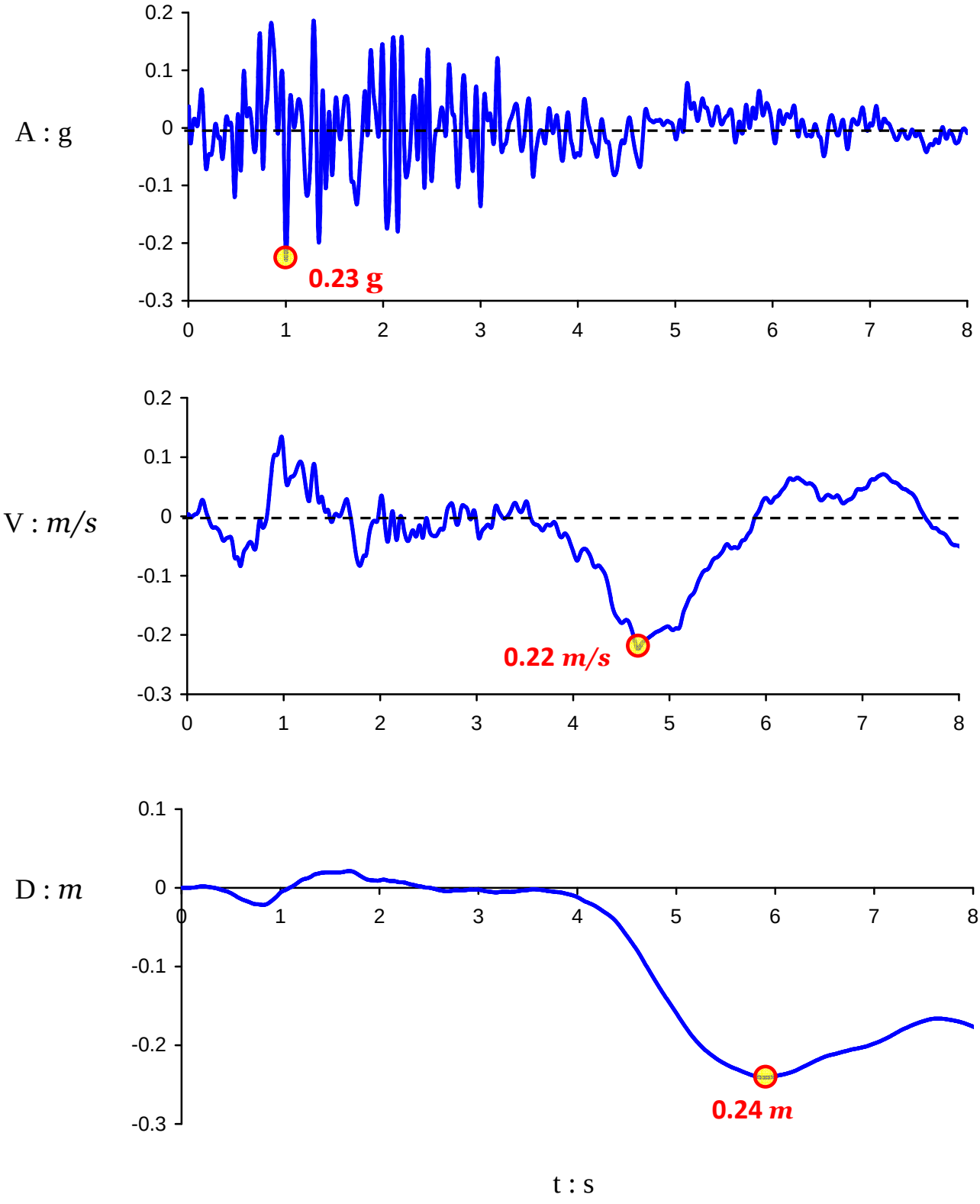

Figure 4.38 *Acceleration, velocity and displacement time-histories of the Duzce-270° vertical ground motion of the 1999 Kocaeli Earthquake. The peak values are circled.*

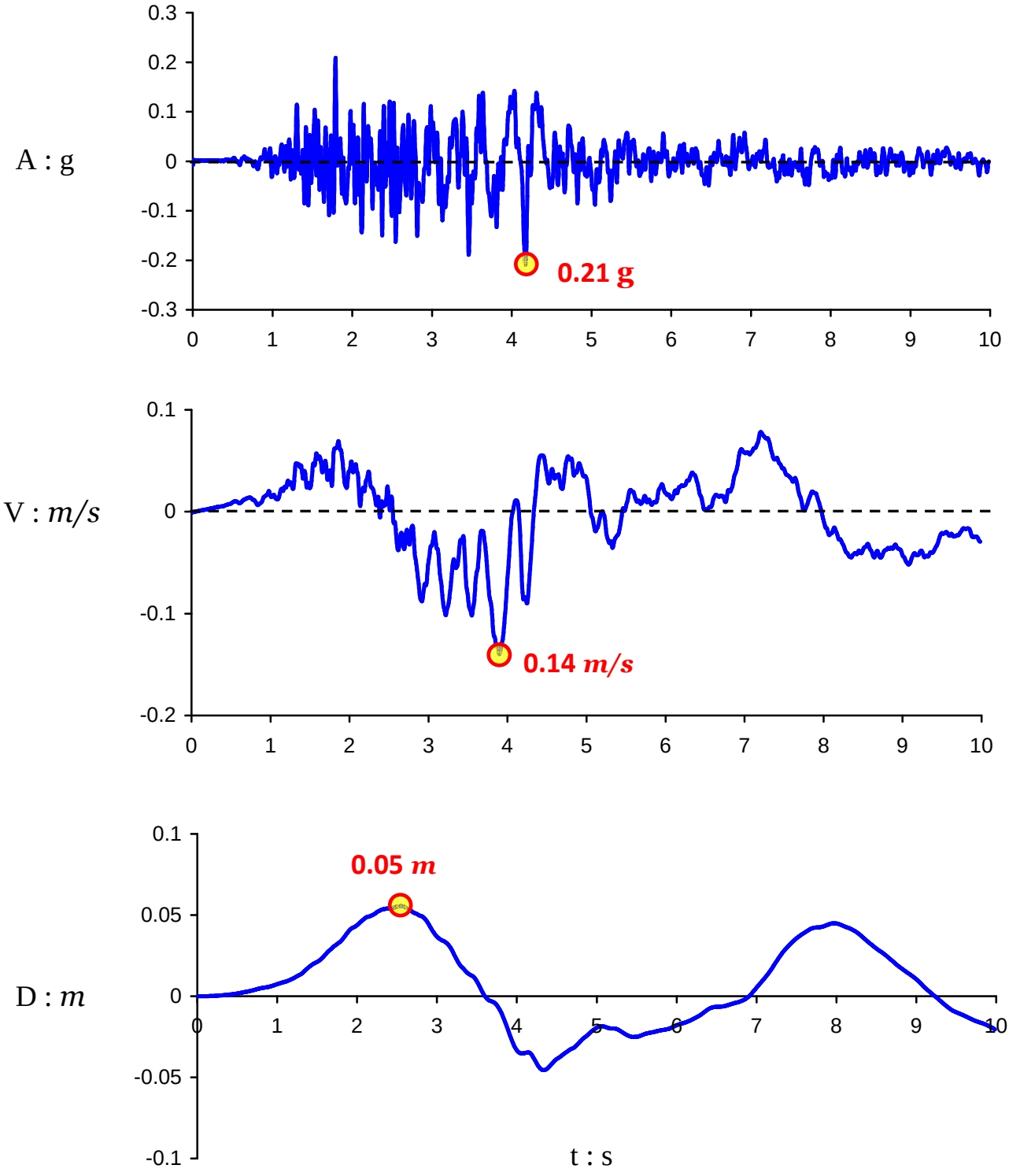

Figure 4.39 *Acceleration, velocity and displacement time-histories of the Gilroy Array No1 vertical ground motion of the 1989 Loma Prieta Earthquake. The peak values are circled.*

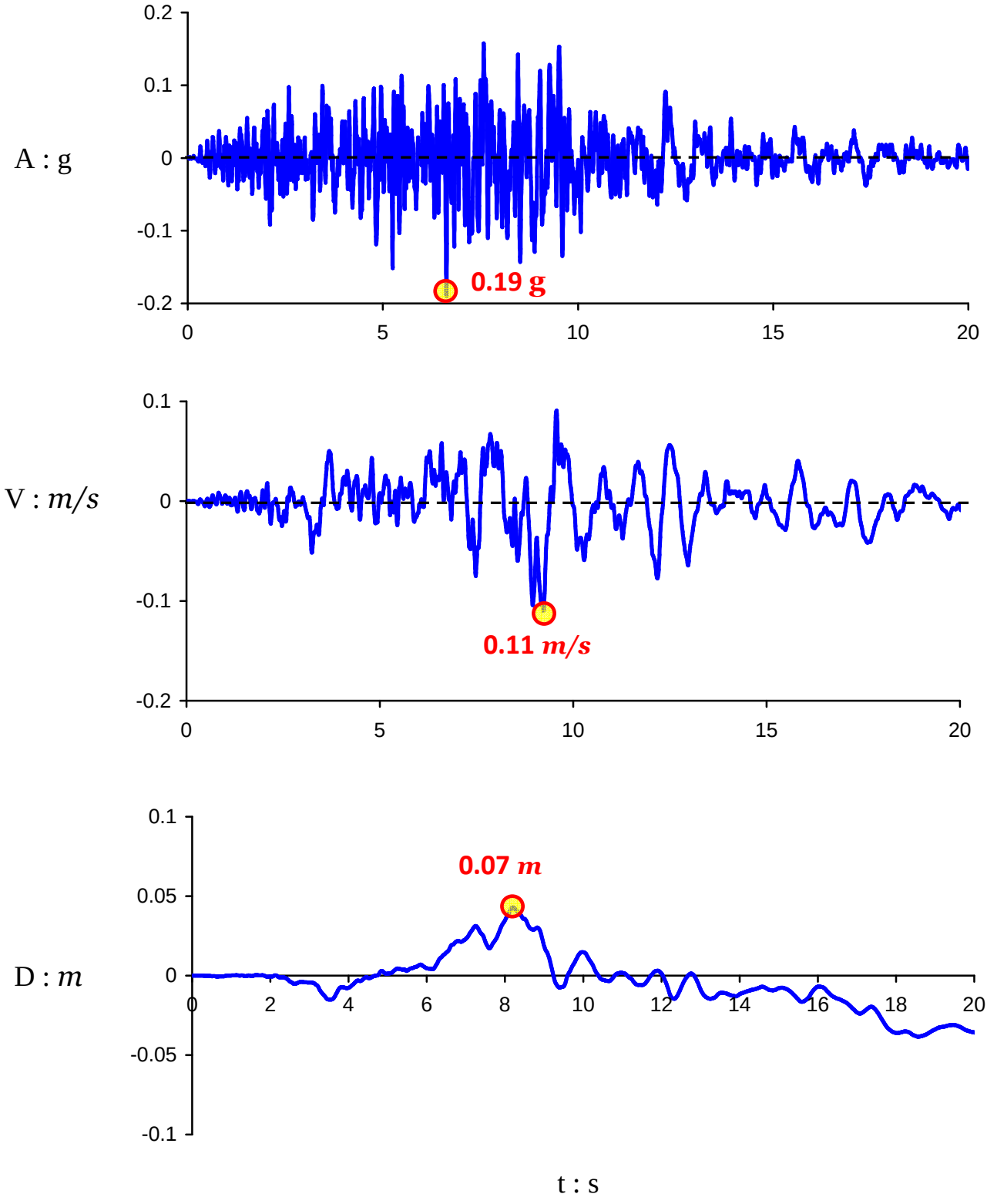

Figure 4.40 *Acceleration, velocity and displacement time-histories of the Lefkada <u>vertical</u> ground motion of the 2003 Lefkada Earthquake. The peak values are circled.*

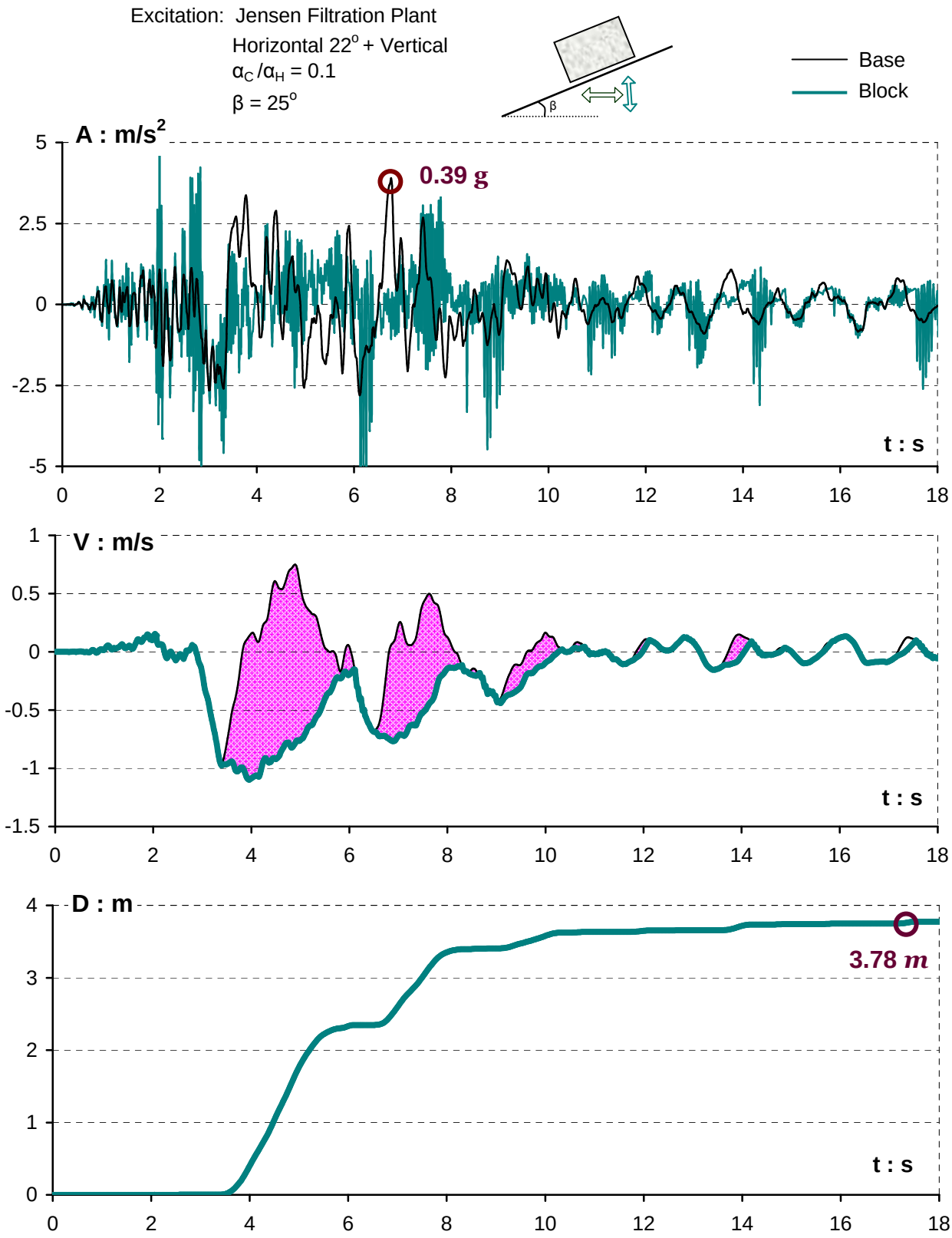

Figure 4.46 *Acceleration, velocity, and sliding displacement time histories of a block rested on a 25⁰ inclined plane subjected simultaneously to: (i) the horizontal component of Jensen 022⁰ record and (ii) the vertical component of the record. Both acceleration components are employed with their normal polarity. The pink shaded areas in velocity represent the sliding periods of the block. (a_C/a_H = 0.1)*

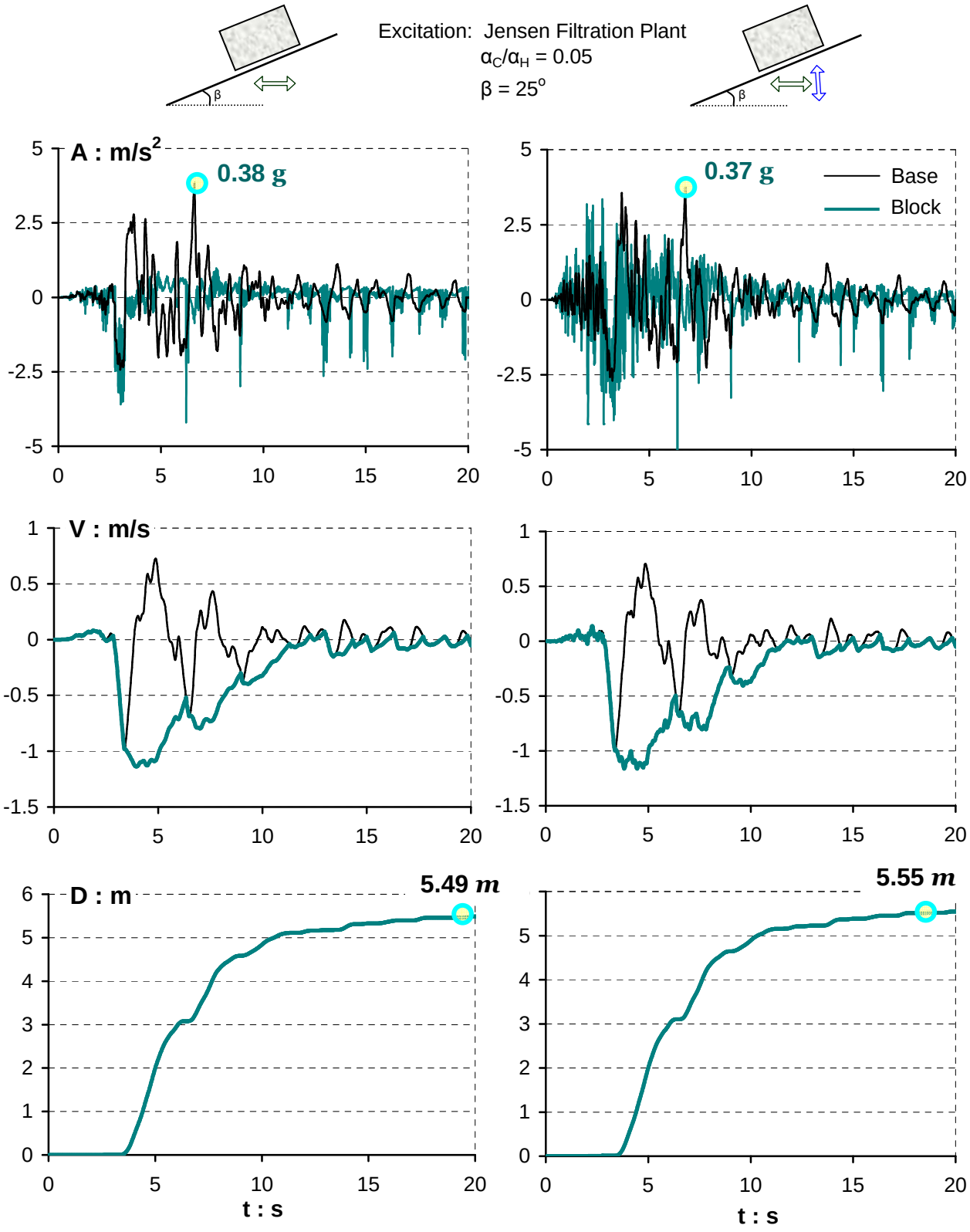

Figure 4.47 *The effect of vertical excitation in case of the Jensen record. On the left is portrayed the response for the horizontally imposed 022° acceleration component. On the right are presented the time histories for simultaneously acted normal polarity horizontal and vertical components of the Jensen record. The difference due to vertical acceleration is almost negligible ~ 1%. (a_C/a_H = 0.05 and β = 25°)*

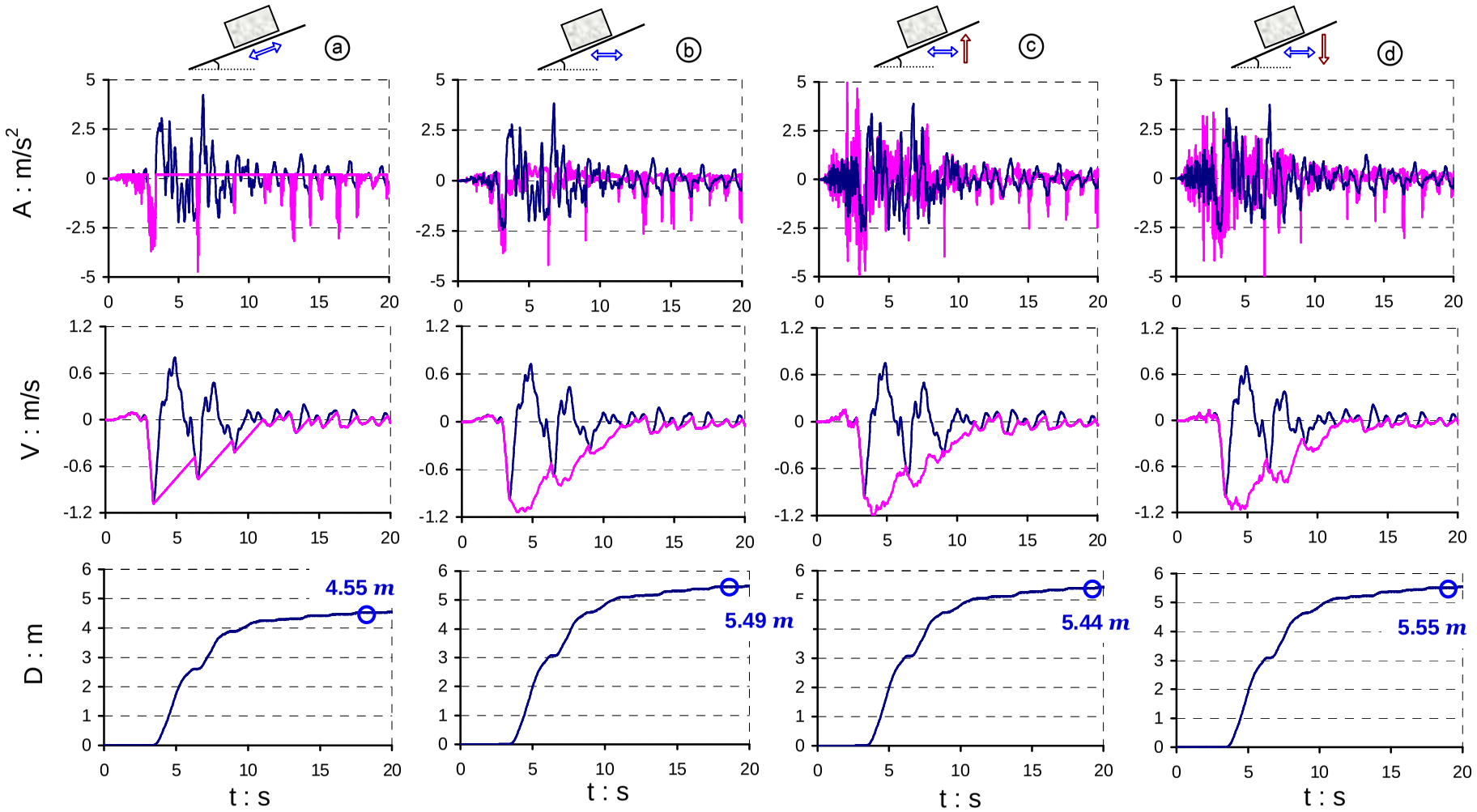

Figure 4.48 *Directionality effect for the Jensen– 022° record: (a) at the left column the horizontal component is acting parallel to the yielding surface, (b) at the second column the horizontal acceleration imposed horizontally to the sliding plane. In the next two columns the plane is triggered by both the vertical and horizontal components: (c) at the third column both components are employed with their normal polarity, and (d) at the right column the vertical acceleration is applied with its reversed polarity.* ($a_C/a_H = 0.05$ *and* $\beta = 25^o$)

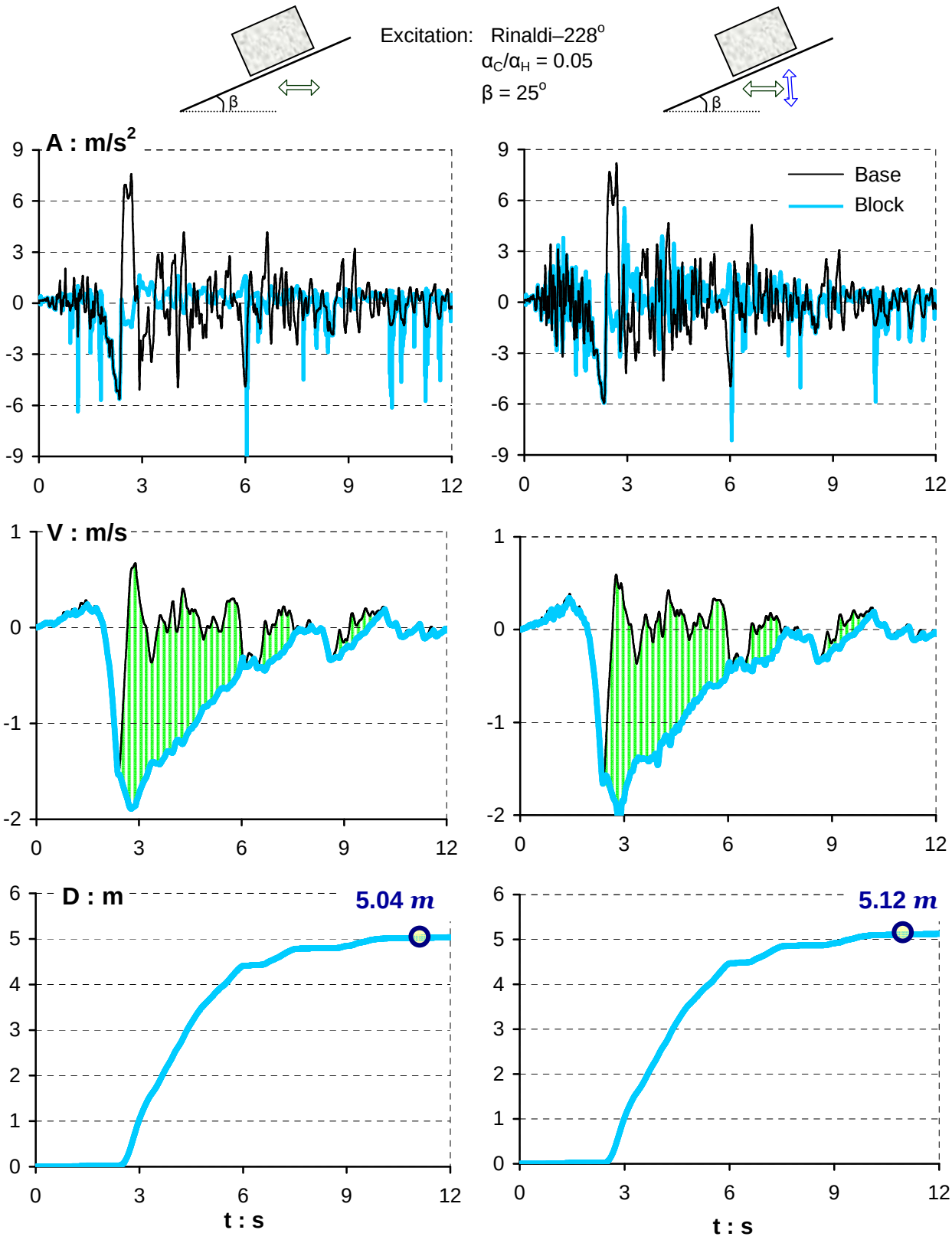

Figure 4.49 *The effect of vertical excitation in case of the reversed polarity Rinaldi record: the response for the horizontally imposed 228° acceleration component (on the left) is just 2% greater than the sliding displacement by simultaneously acted horizontal and vertical components of the Rinaldi record. ($a_C/a_H = 0.05$ and $\beta = 25^o$)*

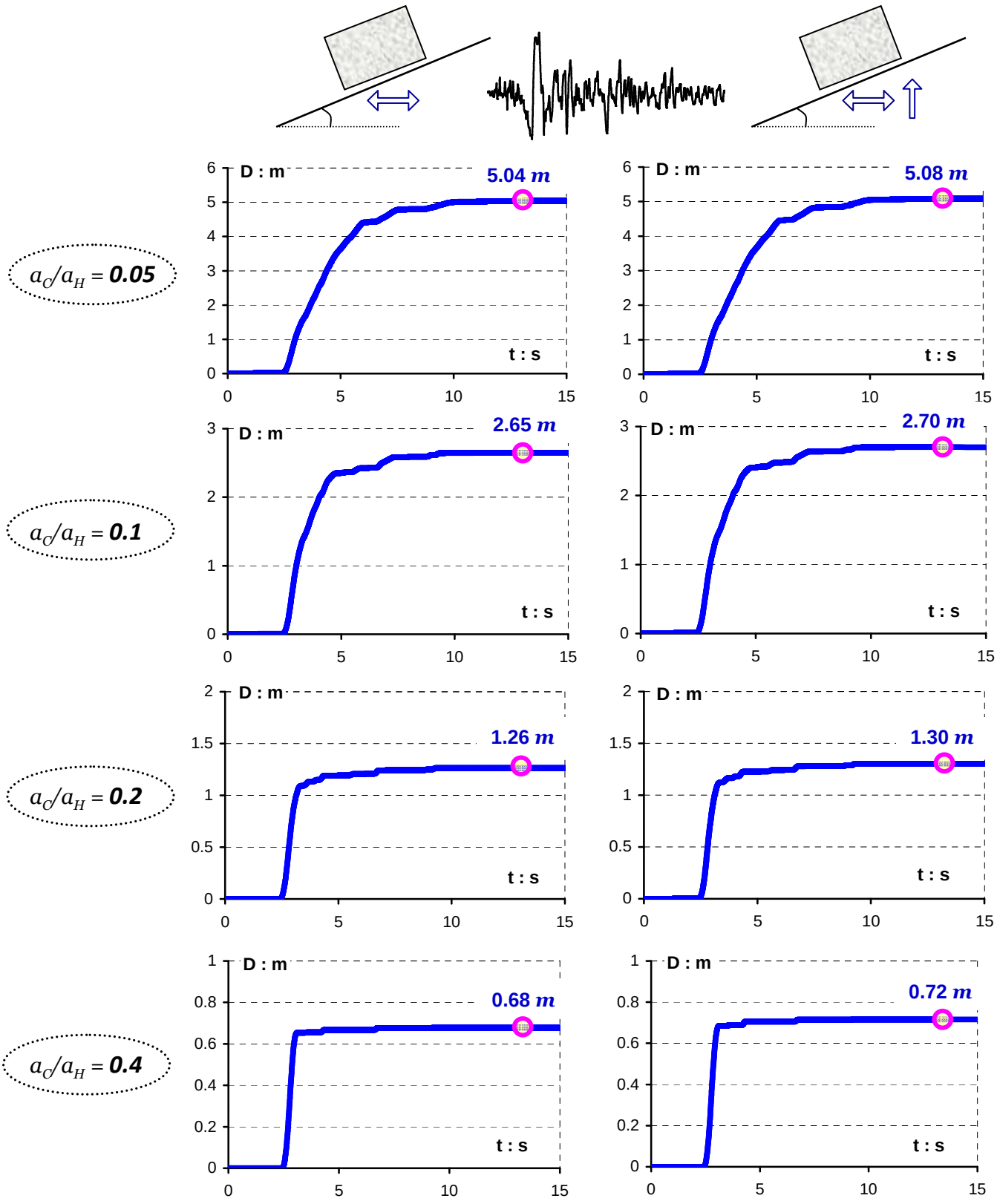

Figure 4.50 *Importance of vertical acceleration on asymmetric sliding for four acceleration ratios, a_C/a_H. The triggering horizontal excitation is the reversed Rinaldi 228° record (left column) and the concurrently acting horizontal and vertical motion (left column). The vertical component is employed with its normal polarity. [$\beta = 25^o$]*

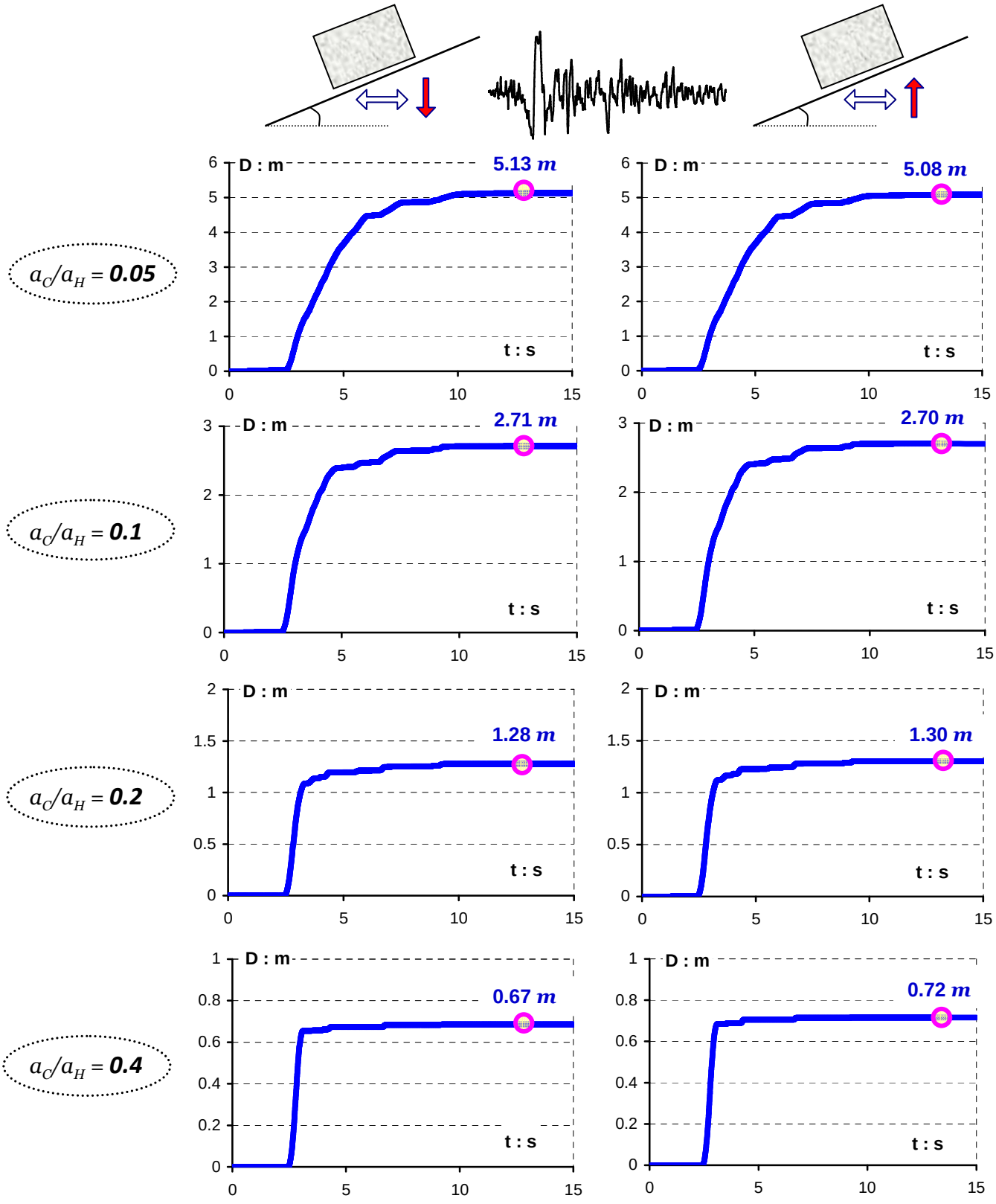

Figure 4.51 *Polarity effect of vertical acceleration on asymmetric sliding for four acceleration ratios, a_C/a_H. The triggering horizontal excitation is the reversed Rinaldi 228° record and is concurrently acting with the vertical motion. [$\beta = 25^o$]*

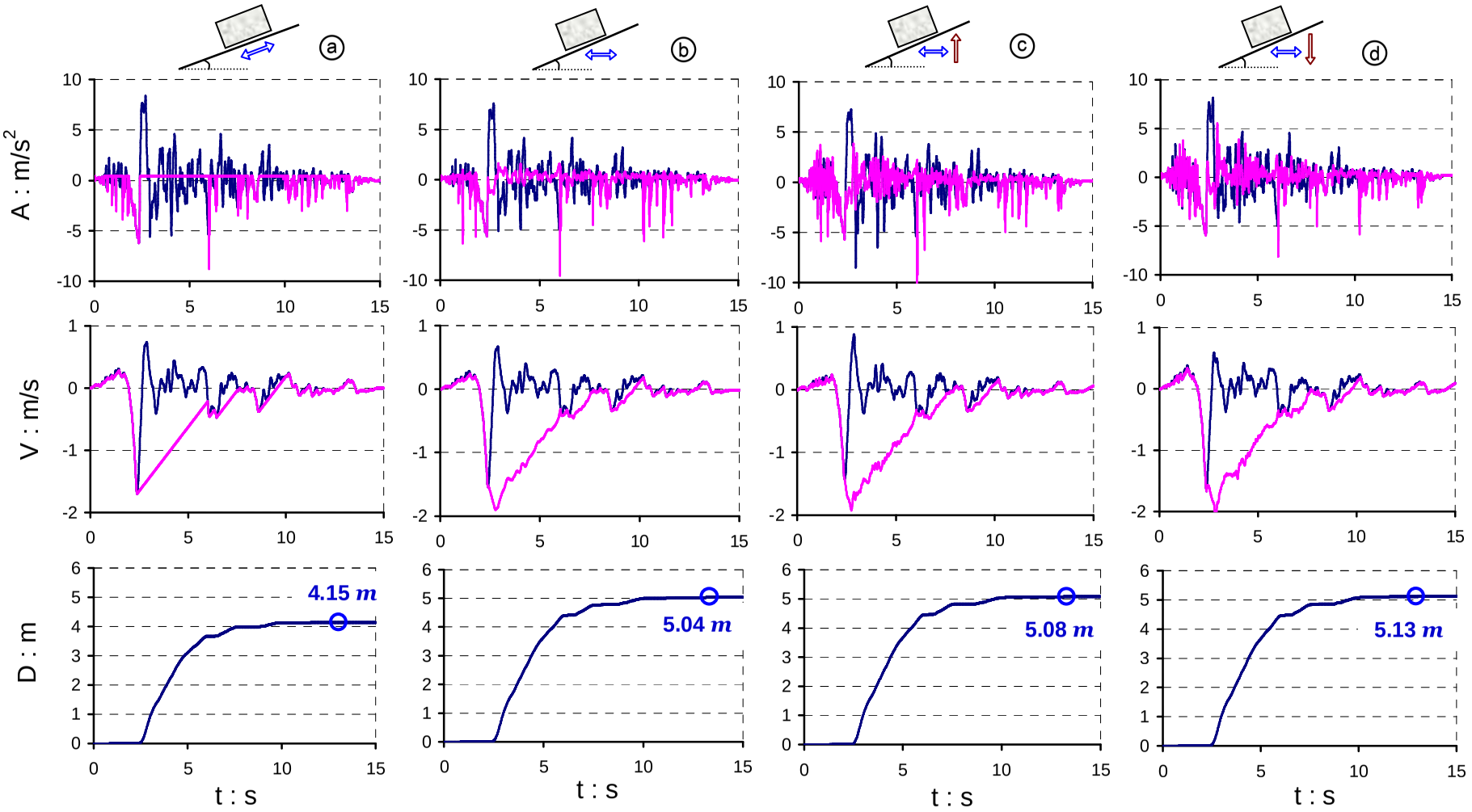

Figure 4.52 *Directionality effect for the Rinaldi– 228° record: (a) at the left column the horizontal component is acting parallel to the yielding surface, (b) at the second column the horizontal acceleration imposed horizontally to the sliding plane. In the next two columns the plane is triggered by both the vertical and horizontal components: (c) at the third column both components are employed with their normal polarity, and (d) at the right column the vertical acceleration is applied with its reversed polarity.* ($a_C/a_H = 0.05$ *and* $\beta = 25^o$)

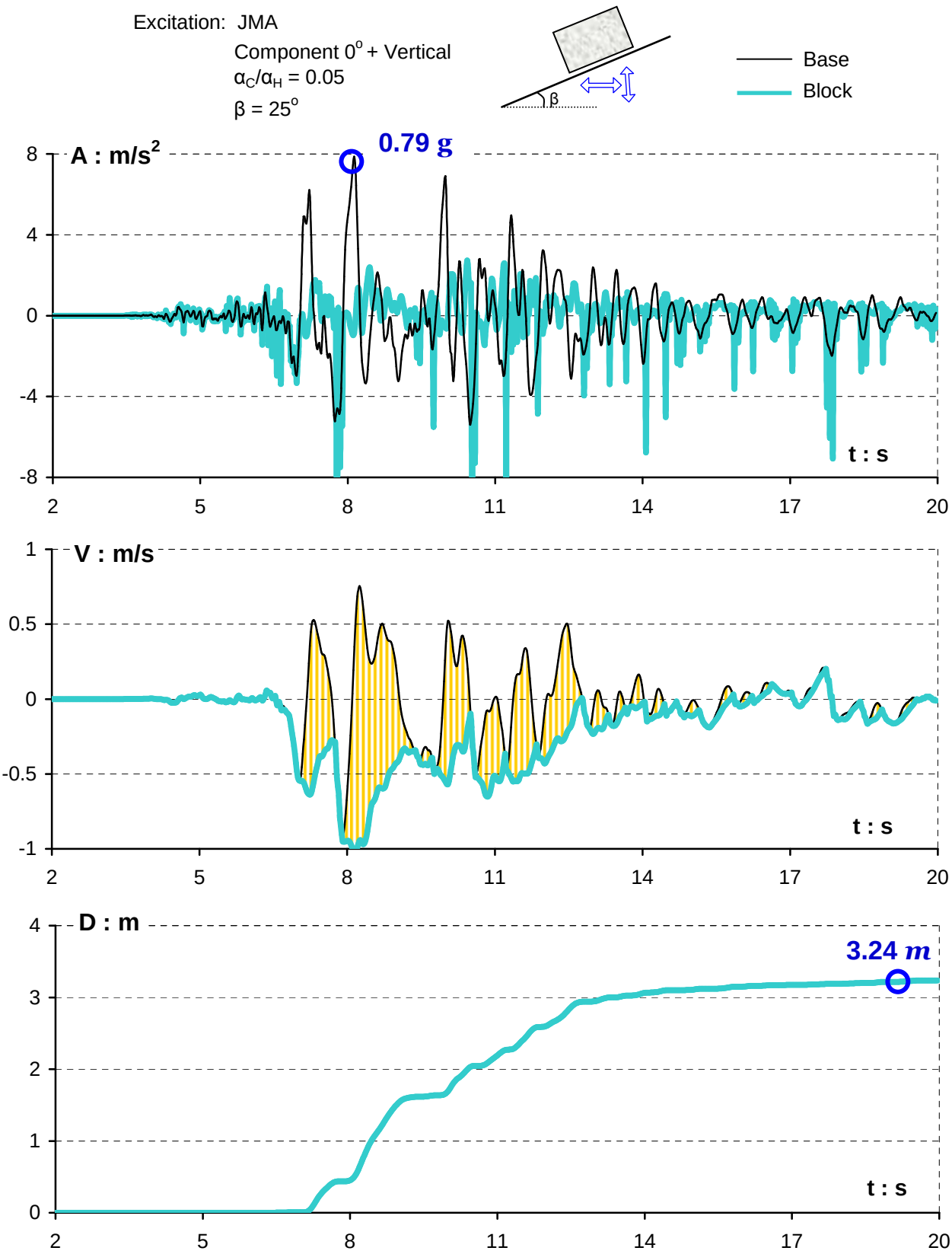

Figure 4.53 *Acceleration, velocity, and sliding displacement time histories of a block rested on an 25⁰ inclined plane subjected simultaneously to: (i) the inverted polarity horizontal component of JMA 0⁰ record and (ii) the normal polarity vertical component of the record. (a_C/a_H = 0.05)*

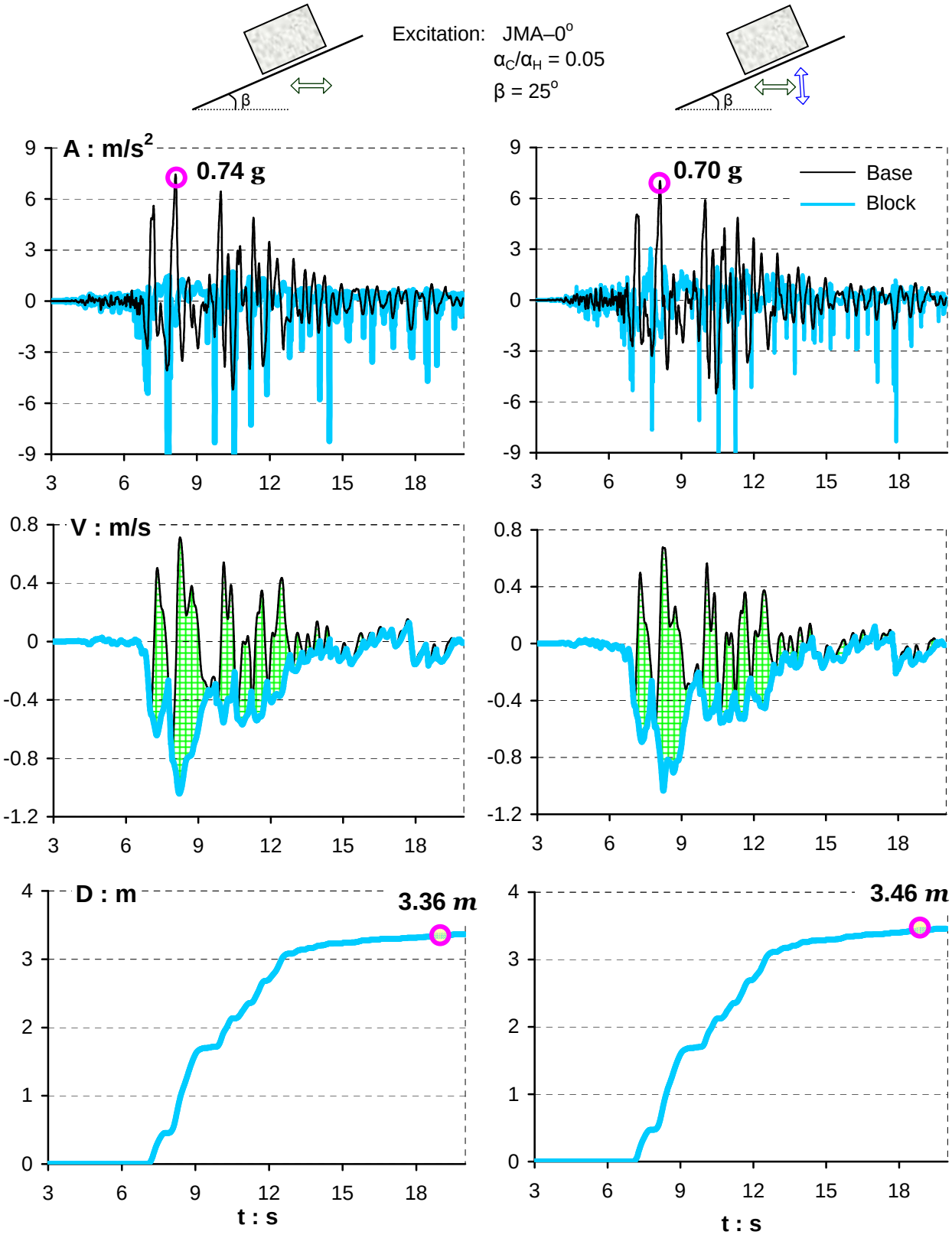

Figure 4.54 *The effect of vertical excitation in case of the reversed polarity horizontal JMA record: the response for the horizontally imposed 0° acceleration component (on the left) is only 3% greater than the sliding displacement by simultaneously acted horizontal and vertical components of the Rinaldi record. The vertical acceleration is employed with its normal polarity. ($a_C/a_H = 0.05$ and $\beta = 25^o$)*

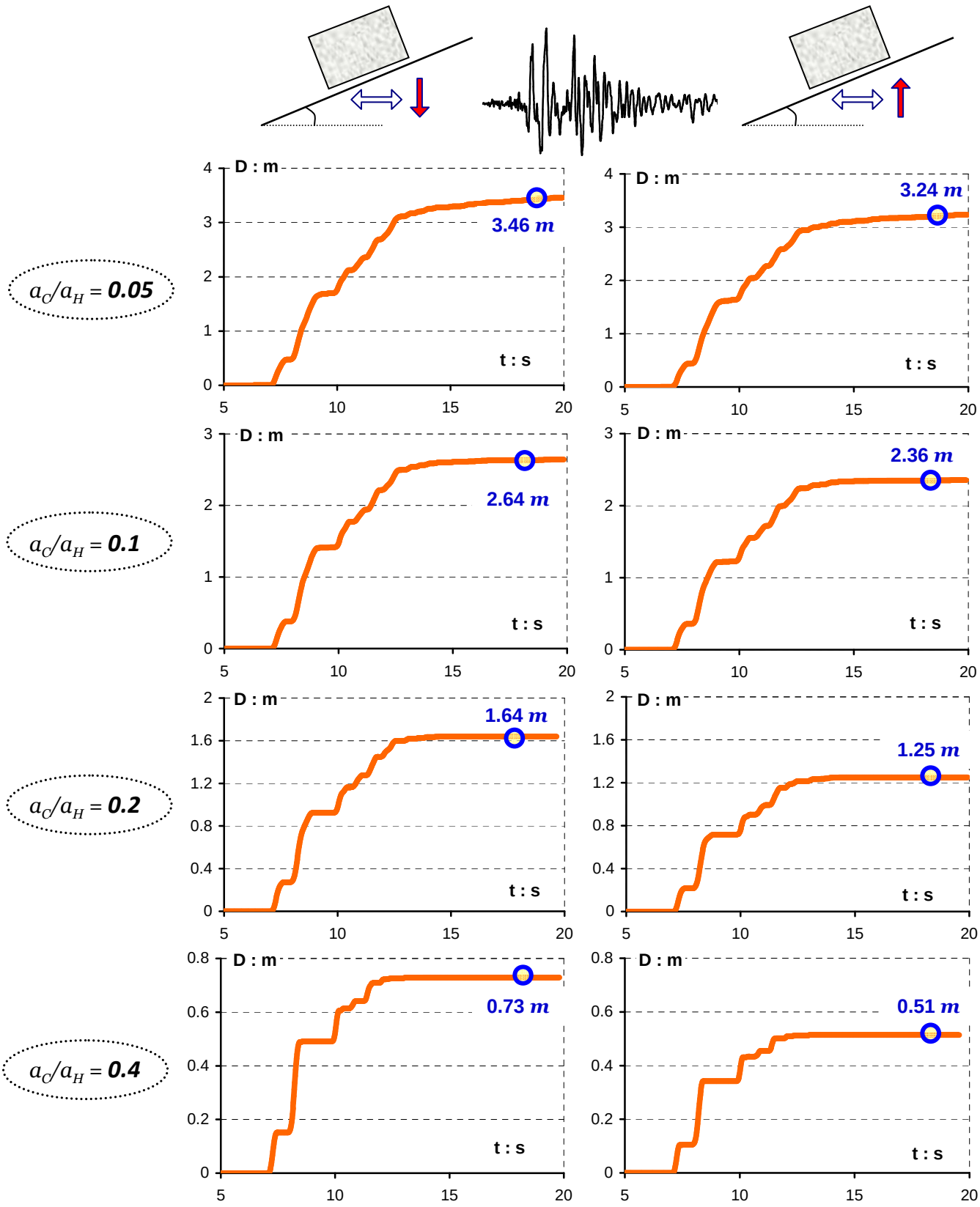

Figure 4.56 *Polarity effect of vertical acceleration on asymmetric sliding for four acceleration ratios, a_C/a_H . The triggering horizontal excitation is the reversed JMA–0° record and is concurrently acting with the vertical motion. [$\beta = 25^o$]*

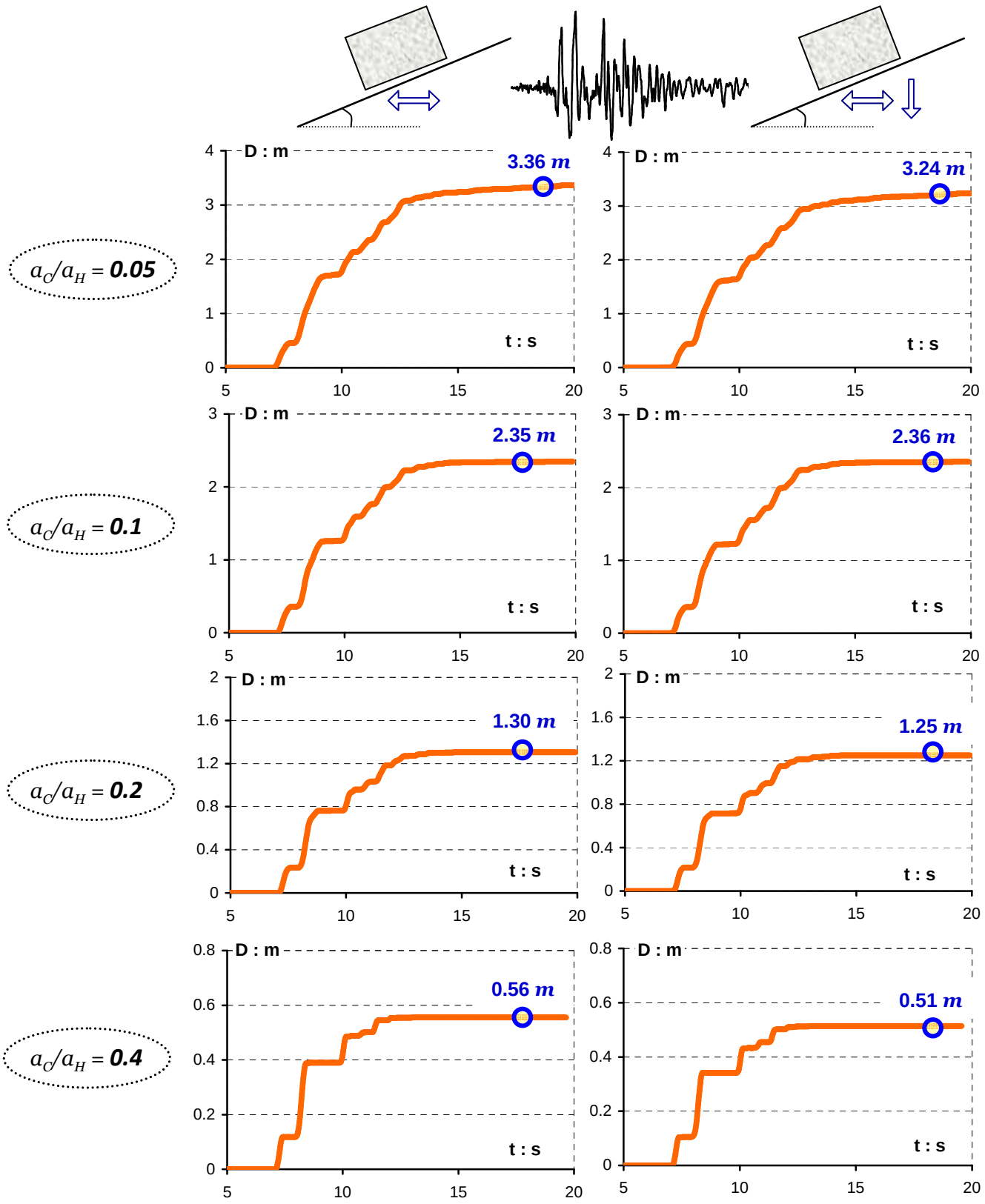

Figure 4.57 *Importance of vertical acceleration on asymmetric sliding for four acceleration ratios, a_C/a_H . The triggering horizontal excitation is the reversed JMA–0° record (left column) and the concurrently acting horizontal and vertical motion (left column). The vertical motion has its normal polarity. [$\beta = 25^o$]*

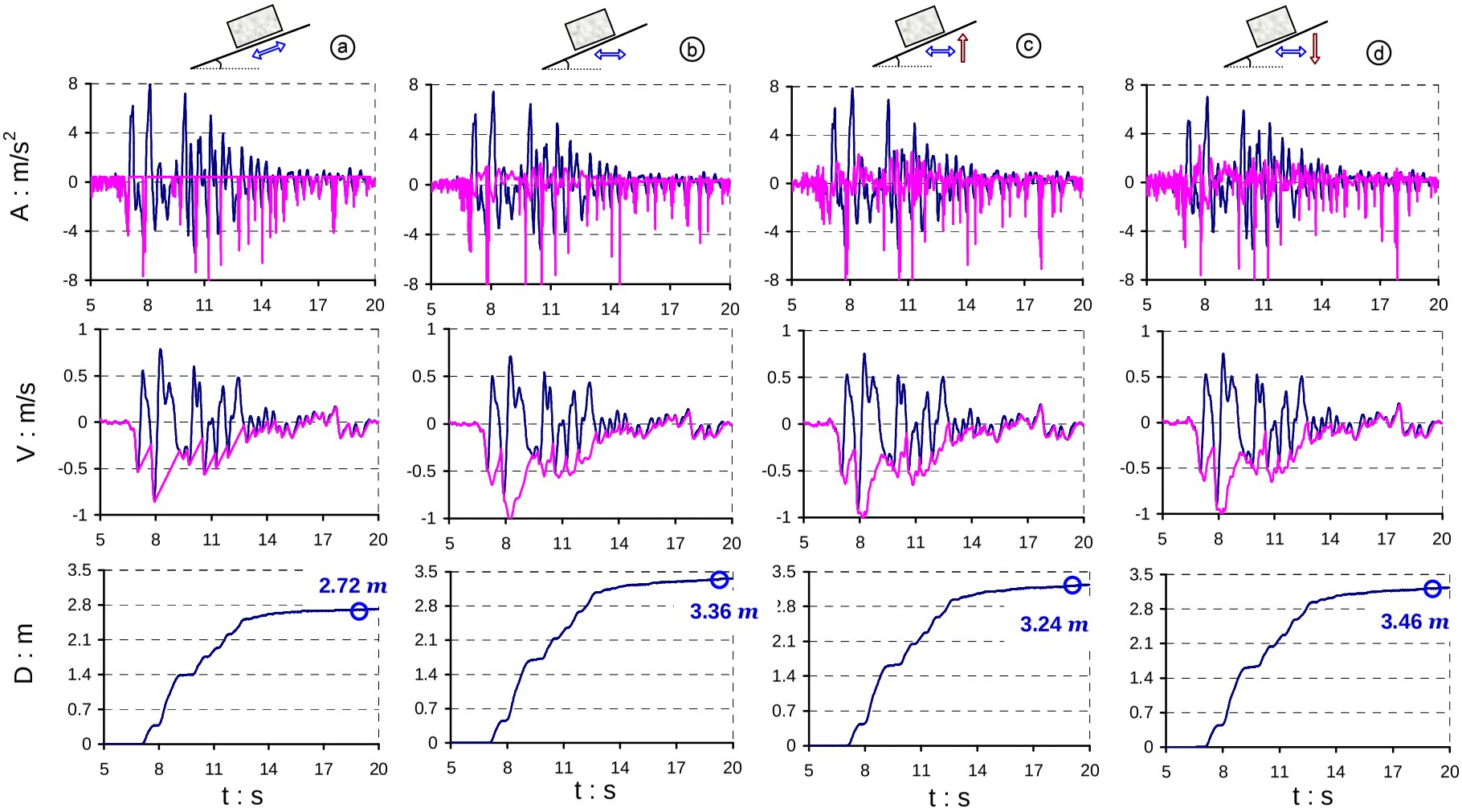

Figure 4.58 *Directionality effect for the JMA– 0° record: (a) at the left column the horizontal component is acting parallel to the yielding surface, (b) at the second column the horizontal acceleration imposed horizontally to the sliding plane. In the next two columns the plane is triggered by both the vertical and horizontal components: (c) at the third column both components are employed with their normal polarity, and (d) at the right column the vertical acceleration is applied with its reversed polarity.* ($a_C/a_H = 0.05$ *and* $\beta = 25^o$)

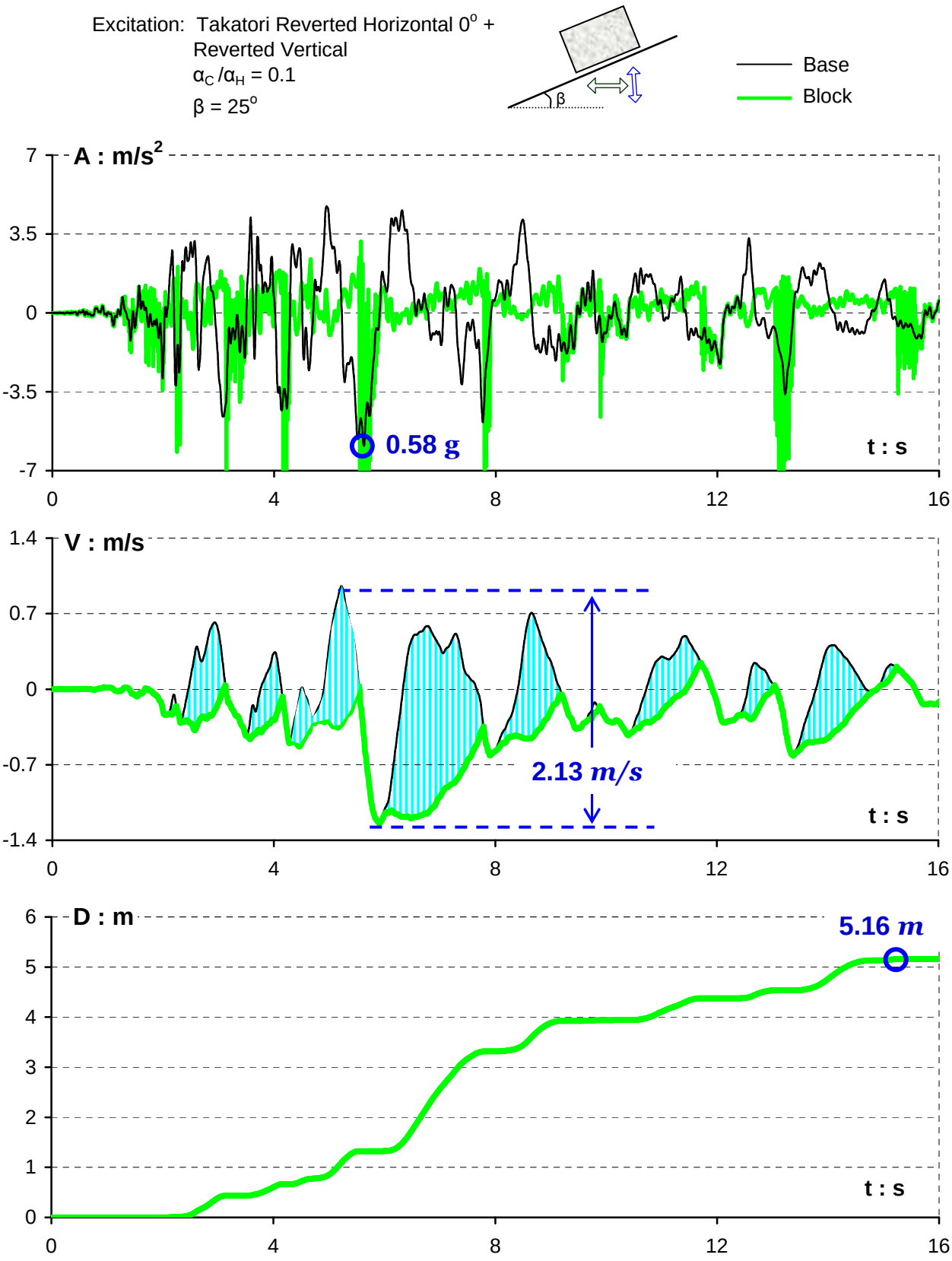

Figure 4.59 *Acceleration, velocity, and sliding displacement time histories of a block rested on an 25^0 inclined plane subjected simultaneously to: (i) the inverted polarity horizontal component of Takatori 0^o record and (ii) the reversed polarity vertical component of the record. ($a_C/a_H = 0.1$)*

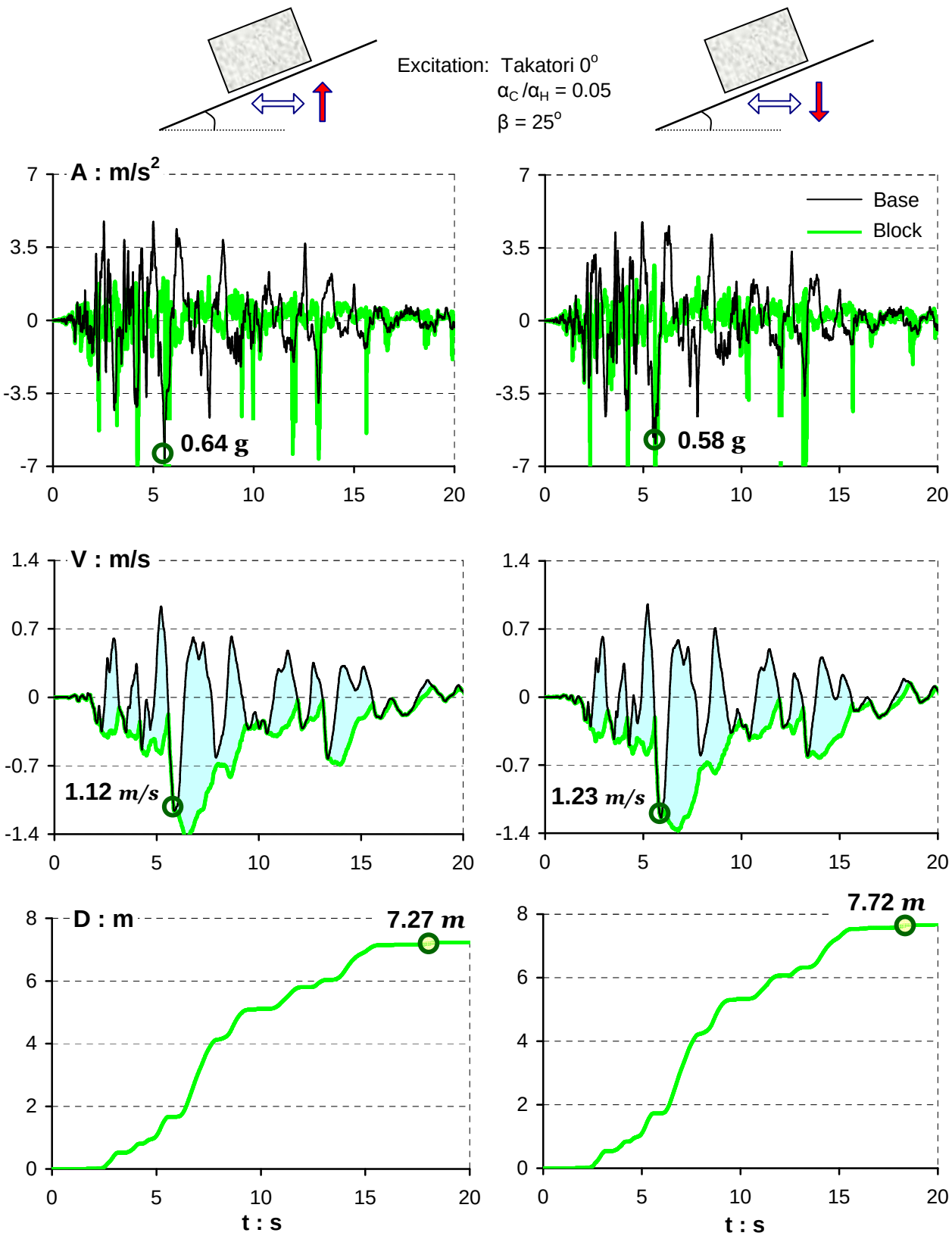

Figure 4.60 *Polarity of vertical excitation in case of the reversed horizontal Takatori–0° record: the response for the normal polarity vertical acceleration (on the left) and for the reversed polarity vertical component (on the right). ($a_C/a_H = 0.05$ and $\beta = 25^o$)*

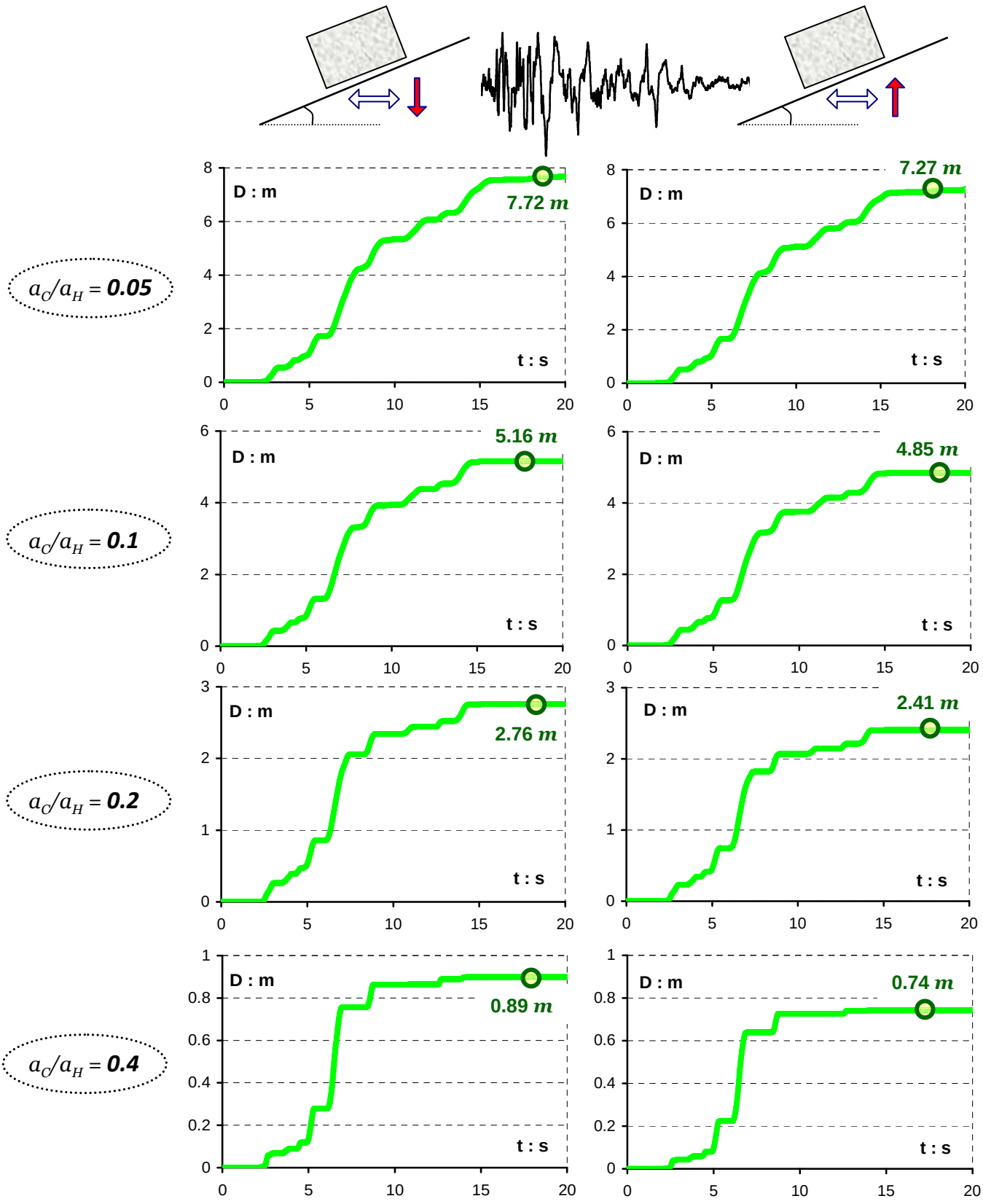

Figure 4.61 *Polarity effect of vertical acceleration on asymmetric sliding for four acceleration ratios, a_C/a_H . The triggering horizontal excitation is the reversed Takatori–0° record and is concurrently acting with the vertical motion. [$\beta = 25^o$]*

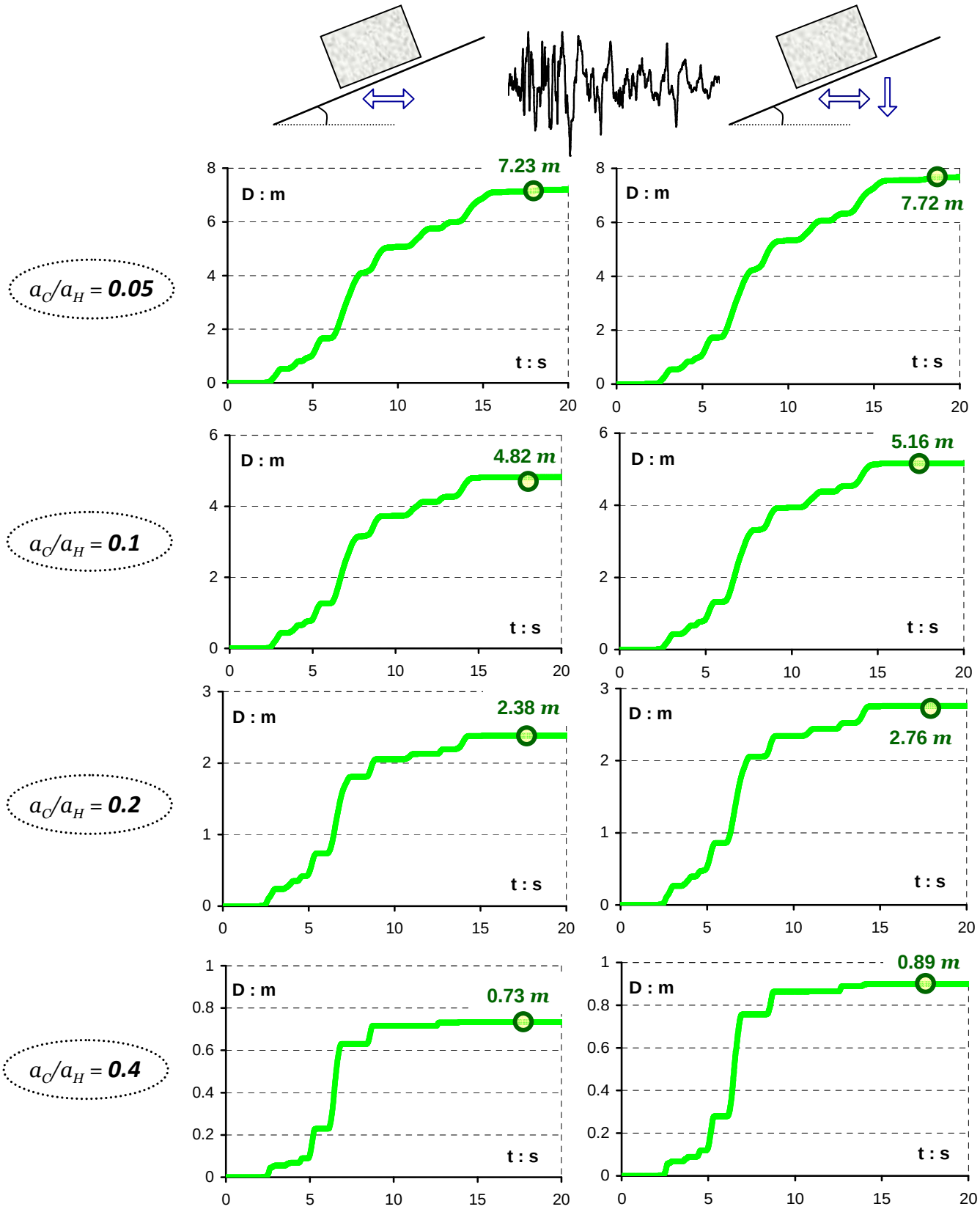

Figure 4.62 *Importance of vertical acceleration on asymmetric sliding for four acceleration ratios, a_C/a_H . The triggering horizontal excitation is the reversed Takatori–0° record (left column) and the concurrently acting horizontal and vertical motion (left column). The vertical motion has its inverted polarity. [$\beta = 25^o$]*

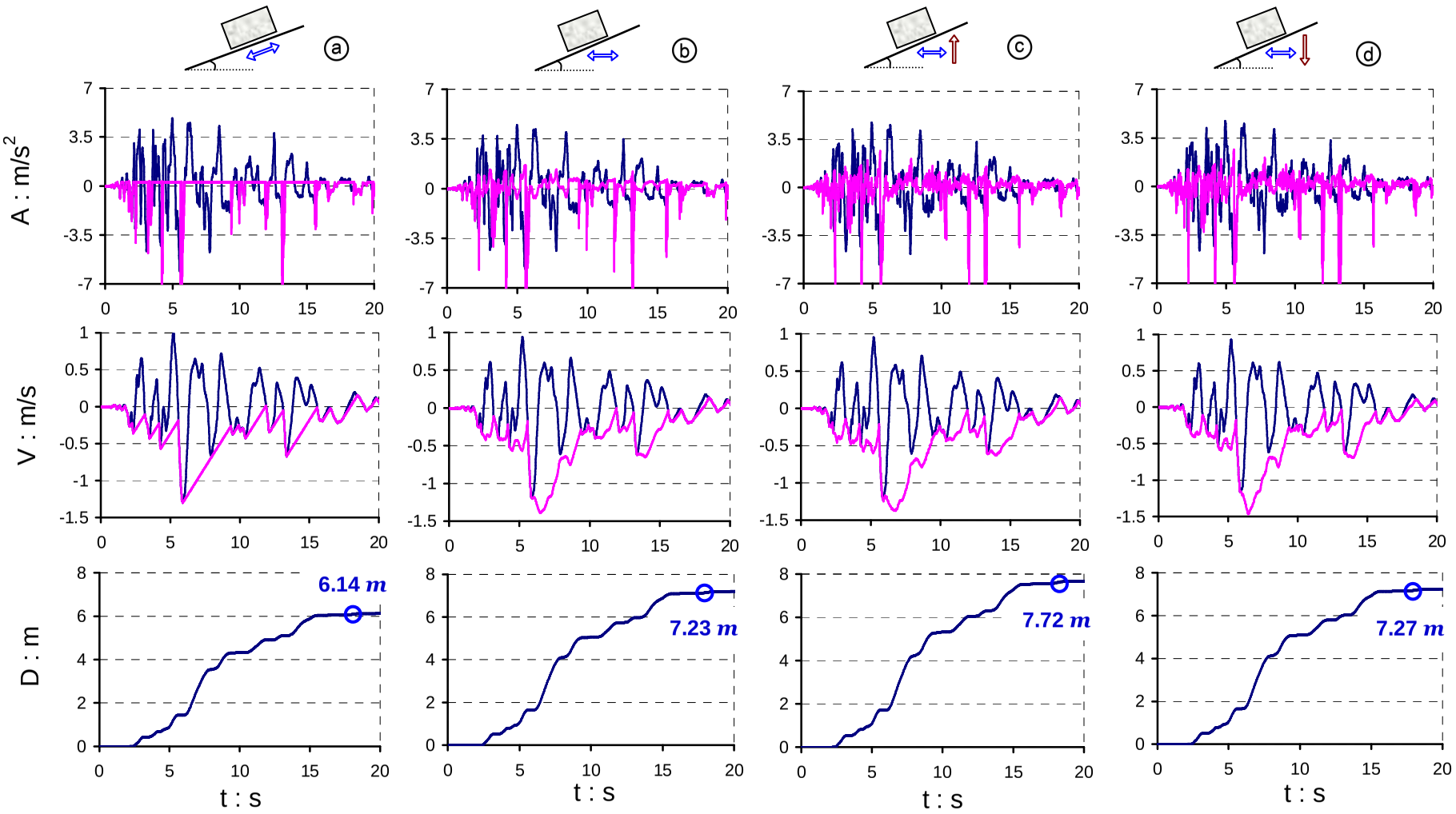

Figure 4.63 *Directionality effect for the Takatori – 0° record: (a) at the left column the horizontal component is acting parallel to the yielding surface, (b) at the second column the horizontal acceleration imposed horizontally to the sliding plane. In the next two columns the plane is triggered by both the vertical and horizontal components: (c) at the third column both components are employed with their normal polarity, and (d) at the right column the vertical acceleration is applied with its reversed polarity.* ($a_C/a_H = 0.05$ *and* $\beta = 25^o$)

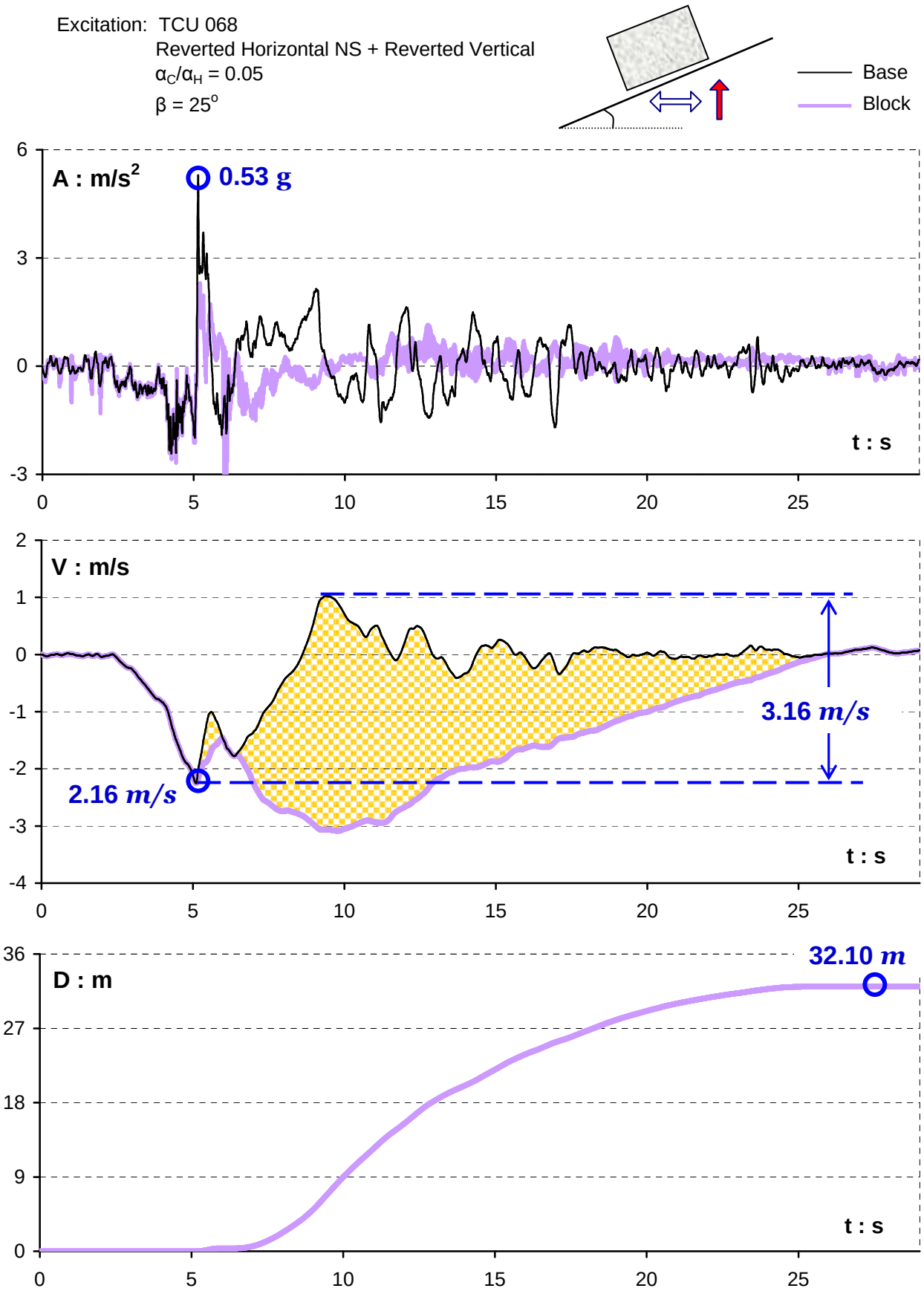

Figure 4.70 *Acceleration, velocity, and sliding displacement time histories of a block rested on an 25⁰ inclined plane subjected simultaneously to the inverted polarity : (i) horizontal component of TCU 068 record and (ii) vertical component.*

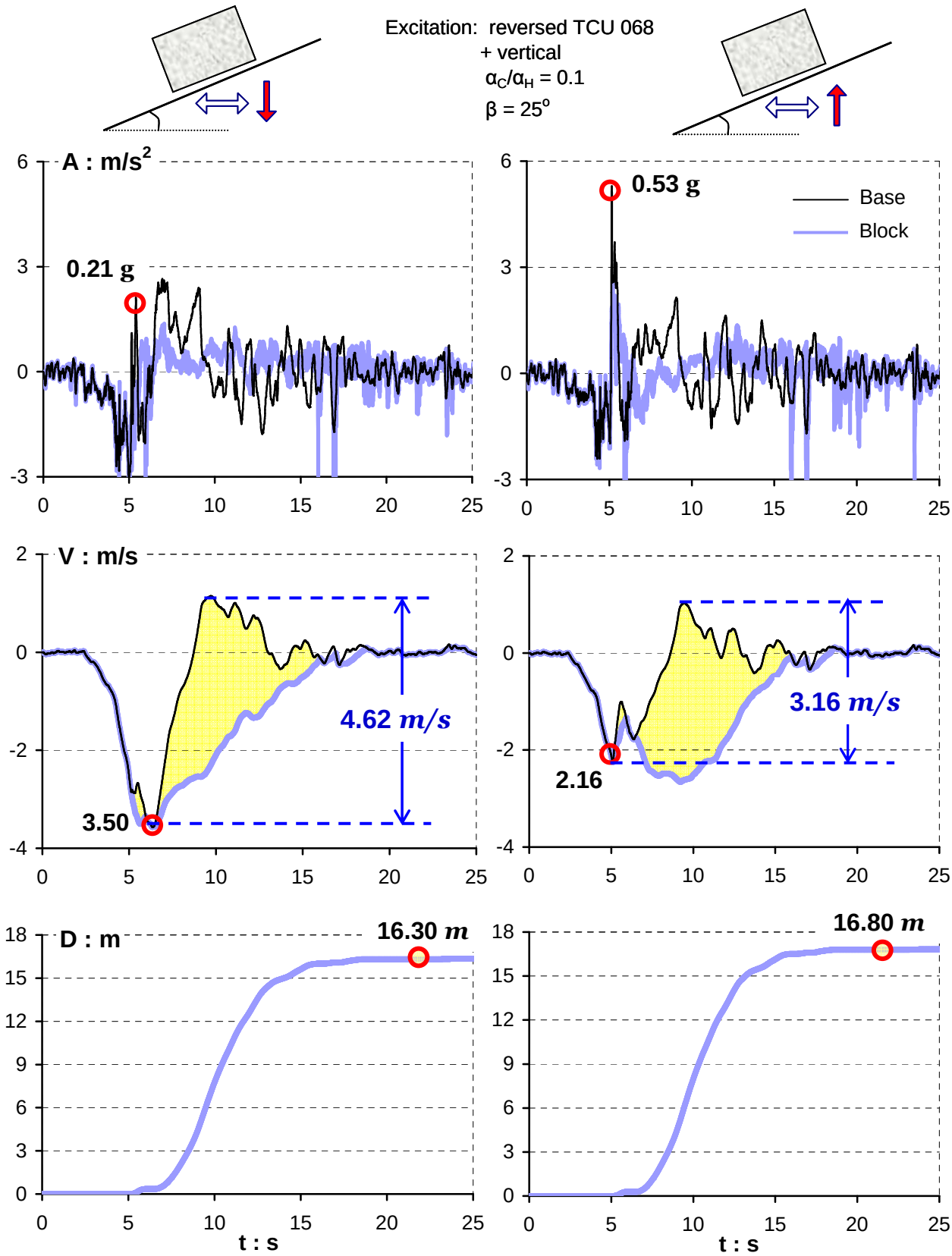

Figure 4.71 *Polarity of vertical excitation in case of the reversed horizontal TCU 068–NS record: the response for the normal polarity vertical acceleration (on the left) and for the reversed polarity vertical component (on the right). (a_C/a_H = 0.1 and β = 25°)*

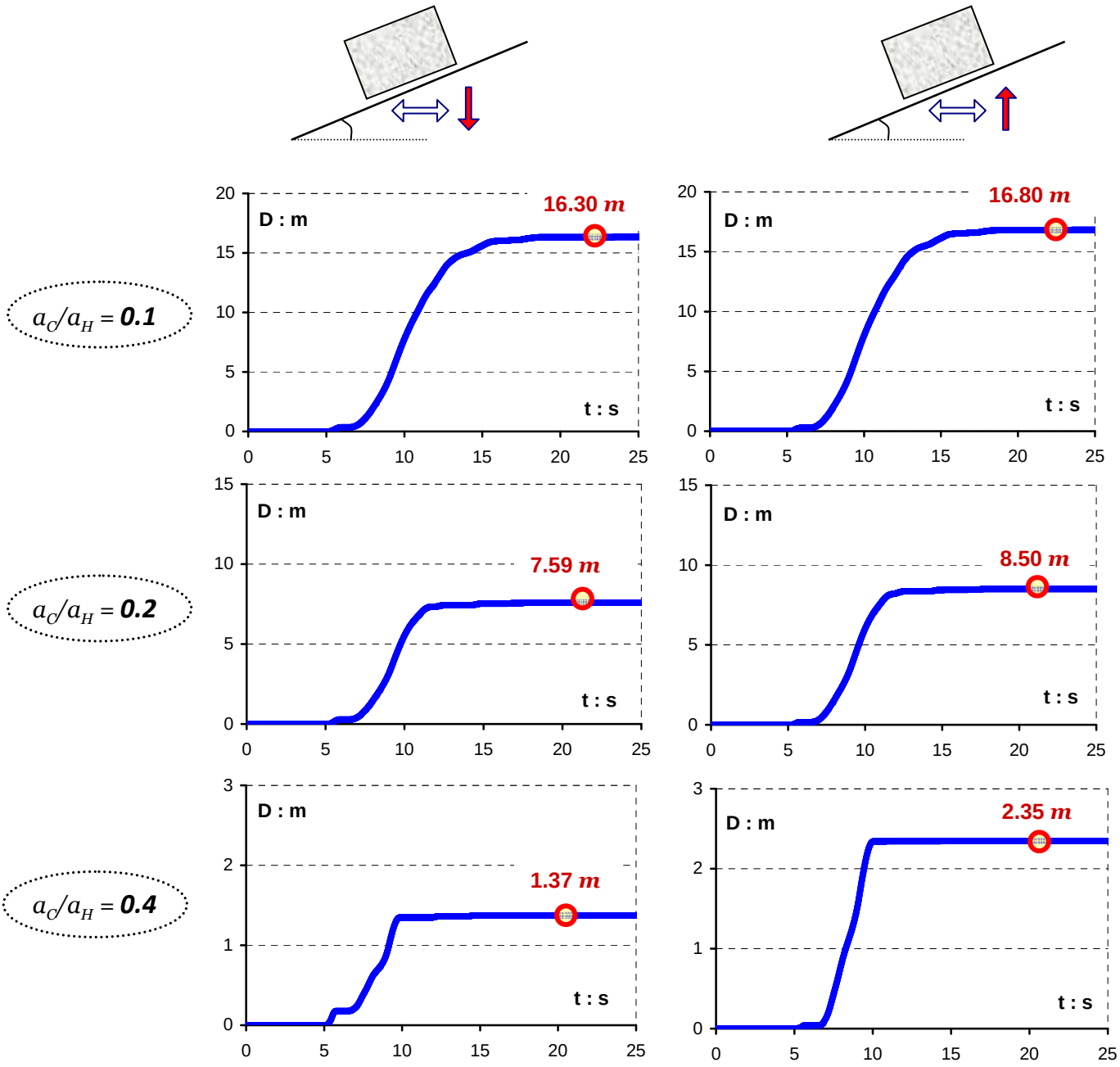

Figure 4.72 *Polarity effect of vertical acceleration on asymmetric sliding for three acceleration ratios, a_C/a_H . The triggering horizontal excitation is the reversed TCU 068–NS record and simultaneously is acting the: normal polarity (left) and inverted polarity (right) vertical component of the record. [$\beta = 25^o$]*

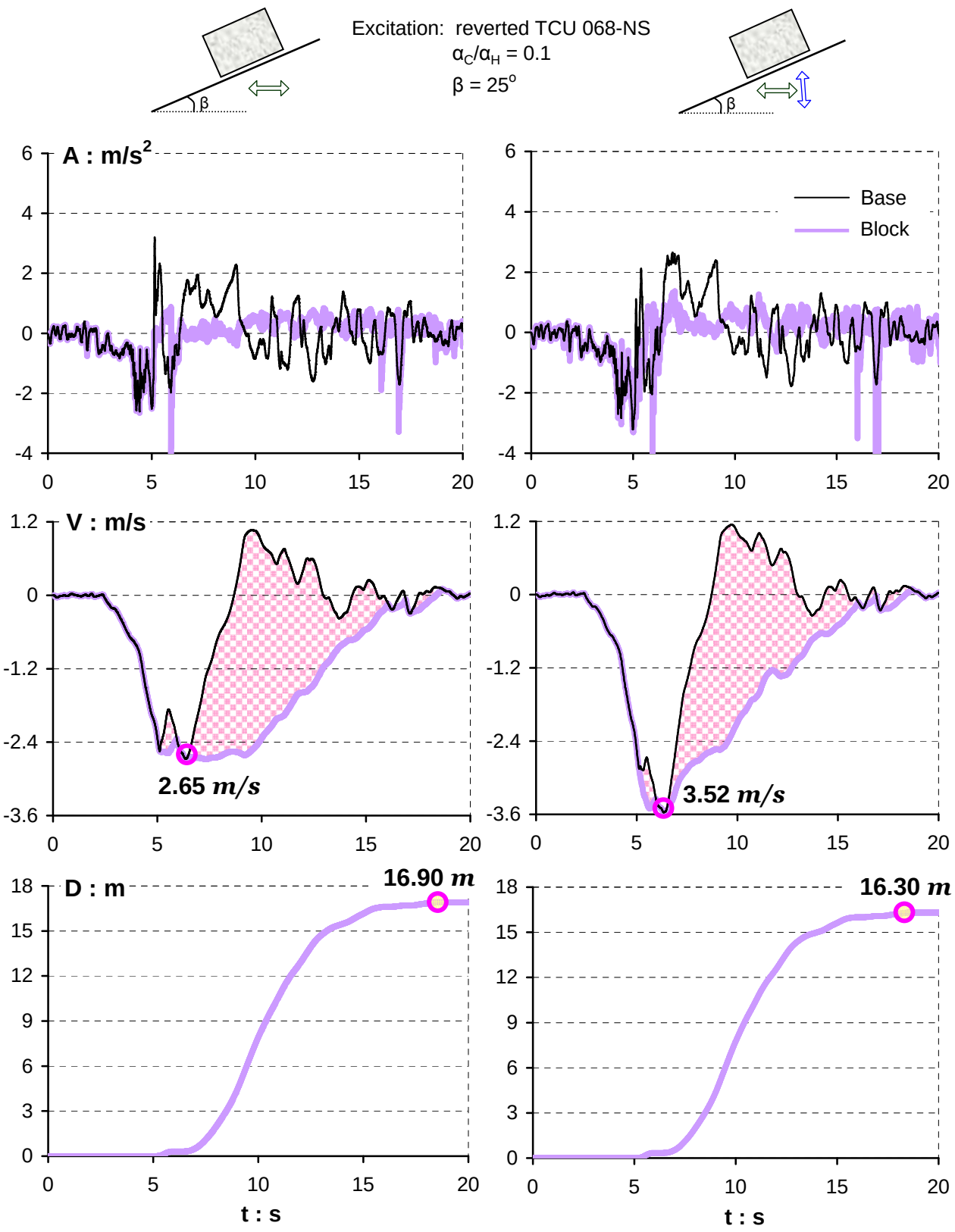

Figure 4.73 *The effect of vertical excitation in case of the reversed polarity horizontal TCU 068–NS record: the response for the horizontally imposed NS acceleration component (on the left) is 4% greater than the sliding displacement by simultaneously acted horizontal and vertical components of the TCU 068 record. The vertical acceleration is employed with its reversed polarity. (a_C/a_H = 0.05 and β = 25°)*

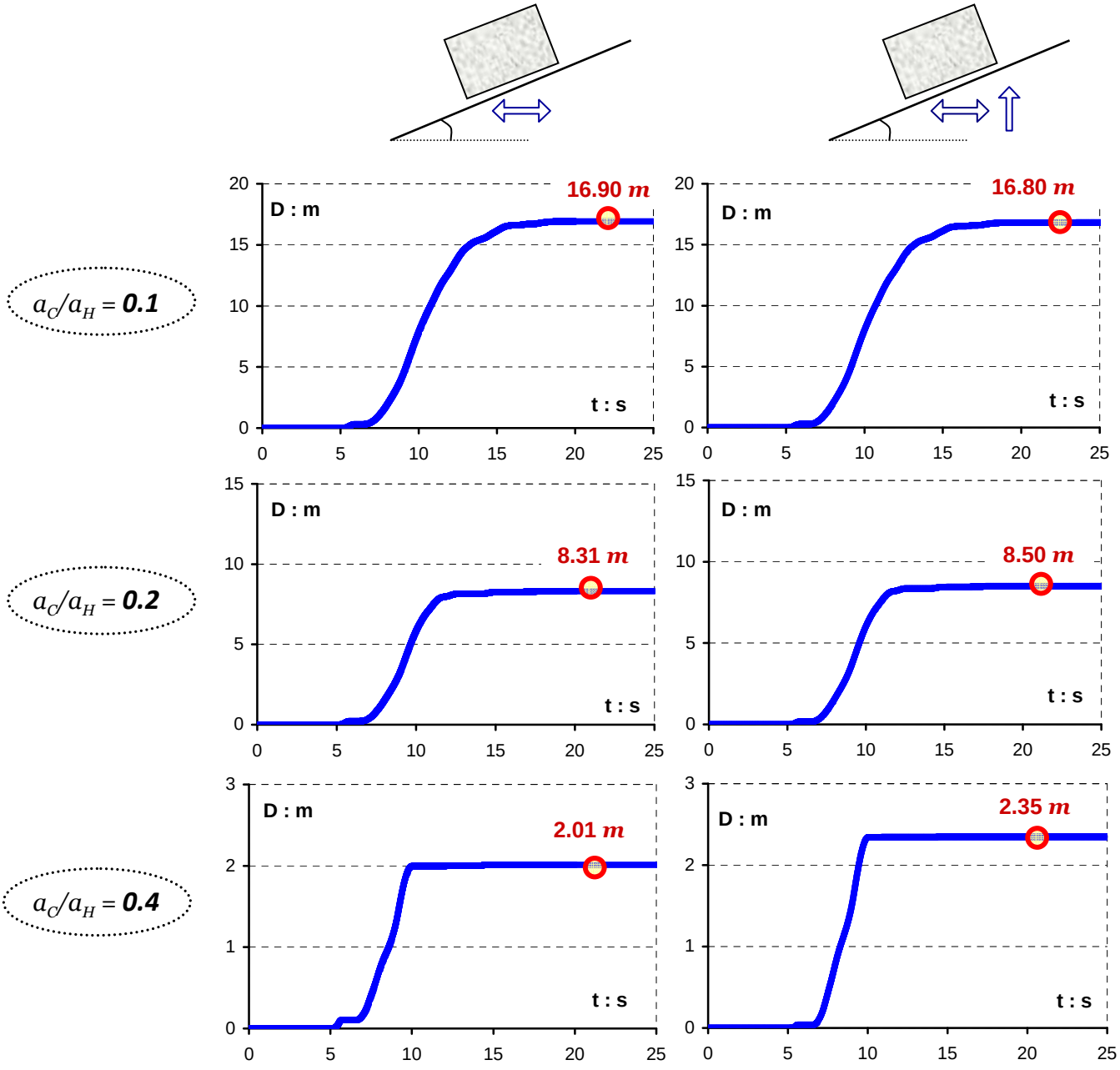

Figure 4.74 *Importance of vertical acceleration on asymmetric sliding for three acceleration ratios, a_C/a_H . The triggering horizontal excitation is the reversed TCU 068–NS record (left column) and the concurrently acting horizontal and vertical motion (left column). The vertical motion has its inverted polarity. [$\beta = 25^o$]*

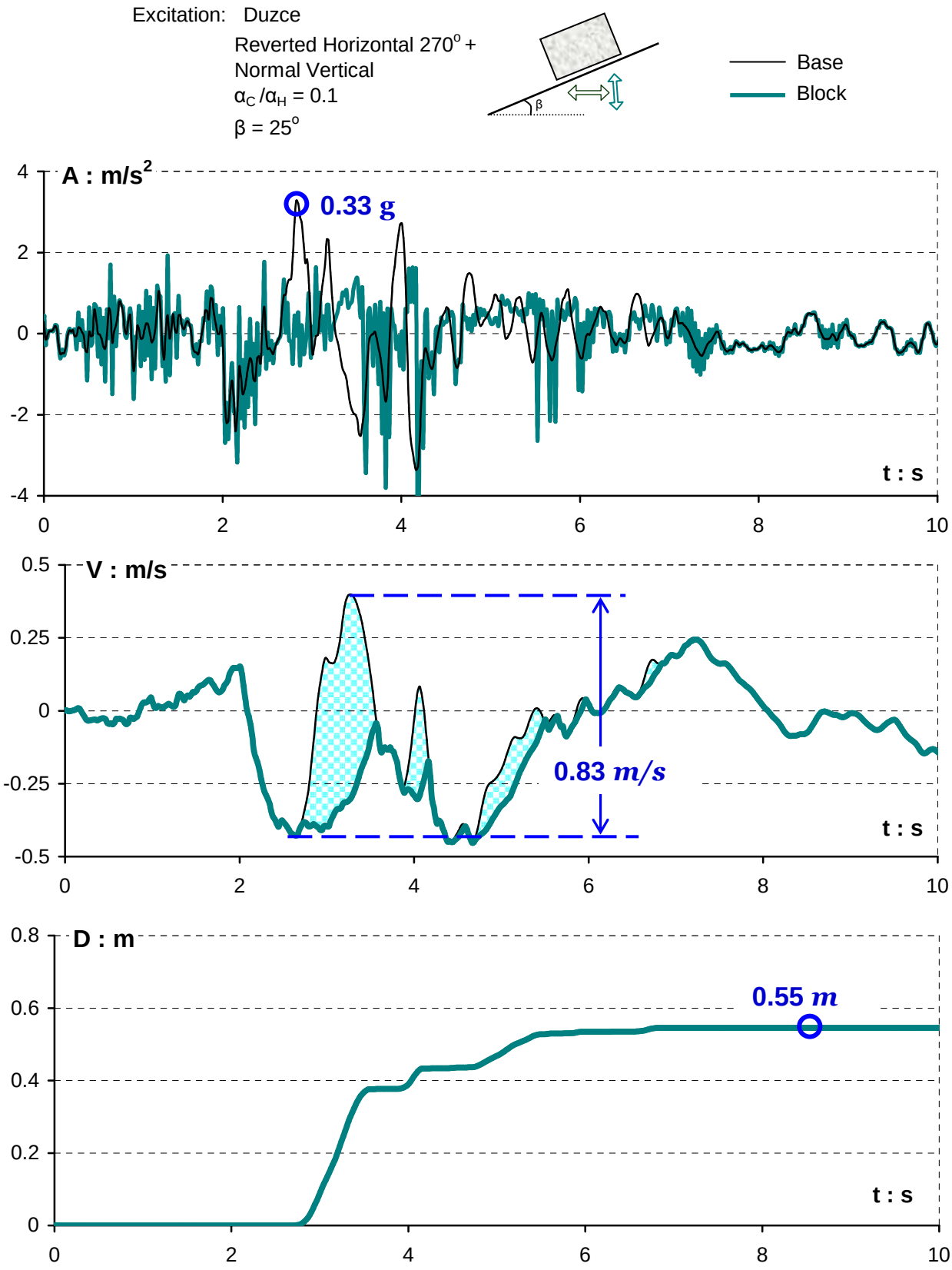

Figure 4.75 *Acceleration, velocity, and sliding displacement time histories of a block rested on an 25⁰ inclined plane subjected simultaneously to the inverted polarity : (i) horizontal component of Duzce 270⁰ record and (ii) vertical component.*

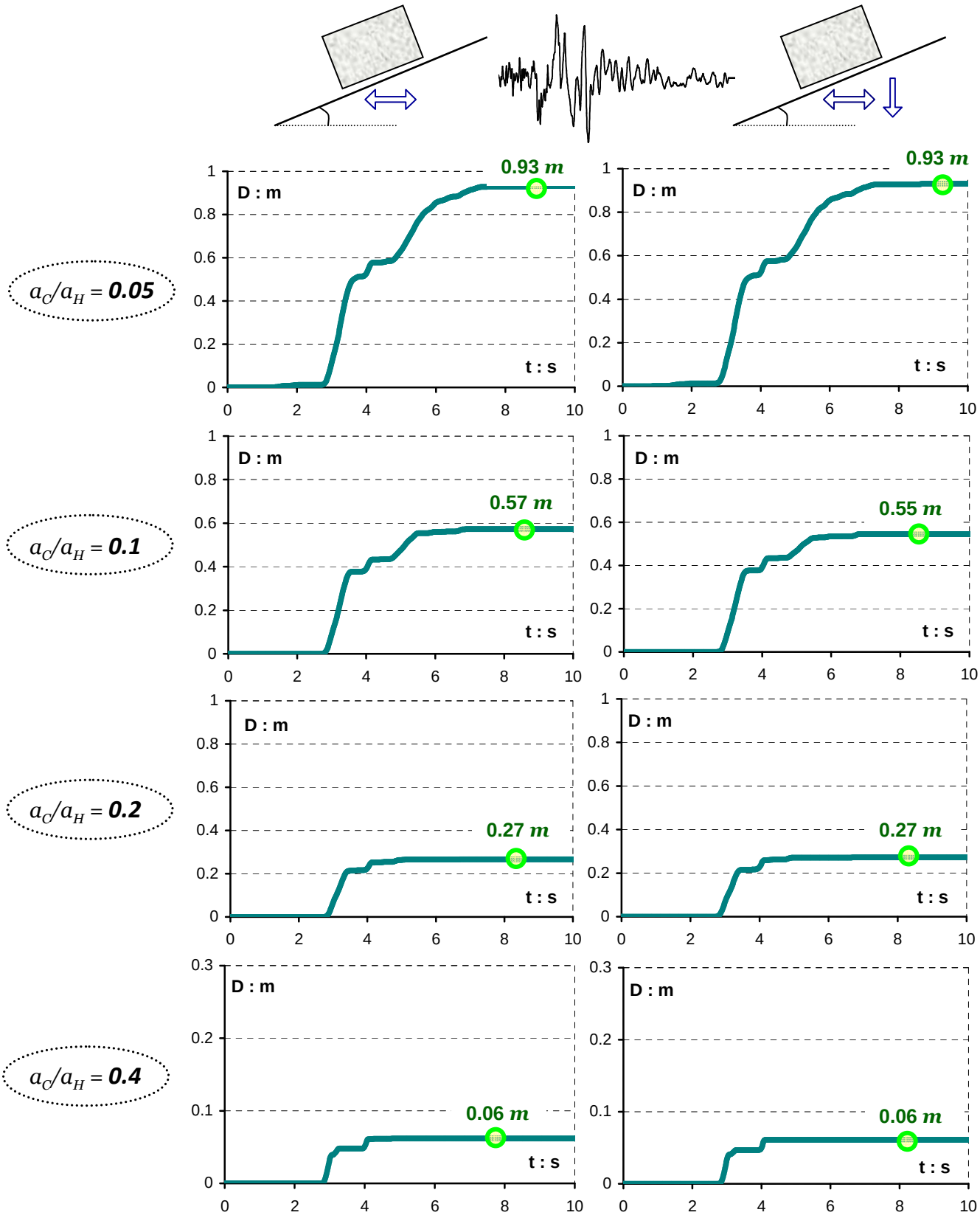

Figure 4.76 *Importance of vertical acceleration on asymmetric sliding for four acceleration ratios, a_C/a_H . The triggering horizontal excitation is the reversed Duzce–270° record (left column) and the concurrently acting horizontal and vertical motion (left column). The vertical motion has its inverted polarity. [$\beta = 25^o$]*

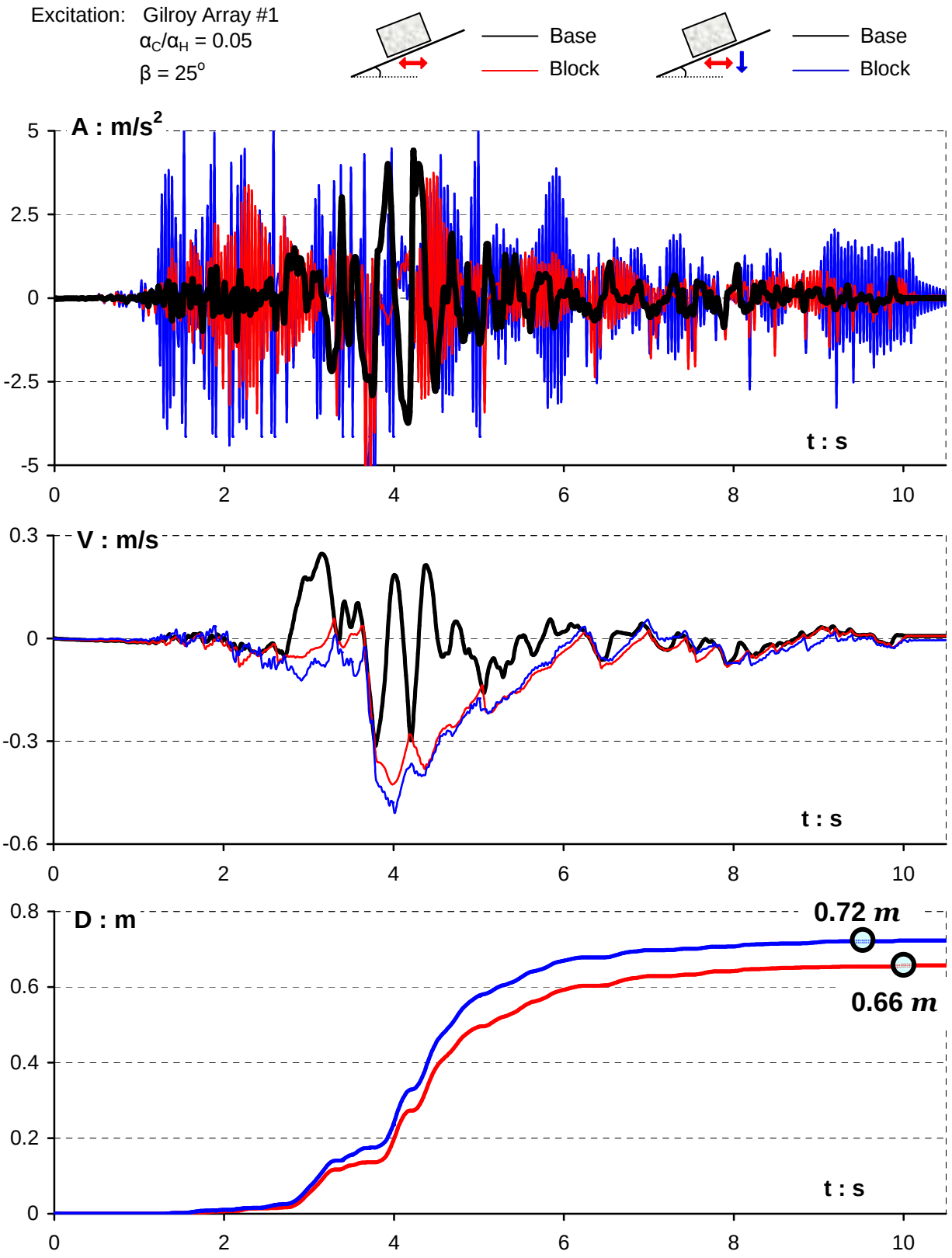

Figure 4.77 *Acceleration, velocity, and sliding displacement time histories of a block rested on an 25^0 inclined plane subjected simultaneously to the normal polarity : (i) horizontal component of Gilroy No1 record [red solid line] and (ii) vertical component [blue solid line].*

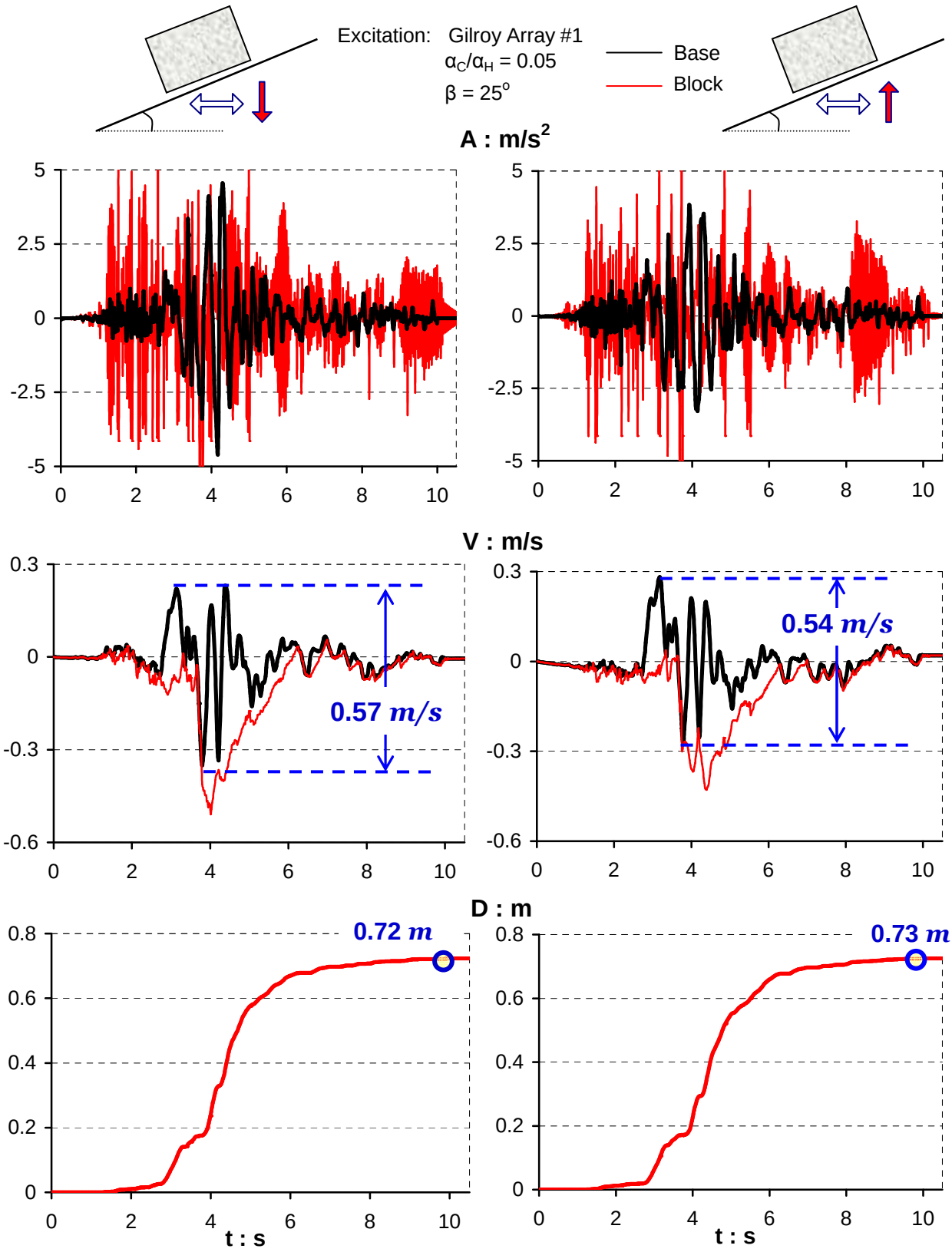

Figure 4.78 *Polarity of vertical excitation in case of the reversed horizontal Gilroy Array No1 record: the response for the normal polarity vertical acceleration (on the left) and for the reversed polarity vertical component (on the right). (a_C/a_H = 0.05 and β = 25°)*

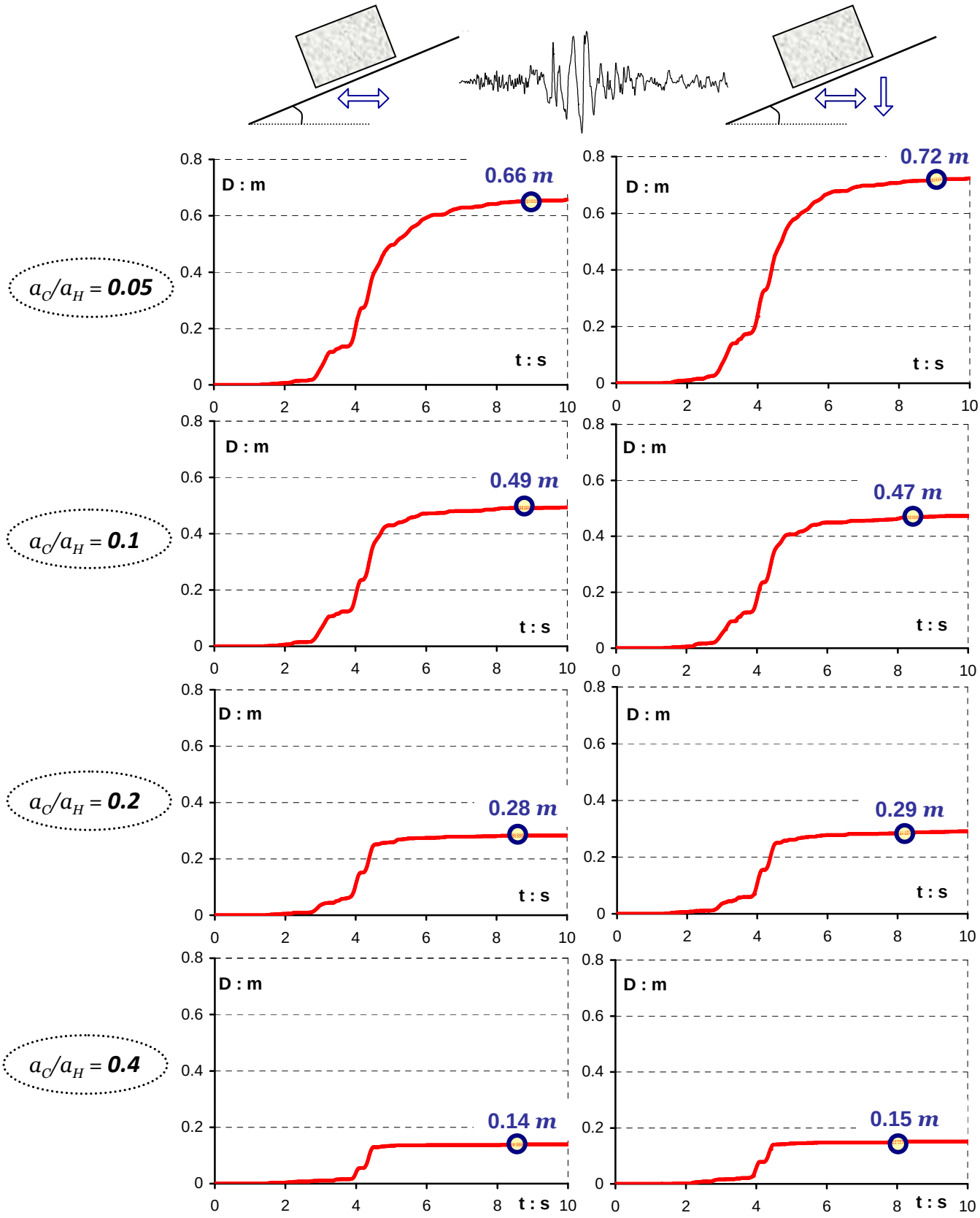

Figure 4.79 *Importance of vertical acceleration on asymmetric sliding for four acceleration ratios, a_C/a_H. The triggering horizontal excitation is the normal polarity Gilroy Array No1 record (left column) and the concurrently acting horizontal and vertical motion (left column). The vertical motion has its normal polarity. [$\beta = 25^o$]*

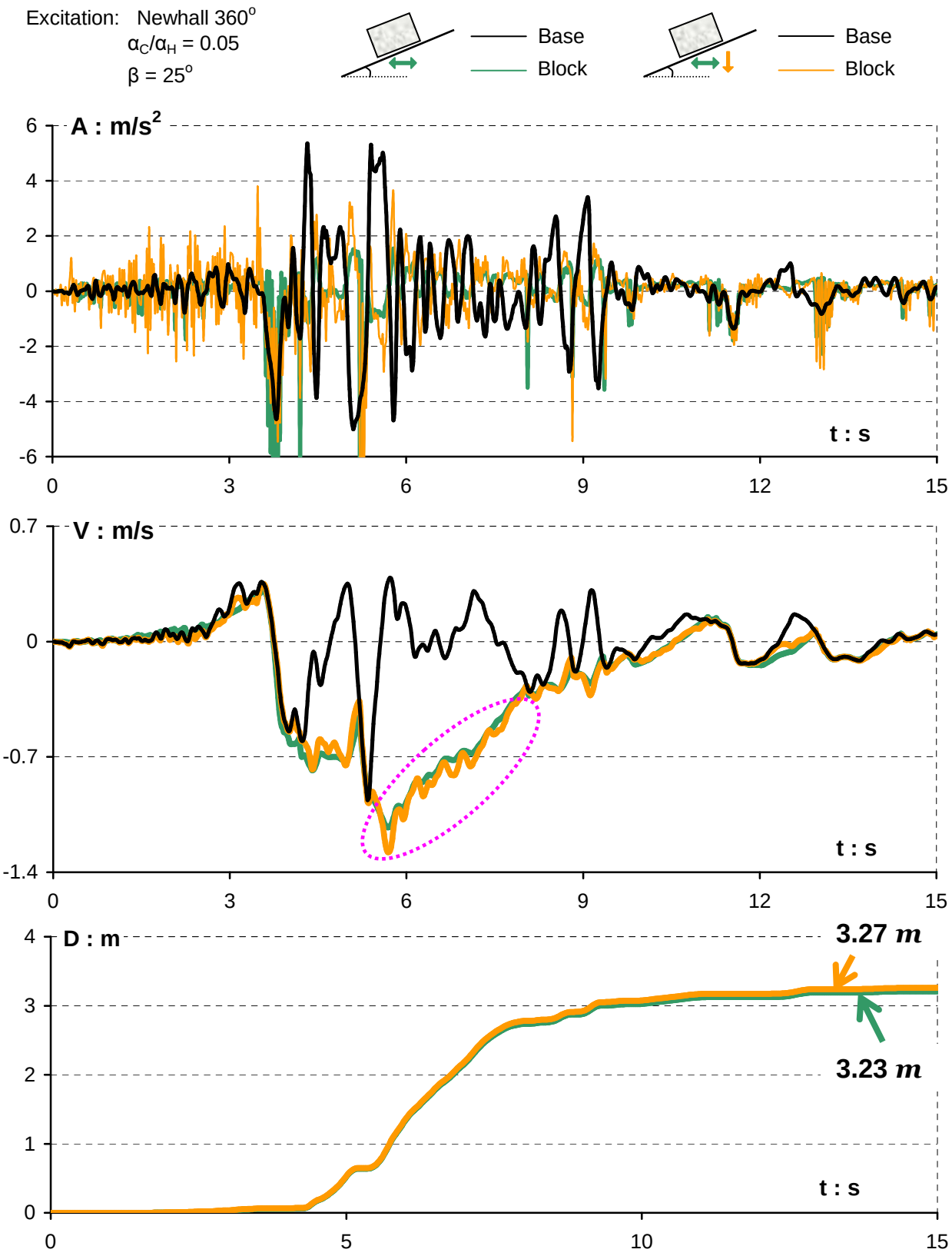

Figure 4.80 *Acceleration, velocity, and sliding displacement time histories of a block rested on an 25⁰ inclined plane subjected simultaneously to the normal polarity : (i) horizontal component of Newhall 360⁰ record [green solid line] and (ii) vertical component [yellow solid line].*

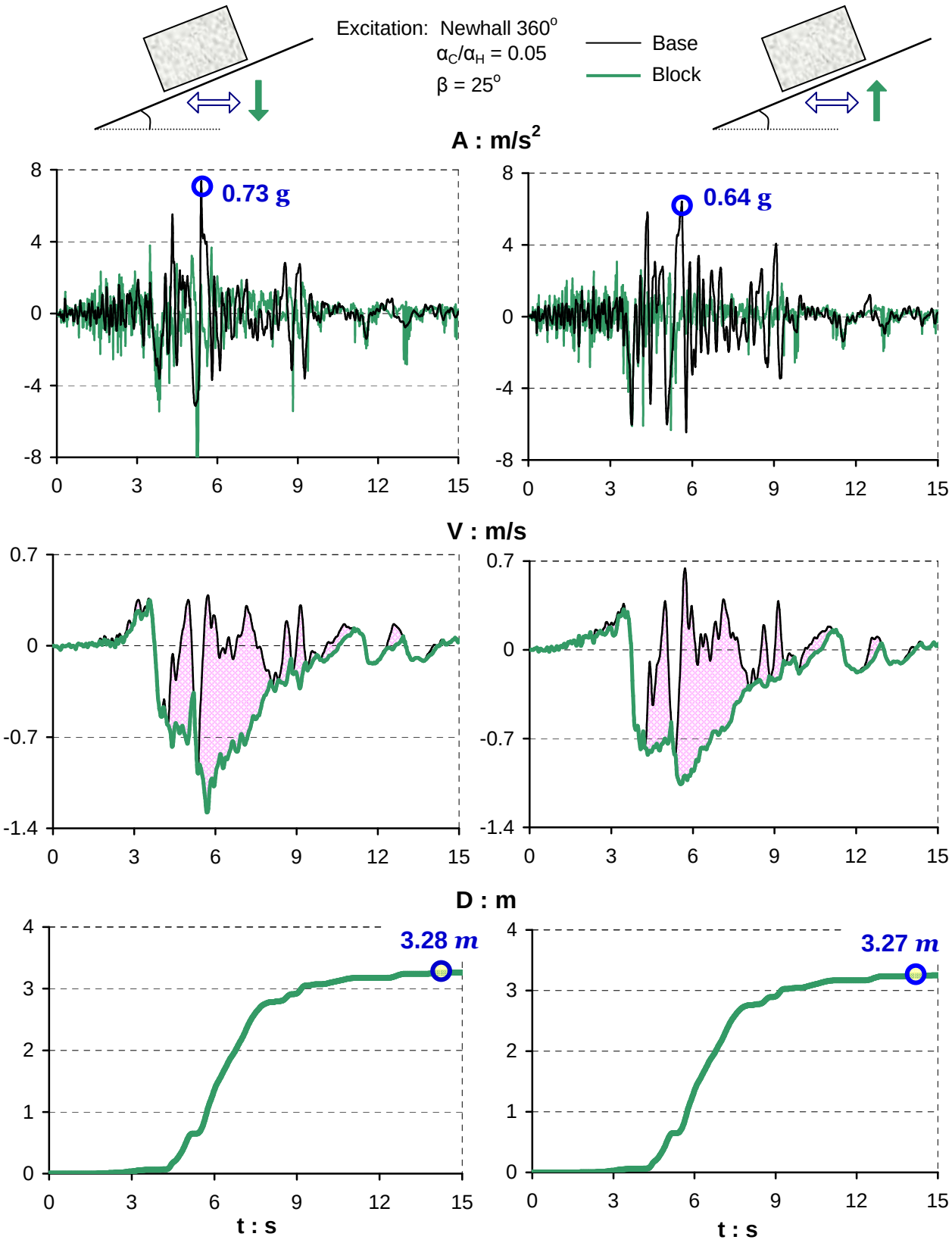

Figure 4.81 *Polarity of vertical excitation in case of the reversed horizontal Newhall 270° record: the response for the normal polarity vertical acceleration (on the left) and for the reversed polarity vertical component (on the right). (a_C/a_H = 0.05 and β = 25°)*

Summary Results

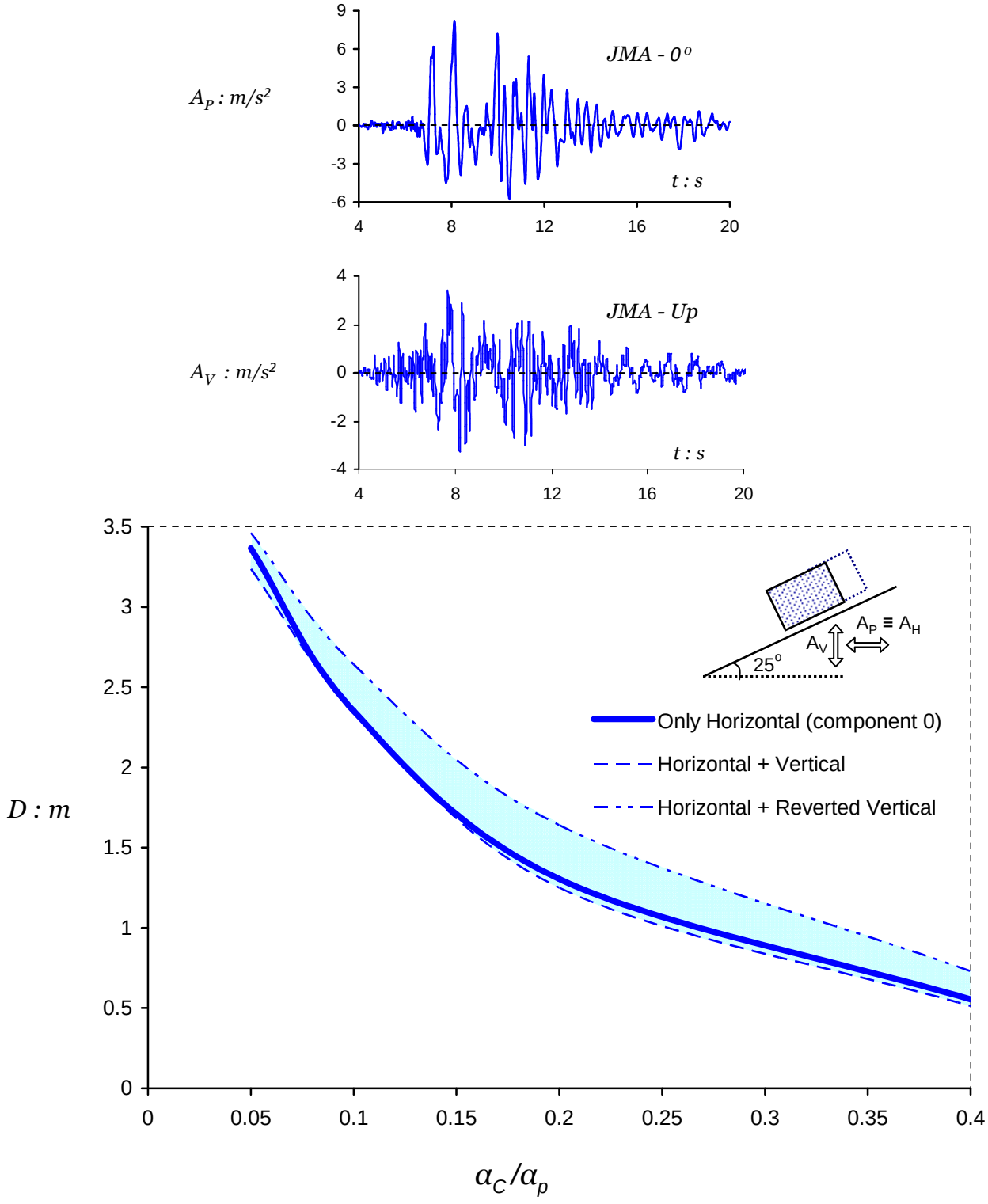

Figure 4.82 *Influence of vertical acceleration on sliding displacement for the Kobe record of JMA. The horizontal component is imposed reversed, because in the reversed polarity the greater slippage is induced. Both polarities of the vertical acceleration is examined.*

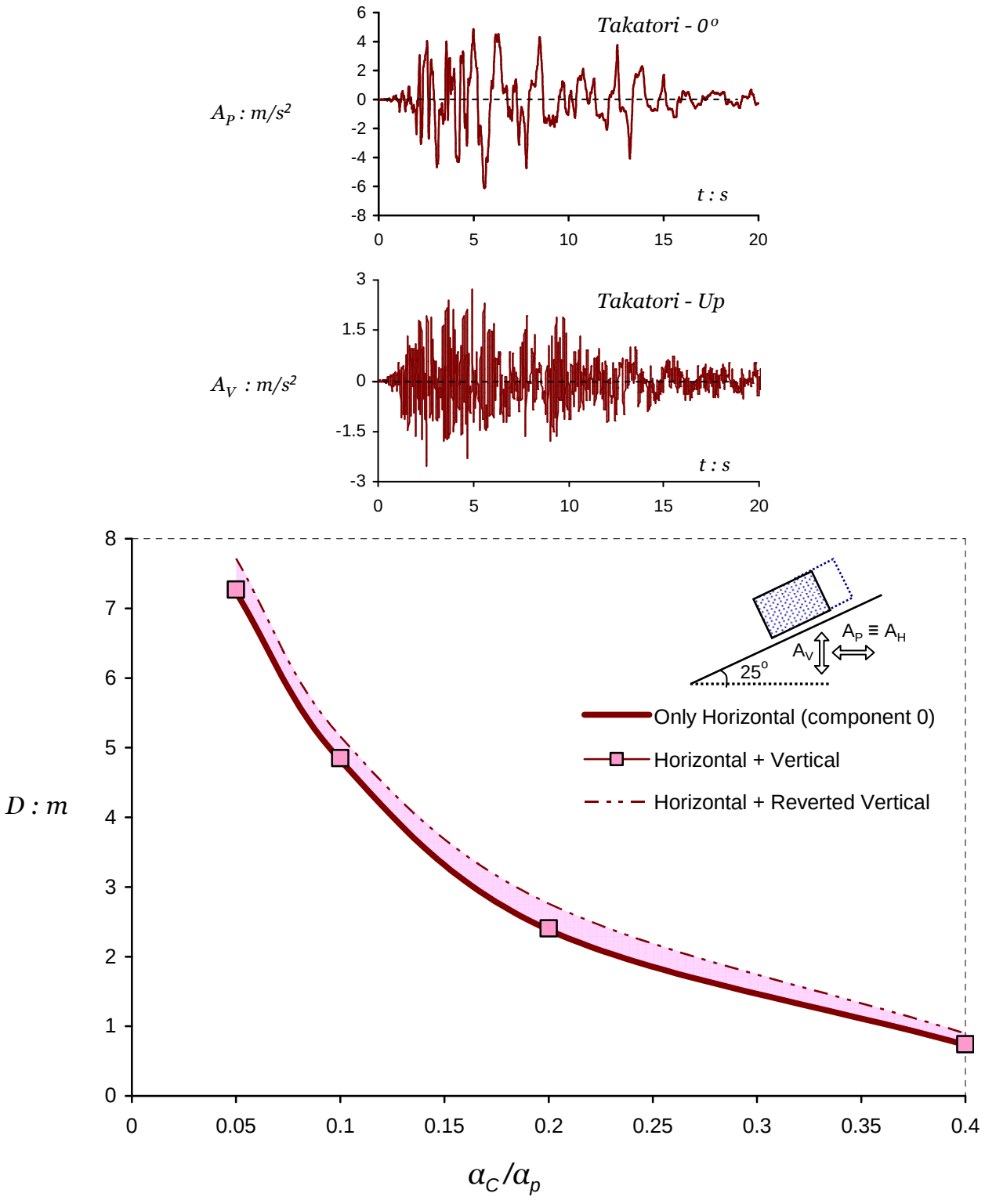

Figure 4.83 *Influence of vertical acceleration on sliding displacement for the Kobe record of Takatori. The horizontal component is imposed reversed, because in the reversed polarity the greater slippage is induced. Both polarities of the vertical acceleration is examined.*

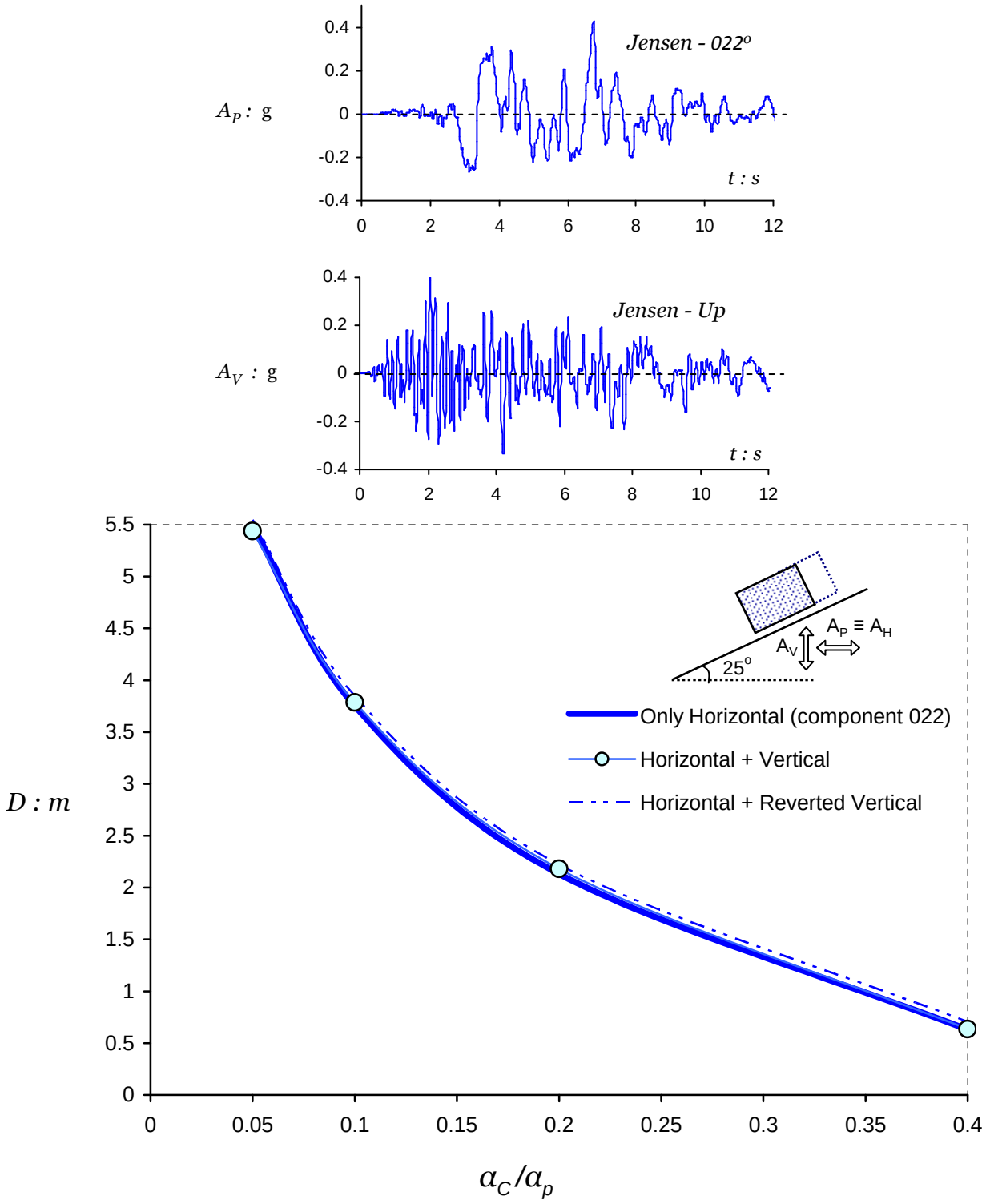

Figure 4.84 *Influence of vertical acceleration on sliding displacement for the Northridge record of Jensen Filtration Plant. The horizontal component is imposed as is, because in this polarity slippage is greater. Both polarities of the vertical acceleration is examined.*

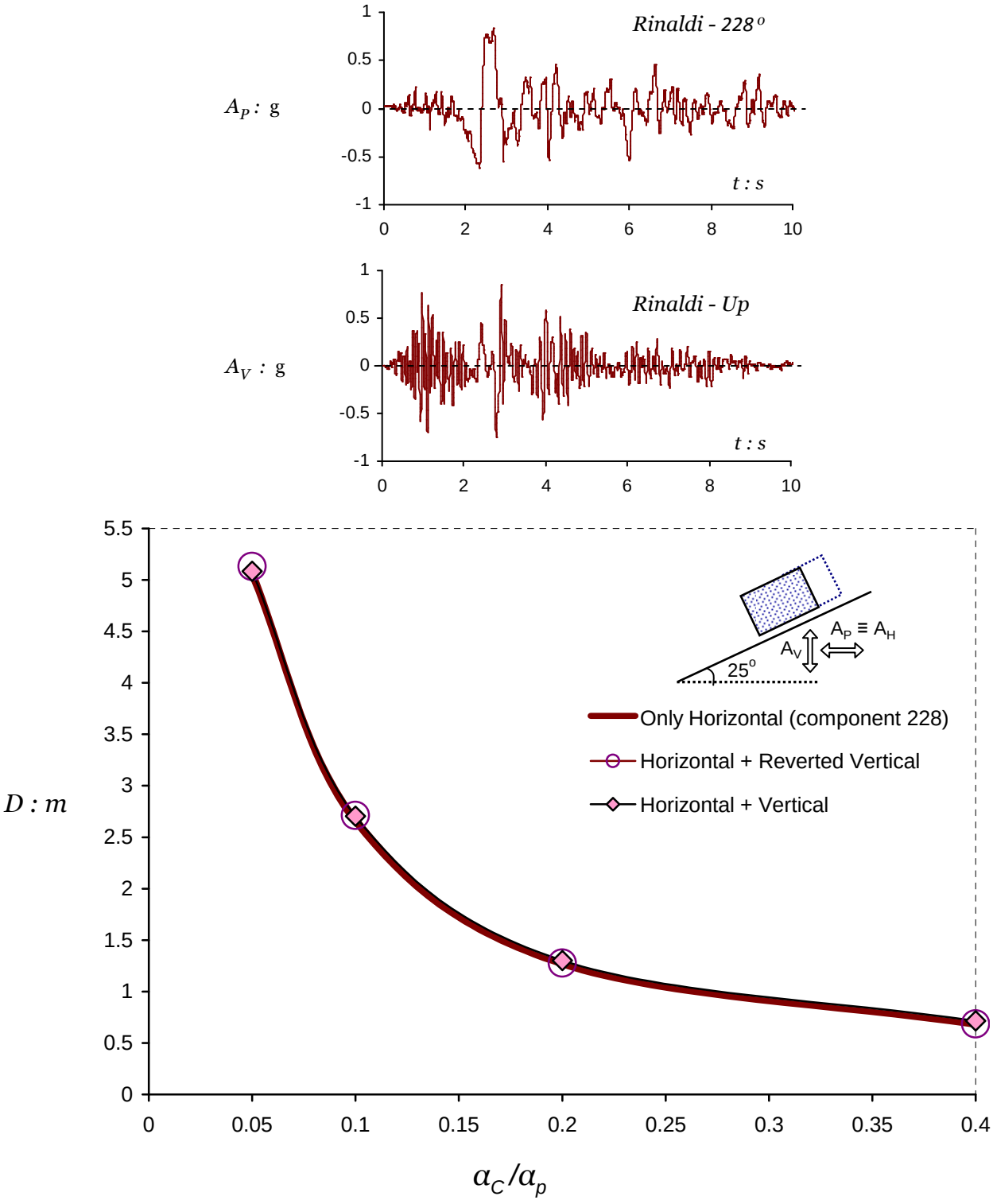

Figure 4.85 *Influence of vertical acceleration on sliding displacement for the Northridge record of Rinaldi. The horizontal component is imposed reversed, because in the reversed polarity the greater slippage is induced. Both polarities of the vertical acceleration is examined.*

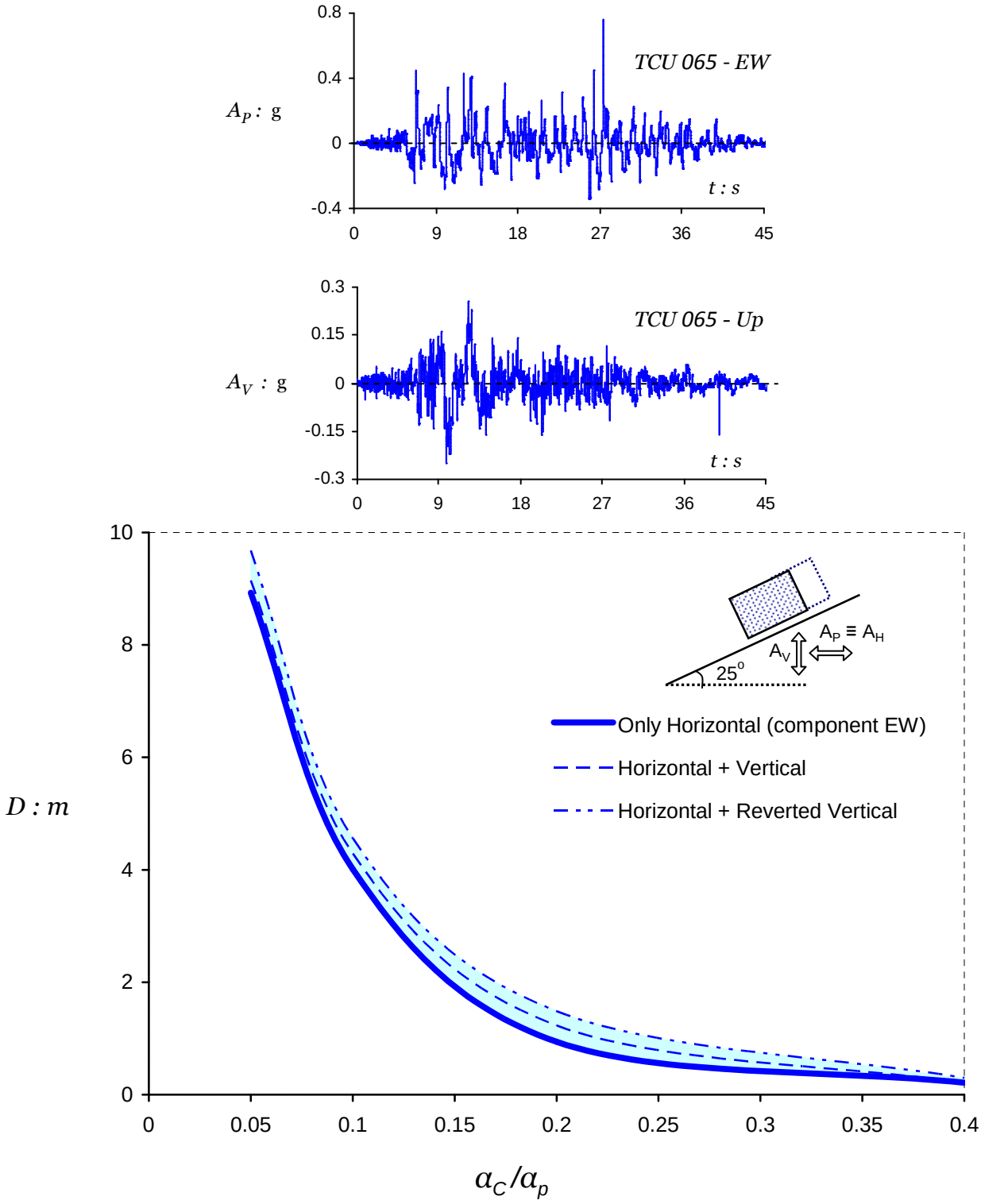

Figure 4.86 *Influence of vertical acceleration on sliding displacement for the Chi-chi record of TCU 065. The horizontal component is imposed as is, because in this polarity slippage is greater. Both polarities of the vertical acceleration is examined.*

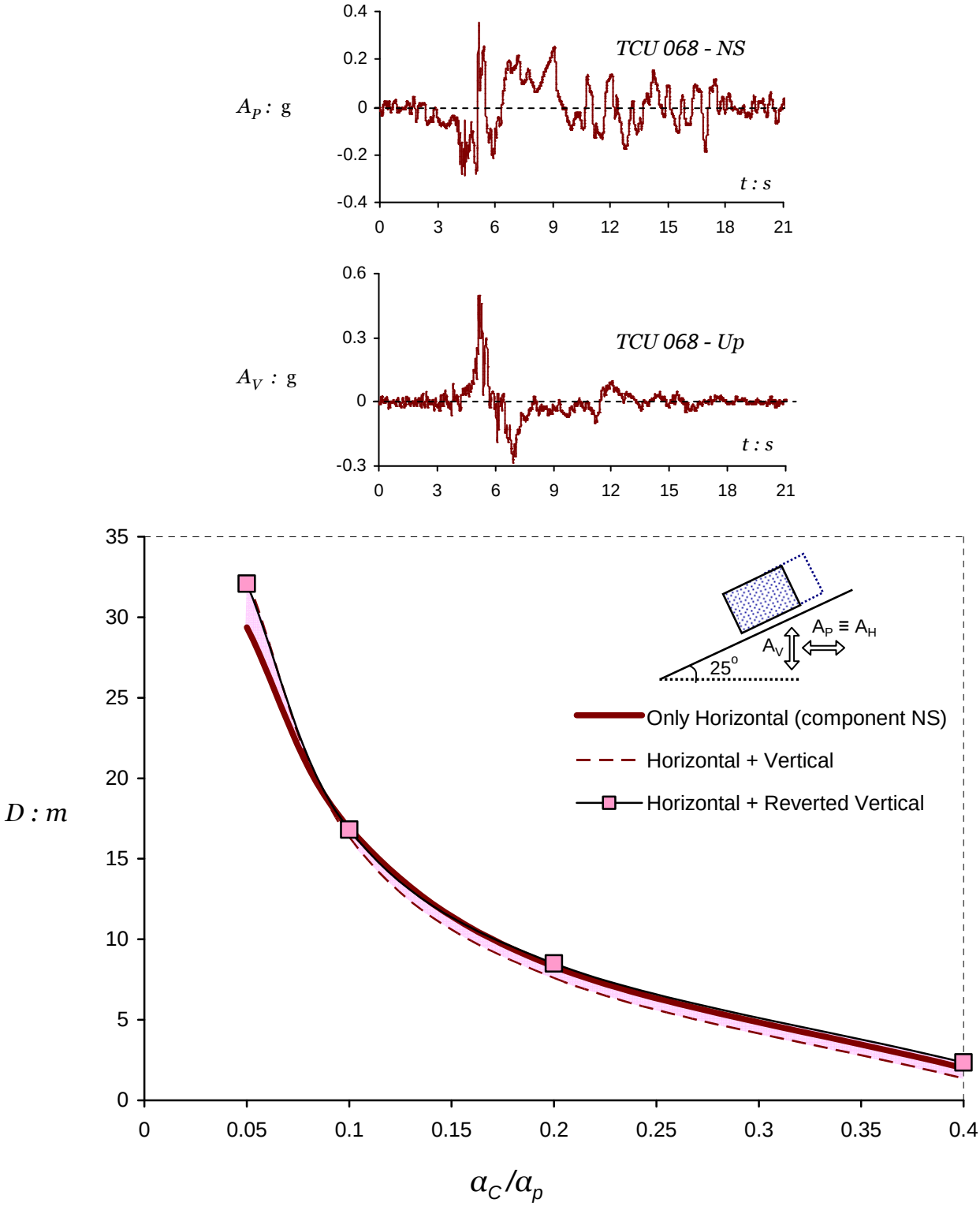

Figure 4.87 *Influence of vertical acceleration on sliding displacement for the Chi-chi record of TCU 068. The horizontal component is imposed reversed, because in the reversed polarity the greater slippage is induced. Both polarities of the vertical acceleration is examined.*

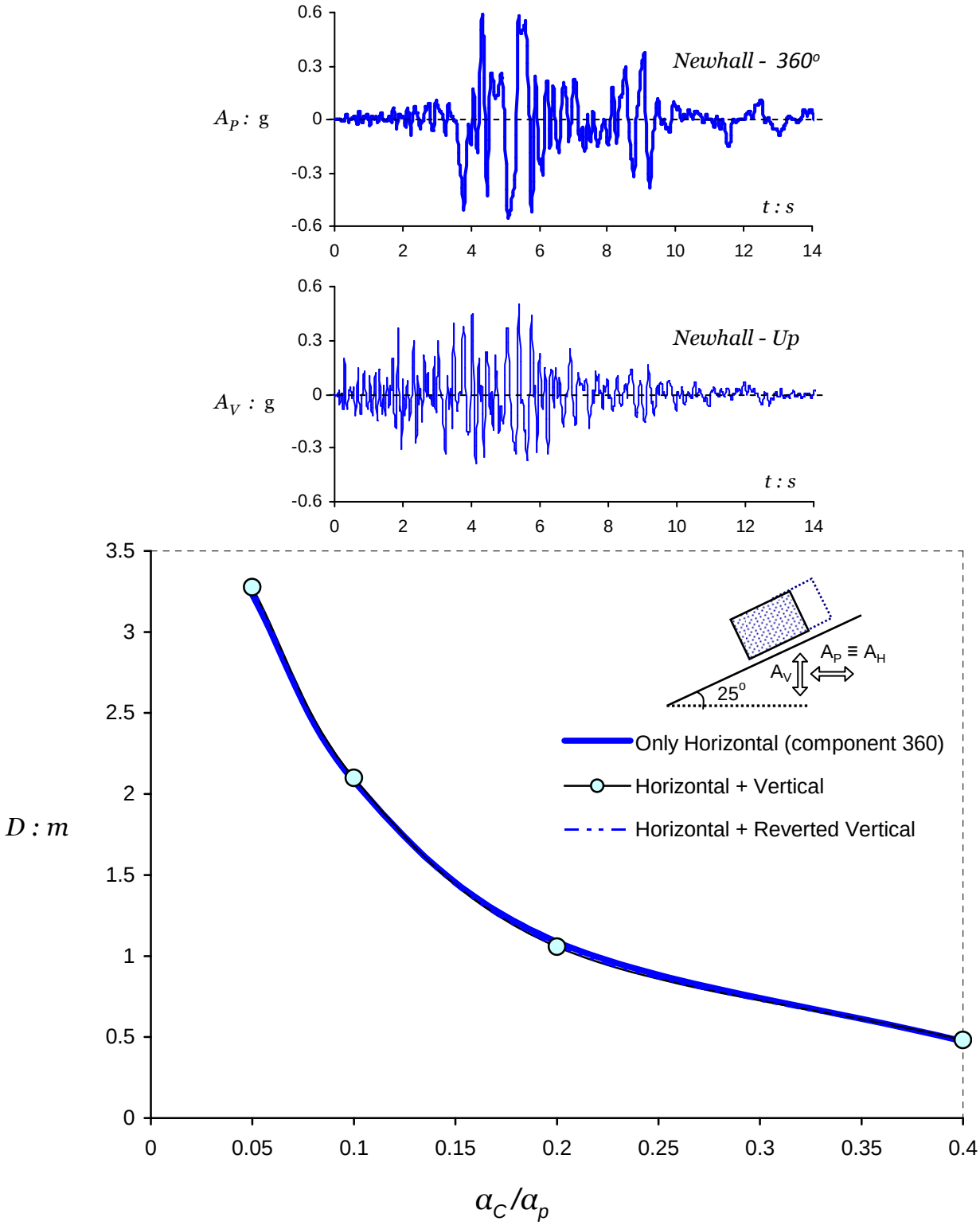

Figure 4.88 *Influence of vertical acceleration on sliding displacement for the Northridge record of Newhall Fire station 360°. The horizontal component is imposed as is, because in this polarity slippage is greater. Both polarities of the vertical acceleration is examined.*

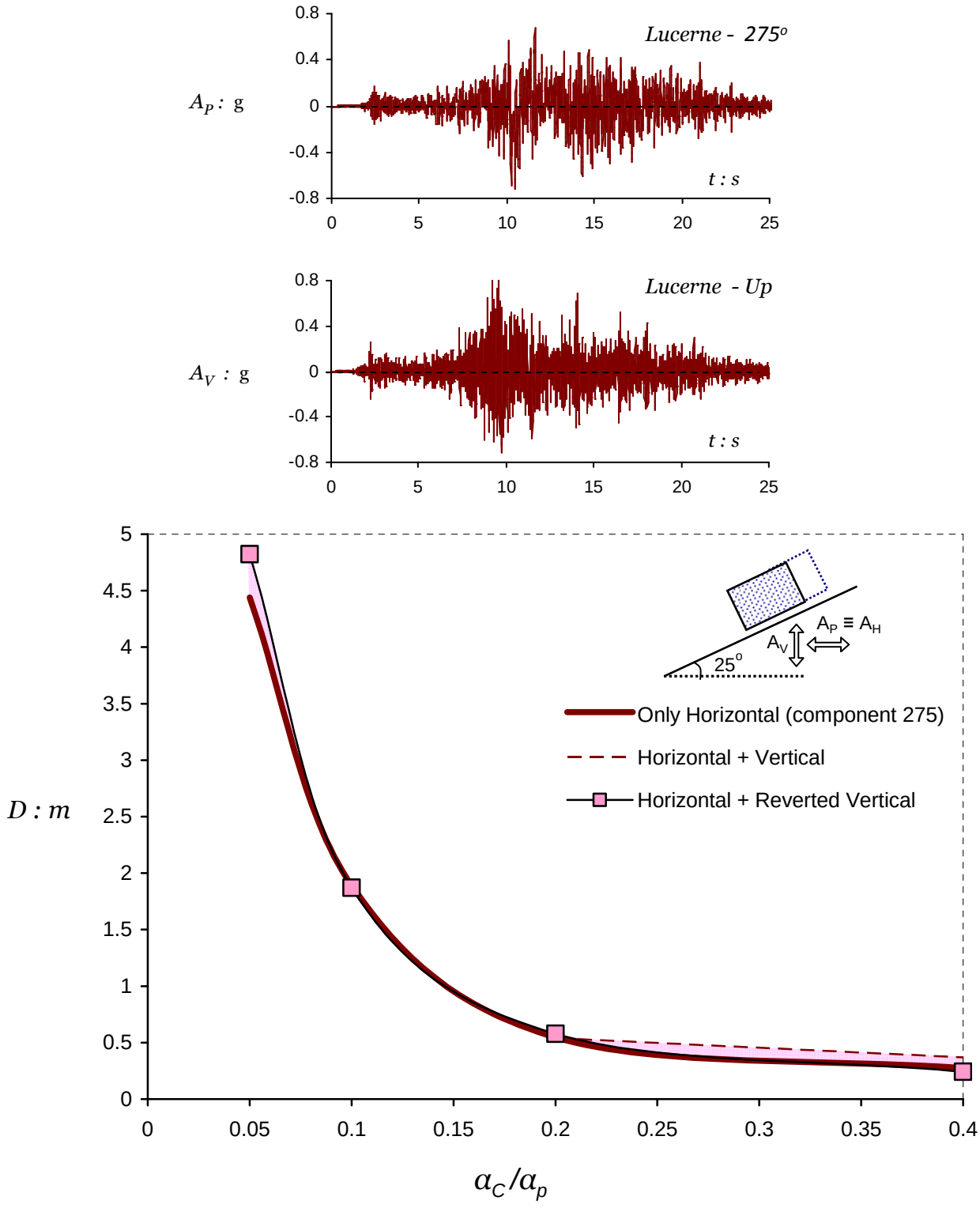

Figure 4.89 *Influence of vertical acceleration on sliding displacement for the Landers record of Lucerne 275°. The horizontal component is imposed as is, because in this polarity the greater slippage is induced. Both polarities of the vertical acceleration is examined.*

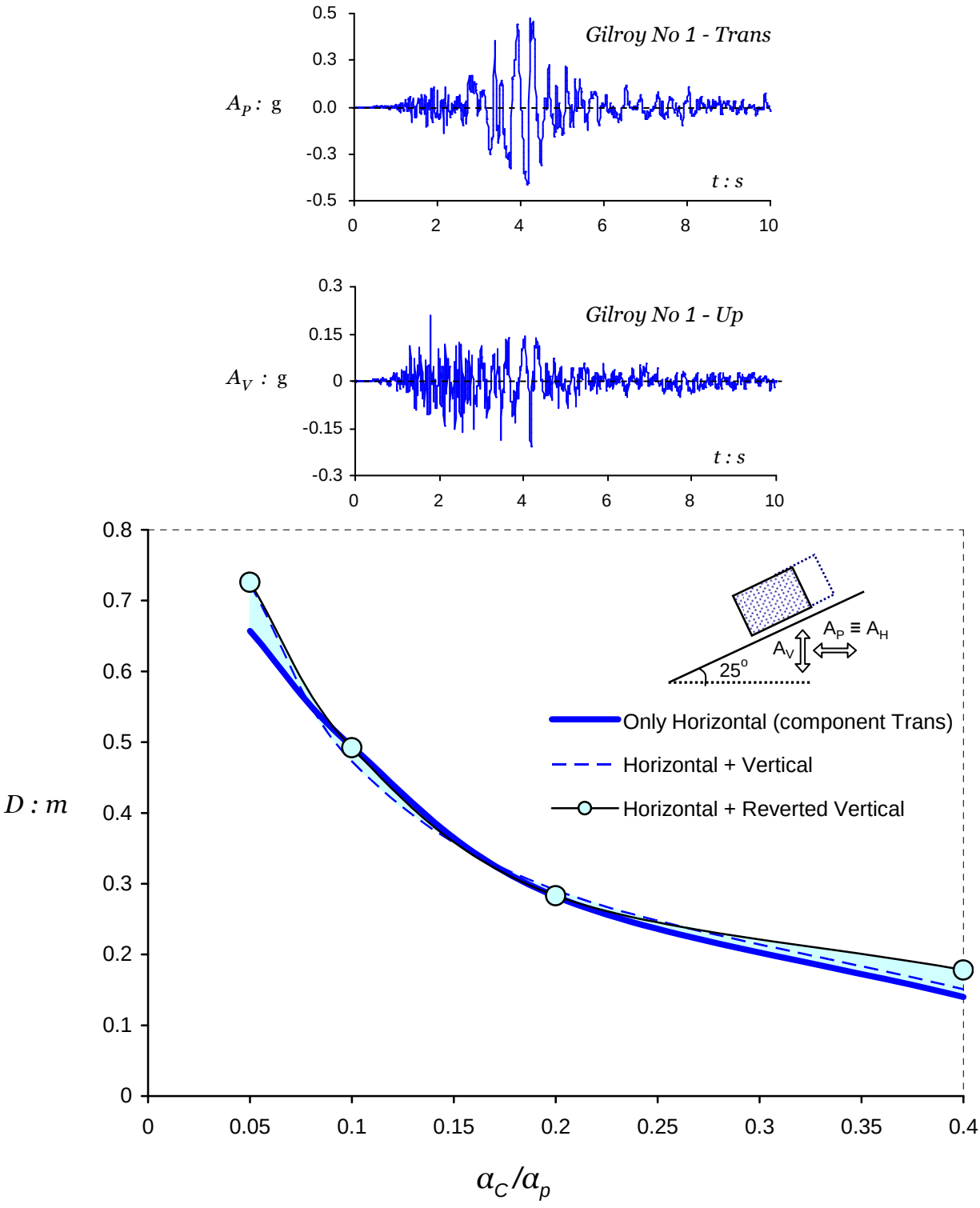

Figure 4.90 *Influence of vertical acceleration on sliding displacement for the Loma Prieta record of Gilroy Array No1. The horizontal component is imposed as is, because in this polarity slippage is greater. Both polarities of the vertical acceleration is examined.*

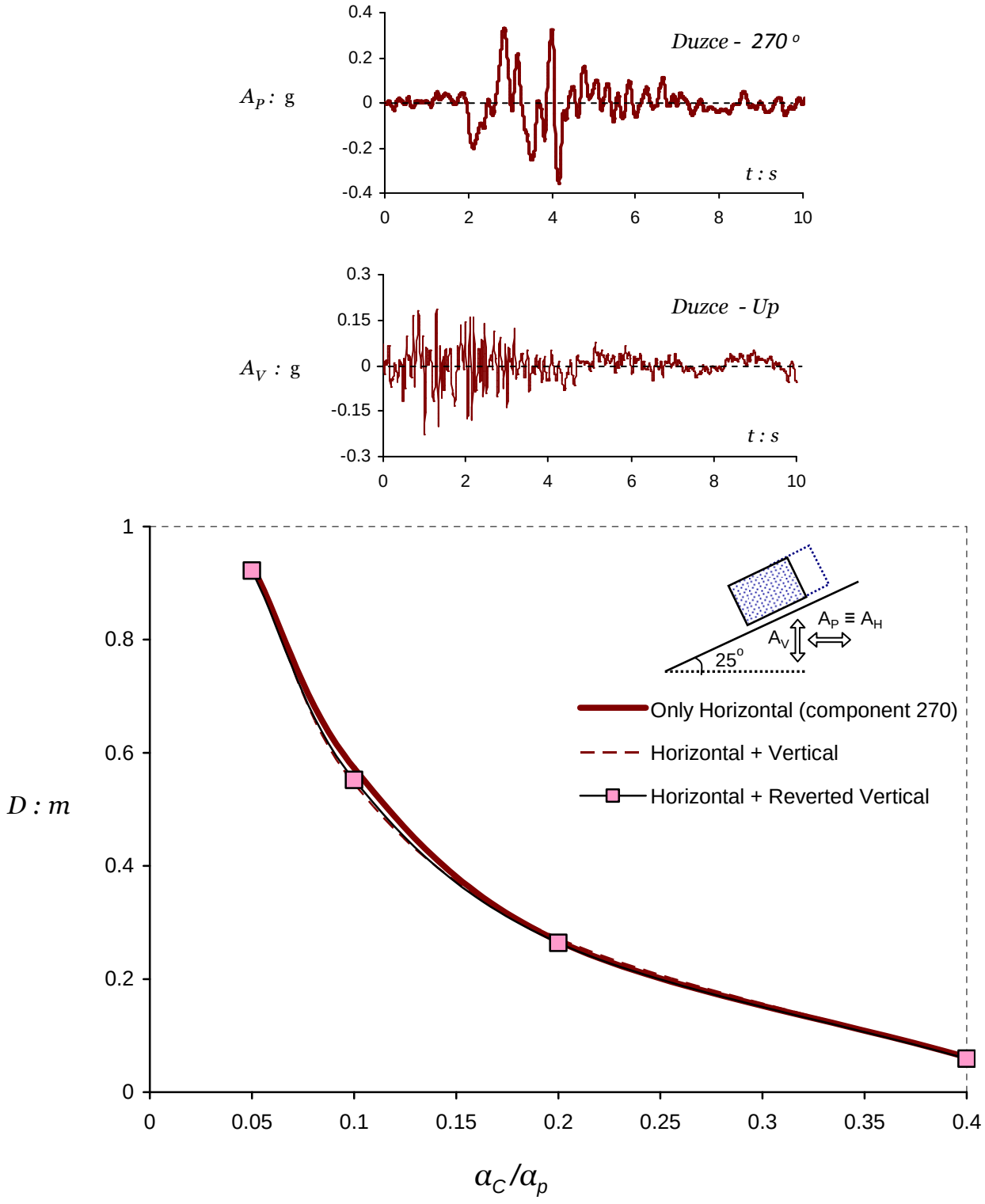

Figure 4.91 *Influence of vertical acceleration on sliding displacement for the Kocaeli record of Duzce 270. The horizontal component is imposed as is, because in this polarity the greater slippage is induced. Both polarities of the vertical acceleration is examined.*

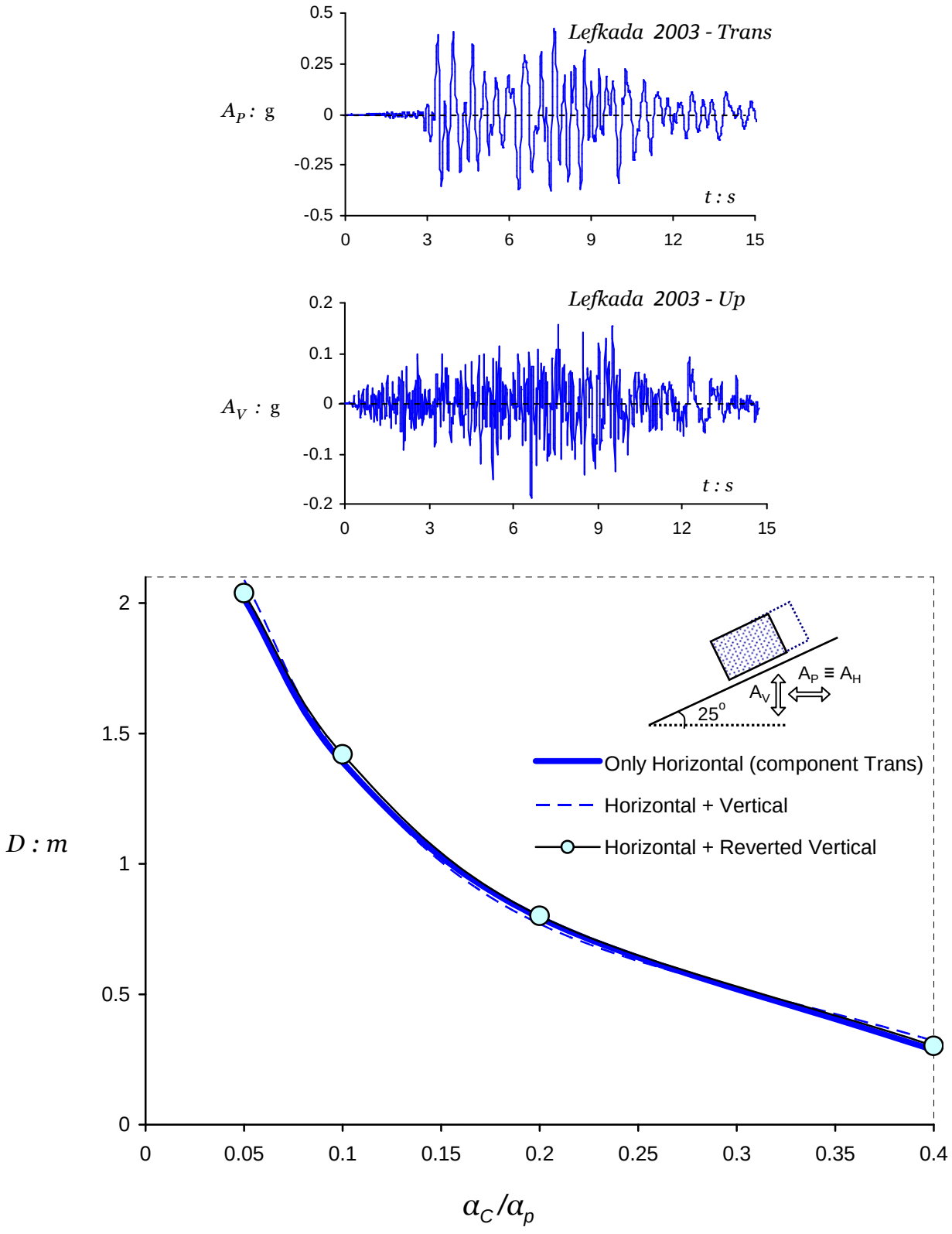

Figure 4.92 *Influence of vertical acceleration on sliding displacement for the Lefkada record of 2003. The horizontal component is imposed as is, because in this polarity slippage is greater. Both polarities of the vertical acceleration is examined.*

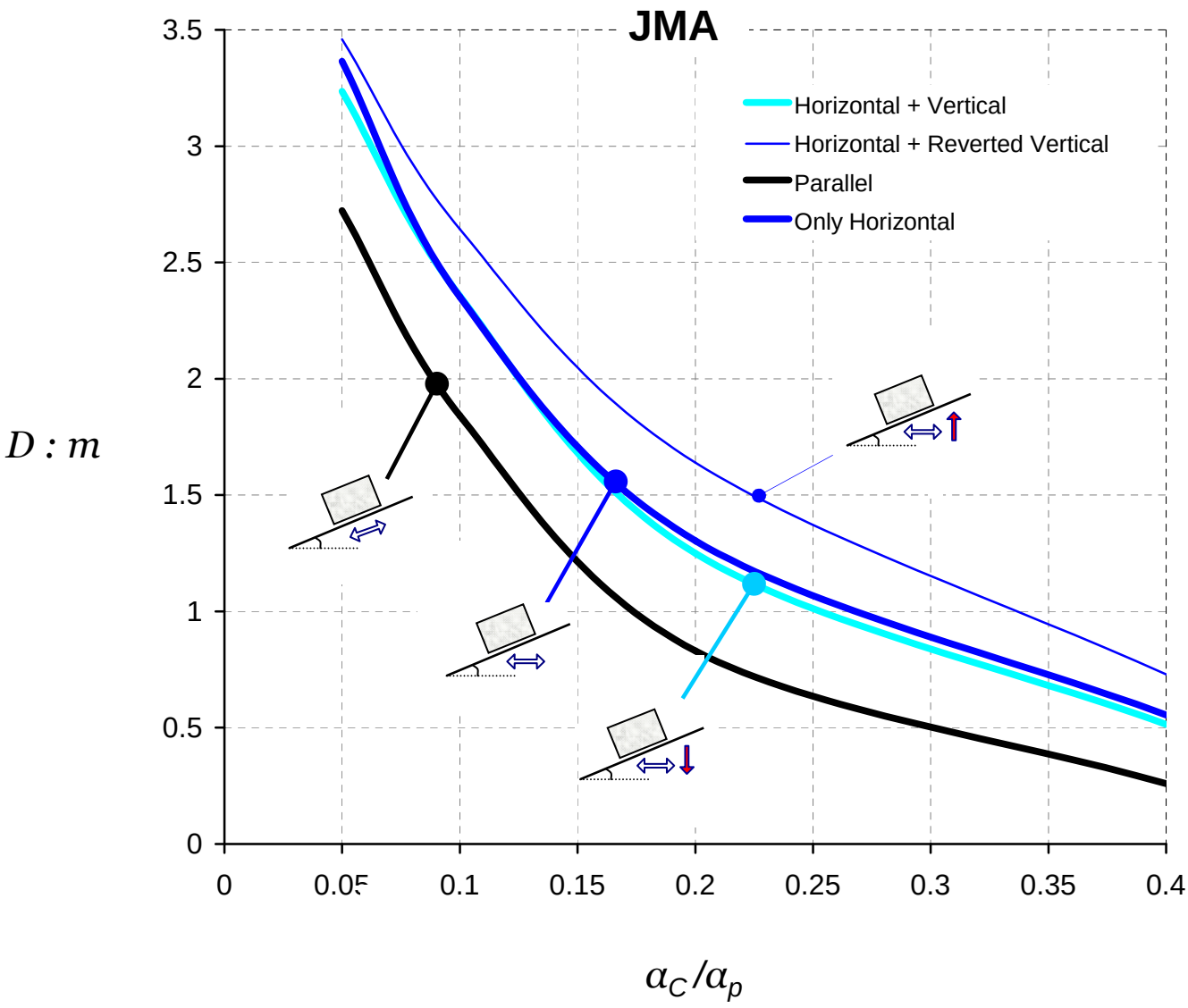

Figure 4.93 *Effect of the JMA record vertical acceleration on sliding displacement as a function of yielding acceleration ratio a_C/a_P. The vertical acceleration is acting simultaneously with the horizontal. Both polarities of the vertical component are examined, whereas the horizontal is imposed with only one polarity: the most detrimental.*

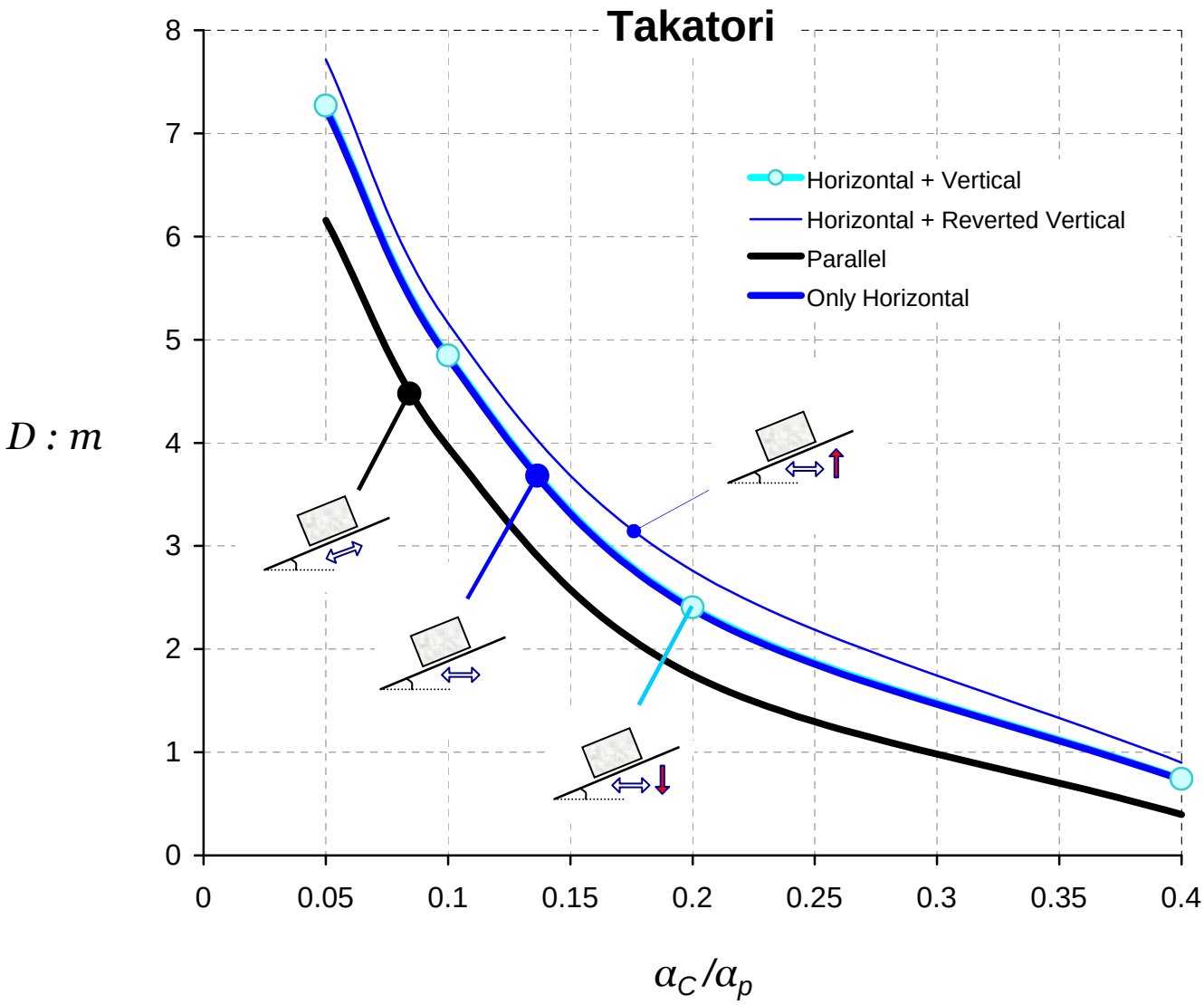

Figure 4.94 *Effect of the Takatori record vertical acceleration on sliding displacement as a function of yielding acceleration ratio a_C/a_P. The vertical acceleration is acting simultaneously with the horizontal. Both polarities of the vertical component are examined, whereas the horizontal is imposed with only one polarity: the most detrimental.*

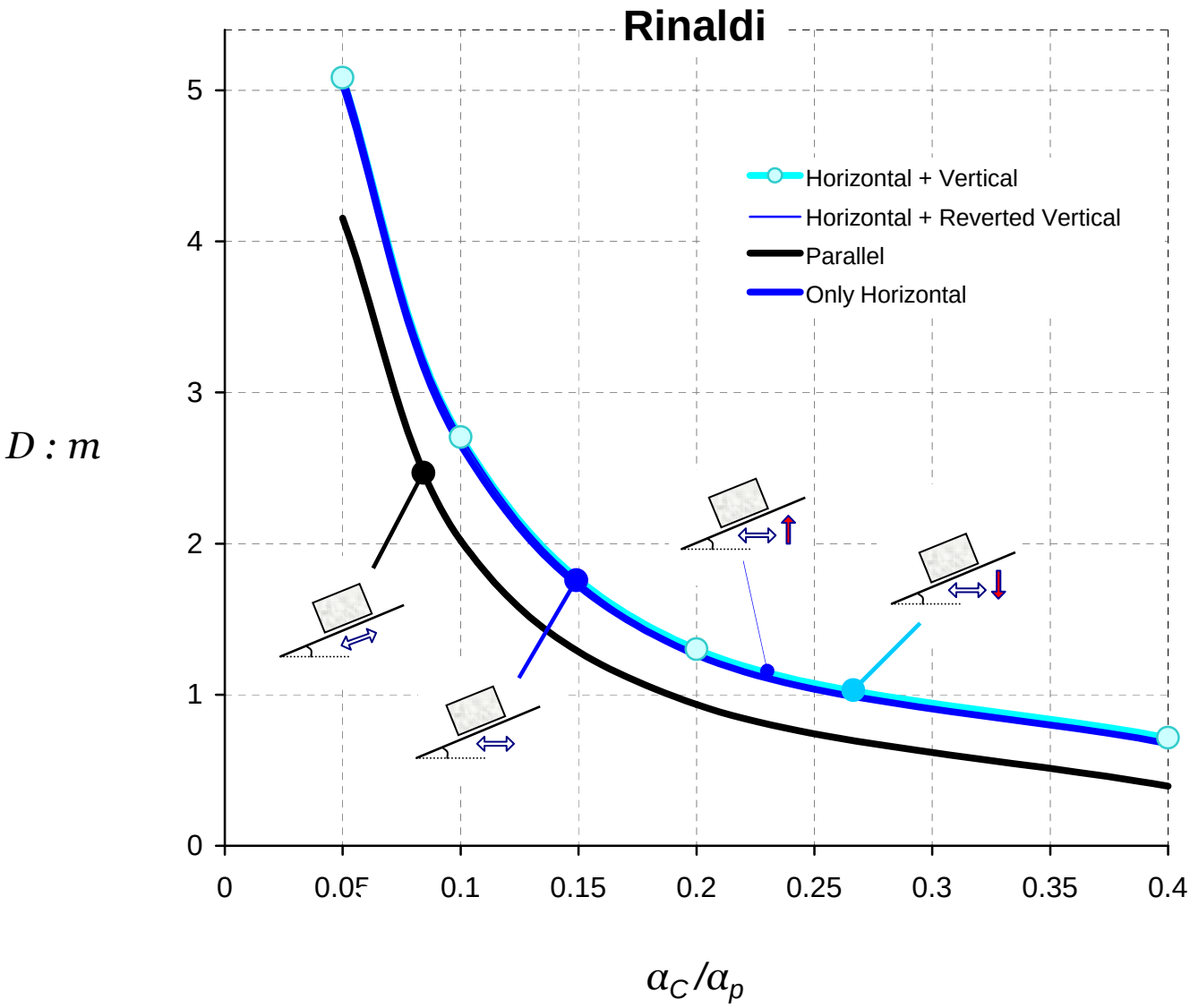

Figure 4.95 *Effect of the Rinaldi record vertical acceleration on sliding displacement as a function of yielding acceleration ratio a_C/a_P. The vertical acceleration is acting simultaneously with the horizontal. Both polarities of the vertical component are examined, whereas the horizontal is imposed with only one polarity: the most detrimental.*

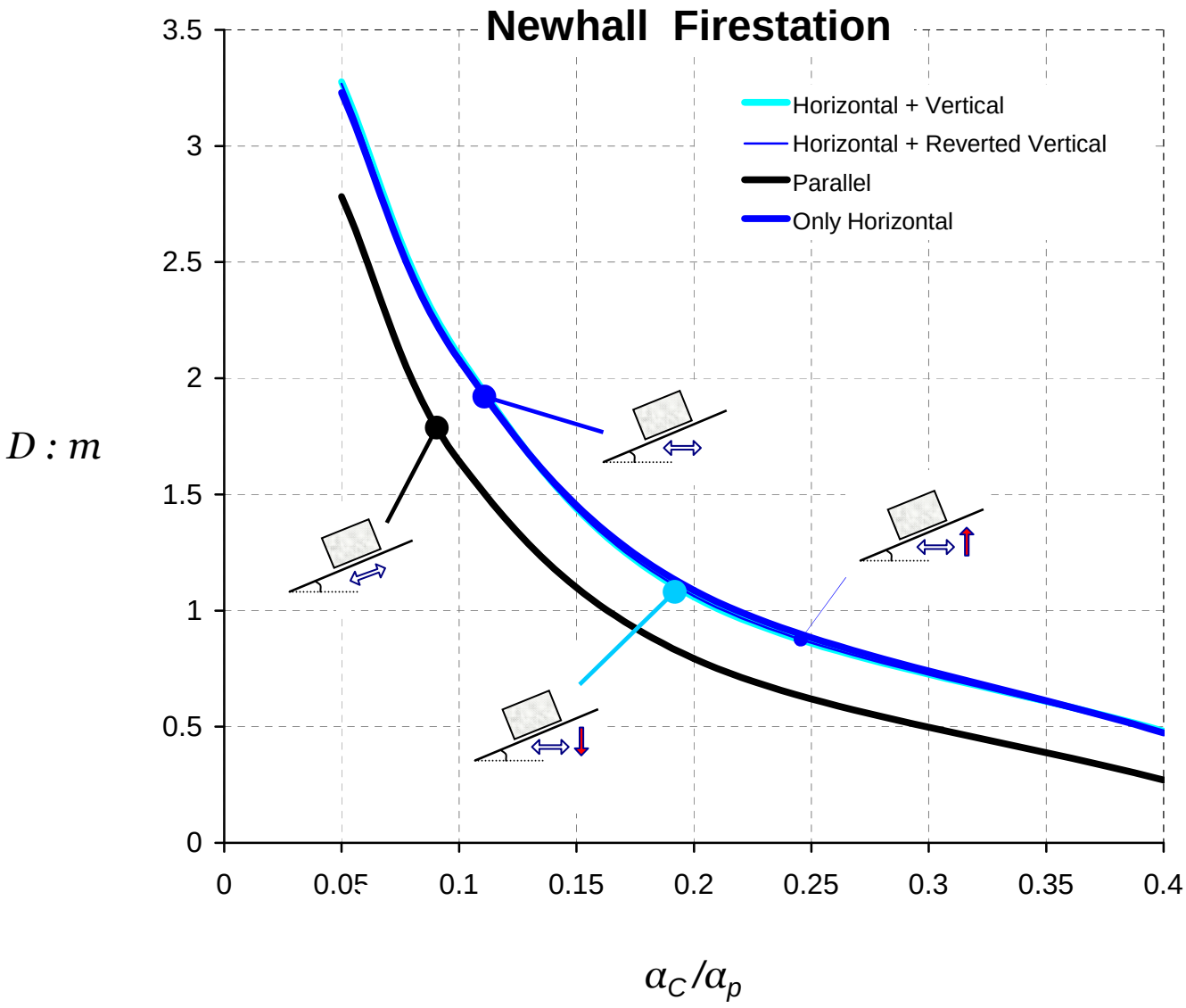

Figure 4.96 *Effect of the Newhall Fire Station record vertical acceleration on sliding displacement as a function of yielding acceleration ratio a_C/a_P. The vertical acceleration is acting simultaneously with the horizontal. Both polarities of the vertical component are examined, whereas the horizontal is imposed with only one polarity: the most detrimental.*

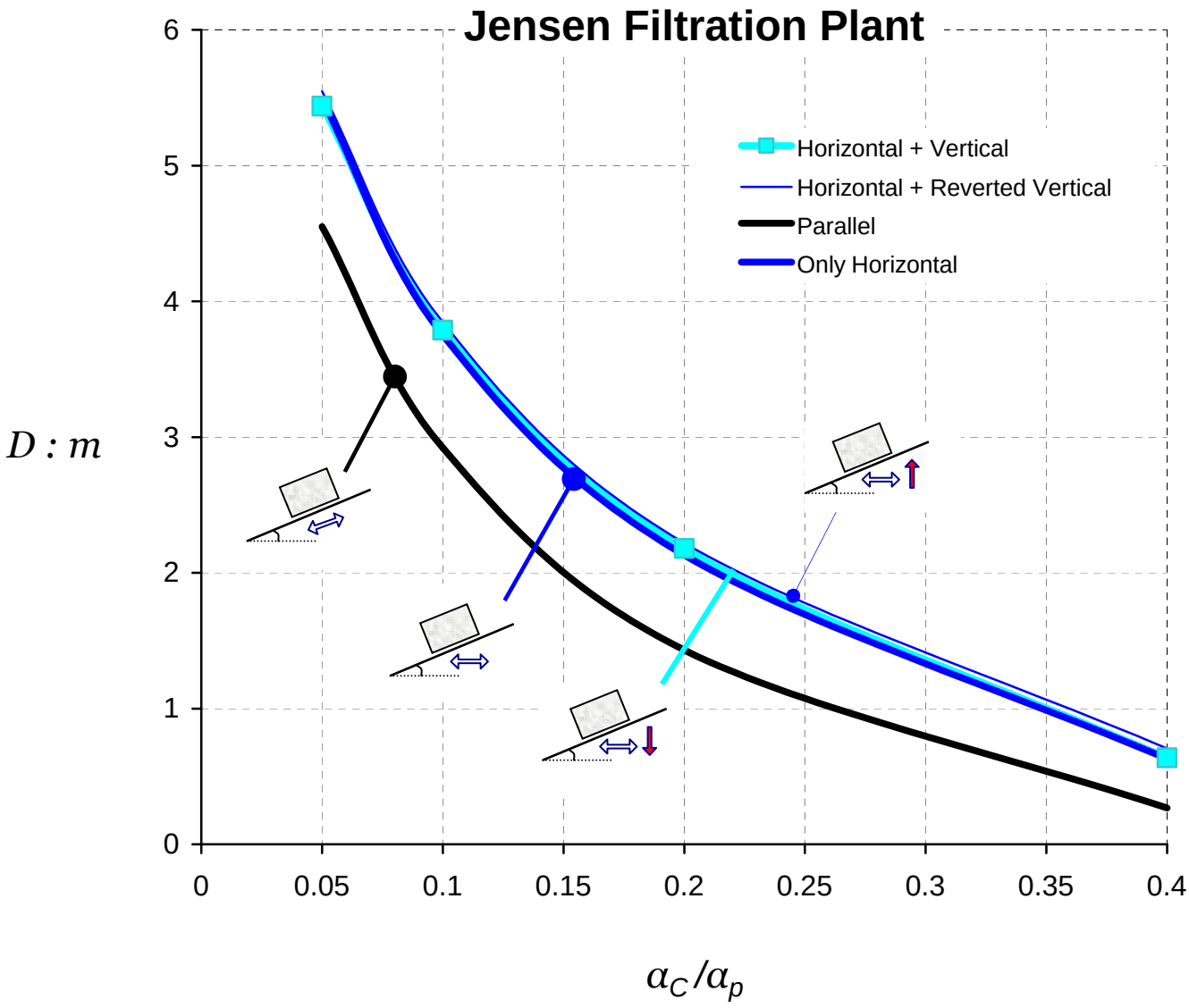

Figure 4.97 *Effect of the Jensen Filtration Plant record vertical acceleration on sliding displacement as a function of yielding acceleration ratio a_C/a_P. The vertical acceleration is acting simultaneously with the horizontal. Both polarities of the vertical component are examined, whereas the horizontal is imposed with only one polarity: the most detrimental.*

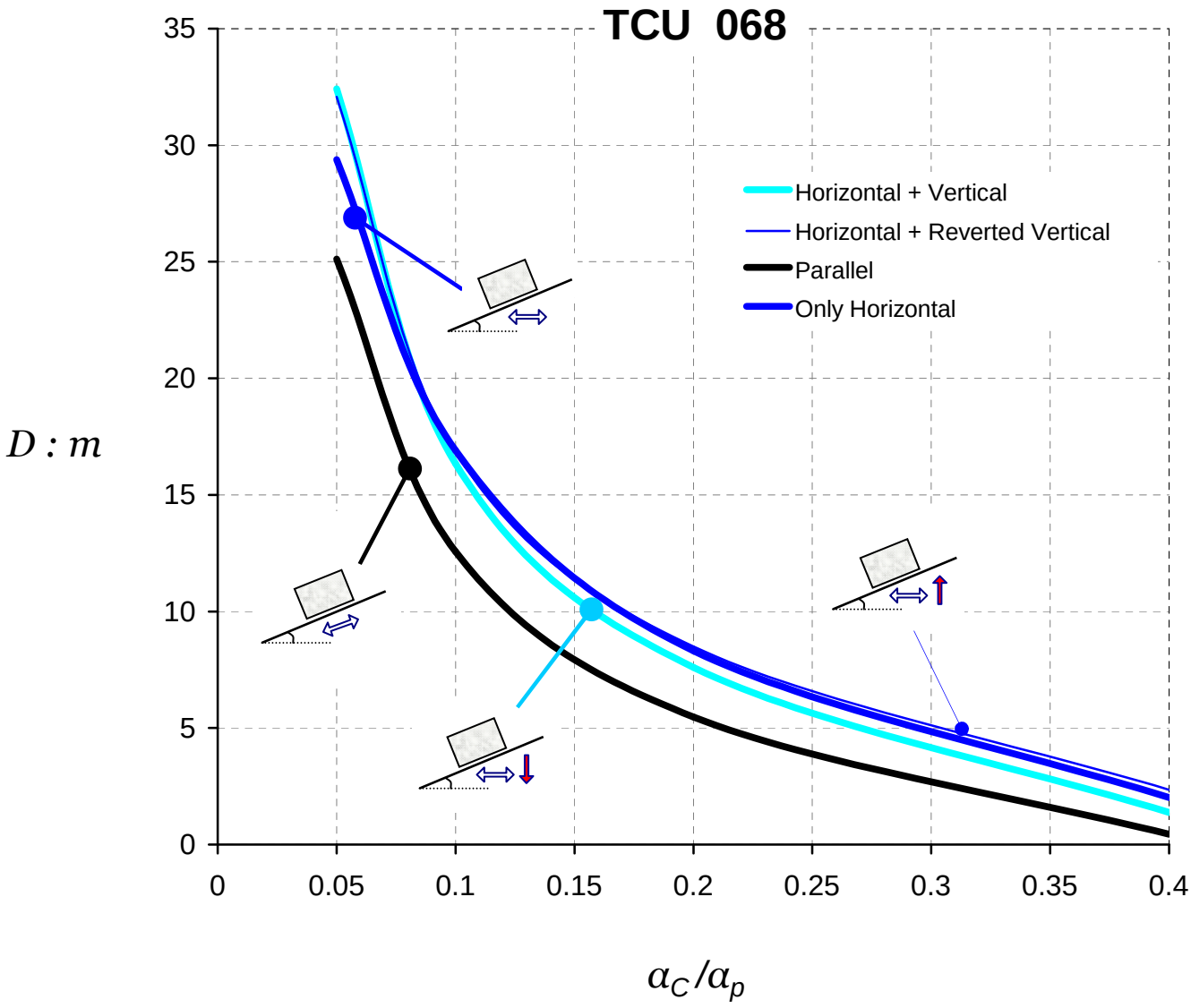

Figure 4.98 *Effect of the TCU–068 record vertical acceleration on sliding displacement as a function of yielding acceleration ratio a_C/a_P. The vertical acceleration is acting simultaneously with the horizontal. Both polarities of the vertical component are examined, whereas the horizontal is imposed with only one polarity: the most detrimental.*

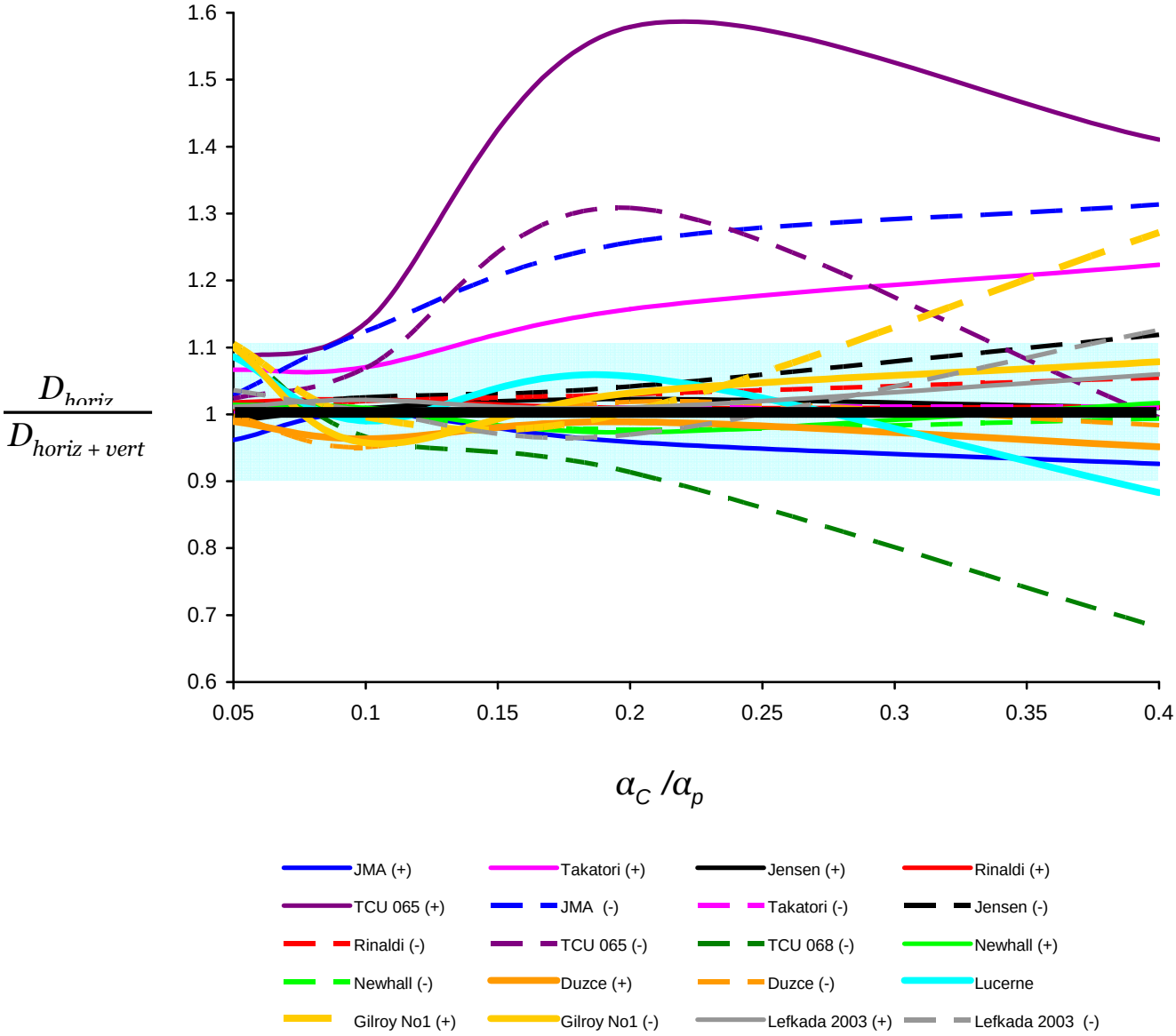

Figure 4.99 *Summary illustration of the influence of vertical acceleration on asymmetric sliding. Depicted are the ratio of slippage induced only by the horizontal component of each acceleration recording station, D_{horiz} , over the slippage triggered by simultaneously acted horizontal and vertical components, $D_{horiz+vert}$, as a function of critical acceleration ratio a_C/a_H. Observe that most curves are enclosed between 0.9 and 1.1 limit values (shaded area) . Therefore, the effect of vertical acceleration even for such detrimental ground motions could be neglected.*

$$\frac{|D_{horiz} - D_{horiz+vert}|}{D_{horiz+vert}} \%$$

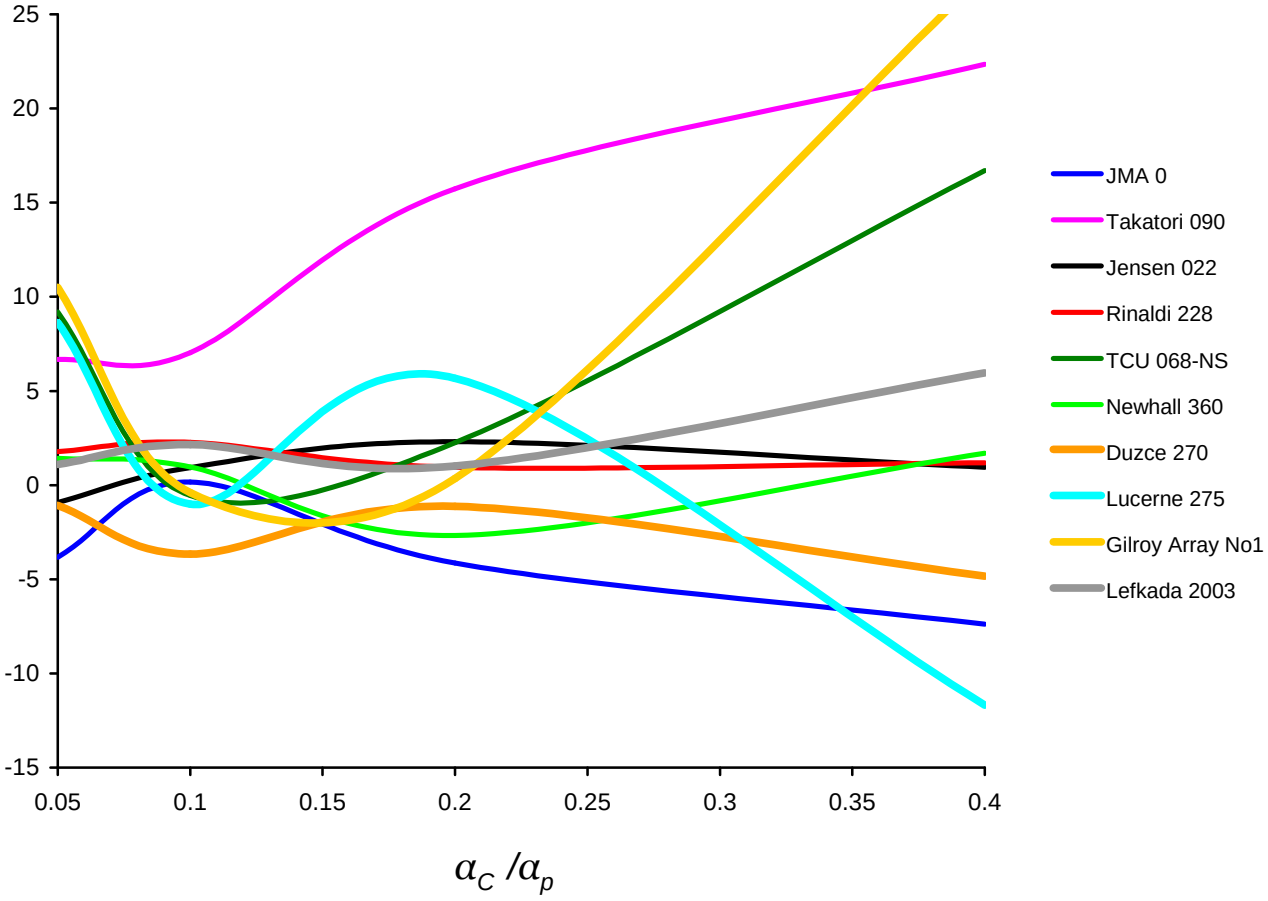

Figure 4.100 *Significance of vertical excitation on sliding as a percentage of the difference in response of the horizontal component induced slippage minus the sliding triggered from both vertical and horizontal components, $D_{horiz} - D_{horiz+vert}$, over $D_{horiz+vert}$ as a function of critical acceleration ratio a_C/a_H. The "error" of ignoring the action of vertical acceleration is for all the studied ground motions lower than 20%.*

Chapter 5

Models of Frictional Behaviour

5.1 Friction in Tribology

When two solids approach each other and come close they will mutually exert short-range forces, which can be modelled by surface tractions on their idealized bounding surfaces. The tangential components of these surface tractions are named frictional forces which obey particular laws: the phenomenological models. A phenomenological model gives a prescription of frictional forces based on known macroscopic, readily observable, quantities: the state variables; and their history if there are memory effects too.

Study of friction phenomena has resulted in a science branch, named Tribology. The phenomenological modelling of frictional interfaces started with Amontons (1699) and Coulomb (1785), who formulated laws for contact friction. Just for encyclopaedic information, in 1699 Guillaume Amontons published his rediscovery of the laws of friction, first put forward by Leonardo da Vinci. Though they were received with some scepticism, the laws were verified by Charles-Augustin de Coulomb in 1781. Both stated that sliding friction force is proportional to the normal force at the sliding surfaces, independent of the sliding speed and the apparent area of contact. These laws are still widely used in modelling and calculating problems with friction, not so much because

these laws are accurate, but more because friction depends on a range of mostly unknown circumstances and we have nothing better at our disposal in most cases.

Eventually, a more scientific approach to the friction phenomena was initiated, with interplay between mechanical, physical, chemical, and metallurgical theory and advanced experimental techniques. It appeared that friction depends on a wide class of circumstances which are not always known or can be controlled, and has some stochastic character. Some important textbooks on the subject are: Bowden & Tabor, 1954, 1964; Rabinowicz, 1951, 1965; Kragelskii, 1965. A good review article is from Tabor, 1981.

In the language of Tribology, contacts between solids are divided in con-formal contacts, where the apparent contact takes place over an extended surface, and counter-formal contacts, which can be divided in line contacts and point contacts. Furthermore, the kind of lubrication between the contacts gives the distinction between dry friction that is pure contact friction, boundary lubrication, full-film lubrication, and mixed lubrication. All combinations of these classifications (amplified by the multitude of possible material combinations) can give their own peculiarities, so it seems that the hope for one simple friction law is idle.

The purpose of this chapter is to show how different phenomenological models that have been proposed for friction can be incorporated into the case of a rigid block sliding on top of an inclined plane, with some reference to the relative intrinsic merits of each model. Bearing in mind the certain degree of arbitrariness in the proposed over the years friction models, we pay attention to desirable properties of models from a computational point of view. The study will be restricted to phenomenological models, applied to systems consisting of rigid bodies, with conformal contacts and dry friction.

5.2 The perfectly plastic Coulomb sliding

The simplest form of a law of friction is the classical Amontons-Coulomb law in which the static and kinetic coefficients of friction are the same. Due to the difficulties associated with the analysis of dry friction systems, most studies have used very simple models to describe it. The simplest and by far the most popular friction model states that during slipping, the friction force is constant in magnitude and acts to oppose the relative sliding motion. For a two-dimensional contact with normal force $F_N < 0$ *(positive if it is a traction force and negative if it is a compressive force) and relative sliding velocity V, this law reads:*

$$\begin{aligned} \mathrm{T} &= -\mu \cdot F_N && \text{for} \quad V > 0 \\ \mu \cdot F_N \le \mathrm{T} &\le -\mu \cdot F_N && \text{for} \quad V = 0 \\ \mathrm{T} &= \mu \cdot F_N && \text{for} \quad V < 0 \end{aligned} \qquad (5.1)$$

A simplification of Coulomb friction is that the friction coefficient is of constant magnitude. In reality, dry friction is inherently nonlinear. Also, dry friction systems are prone to sticking, hence can exhibit dramatically different dynamic behaviour depending on whether a particular friction interface is slipping or sticking.

5.3 Elastoplastic dry friction

The Coulomb assumptions are known to be idealisation of the actual frictional resistance. The friction coefficient is known to depend on numerous system and environmental factors. Furthermore, the normal force across the sliding interface generally depends on the sliding motion itself.

One of the early investigations of non-constant normal forces in a vibration isolation system is by Mercer and Rees (1971), who presented the concept of a "friction mount" where the normal force is varied hydraulically depending on the relative displacement. Later, Tadjbakhsh and Lin (1987) considered the performance of a seismic isolation device in which the normal force varied as a function of the relative displacement and relative velocity between the structure and the foundation.

To illustrate the viscous-like damping attribute of frictional surface with displacement-dependent normal forces, a single-degree-of-freedom (SDOF) oscillator sliding on an inclined plane has been employed as a model. This type of system was studied in detail by Anderson and Ferri (1990). Similar systems were considered by Beucke and Kelly (1985) and by Makris and Constantinou (1991). In these studies, the normal force grows linearly with displacement magnitude; the resistive forces generated by such an arrangement have been termed linear-Coulomb damping or linear-friction damping by some authors.

With an elasto-plastic dry friction system consisting of a rigid block resting on an inclined plane [Figure 5.1(c)] we are dealing in the section 5.5. A series of parametric analyses is performed and results will be presented.

5.4 Exponential law of dry friction

An extension to the classical Coulomb friction model is to make the coefficient, μ, a function of sliding velocity: μ either decreases or increases rapidly with increasing sliding velocity. The dependence on velocity appears to be continuous, but in practical cases, the decrease in friction with increasing speeds may be so steep that the curve is frequently modelled as a discontinuous fall at zero velocity, that is, a distinction between static and kinetic friction at vanishing speeds. This sudden fall has the theoretical and

computational disadvantage that the solution of the equations of motion does not depend in a continuous way on parameters and initial values.

A further extension is that the coefficient of friction, μ, depends on the normal load, which dependence is often weak for hard materials, but may be appreciable for soft material like rubbers and polymers, and also in the cases in which the coefficient of friction depends on the velocity. A decrease in the coefficient of friction with normal stress is observed with granular soils which under small confining stress exhibit much higher angles of internal friction ($\varphi = \arctan\mu$) than at large confinement. This property is of great significance in earth rock-fill dams, as well as in small scale physical model tests in the laboratory.

One of the important characteristics of dry friction (which is not present in other linear or nonlinear mechanical systems) is that of sticking. In the case of free vibration, a response trajectory can terminate in a condition where it is permanently stuck away from the origin of the phase plane. In essence, there is a zone of equilibria rather than an isolated equilibrium at the origin of the state space.

5.5 Parametric analyses for elastoplastic and exponential friction

Figure 5.1 illustrates the various constitutive friction laws examined in this dissertation to describe the contact behaviour of the base-block interface. The simplest form of friction obeys the perfectly plastic Coulomb law, as pictured in Figure 5.1 (b). In the basic form of the Coulomb friction model, two contacting surfaces can carry shear stresses up to a certain magnitude across their interface before they start sliding relative to one another. The friction coefficient can depend on slip rate, contact pressure, temperature, and field variables; that can be manually determined in the GAPUNI element properties on ABAQUS.

Alternatively, the frictional relationship shown in this Figure 5.1 (c) is analogous to elastic-plastic material behaviour without hardening: "dy" corresponds to the yielding elastic displacement limit. Sticking friction corresponds to the elastic regime, and slipping friction corresponds to the plastic regime. The elastic pre-yielding displacement, dy, is taken equal to: dy = 0.01, 0.05, and 0.1 m.

As often experimental data show that friction coefficient that opposes the initiation of sliding from a sticking condition is different from the friction coefficient that opposes established slipping. In the default ABAQUS model the static friction coefficient corresponds to the value given at zero slip rate, and the kinetic friction coefficient corresponds to the value given at the highest slip rate. The transition between static and kinetic friction is defined by the values given at intermediate slip rates. ABAQUS provides a model to specify a static and a kinetic friction coefficient directly. In this model it is assumed that the friction coefficient decays exponentially from the static value to the kinetic value according to the formula:

$$\mu = \mu_{\kappa} + (\mu_s - \mu_{\kappa})\exp(-d_e \dot{\gamma}_{eq}) \qquad (5.2)$$

where μ_{κ} and μ_s are the kinetic and static friction coefficients respectively, d_e is a decay coefficient, and $\dot{\gamma}_{eq}$ is the slip rate. Typically, the static friction coefficient is higher than the kinetic friction coefficient, as sketched in Figure 5.1 (d1). However, the case where the static friction is lower than the kinetic is also studied [Figure 5.1 (d2)]. The particular μ_s and μ_{κ} values utilised in our study will be presented in detail in section 5.5.1.2.

Two types of idealized motions ("wavelets") and three near-fault accelerograms are used as input motions at the inclined base of the sliding system. The idealised motions are the one-cycle sinusoidal pulse and the Ricker wavelet: the former models a typical

fling affected motion, and the latter a directivity affected motion (Figure 5.3). Four characteristic frequencies are utilized for each of these motions as follows:

- *Richer:* f_o *= 0.35, 0.75, 1.5, and 3.5 [Hz]*
- *Sinusoidal:* f_o *= 0.57, 1.25 [Hz]*

These frequencies were selected so that the response spectra of corresponding pairs of these motions are quite similar, resulting in almost the same maximum spectral acceleration at about the same dominant period. As an example, Figure 5.4 illustrates the response spectra of two of the pairs. The selected near-fault records bear forward-directivity and fling effect characteristics. The utilised actual accelerograms namely are: the Rinaldi 228°, the Lucerne 275°, and the TCU 068-NS records. Figure 5.2 portrays all the excitations employed herein.

Finally, we note that the parametric analyses include different values of the critical acceleration ratio: a_C/a_H *= 0.05, 0.1, 0.2, and 0.4.*

5.5.1 Sliding response from idealized wavelets

In the following two sections, the elastoplastic and exponential yielding response will be presented and discussed in terms of acceleration, velocity, and displacement time histories. Again, the sliding system consists of a rigid block resting on a sloping base.

5.5.1.1 Elastoplastic friction response

All the findings of the previous chapters were based on the (extreme) assumption of a perfectly-rigid-plastic interface. Since in most realistic systems some pre-sliding elasticity is unavoidable, the influence of elastic pre-yielding on the response of a mass resting on an inclined plane is investigated herein. The asymmetric sliding response is analysed and the effect of four particular parameters is explored: the critical acceleration ratio, a_C/a_H*, the excitation frequency,* f_o*, the changing polarity of excitation,*

and the magnitude of elastic pre-yielding displacement, dy. The results from the performed parametric analyses are illustrated in Figures 5.5÷5.24. No attempt is made here for a complete dimensional analysis.

At this point, it is important to clarify that the elastoplastic system can not resonate with the input excitations: the natural period of the system, T_n, is an order of magnitude greater than the ground motions predominant period. The mass element in the performed ABAQUS analyses is equal with 1 Mgr. Thus, for each value of dy:

$$k = \frac{T}{dy} = \frac{1}{0.01} = 100\,kN/m \quad \Rightarrow T_n = 2\pi\sqrt{\frac{m}{k}} = 19.86\,s \quad (for\ dy = 0.01m)$$

$$k = \frac{T}{dy} = \frac{1}{0.05} = 20\,kN/m \quad \Rightarrow T_n = 2\pi\sqrt{\frac{m}{k}} = 44.40\,s \quad (for\ dy = 0.05m)$$

$$k = \frac{T}{dy} = \frac{1}{0.1} = 10\,kN/m \quad \Rightarrow T_n = 2\pi\sqrt{\frac{m}{k}} = 62.85\,s \quad (for\ dy = 0.1m)$$

The above natural periods are purposely large, so the trends that have been emerged from the numerical analyses and will be discussed later on, are not affected by frequency content of excitation.

Asymmetric sliding in terms of acceleration, velocity, and displacement time-histories are depicted in Figures 5.5, 5.6, and 5.7, respectively, for a mass on a slope of $\beta = 25^o$. The system is subjected to a Ricker wavelet of peak acceleration 1 g and frequency 0.35 Hz (black solid line). The solid blue line portrays the time-histories corresponding to a rigid-plastic interface with critical ratio of $a_C/a_H = 0.1$. Notice that the mass is moving in unison with the base as long as the critical acceleration a_C is not exceeded. Whenever base acceleration exceeds the critical acceleration, the block slides either downward (usually) or upward (rarely, at about 6.5 s). As a result, a residual yielding displacement of 6.01 m occurs.

The solid pink line illustrates the elastic-plastic response of the same mass-base system. Here, the block can displace elastically up to 0.1 m before yielding. As a consequence, a phase difference between input excitation and induced mass response occurs. It is emphasized that pre-yielding displacement exists in both the upward and downward direction. The block does not rest after the last sliding period at the 11 sec, but continues uphill and downhill undamped elastic oscillations after the end of triggering.

The elastic displacement that precedes every sliding period is graphically marked in Figures 5.8 and 5.9. Notice in Figure 5.9 that the elastic deformation is illustrated with the yellow shadowed areas in the acceleration time histories. The influence of elasticity in sliding systems is not limited to displacements: the velocity of the block is affected as well. As it can be seen in Figure 5.10, when "dy" becomes larger, the velocity of the block which is induced at the elastic part of yielding is greater, leading to increased slippage. Therefore, for a sliding system with dy = 0.1 m the velocity at which the block starts the second slide is 1.26 m/s, whereas for dy = 0.01 m the corresponding velocity is only 0.28 m/s. The force-displacement hysteresis loop in Figure 5.11 shows the two yielding events and the accompanying elastic branches. The same influence of elastoplastic friction on the sliding velocity and its consequent slippage is presented in Figures 5.17, 5.18 and 5.20.

Figures 5.12 and 5.13 demonstrate an astonishing effect: that of the reversal in polarity (i.e., change from + to – direction in which the excitation is applied). This is the same as having two identical slopes, one opposite to the other ("across the street" so to speak), subjected to the same excitation of an one-cycle sinus pulse of 0.57 Hz frequency and 1 g peak amplitude. A few researchers and only in recent years (Fardis et al, 2003; Kramer & Lindwall, 2004; Gazetas et al, 2009) appear to have published on the importance of the polarity of shaking. This has much to do with the asymmetry of

recorded motions, which is what accentuates the importance of polarity. It is mainly the near–fault strong motions which are highly asymmetric due to the contained 'directivity' and 'fling' pulses. But few such motions had been recorded worldwide twenty years ago. Now a large number has become available.

The sliding analysis of Figure 5.12 is simple, but the results are most revealing. For a steep slope (β = 25°), a yield acceleration ratio a_C /a_H = 0.2, and a pre-yielding displacement dy = 0.05 m, we notice the following: When the first sinusoidal acceleration half-pulse is downward [right hand side in Figure 5.12] the block remains almost attached to the base as the inertia force developing in the opposite direction, i.e. uphill, is not enough to overcome the frictional resistance and gravity. The subsequent, second (and last), upward half-pulse acceleration of the base initiates an uninhibited downslope slippage of the block, which lasts for a long time after the excitation has terminated — i.e., $\Delta t \approx 2.4$ sec at $t \approx 5.2$ sec. The result is a huge 7.70 m slippage.

In stark contrast, when the first sinusoidal acceleration half-pulse of the base is upward [left hand side in Figure 5.12] the block starts sliding down slope almost immediately. But it soon comes to a stop after about 1.4 seconds, as the upward base motion decelerates and then reverses. The resulting residual slip is only 3.14 m, almost 2.5 times smaller than the 7.70 m produced with the reverse motion! This difference becomes even more clear in Figure 5.13 where the force-displacement loops are depicted.

The effect of reversing the polarity of shaking is of profound importance especially with 'fling' type motions (as the sinus pulse idealisation studied above). It may not however be as dramatic with 'directivity' affected motions if they contain several "competing" cycles of pulses, as seen in Figures 5.14, 5.15, and 5.21 with the Ricker wavelet.

5.5.1.2 Exponential friction response

To model the sticking effect of yielding interface, a frictional constitutive law is employed which is described by the equation (5.2) and is depicted in Figure 5.25. We assume that yielding initiates when inertial force exceeds the static frictional force T_{static}, and sliding continues with: (i) an exponentially reducing coefficient of friction or (ii) an exponentially increasing coefficient of friction. The final permanent value of friction is $T_{dynamic}$.

As an example, in case of $\mu_{static} = 0.8\mu_{dynamic}$, as in Figure 5.26, the block starts sliding at a 80 percent lower value than the critical one of 0.20 g (see the focused acceleration time history insert, inside the red dashed rectangle). The results of exponential friction parametric analyses, are portrayed in Figures 5.26÷ 5.36. The number "1" in the subscript indicates the downhill motion, and number "2" the uphill.

Figure 5.34 demonstrates the response for an inclined sliding system with $\mu_{slid} = 1.5\mu_{static}$, subjected to a Ricker wavelet of frequency 3.5 Hz. In acceleration time histories, sticking is observed at the beginning of every sliding period where the block acceleration momentarily surpasses the critical value a_C, leading to an "impact-like" behaviour which is demonstrated in the yellow shadowed area of Figure 5.34 (top plot). For the same excitation (Ricker, 0.35 Hz) the force–displacement loops are presented in Figure 5.35 for several types of exponential frictional behaviour.

5.5.2 Sliding response from near-fault ground motions

Results from parametric analyses with strong ground accelerograms as excitation, are displayed in Figures 5.37÷ 5.56. Elastoplastic response of a block resting on an

inclined plane with coefficient of friction $\mu = 0.52$ (or friction angle $\varphi \approx 27^o$) and pre-yielding displacement dy =0.05 m, when subjected to the TCU 068-NS record, is presented in Figure 5.37. Notice that the final slippage at the end of sliding motion reaches 4.69 m. For the same input motion and exactly the same yielding system, the acceleration, velocity, displacement response and friction–displacement loop are portrayed in Figures 5.38, 5.39, 5.40, and 5.41 respectively. In these plots, solid blue line presents the perfectly-plastic system and solid pink line the elastoplastic system of dy = 0.1 m. The main reason for the slippage difference between the perfectly plastic and the elasto-plastic frictional behaviour is graphically described in Figure 5.39 in the velocity time histories: the elastic part of block's motion, before the initiation of plastic displacement, provides the block with velocity larger than its base. As a result, the induced sliding (= 4.93 m) is greater than that of the perfectly-plastic system (= 3.29 m).

This trend seems to be stronger as the pre-yielding displacement dy enlarges (keeping all the other parameters the same). For instance, notice in Figure 5.42 that when dy = 0.05 m the initial velocity of the first slide is 1.54 m/s, whereas for dy = 0.1 m the corresponding velocity is 1.63 m/s. The elasticity influence on sliding velocity is additionally illustrated in Figures 5.47 and 5.48 for the Rinaldi and in Figure 5.55 for the Lucerne record.

In case of taking into account the sticking effect, at the beginning of every yielding cycle an instantaneous impact occurs (see Figures 5.44, 5.49, 5.50, and 5.53). However, these impacts have a negligible influence on the final slippage. A confirmation of the previous statement is given in Figures 5.46 and 5.56 where for the TCU 068-NS and the Lucerne records, respectively, the effects for all the studied frictional laws are presented.

5.5.3 Summary results and conclusions

All numerical results with idealised wavelets and near-fault records as base excitations are summarised in Figures 5.57÷ 5.81. For example, Figure 5.63 depicts the permanent slippage with respect to the critical acceleration ratio, a_C/a_H, for four values of pre-yielding deformation, dy, and four excitation frequencies, f_o. As expected, when the acceleration ratio, a_C/a_H, increases the induced slippage decreases. This general trend is independent of the existence or not of the pre-yielding displacement. Notice that the existence of pre-yielding elasticity may lead to larger or smaller permanent displacements, depending on f_o and a_C/a_H.

Furthermore, in Figure 5.64 observe the influence of frequency on sliding displacement. For frequency, f_o = 0.35 Hz, as the elastic region dy increases so does the slippage D. The same is valid for f_o = 0.75 Hz. However, when f_o increases to 1.50 Hz the response changes. Observe that while slippage becomes greater for pre-yielding region between 0 and 0.01, for larger values of dy the sliding response decreases, in the case of 1.50 Hz. The behaviour is more complicated when the frequency takes the value of 3.50 Hz.

Furthermore, the polarity effect of shaking is of profound importance, especially with 'fling' type motions (as the sinus pulse). As already mentioned, it is not as dramatic with 'directivity' affected motions which usually contain a number of "competing" cycles of pulses, as seen in Figure 5.69 with the Ricker wavelet.

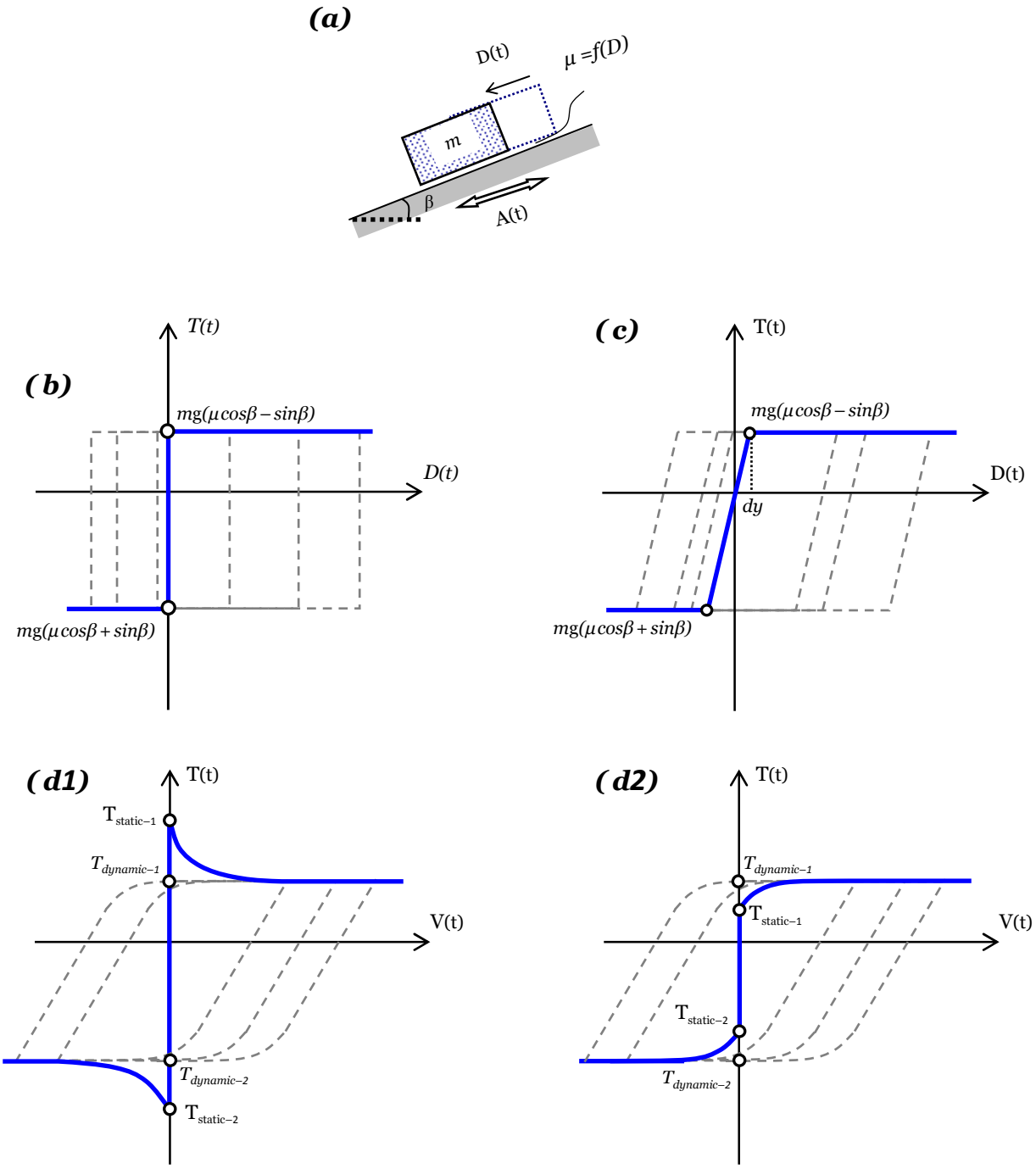

Figure 5.1 *(a) The general frictional analogue studied: sliding on inclined plane undergoing excitation parallel to the slope, (b) ideally rigid-plastic behavior of the interface, (c) elastic-perfectly plastic sliding response, and (d1), (d2) exponential friction law of the interface.*

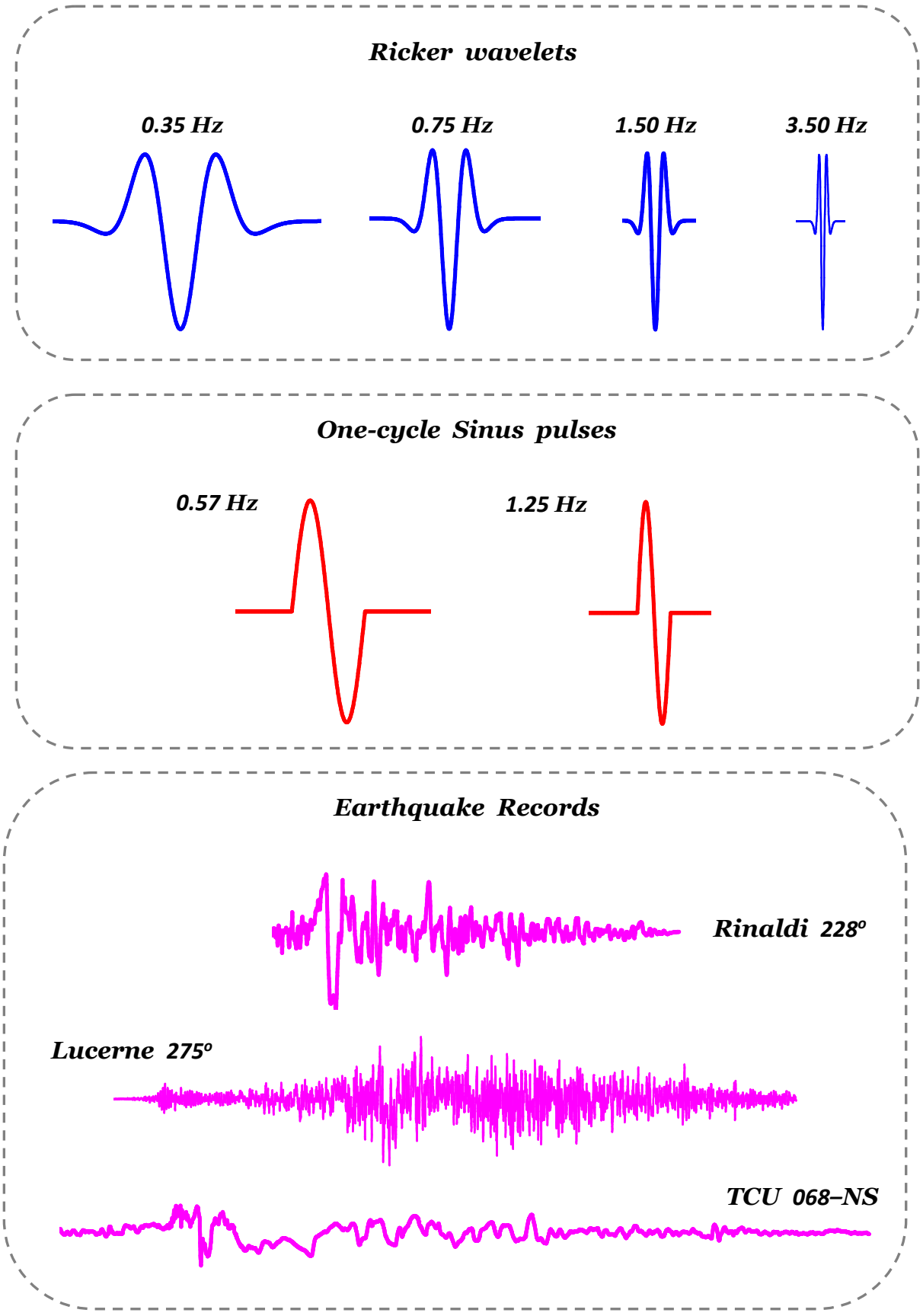

Figure 5.2 *The idealised pulses and records employed as excitation. They are imposed on the top of the inclined plane, triggering the block to slide.*

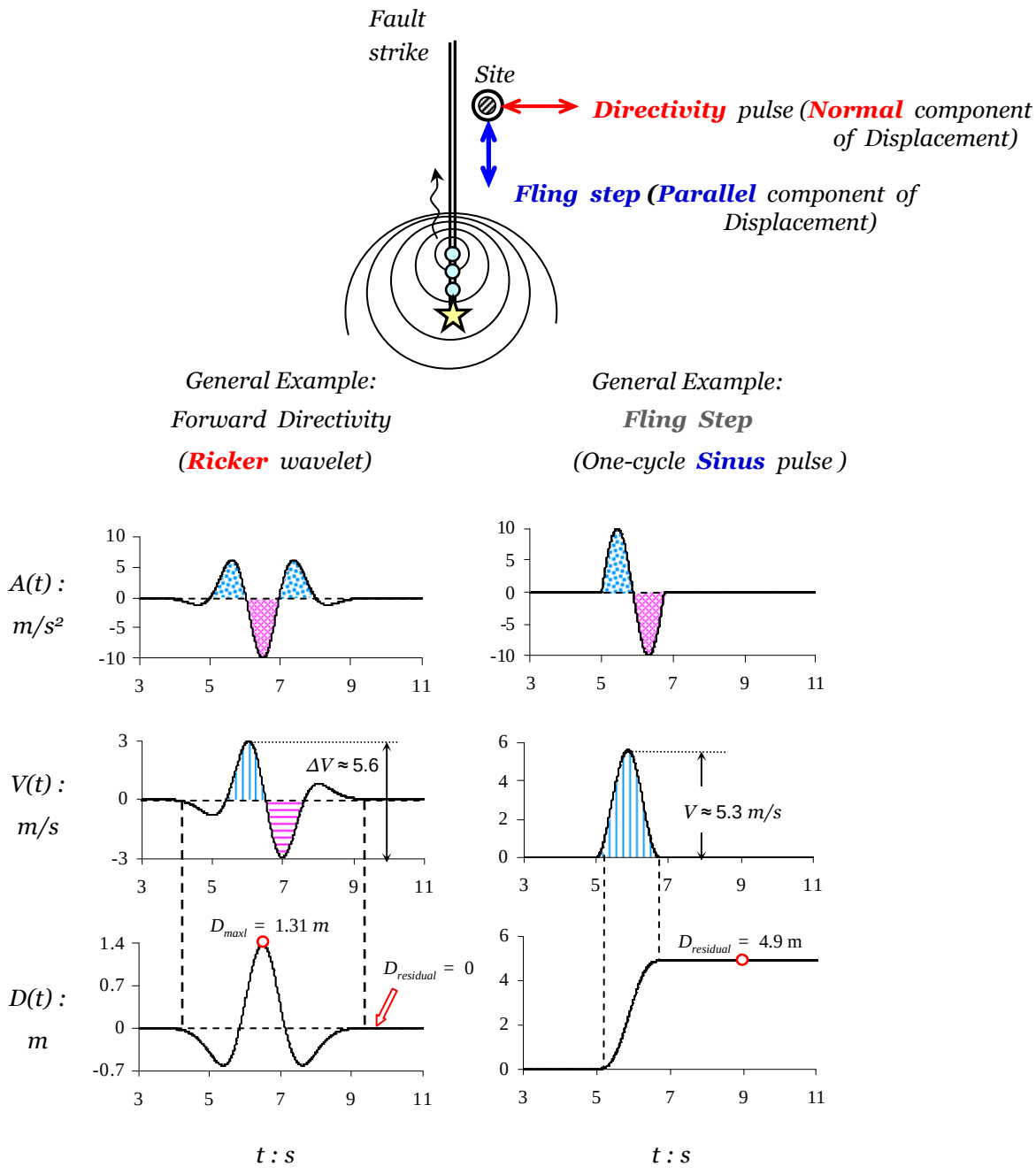

Figure 5.3 *Explanatory sketch of the forward-directivity and fling-step phenomena as reflected in the displacement records; and examples of simple wavelets bearing the "signature" of the two effects.*

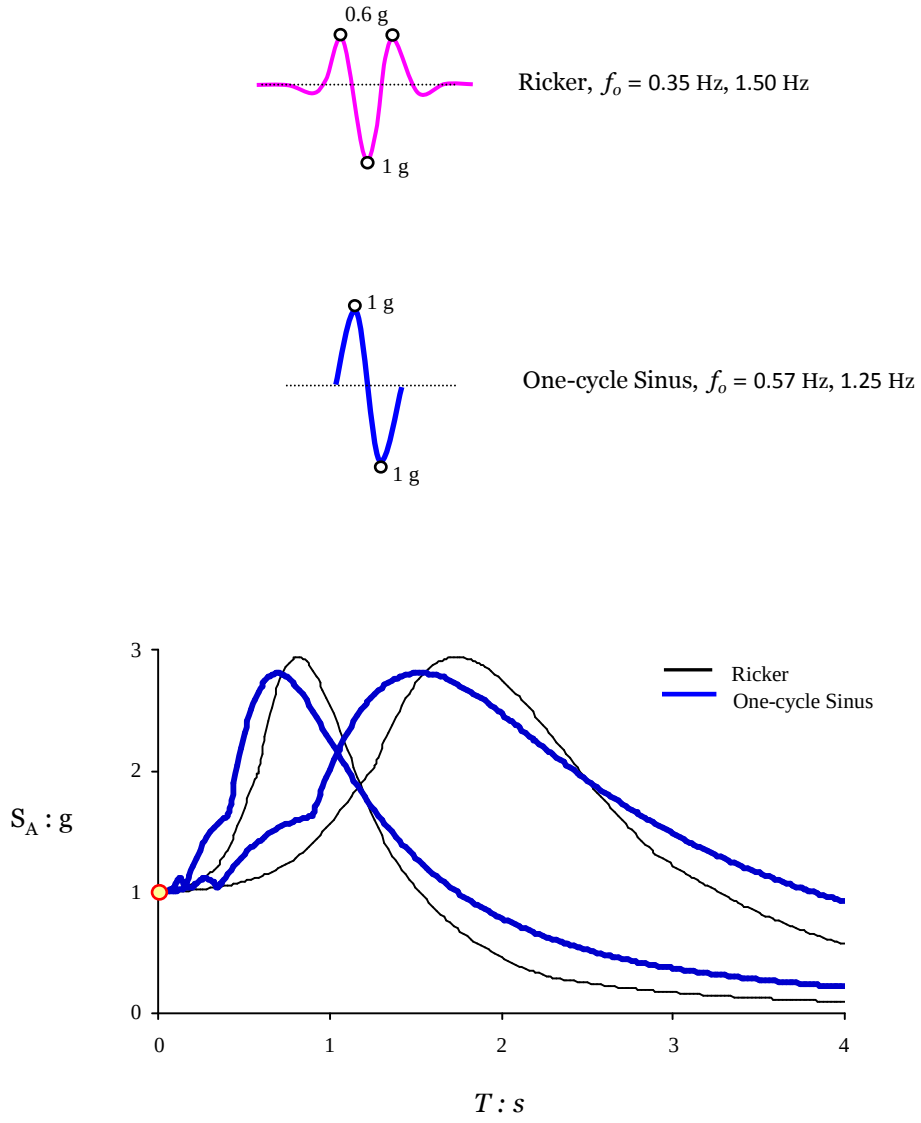

Figure 5.4 *The two idealized time histories used as base excitation, with their response acceleration spectra* S_A *:* g *–* T*. (Peak ground acceleration: 1* g*).*

Asymmetric Sliding on Elasto-Plastic Frictional Interface

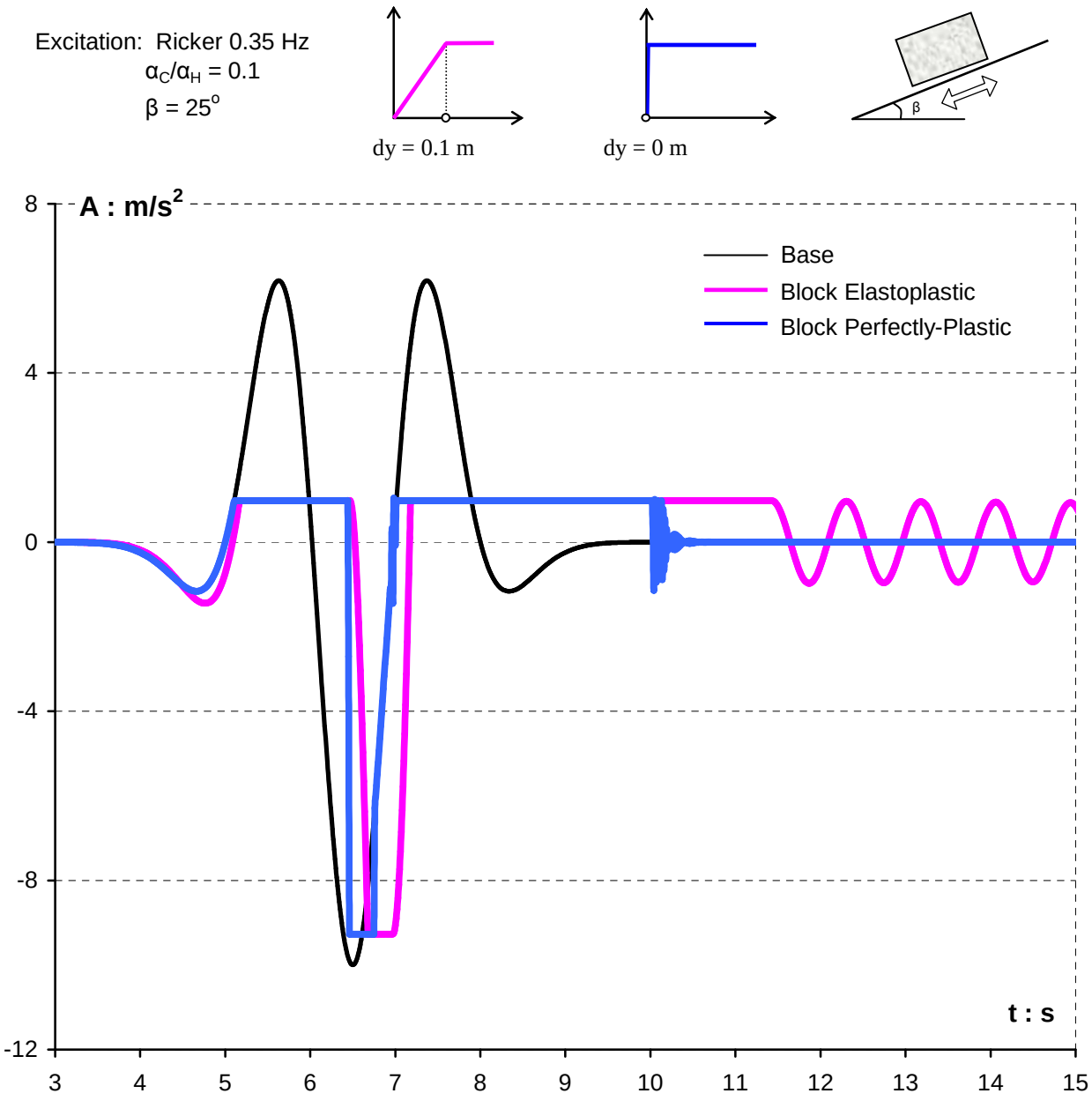

Figure 5.5 *Acceleration time histories of a block rested on a 25^0 inclined plane subjected to a Ricker wavelet of frequency 0.35 Hz. The light blue line represents the block's response when sliding interface is governed by a perfectly-plastic friction law, whereas the solid pink line corresponds to elasto-plastic yielding. ($a_C/a_H = 0.1$)*

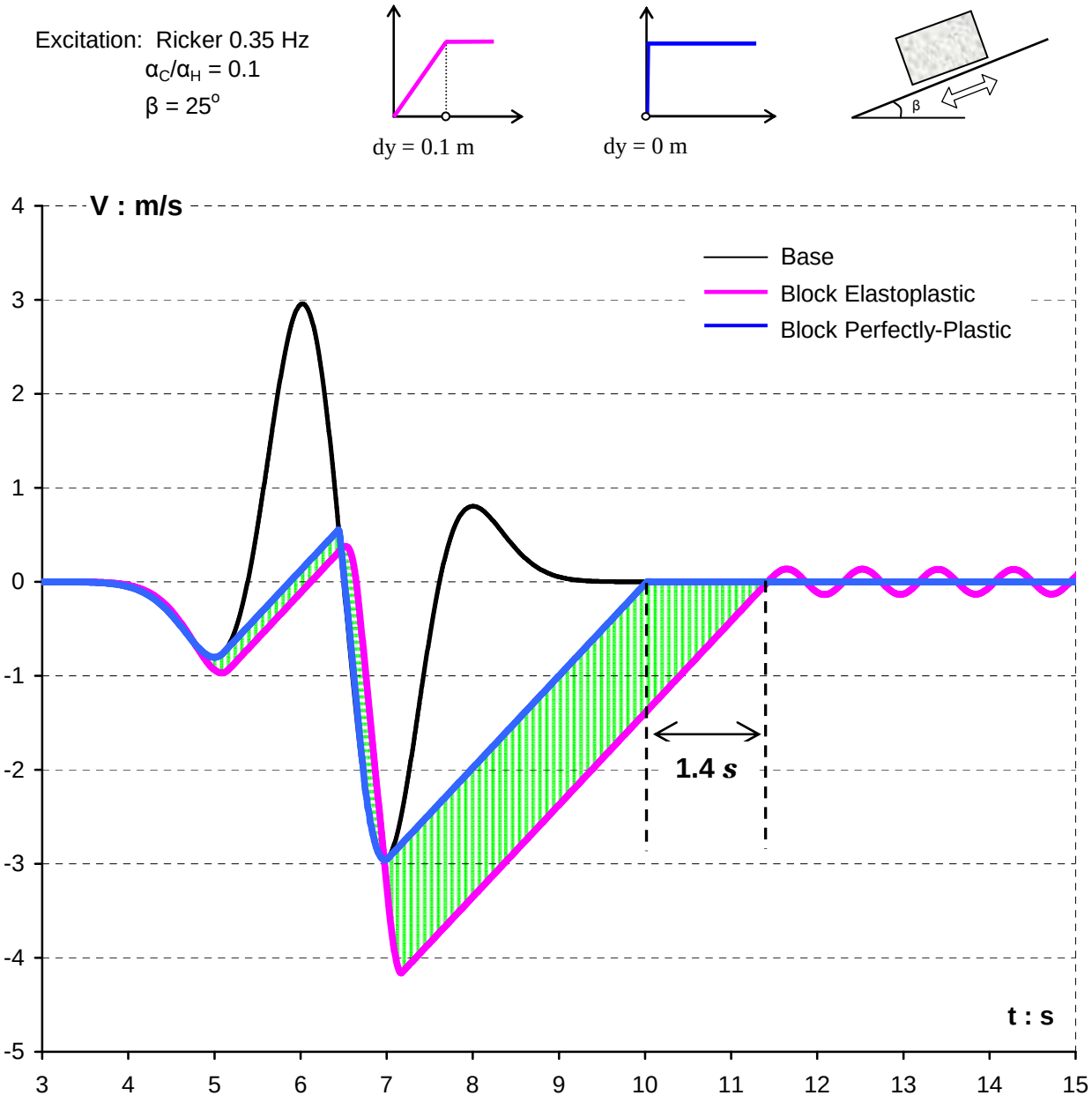

Figure 5.6 *Velocity time histories of a block rested on a 25^0 inclined plane subjected to a Ricker wavelet of frequency 0.35 Hz. The green shaded areas shows the yielding displacement difference between the perfectly-plastic and the elasto-plastic response. ($a_C/a_H = 0.1$)*

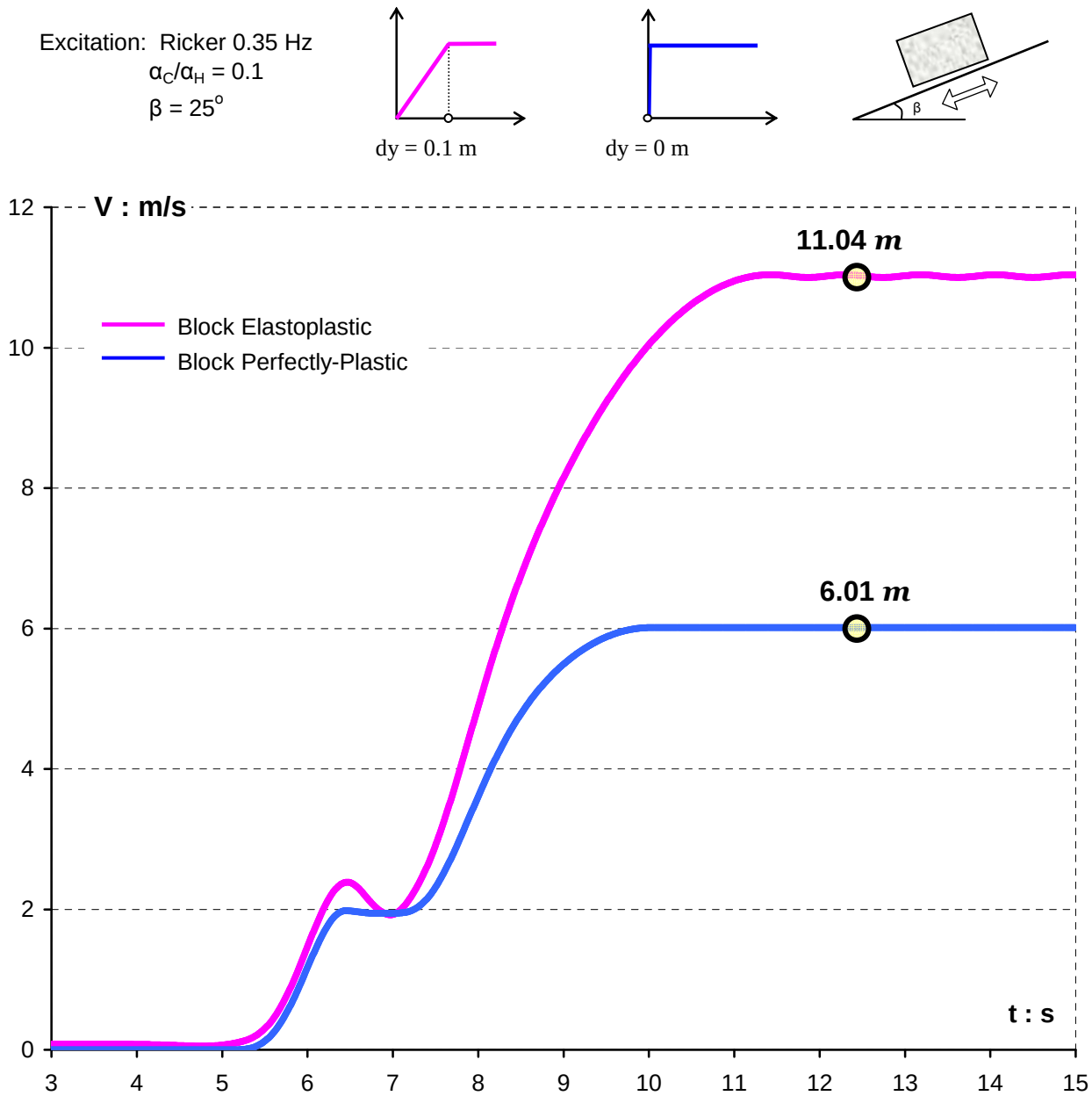

Figure 5.7 *Displacement time histories of a block rested on a 25^0 inclined plane subjected to a Ricker wavelet of frequency 0.35 Hz. The elasto-plastic response with the pink solid line is 84% greater than the perfectly-plastic response with the light blue line. ($a_C/a_H = 0.1$)*

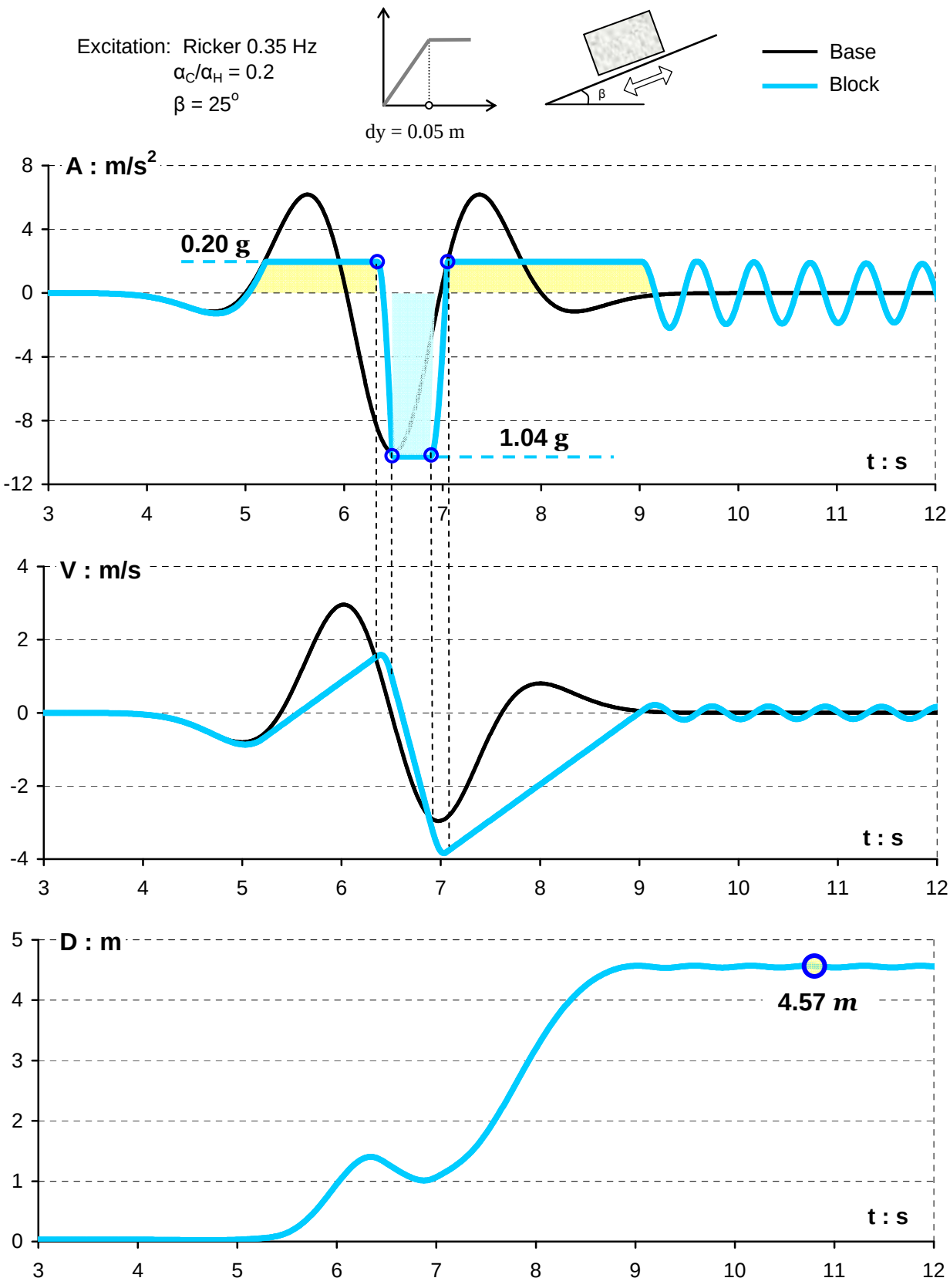

Figure 5.8 *Asymmetric response time histories of a rigid block resting on an 25^0 inclined plane when subjected to a Ricker pulse excitation of frequency 0.35 Hz. The interface between the block and plane is governed by an elasto-plastic frictional law. Block's elastic deformation dy = 0.05 m occurs in advance of yielding initiation. ($a_C/a_H = 0.2$)*

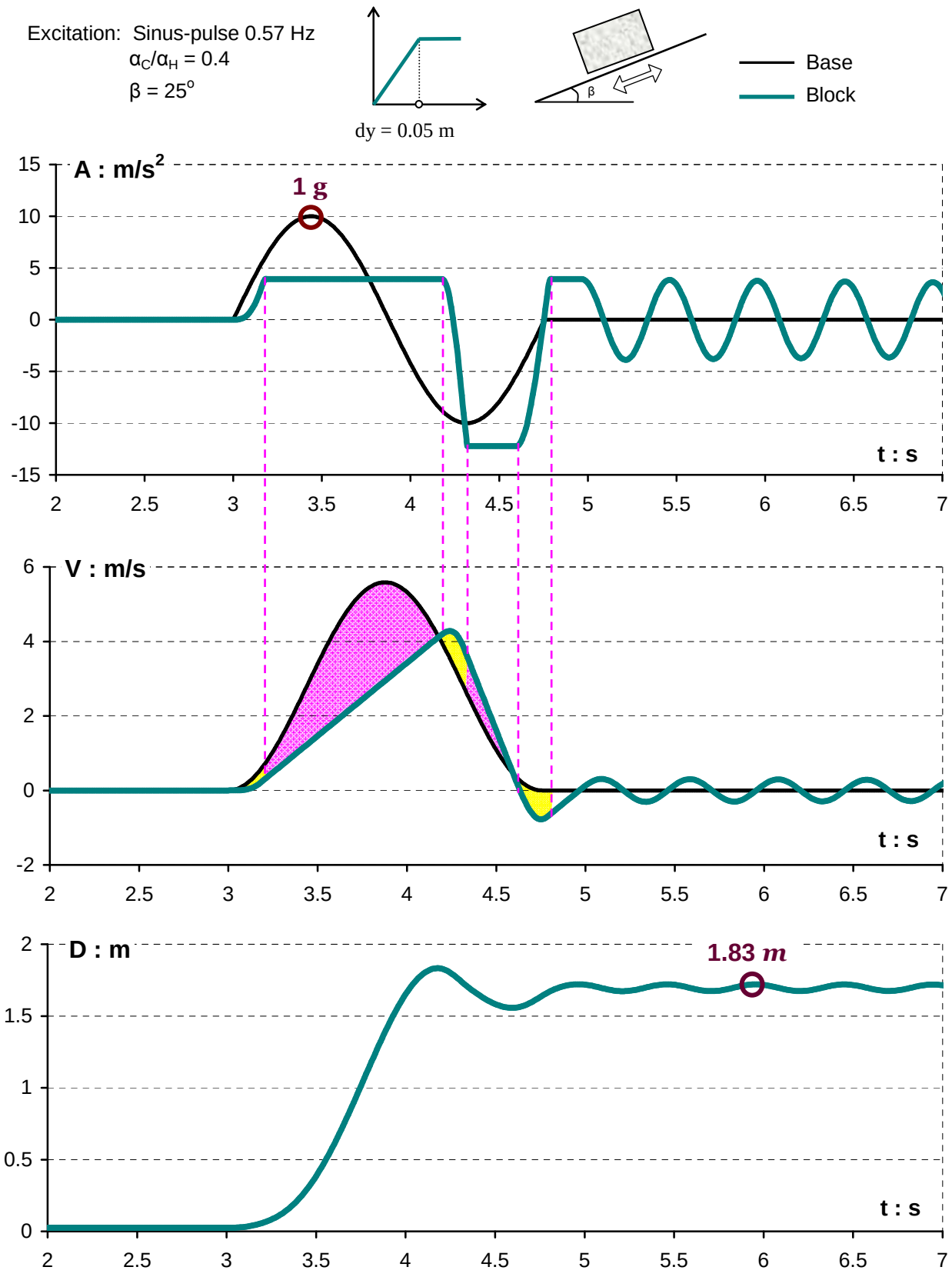

Figure 5.9 *Asymmetric response time histories of a rigid block resting on an 25^0 inclined plane when subjected to one cycle sinus pulse of frequency 0.57 Hz. The yielding interface is governed by an elasto-plastic frictional law, with dy = 0.05 m. The yellow area in the velocity graph corresponds to the elastic part of deformation. However the pink area presents the plastic part of displacement. ($a_C/a_H = 0.4$)*

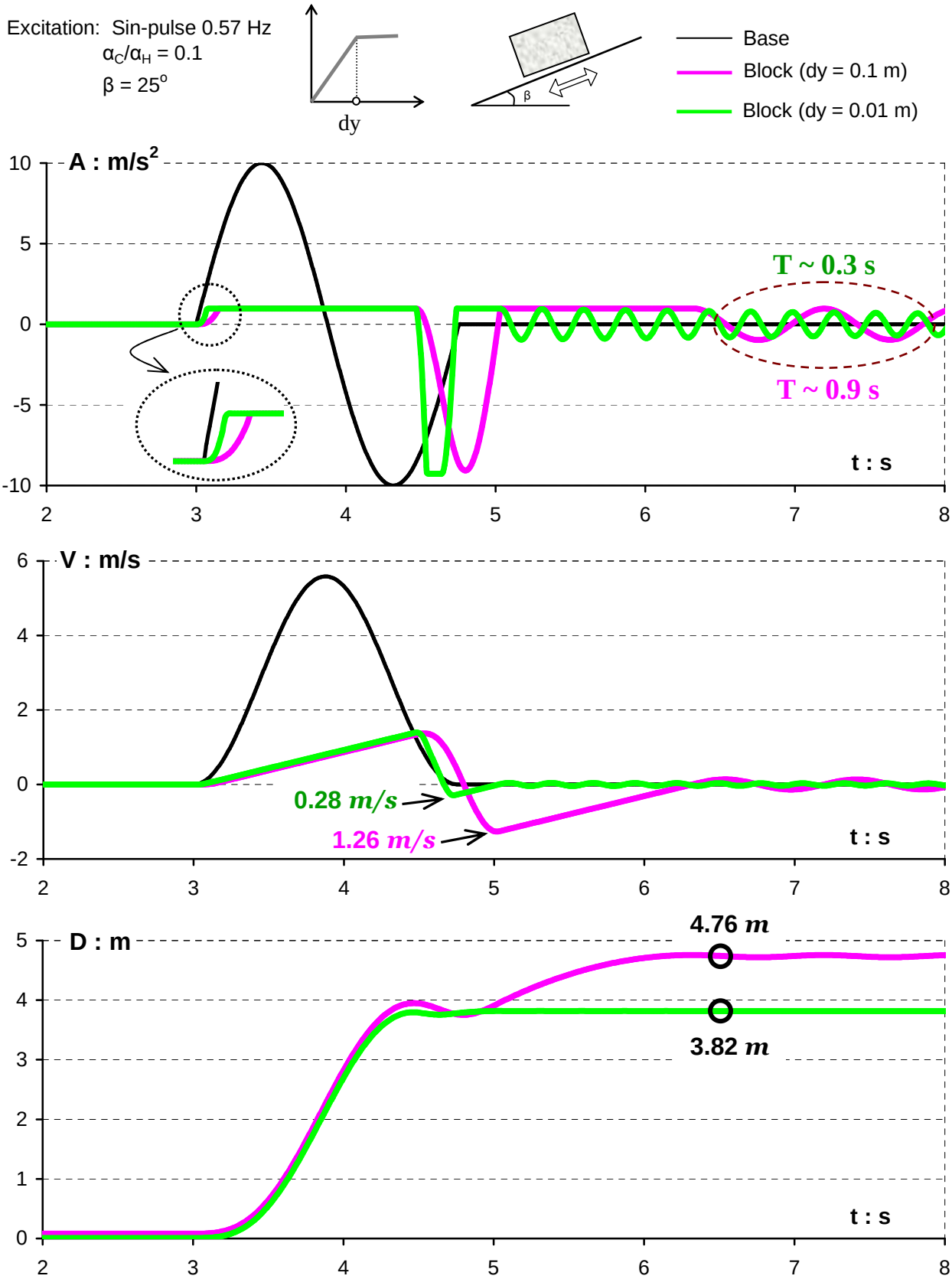

Figure 5.10 *Asymmetric response time histories of a rigid block resting on an 25^0 inclined plane when subjected to one cycle sinus pulse of frequency 0.57 Hz. The light green line presents the elasto-plastic response with dy = 0.01 m; whereas the solid pink line corresponds to dy = 0.1 m. ($a_C/a_H = 0.1$)*

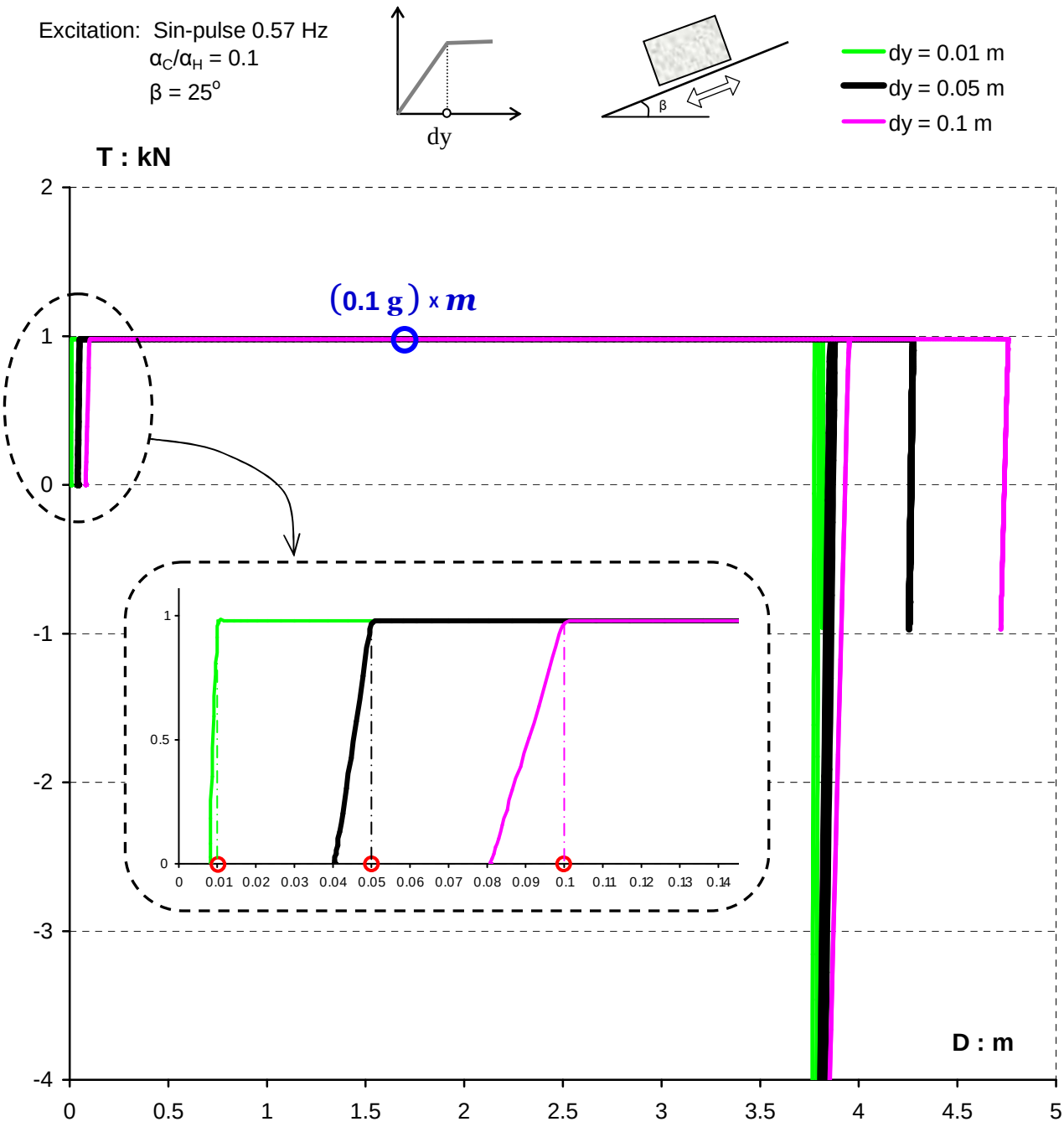

Figure 5.11 *Force-displacement response for an elasto-plastic sliding system with dy = 0.1 m, 0.05 m, and 0.01 m illustrated with the pink, black and light green solid lines respectively [β = 25°, a_C/a_H = 0.1 and an one-cycle sinus pulse of 0.57 Hz frequency]. Notice that in this particular case as the elastic displacement dy increases, the plastic yielding becomes greater too.*

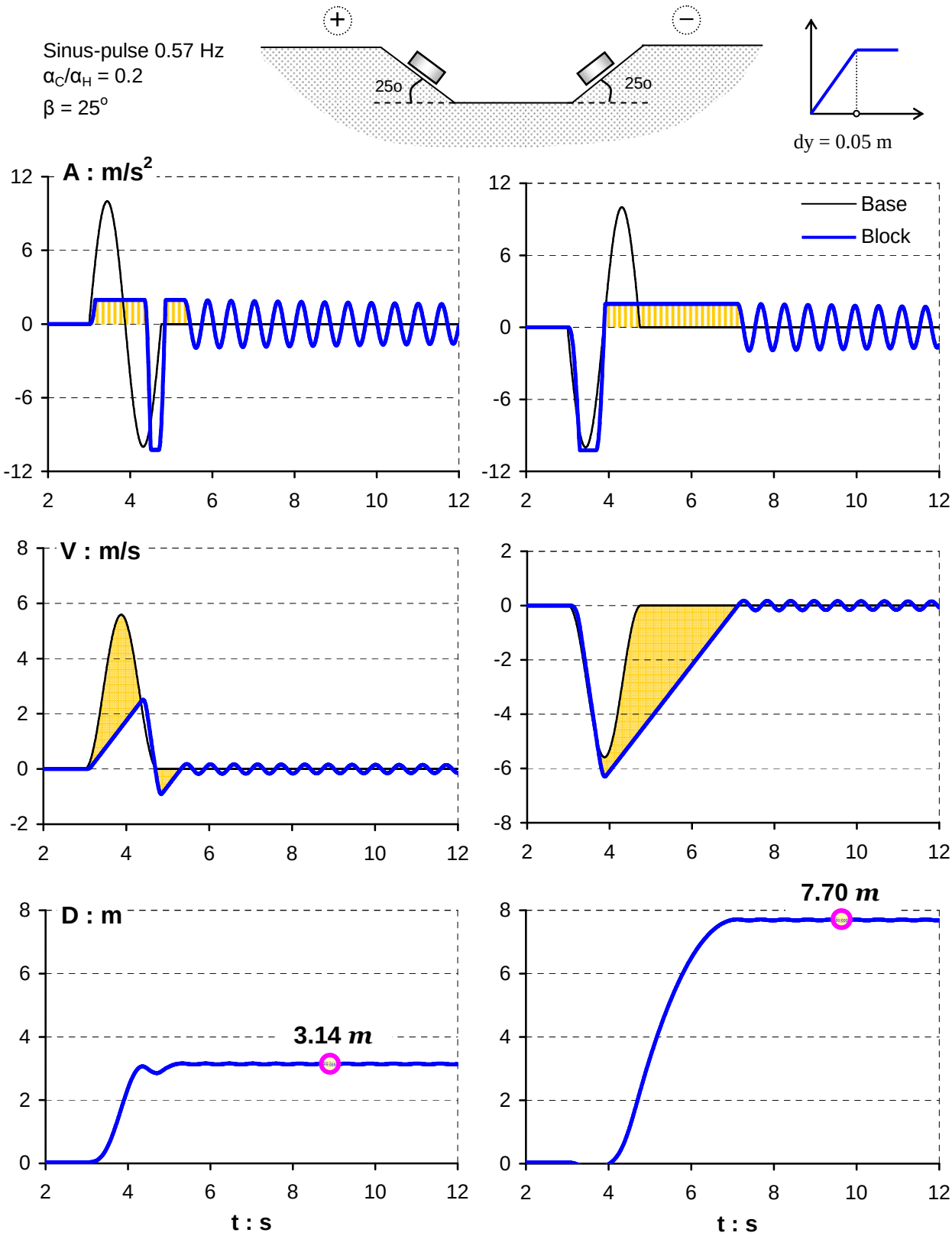

Figure 5.12 *The response difference due to polarity of the applied one-cycle sinus excitation. (a_C/a_H = 0.2).*

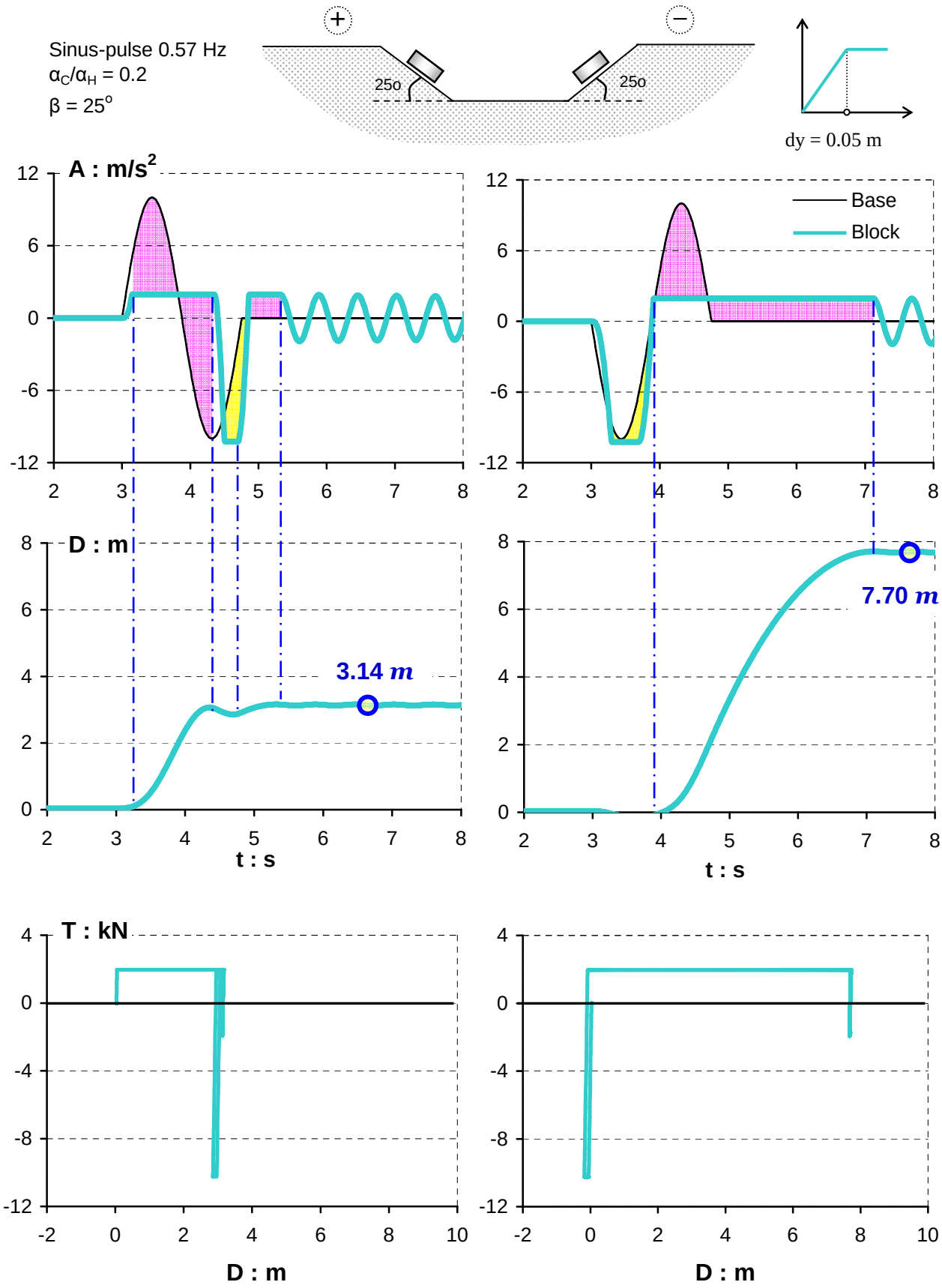

Figure 5.13 *Acceleration and displacement time histories for an elasto-plastic system with maximum elastic deformation of dy = 0.05 m. The third row of figures illustrate the force-displacement response. (Excitation: one-cycle Sinus of 0.57 Hz frequency).*

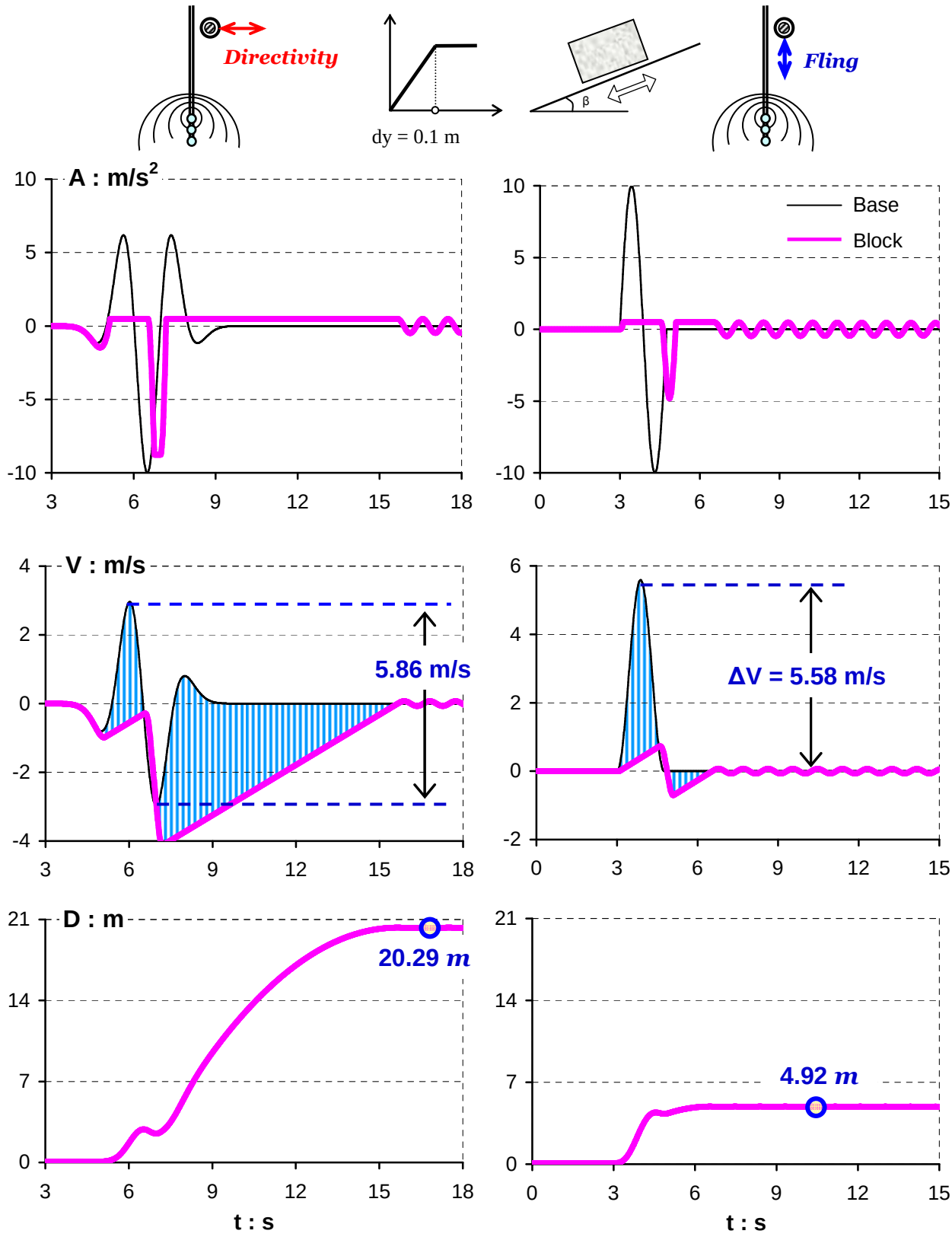

Figure 5.14 *Response comparison between normal polarity imposed Ricker wavelet of 0.35 Hz and one-cycle sinus excitation of 0.57 Hz. Ricker pulse is typical of forward directivity affected motions whereas sinus cycle of fling step effect. In this case, Ricker induces four times greater slippage than the sin-pulse (a_C/a_H = 0.05).*

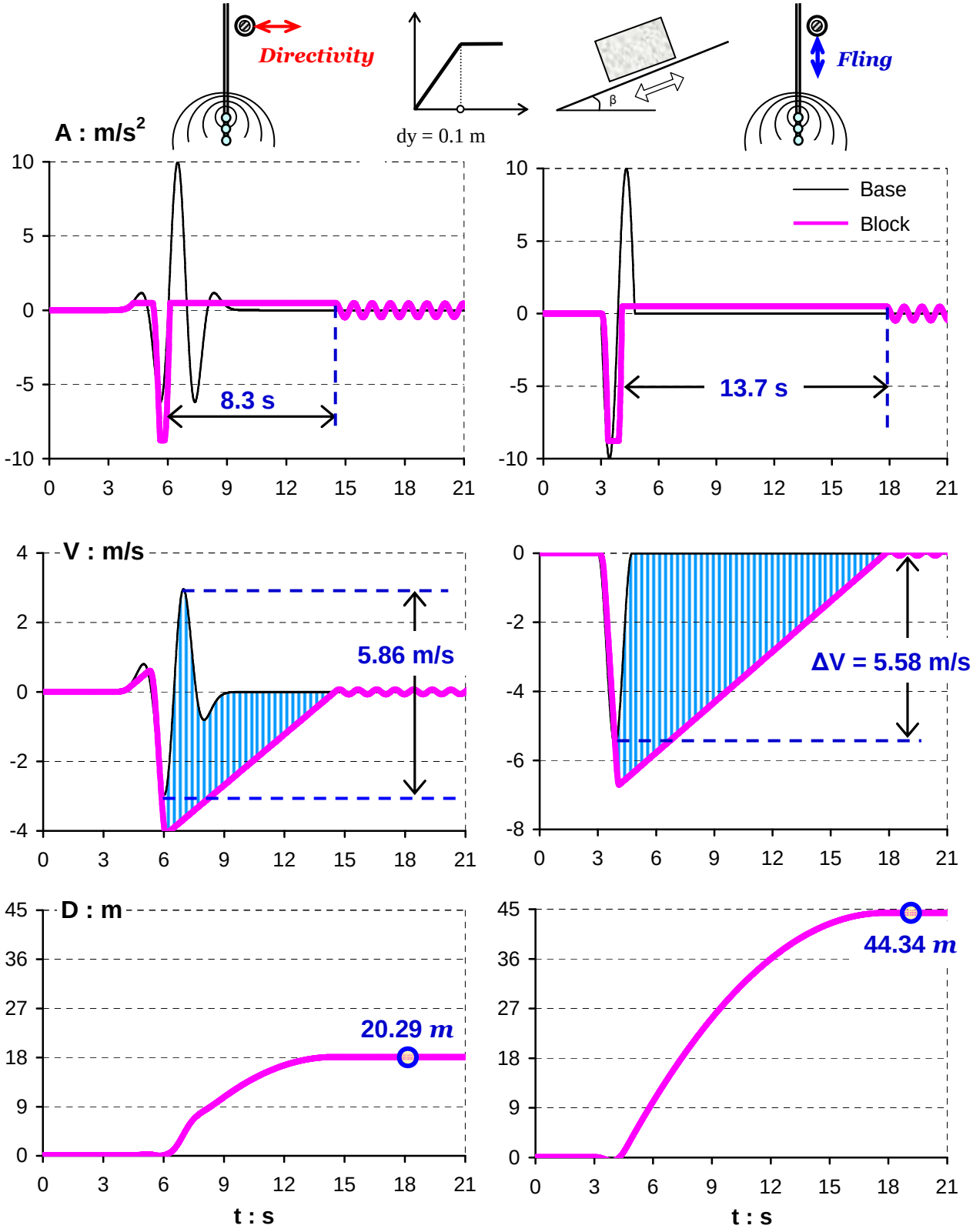

Figure 5.15 *Response comparison between reversed polarity imposed Ricker wavelet of 0.35 Hz and one-cycle sinus excitation of 0.57 Hz. In contrast with the normal polarity excitations, when the polarity is reversed the slippage triggered by sinus is larger than the Ricker induced.* $(a_C/a_H = 0.05)$.

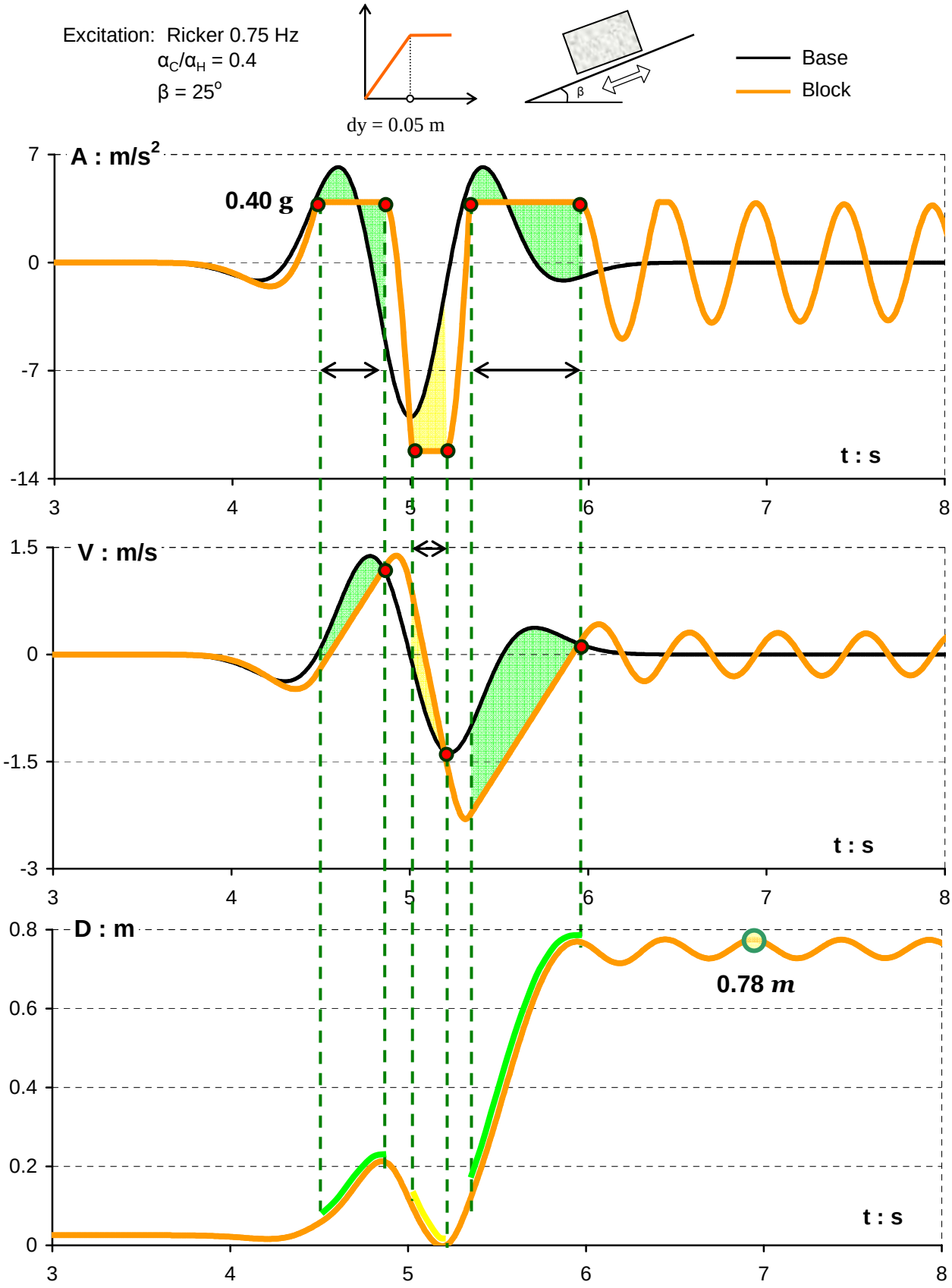

Figure 5.16 *Asymmetric response time histories of a rigid block resting on an 25^0 inclined plane when subjected to a Ricker pulse excitation of frequency 0.75 Hz. The green shaded area illustrates the two downward sliding events and with yellow the upward yielding phase. Block's elastic deformation is dy = 0.05 m. ($a_C/a_H = 0.4$)*

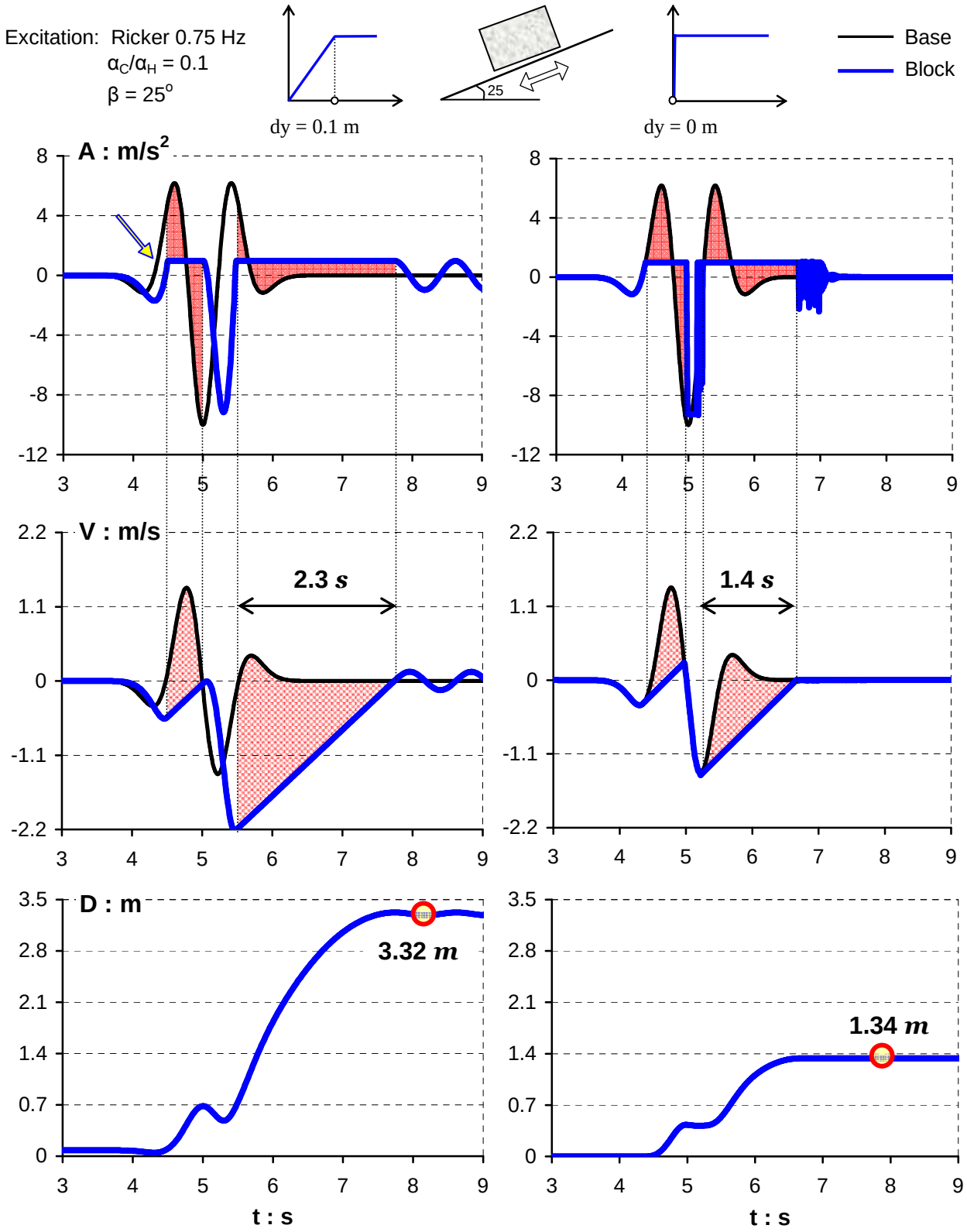

Figure 5.17 *Acceleration, velocity, and displacement time histories for a maximum elastic deformation of dy = 0.1 m are presented at the left, and for dy = 0 are presented at the right. (excitation: Ricker wavelet of frequency f_o = 0.75 Hz)*

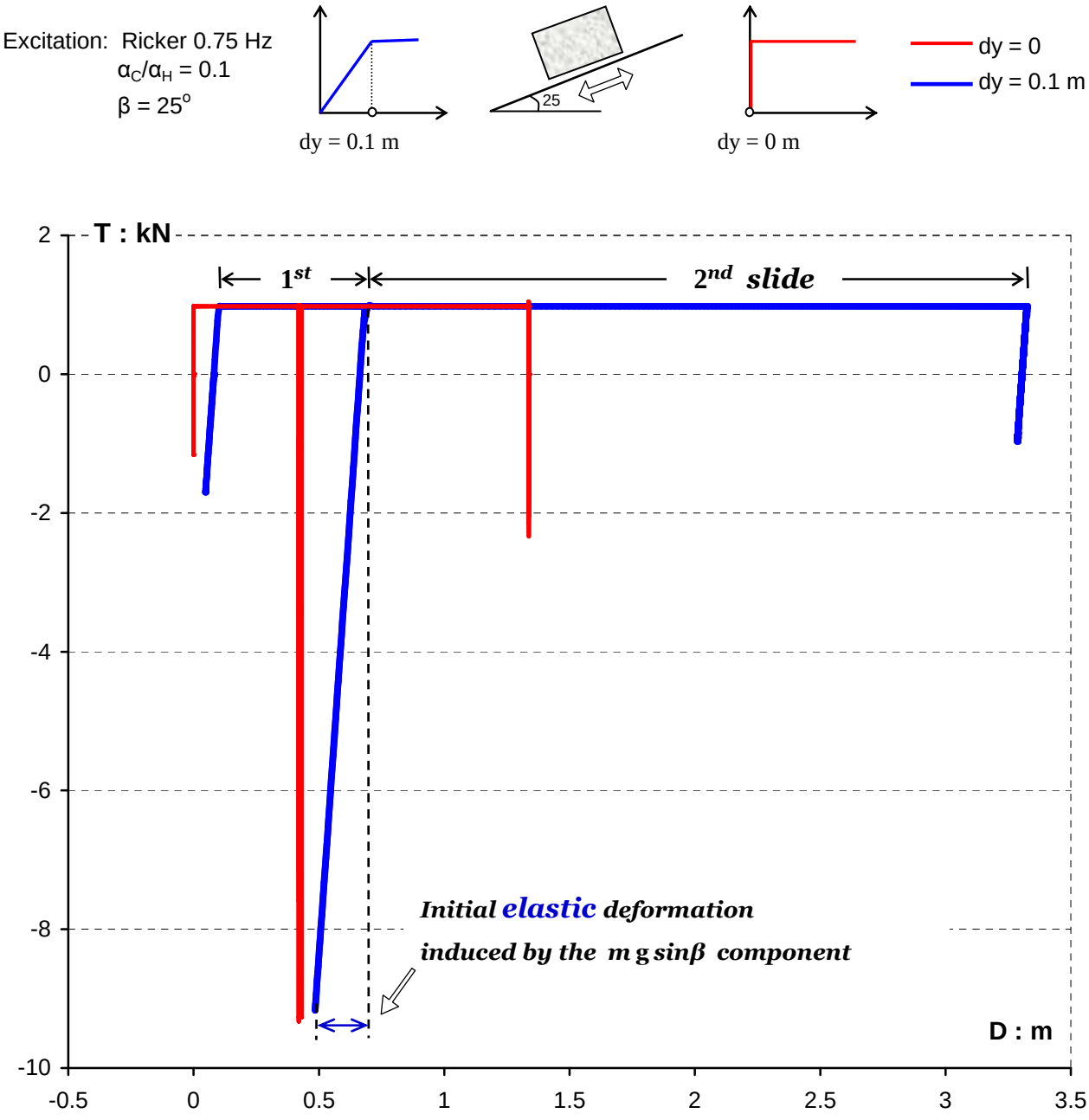

Figure 5.18 *Force-displacement response for the case of: (a) an elasto-plastic sliding system with dy = 0.1 m with the blue solid line, and (b) a perfectly plastic system with the red solid line [β = 25°, a_C/a_H = 0.1 and a Ricker excitation of 0.75 Hz frequency] . Notice that yielding occurs only in one direction, as it was expected.*

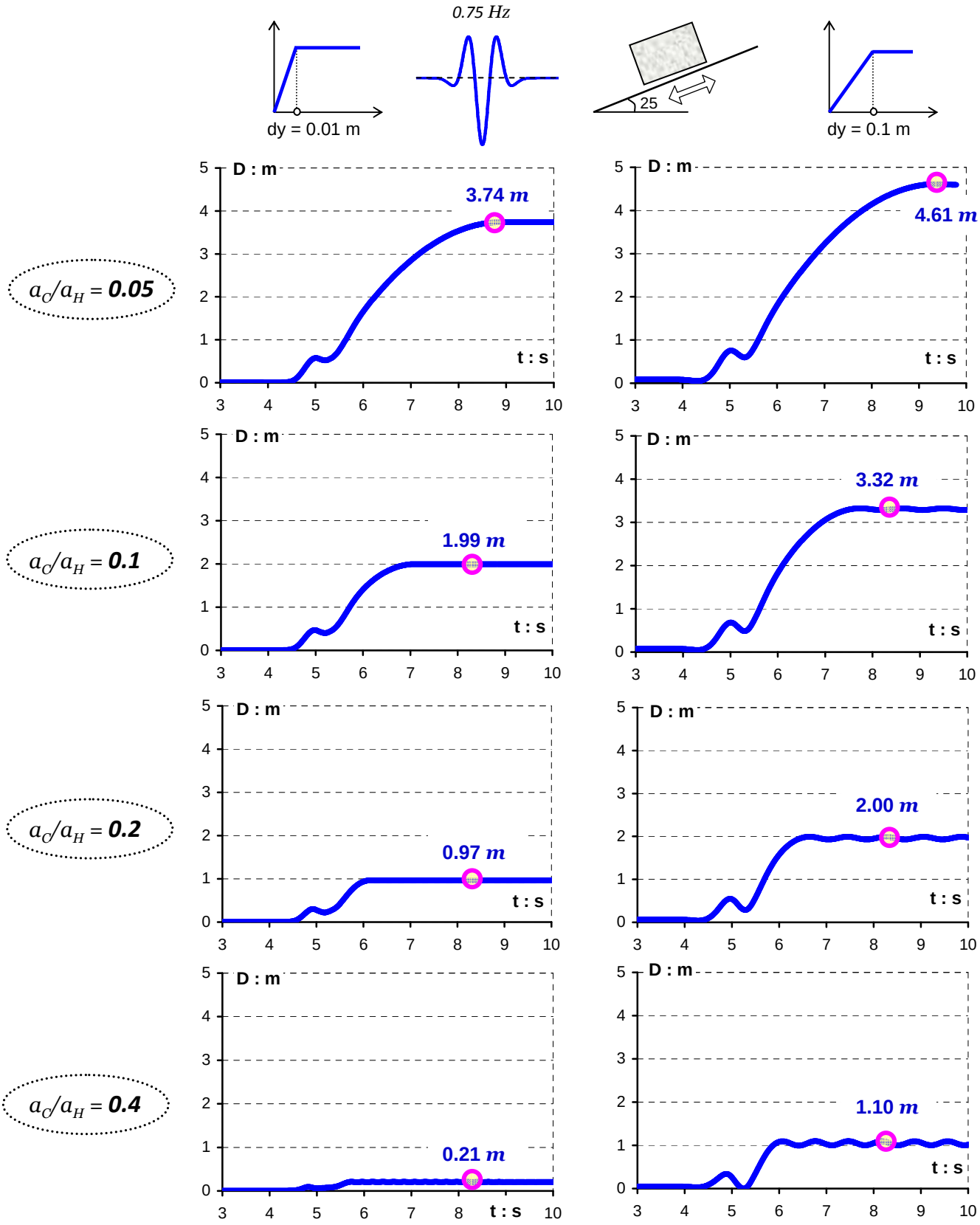

Figure 5.19 *Asymmetric sliding response for four acceleration ratios, a_C/a_H, at the left column for elasto-plastic yielding with dy = 0.01 m and at the right for dy = 0.1 m. The triggering excitation is the Ricker pulse of frequency 0.75 Hz. [$\beta = 25^o$]*

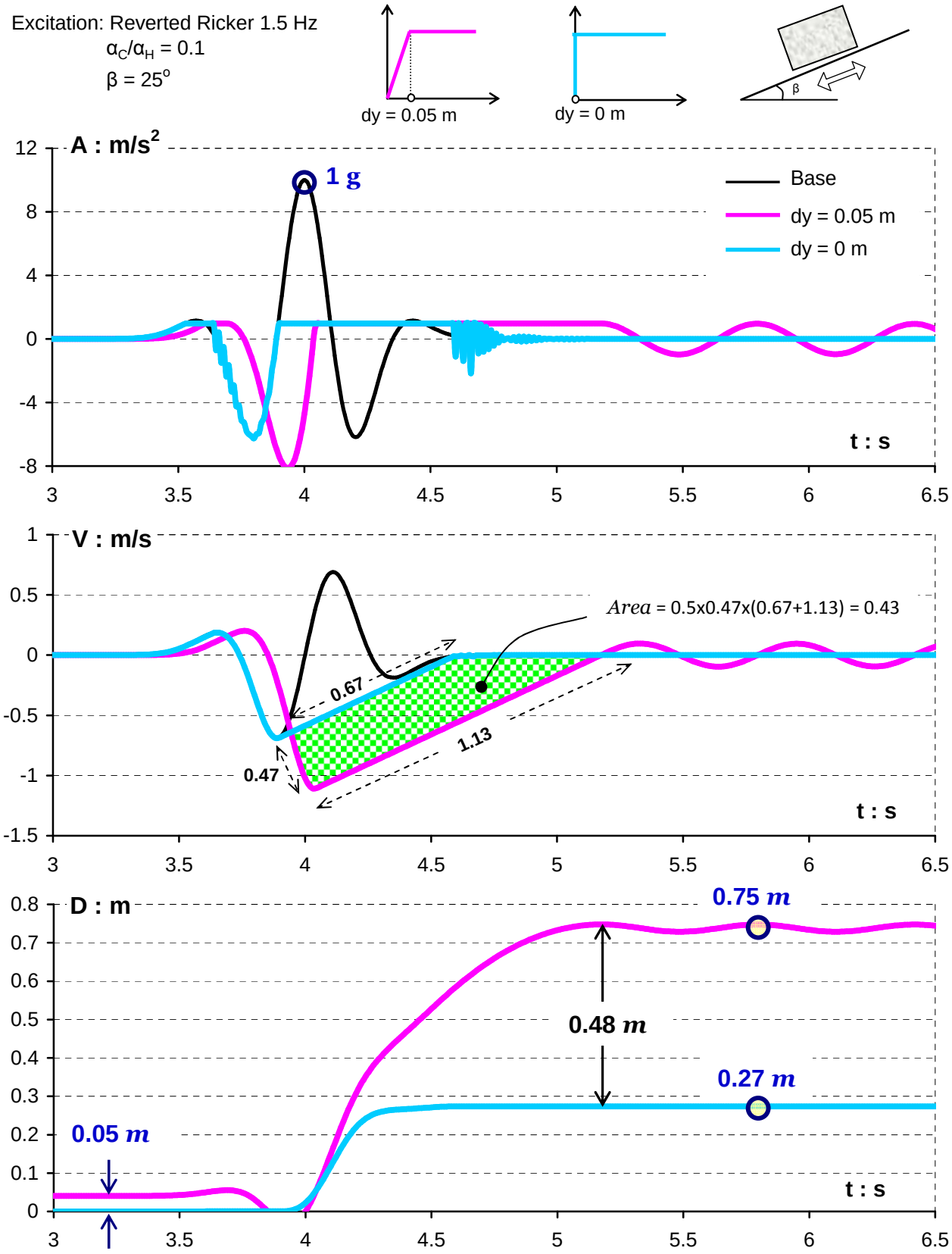

Figure 5.20 *Acceleration, velocity, and sliding displacement time histories of a block rested on a 25^0 inclined plane subjected to the reversed 1.50 Hz Ricker wavelet. The light blue line represents the perfectly plastic block's response, whereas the solid pink line the elasto-plastic sliding response for dy = 0.05 m. ($a_C/a_H = 0.1$)*

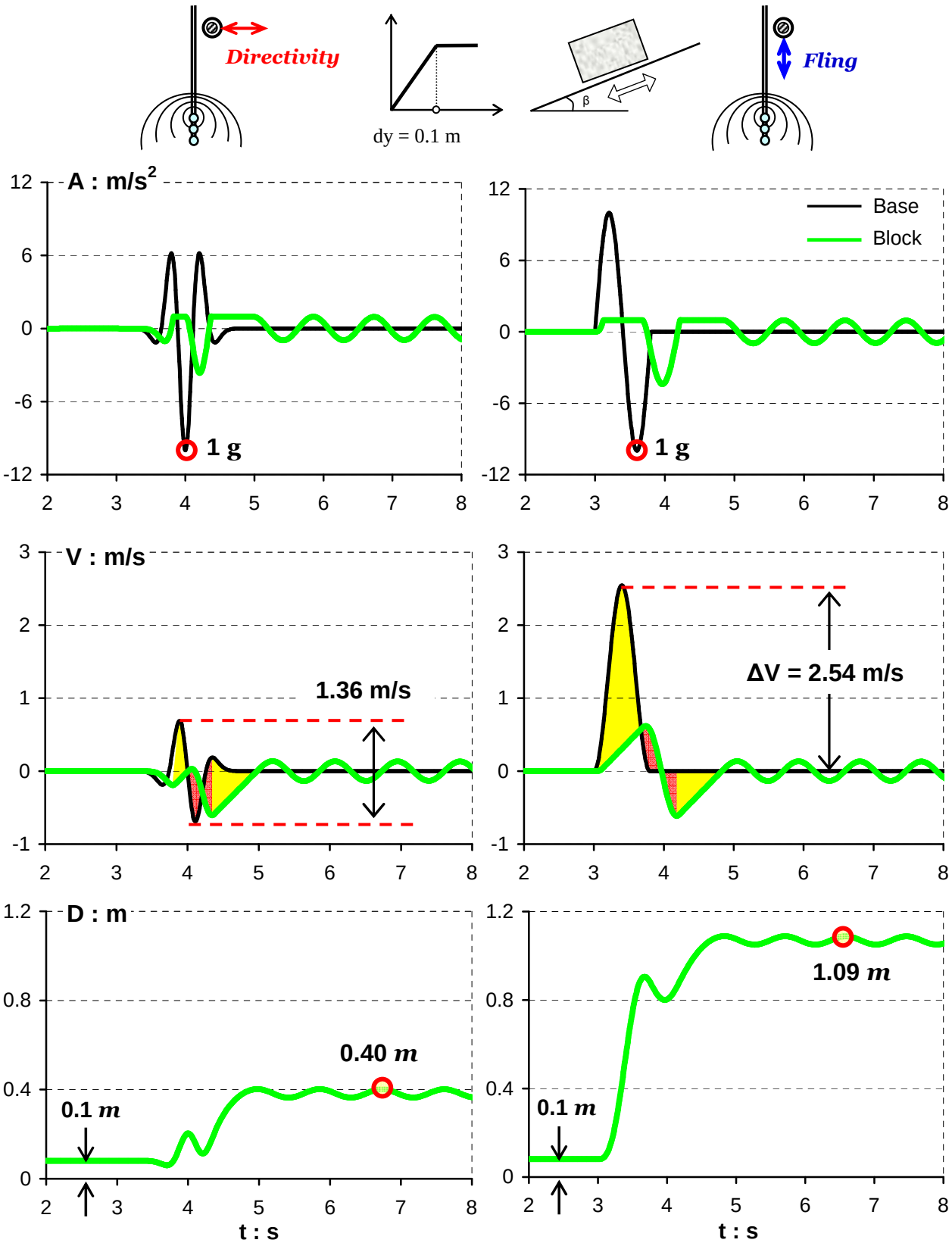

Figure 5.21 *Response comparison between normal polarity imposed Ricker wavelet of 1.50 Hz and one-cycle sinus excitation of 1.25 Hz. The dominance of sinus-pulse induced slippage to the Ricker's response, is generated by the vast difference in the velocity time-histories.* ($a_C/a_H = 0.10$)

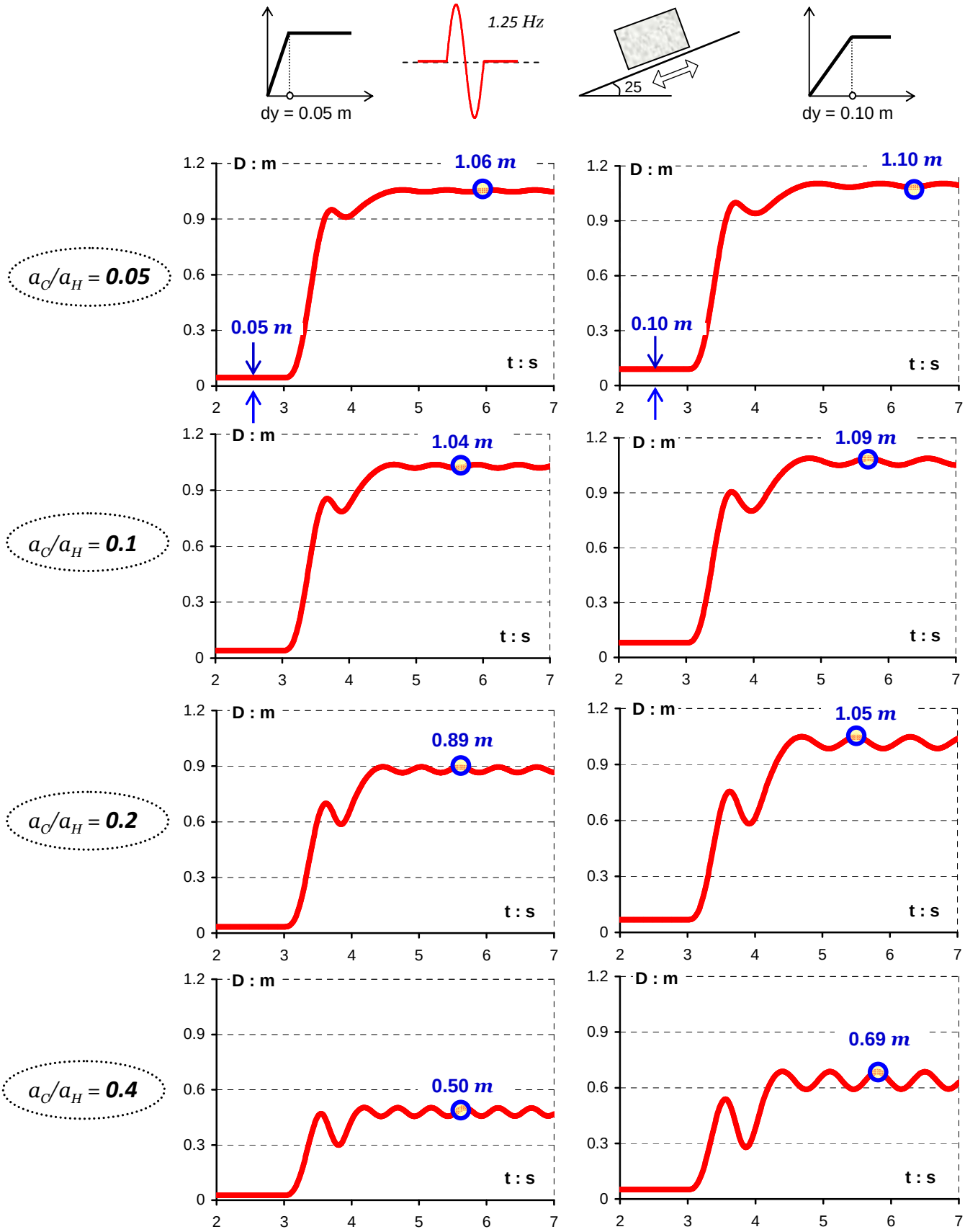

Figure 5.22 *Asymmetric sliding response for four acceleration ratios, a_C/a_H, at the left column for elasto-plastic yielding with dy = 0.05 m and at the right for dy = 0.1 m. The triggering excitation is the one-cycle sinus pulse of frequency 1.25 Hz. [$\beta = 25^o$]*

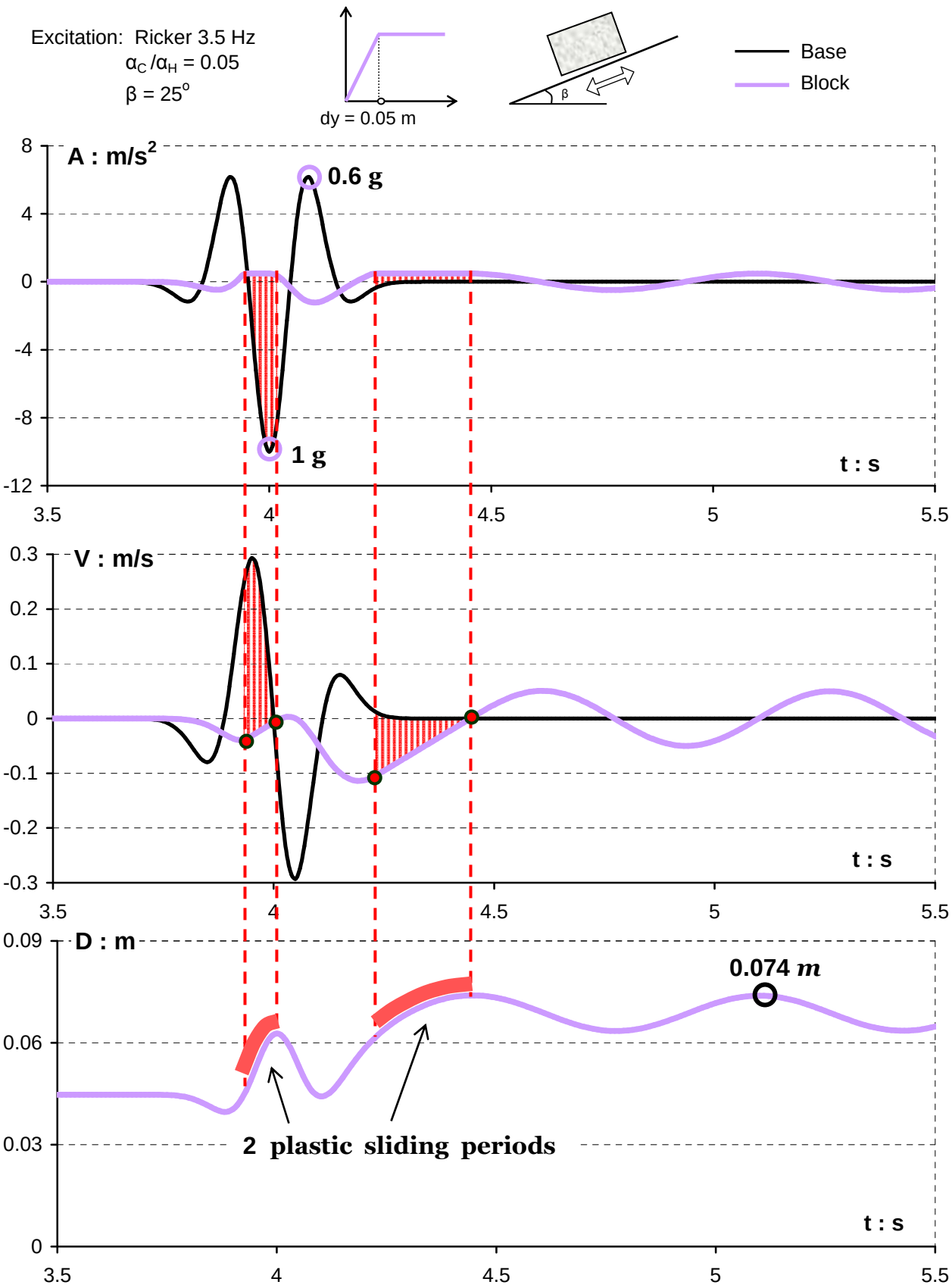

Figure 5.23 *Asymmetric response time histories of a rigid block resting on an 25^0 inclined plane when subjected to a Ricker pulse excitation of frequency 3.50 Hz. The green shaded area illustrates the two downward sliding events and with yellow the upward yielding phase. Block's elastic deformation is dy = 0.05 m. ($a_C/a_H = 0.05$)*

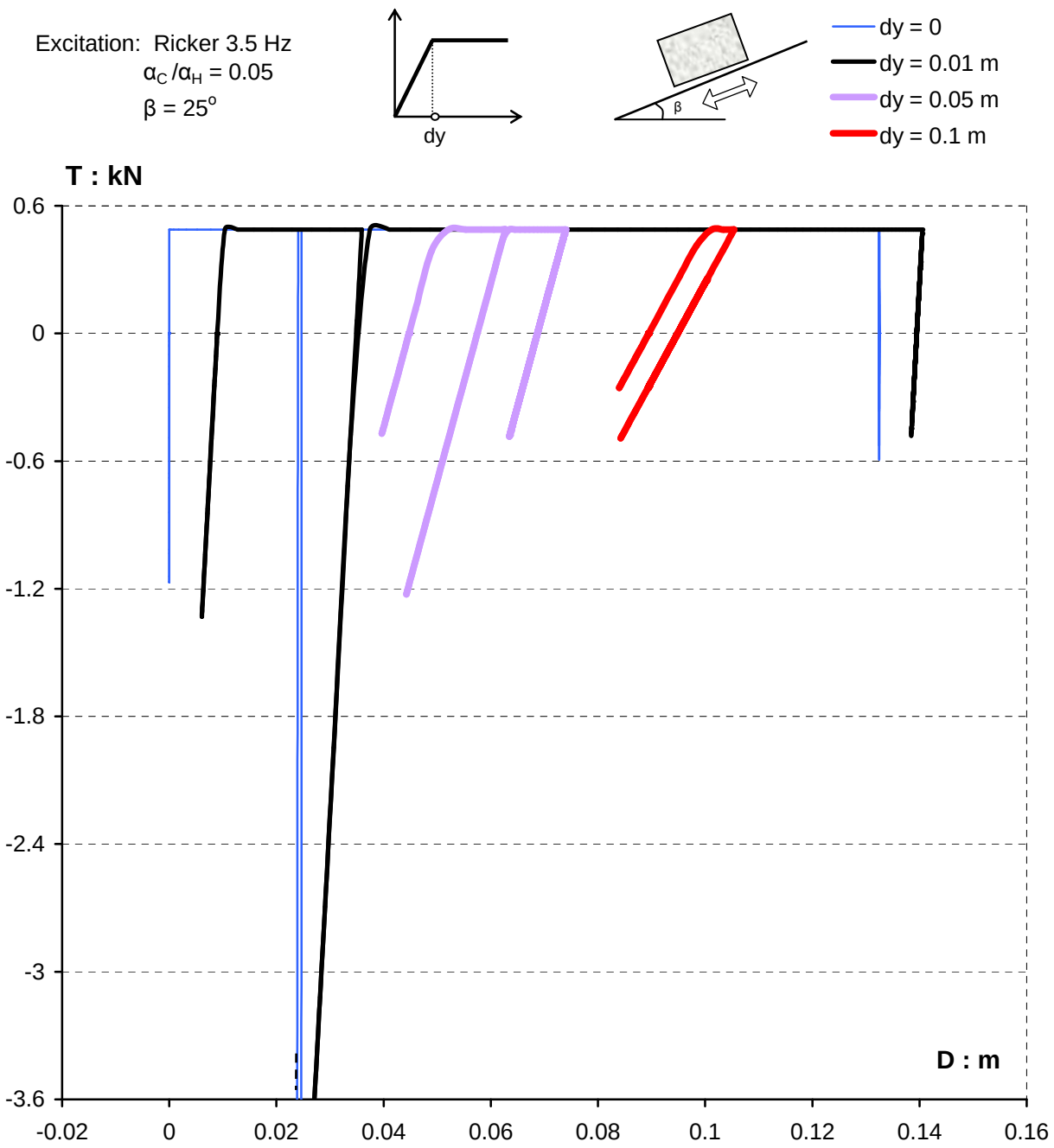

Figure 5.24 *Force-displacement response for the case of: an elasto-plastic sliding system with dy = 0.1 m, 0.05 m, 0.01 m and 0 m pictured with the red, purple, black and blue solid lines respectively [β = 25°, $a_C/a_H = 0.05$ and a Ricker excitation of 3.5 Hz frequency] . Notice that in this particular case as the elastic displacement dy increases, the plastic yielding reduces.*

Asymmetric Sliding on Exponential Related Frictional Interface

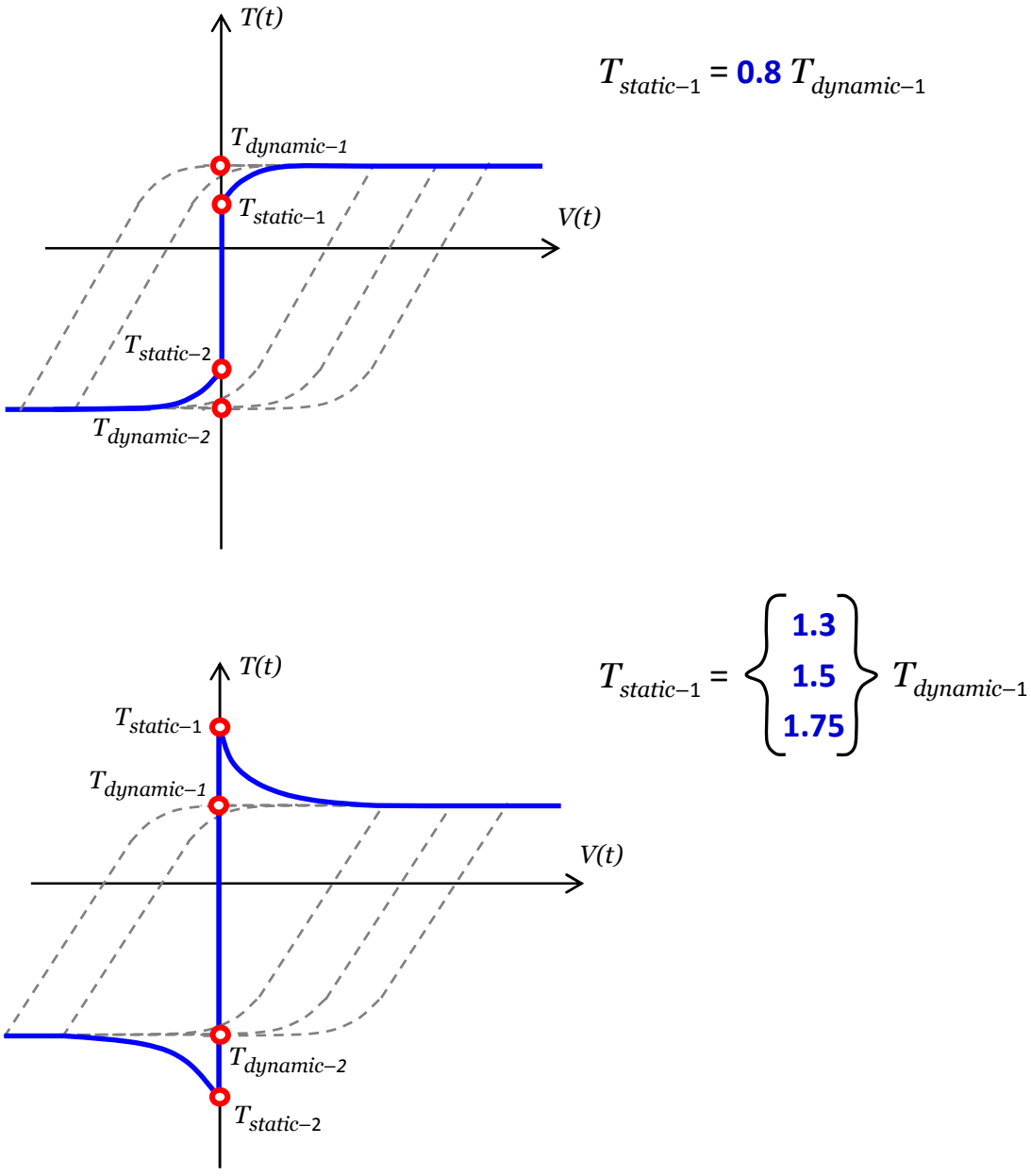

Figure 5.25 *The exponential friction law of the sliding interface is illustrated. The friction force during yielding, $T_{dynamic}$, can be larger (top plot) or smaller (bottom plot) than the initial static friction force, T_{static}.*

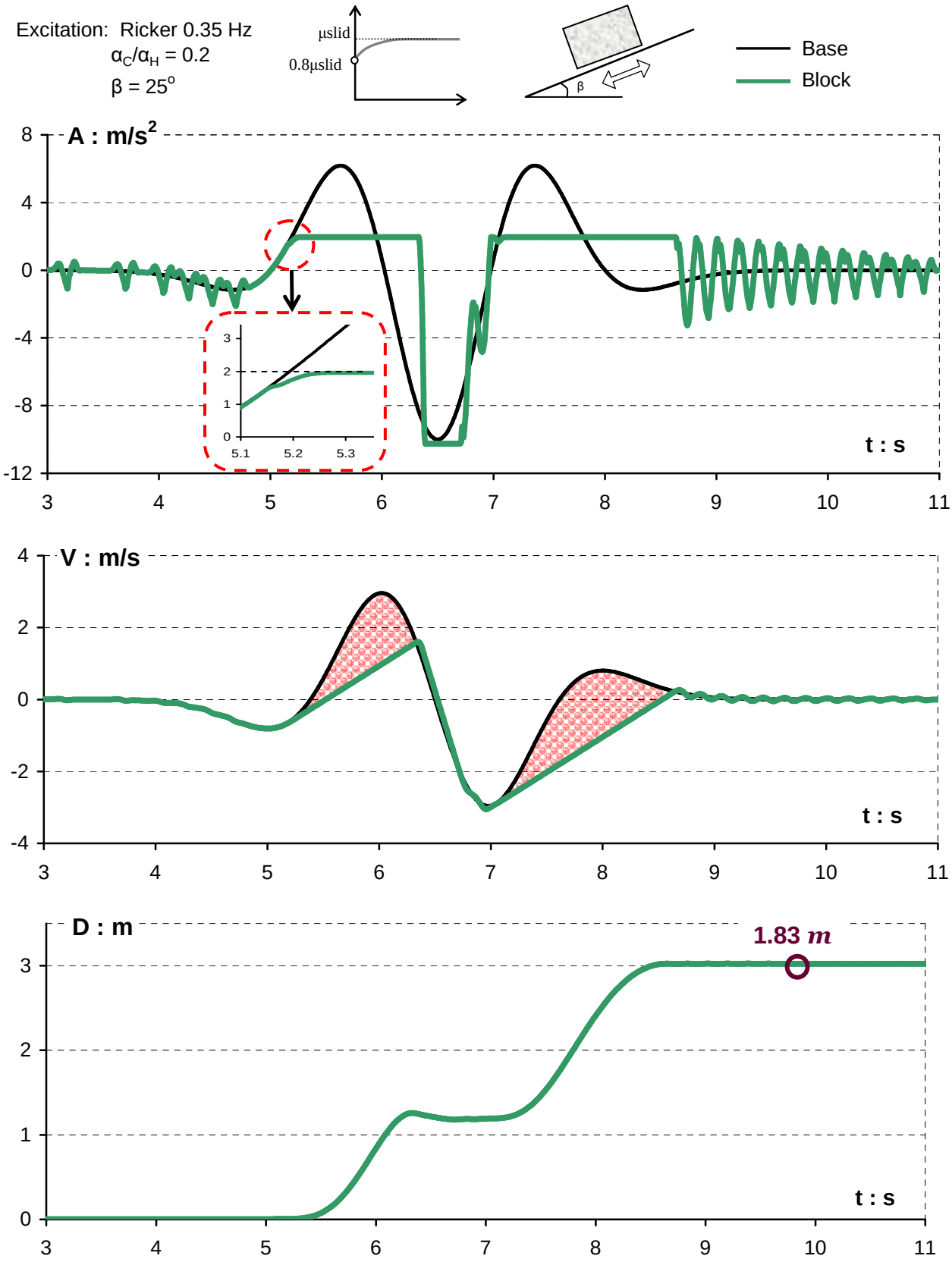

Figure 5.26 *Asymmetric response of a rigid block resting on an 25^0 inclined plane subjected to a Ricker wavelet of frequency 0.35 Hz. Yielding starts at a 20% lower friction value than the dynamic kinetic friction. ($a_C/a_H = 0.2$)*

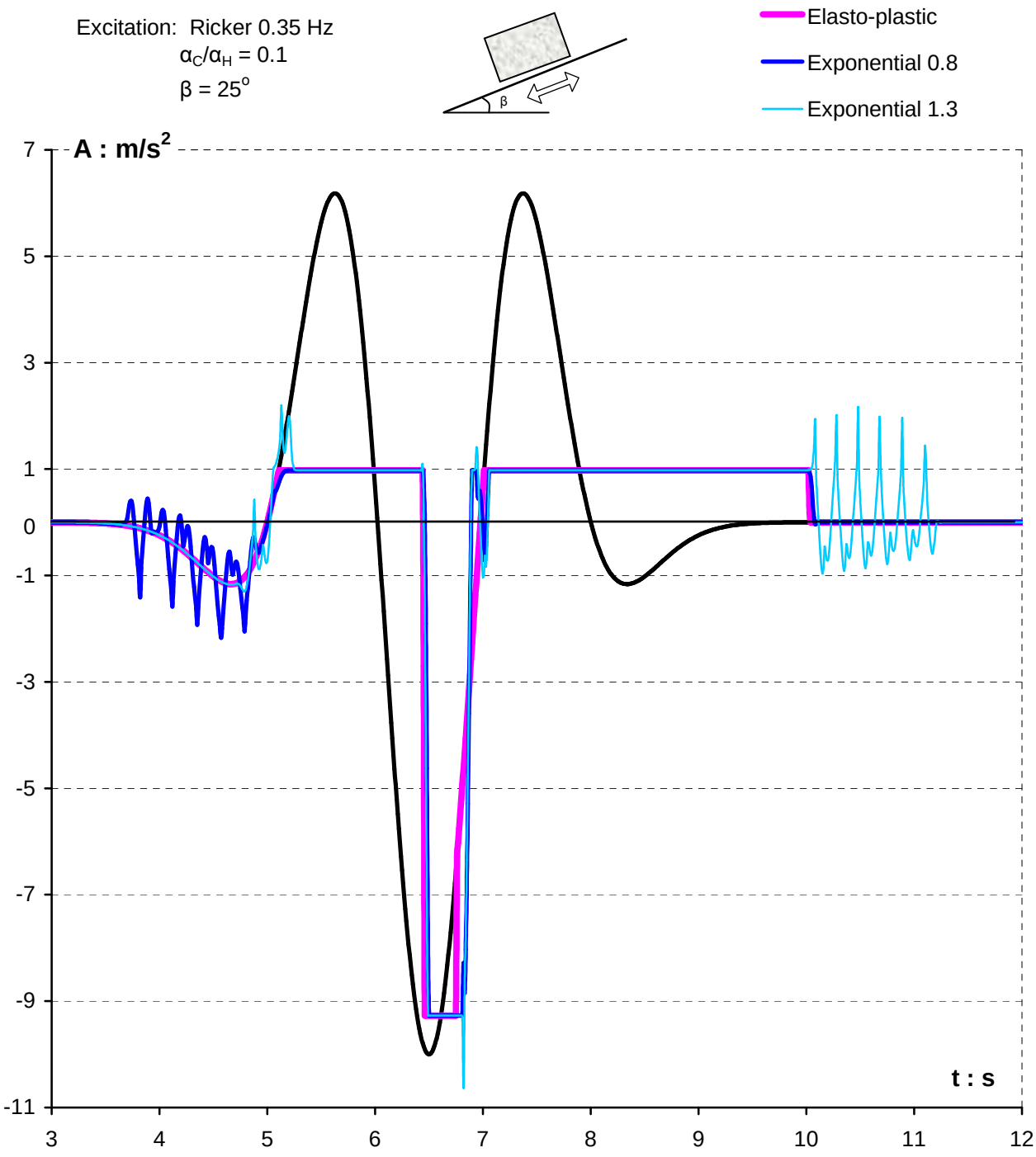

Figure 5.27 *Acceleration time histories of a block rested on a 25^0 inclined plane subjected to a Ricker wavelet of frequency 0.35 Hz. The solid pink line represents the block's response when sliding interface is governed by a perfectly-plastic friction law, whereas the blue and turquoise line corresponds to exponential related yielding with the initial static friction 0.8 times smaller and 1.3 times larger than the kinetic dynamic friction respectively. Observe that duration of sliding periods are almost the same in all three cases. (a_C /a_H = 0.1)*

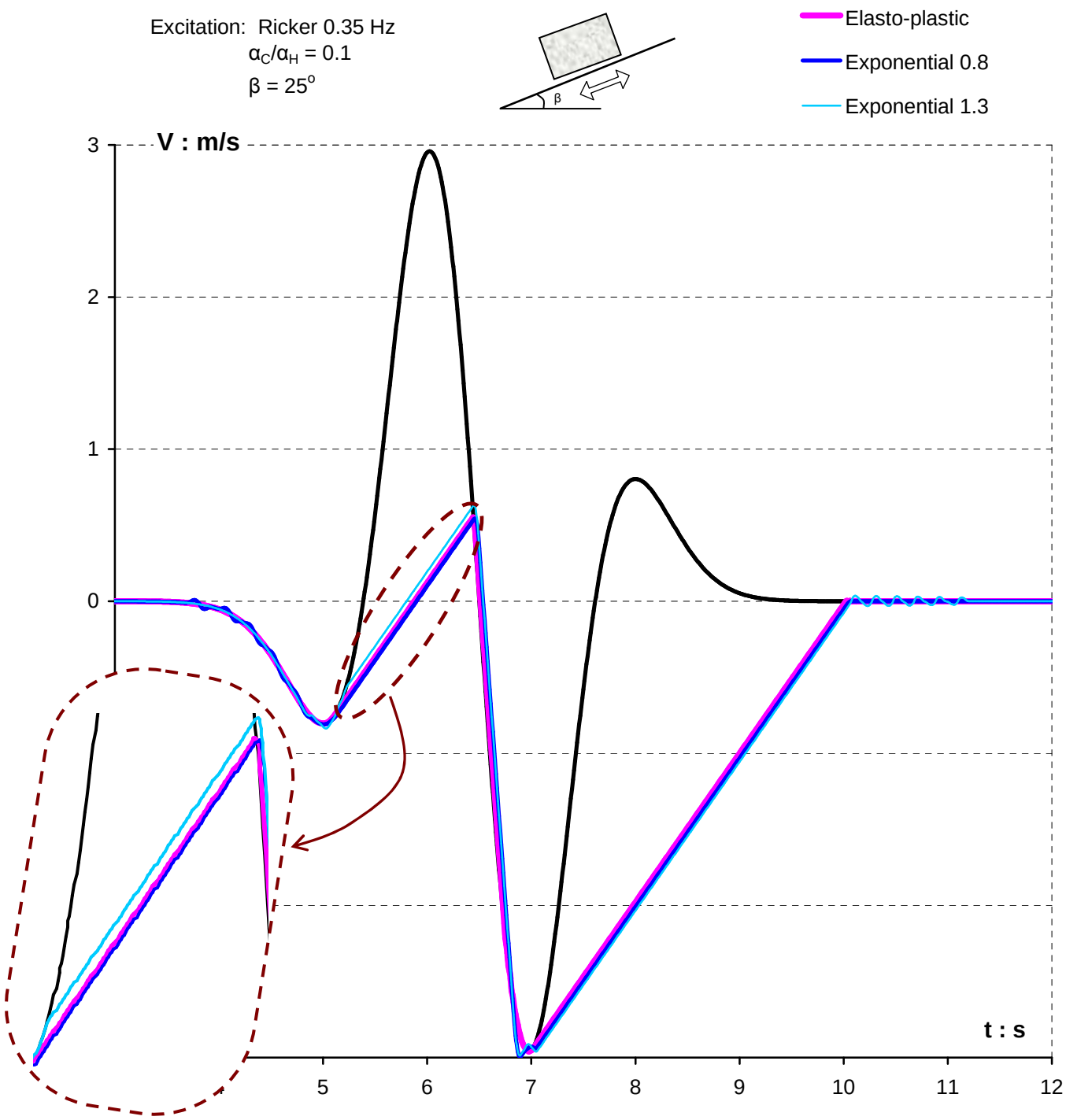

Figure 5.28 *Velocity time histories: the solid pink line represents the block's response when sliding interface is governed by a perfectly-plastic friction law, whereas the blue and turquoise line corresponds to exponential related yielding with the initial static friction 0.8 times smaller and 1.3 times larger than the kinetic dynamic friction respectively. Only one slight difference is noticed at the first sliding, as depicted at the magnified detail.* ($a_C / a_H = 0.1$)

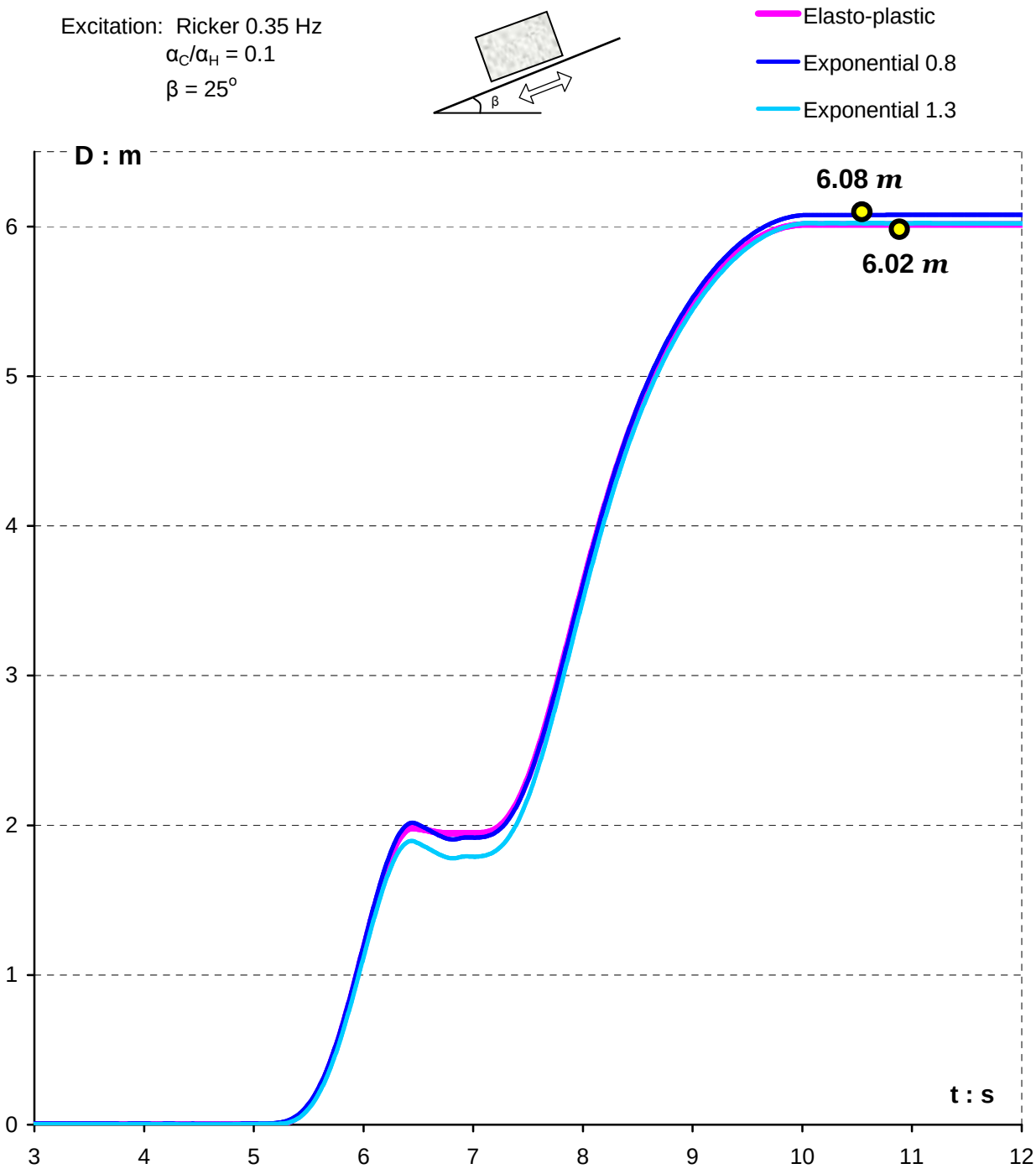

Figure 5.29 *Displacement time histories for perfectly-plastic and exponential related friction. The differences seems to be negligible. (a_C /a_H = 0.1)*

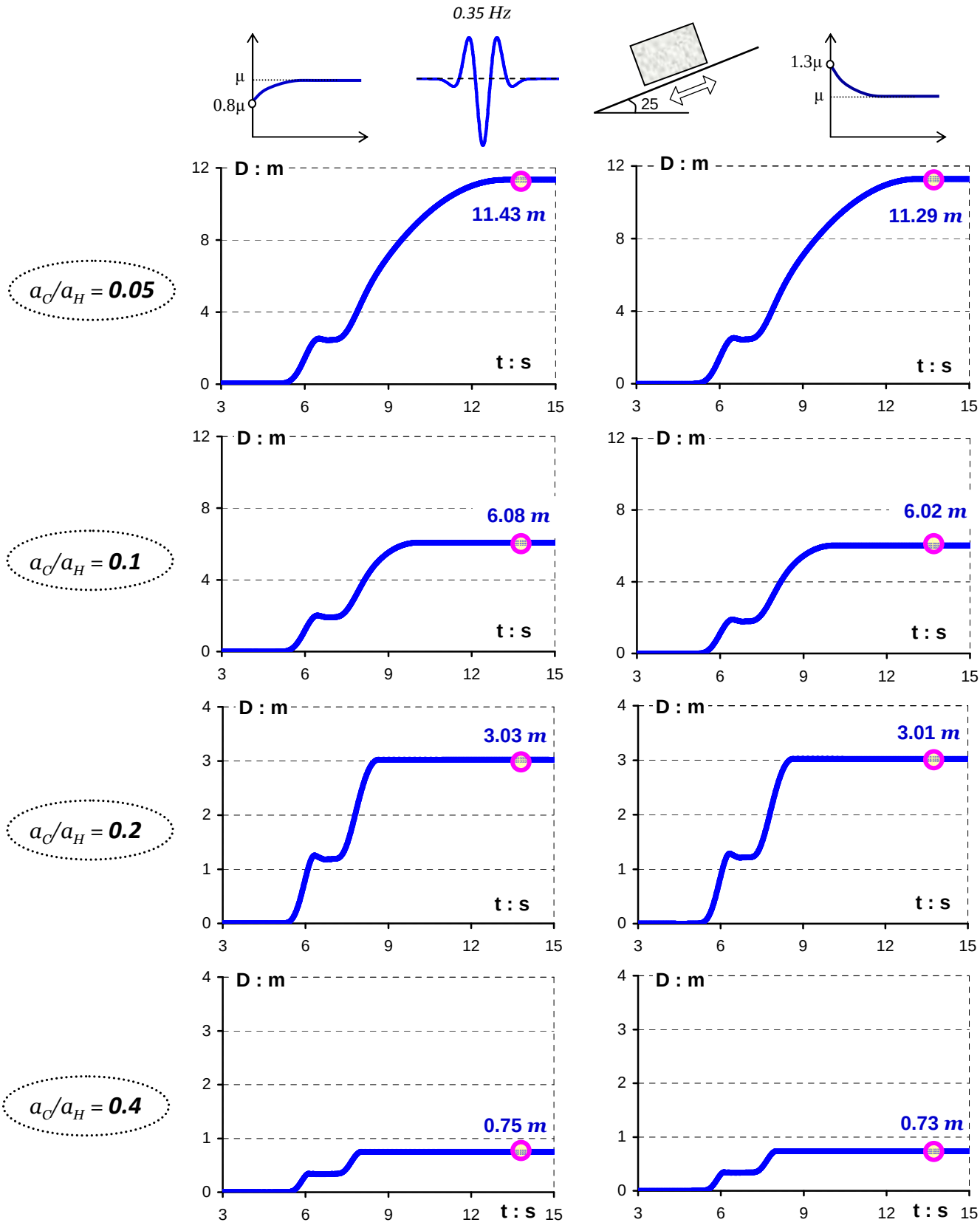

Figure 5.30 *Asymmetric sliding response for four acceleration ratios, a_C/a_H, at the left column for exponential yielding with $\mu_{static} = 0.8\,\mu_{dynamic}$ and at the right for $\mu_{static} = 1.3\,\mu_{dynamic}$. The triggering excitation is the Ricker pulse of frequency 0.35 Hz. [$\beta = 25^o$]*

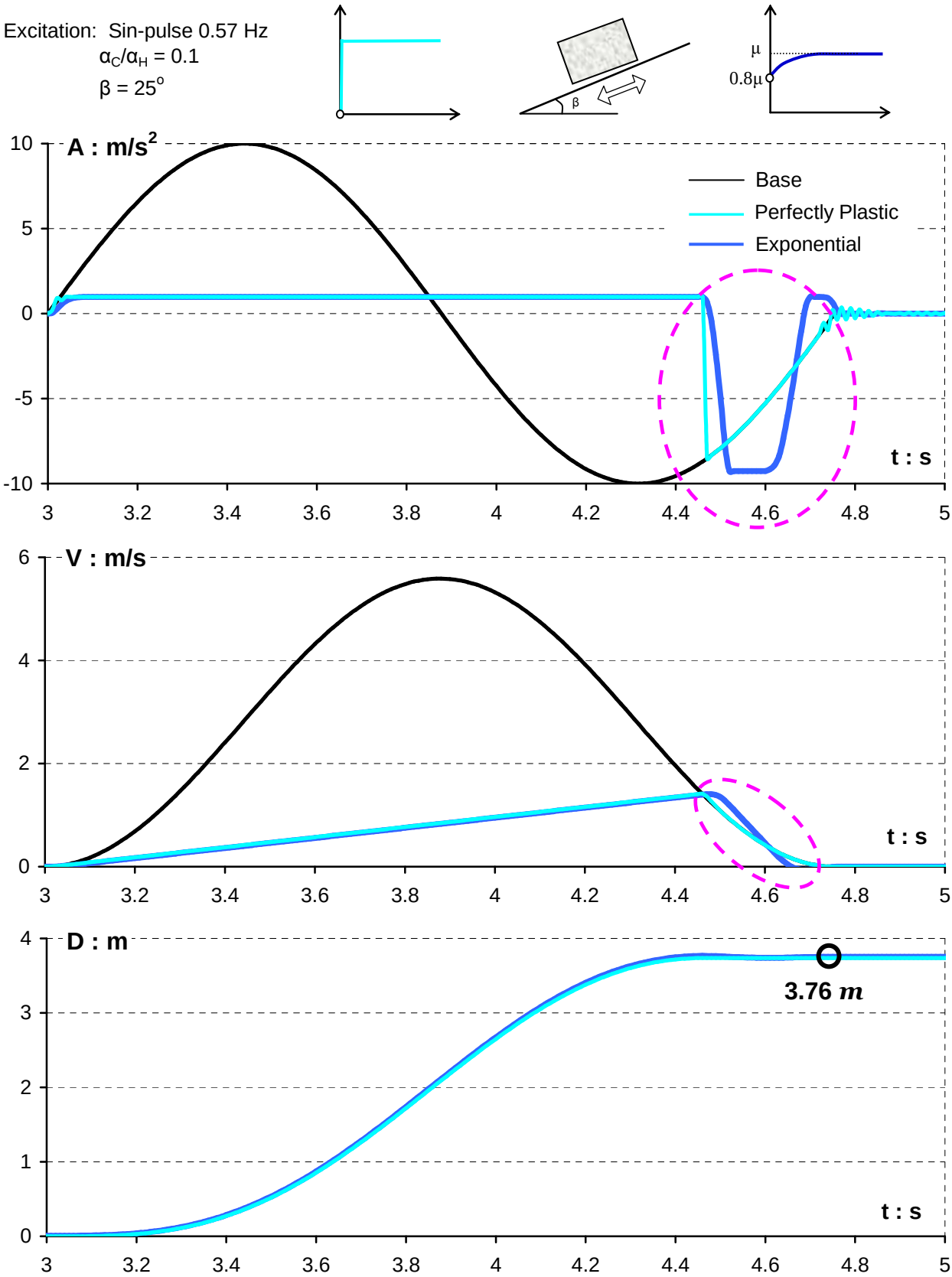

Figure 5.31 *Asymmetric response time histories of a rigid block resting on an 25^0 inclined plane when subjected to one cycle sinus pulse of frequency 0.57 Hz. The turquoise line presents the perfectly-plastic response; whereas the solid blue line corresponds to exponential friction with $\mu_{dynamic} = 0.8\mu_{static}$. The only difference between the two systems is the upward sliding period. ($a_C/a_H = 0.1$)*

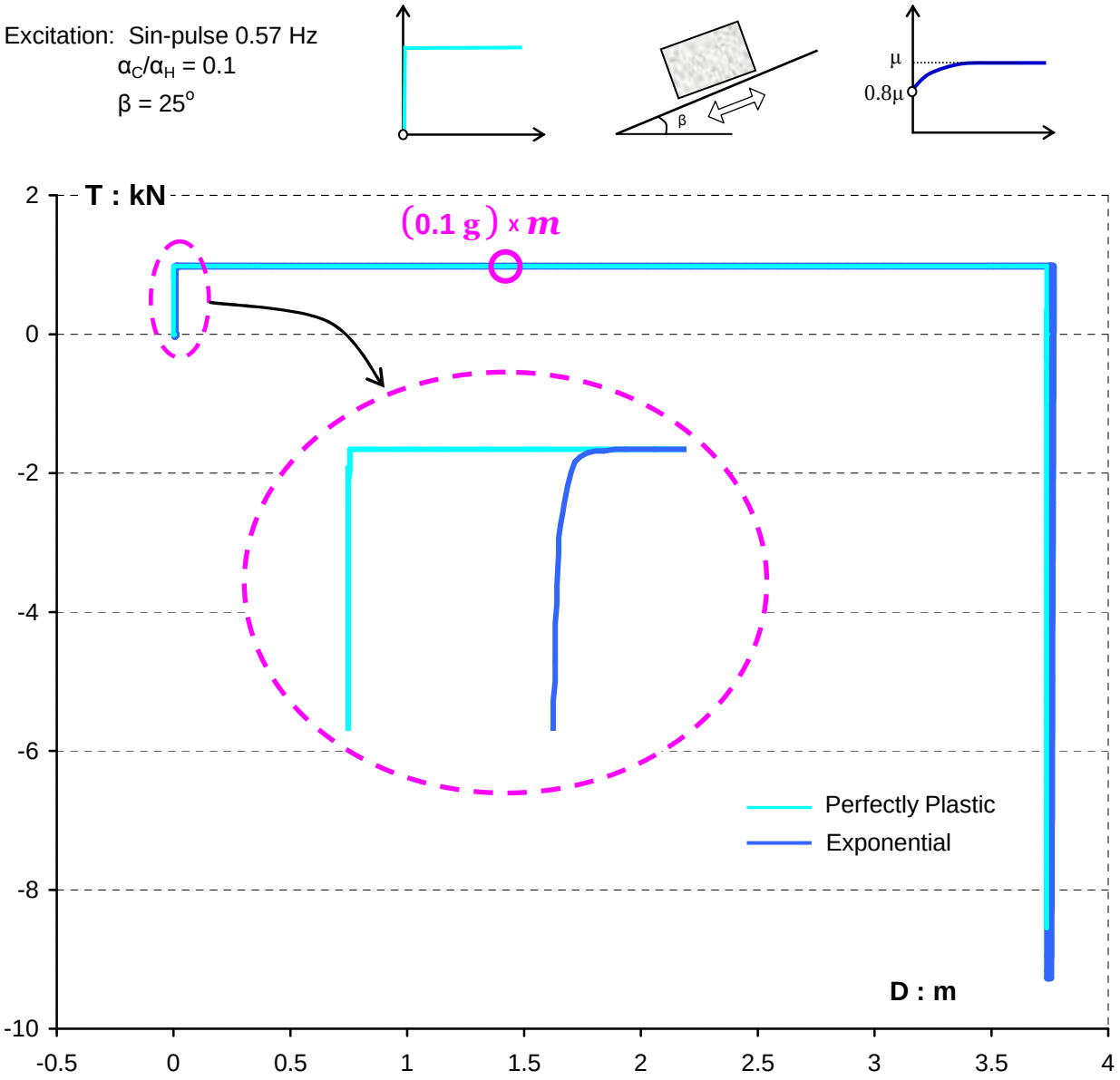

Figure 5.32 *Force-displacement response for a perfectly-plastic sliding system illustrated with the turquoise solid line. Also the solid blue line pictures the friction-displacement response of a system with exponential related yielding law. [β = 25°, a_C /a_H = 0.1 and an one-cycle sinus pulse of 0.57 Hz frequency].*

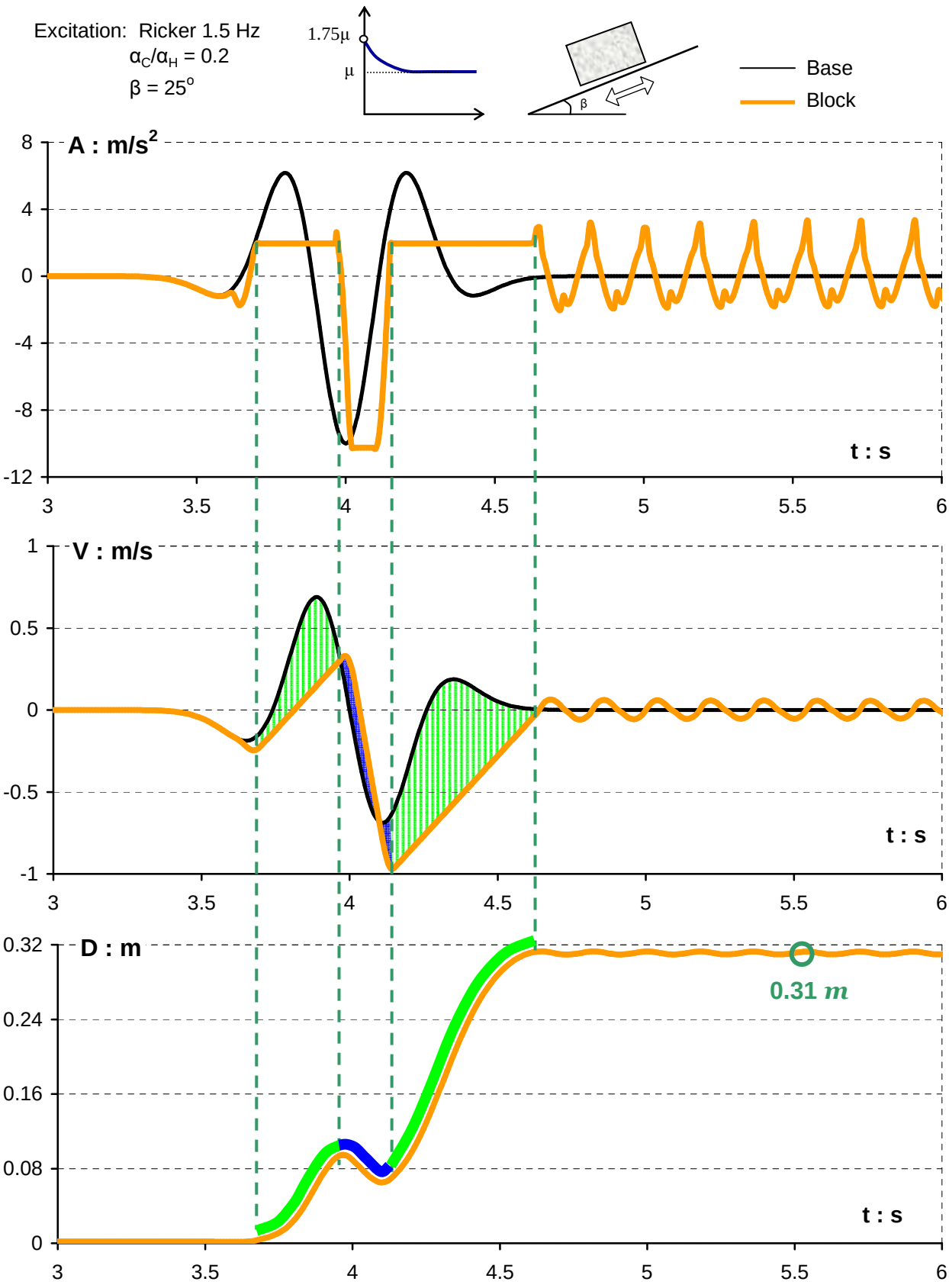

Figure 5.33 *Asymmetric response of a rigid block resting on an 25^0 inclined plane subjected to a Ricker wavelet of frequency 1.5 Hz. Yielding starts at a 75% higher friction value than the dynamic kinetic friction. ($a_C / a_H = 0.2$)*

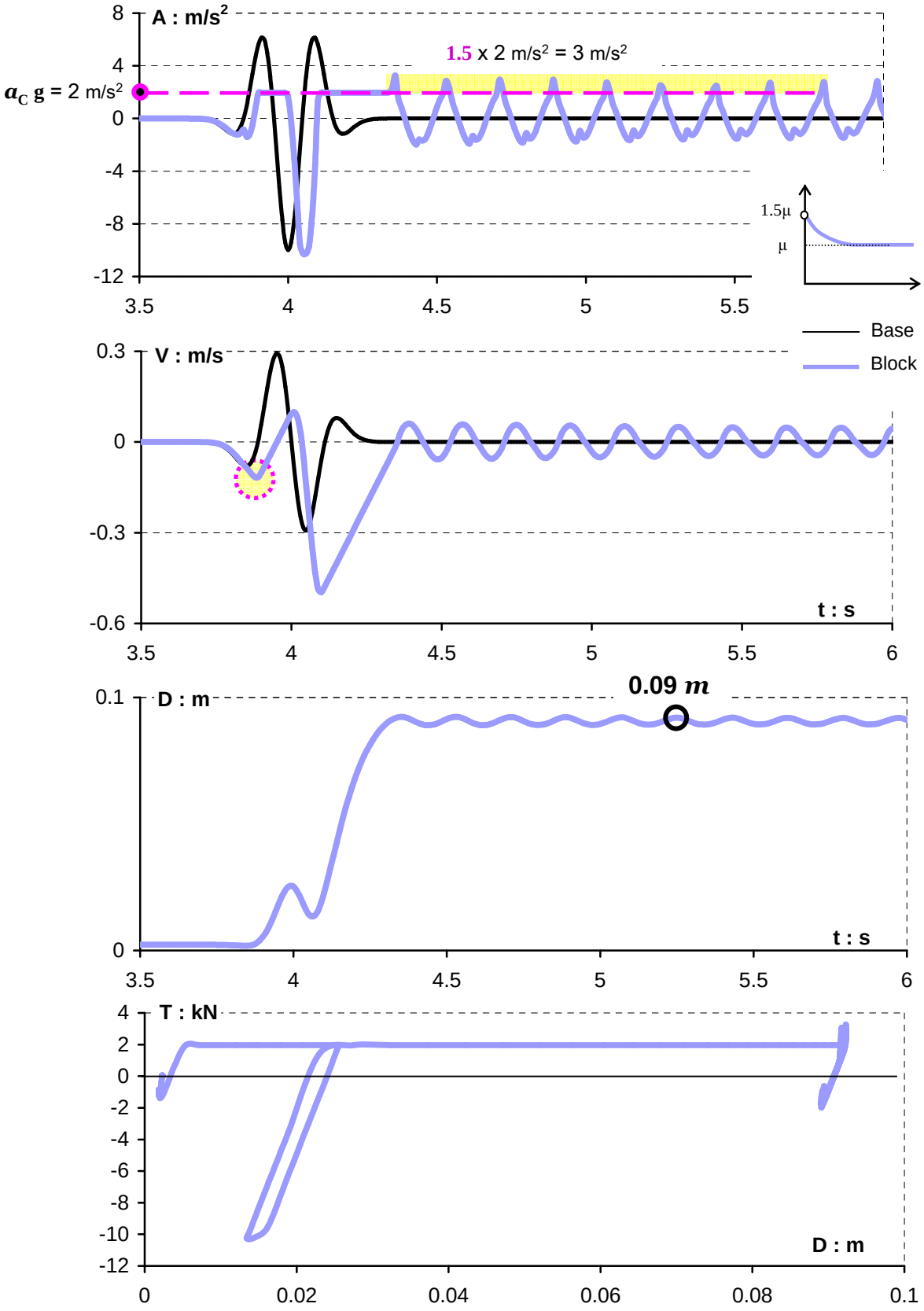

Figure 5.34 *Asymmetric response of a rigid block resting on an 25^0 inclined plane subjected to a Ricker wavelet of frequency 3.5 Hz. Yielding starts at a 50% higher friction value than the dynamic kinetic friction. ($a_C / a_H = 0.2$)*

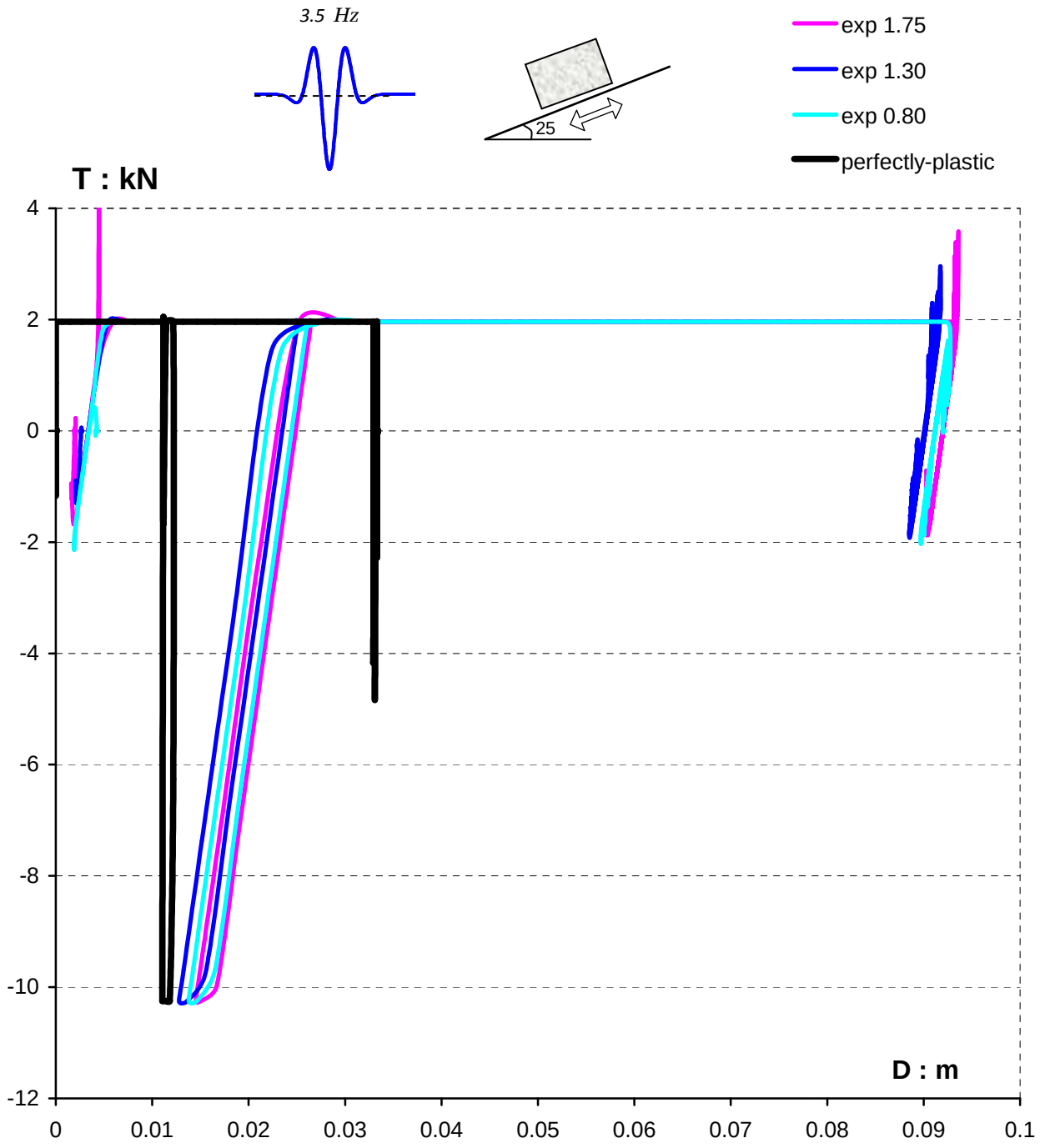

Figure 5.35 *Force-displacement response for the case of: an perfectly-plastic friction sliding system pictured with the bold black line. When the yielding interface is governed by exponential friction with* $\mu_{static} = 0.8\,\mu_{dynamic}$ *the displacement-force loop is illustrated with turquoise line. The pink and the blue lines correspond to* $\mu_{static} = 1.75\,\mu_{dynamic}$ *and* $\mu_{static} = 1.30\,\mu_{dynamic}$ *respectively [*$\beta = 25^{o}$, $a_C / a_H = 0.2$ *and a Ricker excitation of 3.5 Hz frequency] .*

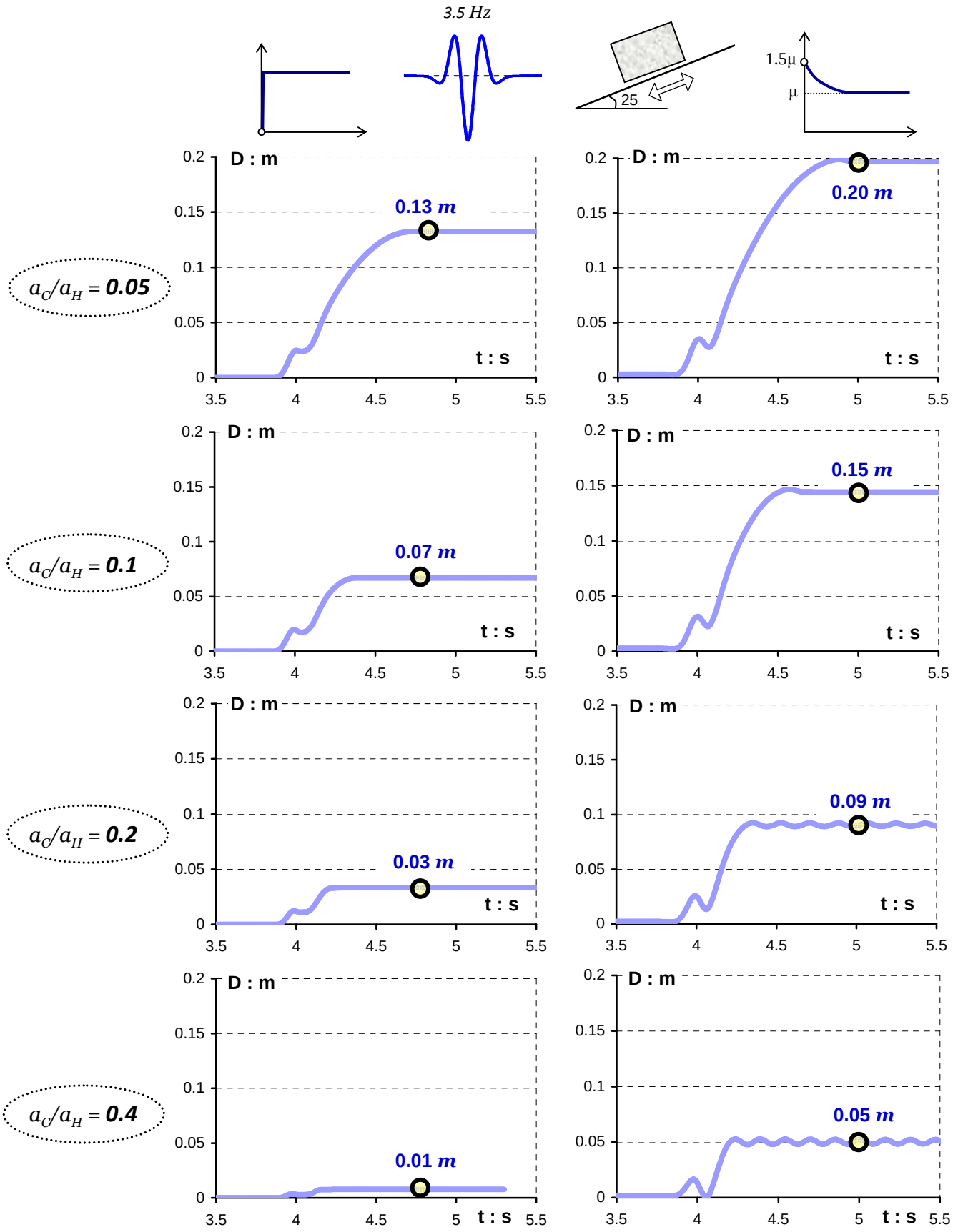

Figure 5.36 *Asymmetric sliding response for four acceleration ratios, a_C/a_H, at the left column for perfectly-plastic friction and at the right for exponential yielding with μ_{static} = 1.5 $\mu_{dynamic}$. The triggering excitation is the Ricker pulse of frequency 3.5 Hz. [$\beta = 25^o$]*

Excitation:
Earthquake Records

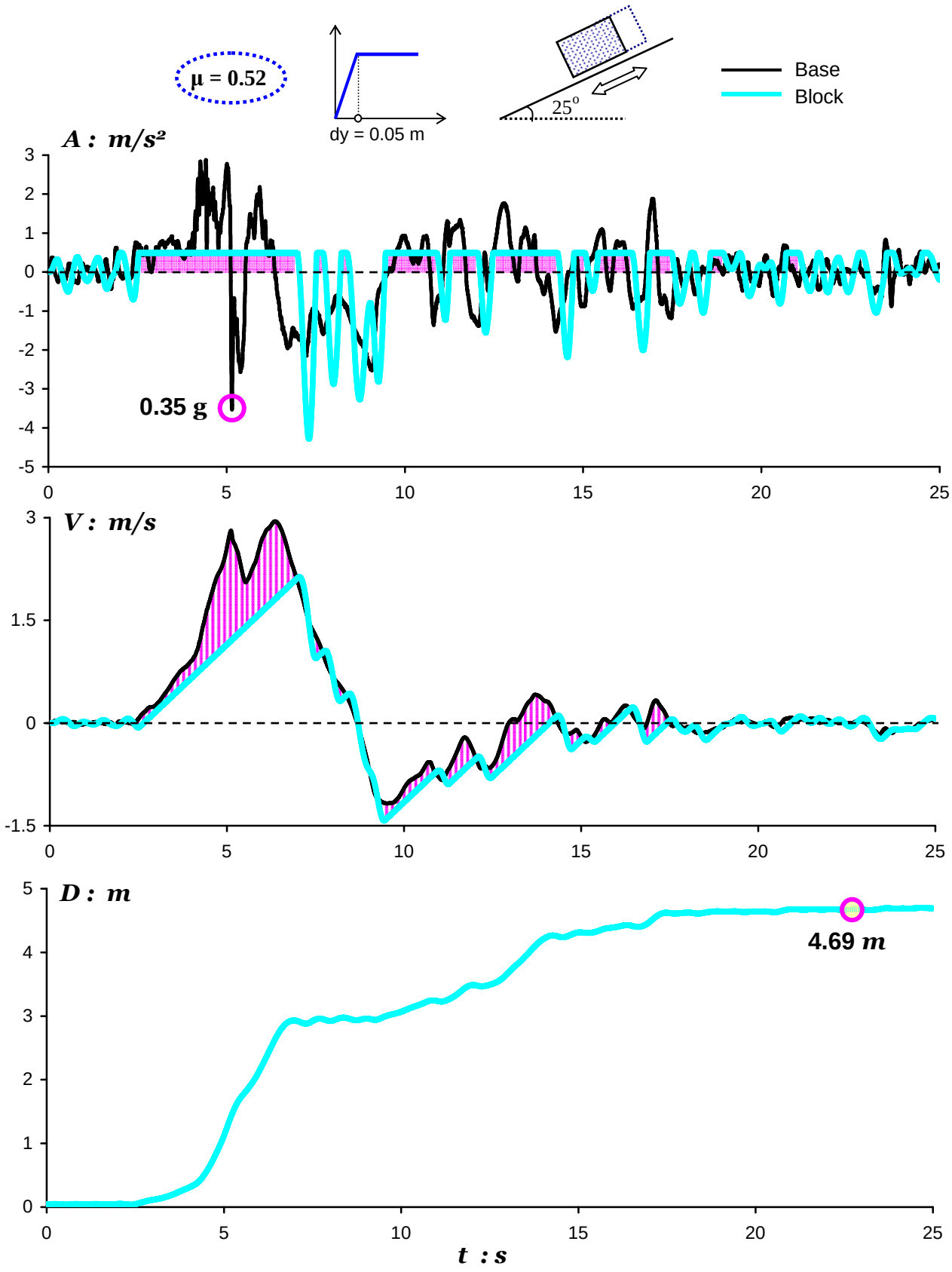

Figure 5.37 *Asymmetric response time histories of a rigid block resting on an 25^0 inclined plane when subjected to the normal polarity TCU 068-NS. Block's elastic deformation is dy = 0.05 m. (friction coefficient μ = 0.52)*

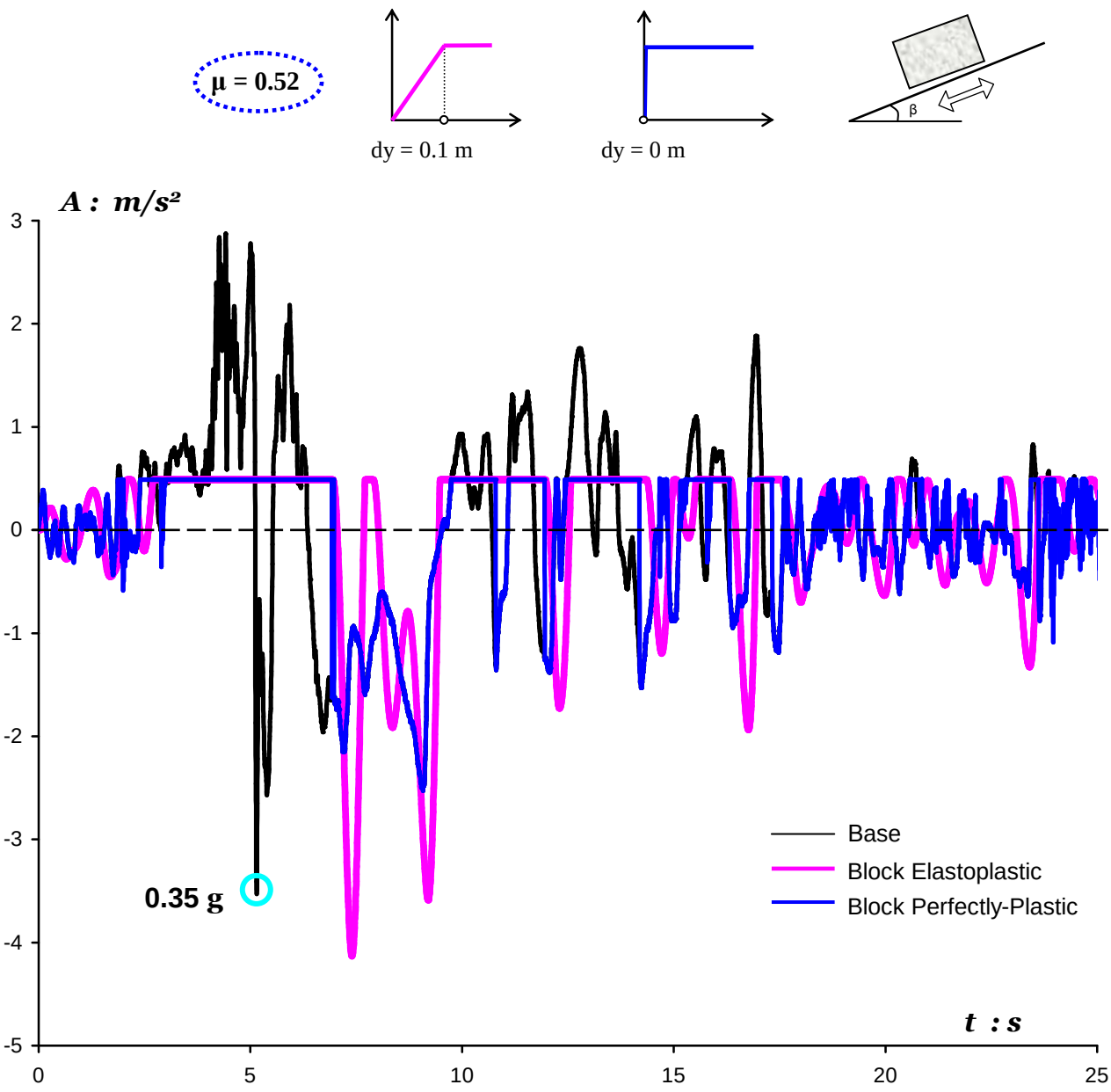

Figure 5.38 *Acceleration time histories of a block rested on a 25^0 inclined plane subjected to the normal polarity TCU 068-NS. The blue line represents the block's response when sliding interface is governed by a perfectly-plastic friction law, whereas the solid pink line corresponds to elasto-plastic yielding with dy = 0.1 m. (friction coefficient μ = 0.52)*

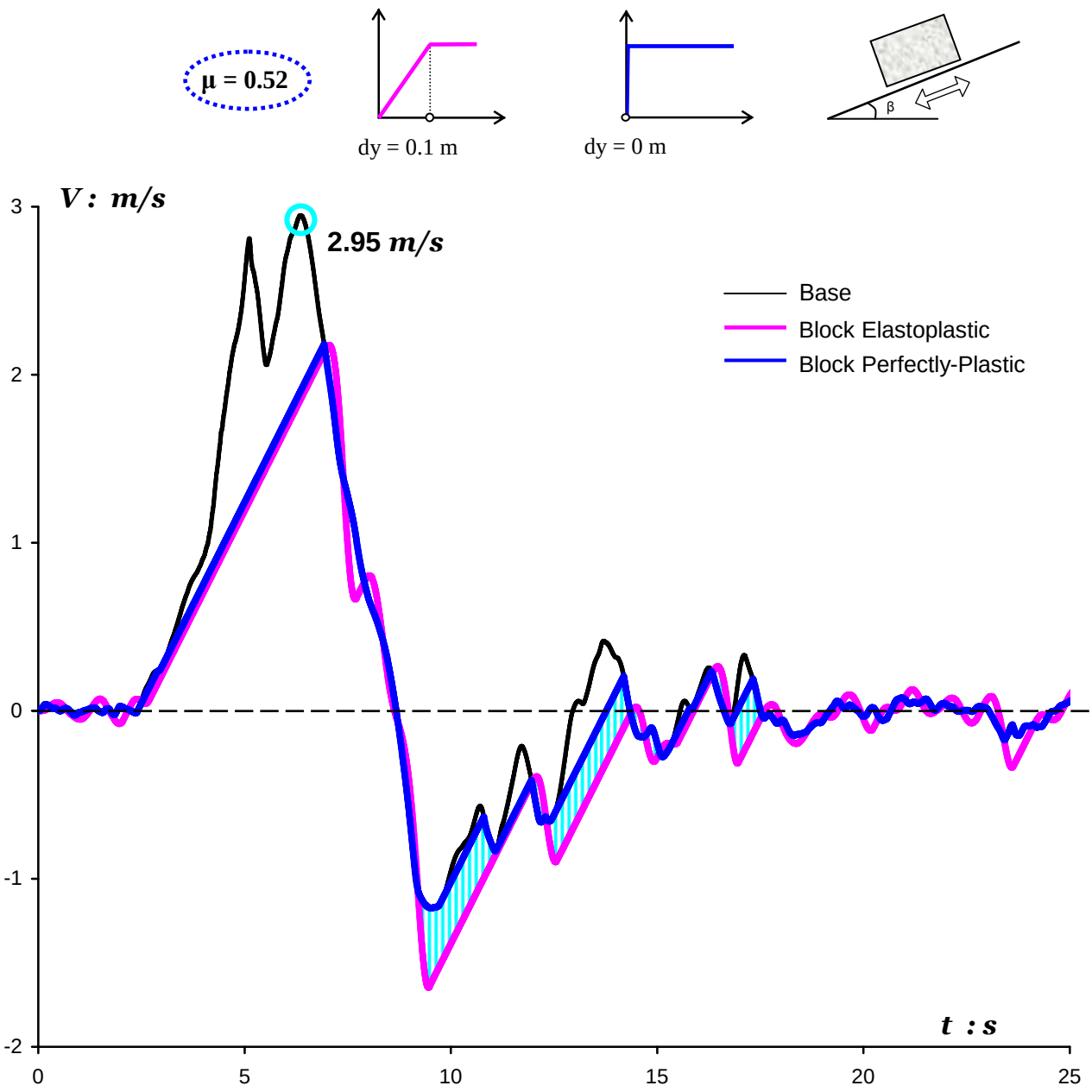

Figure 5.39 *Velocity time histories of a block rested on a 25^0 inclined plane subjected to the normal polarity TCU 068-NS. The turquoise shaded areas shows the yielding displacement difference between the perfectly-plastic and the elasto-plastic response. The blue line represents the block's response when sliding interface is governed by a perfectly-plastic friction law, whereas the solid pink line corresponds to elasto-plastic yielding with dy = 0.1 m. (friction coefficient μ = 0.52)*

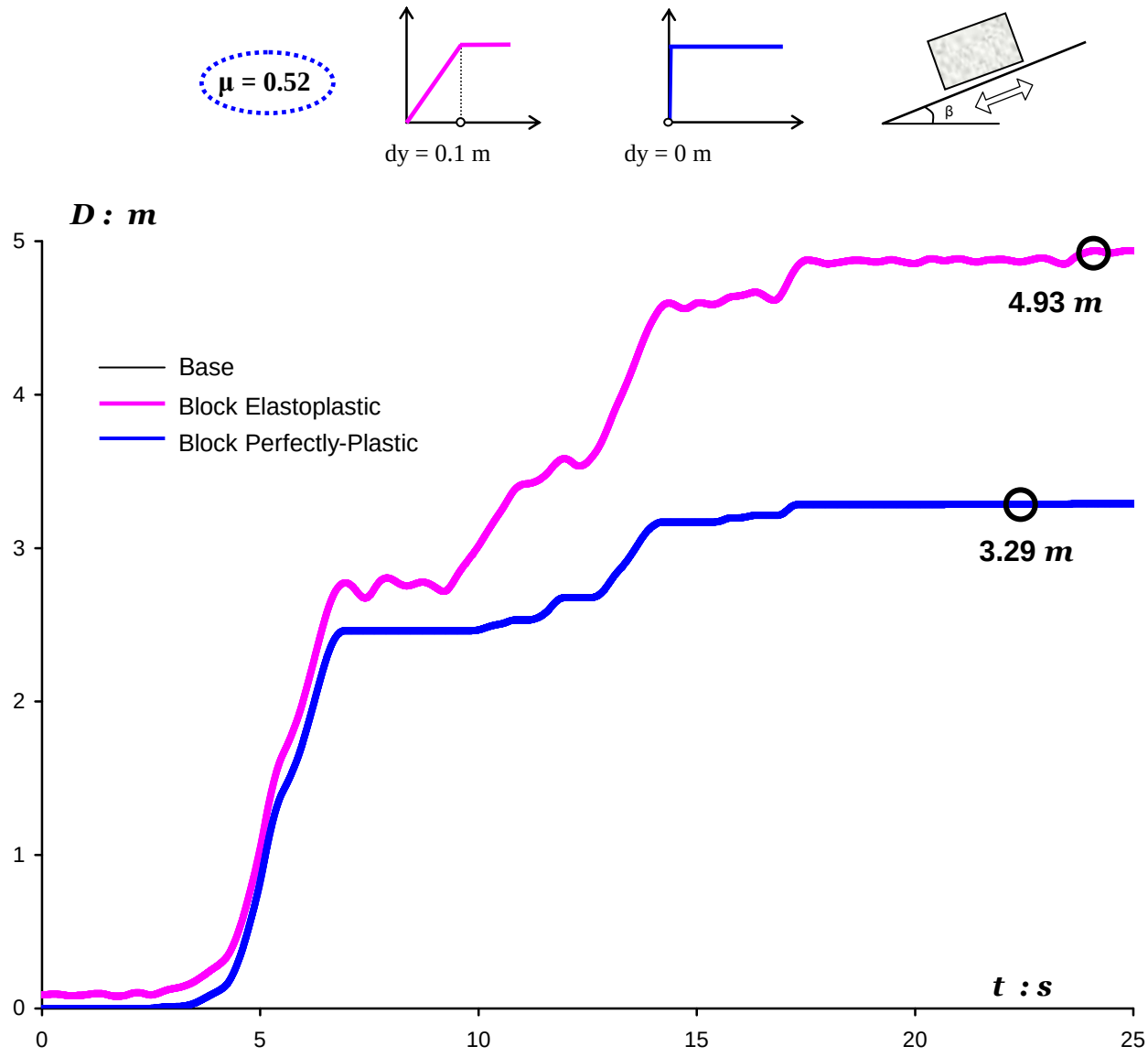

Figure 5.40 *Displacement time histories of a block rested on a 25^0 inclined plane subjected to the normal polarity TCU 068-NS. The elasto-plastic response with the pink solid line is 50% greater than the perfectly-plastic response with the blue line. (friction coefficient μ = 0.52)*

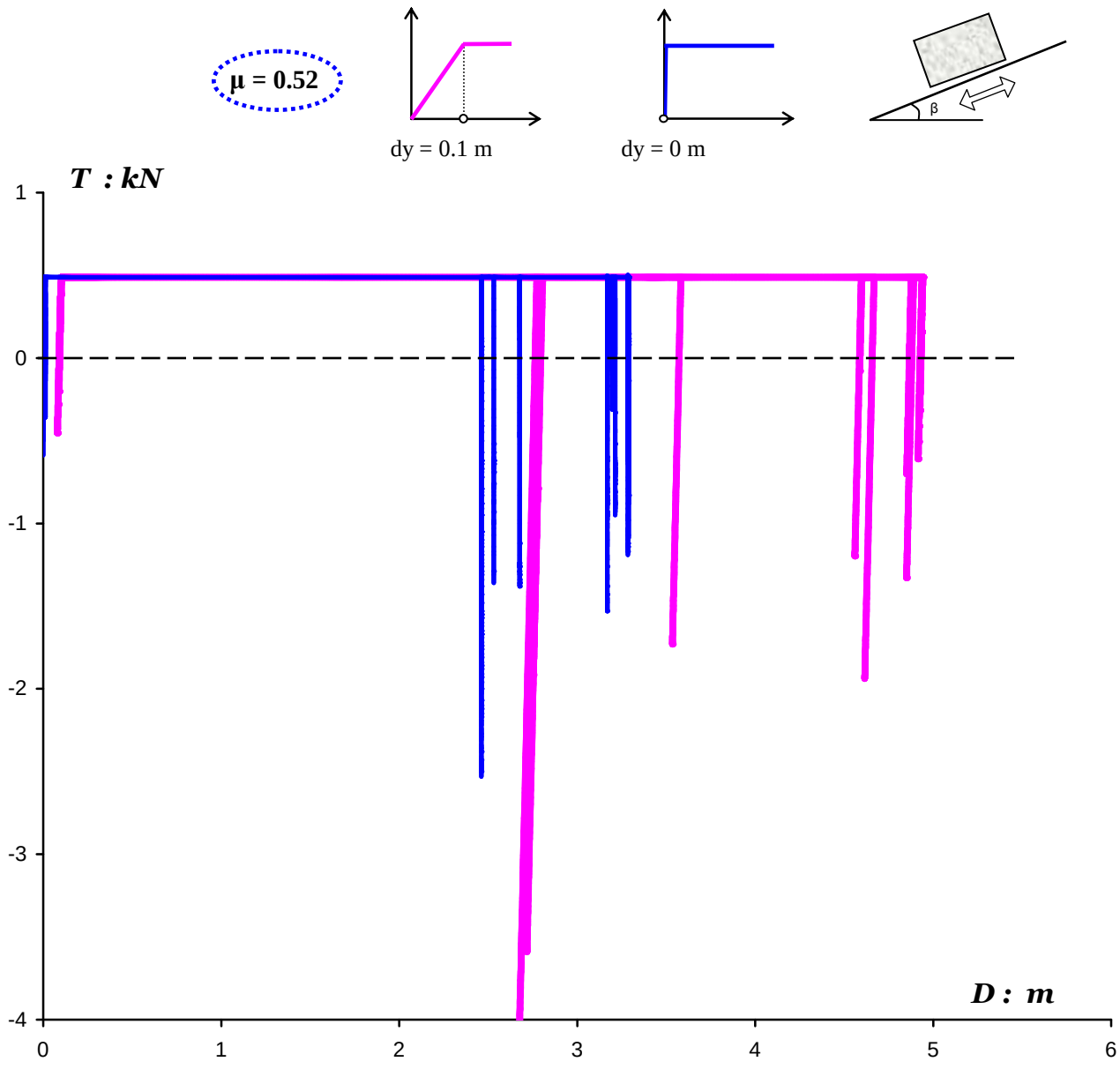

Figure 5.41 *Force-displacement response of a block rested on a 25^0 inclined plane subjected to the normal polarity TCU 068-NS. The blue line represents the block's response when sliding interface is governed by a perfectly-plastic friction law, whereas the solid pink line corresponds to elasto-plastic yielding with dy = 0.1 m. (friction coefficient μ = 0.52)*

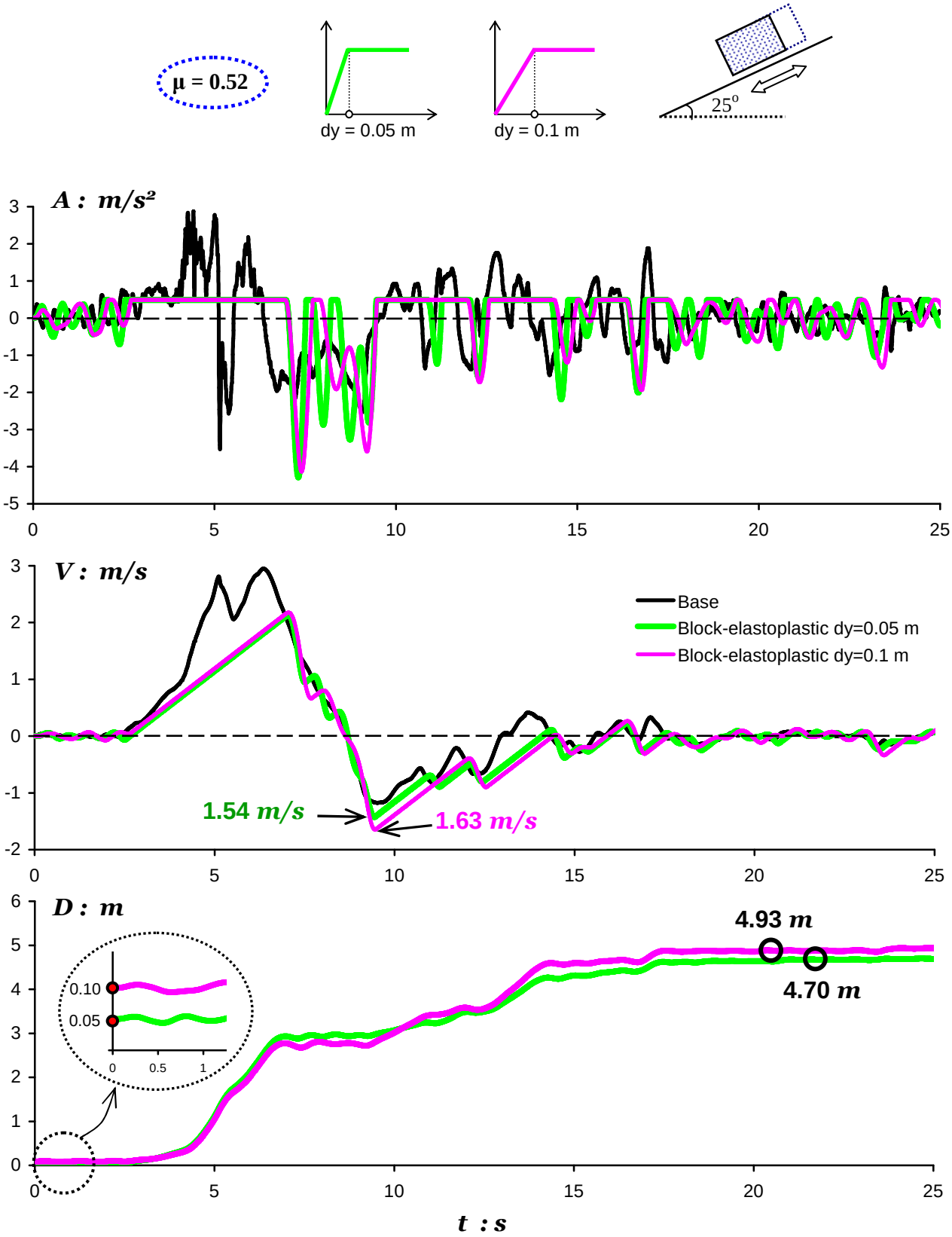

Figure 5.42 *Asymmetric response time histories of a rigid block resting on an 25^0 inclined plane when subjected to the normal polarity TCU 068-NS. The light green line presents the elasto-plastic response with dy = 0.05 m; whereas the solid pink line corresponds to dy = 0.1 m. (friction coefficient μ = 0.52)*

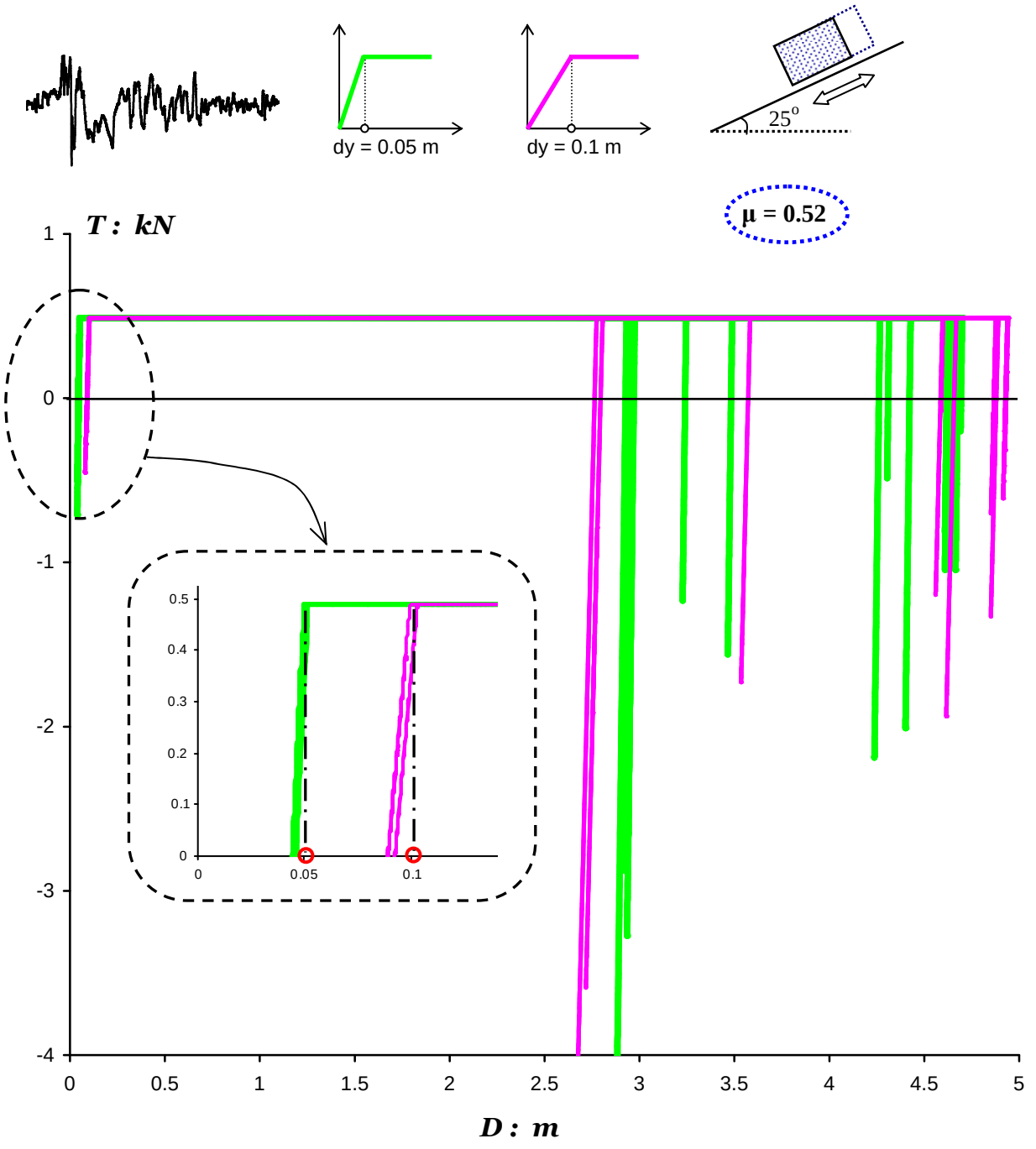

Figure 5.43 *Force-displacement response for an elasto-plastic sliding system with dy = 0.1 m, and 0.05 m illustrated with the light green and pink solid lines respectively [β = 25°, friction coefficient μ = 0.52, normal polarity TCU 068-NS]. Notice that in this particular case as the elastic displacement dy increases, the plastic yielding becomes greater too.*

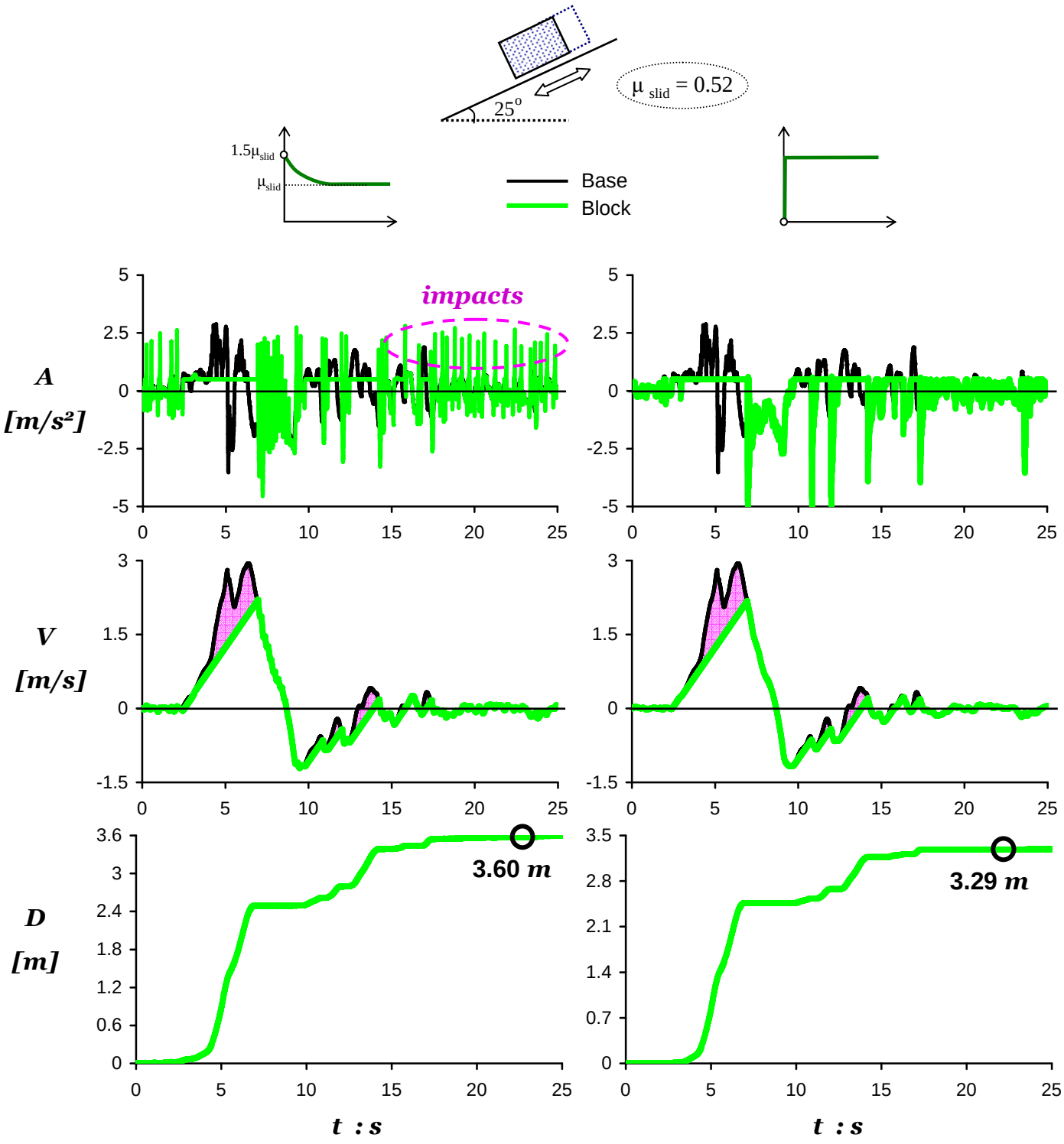

Figure 5.44 *Response time-histories for a perfectly-plastic sliding system on the right column and for an exponentially decreasing friction system on the left [β = 25°, friction coefficient μ_{slid} = 0.52, normal polarity TCU 068-NS]. Notice the small effect of the sliding constitutive law in the particular case.*

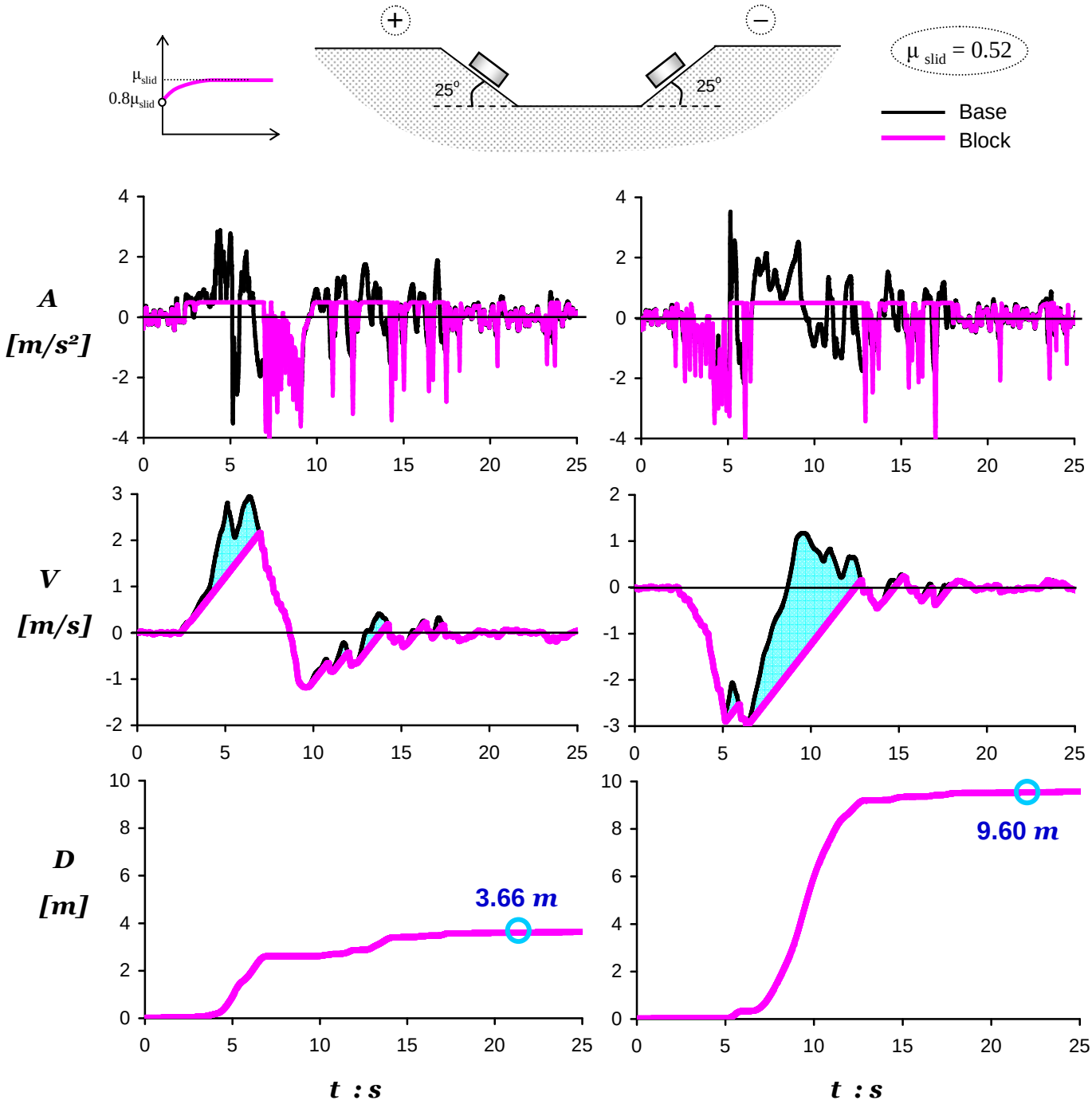

Figure 5.45 *Polarity effect of the TCU 068-NS for a yielding system with exponential friction $\mu_{dynamic} = 0.8\mu_{static}$. By definition, $\mu_{dynamic} = \mu_{slid}$. [$\beta = 25^o$, friction coefficient $\mu_{slid} = 0.52$].*

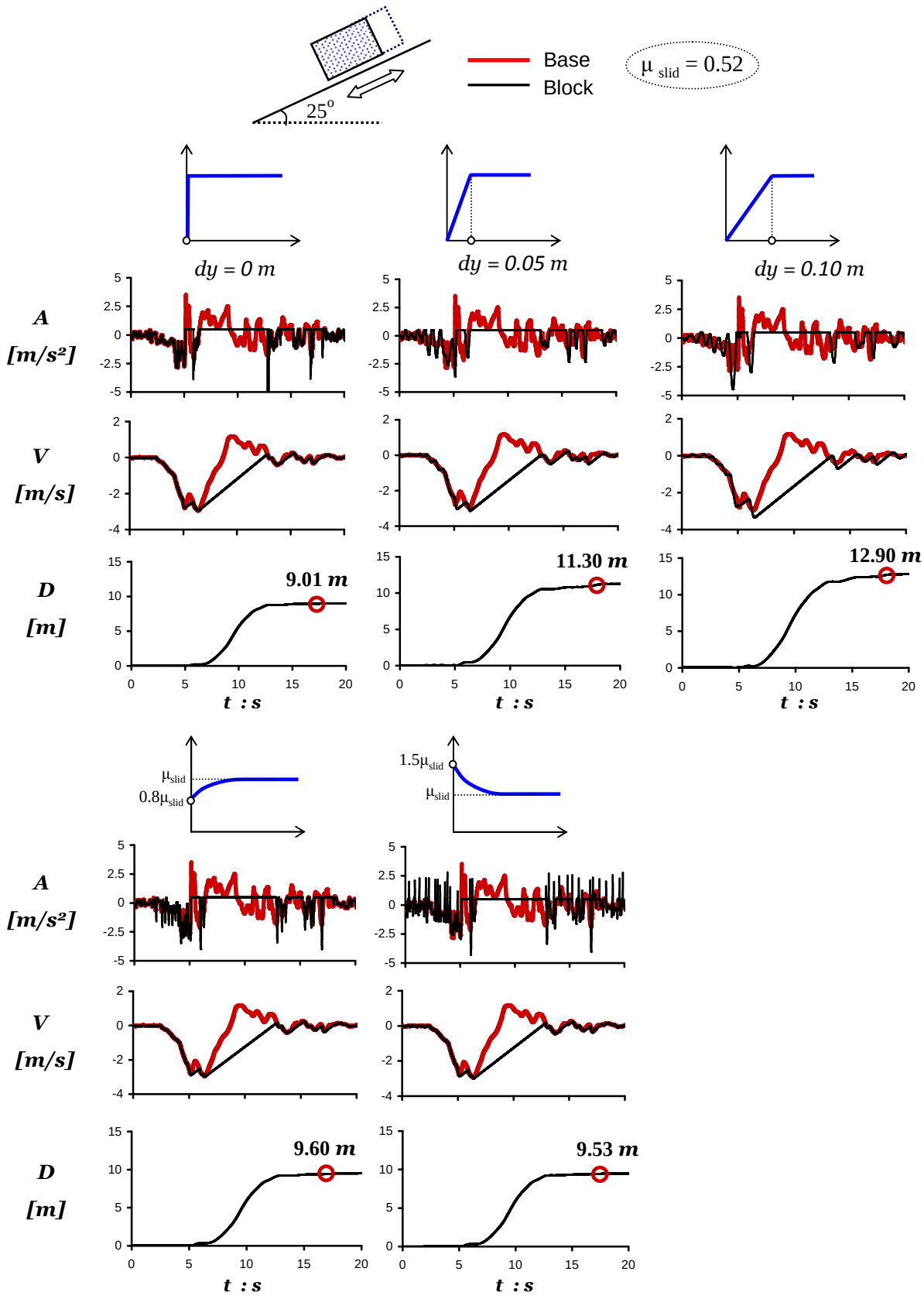

Figure 5.46 *Response time-histories for the five constitutive frictional laws of the yielding interface [β = 25°, friction coefficient μ = 0.52, reversed polarity TCU 068-NS].*

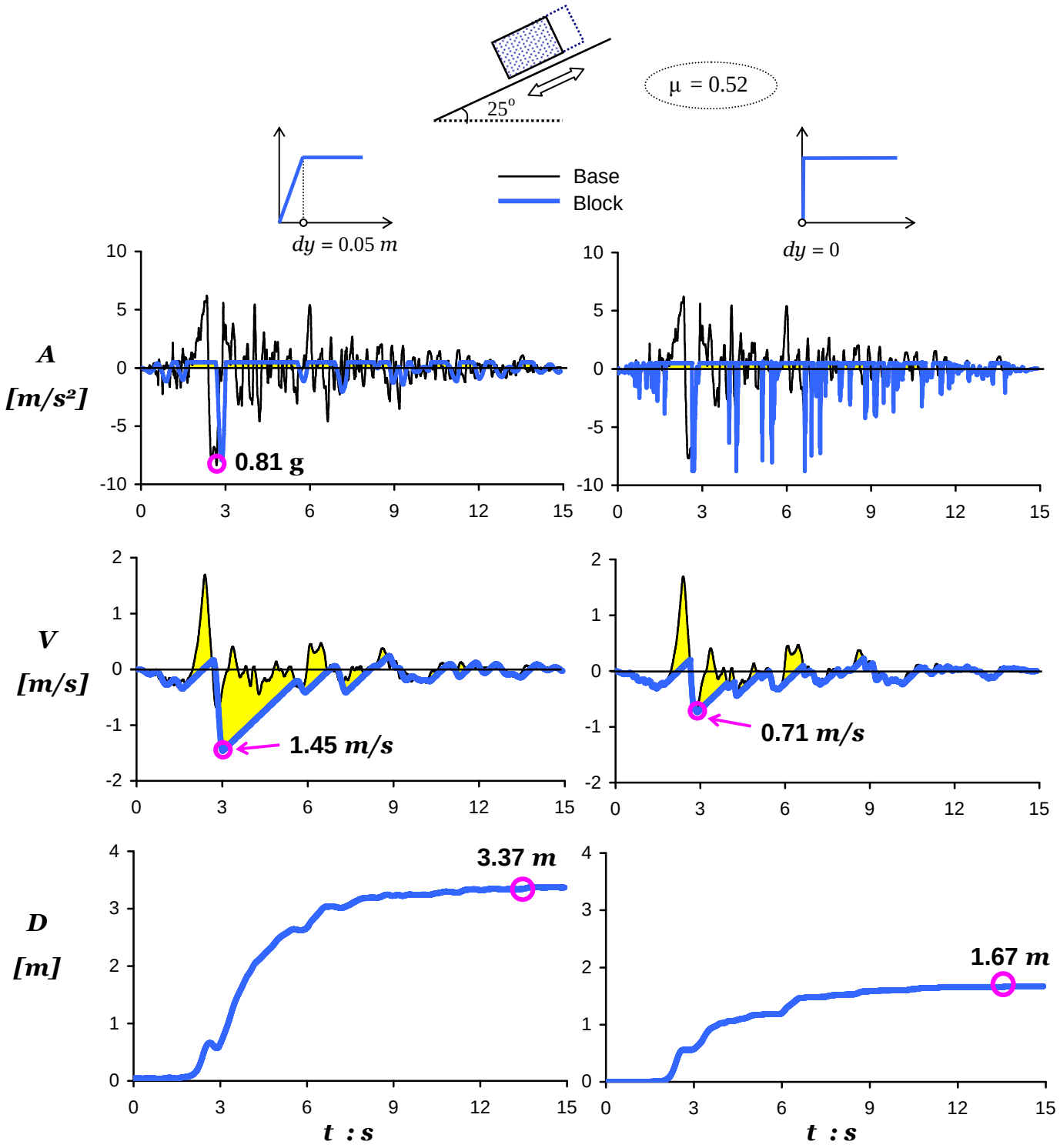

Figure 5.47 *Response time-histories for a perfectly-plastic sliding system on the right column and for an elasto-plastic system with dy = 0.05 m on the left [β = 25°, friction coefficient μ = 0.52, normal polarity Rinaldi 228]. Observe that the elasto-plastic slippage is 100% larger than the perfectly-plastic response.*

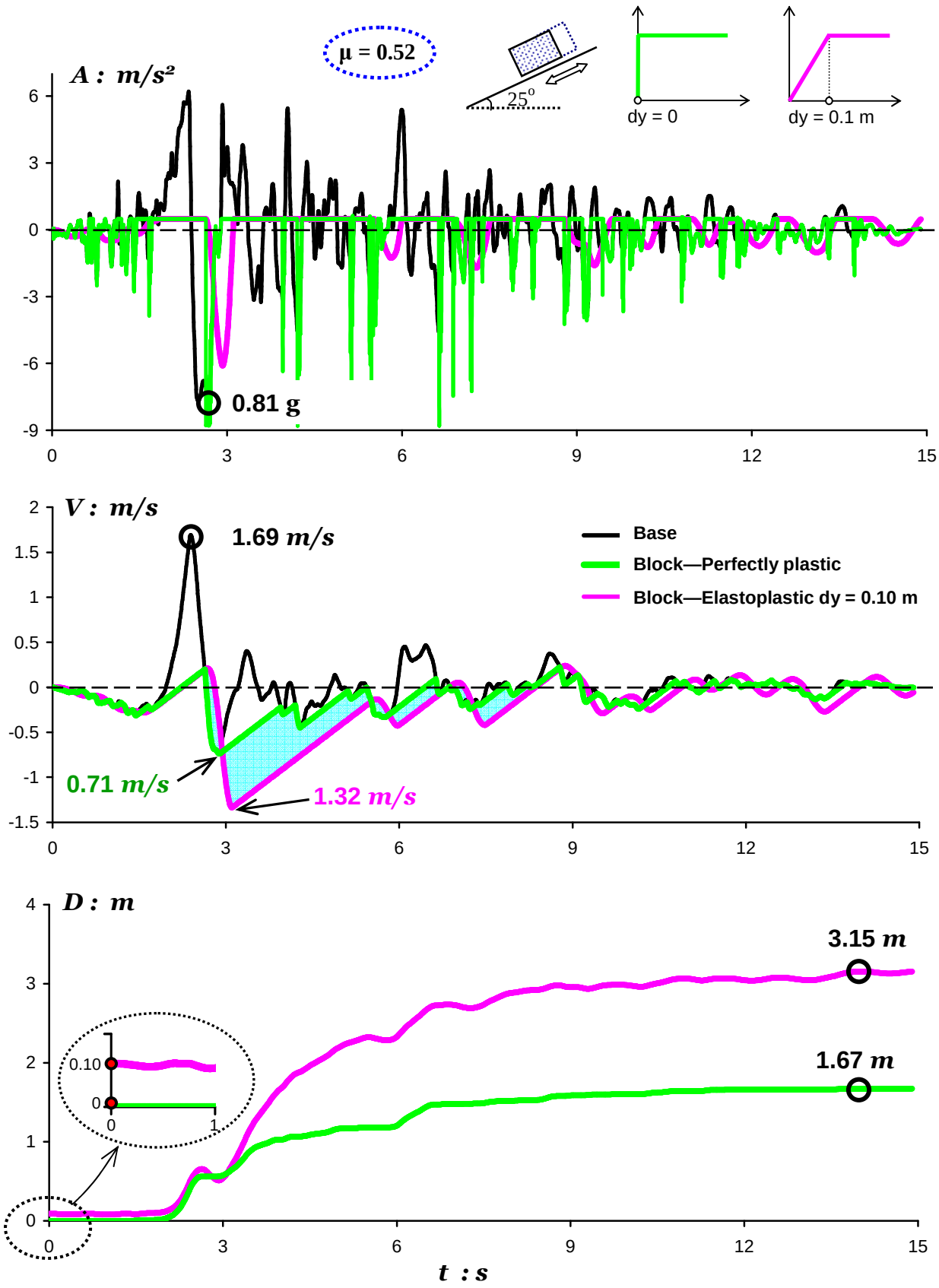

Figure 5.48 *Asymmetric response time histories of a rigid block resting on an 25^0 inclined plane when subjected to the normal polarity Rinaldi 228 record. The light green line presents the perfectly-plastic response with dy = 0; whereas the solid pink line corresponds to dy = 0.10 m. (friction coefficient μ = 0.52)*

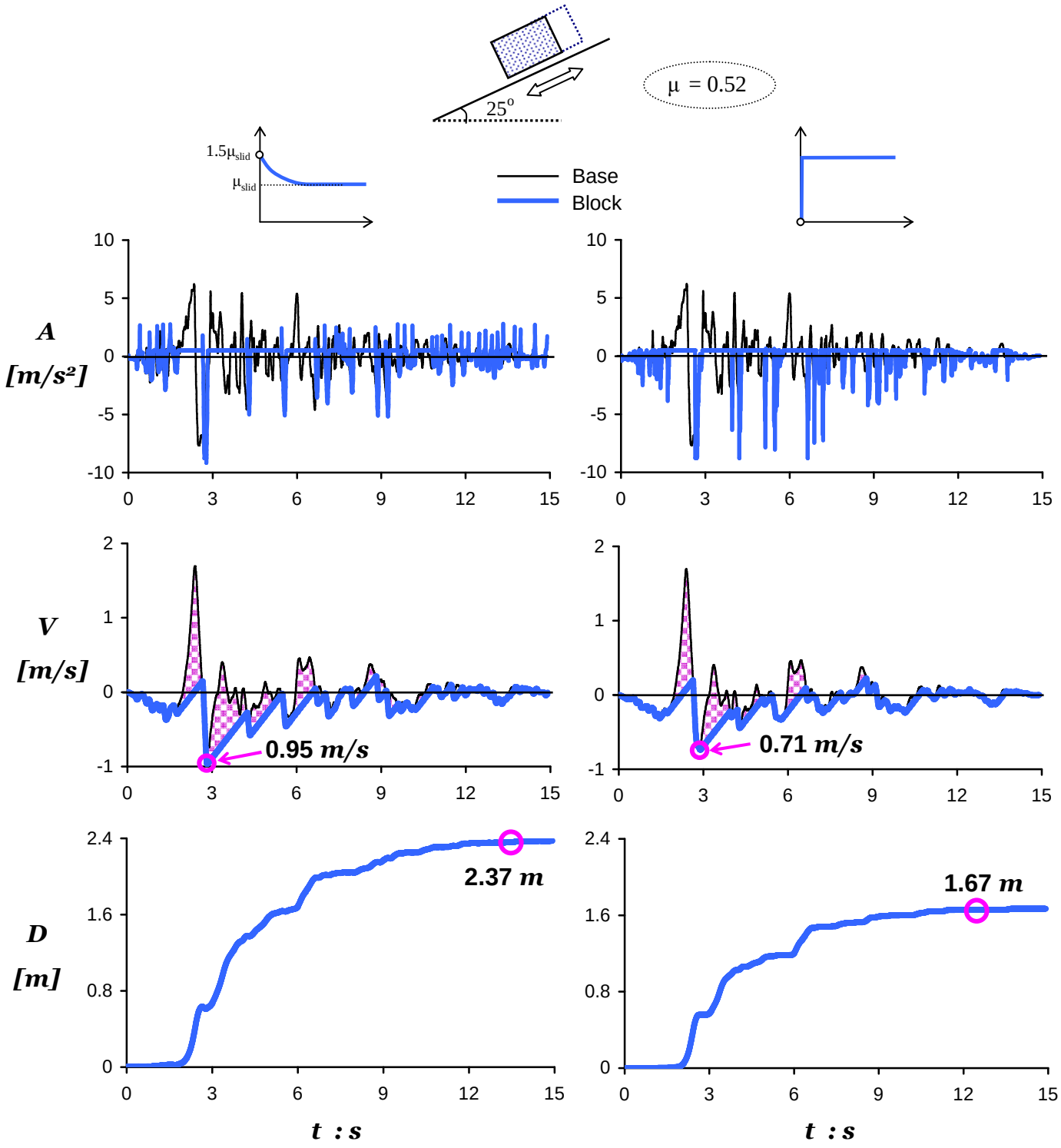

Figure 5.49 *Response time-histories for a perfectly-plastic sliding system on the right column and for exponentially decreased friction interface system on the left [β = 25°, friction coefficient μ = 0.52, normal polarity Rinaldi 228]. Observe that the exponentially friction induced slippage is 42% larger than the perfectly-plastic response.*

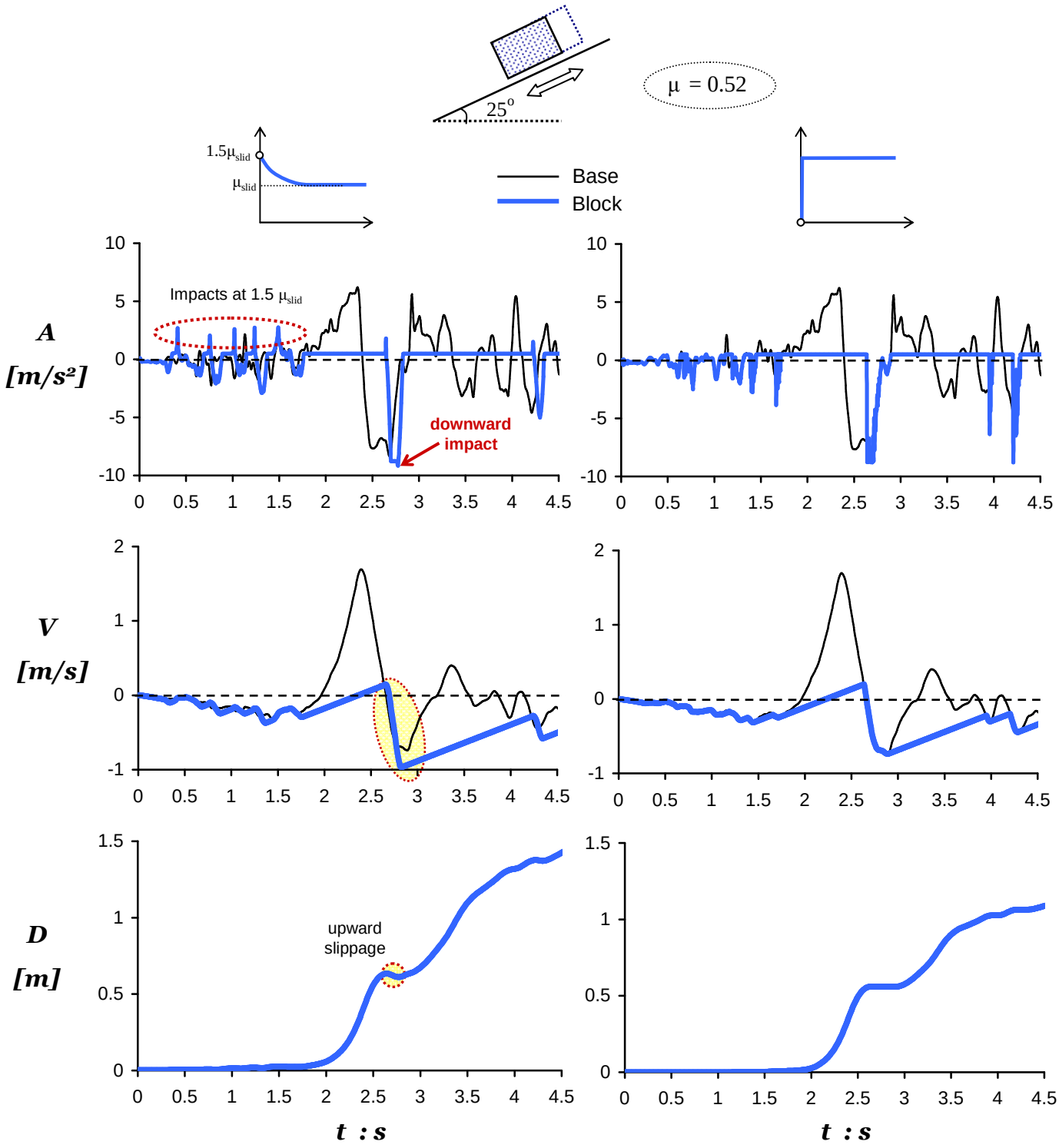

Figure 5.50 *The time-histories of the previous figure focused on the first five seconds of the motion [β = 25°, friction coefficient μ = 0.52, normal polarity Rinaldi 228]. The block's impact when the upward slippage stops, provides the block with greater velocity as pictured inside the circle on the velocity time-history on the left. As a result, larger total downhill displacement occurs.*

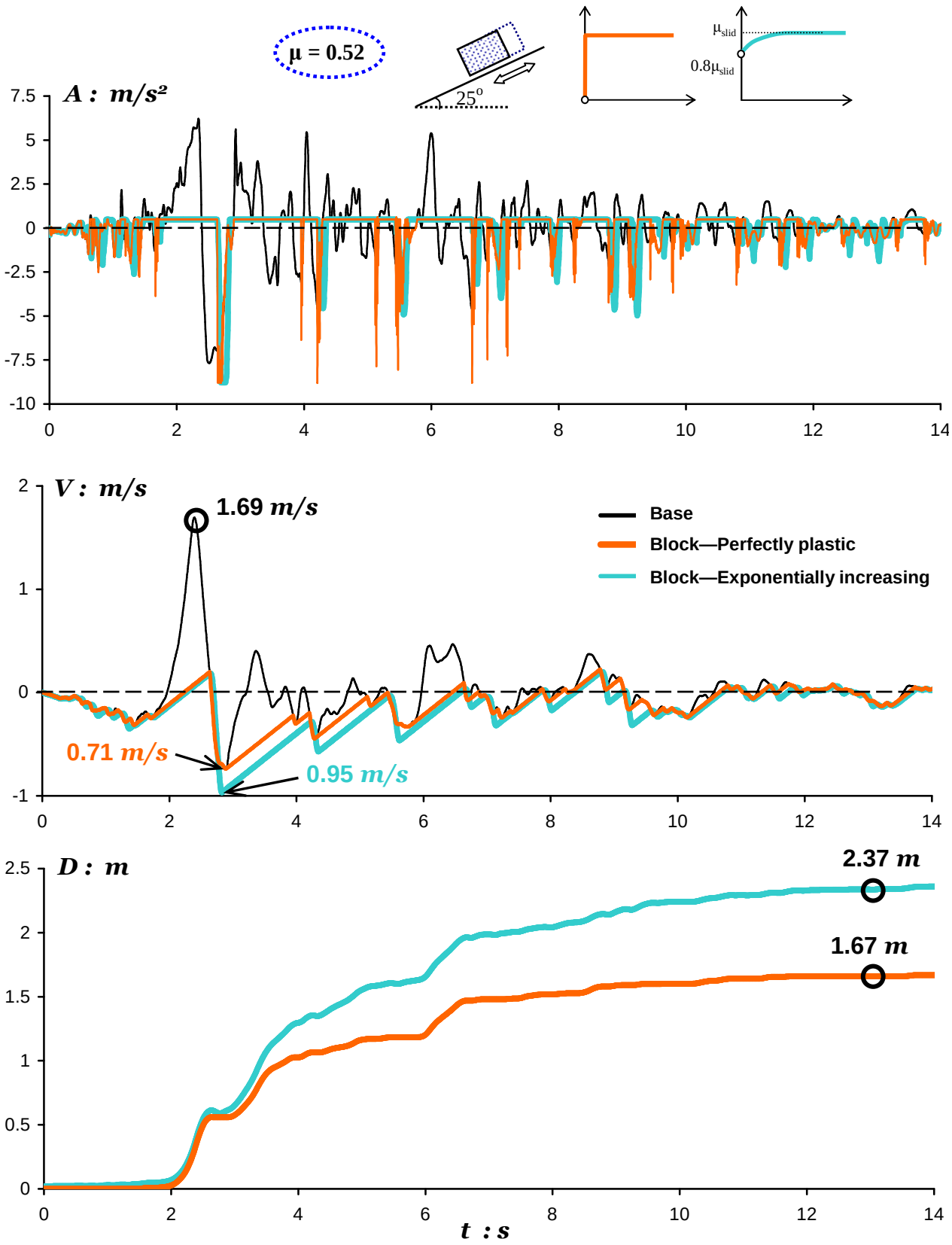

Figure 5.51 *Asymmetric response time histories of a rigid block resting on an 25^0 inclined plane when subjected to the normal polarity Rinaldi 228 record. The orange solid line presents the perfectly-plastic response; whereas the turquoise line corresponds to sliding response for an exponentially increased friction law of the yielding interface . (friction coefficient $\mu = 0.52$)*

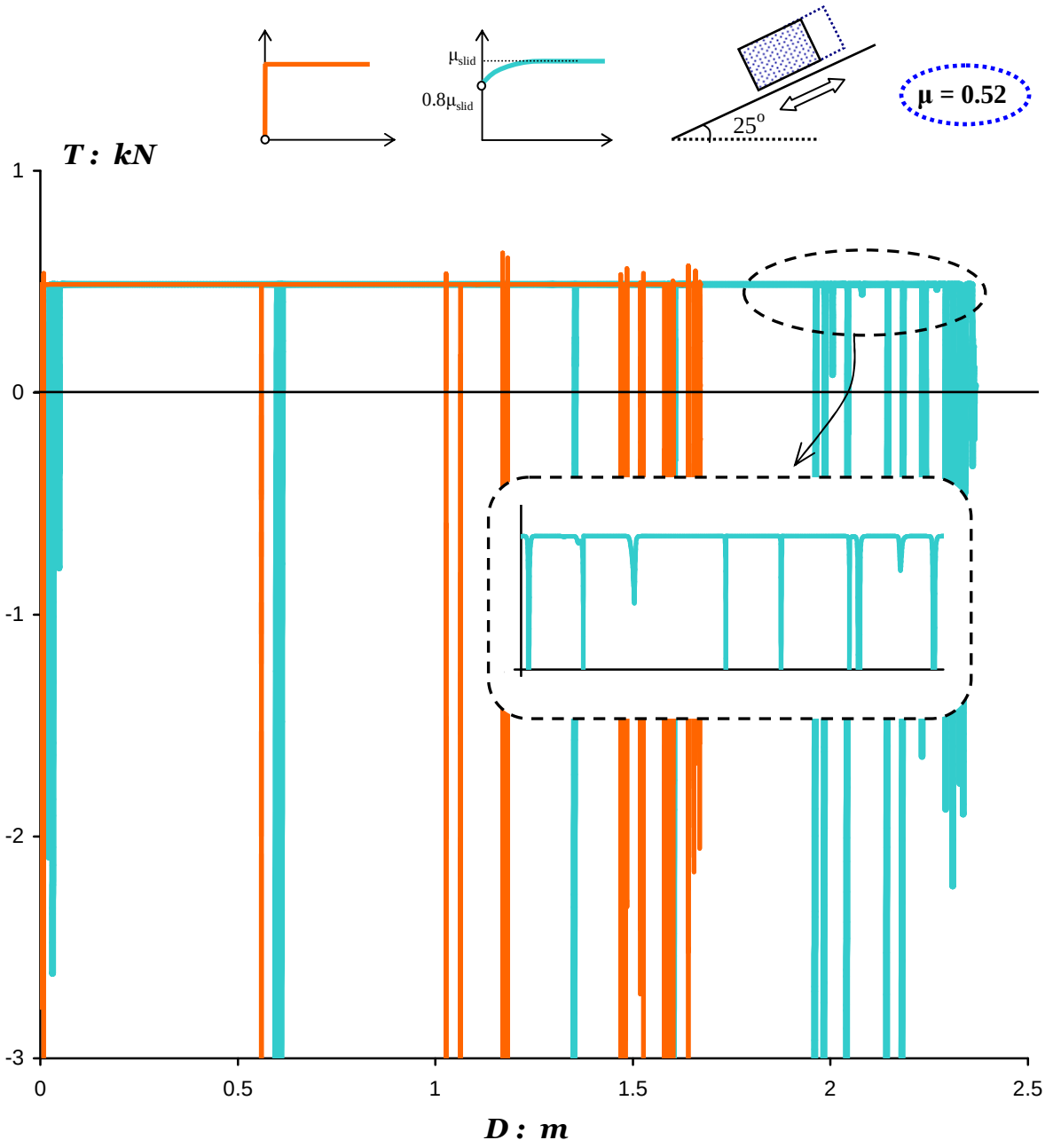

Figure 5.52 *Force-displacement response for a perfectly-plastic sliding system and a sliding system with yielding interface in which $\mu_{static} = 0.8\ \mu_{dynamic}$ illustrated with the solid orange and turquoise lines respectively [$\beta = 25^o$, friction coefficient $\mu = 0.52$, normal polarity Rinaldi 228].*

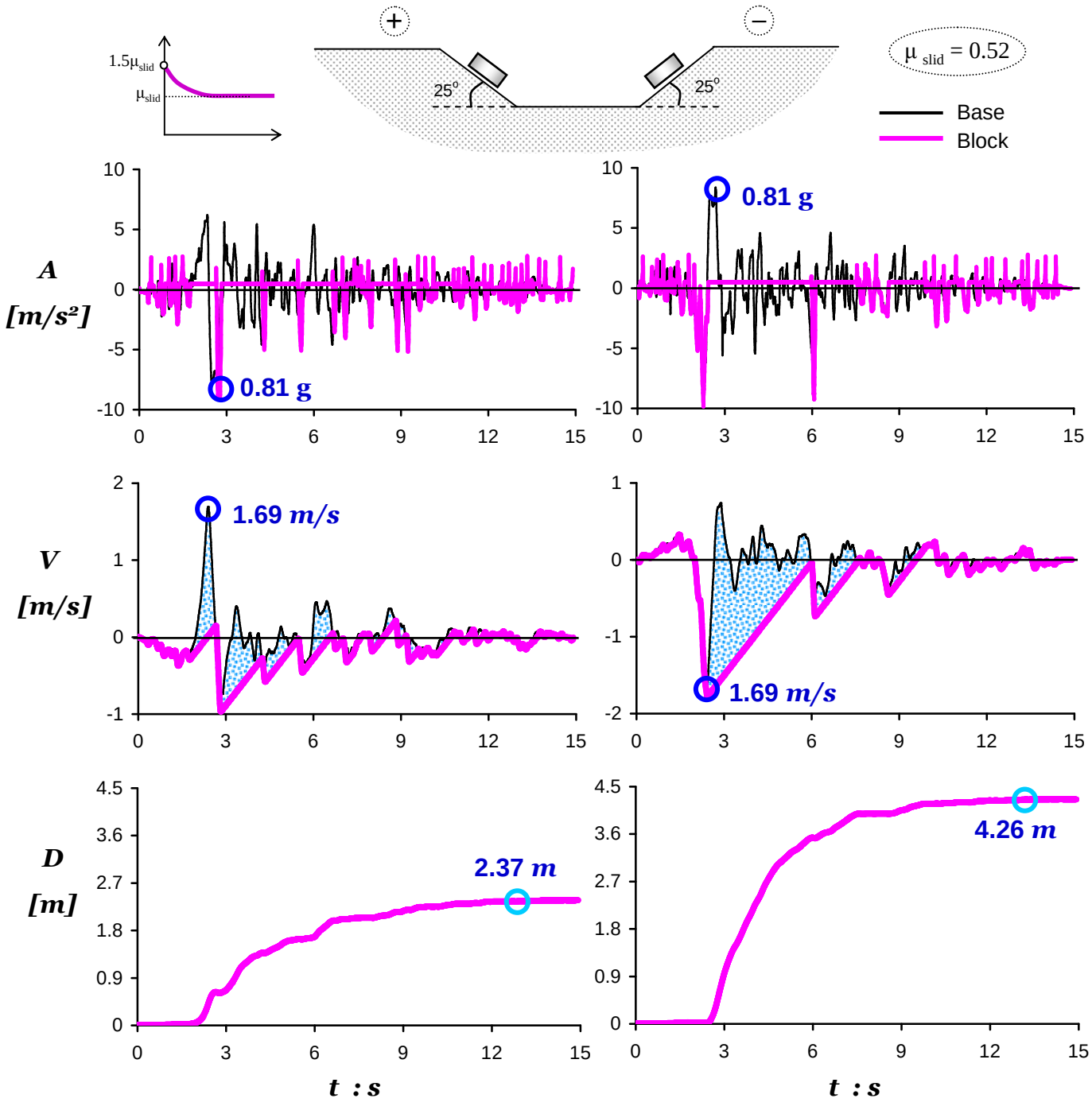

Figure 5.53 *Polarity effect of the Rinaldi 228 for a yielding system with exponential friction* $\mu_{static} = 1.5\mu_{dynamic}$. *By definition,* $\mu_{dynamic} = \mu_{slid}$. *[*$\beta = 25^o$, *friction coefficient* $\mu_{slid} = 0.52$*].*

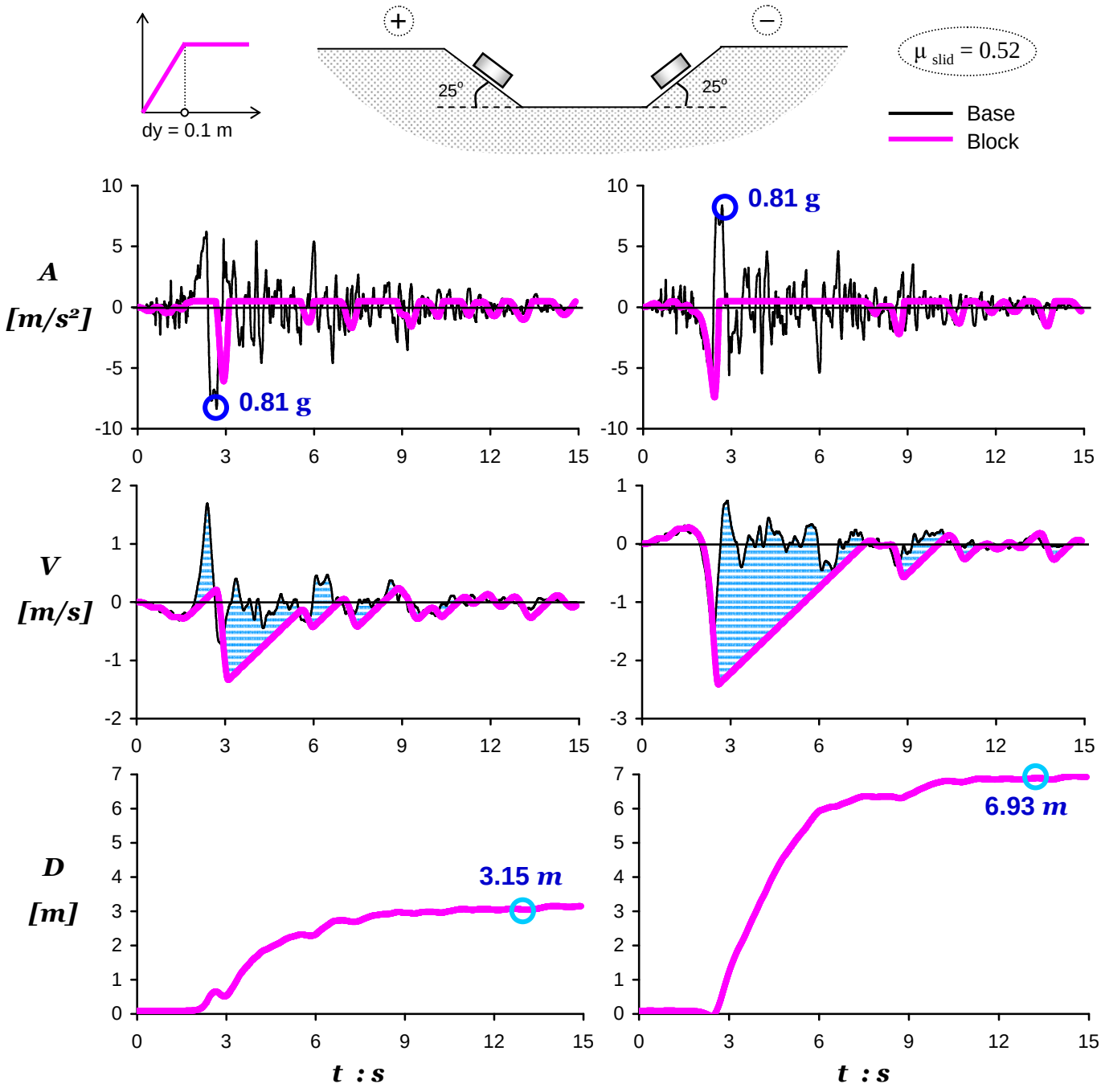

Figure 5.54 *Polarity effect of the Rinaldi 228 for an elasto-plastic sliding system with dy = 0.10 m. [β = 25°, friction coefficient μ_{slid} = 0.52].*

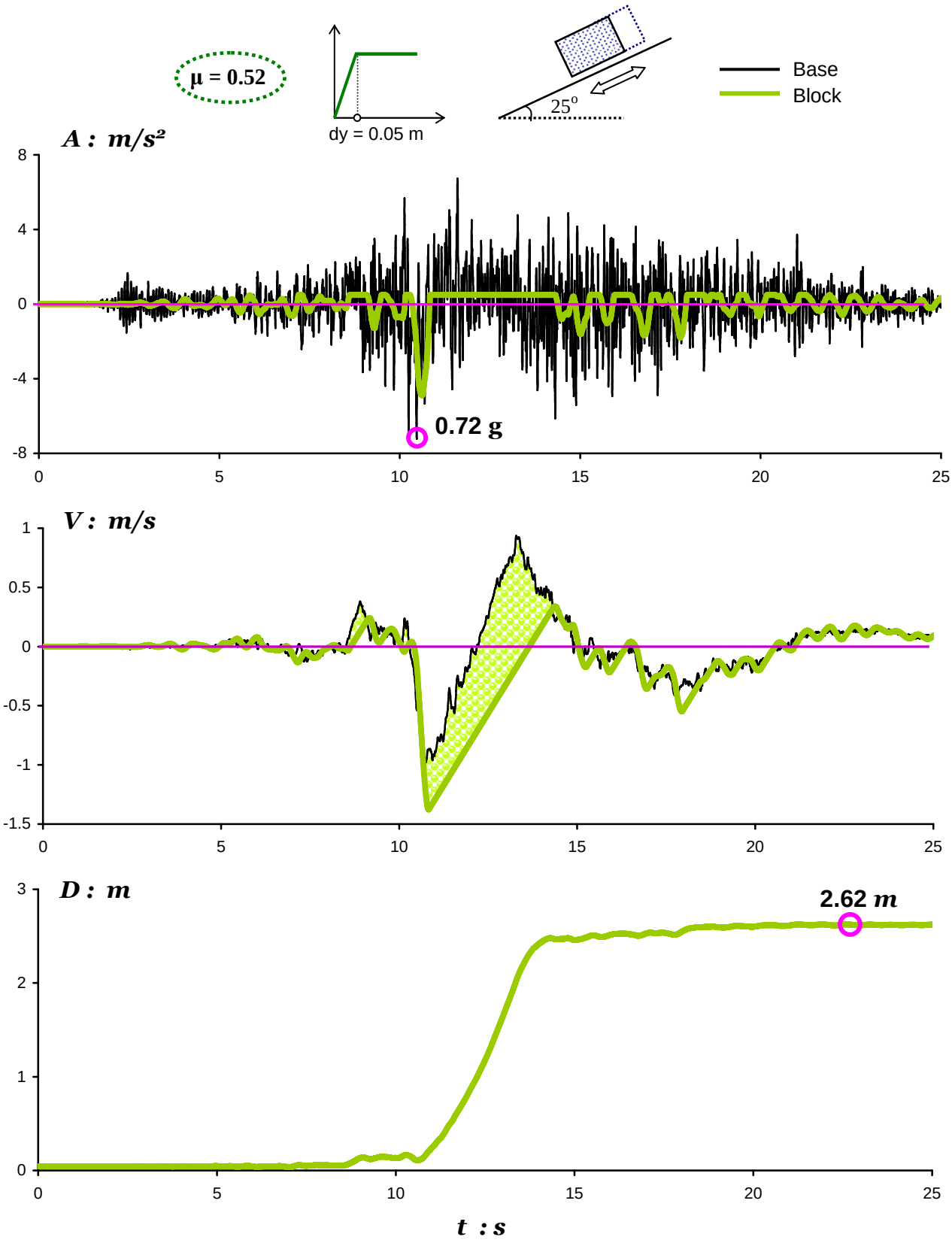

Figure 5.55 *Asymmetric response time histories of a rigid block resting on an 25^0 inclined plane when subjected to the normal polarity Lucerne 275 record. Block's elastic deformation is dy = 0.05 m. (friction coefficient μ = 0.52)*

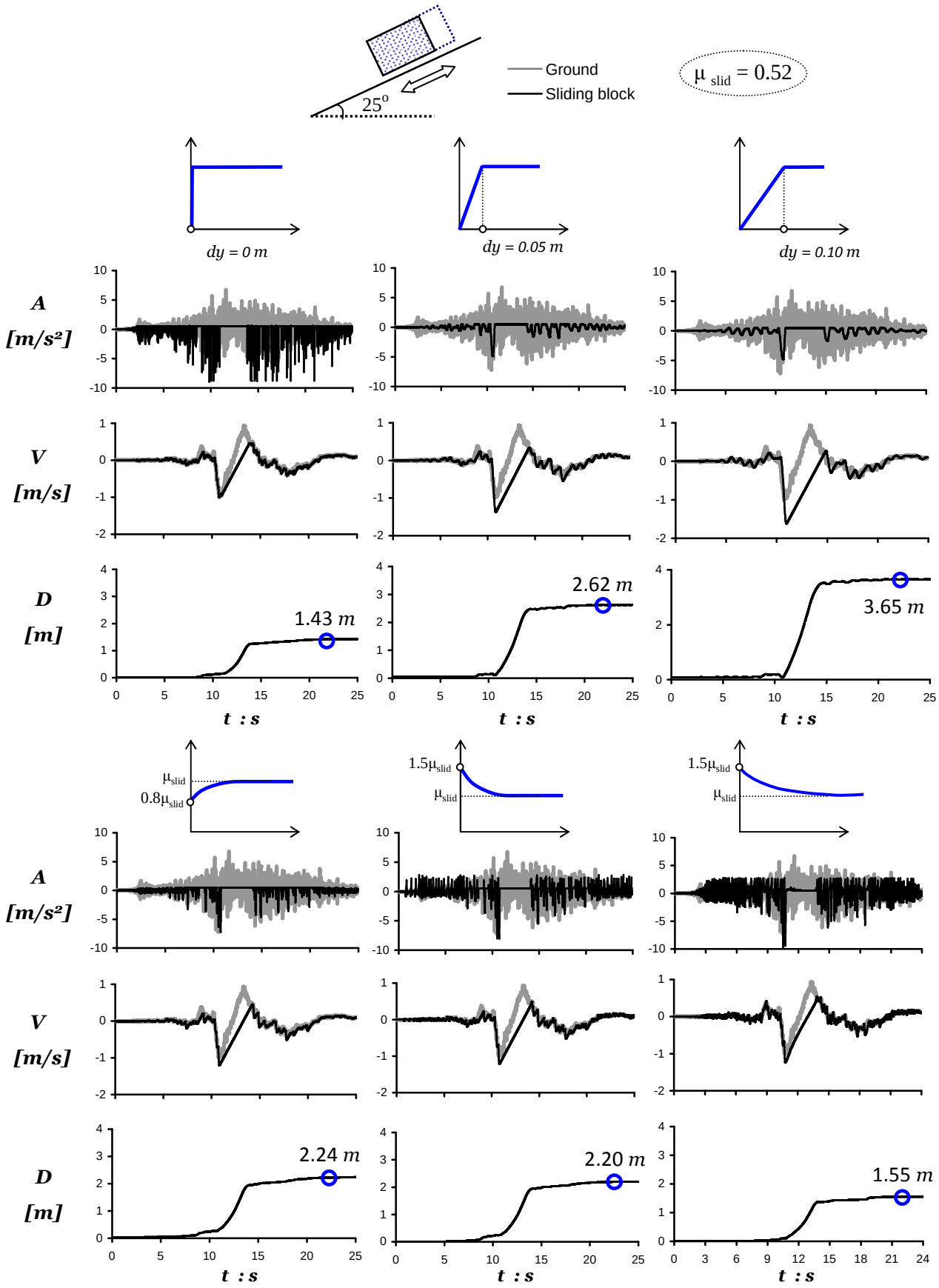

Figure 5.56 *Response time-histories for the five constitutive frictional laws of the yielding interface [β = 25°, friction coefficient μ = 0.52, normal polarity Lucerne 275].*

Summary Results

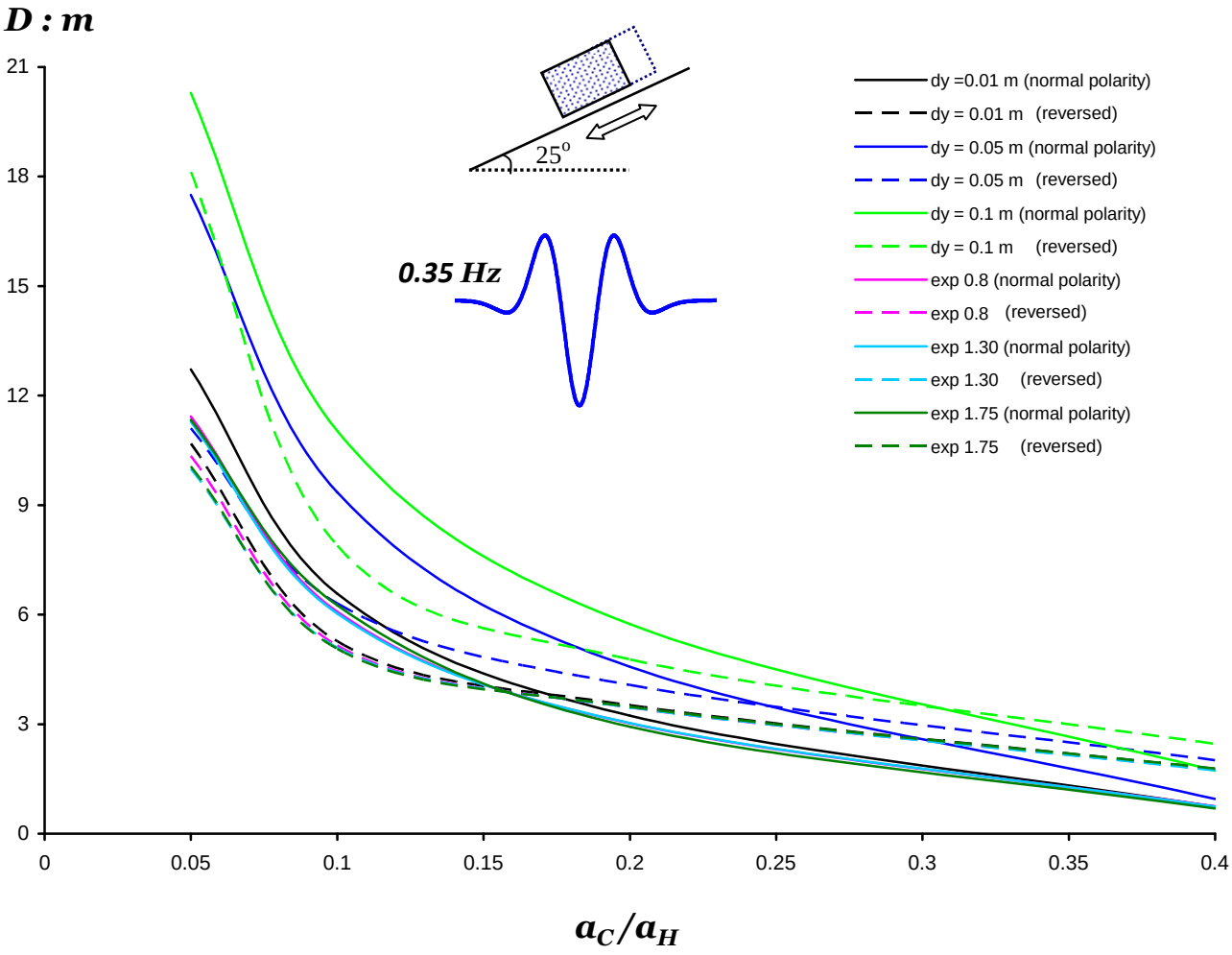

Figure 5.57 *Summary results for all the elasto-plastic and exponential sliding systems when subjected to a 0.35 Hz Ricker wavelet. Excitation is applied with its normal and reversed polarity.*

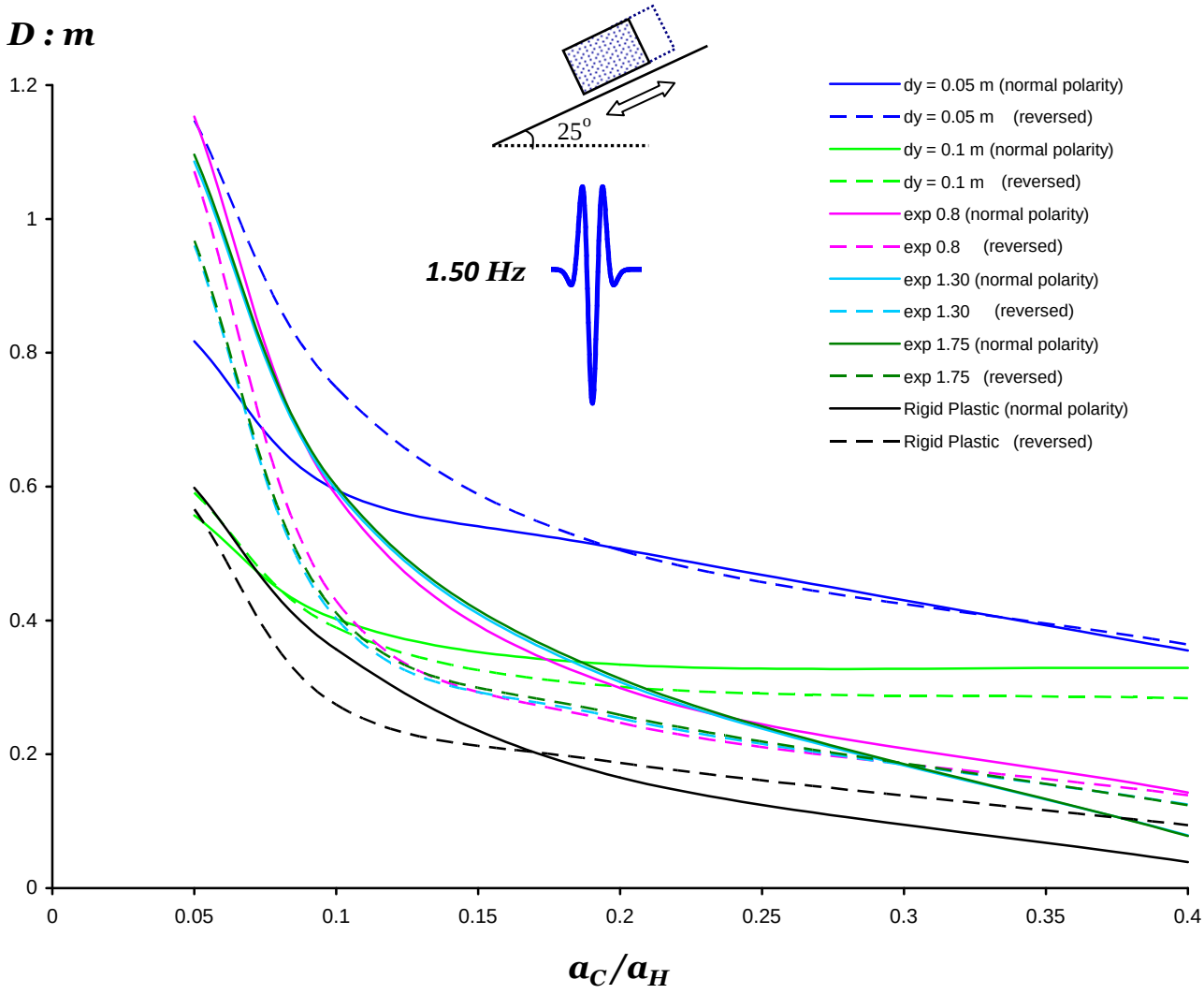

Figure 5.58 *Summary results for all the elasto-plastic and exponential sliding systems when subjected to a 1.5 Hz Ricker wavelet. Excitation is applied with its normal and reversed polarity.*

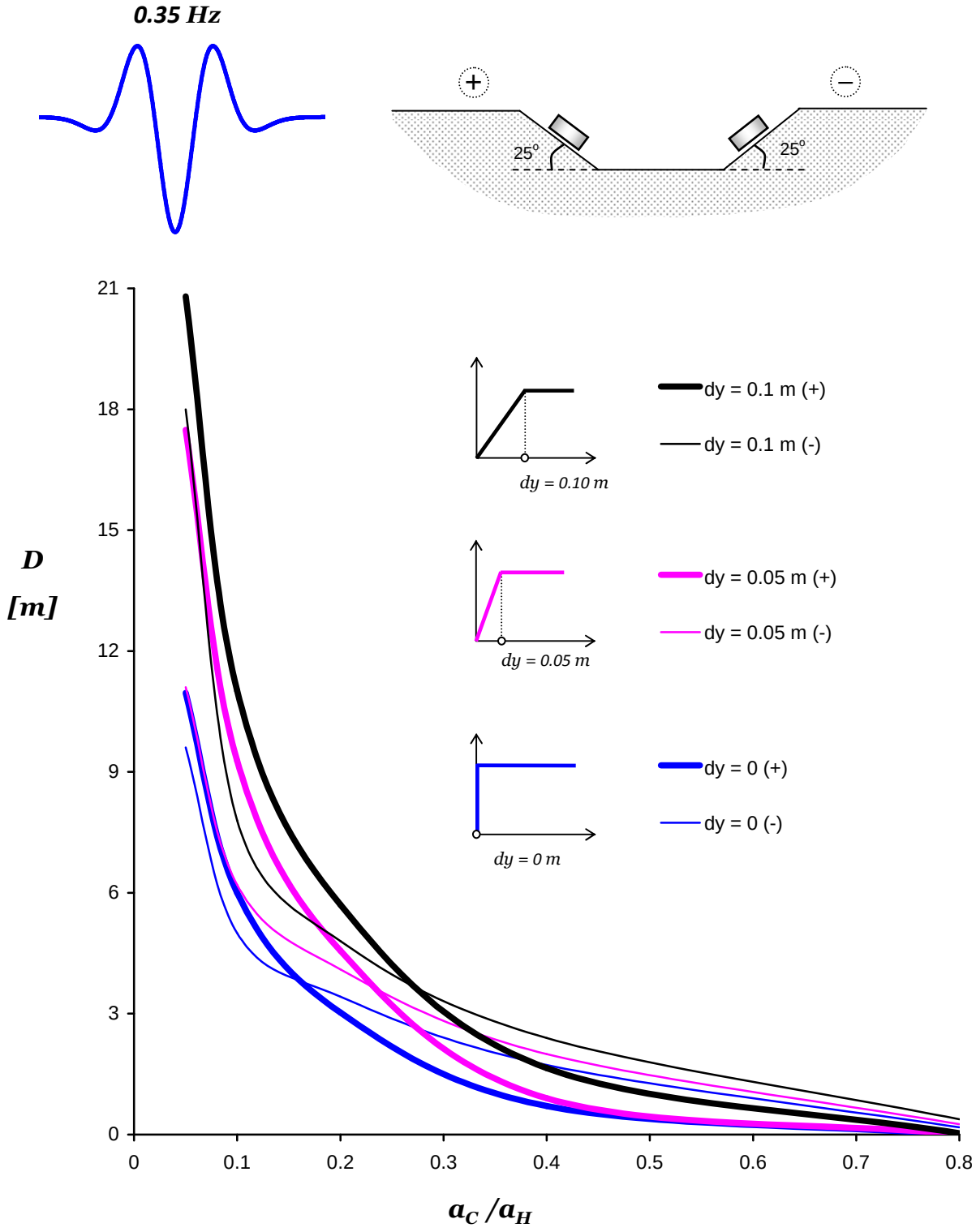

Figure 5.59 *Sliding displacement, D, versus critical acceleration ratio, a_C / a_H, in case of a Ricker pulse excitation of 0.35 Hz frequency for three elasto-plastic yielding systems with dy = 0, 0.05, and 0.10 m. The Ricker wavelet is imposed with its normal and reversed polarity. As the elastic pre-yielding displacement (dy) increases, block's slippage increases too.*

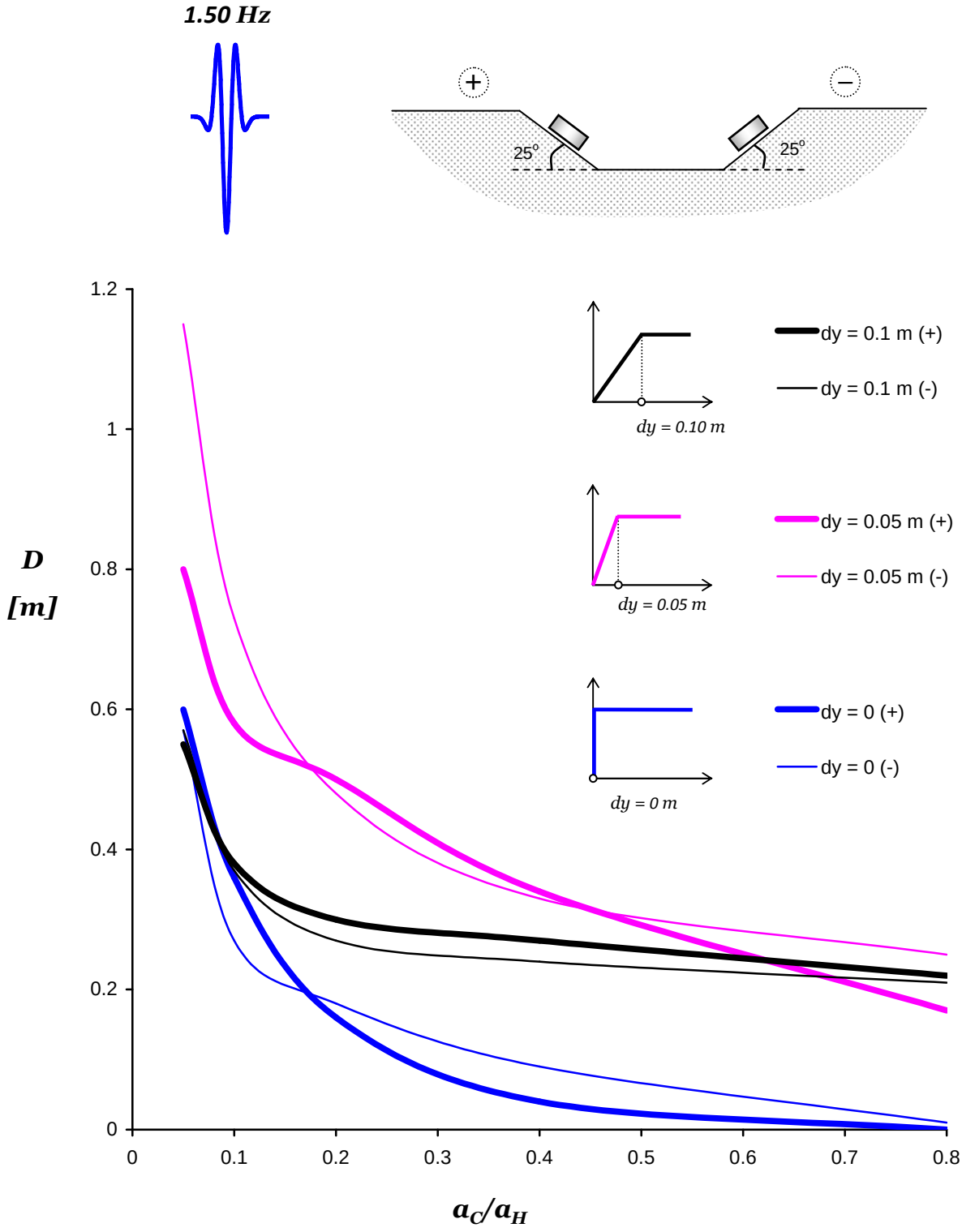

Figure 5.60 *Sliding displacement, D, versus critical acceleration ratio, a_C/a_H, in case of a Ricker pulse excitation of 1.50 Hz frequency for three elasto-plastic yielding systems with dy = 0, 0.05, and 0.10 m. The Ricker wavelet is imposed with its normal and reversed polarity.*

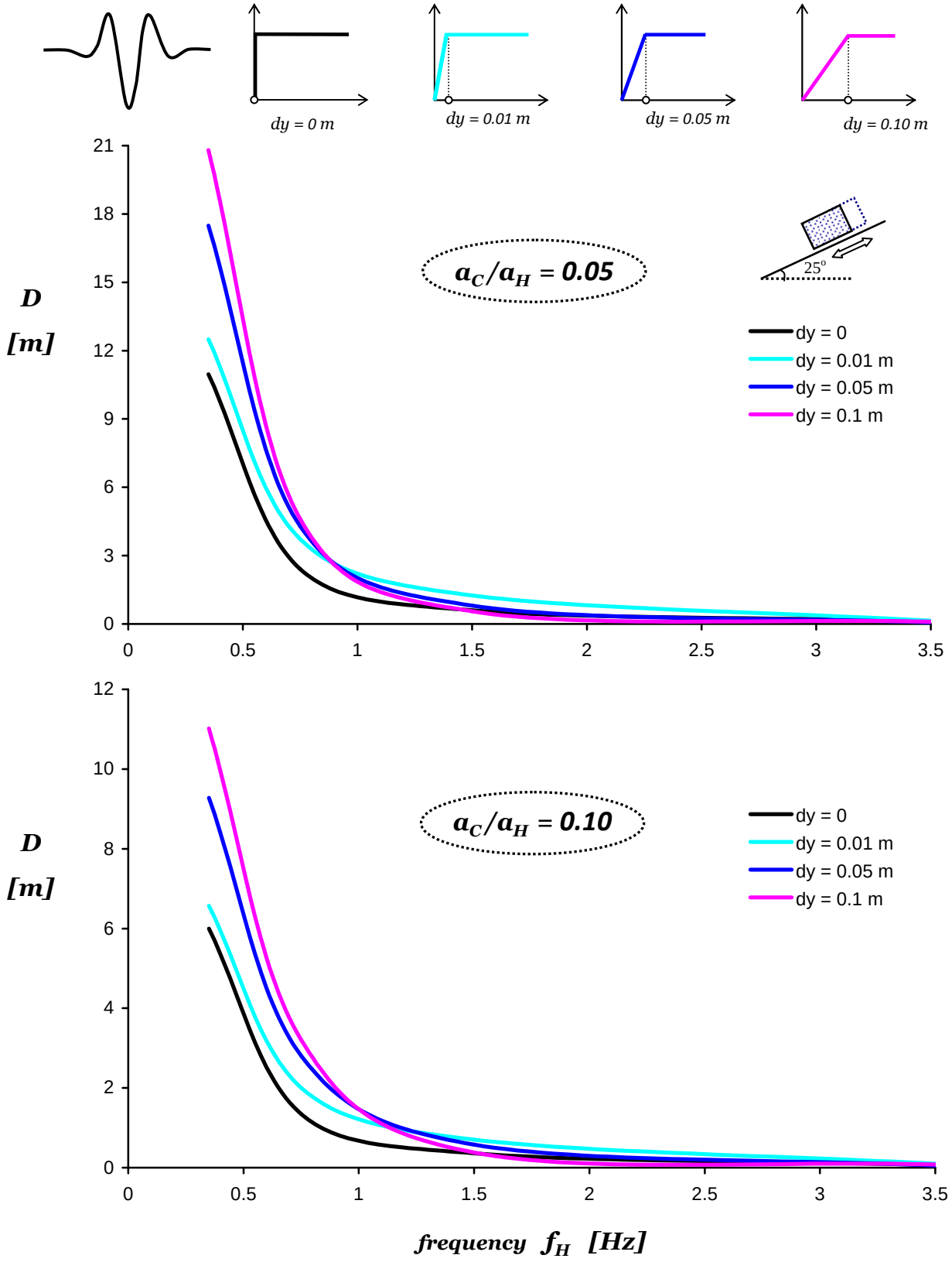

Figure 5.61 *Slippage, D, with respect to excitation's frequency, f_H. The triggering motion is the Ricker wavelet. The top plot pictures the response for critical acceleration ratio: $a_C/a_H = 0.05$ for several elasto-plastic systems with dy = 0, 0.01, 0.05, and 0.10 m. The bottom plot corresponds to $a_C/a_H = 0.10$.*

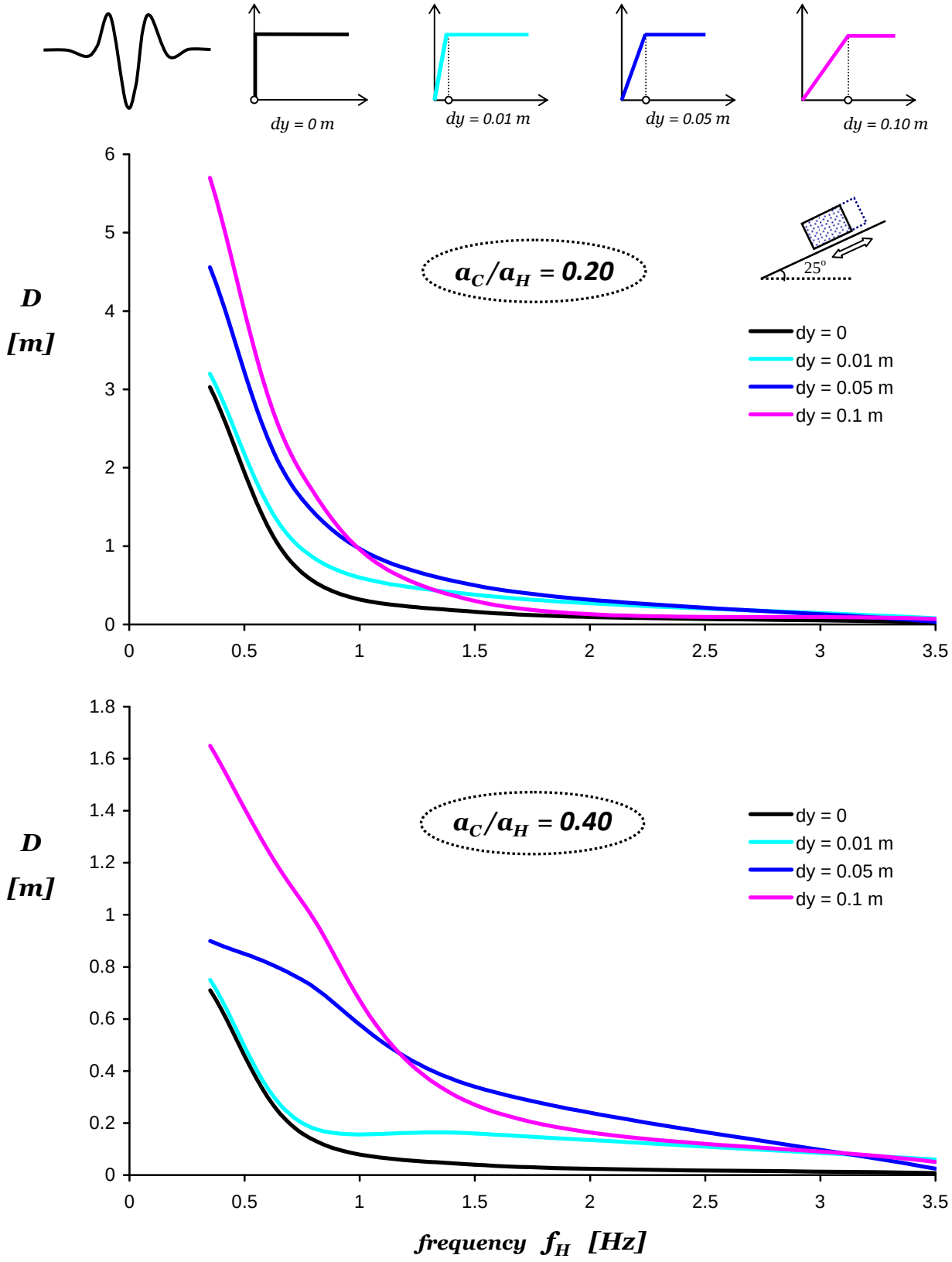

Figure 5.62 *Slippage, D, with respect to excitation's frequency, f_H. The triggering motion is the Ricker wavelet. The top plot pictures the response for critical acceleration ratio: $a_C/a_H = 0.20$ for several elasto-plastic systems with dy = 0, 0.01, 0.05, and 0.10 m. The bottom plot corresponds to $a_C/a_H = 0.40$.*

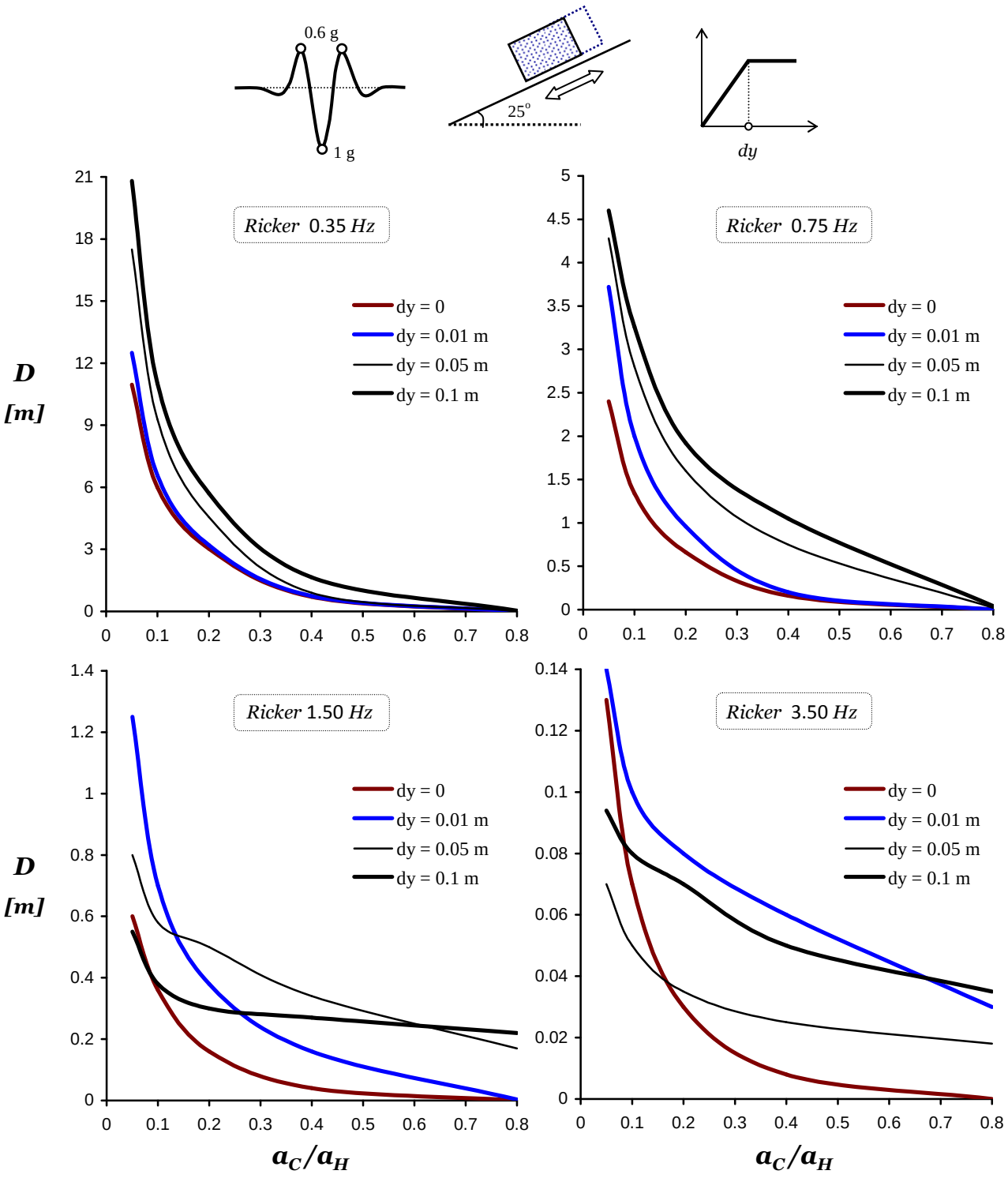

Figure 5.63 *Influence of maximum elastic deformation, dy, on asymmetric sliding response triggered by Ricker wavelets of maximum acceleration 1 g and of different frequencies.*

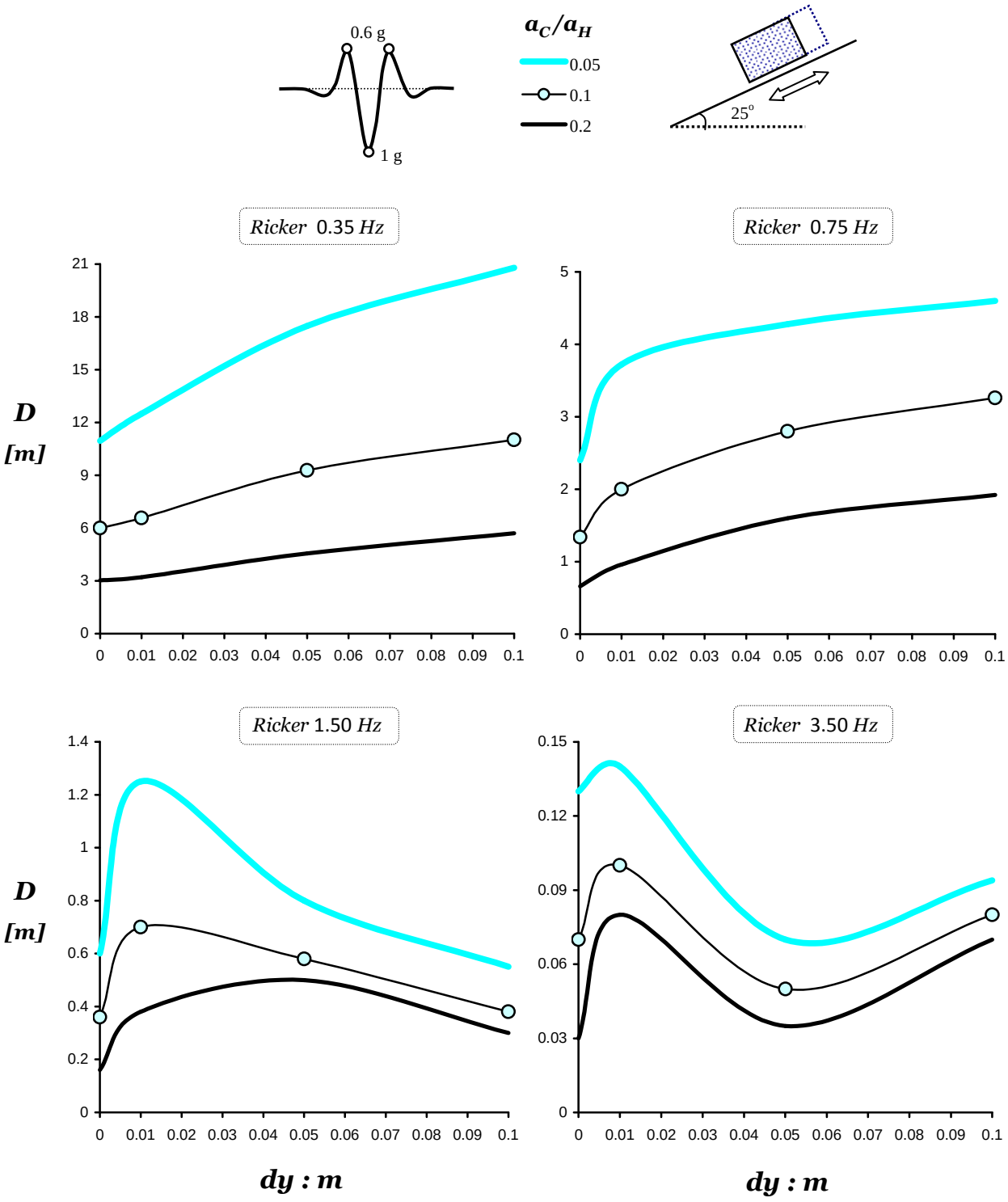

Figure 5.64 *Effect of characteristic frequency, f_H, and of a_C/a_H ratio on maximum slippage with respect to elastic deformation, dy (Excitation: single Ricker wavelet).*

Chapter 6

Effect of Trimmed Records; Sliding on Top of SDOF

6.1 Effect of peak ground acceleration on slippage

As had been shown in previous chapters, for a particular excitation the higher the magnitude of peak acceleration, the larger the slippage. However, the maximum acceleration of a record can not be an efficient indicator of its sliding potential. Other parameters, such as the velocity step, the frequency content, etc. play a far more important role. To demonstrate the deceptive role of peak acceleration on asymmetric sliding, in the sequence we will select particular records that either will be trimmed off their peak acceleration values, or these acceleration pulses will be totally removed, or the whole time history will be replaced by a series of simple pulses. Figures 6.1 ÷ 6.13 portray the results of the aforementioned modifications in accelerograms.

To start with, as illustrated in Figure 6.1, the sliding response of the TCU 052-EW is compared with the response induced by the same record when accelerations are trimmed to 0.20 g. *The original record exhibits a major acceleration pulse of a peak value 0.35* g *and produces a displacement of 8.52 m. By cutting off every acceleration over 0.20* g, *the velocity pulse at 13 sec is reduced substantially but otherwise little difference is observed. As a result, the sliding displacement of the "cropped" record is 8.23 m, only barely lower*

than the 8.52 m of the original ground motion. Figure 6.2 illustrates the elastic spectra and the sliding response of the original and the modified records. The sliding response curves are almost identical. The elastic response spectra display also a small difference, that becomes larger over the period range from 1 sec to 2 sec.

For the NS component of the TCU 068 record, we intervene more drastically on the acceleration time history: the pulse with the peak acceleration is not just trimmed off; it is totally removed (Figure 6.3). Hence, the maximum 0.43 g *acceleration of the original record is deleted and the new peak value is 0.16* g*. Therefore, the velocity sequence which is formed partially by this acceleration pulse is substantially altered. Notice in Figure 6.3 that the maximum velocity of 2.2 m/s is reduced to 1.7 m/s. The duration of the velocity pulse is also shortened from 5.4 sec down to 4.6 sec. The consequence is the slippage of 6.29 m to decrease to 5.68 m; a mere 11% divergence in displacement triggered by a 170% decrease in acceleration and 24 % decrease in velocity. The effect of acceleration modification in elastic spectra is striking: the spectrum from the modified record is much lower than the original record response spectrum throughout the period range up to 3.5 sec (Figure 6.4).*

Next, as can be seen in Figure 6.5, the 1.23 g *peak acceleration of the Pacoima Dam 164^o record is chopped at 0.50* g*. Thus, the 1.15 m/s velocity step is reduced to 0.85 m/s and the induced slippage of 1.76 m to 1.47 m. Impressive is the fact that even though the acceleration time history is trimmed more than 60%, the resulting displacement is only 20% smaller. The elastic response spectrum, as illustrated in Figure 6.6, is slightly lower in the short period range, but for T > 0.5 sec the two spectra are identical—a straight forward result of trimming the high frequency spikes in acceleration.*

Figures 6.7÷6.9 portray the influence on slippage of cropping the major acceleration pulse of the Aegion record. Pay attention to the fact that trimming is applied to a forward-directivity related acceleration pulse, not just to an insignificant acceleration sequence. Also, keep in mind that sliding is performed on a horizontal plane so yielding can occur in both directions. Figure 6.7 depicts the response to the truncated Aegion record, i.e. whose maximum acceleration has been clipped to half: from 0.54 g to 0.27 g. The resulting maximum and residual displacements are greater than those of the original record! On the contrary, if both the positive and negative acceleration peaks are chopped to 0.27 g, the sliding is reduced (Figure 6.8). A clear view of all the results is offered in Figure 6.9, where the elastic and sliding responses for the original and cropped records are summed up.

From the previous discussion, it becomes evident that the peak ground acceleration (as an absolute value independent from the frequency content) plays a secondary role in sliding.

6.2 Approximation of actual records with fitted simple pulses

Another way of investigating the effect of a ground motion on slippage will be presented in this section. In particular, we simulate the TCU 068-NS record through a series of simple rectangular pulses. Figure 6.10 illustrates: (left column) the real record and its consequences on block acceleration, velocity, and slippage; (middle column) approximation of the record with five rectangular pulses, representing almost every major acceleration pulse of the record, along with the consequences on block response; (right column) approximation of the record with only three rectangular pulses (representing only the long-period pulses of the record), along with the consequences on

block response. The TCU 068 NS record is employed in Figure 6.10 with its recorded polarity and in Figure 6.12 with reversed polarity.

Our aim is to explain in more detail the sliding process mechanics and to provide an additional proof of the unique importance of acceleration long-duration pulses in sliding response. By eliminating the acceleration high-frequency spikes of the record and crudely approximating the major pulses with rectangles having the same duration and the average acceleration amplitude over that duration, one obtains the grossly-simplified time histories which are plotted in Figures 6.10 and 6.12. Despite the "innocent" looking peak acceleration of merely 0.14 g, of the latter approximation (right column), this base motion has nearly the same devastating effect with the record when its polarity is reversed: a downward slip of 23.3 m. The similarity with the effects of the actual motion is obvious, an indirect evidence of the dominating role of the long acceleration pulses and the minor importance of the isolated "spikes" of peak-ground acceleration. However, for the original polarity the induced slippage diverges substantially. As can be seen in Figure 6.10, this difference in slippage occurs during the second sliding period of the block. The first yielding period result in almost the same displacement (notice the pink dashed line in Figure 6.10). Nevertheless, the simplified motions trigger larger displacement than the original record. Figures 6.11 and 6.13 depict the elastic and yielding response of the TCU 068 NS ground motion and its simplifications.

One worth-mentioning finding is that motion features such as the sequence of cycles, and "details" of the motion, are often of major importance; sometimes as important as the dominant frequency and the intensity of motion.

6.3 Sliding of a single-degree-of-freedom oscillator: the Whitggar model

Newmark's analogue has been used or extended by a number of authors including Richards & Elms, 1979; Whitman & Lin, 1983; Constantinou et al, 1984; Ambraseys & Menu, 1988; Ambraseys & Srbulov, 1994; Gazetas & Uddin, 1995; Stamatopoulos, 1996; Kramer & Smith, 1997; Mylonakis & Reinhorn, 1997; Rathje & Bray, 2000; Ling, 2001; Fardis et al, 2003; Wartman et al, 2003.

Most of them studied the seismic response of dams and embankments by extending rigid block analysis to single or multiple degree of freedom oscillators which can yield at one of several levels. In the following paragraphs, the single degree of freedom oscillator is presented and analysed.

Figure 6.14 portrays the sliding analogue applied herein with two characteristic geotechnical applications. A new model (named Whitggar) is developed to simulate the dynamic response to earthquake shaking of an embankment of height H and base length 5H and crest length H. We assume that a part of a mass m_2 slides, moving as a rigid block along an inclined sliding surface with coefficient of friction, μ. The rest of the embankment, having a mass m_1, plays the role of a single degree of freedom oscillator (with characteristics T_n , k) on top of which the rigid block rests. The above are schematically described in Figure 6.15. The whole mass of the embankment is equal with:

$$m = \rho \frac{H(5H + H)}{2} = 3\rho H^2 \qquad (6.1)$$

$$m = m_1 + m_2 \qquad (6.2)$$

where ρ is the density of the embankment and a typical value of 2 ton/m^3 is applied.

The natural period of the embankment, if the embankment is dynamically approximated as a soil layer of shear wave velocity V_S = 200 m/s, is given by the expression:

$$T_n \approx \frac{4H}{V_S} = 2\pi\sqrt{\frac{m}{k}} \qquad (6.3)$$

From equations (6.1), (6.2) and (6.3):

$$k = \frac{3\pi^2 V_S^2}{2} \Rightarrow \qquad k \approx 590 \quad kN/m$$

Stiffness, k, is kept constant and is also independent of the height H. Therefore, for any combination of values (m_1, m_2, T_n, H , k) of the Whitggar model, the stiffness k is known. For a given mass ratio m_2/m_1 and height H, equations (6.1) and (6.2) give the masses m_1 and m_2.

Parametric analysis of the Whitggar model is performed with the ABAQUS code. The finite element model comprises a vertical beam of ten distinct elements. On its top, a mass element (m_1) is attached which is connected with a gap element to a second mass (m_2). The earthquake triggering is assigned to the base: idealised Ricker wavelets of frequency 1 and 2 Hz. Near-fault accelerograms are also employed: the Fukiai, Rinaldi, Newhall, and TCU 068 records. The mass ratio m_2/m_1 takes the values of 0.1, 0.5, 1, corresponding to a shallow, medium, deep failure of the dam, respectively. Additionally, the natural period of the system, T_n , is 0.5 or 1 sec. Figures 6.16 ÷ 6.26 present characteristic results from the analyses.

6.3.1 Effect of the oscillator's natural period

By increasing the natural period T_n of the oscillator, the magnitude of acceleration and the subsequent slippage can be either increased (if the predominant period of excitation is closer to T_n), or decreased (if excitation's predominant period is far from the

value T_n). In particular, for two oscillating systems with similar characteristics but different periods (T_1 and T_2) subjected to an excitation of predominant period T_H: for T_1, $T_2 < T_H$, greater slippage is induced to the system with the larger natural period; for T_1, $T_2 > T_H$, greater slippage is occurred to the system with the smaller period.

For instance, Figures 6.17, 6.18, and 6.19 display the acceleration, velocity, and sliding displacement time histories respectively, for the case of two systems with natural periods 0.5 and 1 sec when they are subjected to the Fukiai record. Keep in mind, that the Fukiai record has a predominant period of 0.9 seconds. Thus, the oscillator with the natural period of 1 sec exhibits larger slippage compared with the 0.5 sec system. In stark contrast, for the Ricker excitation of 2 Hz, the system with the smaller natural period of 0.5 sec displays the greater displacement (Figure 6.21); whereas the oscillator of 1 sec suffers no detachment at all of m_2 from its base.

6.3.2 One and two step analyses procedure

As a general rule, the superposition principle states that (for all linear elastic systems) the net response caused by two or more stimuli is equal to the sum of the responses which would have been caused by each stimulus individually. In our case, we study the decoupling of the complete oscillator-slider system (an oscillator with an "internal" sliding surface) into two systems: an 1-sdof system with only one mass, m_1, and a separate system of the mass m_2 on an inclined plane. The second system is excited at its base by the motion experienced by the first system on its mass (a two-step decoupled solution). The question is, how good this decoupling approximation is.

The answer is given through Figures 6.22÷6.26, in which selected results are portrayed comparing the one-step and two-step response.

It is evident that the superposition principle is valid for small mass ratios m_2/m_1 but inadequate for masses m_2 and m_1 of the same order. For example, in Figure 6.23 for $m_2/m_1 = 0.1$, the one-step procedure leads to 1.57 m slippage whereas the two-step system results to 1.60 m displacement: only a 2% divergence between the two systems, almost exactly the same response. Nevertheless, for $m_2/m_1 = 1$, the one-step system leads to 1.13 m but the two-step to 0.84 m (Figure 6.24).

In conclusion, the single degree of freedom sliding system is a strongly non-linear system and superposition is generally ineffective (see also Figure 6.26).

6.3.3 Application of Whitggar model in case of Asteriou dam

Asteriou earth-fill dam is located in Achaia (near the fault of the recent Achaia-Elia earthquake of 2009); it will rise up to 75 m. The main objective of the study is to approximate realistically the nonlinear dynamic response of the dam. 2-D and 3-D finite element analyses were conducted. The 2-D analyses were performed with three different methods: (a) effective stress-inelastic analysis considering the building up of pore water pressures, utilizing the FLAC code; (b) a two-step procedure of an equivalent-linear total stress analysis followed by a simplified calculation of inelastic deformations (employing QUAD4 and SLIDE); and (c) a simplified time-domain analysis of inelastic displacements (WHITGGAR), which combines the response of an equivalent single degree of freedom oscillator with the induced slippage of a Newmark type model. From a practical viewpoint, satisfactory convergence of the three methods is noted. Figures 6.27 ÷ 6.34 illustrate the geometry of Asteriou dam and results from the analyses performed.

Figure 6.27(a) portrays the longitudinal section of Asteriou dam. The body of the dam is built from the limestone of the adjustment area, has a clay core, and is founded on

flysch of adequate strength and permeability properties. Two typical sections Δ6, Δ11 of height 76 m and 54 m respectively are studied (Figures 6.27 b and c). Apart from the finite element model that had been analysed with FLAC, two simplified models of the dam are employed (Figure 6.28) and their results will be discussed herein.

The two-step procedure of simulating the dam's response starts by computing the (amplified) acceleration profile along the dam through wave propagation analysis, and then assessing the induced slippage of a sliding wedge from the dam on a rigid inclined plane, the angle of which with respect to the horizontal is equal to the average angle of the sliding surface. Figure 6.29 depicts the sliding displacement response triggered by the 2003 Lefkada record with the two-step method analysis. The corresponding results with the Whitggar model are shown in Figures 6.30 and 6.32. Furthermore, Figures 6.33 and 6.34 present the comparison of the acceleration outcomes utilizing the Whitggar and FLAC models. Both produce results in reasonable agreement from a practical point of view.

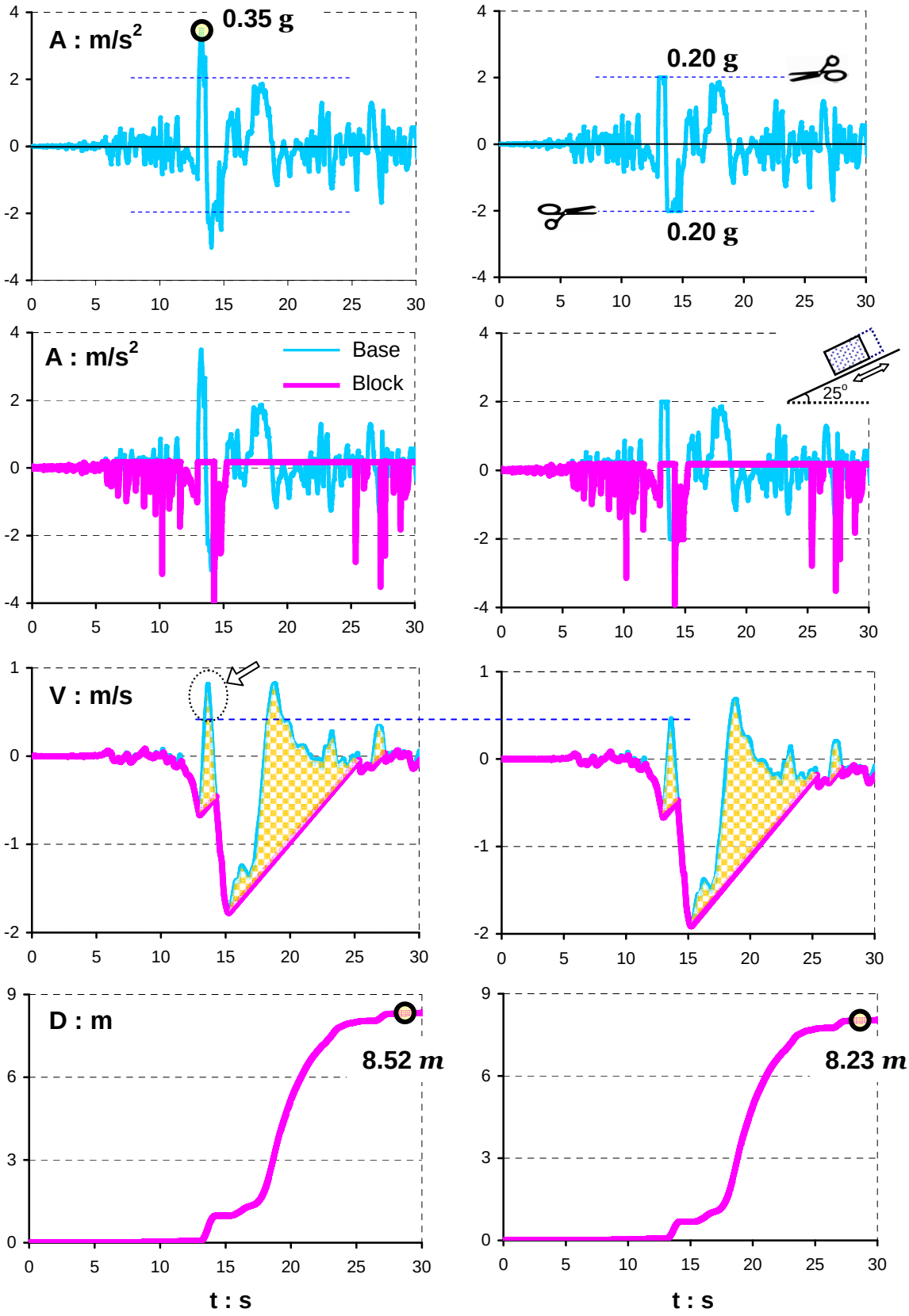

Figure 6.1 *Acceleration, velocity, and sliding displacement time histories triggered by the TCU 052 EW record. Effect of peak acceleration on sliding response: for the plots on the left the excitation applied with its maximum recorded values whereas for those on the right all the acceleration values exceeding 0.2 g are trimmed. ($\beta = 25^o$, $a_C = 0.0175$)*

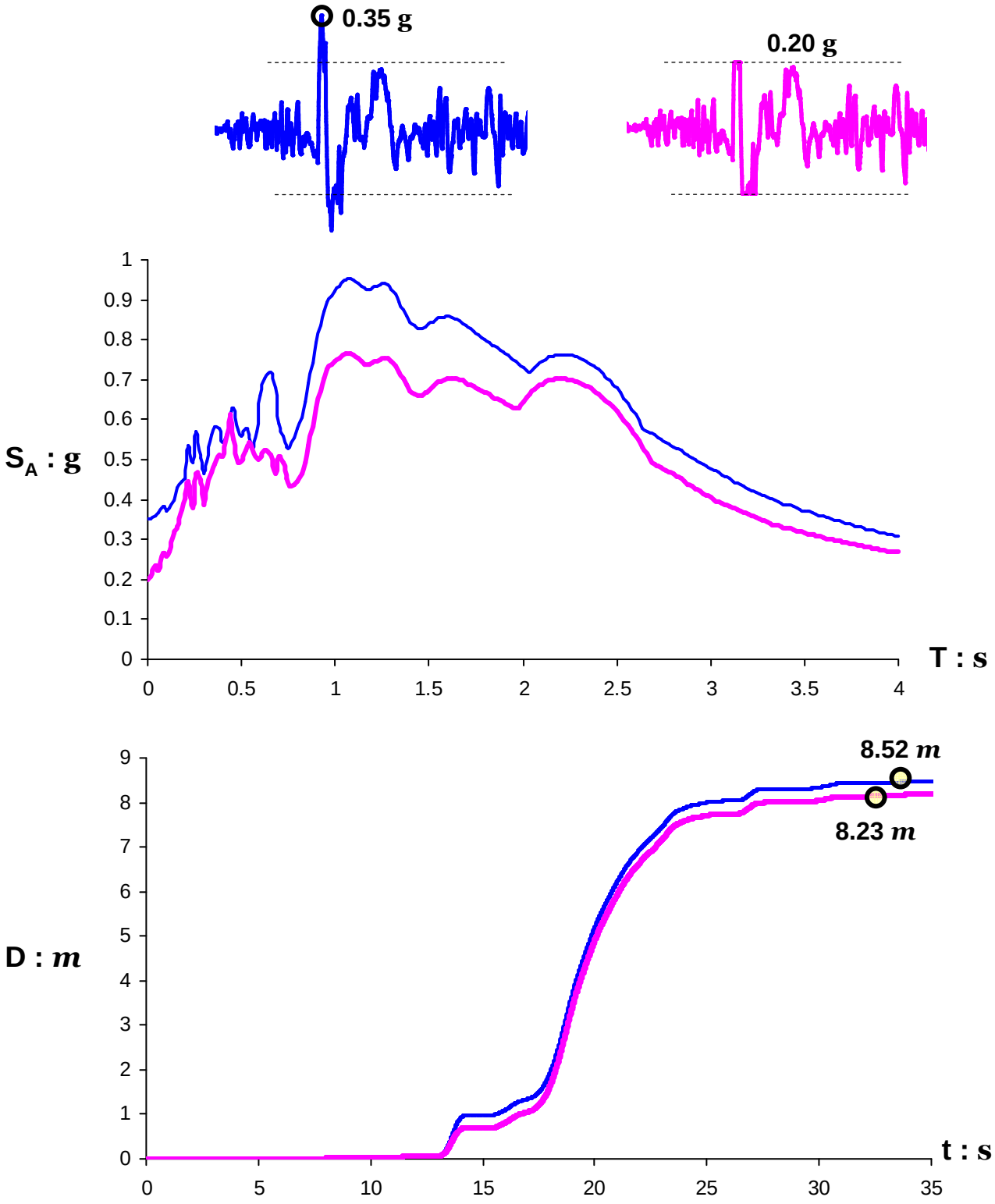

Figure 6.2 *Elastic response spectrum and sliding response induced by the TCU 052 EW of the Chi-chi 1999 earthquake: lines of blue color represent the response triggered by the record as is; whereas lines in pink correspond to the trimmed excitation. ($\beta = 25^{o}$, $a_C = 0.0175$)*

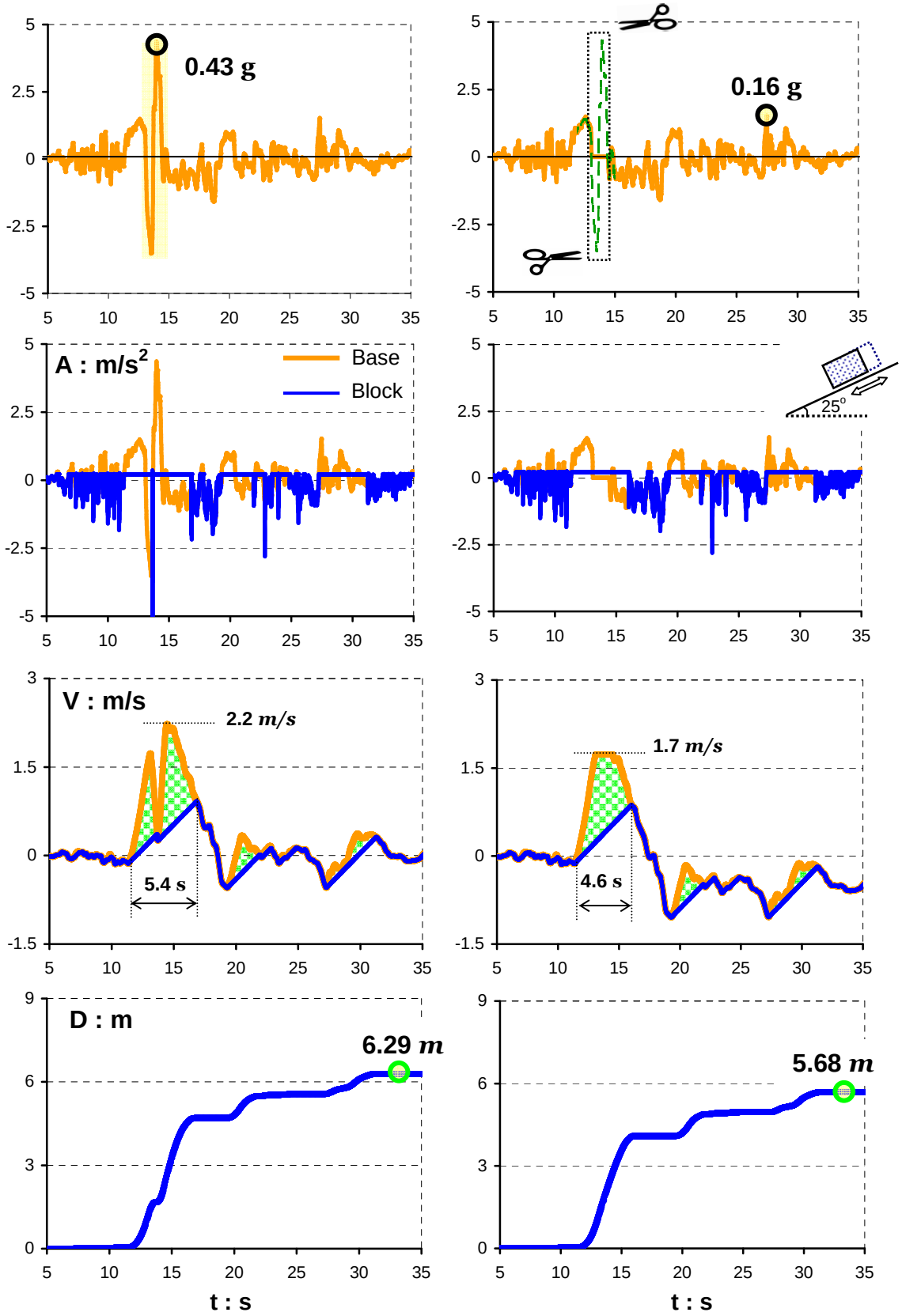

Figure 6.3 *Acceleration, velocity, and sliding displacement time histories triggered by the TCU 052 NS record. The figures on the left depict the response when excitation applied as recorded. Those on the right, illustrate sliding response when the peak acceleration pulse is removed keeping the rest of the record as is. (β = 25°, a_C = 0.021)*

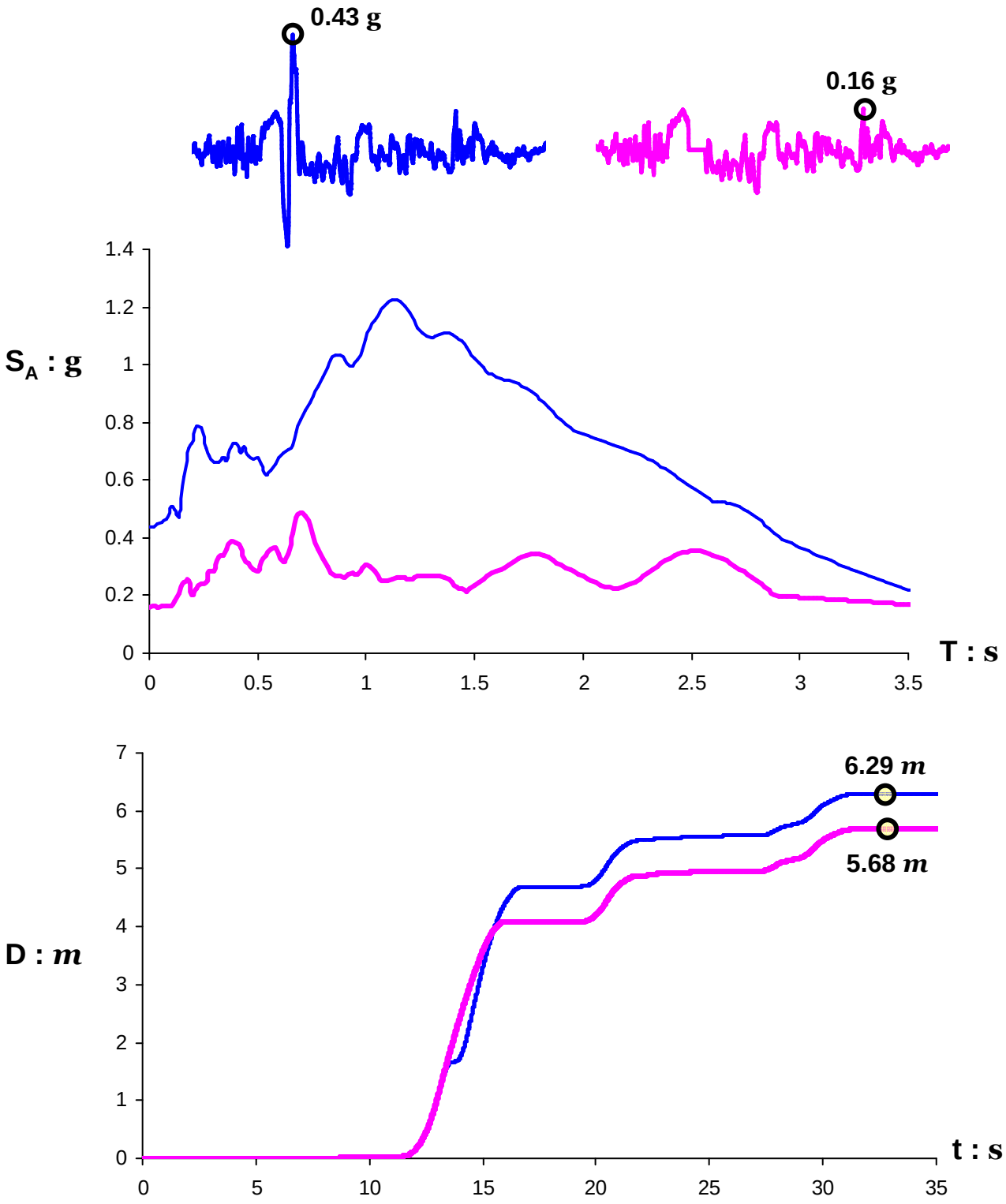

Figure 6.4 *Elastic response spectrum and sliding response induced by the TCU 052 NS of the Chi-chi 1999 earthquake: lines of blue color represent the response triggered by the record as is; whereas lines in pink correspond to the trimmed excitation.*
($\beta = 25^{o}$, $a_C = 0.021$)

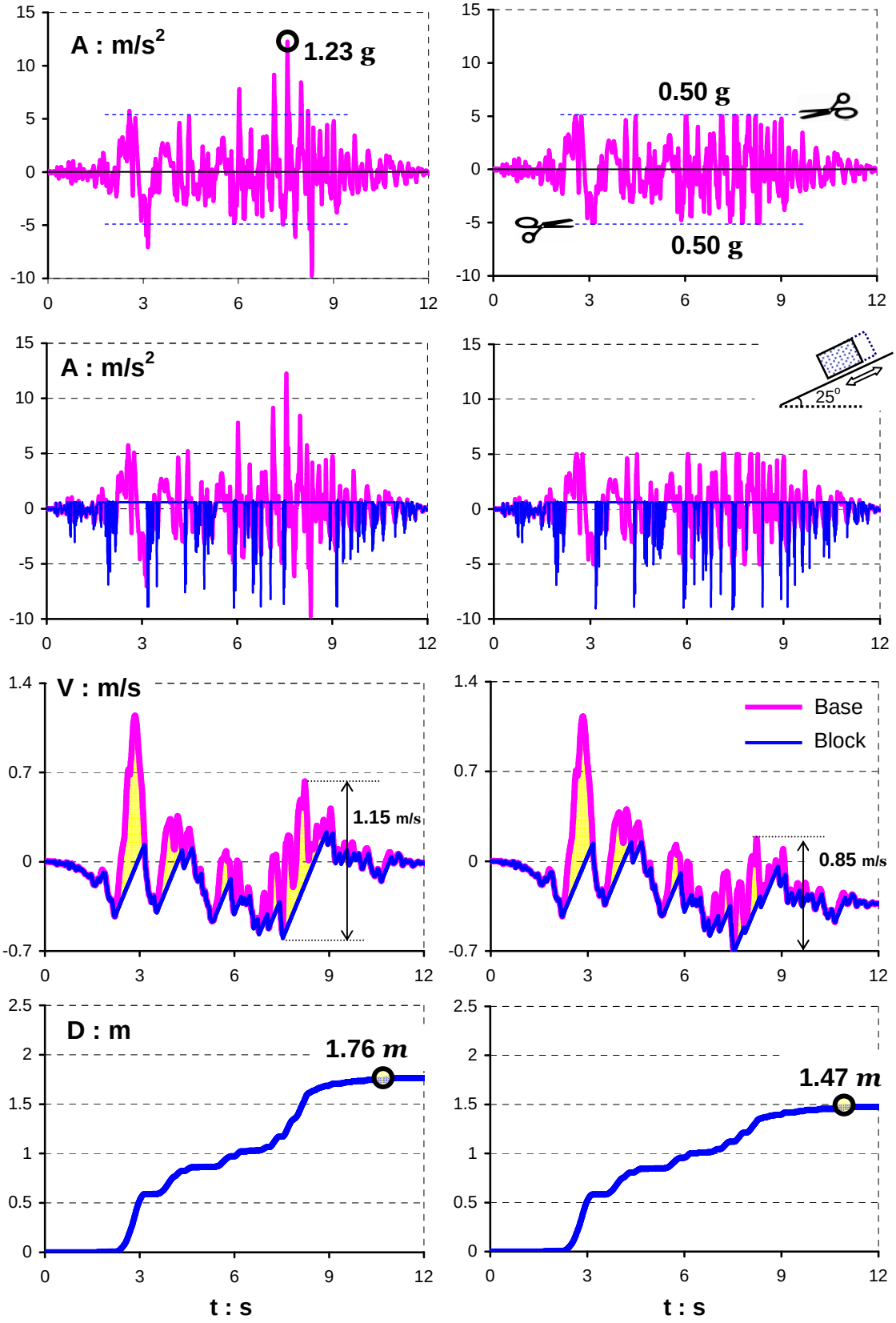

Figure 6.5 *Acceleration, velocity, and sliding displacement time histories triggered by the Pacoima Dam record (component 164°) of the San Fernando 1971 earthquake. Figures on the left handside present the response induced by the record as is. For the figures on the right, all the acceleration values exceeding 0.5 g are trimmed. (β = 25°, a_C = 0.0615)*

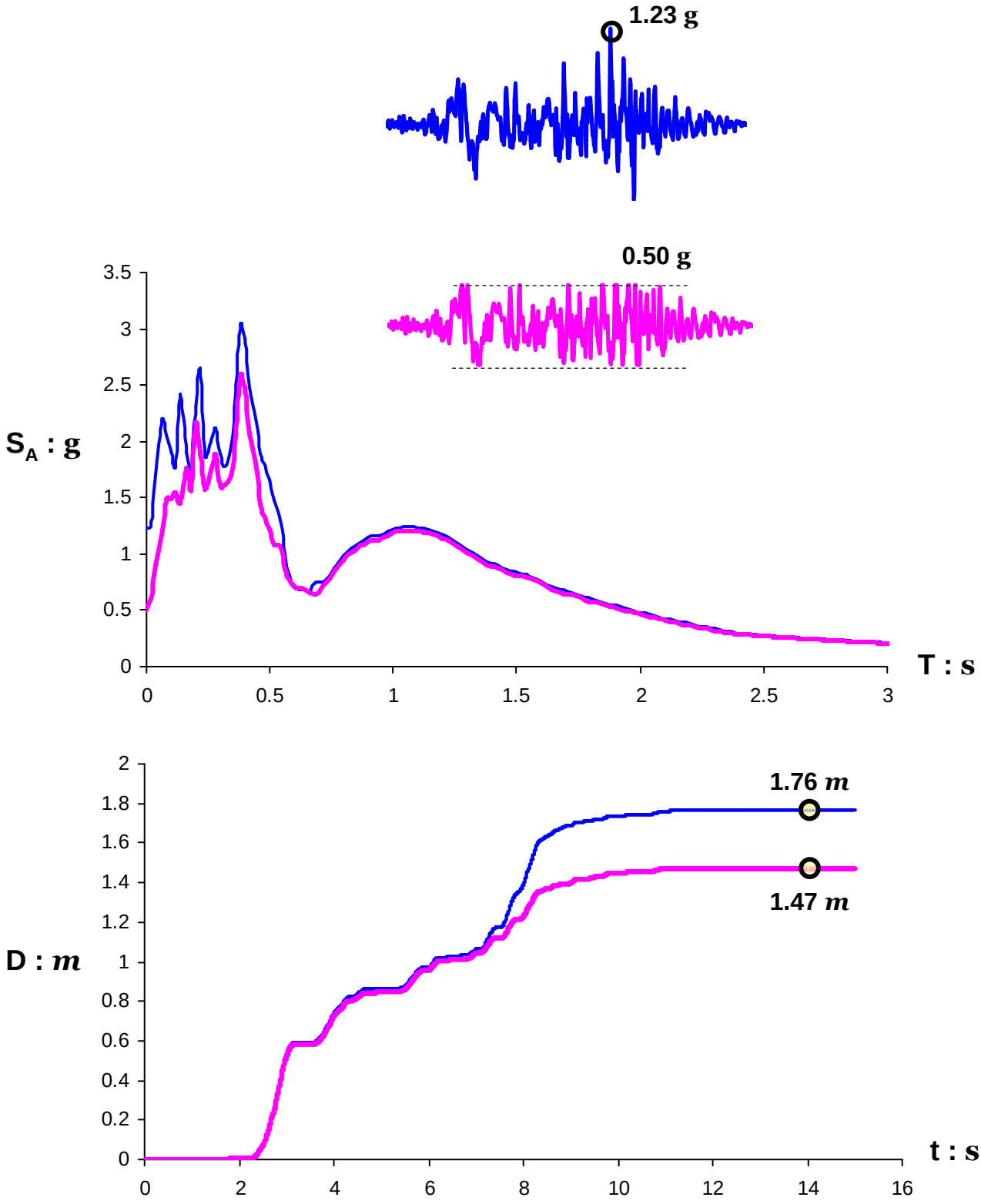

Figure 6.6 *Elastic response spectrum and sliding response induced by the Pacoima Dam record (component 164°) of the San Fernando 1971 earthquake: lines of blue color represent the response triggered by the record as is; whereas lines in pink correspond to the trimmed excitation. (β = 25°, a_C = 0.0615)*

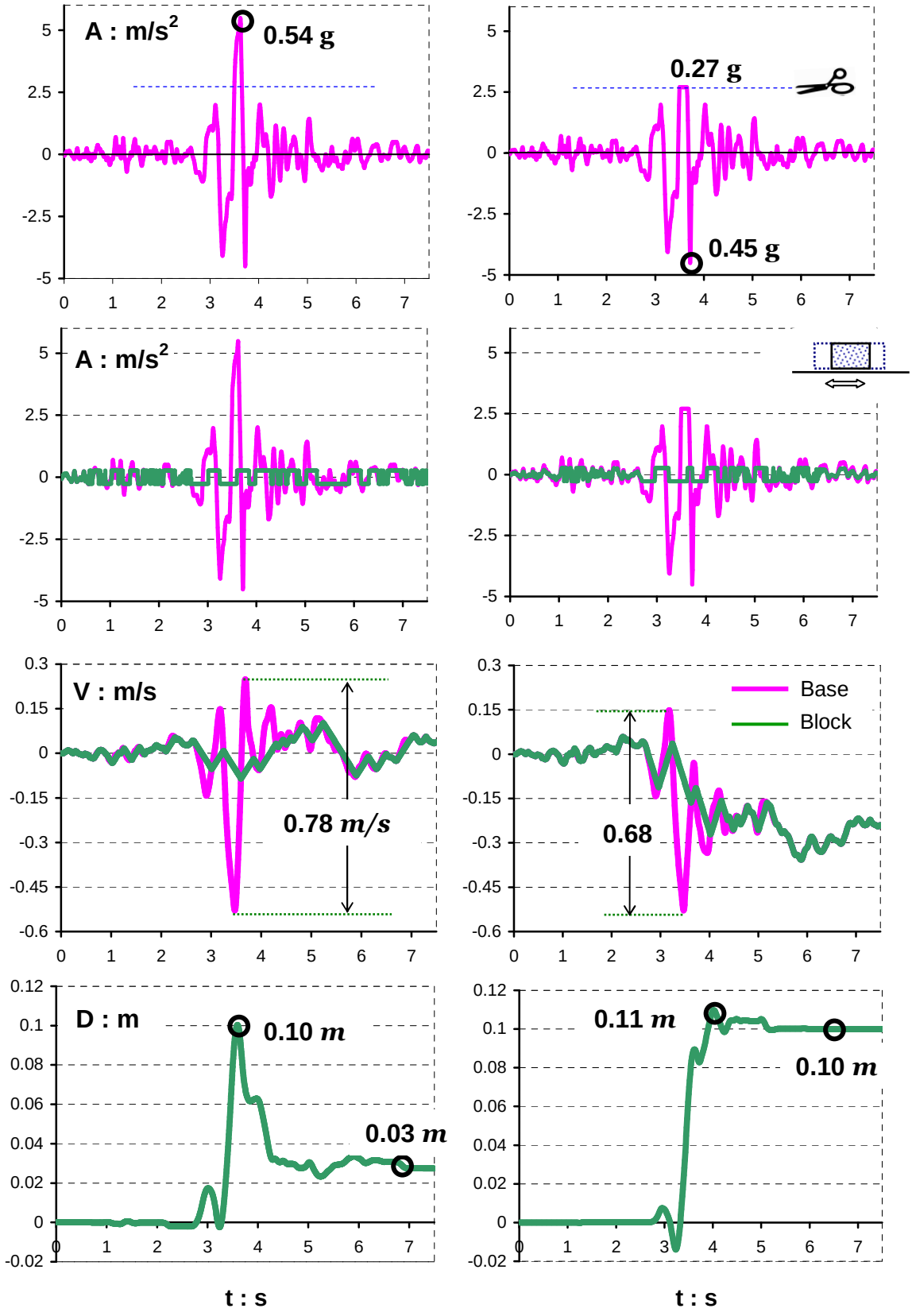

Figure 6.7 *Acceleration, velocity, and sliding displacement time histories triggered by the Aegion record (in the OTE building) of the 1995 earthquake. Figures on the left handside present the response induced by the record as is. For the figures on the right, the maximum acceleration pulse is trimmed to 0.27* g. *($\beta = 0^o$, $a_C/a_H = 0.027$)*

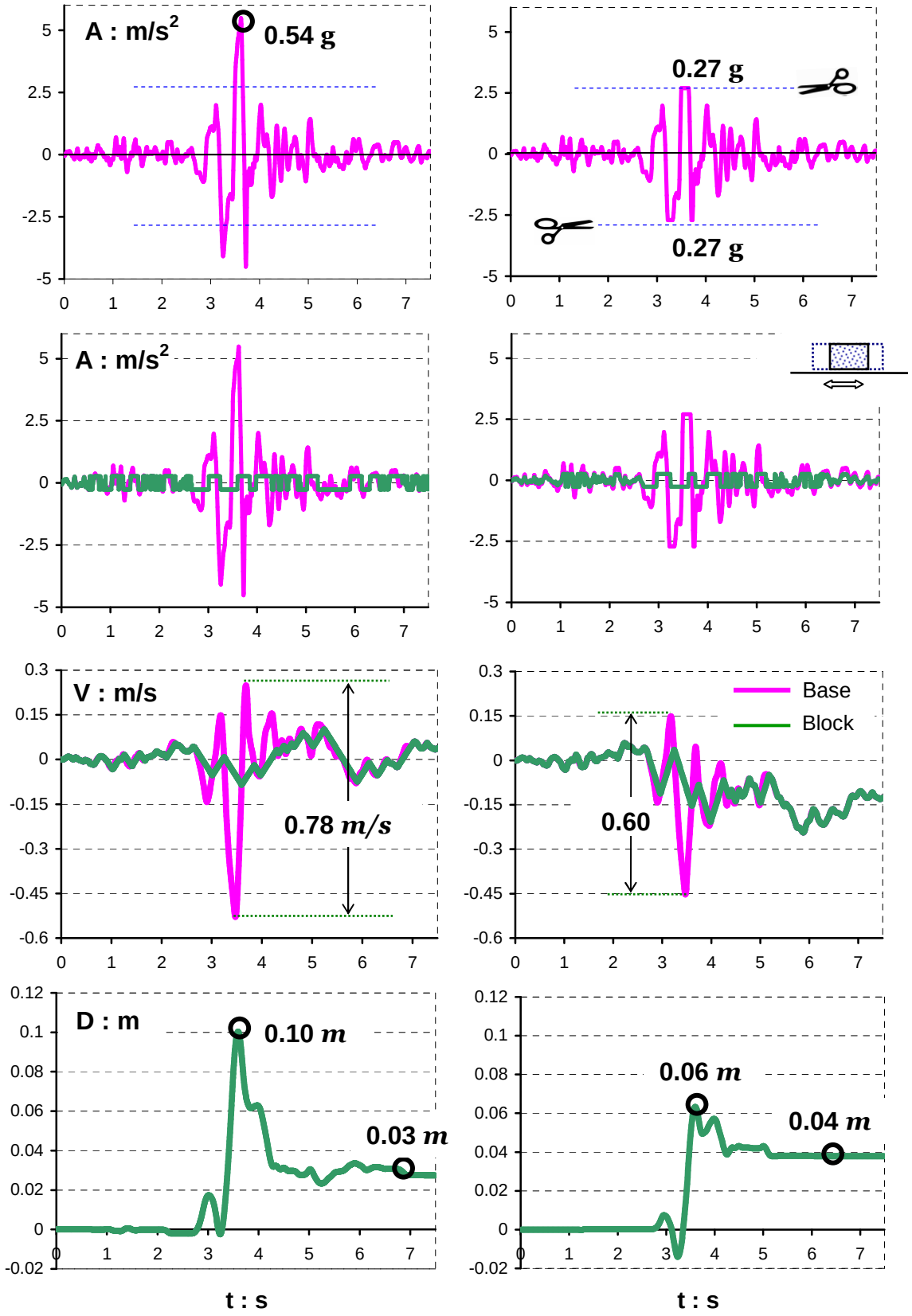

Figure 6.8 *Acceleration, velocity, and sliding displacement time histories triggered by the Aegion record (in the OTE building) of the 1995 earthquake. Figures on the left handside present the response induced by the record as is. For the figures on the right, all the acceleration values exceeding 0.27* g *are trimmed. ($\beta = 0^o$, $a_c/a_H = 0.027$)*

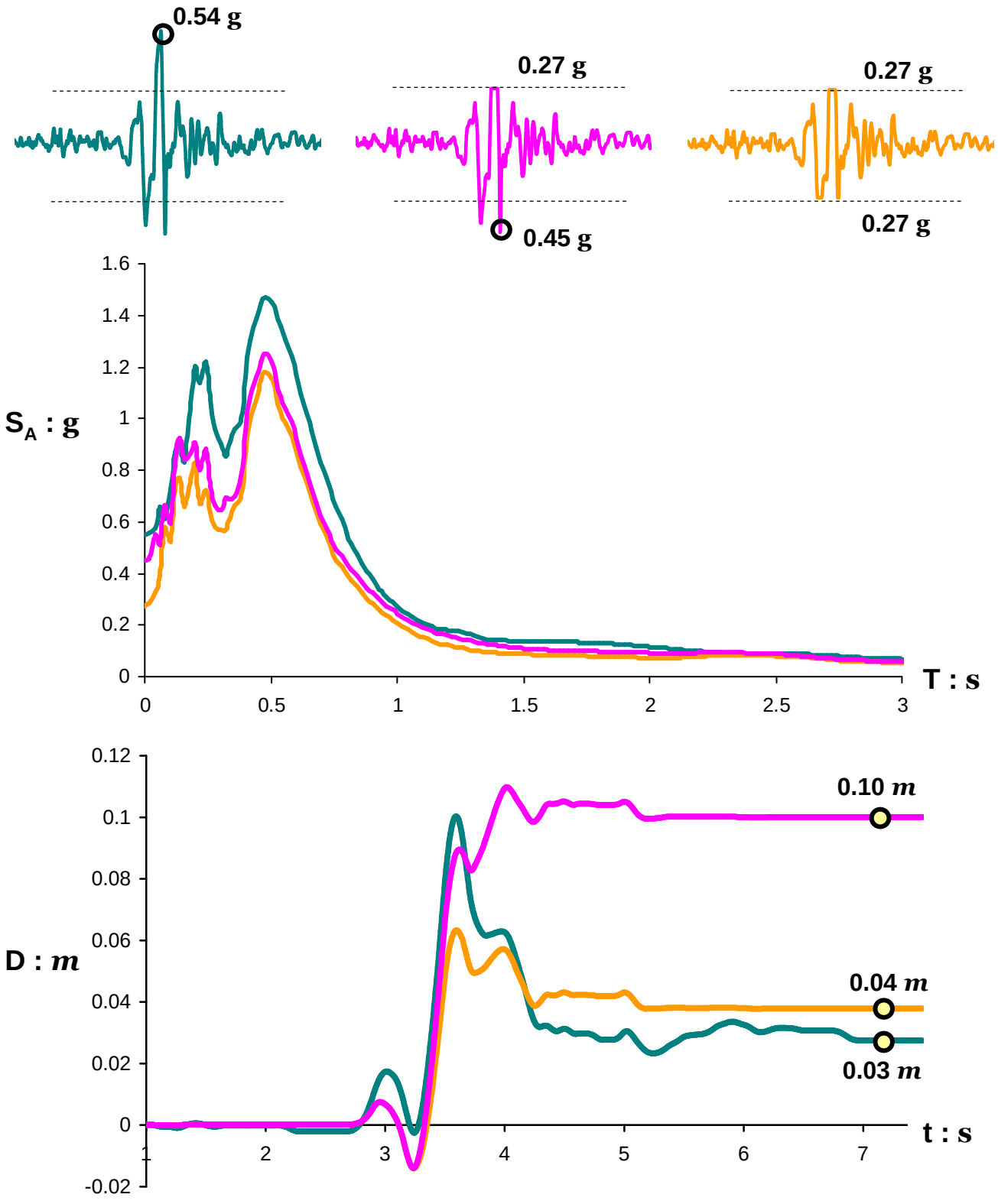

Figure 6.9 *Elastic response spectrum and sliding response induced by the Aegion record (in the OTE building) of the 1995 earthquake : lines of green color represent the response triggered by the record as is; whereas lines in pink and orange correspond to one-sided and both-sided trimmed excitation respectively. ($\beta = 0^o$, $a_C/a_H = 0.027$)*

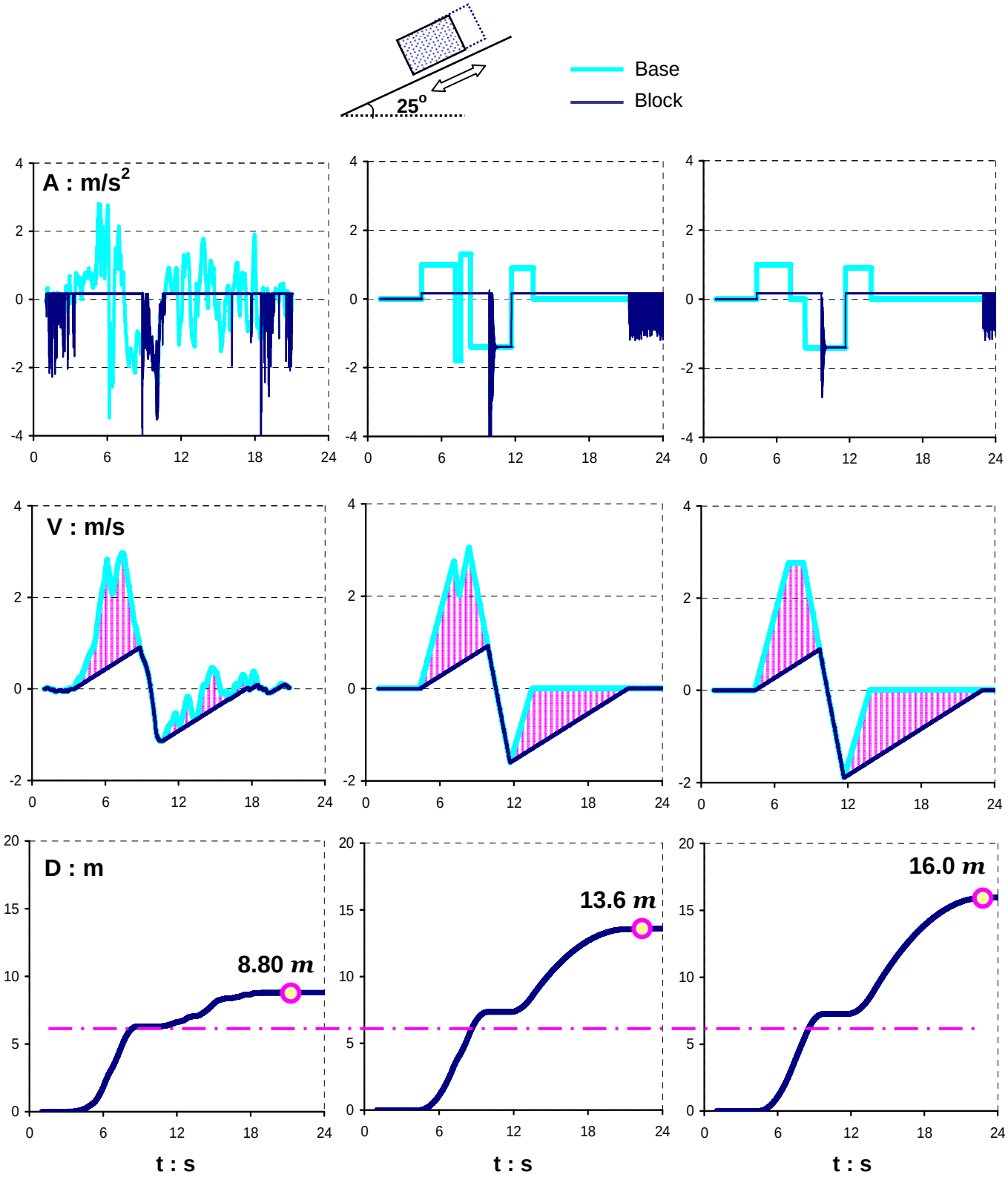

Figure 6.10 *Simple approximation of the TCU 068- NS record through a series of rectangular pulses. The left column plots show the response to the detailed ground motion, whereas the middle and the right column display two simplified accelerations. Even though the first major slippage of nearly 6.5 m (dotted area) is approximated by the simplified motions, the cut off of the details leads to substantial difference in the final result. ($\beta = 25^o$, $a_C/a_H = 0.05$)*

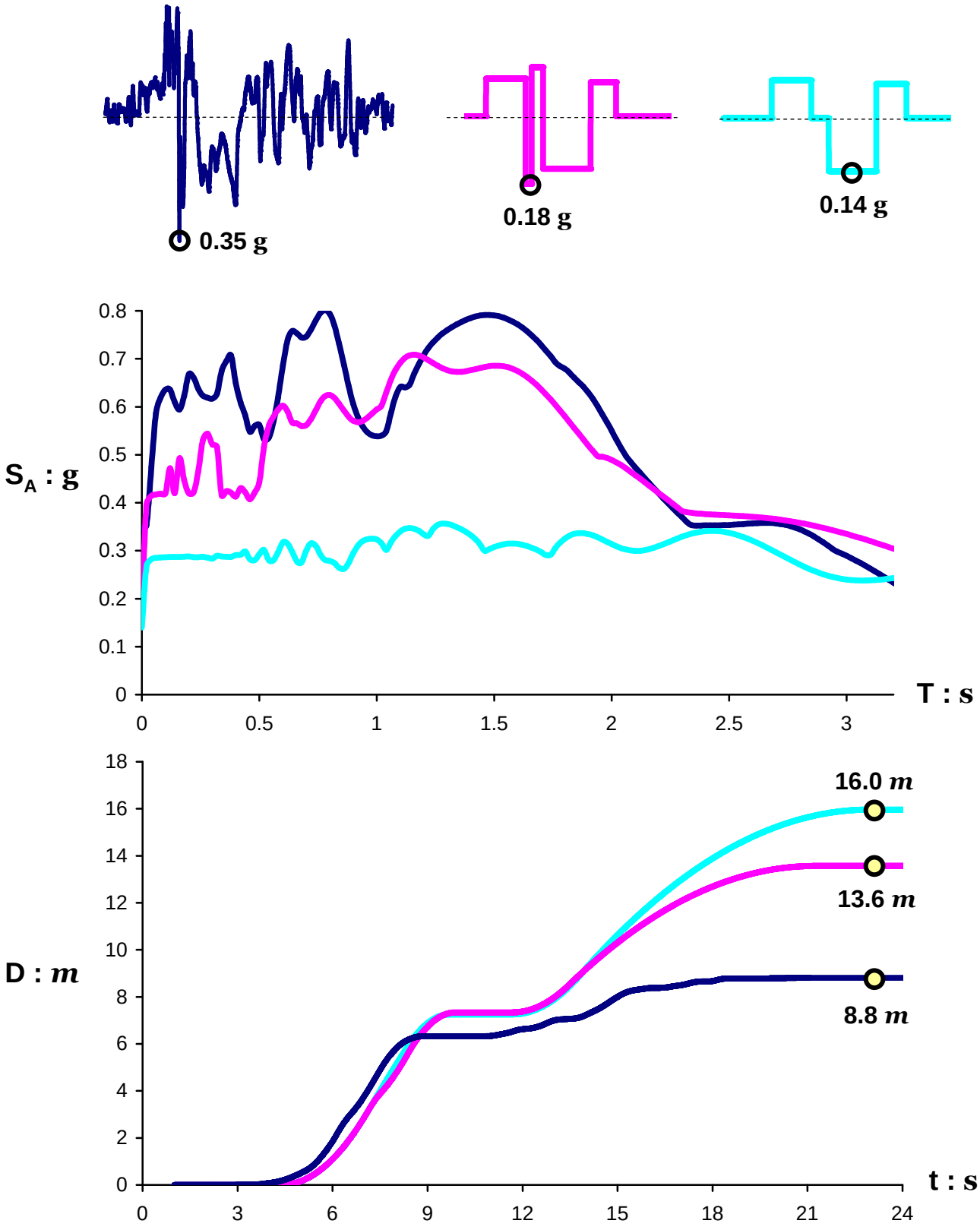

Figure 6.11 *Elastic response spectrum and sliding response induced by the TCU 068-NS record of the Chi-chi 1999 earthquake : lines of green color represent the response triggered by the record as is; whereas lines in pink and orange correspond to simple simulations with rectangular pulses of the original accelerogram. ($\beta = 25^o$, $a_C/a_H = 0.05$)*

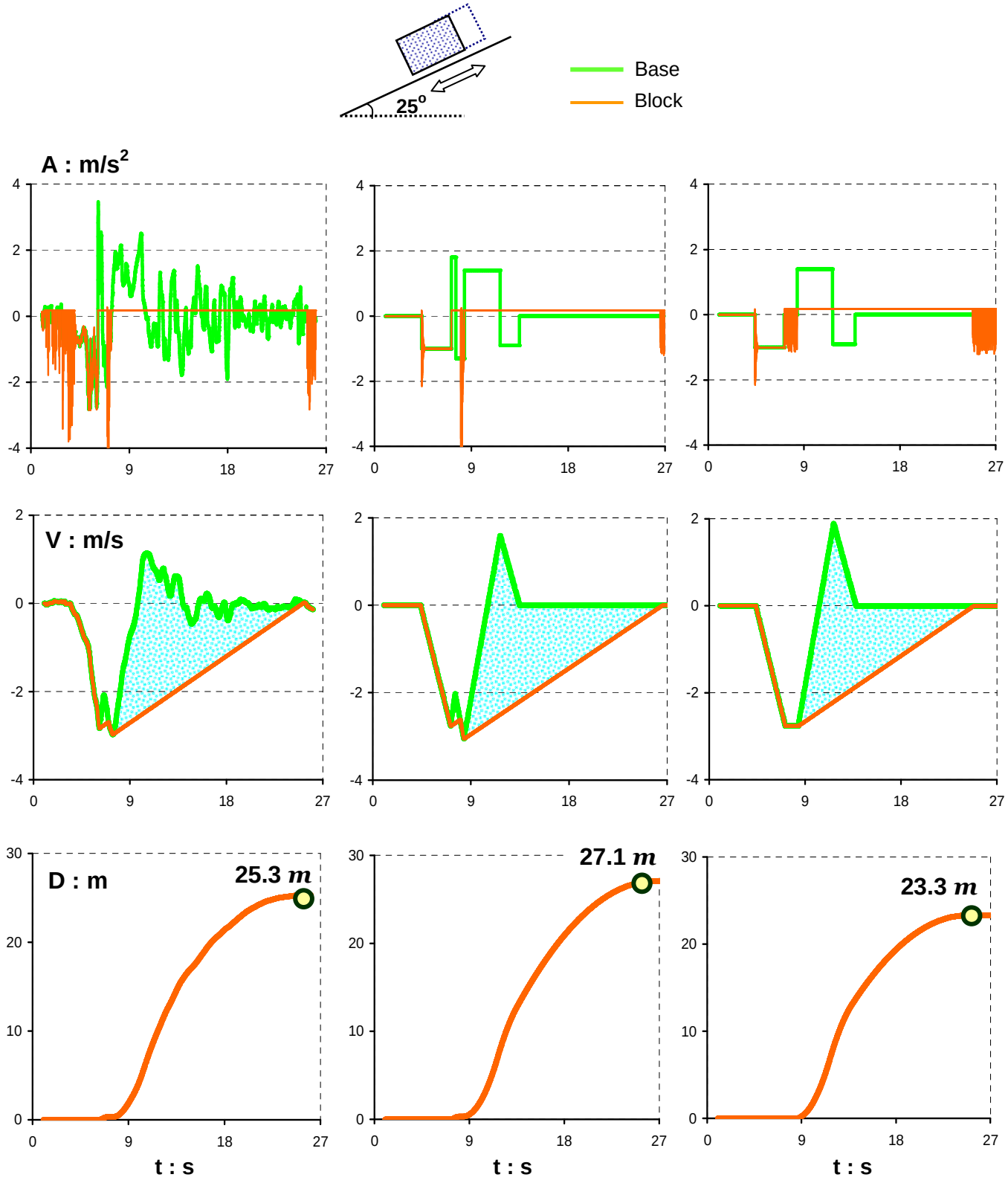

Figure 6.12 *Simple simulation of the reversed TCU 068-NS record through a series of rectangular pulses. The final displacements in all three cases (the actual record and the approximations) are in reasonable agreement. ($\beta = 25^o$, $a_C/a_H = 0.05$)*

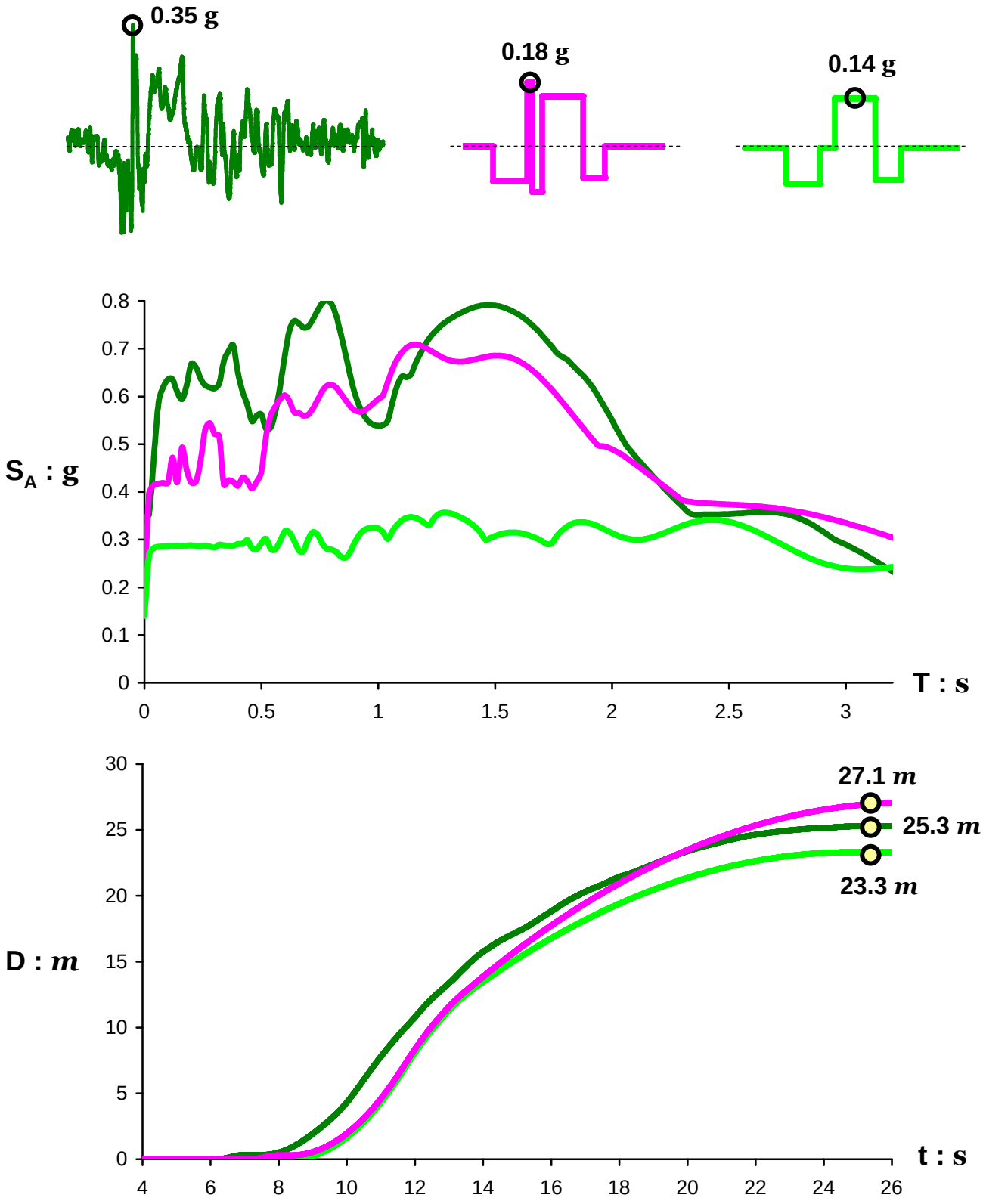

Figure 6.13 *Elastic response spectrum and sliding response induced by the reversed TCU 068-NS record of the Chi-chi 1999 earthquake : lines of green color represent the response triggered by the record as is; whereas lines in pink and orange correspond to simple simulations with rectangular pulses of the original accelerogram.*
($\beta = 25^o$, $a_C/a_H = 0.05$)

References

Abrahamson, N. A. (2000). Effects of rupture directivity on probabilistic seismic hazard analysis, Proceedings, 6th International Conference on Seismic Zonation, Palm Springs, California, Earthquake Engineering Research Institute.

Abrahamson, N. A. (2001). Incorporating Effects of Near Fault Tectonic Deformation into Design Ground Motions, University at Buffalo MCEER: Friedman F. V. Professional Program, http://mceer:buffalo.edu/outreach/pr/Abrahamson.asp

Abrahamson, N. A., and Shedlock, M. K. (1997). Overview, Seismological Research Letters, Vol. 68, No. 1, 9-23.

Aki, K. (1988). Local site effects on strong ground motion, Earthquake Engineering and Soil Dynamics II–Recent advances in ground motion evaluation, Geotechnical Special Publication No.20, J.L. Von Thum (Editor), ASCE, New York, pp. 103–155.

Aki, K., and Richards, P.G. (1980). Quantitative Seismology, Volumes 1 and 2, New York: W. H. Freeman.

Akyüz, H.S., Barka, A., Altunel, E., Hartleb, R., and Sunal, G. (2000). Field observation and slip distribution of the November 12, 1999 Düzce earthquake (M = 7.1), Bolu – Turkey, The 1999 Izmit and Düzce Earthquakes: preliminary results. Istanbul Technical University, pp 63–70.

Alavi, B., and Krawinkler, H. (2000). Consideration of Near-Fault Ground Motion Effects in Seismic Design, Proceedings of the 12th World Earthquake Conference on Earthquake Engineering, New Zealand.

Ambraseys, N.N., and Sarma, S.K. (1967). The Response of Earth Dams to Strong Earthquakes, Géotechnique, 17, pp. 181-213.

Ambraseys, N.N., and Menu, J. (1988). Earthquake induced ground displacements, Earthquake Engineering and Structural Dynamics, Vol. 16, 985-1006.

Ambraseys, N.N., and Srbulov, M. (1994). Attenuation of earthquake-induced ground displacements, Earthquake Engineering and Structural Dynamics, Vol. 23, 467-487.

Amontons, G. (1695). Remarques et expériences physiques sur la construction d'une nouvelle clepsydre, sur les baromètres et hygromètres, Jombert, Paris.

Amontons, G. (1699). Moyen de substituer commodément l'action du Feu à la force des Hommes et des Chevaux pour mouvoir des Machines, Mémoires de l'Académie Royale des Sciences, Paris, pp. 112–126.

Anastasopoulos, I., and Gazetas, G. (2007a). Foundation-Structure Systems over a Rupturing Normal Fault: I. Observations after the Kocaeli 1999 Earthquake, Bulletin of Earthquake Engineering, Vol. 5, No. 3, pp. 253-275.

Anastasopoulos, I., and Gazetas, G. (2007b). Behaviour of Structure–Foundation Systems over a Rupturing Normal Fault: II. Analyses, Experiments, and the Kocaeli Case Histories, Bulletin of Earthquake Engineering, Vol. 5, No. 3, pp. 277-301.

Anderson, J. R., and Ferri, A. A. (1990). Behaviour of a Single-Degree-of-Freedom System with a Generalized Friction Law, Journal of Sound and Vibration, Vol. 140, No. 2, pp. 287-304.

Apostolou, M., Gazetas, G., and Garini, E. (2007). Seismic Response of Simple Slender Structures with Foundation Uplifting. Soil Dynamics and Earthquake Engineering, 27, pp. 642-654.

Araya, R., and Saragoni, R. (1984). Earthquake Accelerogram Destructiveness Potential Factor, Proceedings of the 8th World Conference on Earthquake Engineering, S. Francisco, Vol. 2, pp. 835-841.

Arias, A. (1970). A measure of earthquake intensity, Seismic Design for Nuclear Power Plants (ed. R.J. Hansen), MIT Press, Cambridge, Massachusetts, pp. 438-483.

Avery, H.R., Berrill, J.B., Coursey, P.F., Deam, B.L., Dewe, M.B., François, C.C., Pettinga, J.R., and Yetton, M.D. (2004). The Canterbury University strong-motion recording project. Proceedings 13th World Conference on Earthquake Engineering, Vancouver, B.C., Canada, Paper No. 1335.

Awrejcewicz, J., and Olejnik, P. (2005). Analysis of Dynamic Systems with Various Friction Laws, ASME, Applied Mechanics Reviews, Vol. 58, pp. 389-411.

Berberian, M. (1979). Earthquake faulting and bedding thrust associated with the Tabas Golshan (Iran) earthquake of September 16, 1978, Bulletin of Seismological Society of America, 69, pp. 1861-1887

Berrill, J.B. (2006). The Canterbury Accelerograph Network and other Follies. Proceedings of New Zealand Workshop on Geotechnical Earthquake Engineering, University of Canterbury, Christchurch, New Zealand, 20-21 November.

Berrill, J.B., Davis, R.O., and McCahon, J.F. (1993). Christchurch seismic hazard pilot study. Bull. New Zealand Nat. Soc. Earthquake Eng., 26, pp. 14–27.

Bertero, V.V. (1976). Establishment of design earthquakes : evaluation of present methods, Proceedings, International Symposium of Earthquake Structural Engineering, St. Louis, University of Missouri-Rolla, Vol. 1, pp. 551-580.

Bertero, V.V., Mahin, S.A., and Herrera, R.A. (1978). Aseismic Design Implications of Near-Fault San Fernando Earthquake Records, Earthquake Engineering and Structural Dynamics, Vol. 6, pp. 31-42.

Beucke, K. E., and Kelly, J. M. (1985). Equivalent Linearization for Practical Hysteretic Systems, International Journal of Non-Linear Mechanics, Vol. 23, No. 4, pp. 211-238.

Bolt, B.A. (2004). Earthquakes, W. H. Freeman & Co, Fifth Edition, New York.

Bommer, J. J. and Martinez-Pereira. (1999). The effective duration of earthquake strong motion, Journal of Earthquake Engineering, Vol. 3, No. 2, pp. 127- 172.

Boore, M. D. (2001). Effect of baseline corrections on displacements and response spectra for several Recordings of the 1999 Chi-Chi, Taiwan, Earthquake, Bulletin of the Seismological Society of America, Vol. 91, No. 5, pp. 1199-1211.

Bowden, F. P., and Tabor, D. (1954). The Friction and Lubrication of Solids, revised edition, Clarendon, Oxford.

Bowden, F. P., and Tabor, D. (1964). The Friction and Lubrication of Solids: Part II, Clarendon, Oxford.

Bradley, B.A., Cubrinovski, M., Dhakal, R.P., MacRae, G.A. (2009). Probabilistic seismic performance assessment of a bridge-foundation-soil system. Proceedings of the NZSEE Conference, Christchurch, N. Zealand, 3-5 April.

Bradley, B.A., and Cubrinovski, M. (2011). Near-source strong ground motions observed in the 22–2–11 Christchurch earthquake. Seismological Research Letters; (submitted for the Special Issue on the Christchurch Earthquakes).

Bray, J.D., and Rathje, E.M. (1998). Earthquake-Induced Displacements of Solid-Waste Landfills, Journal of Geotechnical and Geoenvironmental Engineering, ASCE, Vol. 124, pp. 242-253.

Bray, J.D., and Rodriguez-Marek, A. (2004). Characterization of Forward–Directivity Ground Motions in the Near-Fault Region, Soil Dynamics Earthquake Engineering, Vol. 24, pp. 815-828.

Changhai, Z., Shuang, L., Xie, L.L., and Yamin, S. (2007). Study on Inelastic Displacement Ratio Spectra for Near-Fault Pulse-Type Ground Motions, Earthquake Engineering and Engineering Vibration, Springer, Vol. 6, No. 4, pp. 351-356.

Chen, W. F. and Scawthorn, C. (2003). Earthquake Engineering Handbook, CRC Press, Boca Raton, Florida.

Constantinou, M. C., and Gazetas, G. (1987). Probabilistic Seismic Sliding Deformations of Earth Dams and Slopes, Proceedings of the Specialty Conference on Probabilistic Mechanics and Structural Reliability, ASCE, Berkeley, pp. 318-321.

Constantinou, M.C., Gazetas, G., and Tadjbakhsh, I. (1984). Stochastic Seismic Sliding of Rigid Mass against Asymmetric Coulomb Friction, Earthquake Engineering and Structural Dynamics, Vol. 12, pp. 777-793.

Coulomb, C. A. (1785). Théorie des Machines Simples, en Ayant égard au Frottement de Leurs Parties, et a la Roideur des Cordages, Mémoire de Mathématique et de Physique de l'Académie Royale, Paris, pp. 161–342.

Crespellani, T., Madiai, C., & Vannucchi, G. (1998). Earthquake Destructiveness Potential Factor and Slope Stability, Geotechnique, Vol. 48, No. 3, pp. 411-420.

Crespellani, T., Madiai, C., & Vannucchi, G. (1996). Earthquake Destructiveness Potential Factor and Permanent Displacements of Gravity Retaining Walls, Analysis and Design of Retaining Structures Against Earthquakes, Geotechnical special publication No.60, ASCE, pp. 124-133.

Cubrinovski, M., Green, R., Allen, J., Ashford, S., Bowman, E., Bradley, B., Cox, B., Hutchinson, T., Kavazanjian, E., Orense, R., Pender, M., Quigley, M., Wilson, T., Wotherspoon, L. (2010). Geotechnical reconnaissance of the 2010 Darfield (New Zealand) earthquake, Bulletin of the New Zealand Society for Earthquake Engineering, 43, pp. 243-320.

Danay, A., and Adeghe, L. N. (1993). Seismic Induced Slip of Concrete Gravity Dams, Journal of Structural Engineering, ASCE, Vol. 119, No. 1, pp. 1080-1129.

Dakoulas, P., and Gazetas, G. (2008). Insight into Seismic Earth and Water Pressures against Caisson Quay Walls, Geotechnique, Vol. 58, pp. 95-111.

Del Gaudio, V., Pierri, P., and Wasowski, J. (2003). An Approach to Time-Probabilistic Evaluation of Seismically Induced Landslide Hazard, Bulletin of the Seismological Society of America, Vol. 93, pp. 557-569.

Deng, J., Tsutsumi, Y., Kameya, H., and Koseki, J. (2010). A Modified Procedure to Evaluate Earthquake-Induced Displacement of Slopes Containing a Weak Layer, Soils and Foundations, Vol. 50, No. 3, pp. 413-420.

Dupont, P., Armstrong, B., and Hayward, V. (2000). Elasto-plastic Friction Model: Contact Compliance and Stiction, Proceedings of the American Control Conference, Chicago, Illinois, June, pp. 1072-1077.

Elder, D.McG., McCahon, I.F., and Yetton, M.D. (1991). The Earthquake Hazard in Christchurch: a Detailed Evaluation. Research Report to EQC, Soils and Foundations Ltd, Christchurch, N. Z., 131pp.

Erdik, M. (2000). Report on 1999 Kocaeli and Duzce (Turkey) earthquakes. Proceedings of the 3rd International Workshop on Structural Control, Paris—France, 6–8 July, pp. 149–86.

Erdik, M. (2001). Report on 1999 Kocaeli and Düzce (Turkey) Earthquakes. Structural control for civil and infrastructure engineering. Casciati F (ed.) G. Magonette, World Scientific.

Erdik, M., Demircioglu, M., Sesetyan, K., Durukal, E., and Siyahi, B. (2004). Earthquake hazard in Marmara Region, Turkey. Soil Dynamics and Earthquake Engineering, 24, pp. 605–631.

Fardis, N., Georgarakos, P., Gazetas, G., and Anastasopoulos, I. (2003). Sliding Isolation of Structures: Effect of Horizontal and Vertical Acceleration, Proceedings of the FIB International Symposium on "Concrete Structures in Seismic Regions", Athens, Greece (in CD-Rom).

Fenves, G., and Chopra, A. K. (1986). Simplified Analysis for Earthquake Resistant Design of Concrete Gravity Dams, Report UBC/EERC-85/10, University of California, Berkeley.

Franklin, A., and Chang, F. K. (1977). Earthquake Resistance of Earth and Rock-Fill Dams, Report 5: Permanent Displacements of Earth Embankments by Newmark Sliding Block Analysis, Miscellaneous Paper S-71-17, Soils and Pavements Laboratory, U.S. Army Engineer Waterways Experiment Gazetas,

Garini, E., Berrill, J., and Apostolou, M. (2011). Sliding and overturning potential of the Christchurch 2011 earthquake records, Earthquake Engineering and Structural Dynamics, (accepted for possible publication).

Gazetas, G., Garini, E., Anastasopoulos, I., and Georgarakos, T. (2009). Effects of Near–Fault Ground Shaking on Sliding Systems, Journal of Geotechnical and Geoenvironmental Engineering, ASCE, Vol. 135, No. 12, pp. 1906-1921.

Gazetas, G., Apostolou, M., and Anastasopoulos, I. (2003). Seismic uplifting of foundations on soft soil, with examples from Adapazari (Izmit 1999, Earthquake), BGA International Conference on Foundations: Innovations, Observations, Design and Practice, University of Dundee, Scotland, September 2–5, pp 37–50.

Gazetas, G. (1996). Soil Dynamics and Earthquake Engineering: Case Histories. Symeon Publishers, Athens, Greece; Chapter 5: The Aegion 1995 Earthquake, pp. 269-317.

Gazetas, G., and Uddin, N. (1994). Permanent deformation on pre-existing sliding surfaces in dams, Journal of Geotechnical Engineering, ASCE, Vol.120, No.11, pp. 2041–2061.

Gazetas, G. (1987). Seismic response of earth dams: some recent developments, Soil Dynamics and Earthquake Engineering, Vol.6, No.1, pp. 2–47.

Gazetas, G. (1981). A new dynamic model for earth dams evaluated through case histories, Soils and Foundations, Vol.21, No.1, pp. 67–78.

Gazetas, G., Debchaudhury, A., and Gasparini, D.A. (1981). Random Vibration Analysis for the Seismic Response of Earth Dams, Géotechnique, Vol. 31, No.2, pp. 261-277.

Garini, E., Gazetas, G., and Anastasopoulos, I. (2011). Asymmetric 'Newmark' sliding caused by motions containing severe 'directivity' and 'fling' pulses. Geotechnique, 61(9), pp. 733-756.

Gelagoti, F., Kourkoulis, R., Anastasopoulos, I., Tazoh, T., Gazetas, G. (2010). Seismic Wave Propagation in a Very Soft Alluvial Valley: Sensitivity to Ground–Motion Details and Soil Nonlinearity, and Generation of a Parasitic Vertical Component. Bulletin of the Seismological Society of America, 100(6), pp. 3035–3054.

Gerolymos, N., Vardoulakis, I., and Gazetas, G. (2007). A thermo-poro-visco-plastic shear band model for seismic triggering and evolution of catastrophic landslides, Soils and Foundations, Vol. 45, No. 1, pp. 11-25.

Guran, A., Pfeiffer, F., and Popp, K. (2001). Dynamics with Friction: Modelling, analysis and experiment (Part II), World Scientific Publishing Co.

Hall, J.F., Heaton, T.H., Halling, M.W., and Wald, D.J. (1995). Near-Source Ground Motion and its Effects on Flexible Buildings, Earthquake Spectra, Vol. 11, No. 4, pp. 569-605.

Hamada, M., and Wakamatsu, K. (1996). Liquefaction, Ground Deformation and their Caused Damage to Structures, In the 1995 Hyogoken-Nanbu Earthquake, Tokyo, Editors: Committee of Earthquake Engineering, Japan Society of Civil Engineers, pp. 45-91.

Hamada, M., Isoyama, R., and Wakamatsu, K. (1995). The 1995 Hyogoken-Nanbu (Kobe) Earthquake: Liquefaction, Ground Displacement and Soil Condition in Hanshin Area, August 1995, Editors: Association for Development of Earthquake Prediction, Japan.

Hancock, J. and Bommer, J. J. (2005). The effective number of cycles of earthquake ground motion, Earthquake Engineering & Structural Dynamics, 34, pp. 637-664.

Harlow, D. H., White, R. A., Rymer, M. J., and Alvarez, S. G. (1993). The San Salvador

earthquake of 10 October 1986 and its historical context, Bulletin of the Seismological Society of America, Vol. 83, No. 4, pp. 1143-1154.

Harp, E.L., and Jibson, R. W. (1995). Seismic instrumentation of landslides: Building a better model of dynamic landslide behaviour, Bulletin of the Seismological Society of America, Vol. 85, pp. 93-99.

Harp, E.L., and Wilson, R.C. (1995). Shaking intensity thresholds for rock falls and slides: evidence from 1987 Whittier Narrows and Superstition Hills earthquakes, strong motion records, Bulletin of the Seismological Society of America, Vol. 85, pp. 1739-1757.

Hartzell, S. (1980). Faulting process of the May 17, 1976 Gazli, USSR earthquake, Bulletin of the Seismological Society of America, Vol. 70, No. 5, pp. 1715-1736.

Hisada, Y., and Bielak, J. (2003). A Theoretical Method for Computing Near-Fault Ground Motions in Layered Half-Spaces Considering Static Offset Due to Surface Faulting, with a Physical Interpretation of Fling Step and Rupture Directivity, Bulleting of the Seismological Society of America, Vol. 93, No. 3, pp. 1154-1168.

Hong, H. K., Tracy, and Liu, C. S. (2000). Coulomb Friction Oscillator: Modelling and Responses to Harmonic Loads and Base Excitations, Journal of Sound and Vibration, Vol. 229, No. 5, pp. 1171-1192.

Housner, G. V. (1963). The behaviour of Inverted pendulum structures during earthquakes. Bulletin of the Seismological Society of America, 53(2), pp. 403-417.

Housner, G. V. (1952). Spectrum intensities of strong motion earthquakes, Proceedings of the Symposium on Earthquake and Blast Effects on Structures, EERI, Oakland California, pp. 20-36.

Howard, J. K., Tracy, C. A., and Burns, R. G. (2005). Comparing Observed and Predicted Directivity in Near-Source Ground Motion, Earthquake Spectra, Vol. 21, No. 4, pp. 1063-1092.

Huang, C.C., Lee, Y.H., Liu, H.P., Keefer, D.K., and Jibson, R.W. (2001). Influence of Surface-Normal Ground Acceleration on the Initiation of the Jih-Feng-Erh-Shan Landslide during the 1999 Chi-Chi, Taiwan, Earthquake, Bulleting of the Seismological Society of America, Vol. 91, No. 5, pp. 953-958.

Hundal, M. S. (1979). Response of a base excited system with Coulomb and viscous

systems, Journal of Sound and Vibration, Vol. 64, No. 3, pp. 371-378.

Ishihara, K. (1997). Terzaghi Oration: Geotechnical Aspects of the 1995 Kobe Earthquake, Proceedings of the 14th Conference on Soil Mechanics and Foundation Engineering, Hamburg, Vol. 4, pp. 2047-2073.

Ishiyama, Y. (1982). Motions of Rigid Bodies and Criteria for Overturning by Earthquake Excitations. Earthquake Engineering and Structural Dynamics, 10, pp. 630-650.

Iwan, W.D., Huang, C.T., and Guyader, A.C. (2000). Important Features of the Response of Inelastic Structures to Near-Fault Ground Motion, Paper No. 1740, Proceedings of the 12th World Earthquake Conference on Earthquake Engineering, New Zealand.

Jibson, R. (1994). Predicting earthquake-induced landslide displacements using Newmark's sliding block analysis, Transportation Research Record, No.1411, Transportation Research Board, Washington, D.C., pp. 9-17.

Junwu, D., Tong, M., Lee, G.C., Xiaorhai, Q., and Wenting, B. (2004). Dynamic responses under the excitation of pulse sequences, Earthquake Engineering and Engineering Vibration, Springer, Vol. 3, No 2, pp. 157-169.

Kragelskii, I. V. (1965). Friction and Wear, Butterworths, London.

Kramer, S. L. (1996). Geotechnical Earthquake Engineering, Prentice-Hall.

Kramer, S. L., and Lindwall, N. W. (2002). Dimensionality and Directionality Effects of Newmark Stability Analysis, Journal of Geotechnical and Geoenvironmental Engineering, ASCE, Vol. 130, pp. 303-315.

Kramer, S. L., and Smith, M. (1997). Modified Newmark Model for Seismic Displacements of Compliant Slopes, Journal of Geotechnical and Geoenvironmental Engineering, ASCE, Vol. 123, pp. 635–644.

Leger, P., and Katsouli, M. (1989). Seismic Stability of Concrete Gravity Dams, Earthquake Engineering and Structural Dynamics, Vol. 18, pp. 889-902.

Lin, J. S., and Whitman, R. V. (1983). Decoupling Approximation to the Evaluation of Earthquake-Induced Plastic Slip in Earth Dams, Journal of Geotechnical Engineering Division, ASCE, Vol. 11, pp. 667-678.

Ling, H. (2001). Recent applications of sliding block theory to geotechnical design, Soil Dynamics and Earthquake Engineering, ASCE, Vol. 21, pp. 189–197.

Makdisi, F.I., and Seed, H.B. (1978). Simplified Procedure for Estimating Dam And Embankment Earthquake Induced Deformations, Journal of Geotechnical Engineering Division, ASCE, Vol. 104, pp. 849–867.

Makris, N., and Psychogios, T. (2006). Dimensional response analysis of yielding structures with first mode dominated response, Earthquake Engineering Structural Dynamics, Vol.35, pp. 1203-1224.

Makris, N., and Konstantinidis, D. (2005). Seismic response analysis of multidrum classical columns. Earthquake Engineering and Structural Dynamics, 34(10), pp. 1243–1270.

Makris, N., and Konstantinidis, D. (2003). The rocking spectrum and the limitations of practical design methodologies. Earthquake Engineering and Structural Dynamics, 32, pp. 265-289.

Makris, N., and Chang, S. (2000). Effect of viscous, visco-plastic and friction damping on the response of seismic isolated structures. Earthquake Engineering and Structural Dynamics, 29, pp. 85–107.

Makris, N., and Roussos, Y.S. (2000). Rocking Response of Rigid Blocks under Near-Source Ground Motions, Géotechnique, 50, No. 3, pp. 243-262.

Makris, N., and Constantinou, M. C. (1991). Analysis of motions resisted by friction: I. Constant Coulomb and linear/Coulomb friction, Mechanics of Structure and Machine, Vol. 19, No. 4, pp. 477-500.

Marcuson, W.F., III. (1994). An Example of Professional Modesty, The Earth, Engineers, and Education: A Symposium in Honour of Robert V. Whitman, Massachusetts Institute of Technology.

Mavroeidis, P.G., Dong, G., and Papageorgiou, S. A. (2004). Near-Fault Ground Motions, and the Response of Elastic and Inelastic Single-Degree-of-Freedom (SDOF) Systems, Earthquake Engineering and Structural Dynamics, Vol. 33, pp. 1023-1049.

Mavroeidis, P.G., and Papageorgiou, S. A. (2010). Effect of Fault Rupture Characteristics on Near-Fault Strong Ground Motions, Bulleting of the Seismological Society of America, Vol. 100, No. 1, pp. 37-58.

Mavroeidis, P.G., and Papageorgiou, S. A. (2003). A Mathematical Representation of Near-Fault Ground Motions, Bulleting of the Seismological Society of America, Vol. 93, No. 3, pp. 1099-1131.

Mercer, C. A., and Rees, P. L. (1971). An Optimum Shock Isolator, Journal of Sound and Vibration, Vol. 18, No. 4, pp. 511-520.

Mohajer‐Ashjai, A., and Nowroozi, A. A. (1979). The Tabas Earthquake of September 16, 1978 in east‐central Iran, A preliminary field report, Geophysical Research Letters, 6(9), pp. 689-692.

Newmark, N. M. (1965). Effects of Earthquakes on Dams and Embankments, Géotechnique, Vol. 15, No. 2, pp. 139-160.

Pavlou, E.A., and Constantinou, M. C. (2004). Response of Elastic and Inelastic Structures with Damping Systems to Near-Field and Soft-Soil Ground Motions, Engineering Structures, Vol. 26, pp. 1217-1230.

PEER Strong Motion Database. (2002). http://peer.berkeley.edu

Pitarka, A., Somerville, P.G., Fukushima, Y., and Uetake, T. (2002). Ground-Motion Attenuation from the 1995 Kobe Earthquake Based on Simulations Using the Hybrid Green's Function Method, Bulletin of the Seismological Society of America, Vol. 92, pp. 1025-1031.

Pitarka, A., Somerville, P.G., Fukushima, Y., Uetake, T., and Irikura K. (2000). Simulation of Near-Fault Strong-Ground Motion Using Hybrid Green's Functions, Bulletin of the Seismological Society of America, Vol. 90, pp. 566-586.

Pitilakis, K. (2004). Site effects, in Recent Advances in Geotechnical Engineering and Microzonation. A. Ansal (Editor), Kluwer, Hingham, Massachusetts.

Rabinowicz, E. (1951). The nature of the static and kinetic coefficients of friction, Journal of Applied Physics, Vol. 22, pp. 1373-1379.

Rabinowicz, E. (1965). Friction and Wear of Materials, Wiley, New York.

Rathje, E. M., Faraj, F., Russell, S., and Bray, J. D. (2004). Empirical relationships for

frequency content parameters of earthquake ground motions, Earthquake Spectra, 20 (1), pp. 119-144.

Rathje, E. M., and Bray, J. D. (2000). Nonlinear Coupled Seismic Sliding Analysis of Earth Structures, Journal of Geotechnical and Geoenvironmental Engineering, ASCE, Vol. 126 (11), pp. 1002-1014.

Rathje, E.M., and Bray, J.D. (1999). An examination of simplified earthquake-induced displacement procedures for earth structures, Canadian Geotechnical Journal, Vol. 36, pp. 72-87.

Reitherman, R. (2010). Connections: Robert V. Whitman, Oral History Series, Earthquake Engineering Research Institute, Berkeley, California.

Richards, R., and Elms, D.G. (1979). Seismic Behaviour of Gravity Retaining Walls, Journal of Geotechnical Engineering Division, ASCE, Vol. 105, pp. 449-464.

Richards, R., Elms, D.G., and Budhu, M. (1993). Seismic bearing capacity and settlement of foundations, Journal of Geotechnical Engineering, ASCE, Vol. 119, pp. 662-674.

Rodriguez, M. (1994). A measure of the capacity of earthquake ground motions to damage structures, Earthquake Engineering and Structural Dynamics, Vol. 23, No.6, pp. 627-643.

Sarma, S.K. (1975). Seismic Stability of Earth Dams and Embankments, Géotechnique, Vol. 25, No. 4, pp. 743-761.

Sarma, S.K. (1981). Seismic displacement analysis of earth dams, Journal of Geotechnical Engineering Division, ASCE, Vol. 107, pp. 1735-1739.

Sarma, S.K. and Yang, K. S. (1987). An evaluation of strong motion records and a new parameter A95, Earthquake Engineering & Structural Dynamics, 15 (1), pp. 119-132.

Sarma, S.K., and Chen, Y.C. (1995). Seismic bearing capacity of shallow strip footings near sloping ground, Proceedings of the 5th European Conference on Seismic Design Practice, Chester, U.K., Elnashai (ed.), pp. 505-512.

Sarma, S.K. (1999). Seismic bearing capacity of shallow strip footings adjacent to a slope, Earthquake Geotechnical Engineering, Sêco e Pinto (ed.), pp. 309-313.

Sarma, S.K. (1999). Seismic slope stability–The critical acceleration, Earthquake Geotechnical Engineering, Sêco e Pinto (ed.), pp. 1077-1082.

Sarma, S.K., and Kourkoulis, R. (2004). Investigation into the prediction of sliding block displacements in seismic analysis of earth dams, Proceedings of the 13th World Conference on Earthquake Engineering, Vancouver, Canada, paper No 1957.

Sarma, S.K., and Scorer, M. (2009). The effect of vertical accelerations on seismic slope stability, Proceedings of The International Conference on Performance based design in earthquake geotechnical engineering, IS-Tokyo 2009, Editor Kokusho et al, (CD Rom-page 889).

Sasani, M., and Bertero, V.V. (2000). Importance of Severe Pulse-Type Ground Motions in Performance-Based Engineering: Historical and Critical Review, Proceedings of the 12th World Conference on Earthquake Engineering, New Zealand, Paper No 1302.

Sassa, K., Fukuoka, H., Scarascia-Mugnozza, G., and Evans, S. (1996). Earthquake-induced landslides: distribution, motion and mechanisms. Soils & Foundations, Special Issue for the Great Hanshin Earthquake Disaster, pp 53–64.

Sawada, T., Chen, W.F. and Nomachi, S.G. (1993). Assessment of seismic displacements of slopes, Soil Dynamics and Earthquake Engineering, Vol. 12, pp. 357-362.

Seed, H.B., and Martin, G.R. (1966). The Seismic Coefficient In Earth Dam Design, Journal of the Soil Mechanics and Foundation Division, ASCE, Vol. 92, pp. 25-58.

Shen, J., Tsai, M. H., Chang, K.C., and Lee, G.C. (2004). Performance of a Seismically Isolated Bridge under Near-Fault Earthquake Ground Motions, Journal of Structural Engineering, ASCE, Vol. 130, pp. 861-868.

Sideris, P., and Filiatrault, A. (2009). Dynamic analysis of rigid bodies on inclined plane surfaces: application to prediction of merchandise response in steel storage racks under earthquake excitations, COMPDYN, Conference on Computational Methods in Structural Dynamics and Earthquake Engineering, Rhodes, Greece, June 22-24.

Singh, J.P. (1985). Earthquake Ground Motions: Implications for Designing

Structures and Reconciling Structural Damage, Earthquake Spectra, Vol. 1, pp. 239-270.

Sivaselvan, M. V., and Reinhorn, A. M. (2000). Hysteretic models for deteriorating inelastic structures, Journal of Engineering Mechanics, 126, pp. 633-640.

Somerville, P. (2000). Seismic Hazard Evaluation, 12th WCEE 2000, Bulleting of the New Zealand Society of Earthquake Engineering, Vol. 33, pp. 325-346 and pp. 484-491.

Somerville, P. (2003). Characterization of Near Fault Ground Motions for Design, ACI Specialty Conference, U.C. San Diego, American Concrete Institute.

Somerville, P.G., Saikia, C., Wald, D., and Graves, R. (1996). Implications of the Northridge earthquake for strong ground motions from thrust faults, Bulletin of the Seismological Society of America, Vol. 86, pp. 115-125.

Somerville, P.G., Smith, N.F., Graves, R.W. and Abrahamson, N.A. (1997). Modification of Empirical Strong Ground Motion Attenuation Relations to Include the Amplitude and Duration Effects of Rupture Directivity, Seismological Research Letters, Vol. 68, pp. 199-222.

Spudich, P., Hellweg, M. and Lee, W.H.K. (1996). Directional topographic site response at Tarzana observed in aftershocks of the 1994 Northridge, California earthquake: Implications for mainshock motions, Bulletin of the Seismological Society of America, February 1996, Vol. 86, pp. 193-208.

Stamatopoulos, C. A. (1996). Sliding system predicting large permanent co-seismic movements of slopes, Earthquake Engineering and Structural Dynamics, Vol. 25, pp. 1075-1093.

Tadjbakhsh, I. G., and Lin, B. C. (1987). Displacement-Proportional Friction (DPF) in Base Isolation, Earthquake Engineering and Structural Dynamics, Vol. 15, pp. 799-813.

Taflampas, I. (2009). Evaluation of strong ground motion in engineering seismology and structural vulnerability, Ph.D. thesis, National Technical University, Athens, Greece.

Tabor, D. (1981). Friction - the present state of our understanding, ASME, Journal of

Lubrication Technology, Vol. 103, pp. 169-179.

Travasarou, T. (2003). "Optimal Ground Motion Intensity Measures for Probabilistic Assessment of Seismic Slope Displacements", PhD dissertation, Civil and Environmental Engineering, University of California, Berkeley.

Voyagaki, E. L., Mylonakis, G. E., and Psycharis, I. N. (2008, a). Sliding Response of Rigid Blocks on Inclined Plane under Idealised Near-Fault Pulses, Proceedings of the 3rd National Conference on Earthquake Engineering and Engineering Seismology, Athens: Hellenic Society for Earthquake Engineering, G. Gazetas (editor), Paper No 1908.

Voyagaki, E. L., Mylonakis, G. E., and Psycharis, I. N. (2008, b). Sliding Blocks Under Near-fault Pulses: Closed Form Solutions, Geotechnical Earthquake Engineering and Soil Dynamics IV, ASCE Geotechnical Special Publication No 181, Sacramento.

Wartman, J., Bray, J. D., and Seed, R. B. (2003). Inclined Plane Studies of the Newmark Sliding Block Procedure, Journal of Geotechnical and Geo-environmental Engineering, ASCE, Vol. 129 (8), pp. 673-684.

Wen, K. L., Peng, H. Y., Tsai, Y. B., and Chen, K. C. (2001). "Why 1g Was Recorded at TCU129 Site During the 1999 Chi-Chi, Taiwan, Earthquake", Bulleting of Seismological Society of America, Vol.91, No 5, pp. 1255-1266.

Wilson, R. C., and Keefer, D. K. (1983). "Dynamic Analysis of a Slope Failure from the 6 August, 1979 Coyote Lake, California Earthquake", Bulleting of Seismological Society of America, Vol.73, No 3, pp. 863-877.

Xie, L.L., Xu, L.J., and Rondriguez-Marek, A. (2005). Representation of Near-Fault Pulse-Type Ground Motions, Earthquake Engineering and Engineering Vibration, Springer, Vol.4, No.2, pp. 191-199.

Xu, L.J., Rondriguez-Marek, A., and Xie, L.L. (2006). Design Spectra Including Effect of Rupture Directivity in Near-Fault Region, Earthquake Engineering and Engineering Vibration, Springer, Vol. 5, No.2, pp. 159-170.

Yegian, M. K., Harb, J. N., and Kadakal, U. (1998). Dynamic Response Analysis Procedure for Landfills and Geosynthetic Liners, Journal of Geotechnical and Geoenvironmental Engineering, ASCE, Vol. 124 (10), pp. 1027-1033.

Yegian M. K. and Lahlaf A. M (1992). Dynamic Interface Shear Strength Properties of Geomembranes and Geotextiles, Journal of Geotechnical Engineering, ASCE, Vol.118, pp. 760-761.

Yegian, M. K., Marciano, E. A., and Ghahraman, V. G. (1991). Earthquake Induced Permanent Deformations: A Probabilistic Approach, Journal of Geotechnical Engineering, ASCE, Vol.117, pp. 35-50.

Youd, T.L., and Carter, B.L. (2005). Influence on soil softening and liquefaction on spectral acceleration. Journal of Geotechnical and Geoenvironmental Engineering, ASCE; 131(7), pp. 811–825.

Youd, T.L., Bardet, J-P., and Bray, J.D. (2000). Kocaeli, Turkey, Earthquake of August 17, 1999 Reconnaissance Report. Earthquake Spectra Suppl. A, pp 16-456.

Appendix

During the study we also wrote and submitted (in journals) four papers with results from this research. These papers namely are:

1) *Apostolou M., Gazetas G., Garini E. (2007), "Seismic Response of Simple Structures with Foundation Uplift", Journal of Soils Dynamics and Earthquake Engineering, Vol. 27 (7), pp. 642-654.*
2) *Gazetas G., Garini E., Anastasopoulos I., Georgarakos T. (2009) "Effects of Near–Fault Ground Shaking on Sliding Systems", Journal of Geotechnical and Geoenvironmental Engineering, ASCE, Vol. 135, No. 12, pp. 1906-1921.*
3) *Garini E., Gazetas G., Anastasopoulos I. (2011), " Asymmetric 'Newmark' Sliding Caused by Motions Containing Severe 'Directivity' and 'Fling' Pulses", Géotechnique, Vol.61, No. 9, pp. 733-756.*
4) *Gazetas G., Garini E., Berrill J.B., Apostolou M. (2011), "Sliding and Overturning Potential of the Christchurch 2011 Earthquake Records", Earthquake Engineering and Structural Dynamics (accepted for publication)*

Moreover, several conference papers are written (three for Greek and four for international conferences and workshops):

- *Garini E., Gazetas G., Gerolymos N. (2010), " Effect of Pre-Yielding Elasticity on Sliding Triggered by Near-Fault Wavelets ", Proceedings of 6th Hellenic Conference on Geotechnical and Geoenvironmental Engineering, Bolos, 29 September –1 October, Vol. 1, pp. 533-539*
- *Garini E., Gerolymos N., Ziotopoulou K., Gazetas G. (2010), " Seismic Response Analysis of Earthfill Dams using Rigorous and Simplified Methods-The Case of Asterios Dam ", Proceedings of 6th Hellenic Conference on Geotechnical and Geoenvironmental Engineering, Bolos, 29 September –1 October, Vol. 1, pp. 541-548*

- *Garini E., Gazetas G., Gerolymos N. (2009) "Effect of Pre-Yielding Elasticity on Sliding Triggered by Near-Fault Motions Modeled as Idealized Wavelets", Proceedings of 3rd Greece-Japan Workshop on Seismic Design, Observation and Retrofit of Foundations, Santorini, Greece pp. 171-184.*
- *Gazetas G., Garini E., and Georgarakos T. (2008), "Effects of Near–Fault Ground Shaking on Sliding Systems", Conference Proceedings of Geotechnical Earthquake Engineering and Soil Dynamics IV, Sacramento, CA, 18–22 May.*
- *Garini E., Anastasopoulos I., Gazetas G. (2008) "Paradoxical Sliding Behaviour of Block Triggered by Near–Fault Ground Motions", Proceedings of 3rd Hellenic Conference on Earthquake Engineering and Technical Seismology, 5-7 November, Athens, Paper No. 2035 (in CD-Rom).*
- *Garini E., Gazetas G. (2007) "Sliding of Rigid Block on Sloping Plane: The Surprising Role of the Sequence of Long Duration Pulses", Proceedings of 2nd Japan-Greece Workshop on Seismic Design, Observation and Retrofit of Foundations, Tokyo, Japan, pp. 171-184.*
- *Garini E., Gazetas G., Anastasopoulos I. (2007) "Rupture–Directivity and Fling–Step Effects on Newmark Block Sliding", Proceedings of 4th International Conference on Earthquake Geotechnical Engineering, Thessaloniki, Greece, Paper No. 1563 (in CD-Rom).*
- *Garini E., Gerolymos N., Gazetas G. (2006) "Asymmetric Block Sliding from Idealized Pulse Wavelets and Near-fault Ground Motions. ", Proceedings of 5th Hellenic Conference on Geotechnical and Geoenvironmental Engineering, 31 May-2 June, Xanthi, Vol. 2, pp. 121-127.*